# Quarkonium Phenomenology in Vacuum

Dissertation
zur
Erlangung des Doktorgrades
der Naturwissenschaften

vorgelegt beim Fachbereich Physik
der Johann Wolfgang Goethe-Universität
in Frankfurt am Main

von
Denis Parganlija
aus Frankfurt am Main

Frankfurt/Main (12.12.2011)

(D 30)

vom Fachbereich Physik der Johann Wolfgang Goethe-Universität
als Dissertation angenommen

| | |
|---|---|
| Dekan: | Prof. Dr. Michael Huth |
| Gutachter: | Prof. Dr. Dirk-Hermann Rischke |
| | Prof. Dr. Jürgen Schaffner-Bielich |
| Datum der Disputation: | |

# Contents


**1 Introduction** **1**

**2 QCD and Its Symmetries** **7**

2.1 Introduction . . . 7

2.2 The QCD Lagrangian . . . 10

2.3 The Chiral Symmetry . . . 11

2.4 Other QCD Symmetries . . . 16

2.4.1 $\boldsymbol{CP}$ Symmetry . . . 16

2.4.2 $\boldsymbol{Z}$ Symmetry . . . 18

2.4.3 Dilatation Symmetry . . . 18

2.5 Spontaneous Breaking of the Chiral Symmetry . . . 21

2.6 Calculating the Decay Widths . . . 24

2.6.1 Parametrising the Scattering Amplitude . . . 30

2.6.2 Example: Decaying Axial-Vector State I . . . 35

2.6.3 Example: Decaying Axial-Vector State II . . . 37

2.6.4 Example: Decaying Scalar State . . . 39

**3 Review of Scalar Isosinglets** **41**

3.1 The $\boldsymbol{f_0(600)}$ Resonance . . . 41

3.2 The $\boldsymbol{f_0(980)}$ Resonance . . . 44

3.3 The $\boldsymbol{f_0(1370)}$ Resonance . . . 47

3.4 The $\boldsymbol{f_0(1500)}$ Resonance . . . 51

3.5 The $\boldsymbol{f_0(1710)}$ Resonance . . . 52

3.6 The Peculiar Case of $\boldsymbol{f_0(1790)}$ . . . 55

3.7 Consequences for the $\boldsymbol{f_0(1710)}$ Decay Channels . . . 57

3.7.1 The $\boldsymbol{f_0(1710)}$ Decay Widths from Data Preferred by the PDG . . . 57

3.7.2 The $\boldsymbol{f_0(1710)}$ Decay Widths from Alternative BES II Data . . . 60

3.7.3 The $\boldsymbol{f_0(1710)}$ Decay Widths from WA102 Data . . . 61

**4 Construction of a Meson Model** **63**

4.1 General Remarks . . . 63

4.2 The Lagrangian with Global Chiral Symmetry . . . 66

4.3 Large-$N_c$ Behaviour of Model Parameters . . . 72

**5 Two-Flavour Linear Sigma Model** **75**

5.1 The $N_f = 2$ Lagrangian . . . 75

5.1.1 Tree-Level Masses . . . 77

5.1.2 Equivalent Set of Parameters . . . 80

5.2 Decay Widths and $\pi\pi$ Scattering Lengths . . . 80

5.2.1 Decay Width $\rho \to \pi\pi$ . . . 81

5.2.2 Decay Width $f_1(1285) \to a_0\pi$ . . . 83

5.2.3 Decay Width $\sigma_N \to \pi\pi$ . . . 84

5.2.4 Decay Amplitudes $a_0 \to \eta\pi$ and $a_0 \to \eta'\pi$ . . . 85

5.2.5 Decay Width $a_1(1260) \to \pi\gamma$ . . . 87

5.2.6 Decay Width $a_1(1260) \to \sigma_N\pi$ . . . 88

5.2.7 Decay Width $a_1(1260) \to \rho\pi$ . . . 89

5.2.8 Tree-Level Scattering Lengths . . . 91

5.3 Scenario I: Light Scalar Quarkonia . . . 94

5.3.1 Fit procedure . . . 94

5.3.2 Decay Width $\sigma_N \to \pi\pi$ . . . 97

5.3.3 Decays of the $a_1(1260)$ Meson . . . 98

5.3.4 The Case of Isospin-Exact Scattering Lengths . . . 99

5.4 Scenario II: Scalar Quarkonia above 1 GeV . . . 100

5.4.1 Decays of the $a_0(1450)$ Meson . . . 100

5.4.2 Decays of the $f_0(1370)$ Meson . . . 103

5.5 Conclusions from the Two-Flavour Version of the Model . . . 104

5.6 The Full $N_f = 2$ Lagrangian . . . 105

**6 Three-Flavour Linear Sigma Model** **109**

6.1 The $N_f = 3$ Lagrangian . . . 109

6.2 Assigning the Fields . . . 115

6.3 General Discussion of the Model Parameters . . . 116

6.4 Modelling the Chiral Anomaly . . . 117

**7 The Fit Structure** **121**

7.1 Mixing of $\eta$ and $\eta'$ . . . 122

**8 Fit I: Scalars below 1 GeV** **127**

**9 Implications of Fit I** **133**

9.1 Phenomenology in the $I(J^{PC}) = 0(0^{++})$ Channel . . . 133

9.1.1 A Necessary Condition for the Spontaneous Symmetry Breaking . . . 133

9.1.2 A Condition for $\lambda_{1,2}$ from SSB . . . 134

9.1.3 Scalar Isosinglet Masses . . . 135

9.1.4 Decay Width $\sigma_{1,2} \to \pi\pi$ . . . 138

9.1.5 Decay Width $\sigma_{1,2} \to KK$ . . . 142

9.1.6 Decay Width $\sigma_{1,2} \to \eta\eta$ . . . 146

9.2 Decay Amplitude $a_0(980) \to \eta\pi$ . . . 150

9.3 Decay Width $K_0^\star(800) \to K\pi$ . . . 151

9.4 Phenomenology of the Vector and Axial-Vector Mesons in Fit I . . . 153

9.4.1 Decay Width $a_1(1260) \to \rho\pi$ in Fit I . . . 154

9.4.2 Decay Width $a_1(1260) \to f_0(600)\pi$ in Fit I . . . 155

9.4.3 Decay Width $a_1(1260) \to K^\star K \to KK\pi$ in Fit I . . . 155

9.4.4 Decay Width $f_1(1285) \to K^\star K$ in Fit I . . . 156

9.4.5 Decay Width $K^\star \to K\pi$ in Fit I . . . 159

9.4.6 Decay Width $f_1(1420) \to K^\star K$ in Fit I . . . 161

9.4.7 $K_1$ Decays in Fit I . . . 163

9.5 Pion-Pion Scattering Lengths . . . 167

9.6 Conclusions from Fit with Scalars below 1 GeV . . . 174

**10 Fit II: Scalars above 1 GeV** **177**

10.1 Full decay width of $a_0(1450)$ . . . 177

10.2 Implementation of Fit II . . . 178

10.3 Two $K_1$ Fields . . . 183

**11 Implications of Fit II** **185**

11.1 Phenomenology in the $I(J^{PC}) = 0(0^{++})$ Channel . . . 185

11.1.1 Scalar Isosinglet Masses . . . 185

11.1.2 Decay Width $\sigma_{1,2} \to \pi\pi$ . . . 187

11.1.3 Decay Width $\sigma_{1,2} \to KK$ . . . 191
11.1.4 Decay Width $\sigma_{1,2} \to \eta\eta$ . . . 194
11.1.5 Combined Results in the Pion, Kaon and Eta Channels . . . 197
11.1.6 Decay Width $\sigma_{1,2} \to \eta\eta'$ . . . 199
11.1.7 Decay Width $\sigma_{1,2} \to a_1(1260)\pi \to \rho\pi\pi$ . . . 202
11.1.8 Decay Width $\sigma_2 \to \omega\omega$ . . . 204
11.2 Decay Width $K_0^\star(1430) \to K\pi$ . . . 205
11.3 Phenomenology of Vector and Axial-Vector Mesons in Fit II . . . 206
11.3.1 Decay Width $a_1(1260) \to \rho\pi$ in Fit II . . . 207
11.3.2 Decay Width $a_1(1260) \to K^\star K \to KK\pi$ in Fit II . . . 209
11.3.3 Decay Width $\varphi(1020) \to K^+K^-$ in Fit II . . . 209
11.3.4 Decay Width $K^\star \to K\pi$ in Fit II . . . 211
11.3.5 Decay Width $f_1(1285) \to K^\star K$ in Fit II . . . 211
11.3.6 Decay Width $f_1(1420) \to K^\star K$ in Fit II . . . 213
11.3.7 $K_1$ Decays in Fit II . . . 213
11.4 Conclusions from Fit with Scalars above 1 GeV . . . 216

**12 Incorporating the Glueball into the Model** **221**
12.1 Introduction . . . 221
12.2 The Model . . . 222
12.3 Results and Discussion . . . 225
12.3.1 Assigning $\sigma'$ and $G'$ to $f_0(1370)$ and $f_0(1500)$ . . . 225
12.3.2 Assigning $\sigma'_N$ and $G'$ to $f_0(1370)$ and $f_0(1710)$ . . . 228
12.3.3 Scenarios with $\sigma' \equiv f_0(600)$ . . . 230
12.4 Summary of the Results with the Dilaton Field . . . 230

**13 Conclusions** **231**

**14 Zusammenfassung** **235**

**Bibliography** **241**

# 1. Introduction

The human race has always been guided by the quest *So that I may perceive whatever holds // The world together in its inmost folds* – or in the original, German version: *Dass ich erkenne, was die Welt // Im Innersten zusammenhält* [1]. And it has been a long journey: the first strives of the human spirit to understand the inner principles governing nature are as old as civilisation itself. It has been remembered, for example, that more than two and a half millenia ago the ancient Greek philosopher Leucippus claimed nature to possess inner elements of structure, the atoms – or the indivisible ones (as coined by Democritus). An alternative *theory of everything* foresaw the existence of four basic elements (ranging from water to fire) upon which nature is built. Although the idea of the atom is an ancient one, a lot of time passed before the idea of atomic clusters (that is, molecules) was established by Robert Boyle in 1661. Approximately a decade later, Isaac Newton developed the corpuscular theory of light, for which he claimed that it consists of minute particles (corpuscles).

Nowadays the prevalent explanation of the features of light is that of corpuscle-wave duality: the light may behave more as a set of corpuscles or as a wave, depending on the experimental surrounding. Indeed the light corpuscles – the photons – act as transmitters of one of the fundamental forces of nature: the electromagnetic interaction. This interaction is known to affect all particles carrying electric charge (electrons, protons,...). It is essential for the attraction of atomic nuclei (consisting of the positive-charge protons and neutrons that carry no charge) and the electrons, that build a negative-charge cloud around the atomic nuclei and allow for atoms to bind into more complex structures, the molecules.

It has been known since the age of Charles Coulomb ($18^{\text{th}}$ century) that the electromagnetic (back then: only electric) interaction possesses an infinite range – it is inversely proportional to the squared distance between two charges:

$$F_C \sim \frac{1}{r^2}.$$

There is, however, another interaction with such a feature: the gravity. This interaction occurs between objects that possess a mass, be it point-like objects such as electrons (mass $\sim 10^{-31}$ kg or, in units more commonly used in physics nowadays, $\sim 511$ keV) or very large objects such as the sun ($\sim 10^{30}$ kg) or even planetary systems, galaxies and galaxy clusters.

According to Newton's law of universal gravity, the magnitude of this force is also proportional to $1/r^2$. Just as the electromagnetic interaction, gravity is expected to possess its *transmitter particles* (gauge bosons), denoted as gravitons. Newton himself did not coin the name but was reportedly dissatisfied with the *action at a distance* implied by his gravity law (and he expected a *mediator of gravity* to exist). The problem of action at a distance is indeed solved by the introduction of gravitons; however, these particles – if they exist – have remained elusive to experimental observation. The basic difference between photons and gravitons is their spin: photons possess spin one whereas gravitons are expected to possess spin two rendering them rather difficult to examine theoretically [2]. However, gravity without gravitons would mark a special case of an elementary force without gauge particles because not only the electromagnetic interaction but also the other two elementary forces – the strong and the weak interactions – possess their gauge bosons as well.

The weak force has actually been unified with the electromagnetic force into the electroweak one in the groundbreaking work of Glashow, Weinberg, Salam and Ward in the 1960s and 1970s [3]. The ensuing Standard Model of electroweak interactions describes simultaneously the twelve building blocks of nature known to the modern physics:

$$\begin{aligned} \text{6 quarks: } & u \text{ (up)}, d \text{ (down)} \\ & s \text{ (strange)}, c \text{ (charm)} \\ & b \text{ (bottom)}, t \text{ (top)} \end{aligned}$$

and

$$\begin{aligned} \text{6 leptons: } & e \text{ (electron)}, \nu_e \text{ (electron neutrino)} \\ & \mu \text{ (muon)}, \nu_\mu \text{ (muon neutrino)} \\ & \tau \text{ (tau)}, \nu_\tau \text{ (tau neutrino)} \end{aligned}$$

(plus twelve antiparticles). The masses of these particles vary significantly: for example, as we will see in the next chapter, the mass of the $t$ quark is approximately 50000 times larger than the masses of the $u$ and $d$ quarks. Nonetheless, the Standard Model actually starts with the assumption that the particles possess no mass; this includes the gauge bosons of the electroweak interaction, labelled as $W^\pm$ and $Z^0$ as well as the gauge boson of the electromagnetic interaction, the photon [in the language of modern physics: the local $SU(2)_L \times U(1)_Y$ symmetry]. The symmetry is broken by the famous Higgs mechanism that gives mass to all leptons except neutrinos as well as to $W^\pm$ and $Z^0$; the photon remains massless. The predictions of the Standard Model have been confirmed to a high precision by various experiments [4]. Only the Higgs boson has remained elusive at Tevatron as well as at the Large Hadron Collider LHC at CERN (but, if it exists, it should be discovered at the LHC).

There are actually attempts to extend the Standard Model to the physics beyond (again, if such physics exists – this is also, in principle, verifyable at the LHC). One extension is supersymmetry [5], where one assumes that to each observed boson and the as-yet unobserved Higgs (integer-spin particles) there is a supersymmetric fermion counterpart (and analogously for the observed fermion). This renders the lightest of the supersymmetric particles – the LSP – stable under the so-called $R$-parity; the LSP is a candidate for a dark-matter particle.

A further possible extension of the Standard Model is represented by technicolour models [6]. These models are based upon the observation that the Higgs boson – if it exists – would be the only elementary *scalar* particle known to modern physics, i.e., it would possess spin zero. All the other elementary particles are not scalar: the already mentioned quarks and leptons are fermions as they possess spin 1/2 whereas the gauge bosons possess spin 1 or spin 2, depending on the interaction considered. Indeed, until now all scalar states first assumed to be elementary were eventually determined as composite (such as the $\sigma$ meson of the strong interaction, discussed below). For this reason, technicolour models assume the Higgs boson to be composite as well, consisting of so-called *techniquarks*. Techniquarks are expected to be several times heavier than the heaviest observed quark (the $t$ quark) but should in principle also be accessible to the LHC. (Note that there is also a technicolour candidate for the dark matter particle: technicolour-interacting massive particle or TIMP [7].)

The work presented in this thesis will consider a different type of interaction: the strong one. This interaction is responsible for the stability of the nucleons, i.e., protons and neutrons (and thus of atoms and molecules); it is similar to the electromagnetic interaction as it also possesses massless gauge bosons – the *gluons*. Given that the gluons are massless just as the photons, one might expect the range of the strong interaction to be infinite, just as in the case of the electromagnetic one. However the strong interaction actually possesses a very short range ($\sim$ 1 fm = $10^{-15}$ m, the nucleon radius). Additionally, the gluons, while not charged electrically, nonetheless carry a different sort of charge: *colour*. They are transmitters of the strong interaction between quarks; however, their colour charge allows them to not only interact with quarks but also among themselves. It is believed that the colour interaction holds quarks and gluons *confined* within nucleons (which is in turn presumably related to the nucleon stability) – but confinement is an experimental observation without (as yet) a commonly accepted theoretical explanation.

Quarks and gluons were not always confined to nucleons. According to the theory of the Big Bang, an extremely short-lived phase of the primary matter ($10^{-44}$ s), where no complex matter structures existed, was followed by a state of the *quark-gluon* plasma, without confinement of quarks and gluons into nucleons. The expansion of the early universe implied the cooling of the matter, allowing for the first complex structures to be formed by quarks. The simplest ones consisted of one quark ($\bar{q}$) and one antiquark ($q$). Thus the exploration of the $\bar{q}q$ states allows us to gain insight into the early universe – and the work presented in this thesis will have exactly the $\bar{q}q$ states as the main topic.

Of course, there can be no true insight into the state of matter in the early universe from the theoretical standpoint alone; there are various experimental undertakings attempting to recreate the matter as it was shortly after the Big Bang ($\sim$ 13 billion years ago). To this end, heavy ions (Pb, Au) or protons are collided at velocities comparable to the velocity of light; the collisions produce very hot (at least $10^{12}$ K) and/or very dense ($\sim 10^{15}$ g/cm$^3$) matter. Let us mention just three experimental facilities where this is (or will be) accomplished: proton-proton collisions and heavy-ion collisions are performed at the LHC and at the Relativistic Heavy-Ion Collider RHIC in Upton, New York/United States; protons and antiprotons will be collided at the Facility for Antiproton and Ion Research (FAIR), currently being constructed at the Gesellschaft für Schwerionenforschung (GSI) in Darmstadt/Germany.

As already indicated, the work presented in this thesis will be concerned with the strong interaction. Thus in Chapter 2 we describe some basic properties of the theory of strong interactions – the Quantum Chromodynamics (QCD). We introduce the concepts of hadrons, quarks, gluons and colour charge. We observe that the basic equation of QCD – the *QCD Lagrangian* – possesses certain symmetries, most notably the chiral $U(N_f) \times U(N_f)$ symmetry between $N_f$ left-handed and right-handed quark flavours. However, as we discuss in Sec. 2.5, this symmetry is also observed to be broken in vacuum by two mechanisms: explicitly, by non-vanishing quark masses, and spontaneously, by the quark condensate. An additional symmetry-breaking mechanism is the so-called chiral anomaly (a symmetry that is exact classically but broken at the quantum level, discussed in Sec. 2.3).

The spontaneous breaking of the chiral symmetry leads to some profound consequences. Goldstone bosons (for example, the pions) emerge and the masses are generated for a range of mesons. (The pions obtain their mass from the explicit breaking of the chiral symmetry.) Most (but not all) mesons can be described as $\bar{q}q$ states; considering the approximate mass degeneration of the

non-strange [up ($u$) and down ($d$)] quarks, there is one scalar isosinglet state that can be constructed: $\sigma_N = (\bar{u}u + \bar{d}d)/\sqrt{2}$. If we consider the strange quark $s$ as well, then we can construct an additional scalar state: $\sigma_S = \bar{s}s$. However, as we discuss in Chapter 3, experimental data demonstrate that the actual number of scalars is significantly larger: there are six non-strange scalar states [$f_0(600)$ or $\sigma$, $f_0(980)$, $f_0(1370)$, $f_0(1500)$, $f_0(1710)$ and $f_0(1790)$]. Obviously, at most two of them can be $\bar{q}q$ states – but the question is *which two*.

That is the main topic of the work presented in this thesis. In Chapter 4 we develop a generic model of mesons for an arbitrary number of flavours, based on the symmetries of QCD. The model can even be studied for various numbers of colours. Then, in Chapters 5 – 11, we apply the model to investigate scalar $\bar{q}q$ states in the physical spectrum. It is known as the Linear Sigma Model and it incorporates not only the global symmetries of QCD (chiral, $CP$) but also the mechanisms of chiral-symmetry breaking (explicit, spontaneous and the one induced by the chiral anomaly). However, the Linear Sigma Model contains not only scalar states; a realistic model of low-energy QCD will inevitably have to consider other states experimentally established in the region of interest (in our case: up to $\sim 1.8$ GeV). For this reason, our model will also incorporate vector ($\omega$, $\boldsymbol{\rho}$) and axial-vector [$f_1(1285)$, $a_1(1260)$] degrees of freedom from the onset. Then, in Chapter 5, we develop a $U(2)_L \times U(2)_R$ sigma model with scalars (sigma, $\boldsymbol{a}_0$), pseudoscalars (pion and the non-strange component of the physical $\eta$ state), vectors and axial-vectors and describe their phenomenology. The states present in our model are of $\bar{q}q$ structure, as we discuss in Sec. 4.3. Consequently, all our statements about the physical states depend on the assignment of our $\bar{q}q$ model states to the physical ones (conversely, of course, assigning any of our $\bar{q}q$ states to a physical state implies that the given physical state is of $\bar{q}q$ nature).

Given the already mentioned large number of scalar $f_0$ states, we work with two different scenarios in Chapter 5: in Scenario I, Sec. 5.3, we assume that the scalar $\bar{q}q$ states are to be looked for in the energy region below 1 GeV. This implies, for example, that the $f_0(600)$ resonance is a $\bar{q}q$ state. However, this assumption does not appear to be favoured when its implications are compared with experimental data. The $f_0(600)$ resonance is too narrow. Therefore, in Sec. 5.4, we start with a converse assumption (Scenario II): that the scalar $\bar{q}q$ states are actually above 1 GeV [then the $f_0(1370)$ resonance is the scalar $\bar{q}q$ state]. In this scenario, the overall description of the data is decisively better: *the scalar $\bar{q}q$ states appear to be above 1 GeV* rather than, as one might expect, below.

The discussion of Chapter 5 is, however, not conclusive. The reasons are at least twofold: the strange mesons (such as the $K_0^\star$ states) are missing; additionally, the gauge bosons of QCD, the gluons, may, just as quarks, form their own bound states – the glueballs. These states could mix with the scalar $\bar{q}q$ states already present in the model. Thus the question has to be addressed whether the conclusions of Chapter 5 hold once the mentioned strange and glueball states are included into the model. [In principle one could also consider the admixture of the tetraquark ($\bar{q}\bar{q}qq$) states to the scalar resonances; this can be performed in succession to the results regarding quarkonium and glueball phenomenology presented in this thesis.]

For this reason, in Chapters 6 – 11 we present the main part of this work: a sigma model containing scalar, pseudoscalar, vector and axial-vector mesons *both in non-strange and strange sectors*: an $N_f = 3$ model. This is **the first time** that all these states have been considered within a single QCD-based model. Our formalism thus contains, but is not limited to, $\eta$, $\eta'$, $\boldsymbol{\pi}$, $K$ (pseudoscalars); $\omega$, $\varphi(1020)$, $\boldsymbol{\rho}$, $K^\star$ (vectors) and $f_1(1285)$, $f_1(1420)$, $a_1(1260)$, $K_1$ (axial-vectors). The model also contains two scalar isosinglet degrees of freedom $\sigma_N$ (already present

in Chapter 5) and additionally $\sigma_S = \bar{s}s$. We also consider the $\boldsymbol{a}_0$ triplet (already present in Chapter 5) and the scalar-kaon quadruplet $K_S$. (Our scalar state $K_S$ is to be distinguished from the short-lived pseudoscalar $K_S^0$ state that will not be discussed in this work.)

The model parameters are calculated using all masses except those of the two $\sigma$ fields. Then, as in Chapter 5, we distinguish between two possibilities (labelled as Fits I and II in Chapters 6 – 11): in Fit I (Chapters 8 and 9) we discuss whether a reasonable meson phenomenology can be obtained assuming that the scalar $\bar{q}q$ states are below 1 GeV. Thus we work with the assumption that the $f_0(600)$ and $K_0^\star(800)$ resonances are $\bar{q}q$ states (analogously to Scenario I presented in Sec. 5.3). This allows us to consider not only scalar-meson phenomenology, but the broader phenomenology as well – in particular the decays of the axial-vector states [e.g., $f_1(1285)$, $f_1(1420)$ and $a_1(1260)$]. We again obtain a negative result: if the scalars were below 1 GeV, then the axial-vectors would have to have a decay width from 1 GeV up to 20 GeV – several orders of magnitude larger than experimental data. For this reason, we turn to an alternative assignment: that the scalar $\bar{q}q$ states are above 1 GeV. The ensuing fit yields an extremely improved meson phenomenology: almost all the results are consistent with experimental data.

As already indicated, our study is motivated by the phenomenology of the scalar mesons. A realistic description of the scalar states requires the inclusion of vector and axial-vector states as well. Thus our study will also include the phenomenology of these states: indeed, in the more general $N_f = 3$ version of our model in Chapters 8 – 11, we will calculate widths of all experimentally observed two-body decays of mesons for which there exist vertices in the model. This will be performed in both (pseudo)scalar as well as (axial-)vector channels. In addition, three-body and four-body decay widths will also be calculated utilising sequential decays; $\pi\pi$ scattering lengths will be calculated as well. This will in turn provide us with an extremely powerful agent of discrimination between the two assignments where, respectively, the scalar states are below and above 1 GeV.

Before the summary and outlook of the work are presented in Chapter 13, we present another extension of the $N_f = 2$ model of Chapter 5 to $N_f = 2 +$ scalar glueball in Chapter 12. Although Chapter 12 does not present results with strange degrees of freedom, it is still another valuable test of the assertion obtained in Chapter 5: that the scalar $\bar{q}q$ states are above, rather than below, 1 GeV.

# 2. QCD and Its Symmetries

## 2.1 Introduction

A large multitude of new particles was discovered in the 1950s and 1960s. There were usually referred to as *elementary*, implying that they possessed no inner structure; however, their decay patterns and large numbers imposed two questions:

- Why do we observe that the newly discovered particles do not decay into all other particles into which their decays would be kinematically alowed?
- Is there a classfication scheme for the new particles, but also for the already known ones, such as protons and neutrons?

In other words: Is there a force binding more elementary blocks into the observed particles?
A classification scheme was proposed by M. Gell-Mann [8] and G. Zweig [9] in 1964 using the $SU(3)$ flavour symmetry. Zweig proposed the particle substructure elements to be denoted as *aces* whereas, according to Gell-Mann's classification, if one considers a unitary triplet $t$ consisting of an isotopic singlet $s$ of electric charge $z$ and an isotopic doublet $(u, d)$ with charges $z + 1$ and $z$ respectively, then

> *We can dispense entirely with the basic baryon b if we assign to the triplett the following properties*: *spin* $\frac{1}{2}$, $z = -\frac{1}{3}$ *and baryon number* $\frac{1}{3}$.
> *We then refer to members* $u^{\frac{2}{3}}$, $d^{-\frac{1}{3}}$, *and* $s^{-\frac{1}{3}}$ *of the triplet as "quarks" and the members of the anti-triplet as anti-quarks.*

Therefore the particles originally denoted as elementary (protons, neutrons, hyperons,...) were suggested to possess an inner structure. Strictly speaking, they are then no longer *elementary* as this role is thereafter played by their substructure partons, the quarks, but nonetheless they are still sometimes referred to as elementary. All the particles containing quarks are subject to the so-called strong interaction, described by

**Quantum Chromodynamics (QCD).**

We will discuss the Lagrangian of QCD later in this chapter. At this point we note that, due to the electric charge of the quarks, the electromagnetic interaction also plays a certain, though subdominant, role in quark interactions. The reason is that the fine-structure constant of the electromagnetic interaction (that encodes the strength of the electromagnetic coupling) $\alpha = 1/137.035999679(94)$ [10] is two orders of magnitude smaller than the fine-structure constant of the strong interaction $\alpha_s \sim 1$ in vacuum. Additionally, the quarks can also interact weakly, by exchanging weak bosons [4]; this mechanism is responsible for the $\beta$ decay of nucleons.
The particles containing quarks are known as *hadrons* (Greek – $\alpha\delta\rho\acute{o}\varsigma$: strong). Hadrons are classified into two groups according to their spin:

- *Fermionic* hadrons are known as *baryons* (Greek – $\beta\alpha\rho\acute{\upsilon}\varsigma$, heavy: the lightest baryon, the proton, is approximately 1836 heavier than the electron).
- *Bosonic* hadrons are known as *mesons* from the Greek word – $\mu\acute{\varepsilon}\sigma o\varsigma$, the middle one: the first discovered meson was the pion [11], approximately 280 times heavier than the electron but still lighter than the proton; the name has remained although it is an experimental fact nowadays that baryons and mesons typically accommodate the same mass region. Note that the mesons are sometimes defined in terms of their quark structure as antiquark-quark states. This definition is improper because not all mesons are $\bar{q}q$ states (some of them may be of $\bar{q}\bar{q}qq$ structure, or even represent bound states of other mesons). Consequently, this work will utilise the definition of mesons based on their spin.

Current high-energy experimental data suggest that (as already indicated) there are six building blocks of hadrons – i.e., six quark *flavours* with the following masses according to the Particle Data Group (PDG) [10]:

$$\begin{aligned} m_u &= (1.7 - 3.1)\ \text{MeV};\ m_d = (4.1 - 5.7)\ \text{MeV};\\ m_s &= (80 - 130)\ \text{MeV};\\ m_c &= 1.29^{+0.05}_{-0.11}\ \text{GeV};\ m_b = 4.19^{+0.18}_{-0.06}\ \text{GeV};\\ m_t &= (172.9 \pm 0.6 \pm 0.9)\ \text{GeV}. \end{aligned}$$

These values are the estimates of the so-called current quark masses. The values of $m_{u,d,s}$ are not a product of direct experimental observations but obtained either in lattice calculations [12] or in first-principle calculations [13] at the scale $\mu \approx 2$ GeV. Indeed, to our knowledge, there has recently been only one article by an experimental collaboration regarding the light-quark masses: the results of the ALEPH Collaboration suggest $m_s = 176^{+46}_{-57}$ MeV (at $\mu \approx 2$ GeV) from a $\tau$-decay analysis [14]. Similarly, the value of $m_c$ is also predominantly determined in theoretical calculations [15] although the BABAR Collaboration has recently claimed $m_c = (1.196 \pm 0.059 \pm 0.050)$ GeV from $B$ decays [16]. The value of $m_t$ stems from direct top-event observations published by the Tevatron Electroweak Working Group (see Ref. [17] for the latest data and references therein for the older ones). Similar is true for the $b$ quark [10]. Note that the current $u$, $d$ masses need to be distinguished from their constituent masses $\sim 300$ MeV $\simeq m_p/3$ where $m_p$ denotes the mass of the proton.

Quarks carry electric charges as follows

$$u, c, t \leftrightarrow \frac{2}{3}e, \tag{2.1}$$

$$d, s, b \leftrightarrow -\frac{1}{3}e, \tag{2.2}$$

where $e$ denotes the elementary electric charge. Following the Gell-Mann–Zweig classification, a proton is a state containing two $u$ quarks and one $d$ quark (with the charge $2 \cdot 2e/3 - e/3 = e$). Given that the total spin of the proton reads $1/2$, then the spin-flavour wave function of this particle can be written as

$$|p\rangle = \frac{1}{\sqrt{3}}(|u_\uparrow u_\uparrow d_\downarrow\rangle + |u_\uparrow u_\downarrow d_\uparrow\rangle + |u_\downarrow u_\uparrow d_\uparrow\rangle). \tag{2.3}$$

An analogous relation holds for the neutron upon substituting $u \longleftrightarrow d$. These relations comply with W. Pauli's Spin-Statistics Theorem [18]. However, in 1965 a baryon with charge $q = 2e$ and spin 3/2 was discovered [19]; the particle could readily be described in terms of $u$ and $d$ quark flavours with spin 1/2, but only if the Pauli Principle were violated. The particle was labelled as $\Delta^{++}$ [or, nowadays, $\Delta(1232)$] and, given the charge, its spin-flavour wave function had to be composed as

$$|\Delta^{++}\rangle = |u_\uparrow u_\uparrow u_\uparrow\rangle. \tag{2.4}$$

The solution to this paradox was found by introducing an additional degree of freedom for quarks: colour. If we assume that each quark comes in three colours, red ($r$), green ($g$) and blue ($b$), then the three quarks contained in $\Delta^{++}$ can be combined in the following antisymmetric way in the colour space:

$$|\Delta^{++}\rangle_{\text{colour}} = \frac{1}{\sqrt{6}}|u_r u_g u_b + u_g u_b u_r + u_b u_r u_g - u_g u_r u_b - u_b u_g u_r - u_r u_b u_g\rangle. \tag{2.5}$$

Indeed, assuming that any baryon $B$ contains three quarks $q_{1,2,3}$, then the colour wave function of such a composite object can be antisymmetrised as

$$\begin{aligned}|B\rangle_{\text{colour}} = \frac{1}{\sqrt{6}}|&q_{1r}q_{2g}q_{3b} + q_{1g}q_{2b}q_{3r} + q_{1b}q_{2r}q_{3g}\\ &- q_{1g}q_{2r}q_{3b} - q_{1b}q_{2g}q_{3r} - q_{1r}q_{2b}q_{3g}\rangle\end{aligned} \tag{2.6}$$

or simply

$$|B\rangle_{\text{colour}} = \frac{1}{\sqrt{6}}\varepsilon^{\alpha\beta\gamma}|q_{1\alpha}q_{2\beta}q_{3\gamma}\rangle, \tag{2.7}$$

where $\varepsilon^{\alpha\beta\gamma}$ denotes the totally antisymmetric tensor and $\alpha, \beta, \gamma \in \{r, g, b\}$.
Then the direct product of the $\Delta^{++}$ flavour-spin wave function (2.4) with the corresponding colour wave function (2.5) yields a total wave function that is antisymmetric under exchange of two quarks – in accordance with the Pauli Principle.

This is of course valid under the assumption that there are three quark colours in nature. This statement cannot be validated in vacuum – it is an experimental fact that quarks do not appear as free particles in vacuum but that they are *confined* within hadrons. There is (at least for now) no analytic proof of confinement from QCD. However, there are indirect methods from hadron decays allowing us to determine the number of quark colours.

*Experiment 1.* The neutral pion decays into $2\gamma$ via a triangular quark loop; the branching ratio is $\sim 100\%$ [10]. The Standard Model determines the corresponding decay width as [4]

$$\Gamma_{\pi^0\to 2\gamma} = \frac{\alpha^2 m_\pi^3}{64\pi^3 f_\pi^2}\left(\frac{N_c}{3}\right)^2 \equiv 7.73\text{ eV}\cdot\left(\frac{N_c}{3}\right)^2, \tag{2.8}$$

where $N_c$ denotes the number of colours and $f_\pi = 92.4$ MeV is the pion decay constant. The experimental result reads $\Gamma^{\text{exp}}_{\pi^0\to 2\gamma} = (7.83 \pm 0.37)$ eV [10] and it can only be described by the

Standard Model if $N_c = 3$.

*Experiment 2.* Consider the ratio of the cross-sections for the processes $e^+e^- \to \gamma$ (or $Z$) $\to \bar{q}q$ $\to$ hadrons and $e^+e^- \to \mu^+\mu^-$. The ratio reads [4]

$$\frac{\sigma(e^+e^- \to \gamma, Z \to \bar{q}q \to)}{\sigma(e^+e^- \to \mu^+\mu^-)} = \begin{cases} \frac{2}{3}N_c & (N_f = 3) \\ \frac{10}{9}N_c & (N_f = 4) \\ \frac{11}{9}N_c & (N_f = 5). \end{cases}$$

The best correspondence with experimental data is obtained if $N_c = 3$ [4]. We thus conclude that the physical world contains three quarks colours. Note, however, that QCD with two colours can be explored nonetheless, at least from the theoretical standpoint, see, e.g., Ref. [20]. Additionally, the limit of a large number of colours (large-$N_c$ limit) has also been subject of many studies [21, 22] and represents a valuable tool of model building (see Sec. 4.3 for the application to the model presented in this work).

Now that we know the number of colours, it is possible to build colour-neutral meson states:

$$|M\rangle_{\text{colour}} = \frac{1}{\sqrt{3}}|\bar{q}_{\bar{r}}q_r + \bar{q}_{\bar{g}}q_g + \bar{q}_{\bar{b}}q_b\rangle. \tag{2.9}$$

## 2.2 The QCD Lagrangian

In the previous section we have seen that the necessity to introduce a colour degree of freedom for quarks arises from the requirement of an antisymmetric baryon wave function (that adheres to the Pauli Principle). It has allowed us to construct putative colour wave functions for baryons (2.7) as well as meson $\bar{q}q$ states (2.9). In this section we construct a Lagrangian containing quarks and considering their flavour and colour degrees of freedom.

The Lagrangian is constructed utilising the local (gauge) $SU(N_c = 3)$ symmetry [23]. A quark field $q_f$ in the fundamental representation transforms under the local $SU(3)$ symmetry as

$$q_f \to q'_f = \exp\left\{-i\sum_{a=1}^{N_c^2-1}\alpha^a(x)t_a\right\}q_f \equiv Uq_f, \tag{2.10}$$

where $t_a = \lambda_a/2$ denotes the generators of the $SU(3)$ group, $\lambda_a$ are the Gell-Mann matrices and $\alpha^a(x)$ are the parameters of the group. Let us remember that the Dirac Lagrangian for a free fermion $\psi$ possesses this form:

$$\mathcal{L}_{Dirac} = \bar{\psi}(i\gamma^\mu\partial_\mu - m_\psi)\psi. \tag{2.11}$$

Then, in analogy to the Dirac Lagrangian, we can construct the following Lagrangian involving the quark flavours considering the requirement that the Lagrangian is *locally* $SU(3)_c$ *symmetric* (sum over flavour index $f$ is implied):

$$\mathcal{L}_q = \bar{q}_f(i\gamma^\mu D_\mu - m_f)q_f \tag{2.12}$$

where $m_f$ denotes the mass of the quark flavour $q_f$,

$$D_\mu = \partial_\mu - ig\mathcal{A}_\mu \tag{2.13}$$

represents the $SU(3)$ covariant derivative with the eight gauge fields $A^a_\mu$

$$\mathcal{A}_\mu = \sum_{a=1}^{N_c^2-1} A^a_\mu t_a, \tag{2.14}$$

referred to as *gluons*. The (adjoint) gluon fields transform as follows under the local $SU(3)$ group:

$$\mathcal{A}_\mu \to \mathcal{A}'_\mu = U\mathcal{A}_\mu U^\dagger - \frac{i}{g}\,(\partial_\mu U)\,U^\dagger. \tag{2.15}$$

The Lagrangian (2.12) is invariant under transformations (2.10) and (2.15). It is possible to construct an additional gauge invariant term involving only gluons [24]:

$$\mathcal{L}_g = -\frac{1}{4}\,G^a_{\mu\nu}G^{\mu\nu}_a \tag{2.16}$$

(sum over gluon-field index $a$ is implied) where the field strength tensor $G^a_{\mu\nu}$ is defined as

$$G^a_{\mu\nu} = \partial_\mu A^a_\nu - \partial_\nu A^a_\mu + g f^{abc} A^b_\mu A^c_\nu \tag{2.17}$$

and $f^{abc}$ denote the antisymmetric structure constants of the $SU(3)$ group.
The sum of the two Lagrangians (2.12) and (2.16) yields the *QCD Lagrangian*:

$$\mathcal{L}_{QCD} = \bar{q}_f(i\gamma^\mu D_\mu - m_f)q_f - \frac{1}{4}G^a_{\mu\nu}G^{\mu\nu}_a. \tag{2.18}$$

### 2.3 The Chiral Symmetry

In addition to the local $SU(3)_c$ colour symmetry, the QCD Lagrangian also exhibits a global symmetry if quarks are massless – the chiral symmetry. To ascertain this symmetry in the Lagrangian (2.12) in the limit $m_f = 0$, let us first define the following left-handed and right-handed operators $\mathcal{P}_{R,\,L}$:

$$\mathcal{P}_{R,\,L} = \frac{1 \pm \gamma_5}{2}, \tag{2.19}$$

where $\mathcal{P}_R$ has the plus sign in the denominator and $\gamma_5$ is a matrix defined in terms of the other Dirac matrices as

$$\gamma_5 = i\gamma_0\gamma^1\gamma^2\gamma^3, \tag{2.20}$$

with (in the chiral representation)

$$\gamma_0 = \begin{pmatrix} 0 & 1_2 \\ 1_2 & 0 \end{pmatrix}, \quad \boldsymbol{\gamma} = \begin{pmatrix} 0 & \boldsymbol{\sigma} \\ -\boldsymbol{\sigma} & 0 \end{pmatrix} \tag{2.21}$$

and $\boldsymbol{\sigma}$ denotes the triplet of the Pauli matrices. Thus we obtain

$$\gamma_5 = \begin{pmatrix} -1_2 & 0 \\ 0 & 1_2 \end{pmatrix}. \tag{2.22}$$

Consequently, the two operators $\mathcal{P}_{R,\,L}$ possess the following form, justifing their labels as right-handed and left-handed

$$\mathcal{P}_R = \begin{pmatrix} 0 & 0 \\ 0 & 1_2 \end{pmatrix}, \quad \mathcal{P}_L = \begin{pmatrix} 1_2 & 0 \\ 0 & 0 \end{pmatrix}. \tag{2.23}$$

By definition (2.20), the $\gamma_5$ matrix has the feature that $\gamma_5^2 = 1$ (i.e., unit matrix). This is demonstrated using the well-known anticommutation formula of the Dirac matrices

$$\{\gamma_\mu, \gamma_\nu\} = 2g_{\mu\nu}, \tag{2.24}$$

where $g_{\mu\nu} = \mathrm{diag}(1, -1, -1, -1)$ denotes the metric tensor

$$\begin{aligned} \gamma_5^2 &= -\gamma_0\gamma^1\gamma^2\gamma^3\gamma_0\gamma^1\gamma^2\gamma^3 = \gamma_0^2\gamma^1\gamma^2\gamma^3\gamma^1\gamma^2\gamma^3 \\ &= \gamma^1\gamma^2\gamma^3\gamma^1\gamma^2\gamma^3 = (\gamma^1)^2\gamma^2\gamma^3\gamma^2\gamma^3 = -\gamma^2\gamma^3\gamma^2\gamma^3 \\ &= (\gamma^2)^2(\gamma^3)^2 = 1. \end{aligned} \tag{2.25}$$

Additionally,

$$\{\gamma_\mu, \gamma_5\} = 0. \tag{2.26}$$

Consequently,

$$\mathcal{P}_{R,\,L}^2 = \frac{(1 \pm \gamma_5)^2}{4} = \frac{1 \pm \gamma_5}{2} = \mathcal{P}_{R,\,L} \tag{2.27}$$

and

$$\mathcal{P}_R\mathcal{P}_L = 0. \tag{2.28}$$

$\mathcal{P}_{R,\,L}$ are therefore projection operators – we refer to them as *chirality projection operators*. Utilising these operators allows us to decompose a quark flavour $q_f$ into two components, a left-handed and a right-handed one:

$$q_f = (\mathcal{P}_R + \mathcal{P}_L)\, q_f = q_{f\,R} + q_{f\,L}. \tag{2.29}$$

Analogously for the antiquarks:

$$\bar{q}_f = \bar{q}_f\, (\mathcal{P}_L + \mathcal{P}_R) = \bar{q}_{f\,R} + \bar{q}_{f\,L}. \tag{2.30}$$

Using Eq. (2.19) we obtain from the Lagrangian (2.12)

$$\begin{aligned} \mathcal{L}_q &= \bar{q}_f(i\gamma^\mu D_\mu - m_f)q_f \overset{\mathcal{P}_R+\mathcal{P}_L=1}{=} \bar{q}_f(\mathcal{P}_R + \mathcal{P}_L)(i\gamma^\mu D_\mu - m_f)(\mathcal{P}_R + \mathcal{P}_L)q_f \\ &\overset{(\mathcal{P}_R+\mathcal{P}_L)^2=1}{=} \bar{q}_f(\mathcal{P}_R\mathcal{P}_R + \mathcal{P}_L\mathcal{P}_L)(i\gamma^\mu D_\mu - m_f)(\mathcal{P}_R + \mathcal{P}_L)q_f \\ &\overset{\text{Eqs. (2.26), (2.27), (2.28)}}{=} \bar{q}_f\mathcal{P}_R i\gamma^\mu D_\mu \mathcal{P}_L q_f + \bar{q}_f\mathcal{P}_L i\gamma^\mu D_\mu \mathcal{P}_R q_f - \bar{q}_f\mathcal{P}_R m_f \mathcal{P}_R q_f - \bar{q}_f\mathcal{P}_L m_f \mathcal{P}_L q_f \\ &= q_f^\dagger\gamma_0\mathcal{P}_R i\gamma^\mu D_\mu \mathcal{P}_L q_f + q_f^\dagger\gamma_0\mathcal{P}_L i\gamma^\mu D_\mu \mathcal{P}_R q_f - q_f^\dagger\gamma_0\mathcal{P}_R m_f \mathcal{P}_R q_f - q_f^\dagger\gamma_0\mathcal{P}_L m_f \mathcal{P}_L q_f \\ &\overset{\text{Eq. (2.26)}}{=} q_f^\dagger\mathcal{P}_L\gamma_0 i\gamma^\mu D_\mu \mathcal{P}_L q_f + q_f^\dagger\mathcal{P}_R\gamma_0 i\gamma^\mu D_\mu \mathcal{P}_R q_f - q_f^\dagger\mathcal{P}_L\gamma_0 m_f \mathcal{P}_R q_f - q_f^\dagger\mathcal{P}_R\gamma_0 m_f \mathcal{P}_L q_f \\ &\equiv \bar{q}_{f\,L} i\gamma^\mu D_\mu q_{f\,L} + \bar{q}_{f\,R} i\gamma^\mu D_\mu q_{f\,R} - \bar{q}_{f\,L} m_f q_{f\,R} - \bar{q}_{f\,R} m_f q_{f\,L}. \end{aligned} \tag{2.31}$$

Then the Lagrangian (2.31) less the terms $\sim m_f$ is symmetric under the following, global $U(N_f)\times U(N_f)$ transformations of the quark fields in the flavour space ($t_i$: group generators)

$$q_{f\,L} \longrightarrow q'_{f\,L} = U_L q_{f\,L} = \exp\left\{-i\sum_{i=0}^{N_f^2-1}\alpha_L^a t^a\right\} q_{f\,L}, \tag{2.32}$$

$$q_{f\,R} \longrightarrow q'_{f\,R} = U_R q_{f\,R} = \exp\left\{-i\sum_{i=0}^{N_f^2-1}\alpha_R^a t^a\right\} q_{f\,R}. \tag{2.33}$$

This symmetry is referred to as the *chiral symmetry*. As evident from Eq. (2.31), the terms proportional to $m_f$ break the chiral symmetry explicitly, i.e., the symmetry is exact only in the case of vanishing quark masses: $m_f = 0$.
According to the Noether Theorem [25], a conserved current $J^\mu$ is implied by a global symmetry (and vice versa) in a Lagrangian $\mathcal{L}(\varphi(x^\mu))$ that is invariant under transformations of the form $\varphi(x) \to \varphi'(x) = \varphi(x) + \delta\varphi(x)$ and $x \to x'(x) = x + \delta x$ with

$$J^\mu = \frac{\partial\mathcal{L}}{\partial(\partial_\mu\varphi)}\delta\varphi + \delta x^\mu \mathcal{L}. \tag{2.34}$$

Thus the mentioned $U(N_f)_L \times U(N_f)_R$ implies the existence of the conserved left-handed and right-handed currents $L^\mu$ and $R^\mu$. It is usual, however, to work instead with currents of definitive parity $P$: the vector current $V^\mu = (L^\mu + R^\mu)/2$

$$P : V^0(t,\boldsymbol{x}) \longrightarrow V^0(t,-\boldsymbol{x}), \tag{2.35}$$

$$P : V^i(t,\boldsymbol{x}) \longrightarrow -V^i(t,-\boldsymbol{x}) \tag{2.36}$$

($i$ denotes the spatial index) and the axial-vector current $A^\mu = (L^\mu - R^\mu)/2$

$$P : A^i(t,\boldsymbol{x}) \longrightarrow A^i(t,-\boldsymbol{x}), \tag{2.37}$$

$$P : A^0(t,\boldsymbol{x}) \longrightarrow -A^0(t,-\boldsymbol{x}). \tag{2.38}$$

Indeed the chiral group $U(N_f)_L \times U(N_f)_R$ is isomorphic to the group $U(N_f)_V \times U(N_f)_A$ of the unitary vector and axial-vector transformations. From the features of the unitary groups we know that $U(N_f)_V \times U(N_f)_A \equiv U(1)_V \times SU(N_f)_V \times U(1)_A \times SU(N_f)_A$. Let us now discuss the currents obtained from the Lagrangian (2.12) without gluon fields ($\mathcal{A}_\mu = 0$) under the stated four transformations.

- $U(1)_V$ implies $\alpha_L^0 = \alpha_R^0 = \alpha_V^0/2$ in Eqs. (2.32) and (2.33):

$$U_{1V} = \exp(-i\alpha_V^0 t^0), \tag{2.39}$$

  i.e., $U_{1V} = U_{1L} = U_{1R}$. We define $t^0 = 1_{N_f}/\sqrt{2N_f}$ [we denote the other generators of the unitary group $U(N_f)$ as $t^i$ with $i = 1,\ldots,N_f$]. It is clear that the Lagrangian (2.12) is symmetric under the transformation (2.39). The corresponding conserved current

obtained by inserting the Lagrangian (2.12) into Eq. (2.34) and considering infinitesimal transformation $U_V \approx 1 - i\alpha_V^0 t^0$ reads

$$V_0^\mu = \frac{\partial \mathcal{L}}{\partial(\partial_\mu q_f)} \delta q_f = \bar{q}_f \gamma^\mu \alpha_V^0 t^0 q_f. \tag{2.40}$$

The parameter $\alpha_V^0$ can be discarded because the current is conserved:

$$\partial_\mu V_0^\mu = 0. \tag{2.41}$$

Similarly, the generator $t^0$ is proportional to the unit matrix and the corresponding proportionality constant can be absorbed into $\alpha_V^0$. Thus we obtain

$$V_0^\mu = \bar{q}_f \gamma^\mu q_f. \tag{2.42}$$

The zero component of the current reads

$$V_0^0 = \bar{q}_f \gamma^0 q_f \tag{2.43}$$

and it corresponds exactly to the one that we could have obtained also from the Dirac equation (2.11). Then we know, however, that integration over $V_0^0$ yields a conserved charge $Q$

$$Q = \int \mathrm{d}^3 x \bar{q}_f \gamma^0 q_f \tag{2.44}$$

corresponding to the baryon-number conservation.

- Group parameters for $SU(N_f)_V$ are obtained for $\alpha_L^i = \alpha_R^i = \alpha_V^i/2$ with $i = 1, ..., N_f^2 - 1$ or in other words

$$U_V = \exp(-i\alpha_V^i t^i), \tag{2.45}$$

i.e., $U_V = U_L = U_R$. Infinitesimally,

$$U_V \approx 1 - i\alpha_V^i t^i. \tag{2.46}$$

Varying the quark fields $q_f$ in the Lagrangian (2.12) under the transformation (2.46) yields (we consider only terms up to order $\alpha_V^i$, not higher-order ones):

$$\begin{aligned}
\mathcal{L}_q &= i q_f^\dagger (1 + i\alpha_V^i t^i)\gamma^0 \gamma^\mu \partial_\mu (1 - i\alpha_V^i t^i) q_f \\
&\quad - q_f^\dagger (1 + i\alpha_V^i t^i)\gamma^0 m_f (1 - i\alpha_V^i t^i) q_f \\
&= i\bar{q}_f \gamma^\mu \partial_\mu q_f - i\alpha_V^i (\bar{q}_f \, i \, t^i \, \gamma^\mu \partial_\mu \, q_f - \bar{q}_f \, i \, t^i \, \gamma^\mu \, \partial_\mu \, q_f) \\
&\quad - \bar{q}_f m_f q_f - i\alpha_V^i (\bar{q}_f \, [t^i, m_f] \, q_f) \\
&= i\bar{q}_f \gamma^\mu \partial_\mu q_f - \bar{q}_f m_f q_f - i\alpha_V^i (\bar{q}_f \, [t^i, m_f] \, q_f).
\end{aligned} \tag{2.47}$$

The Lagrangian is only invariant under the vector transformations if the quark masses are degenerate. The conserved vector current from Eq. (2.47) and the Noether Theorem is

$$V^i = \bar{q}_f \gamma^\mu t^i q_f \tag{2.48}$$

but, as already indicated, the divergence of the current

$$\partial^\mu V^i_\mu = i\bar{q}_f\,[t^i, m_f]\,q_f \tag{2.49}$$

is zero only in the case of degenerate quark masses.

- An element of $SU(N_f)_A$ is given by

$$U_A = \exp(-i\alpha^i_A\gamma_5 t^i), \tag{2.50}$$

where $U_A = U_L = U_R^\dagger$. [$SU(N_f)_A$ is actually not a group because it is not closed with regard to the product of two elements but this is not a problem here because the $SU(N_f)_A$ symmetry is spontaneously broken, see below.] The infinitesimal transformation reads

$$U_A \approx 1 - i\alpha^i_A\gamma_5 t^i. \tag{2.51}$$

Varying the quark fields $q_f$ in the Lagrangian (2.12) under the transformation (2.46) yields

$$\begin{aligned}
\mathcal{L}_q &= iq_f^\dagger(1 + i\alpha^i_A\gamma_5 t^i)\gamma^0\gamma^\mu\partial_\mu(1 - i\alpha^i_A\gamma_5 t^i)q_f \\
&\quad - q_f^\dagger(1 + i\alpha^i_A\gamma_5 t^i)\gamma^0 m_f(1 - i\alpha^i_A\gamma_5 t^i)q_f \\
&= i\bar{q}_f\gamma^\mu\partial_\mu q_f - i\alpha^i_A(\bar{q}_f\, i\, t^i\,\gamma^\mu\partial_\mu\,\gamma_5\, q_f - q_f^\dagger\, i\, t^i\,\gamma_5\,\gamma_0\,\gamma^\mu\,\partial_\mu\, q_f) \\
&\quad - \bar{q}_f m_f q_f + i\alpha^i_A(\bar{q}_f\ \{t^i, m_f\}\gamma_5\, q_f) \\
&\overset{\text{Eq. (2.26)}}{=} i\bar{q}_f\gamma^\mu\partial_\mu q_f - \bar{q}_f m_f q_f + i\alpha^i_A(\bar{q}_f\ \{t^i, m_f\}\gamma_5\, q_f).
\end{aligned} \tag{2.52}$$

Thus the axial-vector current

$$A^i = \bar{q}_f\gamma^\mu\gamma_5 t^i q_f \tag{2.53}$$

is only conserved if all quark masses are zero:

$$\partial^\mu A^i_\mu = i\bar{q}_f\,\{t^i, m_f\}\,q_f. \tag{2.54}$$

- Let us now turn to the axial-vector singlet transformation $U(1)_A$. It has the following form:

$$U_{1A} = \exp(-i\alpha^0_A\gamma_5 t^0) \tag{2.55}$$

or infinitesimally

$$U_{1A} \approx 1 - i\alpha^0_A\gamma_5 t^0. \tag{2.56}$$

Then the Lagrangian (2.12) transforms under $U(1)_A$ as follows:

$$\begin{aligned}
\mathcal{L}_q &= iq_f^\dagger(1 + i\alpha^0_A\gamma_5 t^0)\gamma^0\gamma^\mu\partial_\mu(1 - i\alpha^0_A\gamma_5 t^0)q_f \\
&\quad - q_f^\dagger(1 + i\alpha^0_A\gamma_5 t^0)\gamma^0 m_f(1 - i\alpha^0_A\gamma_5 t^0)q_f \\
&= i\bar{q}_f\gamma^\mu\partial_\mu q_f - i\alpha^0_A(\bar{q}_f\, i\, t^0\,\gamma^\mu\partial_\mu\,\gamma_5\, q_f - q_f^\dagger\, i\, t^0\,\gamma_5\,\gamma_0\,\gamma^\mu\,\partial_\mu\, q_f) \\
&\quad - \bar{q}_f m_f q_f + i\alpha^0_A(\bar{q}_f\ \{t^0, m_f\}\gamma_5\, q_f) \\
&\overset{\text{Eq. (2.26)}}{=} i\bar{q}_f\gamma^\mu\partial_\mu q_f - \bar{q}_f m_f q_f + i\alpha^0_A(\bar{q}_f\, m_f\,\gamma_5\, q_f).
\end{aligned} \tag{2.57}$$

Thus the axial-vector singlet current

$$A^0 = \bar{q}_f \, \gamma^\mu \gamma_5 \, q_f \tag{2.58}$$

appears to be conserved in the limit $m_f = 0$:

$$\partial^\mu A^0_\mu = i\bar{q}_f \, m_f \, \gamma_5 q_f . \tag{2.59}$$

It is, however, only conserved classically. Considering quantum fluctuations one sees that it is actually not conserved [26]:

$$\partial^\mu A^0_\mu|_{m_f=0} = -\frac{g^2 N_f}{32\pi^2} G^a_{\mu\nu} \tilde{G}^{\mu\nu}_a , \tag{2.60}$$

where $\tilde{G}^{\mu\nu}_a$ denotes the dual field-strength tensor $\tilde{G}^{\mu\nu}_a = \varepsilon^{\mu\nu\rho\sigma} G^a_{\rho\sigma}/2$. Symmetries valid on the classical level but broken on the quantum level are referred to as anomalies – Eq. (2.60) indicates the *chiral anomaly*, a very important feature of QCD that has to be considered also when a model is built (see Sec. 6.4 for the discussion of the chiral-anomaly term in our model). Nonetheless, given that even the $u$ and $d$ quarks possess non-vanishing mass values, we observe from Eq. (2.59) that, even classically, the axial-vector singlet current is conserved only partially (PCAC).

Let us then summarise the results of this section as follows: we observe a $U(N_f)_L \times U(N_f)_R$ chiral symmetry in the QCD Lagrangian with $N_f$ flavours (2.18); the symmetry is isomorphic to the $U(N_f)_V \times U(N_f)_A \equiv U(1)_V \times SU(N_f)_V \times U(1)_A \times SU(N_f)_A$ symmetry and, in the limit of vanishing quark masses, it appears to be exact (apart from the chiral anomaly). For non-vanishing but degenerate quark masses, the symmetry is broken explicitly to $U(N_f)_V \times U(N_f)_A \to U(1)_V \times SU(N_f)_V$ and for non-degenerate quark masses it is broken to $U(N_f)_V \times U(N_f)_A \to U(1)_V$. Thus, by discussing the properties of the QCD Lagrangian only, we conclude that the magnitude of the symmetry breaking in nature should not be large if we consider $u$ and $d$ quarks only because their masses are small. However, we will see later on that there is another mechanism of chiral symmetry breaking, the spontaneous one, that leads to a variety of new conclusions.

Before we turn to the spontaneous breaking of the chiral symmetry, let us first briefly discuss other symmetries of the QCD Lagrangian.

## 2.4 Other QCD Symmetries

### 2.4.1 *CP* Symmetry

The parity transformation for fermions (and thus also for quarks) reads

$$q(t, \boldsymbol{x}) \xrightarrow{P} \gamma^0 q(t, -\boldsymbol{x}) \tag{2.61}$$

and thus

$$q^\dagger(t, \boldsymbol{x}) \xrightarrow{P} q^\dagger(t, -\boldsymbol{x})\gamma^0 . \tag{2.62}$$

If we transform the quark part of the QCD Lagrangian (2.12), then we obtain for $\mu = i \in \{1,2,3\}$

$$\begin{aligned}
\mathcal{L}_q &= \bar{q}_f(t,\boldsymbol{x}) i\gamma^i D_i q_f(t,\boldsymbol{x}) - \bar{q}_f(t,\boldsymbol{x}) m_f q_f(t,\boldsymbol{x}) \\
&\overset{P}{\to} q_f^\dagger(t,-\boldsymbol{x})\gamma^0\gamma^0 i\gamma^i(-D_i)\gamma^0 q_f(t,-\boldsymbol{x}) - q_f^\dagger(t,-\boldsymbol{x})\gamma^0\gamma^0 m_f \gamma^0 q_f(t,-\boldsymbol{x}) \\
&\overset{\text{Eq. (2.24)}}{=} q_f^\dagger(t,-\boldsymbol{x})\gamma^0 i\gamma^i D_i q_f(t,-\boldsymbol{x}) - q_f^\dagger(t,-\boldsymbol{x}) m_f q_f(t,-\boldsymbol{x}) \\
&= \bar{q}_f(t,-\boldsymbol{x}) i\gamma^i D_i q_f(t,-\boldsymbol{x}) - \bar{q}_f(t,-\boldsymbol{x}) m_f q_f(t,-\boldsymbol{x}).
\end{aligned} \tag{2.63}$$

The parity conservation is trivially fulfilled in the case $\mu = 0$ due to Eq. (2.24). The gauge part of the QCD Lagrangian (2.16) is obviously parity-conserving.
The charge conjugation of quarks $S_C$ is such that

$$q \overset{C}{\to} S_C \bar{q}^t = S_C (\gamma^0)^t q^* \tag{2.64}$$

where the superscript $t$ denotes the transposed function and $S_C^{-1}\gamma^\mu S_C = (-\gamma^\mu)^t$. (In the case of the Dirac notation, $S_C = -i\gamma^2\gamma^0$.) We note that, due to $S_C^{-1} = S_C^\dagger$ (unitary transformation),

$$S_C^\dagger \gamma^\mu S_C = (-\gamma^\mu)^t \Rightarrow S_C^\dagger \gamma^\mu = (-\gamma^\mu)^t S_C^{-1}. \tag{2.65}$$

Additionally,

$$q^\dagger \overset{C}{\to} [S_C(\gamma^0)^t q^*]^\dagger = q^t (\gamma^0)^* S_C^\dagger. \tag{2.66}$$

Let us consider how the quark part of the QCD Lagrangian (2.12) transforms under charge conjugation. Note that $D_\mu = \partial_\mu - ig\mathcal{A}_\mu$ contains gluon fields transforming as odd under $C$. Remember that the quarks are fermions and therefore any commutation of the quark fields in the following lines yields an additional minus sign.

$$\begin{aligned}
\mathcal{L}_q &= \bar{q}_f i\gamma^\mu D_\mu q_f - \bar{q}_f m_f q_f \\
&\overset{C}{\to} i q_f^t (\gamma^0)^* S_C^\dagger \gamma^0 \gamma^\mu (\partial_\mu + ig\mathcal{A}_\mu) S_C (\gamma^0)^t q_f^* - q_f^t (\gamma^0)^* S_C^\dagger \gamma^0 m_f S_C (\gamma^0)^t q_f^* \\
&\overset{\text{Eq. (2.65)}}{=} i q_f^t (\gamma^0)^* (-\gamma^0)^t S_C^{-1} \gamma^\mu S_C (\partial_\mu + ig\mathcal{A}_\mu)(\gamma^0)^t q_f^* - q_f^t (\gamma^0)^* (-\gamma^0)^t S_C^{-1} m_f S_C (\gamma^0)^t q_f^* \\
&\overset{S_C^{-1}\gamma^\mu S_C = (-\gamma^\mu)^t}{=} i q_f^t (\gamma^0)^* (\gamma^0)^t (\gamma^\mu)^t (\partial_\mu + ig\mathcal{A}_\mu)(\gamma^0)^t q_f^* - q_f^t (\gamma^0)^* (-\gamma^0)^t m_f (\gamma^0)^t q_f^* \\
&\overset{\gamma^0(\gamma^0)^\dagger = 1}{=} i q_f^t (\gamma^\mu)^t (\gamma^0)^t \partial_\mu q_f^* + i q_f^t (\gamma^\mu)^t (ig) \mathcal{A}_\mu (\gamma^0)^t q_f^* - q_f^t (\gamma^0)^* (-\gamma^0)^t m_f (\gamma^0)^t q_f^* \\
&= \left[ i q_f^t (\gamma^\mu)^t (\gamma^0)^t \partial_\mu q_f^* \right]^t + \left[ i q_f^t (\gamma^\mu)^t (ig) \mathcal{A}_\mu (\gamma^0)^t q_f^* \right]^t + \left[ q_f^t m_f (\gamma^0)^t q_f^* \right]^t \\
&= -i(\partial_\mu \bar{q}_f)\gamma^\mu q_f - i\bar{q}_f \gamma^\mu (ig\mathcal{A}_\mu) q_f - \bar{q}_f m_f q_f \\
&\equiv i\bar{q}_f \gamma^\mu \partial_\mu q_f - i\bar{q}_f \gamma^\mu (ig\mathcal{A}_\mu) q_f - \bar{q}_f m_f q_f \\
&= i\bar{q}_f \gamma^\mu D_\mu q_f - \bar{q}_f m_f q_f,
\end{aligned} \tag{2.67}$$

where we have used $(\gamma^0)^*(\gamma^0)^t = [\gamma^0(\gamma^0)^\dagger]^t = 1^t = 1$ and also the well-known feature that the following equality holds for an $(N \times N)$ matrix $M$, $(1 \times N)$ vector $\boldsymbol{v}$ and $(N \times 1)$ vector $\boldsymbol{u}$ under transposition:

$$\boldsymbol{v} M \boldsymbol{u} = (\boldsymbol{v} M \boldsymbol{u})^t \tag{2.68}$$

because the result of the multiplication is a number.

Then the QCD Lagrangian (2.18) is unchanged under $P$ and $C$ transformations (2.61), (2.62), (2.64) and (2.66) – the strong interaction is $CP$ *invariant*. [A review of a possible, although small, $CP$ violation in strong interactions may be found, e.g., in Ref. [27].]

### 2.4.2 $Z$ Symmetry

This symmetry is a discrete one. The general form of a special unitary $N_f \times N_f$ matrix $U$ contains also the centre elements $Z_n$ (sometimes referred to simply as $Z$):

$$U = Z_n \exp(-i\alpha^i t^i),\ i = 1, ..., N_f^2 - 1 \tag{2.69}$$

where

$$Z_n = \exp\left(-i\frac{2\pi n}{N_c}t^0\right),\ n = 0, 1, ...N_c - 1. \tag{2.70}$$

The determinant of $Z_n$ reads

$$\det Z_n = \left[\exp\left(-i\frac{2\pi n}{N_c}\right)\right]^{N_c} = 1. \tag{2.71}$$

For this reason, $Z_n$ is (as already indicated) a member of the $SU(N_f)$ group. The quarks and gluons transform under the $Z$ group as

$$q_f \to q_f^{'} = Z_n q_f, \tag{2.72}$$
$$A_\mu \to A'_\mu = Z_n A_\mu Z_n^\dagger \tag{2.73}$$

and the Yang-Mills Lagrangian (2.16) is invariant under these transformations. The $Z$ symmetry is not exact in the presence of quarks because it does not fulfill the necessary antisymmetric boundary conditions. Additionally, note that the symmetry is spontaneously broken in the gauge (i.e., gluon) sector of QCD at large temperatures. This is an order parameter for the deconfinement. The order parameter is usually represented (in models such as the NJL model [28] but also in first-principle calculations) by the so-called Polyakov loop (see Ref. [29] for Polyakov-loop extended NJL model).

### 2.4.3 Dilatation Symmetry

This is a symmetry of the gauge (or Yang-Mills – YM) sector of QCD, Eq. (2.16). The dilatation (or scale) transformation is defined as

$$x^\mu \to x'^\mu = \lambda^{-1} x^\mu, \tag{2.74}$$

where $\lambda$ denotes a scale parameter. Then, for dimensional reasons, the gauge fields in Eq. (2.16) have to transform as

$$A^a_\mu(x) \to A^{a\prime}_\mu(x') = \lambda A^a_\mu(x). \tag{2.75}$$

Consequently, the Lagrangian (2.16) obtains a factor $\lambda^4$ under the transformations (2.74) and (2.75)

$$\mathcal{L}_g \to \lambda^4 \mathcal{L}_g \tag{2.76}$$

but the action

$$S_g = \int \mathrm{d}^4 x \mathcal{L}_g \tag{2.77}$$

is invariant. This symmetry is known as the *dilatation* or *trace symmetry*. (Strictly speaking, the notion of a symmetry always requires the action $S$ to be invariant under a transformation rather than the Lagrangian $\mathcal{L}$ but in all the other examples discussed in this chapter there is no transformation of space-time $x$. For this reason, in all the other cases, the symmetry of the Lagrangian is simultaneously the symmetry of the action as well.)
Consequently, the obtained conserved current reads

$$J^\mu = x_\nu T^{\mu\nu}, \tag{2.78}$$

where $T^{\mu\nu}$ is the energy-momentum tensor of the gauge-field Lagrangian (2.16):

$$T^{\mu\nu} = \frac{\partial \mathcal{L}_g}{\partial(\partial_\mu A_\xi)} \partial^\nu A^\xi - g^{\mu\nu} \mathcal{L}_g. \tag{2.79}$$

Therefore,

$$\partial_\mu J^\mu = T^\mu_\mu = 0. \tag{2.80}$$

Similarly to the singlet axial current (2.59), the dilatation symmetry is broken both classically and at the quantum level. On the classical level, the dilatation-symmetry breaking is induced by the inclusion of quark degrees of freedom. We observe from Eq. (2.12) that the quark fields have to transform in the following way so that the dilatation symmetry is fulfilled in the limit $m_f = 0$:

$$q_f \to q'_f = \lambda^{3/2} q_f. \tag{2.81}$$

If we consider $m_f \neq 0$, then we observe that the dilatation symmetry is broken explicitly by non-vanishing quark masses:

$$T^\mu_\mu = \sum_{f=1}^{N_f} m_f \bar{q} q, \tag{2.82}$$

unlike Eq. (2.80). The degree of the dilatation-symmetry breaking is of course small if one considers only light quarks and the symmetry is exact if one considers $m_f = 0$.
However, at the quantum level (calculating gluon loops), the symmetry is never exact. The strong coupling $g$ is known to change with scale $\mu$ (e.g., centre-of-mass energy) upon renormalisation of QCD [30]: $g \to g(\mu)$. Perturbative QCD then yields

$$\partial_\mu J^\mu = T^\mu_\mu = \frac{\beta(g)}{4g} G^a_{\mu\nu} G^{\mu\nu}_a \neq 0, \tag{2.83}$$

where $\beta(g)$ denotes the famous $\beta$-function of QCD

$$\beta(g) = \mu \frac{\partial g}{\partial \mu} \tag{2.84}$$

that demonstrates how the strong coupling changes with the scale. At 1-loop level:

$$\beta(g) = -bg^3 = -\frac{11N_c - 2N_f}{48\pi^2} g^3. \tag{2.85}$$

If the strong coupling did not change ($g = \text{const.} = g_0$), then the dilatation symmetry would not be broken and we would retrieve the result of Eq. (2.80). Solving the differential Eq. (2.85) yields

$$g^2(\mu) = \frac{g_*^2}{1 + 2bg_*^2 \log \frac{\mu}{\mu_*}}. \tag{2.86}$$

Given that $b > 0$ for $N_f < 11N_c/2$ [see Eq. (2.85)], the coupling decreases with the increasing scale. Thus, at small scales, the coupling is strong: this is a sign of confinement. However, we also observe that, at a certain scale, one can expect the interaction strength between quarks and gluons to decrease sufficiently as to allow for the partons to no longer be confined within hadrons – *asymptotic freedom*. Note also that Eq. (2.86) implies that the strong coupling $g$ decreases with the number of colours, a result of major impact also for deliberations in this work (see Sec. 4.3).

Note that Eq. (2.86) possesses a pole (the so-called Landau pole) at

$$\mu_L \equiv \Lambda_{\text{Landau}} = \mu_* \exp\left(-\frac{1}{2bg_*^2}\right). \tag{2.87}$$

Then we can transform Eq. (2.86) as

$$g^2(\mu) = \frac{1}{2b \log \frac{\mu}{\Lambda_{\text{Landau}}}}. \tag{2.88}$$

Of course, this result does not imply that the strong coupling $g$ diverges at $\mu = \mu_L$ but rather indicates that QCD is a strongly bound theory in the vicinity of the pole. The value of the pole itself is, unfortunately, unknown because an initial value of $\mu$ [needed to solve Eq. (2.85)] is unknown as well. However, this nonetheless implies that a scale is generated in a dimensionless theory via renormalisation – a mechanism known as the *dimensional transmutation*.

The breaking of the dilatation (scale) invariance is labelled as the *trace anomaly*. It leads to the generation of a gluon condensate due to the non-vanishing vacuum expectation value of the gluon fields:

$$\left\langle T_\mu^\mu \right\rangle = -\left\langle \frac{11N_c - 2N_f}{48} \frac{\alpha_s}{\pi} G^a_{\mu\nu} G_a^{\mu\nu} \right\rangle \sim -\frac{11N_c - 2N_f}{48} C^4, \tag{2.89}$$

where $\alpha_s = g^2/(4\pi)$ is the strong fine-structure constant and the values

$$C^4 \simeq (300 - 600 \text{ MeV})^4 \tag{2.90}$$

have been obtained through QCD sum rules (lower range of the interval) [31] and lattice simulations (higher range of the interval) [32].

This raises the possibility to study glueball fields – bound states of two (or more) gluons. We will present a calculation involving, among others, a scalar glueball and a $\bar{q}q$ state in Chapter 12.

## 2.5 Spontaneous Breaking of the Chiral Symmetry

Until now we have only considered quarks and gluons as degrees of freedom. In this section we turn to structures that are composed of quarks. Concretely, we will be working with $\bar{q}q$ mesons (flavour index $f$ suppressed). These states are colour-neutral therefore trivially fulfilling the confinement.

States containing an antiquark and a quark can be classified according to their quantum numbers: total spin $J = L + S$ (where $L$ denotes the relative orbital angular momentum of the two quarks and $S$ denotes their relative spin), parity $P$, Eqs. (2.61) and (2.62), and charge conjugation $C$, Eq. (2.64) and (2.66). Let us restrict ourselves to the case of the light quarks $u$ and $d$ only, i.e., $\bar{q} \equiv (\bar{u}, \bar{d})$ and $q$ the corresponding column vector; states with heavier quarks are discussed analogously.

First we can define a state [33]:

$$\bar{q}q \tag{2.91}$$

for which we observe that it transforms as follows under parity, Eqs. (2.61) and (2.62):

$$\bar{q}(t,\boldsymbol{x})q(t,\boldsymbol{x}) \overset{P}{\to} q^\dagger(t,-\boldsymbol{x})\gamma^0\gamma^0\gamma^0 q(t,-\boldsymbol{x}) \overset{\text{Eq. (2.24)}}{=} \bar{q}(t,-\boldsymbol{x})q(t,-\boldsymbol{x}) \tag{2.92}$$

and under charge conjugation, Eqs. (2.64) and (2.66), as

$$\begin{aligned}
\bar{q}q &\overset{C}{\to} q^t i(\gamma^0)^*\gamma^2\gamma^0\gamma^0(-i)\gamma^2\gamma^0(\gamma^0)^t q^* \\
&\overset{\text{Eq. (2.24)}}{=} q^t(\gamma^0)^*\gamma^2\gamma^2\gamma^0(\gamma^0)^t q^* = -q^t(\gamma^0)^*\gamma^0(\gamma^0)^t q^* \\
&\overset{!}{=} [-q^t(\gamma^0)^*\gamma^0(\gamma^0)^t q^*]^t = q^\dagger\gamma^0(\gamma^0)^t(\gamma^0)^\dagger q = \bar{q}q.
\end{aligned} \tag{2.93}$$

The $\bar{q}q$ state is therefore unchanged under parity and charge conjugation, and it obviously carries no (total) spin. It is therefore a scalar. Note, however, that the mere fact of having $J = 0$ does not necessarily imply that $L$ and $S$ vanish as well. Indeed one can demonstrate [34] that, for a system of an antiquark and a quark,

$$P = (-1)^{L+1} \tag{2.94}$$

and

$$C = (-1)^{L+S}. \tag{2.95}$$

For this reason, $P = 1 = C$ implies $L = 1 = S$. In other words: the scalar $\bar{q}q$ state is a $P$-wave state. We can denote it as $\sigma_N$, alluding to the famous $\sigma$ meson (see Sec. 3.1), or in other words

$$\sigma_N \equiv \bar{q}q. \tag{2.96}$$

If we define a state

$$i\bar{q}\gamma_5 q, \tag{2.97}$$

then we observe that it transforms as follows under parity

$$i\bar{q}(t,\boldsymbol{x})\gamma_5 q(t,\boldsymbol{x}) \overset{P}{\to} iq^\dagger(t,-\boldsymbol{x})\gamma^0\gamma^0\gamma_5\gamma^0 q(t,-\boldsymbol{x}) \overset{\text{Eq. (2.24)}}{=} -i\bar{q}(t,-\boldsymbol{x})\gamma_5 q(t,-\boldsymbol{x}) \tag{2.98}$$

and under charge conjugation (here exemplary for the Dirac notation) as:

$$\begin{aligned} i\bar{q}(t,\boldsymbol{x})\gamma_5 q(t,\boldsymbol{x}) &\overset{C}{\to} iq^t i\gamma^0\gamma^2\gamma^0\gamma^0\gamma_5(-i)\gamma^2 q^* \\ &\overset{\text{Eq. (2.24)}}{=} iq^t i\gamma^0\gamma^2\gamma_5(-i)\gamma^2 q^* \overset{\text{Eq. (2.26)}}{=} -iq^t\gamma^0\gamma^2\gamma^2\gamma_5 q^* \\ &= iq^t\gamma^0\gamma_5 q^* \overset{!}{=} (iq^t\gamma^0\gamma_5 q^*)^t = -iq^\dagger\gamma_5\gamma^0 q = i\bar{q}\gamma_5 q. \end{aligned} \tag{2.99}$$

The state $\bar{q}\gamma_5 q$ is thus $P$-odd and $C$-even: it is a pseudoscalar and we label the state as $\eta_N$, alluding to the physical $\eta$ field: $\eta_N = \bar{q}\gamma_5 q$. [Note, however, that the field defined in Eq. (2.97) cannot be exactly the physical $\eta$ field because we have restricted ourselves to two flavours, i.e., non-strange quarks, see Sec. 7.1.] Similarly, we define a pion-like state

$$\boldsymbol{\pi} \equiv i\bar{q}\boldsymbol{t}\gamma_5 q \tag{2.100}$$

considering that the pion is an isospin triplett. The calculation of the behaviour of the state in Eq. (2.100) under parity and charge conjugation is analogous to the one demonstrated in Eqs. (2.98) and (2.99).

Let us now define a state

$$\bar{q}\gamma^\mu q \tag{2.101}$$

for which we observe that it transforms as follows under parity

$$\begin{aligned} \bar{q}(t,\boldsymbol{x})\gamma^\mu q(t,\boldsymbol{x}) &\overset{P}{\to} q^\dagger(t,-\boldsymbol{x})\gamma^0\gamma^0\gamma^\mu\gamma^0 q(t,-\boldsymbol{x}) \\ &\overset{\text{Eq. (2.24)}}{=} \begin{cases} \bar{q}(t,-\boldsymbol{x})\gamma^0 q(t,-\boldsymbol{x}) \text{ for } \mu = 0 \\ -\bar{q}(t,-\boldsymbol{x})\gamma^i q(t,-\boldsymbol{x}) \text{ for } \mu = i \in \{1,2,3\} \end{cases} \end{aligned} \tag{2.102}$$

or, in other words, the temporal component is parity-even whereas the spatial components are parity-odd. Additionally, we observe that the state is odd under the $C$-transformation [the calculation is analogous to the one in Eq. (2.99)]. Given that the field combination $\bar{q}\gamma^\mu q$ possesses spin 1, we label it as a vector state that we denote as $\omega_N^\mu$. Consequently, the state

$$\boldsymbol{\rho}^\mu \equiv \bar{q}\boldsymbol{t}\gamma^\mu q \tag{2.103}$$

is an isospin-triplett vector state [just as the $\rho(770)$ meson].

Finally, the states

$$f_{1N}^\mu \equiv \bar{q}\gamma_5\gamma^\mu q \tag{2.104}$$

and

$$\boldsymbol{a}_1^\mu \equiv \bar{q}\boldsymbol{t}\gamma_5\gamma^\mu q \tag{2.105}$$

are even under both parity and charge conjugation and additionally have spin 1: we label them as axial-vectors.

Let us now discuss the behaviour of these states under vector and axial-vector transformations. We observe, for example, that the vector transformation (2.46) of the pion field $\boldsymbol{\pi}$ (2.100) yields

$$\begin{aligned}\boldsymbol{\pi} \equiv i\bar{q}\boldsymbol{t}\gamma_5 q &\overset{V}{\to} iq^\dagger\,(1 + i\,\boldsymbol{\alpha}_V\cdot\boldsymbol{t})\,\gamma_0\,\boldsymbol{t}\,\gamma_5\,(1 - i\,\boldsymbol{\alpha}_V\cdot\boldsymbol{t})\,q \\ &= i\bar{q}\boldsymbol{t}\gamma_5 q + iq^\dagger\,(i\,t^i\,t^j\,\alpha_V^i - i\,t^j\,t^i\,\alpha_V^i)\,\gamma_0\,\gamma_5\,q \\ &= i\bar{q}\boldsymbol{t}\gamma_5 q - iq^\dagger\alpha_V^i\,\varepsilon^{ijk}\,t^k\,\gamma_0\,\gamma_5\,q \\ &= i\bar{q}\boldsymbol{t}\gamma_5 q - i\varepsilon^{ijk}\,\alpha_V^i\,\bar{q}\,t^k\,\gamma_5\,q \\ &\equiv \boldsymbol{\pi} + i\varepsilon^{ijk}\,\alpha_V^j\,\bar{q}\,t^k\,\gamma_5\,q \equiv \boldsymbol{\pi} + \boldsymbol{\alpha}_V\times\boldsymbol{\pi},\end{aligned} \tag{2.106}$$

where we have used the commutator $[t^i, t^j] = i\varepsilon^{ijk}t^k$.
Analogously to Eq. (2.106), we obtain from Eqs. (2.96), (2.103) and (2.105):

$$\sigma \overset{V}{\to} \sigma, \tag{2.107}$$

$$\boldsymbol{\rho}^\mu \overset{V}{\to} \boldsymbol{\rho}^\mu + \boldsymbol{\alpha}_V\times\boldsymbol{\rho}^\mu, \tag{2.108}$$

$$\boldsymbol{a}_1^\mu \overset{V}{\to} \boldsymbol{a}_1^\mu + \boldsymbol{\alpha}_V\times\boldsymbol{a}_1^\mu. \tag{2.109}$$

Thus the vector transformation corresponds to a rotation in the isospin space; as we have seen in Sec. 2.3, the QCD Lagrangian is invariant under this transformation (for degenerate quark masses) – the conserved vector current can thus be identified with an isospin current.

However, the behaviour of our composite fields is quite different under axial transformations (2.51). Let us again first study the $\boldsymbol{\pi}$ field:

$$\begin{aligned}\boldsymbol{\pi} = i\bar{q}\boldsymbol{t}\gamma_5 q &\overset{A}{\to} iq^\dagger\,(1 + i\,\gamma_5\,\boldsymbol{\alpha}_A\cdot\boldsymbol{t})\,\gamma_0\,\boldsymbol{t}\,\gamma_5\,(1 - i\,\gamma_5\,\boldsymbol{\alpha}_A\cdot\boldsymbol{t})\,q \\ &= i\bar{q}\boldsymbol{t}\gamma_5 q + iq^\dagger\,(i\,\gamma_5\,\gamma_0\,\gamma_5\,t^i\,t^j\,\alpha_A^i - i\,\gamma_0\,\gamma_5^2\,t^j\,t^i\,\alpha_A^i)\,q \\ &\overset{\text{Eq. (2.26)}}{=} \boldsymbol{\pi} + q^\dagger\,\gamma_0\,\alpha_A^i\,(t^i\,t^j + t^j\,t^i)q \\ &= \boldsymbol{\pi} + q^\dagger\,\gamma_0\,\alpha_A^i\,\{t^i, t^j\}\,q \equiv \boldsymbol{\pi} + \boldsymbol{\alpha}_A\sigma,\end{aligned} \tag{2.110}$$

where we have used the anticommutator $\{t^i, t^j\} = \delta^{ij}t^0$. Analogously to Eq. (2.110) we obtain from Eqs. (2.96), (2.103) and (2.105):

$$\sigma \overset{A}{\to} \sigma - \boldsymbol{\alpha}_A\cdot\boldsymbol{\pi}, \tag{2.111}$$

$$\boldsymbol{\rho}^\mu \overset{A}{\to} \boldsymbol{\rho}^\mu + \boldsymbol{\alpha}_A\times\boldsymbol{a}_1^\mu, \tag{2.112}$$

$$\boldsymbol{a}_1^\mu \overset{A}{\to} \boldsymbol{a}_1^\mu - \boldsymbol{\alpha}_A\times\boldsymbol{\rho}^\mu. \tag{2.113}$$

Thus the scalar state $\sigma$ is connected to the pseudoscalar state $\boldsymbol{\pi}$ via the axial transformation (and vice versa); the vector state $\boldsymbol{\rho}^\mu$ is connected to the axial-vector state $\boldsymbol{a}_1^\mu$ (and vice versa) in the same way. As we have discussed in Sec. 2.3, the axial symmetry $SU(N_f)_A$ is exact within the QCD Lagrangian, up to the explicit breaking due to non-vanishing quark masses. This implies that, in the limit of small $u$, $d$ quark masses, the breaking of the axial symmetry is virtually negligible. Consequently, given that the scalar and the pseudoscalar can be rotated into each other (just as the vector and the axial-vector), one would expect these states to possess the same masses. *Experimentally, this is not the case.* If we assign our vector state $\boldsymbol{\rho}^\mu$ to the lowest observed vector excitation, the $\rho(770)$ meson with a mass of $m_{\rho(770)} = (775.49 \pm 0.34)$ MeV and

our axial-vector state $\boldsymbol{a}_1^\mu$ to the lowest observed axial-vector excitation, the $a_1(1260)$ meson with a mass of $\sim 1230$ MeV [10], then we observe that the mass difference of these two states is of the order of the $\rho(770)$ mass itself. Such a large magnitude of symmetry breaking cannot originated from the (small) quark masses. The symmetry must have been broken by a different mechanism – *spontaneously* – because, evidently, the axial symmetry realised in the QCD Lagrangian is not realised in the vacuum states of QCD.
Then the chiral symmetry $U(N_f)_V \times U(N_f)_A \equiv U(1)_V \times SU(N_f)_V \times U(1)_A \times SU(N_f)_A$ discussed in Sec. 2.3 is spontaneously broken to $U(1)_V \times SU(N_f)_V \times U(1)_A$ in the case of vanishing quark masses [with the caveat of the $U(1)_A$ anomaly (2.60)]. If the quark masses are non-vanishing but degenerate then the symmetry is broken to $U(1)_V \times SU(N_f)_V$ and otherwise the chiral symmetry is completely broken to $U(1)_V$, indicating baryon-number conservation.

The spontaneous breaking of the chiral symmetry has at least two important consequences. According to the Goldstone Theorem [35], one expects $N_f^2 - 1$ massless pseudoscalar bosons to emerge as consequence of the spontaneous breaking of a global symmetry. This is indeed observed: e.g., for $N_f = 2$, three pions were discovered a long time ago [11] and their masses of $\sim 140$ MeV are several times smaller than the mass of the first heavier meson. Their non-vanishing mass arises due to the explicit breaking of the chiral symmetry, rendering them pseudo-Goldstone bosons. For $N_f = 3$, experimental observations yield five additional pseudoscalar Goldstone states: four kaons and the $\eta$ meson. Note, however, that the latter mixes with a heavier $\eta'$ state that would also represent a Goldstone mode of QCD if the chiral anomaly (2.60) were not present.
Additionally, the mechanism of spontaneous chiral-symmetry breaking is based on the existence of the chiral condensate [36]

$$\langle \bar{q}q \rangle = \langle 0|\bar{q}q|0\rangle = -i\mathrm{Tr} \lim_{y \to x^+} S_F(x,y) \tag{2.114}$$

where $S_F(x,y)$ denotes the full quark propagator. Then utilising Eqs. (2.29), (2.30) and (2.28) we obtain

$$\langle \bar{q}q \rangle = \langle (\bar{q}_L + \bar{q}_R)(q_L + q_R) \rangle = \langle \bar{q}_R q_L + \bar{q}_L q_R \rangle \neq 0. \tag{2.115}$$

The existence of the quark condensate is a consequence of vacuum polarisation by means of the strong interaction. The chiral condensate is a measure of the magnitude of the spontaneous chiral-symmetry breaking – for $\langle \bar{q}q \rangle \to 0$, the axial symmetry is exact again. It is expected that the quark condensate will diminish at non-zero values of temperature and baryon density; the restoration of the chiral symmetry (the so-called chiral phase transition) thus denotes the point where the chiral-symmetry breaking is no longer present (at a temperature $T_c \sim 190$ MeV [37]). The chiral phase transition may occur simultaneously with the deconfinement; however, it is as yet not known whether this is actually the case.

## 2.6 Calculating the Decay Widths

As already indicated, mesons are very unstable particles. The typical lifetime of a meson is $(10^{-24} - 10^{-25})$ s, with some notable exceptions such as the pion with the mean lifetime of approximately $10^{-8}$ s. This work will analyse various two-body decays of mesons into final states as well as into states that themselves decay further (sequential decays). For this reason it

is necessary to develop a formalism that allows us to calculate the corresponding decay widths, denoted as $\Gamma$; these are related to the time $\tau$ necessary for a particle to decay with the following relation

$$\tau = \Gamma^{-1}. \tag{2.116}$$

(There may be deviations from this law under certain conditions which we do not consider here; see Ref. [38].)

Let us in the following derive a formula for the decay width $\Gamma_{\chi\to\varphi_1\varphi_2}$ of a particle $\chi$ decaying into particles $\varphi_1$and $\varphi_2$.

$$\begin{aligned}\mathcal{L}_{\chi\varphi_1\varphi_2} = &\frac{1}{2}(\partial_\mu\chi)^2 - \frac{1}{2}m_\chi^2\chi^2 + \frac{1}{2}(\partial_\mu\varphi_1)^2 - \frac{1}{2}m_{\varphi_1}^2\varphi_1^2 \\ &+ \frac{1}{2}(\partial_\mu\varphi_2)^2 - \frac{1}{2}m_{\varphi_2}^2\varphi_2^2 + g\chi\varphi_1\varphi_2\end{aligned} \tag{2.117}$$

where the last term, $g\chi\varphi_1\varphi_2$, denotes the interaction of the field $\chi(X)$ with the fields $\varphi_1(X)$ and $\varphi_2(X)$; $x$ denotes the Minkowski space-time vector. Let us, for simplicity, assume that $\varphi_1 = \varphi_2 \equiv \varphi$. Let us also assume that $m_\chi > 2m_\varphi$ rendering the tree-level decay $\chi \to 2\varphi$ possible.

The decay amplitude obtained from the Lagrangian in Eq. (2.117) then reads:

$$-i\mathcal{M}_{\chi\to 2\varphi} = i2g \tag{2.118}$$

where the symmetry factor of two appears due to the new form of the interaction part of the Lagrangian (2.117): $g\chi\varphi_1\varphi_2 \overset{\varphi_1=\varphi_2}{\to} g\chi\varphi^2$.

Let us consider the scalar fields $\chi$ and $\varphi$ as confined in a cube of length $L$ and volume $V = L^3$. Let us furthermore denote the 4-momenta of $\chi$ and $\varphi$ as $P$ and $K$, respectively; then it is known from Quantum Mechanics that their 3-momenta are quantised: $\boldsymbol{p} = 2\pi\boldsymbol{n}_P/L$, $\boldsymbol{k} = 2\pi\boldsymbol{n}_K/L$. We denote the corresponding energies as $E_{\boldsymbol{p}} = \sqrt{m_\chi^2 + \boldsymbol{p}^2}$ and $E_{\boldsymbol{k}} = \sqrt{m_\varphi^2 + \boldsymbol{k}^2}$. It is also known from Quantum Field Theory that a free scalar bosonic field can be decomposed in terms of creation and annihilation operators (respectively $\hat{a}^\dagger$, $\hat{b}^\dagger$ and $\hat{a}$, $\hat{b}$) utilising the following Fourier transformation:

$$\hat{\chi}(X) = \int \frac{\mathrm{d}^3\boldsymbol{p}}{\sqrt{(2\pi)^3}}\frac{1}{\sqrt{2E_{\boldsymbol{p}}}}\left[\hat{b}\,(\boldsymbol{p})\,e^{-iP\cdot X} + \hat{b}^\dagger(\boldsymbol{p})e^{iP\cdot X}\right] \tag{2.119}$$

and

$$\hat{\varphi}(X) = \int \frac{\mathrm{d}^3\boldsymbol{k}}{\sqrt{(2\pi)^3}}\frac{1}{\sqrt{2E_{\boldsymbol{k}}}}\left[\hat{a}(\boldsymbol{k})e^{-iK\cdot X} + \hat{a}^\dagger(\boldsymbol{k})e^{iK\cdot X}\right]. \tag{2.120}$$

The operators obey the following commutation relations:

$$[\hat{a}(\boldsymbol{k}_1), \hat{a}(\boldsymbol{k}_2)] = [\hat{a}^\dagger(\boldsymbol{k}_1), \hat{a}^\dagger(\boldsymbol{k}_2)] = 0, \tag{2.121}$$

$$[\hat{a}(\boldsymbol{k}_1), \hat{a}^\dagger(\boldsymbol{k}_2)] = \delta^{(3)}(\boldsymbol{k}_1 - \boldsymbol{k}_2), \tag{2.122}$$

$$[\hat{b}(\boldsymbol{p}_1), \hat{b}(\boldsymbol{p}_2)] = [\hat{b}^\dagger(\boldsymbol{p}_1), \hat{b}^\dagger(\boldsymbol{p}_2)] = 0, \tag{2.123}$$

$$[\hat{b}(\boldsymbol{p}_1), \hat{b}^\dagger(\boldsymbol{p}_2)] = \delta^{(3)}(\boldsymbol{p}_1 - \boldsymbol{p}_2). \tag{2.124}$$

The $\chi$ resonance represents our initial state $|i\rangle$:

$$|i\rangle = \sqrt{\frac{(2\pi)^3}{V}}\hat{b}^\dagger(\boldsymbol{p})\,|0\rangle \tag{2.125}$$

whereas the two $\varphi$ resonances are our final states:

$$|f\rangle = \frac{(2\pi)^3}{V}\hat{a}^\dagger(\boldsymbol{k}_1)\hat{a}^\dagger(\boldsymbol{k}_2)\,|0\rangle\,. \tag{2.126}$$

The volume appears in the definition of the initial and final states to ensure their correct normalisation:

$$\begin{aligned}\langle i\,|i\rangle &= \frac{(2\pi)^3}{V}\langle 0\left|\hat{b}(\boldsymbol{p})\hat{b}^\dagger(\boldsymbol{p})|0\right\rangle \overset{\text{Eq. (2.124)}}{=} \frac{(2\pi)^3}{V}\langle 0\left|\delta^{(3)}(0)-\hat{b}^\dagger(\boldsymbol{p})\hat{b}(\boldsymbol{p})|0\right\rangle \\ &= \frac{(2\pi)^3}{V}\langle 0\left|\delta^{(3)}(0)|0\right\rangle = \frac{(2\pi)^3}{V}\delta^{(3)}(0) = 1,\end{aligned} \tag{2.127}$$

under the following normalisation condition for the $\delta$ distribution:

$$\delta^{(3)}(0) = \lim_{V\to\infty}\frac{V}{(2\pi)^3}, \tag{2.128}$$

obtained from the well-known Fourier transformation

$$\delta^{(3)}(\boldsymbol{p}) = \int\frac{\mathrm{d}^3\boldsymbol{x}}{(2\pi)^3}e^{i\boldsymbol{p}\cdot\boldsymbol{x}} \tag{2.129}$$

for $\boldsymbol{p}=0$. [As an equivalence but not equality, we can state simply $\delta^{(3)}(0)\equiv\frac{V}{(2\pi)^3}$.] The calculation of Eq. (2.127) can likewise be repeated for the final state $|f\rangle$ (2.126).
The corresponding element of the scattering matrix then reads

$$\langle f|\,\mathcal{S}\,|i\rangle\,, \tag{2.130}$$

with the scattering-matrix operator

$$\mathcal{S} = \hat{T}e^{-i\int d^4X\mathcal{H}(X)}, \tag{2.131}$$

where $\hat{T}$ denotes the time-ordering operator and $\mathcal{H}(X)$ is the interaction Hamiltonian that depends on the interaction part of the Lagrangian (2.117):

$$\mathcal{H} = -g\chi(X)\varphi^2(X). \tag{2.132}$$

For a small coupling, we can consider the scattering matrix up to the first order only:

$$\mathcal{S}^{(1)} = -i\int d^4X\hat{T}[\mathcal{H}(X)]. \tag{2.133}$$

Let us now calculate the expectation value of $\mathcal{S}^{(1)}$ in terms of the initial and final states:

$$\begin{aligned}\langle f|\,\mathcal{S}^{(1)}\,|i\rangle &= \langle f|\,ig\int\mathrm{d}^4X\hat{T}[\varphi^2(X)\chi(X)]\,|i\rangle \\ &= i\left[\frac{(2\pi)^3}{V}\right]^{3/2}g\,\langle 0|\,\hat{a}(\boldsymbol{k}_1)\hat{a}(\boldsymbol{k}_2)\int\mathrm{d}^4X\hat{T}[\varphi^2(X)\chi(X)]\hat{b}^\dagger(\boldsymbol{p})\,|0\rangle\,.\end{aligned} \tag{2.134}$$

Inserting Eqs. (2.119) and (2.120) into Eq. (2.134) and performing time-ordered product of creation and annihilation operators we obtain

$$\begin{aligned}
\langle f|\,\mathcal{S}^{(1)}\,|i\rangle &= i\left[\frac{(2\pi)^3}{V}\right]^{3/2} g\frac{1}{\sqrt{2E_{\boldsymbol{p}}}}\frac{1}{\sqrt{2E_{\boldsymbol{k}_1}}}\frac{1}{\sqrt{2E_{\boldsymbol{k}_2}}}\int \mathrm{d}^4X\frac{\mathrm{d}^3\boldsymbol{p}}{\sqrt{(2\pi)^3}}\frac{\mathrm{d}^3\boldsymbol{k}_1}{\sqrt{(2\pi)^3}}\frac{\mathrm{d}^3\boldsymbol{k}_2}{\sqrt{(2\pi)^3}}\\
&\times\langle 0|\,\hat{a}(\boldsymbol{k}_1)\hat{a}(\boldsymbol{k}_2)\left[\hat{b}\,(\boldsymbol{p})\,e^{-iP\cdot X}+\hat{b}^\dagger(\boldsymbol{p})e^{iP\cdot X}\right]\\
&\times\left[\hat{a}(\boldsymbol{k}_1)e^{-iK_1\cdot X}+\hat{a}^\dagger(\boldsymbol{k}_1)e^{iK_1\cdot X}\right]\left[\hat{a}(\boldsymbol{k}_2)e^{-iK_2\cdot X}+\hat{a}^\dagger(\boldsymbol{k}_2)e^{iK_2\cdot X}\right]\hat{b}^\dagger(\boldsymbol{p})\,|0\rangle\\
&= i\left[\frac{(2\pi)^3}{V}\right]^{3/2} g\frac{1}{\sqrt{2E_{\boldsymbol{p}}}}\frac{1}{\sqrt{2E_{\boldsymbol{k}_1}}}\frac{1}{\sqrt{2E_{\boldsymbol{k}_2}}}\int \mathrm{d}^4X\frac{\mathrm{d}^3\boldsymbol{p}}{\sqrt{(2\pi)^3}}\frac{\mathrm{d}^3\boldsymbol{k}_1}{\sqrt{(2\pi)^3}}\frac{\mathrm{d}^3\boldsymbol{k}_2}{\sqrt{(2\pi)^3}}\\
&\times\langle 0|\,\hat{a}(\boldsymbol{k}_2)\hat{a}(\boldsymbol{k}_1)\hat{a}(\boldsymbol{k}_1)\hat{a}(\boldsymbol{k}_2)\hat{b}\,(\boldsymbol{p})\,\hat{b}^\dagger\,(\boldsymbol{p})\,e^{-i(K_1+K_2+P)\cdot X}\\
&+\hat{a}(\boldsymbol{k}_2)\hat{a}(\boldsymbol{k}_1)\hat{a}^\dagger(\boldsymbol{k}_1)\hat{a}(\boldsymbol{k}_2)\hat{b}\,(\boldsymbol{p})\,\hat{b}^\dagger\,(\boldsymbol{p})\,e^{i(K_1+K_2-P)\cdot X}\\
&+\hat{a}(\boldsymbol{k}_2)\hat{a}(\boldsymbol{k}_1)\hat{a}(\boldsymbol{k}_1)\hat{a}^\dagger(\boldsymbol{k}_2)\hat{b}\,(\boldsymbol{p})\,\hat{b}^\dagger\,(\boldsymbol{p})\,e^{-i(K_1-K_2+P)\cdot X}\\
&+\hat{a}(\boldsymbol{k}_2)\hat{a}(\boldsymbol{k}_1)\hat{a}(\boldsymbol{k}_1)\hat{a}(\boldsymbol{k}_2)\hat{b}^\dagger\,(\boldsymbol{p})\,\hat{b}^\dagger\,(\boldsymbol{p})\,e^{-i(K_1+K_2-P)\cdot X}\\
&+\hat{a}(\boldsymbol{k}_2)\hat{a}(\boldsymbol{k}_1)\hat{a}^\dagger(\boldsymbol{k}_1)\hat{a}(\boldsymbol{k}_2)\hat{b}^\dagger\,(\boldsymbol{p})\,\hat{b}^\dagger\,(\boldsymbol{p})\,e^{i(K_1+K_2+P)\cdot X}\\
&+\hat{a}(\boldsymbol{k}_2)\hat{a}(\boldsymbol{k}_1)\hat{a}(\boldsymbol{k}_1)\hat{a}^\dagger(\boldsymbol{k}_2)\hat{b}^\dagger\,(\boldsymbol{p})\,\hat{b}^\dagger\,(\boldsymbol{p})\,e^{-i(K_1-K_2-P)\cdot X}\\
&+\hat{a}(\boldsymbol{k}_2)\hat{a}(\boldsymbol{k}_1)\hat{a}^\dagger(\boldsymbol{k}_1)\hat{a}^\dagger(\boldsymbol{k}_2)\hat{b}^\dagger\,(\boldsymbol{p})\,\hat{b}^\dagger\,(\boldsymbol{p})\,e^{i(K_1+K_2+P)\cdot X}\\
&+\hat{a}(\boldsymbol{k}_2)\hat{a}(\boldsymbol{k}_1)\hat{a}^\dagger(\boldsymbol{k}_1)\hat{a}^\dagger(\boldsymbol{k}_2)\hat{b}\,(\boldsymbol{p})\,\hat{b}^\dagger\,(\boldsymbol{p})\,e^{i(K_1+K_2-P)\cdot X}\,|0\rangle\,. \qquad (2.135)
\end{aligned}$$

Only the term in the last line remains as all the other terms are proportional to $\hat{a}(\boldsymbol{k}_{1,2})\,|0\rangle=0$, to $\langle 0|\,\hat{b}^\dagger\,(\boldsymbol{p})=0$ or to

$$\begin{aligned}
&\hat{a}(\boldsymbol{k}_2)\hat{a}(\boldsymbol{k}_1)\hat{a}(\boldsymbol{k}_1)\hat{a}^\dagger(\boldsymbol{k}_2)\hat{b}\,(\boldsymbol{p})\,\hat{b}^\dagger\,(\boldsymbol{p})\,|0\rangle\\
&\overset{\text{Eq. (2.124)}}{=}\hat{a}(\boldsymbol{k}_2)\hat{a}(\boldsymbol{k}_1)\hat{a}(\boldsymbol{k}_1)\hat{a}^\dagger(\boldsymbol{k}_2)[\delta^{(3)}(0)+\hat{b}^\dagger\,(\boldsymbol{p})\,\hat{b}\,(\boldsymbol{p})]\,|0\rangle\\
&\overset{\text{Eq. (2.122)}}{=}\hat{a}(\boldsymbol{k}_2)\hat{a}(\boldsymbol{k}_1)[\delta^{(3)}(\boldsymbol{k}_1-\boldsymbol{k}_2)+\hat{a}^\dagger(\boldsymbol{k}_1)\hat{a}(\boldsymbol{k}_2)]\delta^{(3)}(0)\,|0\rangle=0. \qquad (2.136)
\end{aligned}$$

We therefore obtain

$$\begin{aligned}
\langle f|\,\mathcal{S}^{(1)}\,|i\rangle &= i\left[\frac{(2\pi)^3}{V}\right]^{3/2} g\frac{1}{\sqrt{2E_{\boldsymbol{p}}}}\frac{1}{\sqrt{2E_{\boldsymbol{k}_1}}}\frac{1}{\sqrt{2E_{\boldsymbol{k}_2}}}\int \mathrm{d}^4X\frac{\mathrm{d}^3\boldsymbol{p}}{\sqrt{(2\pi)^3}}\frac{\mathrm{d}^3\boldsymbol{k}_1}{\sqrt{(2\pi)^3}}\frac{\mathrm{d}^3\boldsymbol{k}_2}{\sqrt{(2\pi)^3}}\\
&\times\langle 0|\,\hat{a}(\boldsymbol{k}_2)\hat{a}(\boldsymbol{k}_1)\hat{a}^\dagger(\boldsymbol{k}_1)\hat{a}^\dagger(\boldsymbol{k}_2)\hat{b}\,(\boldsymbol{p})\,\hat{b}^\dagger\,(\boldsymbol{p})\,e^{i(K_1+K_2-P)\cdot X}\,|0\rangle\,. \qquad (2.137)
\end{aligned}$$

Eq. (2.127) implies that our creation and annihilation operators are normalised as

$$\langle 0\left|\hat{b}(\boldsymbol{p})\hat{b}^\dagger(\boldsymbol{p})|0\right\rangle=\frac{V}{(2\pi)^3} \qquad (2.138)$$

and consequently Eq. (2.137) gains the following form:

$$\langle f|\,\mathcal{S}^{(1)}\,|i\rangle = i\left[\frac{(2\pi)^3}{V}\right]^{3/2} g\frac{1}{\sqrt{2E_{\boldsymbol{p}}}}\frac{1}{\sqrt{2E_{\boldsymbol{k}_1}}}\frac{1}{\sqrt{2E_{\boldsymbol{k}_2}}}\frac{V^3}{(2\pi)^9} \times \int \mathrm{d}^4X \frac{\mathrm{d}^3\boldsymbol{p}}{\sqrt{(2\pi)^3}}\frac{\mathrm{d}^3\boldsymbol{k}_1}{\sqrt{(2\pi)^3}}\frac{\mathrm{d}^3\boldsymbol{k}_2}{\sqrt{(2\pi)^3}} e^{i(K_1+K_2-P)\cdot X}. \tag{2.139}$$

If we consider the quantised version of the 3-momenta of the particles involved, then the usual box normalisation yields $\boldsymbol{p} = 2\pi\boldsymbol{n}_P/L$ and $\boldsymbol{k} = 2\pi\boldsymbol{n}_K/L$, i.e.,
$\Delta\boldsymbol{p} = 2\pi\Delta\boldsymbol{n}_P/L$ and $\Delta\boldsymbol{k} = 2\pi\Delta\boldsymbol{n}_K/L$. Substituting $\Delta\boldsymbol{p} \to \mathrm{d}\boldsymbol{p}$ and $\Delta\boldsymbol{k} \to \mathrm{d}\boldsymbol{k}$ yields $\int\mathrm{d}^3\boldsymbol{p} = (2\pi)^3/V = \int\mathrm{d}^3\boldsymbol{k}$ and thus

$$\begin{aligned}
\langle f|\,\mathcal{S}^{(1)}\,|i\rangle &= i\left(\frac{1}{V}\right)^{3/2} g\frac{1}{\sqrt{2E_{\boldsymbol{p}}}}\frac{1}{\sqrt{2E_{\boldsymbol{k}_1}}}\frac{1}{\sqrt{2E_{\boldsymbol{k}_2}}}\frac{V^3}{(2\pi)^9}\int \mathrm{d}^4X \frac{(2\pi)^9}{V^3} e^{i(K_1+K_2-P)\cdot X} \\
&= i\left(\frac{1}{V}\right)^{3/2} g\frac{1}{\sqrt{2E_{\boldsymbol{p}}}}\frac{1}{\sqrt{2E_{\boldsymbol{k}_1}}}\frac{1}{\sqrt{2E_{\boldsymbol{k}_2}}}\int \mathrm{d}^4X e^{i(K_1+K_2-P)\cdot X} \\
&\equiv \frac{1}{V^{3/2}}\frac{ig}{\sqrt{2E_{\boldsymbol{k}_1}2E_{\boldsymbol{k}_2}2E_{\boldsymbol{p}}}}\int \mathrm{d}^4X e^{i(P-K_1-K_2)X} \\
&= \frac{\sqrt{s_f}}{V^{3/2}}\frac{-i\mathcal{M}_{\chi\to 2\varphi}}{\sqrt{2E_{\boldsymbol{k}_1}2E_{\boldsymbol{k}_2}2E_{\boldsymbol{p}}}}(2\pi)^4\delta^{(4)}(P-K_1-K_2)
\end{aligned} \tag{2.140}$$

where in the last line we have substituted the coupling $g$ by the decay amplitude $-i\mathcal{M}_{\chi\to 2\varphi}$ (2.118) multiplied by a symmetry factor $\sqrt{s_f}$ (in our case $s_f = 2$ because the decay $\chi \to 2\varphi$ contains two identical particles). The delta distribution $\delta^{(4)}(P-K_1-K_2)$ corresponds to energy-momentum conservation at each vertex.
The probability for the decay $\chi \to 2\varphi$ corresponds to the squared modulus of the scattering matrix:

$$\left|\langle f|\,\mathcal{S}^{(1)}\,|i\rangle\right|^2 = \frac{s_f}{V^3}\frac{1}{2E_{\boldsymbol{k}_1}2E_{\boldsymbol{k}_2}2E_{\boldsymbol{p}}}(2\pi)^8[\delta^{(4)}(P-K_1-K_2)]^2\left|-i\mathcal{M}_{\chi\to 2\varphi}\right|^2. \tag{2.141}$$

The square of the delta distribution can be calculated as follows:

$$\begin{aligned}
&(2\pi)^8[(\delta^{(4)}(P-K_1-K_2)]^2 \\
&= (2\pi)^4\delta^{(4)}(P-K_1-K_2)\int \mathrm{d}^4X e^{iX(P-K_1-K_2)} \\
&= (2\pi)^4\delta^{(4)}(P-K_1-K_2)\int \mathrm{d}^4X \\
&= (2\pi)^4\delta^{(4)}(P-K_1-K_2)\int \mathrm{d}^3\boldsymbol{x}\int_0^t dt \\
&= (2\pi)^4\delta^{(4)}(P-K_1-K_2)Vt.
\end{aligned} \tag{2.142}$$

Integrating over $\boldsymbol{k}_{1,2}$ we obtain

$$\int\int \left|\langle f|\,\mathcal{S}^{(1)}\,|i\rangle\right|^2 \frac{V}{(2\pi)^3}\mathrm{d}^3\boldsymbol{k}_1\frac{V}{(2\pi)^3}\mathrm{d}^3\boldsymbol{k}_2$$
$$= (2\pi)^4\frac{s_f}{V^2}\int\int\frac{|-i\mathcal{M}_{\chi\to 2\varphi}|^2}{2E_{\boldsymbol{k}_1}2E_{\boldsymbol{k}_2}2E_{\boldsymbol{p}}}\delta^{(4)}(P-K_1-K_2)\frac{V}{(2\pi)^3}\mathrm{d}^3\boldsymbol{k}_1\frac{V}{(2\pi)^3}\mathrm{d}^3\boldsymbol{k}_2 t$$
$$= \Gamma t \tag{2.143}$$

where we have defined the decay width for the process $\chi \to 2\varphi$ as

$$\Gamma_{\chi\to 2\varphi} = \frac{s_f}{(2\pi)^2}\int\int\frac{|-i\mathcal{M}_{\chi\to 2\varphi}|^2}{2E_{\boldsymbol{k}_1}2E_{\boldsymbol{k}_2}2E_{\boldsymbol{p}}}\delta^{(4)}(P-K_1-K_2)\mathrm{d}^3\boldsymbol{k}_1\mathrm{d}^3\boldsymbol{k}_2. \tag{2.144}$$

Consequently, the probability to find two particles at the time $t$ is $P_{2\varphi}(t) = \Gamma_{\chi\to 2\varphi}t$. Then the probability to find the particle $\chi$ at the same time point is

$$P_\chi(t) = 1 - \Gamma_{\chi\to 2\varphi}t \tag{2.145}$$

or, if $\Gamma_{\chi\to 2\varphi} \ll t$

$$P_\chi(t) = e^{-\Gamma_{\chi\to 2\varphi}t}. \tag{2.146}$$

Consequently, we define the median life-time of the particle $\chi$ as

$$\tau = \Gamma^{-1}_{\chi\to 2\varphi}. \tag{2.147}$$

The latter expression is valid in the rest frame of the decaying particle; the life-time of the particle in the laboratory frame reads

$$\tau' = \gamma\tau, \tag{2.148}$$

where $\gamma = (1-v^2)^{-1/2}$. We also know that the 4-vectors of all the particles involved have this form: $P = (m_\chi, \mathbf{0})$, $K_1 = (E_{\boldsymbol{k}_1}, \boldsymbol{k}_1)$ and $K_2 = (E_{\boldsymbol{k}_2}, \boldsymbol{k}_2)$. Given that $|\boldsymbol{k}_2| = |\boldsymbol{k}_1|$, we obtain $E_{\boldsymbol{k}_1} = E_{\boldsymbol{k}_2}$. Let us then rewrite $\delta^{(4)}(P-K_1-K_2)$ as follows:

$$\begin{aligned}\delta^{(4)}(P-K_1-K_2) &= \delta^{(3)}(\boldsymbol{k}_1+\boldsymbol{k}_2)\delta(m_\chi - E_{\boldsymbol{k}_1} - E_{\boldsymbol{k}_2}) \\ &= \delta^{(3)}(\boldsymbol{k}_1+\boldsymbol{k}_2)\delta(m_\chi - 2E_{\boldsymbol{k}_1}).\end{aligned} \tag{2.149}$$

Then integrating over $d^3\boldsymbol{k}_2$ in Eq. (2.144) we obtain

$$\Gamma = \frac{1}{2(2\pi)^2}\int\frac{|-i\mathcal{M}|^2}{(2E_{\boldsymbol{k}_1})^2 2m_\chi}\delta(m_\chi - 2E_{\boldsymbol{k}_1})\mathrm{d}^3\boldsymbol{k}_1. \tag{2.150}$$

Energy-momentum conservation implies

$$|\boldsymbol{k}_1| = \sqrt{\frac{m_\chi^2}{4} - m_\varphi^2} \equiv k_f \tag{2.151}$$

and therefore the $\delta$ distribution in Eq. (2.150) can be expressed in the following way using the generic identity $\delta(g(x)) = \sum_i \delta(x-x_i)/|g'(x_i)|$ where $g(x_i) = 0$:

$$\delta(m_\chi - 2E_{\boldsymbol{k}_1}) = \frac{4m_\chi}{k_f}\delta\left(|\boldsymbol{k}_1| - k_f\right). \tag{2.152}$$

Let us then perform the integral in Eq. (2.150) using the spherical coordinates: $d^3\boldsymbol{k}_1 \equiv \boldsymbol{k}_1^2 \mathrm{d}|\boldsymbol{k}_1|\mathrm{d}\Omega$. Integrating over $\mathrm{d}|\boldsymbol{k}_1|$ yields

$$\Gamma = \frac{k_f}{32\pi^2 m_\chi^2} \int d\Omega \, |-i\mathcal{M}|^2 \tag{2.153}$$

and, if the decay amplitude does not depend on $\Omega$

$$\Gamma = \frac{k_f}{8\pi m_\chi^2} \, |-i\mathcal{M}|^2 \, . \tag{2.154}$$

We have to ensure that there is no double counting in case of a decay into identical particles. This is performed by introducing a symmetry factor $s_f$ into the formula for the decay width:

$$\Gamma = s_f \frac{k_f}{8\pi m_\chi^2} \, |-i\mathcal{M}|^2 \, . \tag{2.155}$$

In the decay discussed in this section, the assumption was made that the particle $\chi$ decays into two identical particles $\varphi$. Consequently $s_f = 1/2$ and from Eq. (2.155) we obtain:

$$\Gamma_{\chi \to 2\varphi} = \frac{k_f}{4\pi m_\chi^2} g^2 . \tag{2.156}$$

### 2.6.1 Parametrising the Scattering Amplitude

Two scattering particles will in general form an intermediate state before the scattering products subsequently arise (see, e.g., Sec. 5.2.8 where $\pi\pi$ scattering entails contributions of the form $\pi\pi \to \sigma_N \to \pi\pi$ and $\pi\pi \to \rho \to \pi\pi$, i.e., with intermediate scalar and vector particles, respectively). A scattering amplitude $\mathcal{M}$ of the incoming two particles (or, equivalently, the decay amplitude of the intermediate particle into the incoming two particles) is in general a complex-valued quantity; we expect it to depend on the centre-of-mass momentum $p$. Let us then decompose $\mathcal{M}$ in terms of $p$ and a quantity of dimension $[E^{-1}]$ that we will refer to as scattering length $a$ as follows [39]:

$$\mathcal{M} = \mathcal{M}(p) = \frac{N}{-a^{-1} - ip}, \tag{2.157}$$

with $N$ a constant of dimension $[E^2]$ that assures $[\mathcal{M}] = [E]$; $N$ could in principle also be a function (see for instance Ref. [40] and references therein for explicit ways how to parametrise a scattering amplitude) but the exact nature of $N$ is not important for the statements in this section. It is obvious that the limit where $p = 0$ leads to $\mathcal{M}(p) \sim -a$. If we restrict ourselves to the behaviour of $\mathcal{M}$ close to threshold, then we observe in Eq. (2.157) that the function is analytic in this energy region (i.e., $p \sim 0$) except for a pole at $p = ia^{-1} \equiv ip_0$ (i.e., $p_0 \equiv a^{-1}$). The value of the scattering length can be determined from the scattering amplitude, with the latter being a measurable quantity (for examples regarding the $\pi\pi$ scattering see also Refs. [41, 42, 43]). The scattering length can have both positive or negative signs. If $a < 0$, then the pole is found in the lower half of the complex $p$ plane ($\mathrm{Im}\, p < 0$); the pole corresponds to a "virtual state" [39] or, in the language of the hadronic physics, to a resonance. The lower half-plane is usually denoted as the second (unphysical) sheet. Conversely, $a > 0$ implies the existence of a pole in the upper half-plane (denoted as the first, or physical, sheet); it corresponds to a bound state. It is known, for example, that the proton-neutron scattering produces such a bound state (deuteron) in the ${}^3S$ channel. Conversely, $a < 0$ is also possible in the $pn$ scattering, leading to a ${}^1S$ virtual state.

The $p$ plane can also be mapped onto the complex $s$ plane, where $s$ denotes the Mandelstam variable $s = 4(m^2 + p^2)$ with $m$ being the mass of the incoming particles (taken for simplicity to be identical). Thus the condition $s \geq 4m^2$ holds in any given experimental environment, notwithstanding whether it explores a virtual or a bound state. However, the mentioned two types of states do not behave in the same way below threshold. Although not accessible to experiments, the region below threshold nonetheless can be explored mathematically by means of analytic continuation $p \to i\tilde{p}$ (with $\tilde{p}$ a positive, real number) yielding from Eq. (2.157)

$$\mathcal{M} \sim \frac{1}{\tilde{p} - p_0}. \tag{2.158}$$

Then there are two possibilities (see Fig. 2.1): (i) if $p_0 > 0$, i.e., $a > 0$ (bound state), then $|\mathcal{M}|^2$ exhibits a pole at $\tilde{p} = p_0$, i.e., $s_0 = 4(m^2 - p_0^2)$; (ii) if $p_0 < 0$, i.e., $a < 0$ (virtual state), then $|\mathcal{M}|^2$ exhibits a cusp at the point $\tilde{p} = 0$, i.e., $s = 4m^2$. Thus the behaviour of the two types of states is fundamentally different below threshold; the dependence of $|\mathcal{M}|^2$ on $s$ is a strong indicator whether particle scattering has yielded a bound state or a virtual-type state.

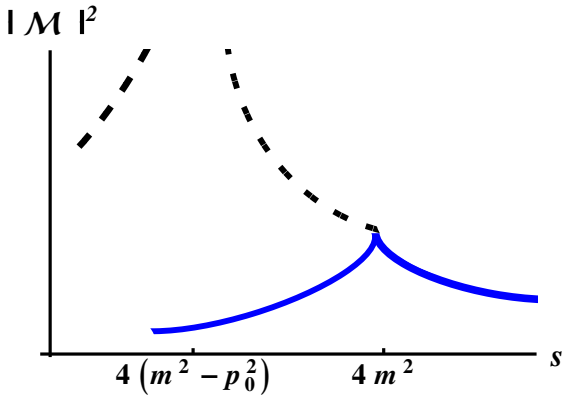


**Figure 2.1:** Behaviour of $|\mathcal{M}|^2$ for a bound state (dashed line) and a virtual state (full line).

Let us explore the behaviour of the decay amplitude on a concrete example. As demonstrated in Eq. (2.155), the square of the decay amplitude is necessary for the decay width of an unstable state to be calculated. Similarly to the Lagrangian (2.117), let us consider a decay of a resonance $S \to 2\varphi$ [44]:

$$\mathcal{L}_{S\varphi\varphi} = \frac{1}{2}(\partial_\mu S)^2 - \frac{1}{2}m_S^2 S^2 + \frac{1}{2}(\partial_\mu \varphi)^2 - \frac{1}{2}m_\varphi^2 \varphi^2 + gS\varphi^2. \tag{2.159}$$

Let us also introduce the tree-level decay width for the process $S \to 2\varphi_1$ as

$$\Gamma_{S,0}(x_S, m_\varphi, g) = \frac{\sqrt{\frac{x_S^2}{4} - m_\varphi^2}}{8\pi x_S^2}(\sqrt{2}g)^2\theta(x_S - 2m_\varphi), \tag{2.160}$$

where $x_S$ denotes the running mass of the state $S$ and the $\theta$-function implements the tree-level condition that $S$ is above the $2\varphi$ threshold. The decay width of Eq. (2.160) can in principle be calculated by setting $x_S = m_S$; however, quantum fluctuations are known to modify the value of $m_S$ (see below) and consequently we evaluate $\Gamma_{S,0}(x_S, m_\varphi, g)$ at the physical value of the $S$

mass (let us denote it as $m$) rather than at the value of the Lagrangian parameter $m_S$. The total decay width of the state $S$ is then

$$\Gamma_S(m) \equiv \Gamma_{S,0}(m, m_\varphi, g). \tag{2.161}$$

Note that the quantity $\tau_{BW} \equiv 1/\Gamma_S(m)$ represents the so-called Breit-Wigner mean life-time of the particle $S$.

In general, a calculation of the decay width may be performed at tree level (see Sections 2.6.2 – 2.6.4). However, the optical theorem allows us to relate the tree-level decay width with the self-energy of the decaying particle $S$. To this end, we first have to evaluate the propagator $G_S(p^2)$ of the state $S$ (with $p$ the centre-of-mass momentum)

$$G_S(p^2) = \frac{1}{p^2 - m_S^2 + (\sqrt{2}g)^2\Sigma(p^2, m_\varphi^2) + i\epsilon} \tag{2.162}$$

by integrating over the loop diagram presented in Fig. 2.2 to obtain the self-energy

$$\Sigma(p^2, m_\varphi^2) = -i \int \frac{\mathrm{d}^4 q}{(2\pi)^4} \frac{1}{\left[\left(\frac{p}{2} + q\right)^2 - m_\varphi^2 + i\varepsilon\right]\left[\left(\frac{p}{2} - q\right)^2 - m_\varphi^2 + i\varepsilon\right]}. \tag{2.163}$$

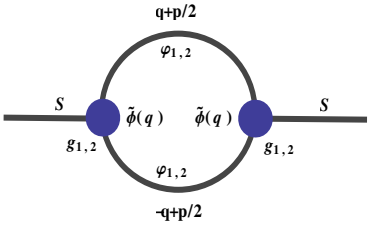


**Figure 2.2:** Self-energy diagram for the decay process $S \to \phi_{1,2}\phi_{1,2}$; $\tilde{\phi}$ is the vertex function, required for regularisation of the self-energy diagram.

The integral stated in Eq. (2.163) has to be regularised because its real part is divergent (the imaginary part is convergent). The regularisation is performed by introducing a function $\tilde{\phi}(q)$ at every vertex in the loop diagram of Eq. (2.162), see Fig. 2.2. Then we regularise $\Sigma(p^2, m_\varphi^2)$ in the following way:

$$\Sigma(p^2, m_\varphi^2) = -i \int \frac{\mathrm{d}^4 q}{(2\pi)^4} \frac{\left[\tilde{\phi}(q)\right]^2}{\left[\left(\frac{p}{2} + q\right)^2 - m_\varphi^2 + i\varepsilon\right]\left[\left(\frac{p}{2} - q\right)^2 - m_\varphi^2 + i\varepsilon\right]}. \tag{2.164}$$

The function $\tilde{\phi}(q)$ is also referred to as the vertex function. It does not have a unique form; it can be defined for example as $\tilde{\phi}(q) = \theta(\Lambda^2 - q^2)$ with the cutoff $\Lambda$ [$q$ represents the off-shell momentum of the state $\varphi$], $\tilde{\phi}(x_S) = \theta(\sqrt{\Lambda^2 + m_\varphi^2} - x_S/2)$ [38], $\tilde{\phi}(q) = 1/[1 + (q/\Lambda)^2]$ as in Ref.

[45] or $\tilde{\phi}(q) = 1/(1 + \boldsymbol{q}^2/\Lambda^2)$ [46]. Different choices of $\tilde{\phi}(q)$ do not change qualitative statements of the given model [44].
We can simplify Eq. (2.162) by introducing the loop function

$$\Pi(p^2) = (\sqrt{2}g)^2 \Sigma(p^2, m_\varphi^2) \tag{2.165}$$

obtaining

$$G_S(p^2) = \frac{1}{p^2 - m_S^2 + \Pi(p^2) + i\epsilon}. \tag{2.166}$$

The optical theorem relates the tree-level decay width in Eq. (2.161), evaluated at any value of the running mass $x_S$, with the imaginary part of the loop function $\Pi(p^2 = x_S^2)$:

$$\operatorname{Im}\Pi(x_S^2) = x_S \Gamma_S(x_S) \left[\tilde{\phi}(q = (0, \boldsymbol{q}))\right]^2 \tag{2.167}$$

with the energy-momentum conservation at vertex yielding $\boldsymbol{q}^2 = x_S^2/4 - m_\varphi^2$. Spatial isotropy implies that $\tilde{\phi}(q = (0, \boldsymbol{q}))$ has to be a function of $\boldsymbol{q}^2$. As a consequence,

$$\Gamma_S(m) \to \Gamma_S(m) \left[\tilde{\phi}(q = (0, \boldsymbol{q}))\right]^2, \tag{2.168}$$

i.e., for the decay widths in Eq. (2.160)

$$\Gamma_{S,0}(x_S, m_\varphi, g) \to \Gamma_{S,0}(x_S, m_\varphi, g) \left[\tilde{\phi}(q = (0, \boldsymbol{q}))\right]^2. \tag{2.169}$$

We define the *spectral function* $d_S(x_S)$ of the resonance $S$ as the imaginary part of the propagator (2.166)

$$d_S(x_S) = \frac{2x_S}{\pi} \left| \lim_{\varepsilon \to 0} \operatorname{Im} G_S(x_S^2) \right|, \tag{2.170}$$

i.e.,

$$d_S(x_S) = \frac{2x_S}{\pi} \left| \lim_{\varepsilon \to 0} \frac{\operatorname{Im}\Pi(x_S^2) + \varepsilon}{\left[x_S^2 - m_S^2 + \operatorname{Re}\Pi(x_S^2)\right]^2 + \left[\operatorname{Im}\Pi(x_S^2) + \varepsilon\right]^2} \right|. \tag{2.171}$$

The differential value $d_S(x_S)\mathrm{d}x_S$ is interpreted as the probability that the resonance $S$ will have a mass between $x_S$ and $x_S + \mathrm{d}x_S$. For this reason, the spectral function $d_S(x_S)$ has to be normalised properly:

$$\int_0^\infty \mathrm{d}x_S d_S(x_S) \stackrel{!}{=} 1. \tag{2.172}$$

The renormalised (physical) mass $m$ of the resonance $S$ is usually defined as the zero of the real part of the resonance propagator, i.e., from the implicit equation

$$m^2 - m_S^2 + \operatorname{Re}\Pi(m^2) = 0. \tag{2.173}$$

It is common that $\operatorname{Re}\Pi(m^2) > 0$ – in other words, quantum fluctuations usually decrease the value of the model mass $m_S$ to the physical mass value $m$. Note, however, that Eq. (2.173) is not the only way to define the regularised mass: the mass can also be defined as the position of

the minimum of $\mathrm{Im}\, G_S(x_S^2)$ but this definition leads to qualtiatively the same results (see Ref. [47] for an explicit example of the $a_1$ mass calculation).

There is an important approximation of Eq. (2.171). The approximation is obtained by neglecting the real part of the loop function (justified for resonances that are not too broad): $\mathrm{Re}\,\Pi(m^2) = 0$, using Eq. (2.167) without the vertex function $\tilde{\phi}$ [that is no longer necessary because the divergent, real part of $\Pi(m^2)$ is set to zero and $\mathrm{Im}\,\Pi(m^2)$ is convergent] and setting $\varepsilon \to 0$:

$$d_S(x_S) = \bar{N}_S \frac{x_S^2 \Gamma_S(x_S)}{(x_S^2 - m^2)^2 + [x_S \Gamma_S(x_S)]^2} \theta(x_S - 2m_{\varphi_{1,2}}), \tag{2.174}$$

where the constant $2/\pi$ from Eq. (2.171) has been absorbed into $\bar{N}_S$, the normalisation constant obtained from the condition (2.172). Note that, conversely, the $\theta$ function in Eq. (2.174) is no longer absorbed into $\Gamma_S(x_S)$ as was the case in Eq. (2.160). Eq. (2.174) can be simplified further by approximating $\Gamma_S(x_S)$ with the experimental value $\Gamma_S^{\mathrm{exp}}$, i.e., by neglecting the functional dependence of $\Gamma_S(x_S)$ on $x_S$:

$$d_S(x_S) = N_S \frac{x_S^2 \Gamma_S^{\mathrm{exp}}}{(x_S^2 - m^2)^2 + \left(x_S \Gamma_S^{\mathrm{exp}}\right)^2} \theta(x_S - 2m_{\varphi}). \tag{2.175}$$

Equation (2.175) is known as the relativistic Breit-Wigner limit of the spectral function (or simply the relativistic Breit-Wigner spectral function). The relativistic Breit-Wigner spectral function will be used throughout this work to calculate decays via off-shell particles (see, e.g., Sections 2.6.2 and 2.6.4).

Let us finally note that, in the case of our resonance $S$, the scattering amplitude discussed in Eq. (2.157) can also be parametrised in terms of the Mandelstam variable $s = p^2$ with a pole at $s_0 = (m - i\Gamma_S/2)^2$. The parametrisation can be motivated in the following way: let our starting point be the propagator (2.166) where the loop function $\Pi$ is evaluated at the physical mass value $m$:

$$\begin{aligned} \frac{1}{p^2 - m_S^2 + \Pi(m^2)} &= \frac{1}{p^2 - m_S^2 + \mathrm{Re}\,\Pi(m^2) + i\,\mathrm{Im}\,\Pi(m^2)} \\ &\overset{\text{Eq. (2.167)}}{=} \frac{1}{p^2 - m_S^2 + \mathrm{Re}\,\Pi(m^2) + im\Gamma_S(m)} \overset{\text{Eq. (2.173)}}{=} \frac{1}{p^2 - m^2 + im\Gamma_S(m)}. \end{aligned} \tag{2.176}$$

Let us assume that our resonance $S$ fulfills the condition $\Gamma_S^2(m) \ll m^2$, i.e., $\Gamma_S^2(m)/m^2 \ll 1$. Then we can add the term $\Gamma_S^2(m)/4$ to the denominator:

$$\frac{1}{p^2 - m^2 + im\Gamma_S(m)} \simeq \frac{1}{p^2 - m^2 + im\Gamma_S(m) + \frac{\Gamma_S^2(m)}{4}} \tag{2.177}$$

$$= \frac{1}{p^2 - \left[m - \frac{i}{2}\Gamma_S(m)\right]^2}. \tag{2.178}$$

Substituting $p^2 = s$ and $s_0 = (m - i\Gamma_S/2)^2$, we obtain the following expression

$$\frac{1}{p^2 - \left[m - \frac{i}{2}\Gamma_S(m)\right]^2} = \frac{1}{s - s_0}. \tag{2.179}$$

Consequently, *if* an experimentally determined scattering amplitude can be parametrised as

$$\mathcal{M} \sim \frac{1}{s - s_0}, \tag{2.180}$$

then it evidently contains a pole at $s = s_0$ describing a resonance with mass $m$ and decay width $\Gamma_S(m)$. This is a well-known criterion that allows one to ascertain whether scattering data entail a resonance signal.
Applications of the discussion in this section are presented in the following, where some exemplary tree-level decay widths are calculated.

### 2.6.2 Example: Decaying Axial-Vector State I

Let us consider a decay process of the form $A \to V\tilde{P}$ where $A$, $V$ and $\tilde{P}$ denote an axial-vector, a vector and a pseudoscalar state, respectively, with the following interaction Lagrangian describing the decay of the axial-vector state into neutral modes:

$$\begin{aligned}\mathcal{L}_{AV\tilde{P}} &= A_{AV\tilde{P}} A^{\mu 0} V^0_\mu \tilde{P}^0 \\ &\quad + B_{AV\tilde{P}} \left[ A^{\mu 0} \left( \partial_\nu V^0_\mu - \partial_\mu V^0_\nu \right) \partial^\nu \tilde{P}^0 + \partial^\nu A^{\mu 0} \left( V^0_\nu \partial_\mu \tilde{P}^0 - V^0_\mu \partial_\nu \tilde{P}^0 \right) \right].\end{aligned} \tag{2.181}$$

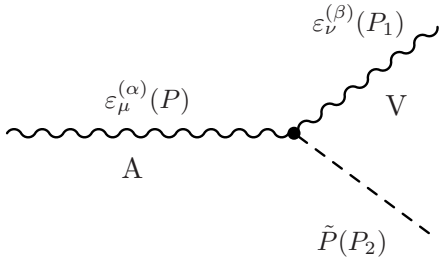


**Figure 2.3:** Decay process $A \to V\tilde{P}$.

We will consider the possible decay of the axial-vector state into charged modes at the end of this section. For now, let us consider a generic decay process of the form $A \to V^0 P^0$.
Let us then denote the momenta of $A$, $V$ and $\tilde{P}$ as $P$, $P_1$ and $P_2$, respectively. The stated decay process involves two vector states: $A$ and $V$. We therefore have to consider the corresponding polarisation vectors; let us denote them as $\varepsilon^{(\alpha)}_\mu(P)$ for $A$ and $\varepsilon^{(\beta)}_\nu(P_1)$ for $V$. Then, upon substitutions $\partial^\mu \to -iP^\mu$ for the decaying particle and $\partial^\mu \to iP^\mu_{1,2}$ for the decay products, we obtain the following Lorentz-invariant $AV\tilde{P}$ scattering amplitude $-i\mathcal{M}^{(\alpha,\beta)}_{A\to V^0\tilde{P}^0}$:

$$\begin{aligned}-i\mathcal{M}^{(\alpha,\beta)}_{A\to V^0\tilde{P}^0} &= \varepsilon^{(\alpha)}_\mu(P)\varepsilon^{(\beta)}_\nu(P_1) h^{\mu\nu}_{AV\tilde{P}} = i\varepsilon^{(\alpha)}_\mu(P)\varepsilon^{(\beta)}_\nu(P_1) \\ &\quad \times \{A_{AV\tilde{P}} g^{\mu\nu} + B_{AV\tilde{P}} [P_1^\mu P_2^\nu + P_2^\mu P^\nu - (P_1 \cdot P_2) g^{\mu\nu} - (P \cdot P_2) g^{\mu\nu}]\}\end{aligned} \tag{2.182}$$

with

$$h^{\mu\nu}_{AV\tilde{P}} = i\left\{A_{AV\tilde{P}}g^{\mu\nu} + B_{AV\tilde{P}}[P_1^\mu P_2^\nu + P_2^\mu P^\nu - (P_1\cdot P_2)g^{\mu\nu} - (P\cdot P_2)g^{\mu\nu}]\right\}, \tag{2.183}$$

where $h^{\mu\nu}_{AV\tilde{P}}$ denotes the $AV\tilde{P}$ vertex.

It will be necessary to determine the square of the scattering amplitude in order to calculate the decay width. We note that the scattering amplitude in Eq. (2.182) depends on the polarisation vectors $\varepsilon^{(\alpha)}_\mu(P)$ and $\varepsilon^{(\beta)}_\nu(P_1)$; therefore, it is necessary to calculate the average of the squared amplitude for all polarisation values. Let us denote the masses of the vectors states $A$ and $V$ as $m_A$ and $m_V$, respectively. Then the averaged squared amplitude $|-i\bar{\mathcal{M}}|^2$ is determined as follows:

$$\begin{aligned}-i\mathcal{M}^{(\alpha,\beta)}_{A\to V^0\tilde{P}^0} = \varepsilon^{(\alpha)}_\mu(P)\varepsilon^{(\beta)}_\nu(P_1)h^{\mu\nu}_{AV\tilde{P}} \Rightarrow \left|-i\bar{\mathcal{M}}_{A\to V^0\tilde{P}^0}\right|^2 &= \frac{1}{3}\sum_{\alpha,\beta=1}^{3}\left|-i\mathcal{M}^{(\alpha,\beta)}_{A\to V^0\tilde{P}^0}\right|^2 \\ &= \frac{1}{3}\sum_{\alpha,\beta=1}^{3}\varepsilon^{(\alpha)}_\mu(P)\varepsilon^{(\beta)}_\nu(P_1)h^{\mu\nu}_{AVP}\varepsilon^{(\alpha)}_\kappa(P)\varepsilon^{(\beta)}_\lambda(P_1)h^{*\kappa\lambda}_{AV\tilde{P}}.\end{aligned} \tag{2.184}$$

Given that

$$\sum_{\alpha=1}^{3}\varepsilon^{(\alpha)}_\mu(P)\varepsilon^{(\alpha)}_\kappa(P) = \left(-g_{\mu\kappa} + \frac{P_\mu P_\kappa}{m_A^2}\right) \tag{2.185}$$

[an analogous equation holds for $\varepsilon^{(\beta)}$], we then obtain from Eq. (2.184):

$$\begin{aligned}|-i\bar{\mathcal{M}}_{A\to V^0\tilde{P}^0}|^2 &= \frac{1}{3}\left(-g_{\mu\kappa} + \frac{P_\mu P_\kappa}{m_A^2}\right)\left(-g_{\nu\lambda} + \frac{P_{1\nu}P_{1\lambda}}{m_V^2}\right)h^{\mu\nu}_{AV\tilde{P}}h^{*\kappa\lambda}_{AV\tilde{P}} \\ &= \frac{1}{3}\left[h_{\mu\nu AV\tilde{P}}h^{*\mu\nu}_{AV\tilde{P}} - \frac{\left(h^{\mu\nu}_{AV\tilde{P}}P_\mu\right)\left(h^{*\kappa}_{\nu AV\tilde{P}}P_\kappa\right)}{m_A^2} - \frac{\left(h^{\mu\nu}_{AV\tilde{P}}P_{1\nu}\right)\left(h^{*\lambda}_{\mu AV\tilde{P}}P_\lambda\right)}{m_V^2}\right. \\ &\quad \left. + \frac{\left(h^{\mu\nu}_{AV\tilde{P}}P_\mu P_{1\nu}\right)\left(h^{*\mu\nu}_{AV\tilde{P}}P_\mu P_{1\nu}\right)}{m_V^2 m_A^2}\right] \\ &= \frac{1}{3}\left[\left|h^{\mu\nu}_{AV\tilde{P}}\right|^2 - \frac{\left|h^{\mu\nu}_{AV\tilde{P}}P_\mu\right|^2}{m_A^2} - \frac{\left|h^{\mu\nu}_{AV\tilde{P}}P_{1\nu}\right|^2}{m_V^2} + \frac{\left|h^{\mu\nu}_{AV\tilde{P}}P_\mu P_{1\nu}\right|^2}{m_V^2 m_A^2}\right].\end{aligned} \tag{2.186}$$

Equation (2.186) contains the metric tensor $g_{\mu\nu} = \mathrm{diag}(1,-1-1,-1)$. The decay width for the process $A\to V^0\tilde{P}^0$ then reads

$$\Gamma_{A\to V^0\tilde{P}^0} = \frac{k(m_A,m_V,m_{\tilde{P}})}{8\pi m_A^2}|-i\bar{\mathcal{M}}_{A\to V^0\tilde{P}^0}|^2. \tag{2.187}$$

A non-singlet axial-vector field will in general also posses charged decay channels. Therefore, in addition to the decay process considered in Eq. (2.187), we have to consider the contribution of

the charged modes from the process $A \to V^{\pm}\tilde{P}^{\mp}$ to the full decay width as well. To this end, we multiply the neutral-mode decay width of Eq. (2.187) with an isospin factor $I$, i.e., we set $\Gamma_{A\to V\tilde{P}} = \Gamma_{A\to V^0\tilde{P}^0} + \Gamma_{A\to V^{\pm}\tilde{P}^{\mp}} \equiv I\Gamma_{A\to V^0\tilde{P}^0}$, and obtain the following equation for the full decay width:

$$\Gamma_{A\to V\tilde{P}} = I\frac{k(m_A, m_V, m_{\tilde{P}})}{8\pi m_A^2}|-i\bar{\mathcal{M}}_{A\to V^0\tilde{P}^0}|^2. \tag{2.188}$$

The exact value of $I$ can be determined from isospin deliberations, or simply from the interaction Lagrangian of a given decay process (as we will see in later in this work).
Note that an off-shell vector state can also be considered within our formalism upon introducing the corresponding spectral function as in Eq. (2.175)

$$d_V(x_V) = N_V \frac{x_V^2\Gamma_V^{\text{exp}}}{(x_V^2 - m_V^2)^2 + \left(x_V\Gamma_V^{\text{exp}}\right)^2}\,\theta(m_A - m_V - m_{\tilde{P}}) \tag{2.189}$$

with $x_V$ and $\Gamma_V^{\text{exp}}$ denoting the off-shell mass and the tree-level width of the vector state $V$, respectively, and $N_V$ determined such that $\int_0^{\infty} \mathrm{d}x_V\, d_V(x_V) = 1$. This allows us to calculate the decay width for a sequential decay of the form $A \to V\tilde{P} \to \tilde{P}_1\tilde{P}_2\tilde{P}$, i.e., to consider an off-shell decay of the vector particle that possesses this assumed form: $V \to \tilde{P}_1\tilde{P}_2$. Then Eq. (2.188) is modified as

$$\Gamma_{A\to V\tilde{P}\to\tilde{P}_1\tilde{P}_2\tilde{P}} = \int\limits_{m_{\tilde{P}_1}+m_{\tilde{P}_2}}^{m_A-m_{\tilde{P}}} \mathrm{d}x_V\, I\frac{k(m_A, x_V, m_{\tilde{P}})}{8\pi m_A^2}\, d_V(x_V)|-i\bar{\mathcal{M}}_{A\to V^0\tilde{P}^0}|^2 \tag{2.190}$$

with $k(m_A, x_V, m_{\tilde{P}})$ from Eq. (5.30).
Note that Eqs. (2.188) and (2.190) will be very useful, e.g., in Sections 9.4.1, 9.4.4, 9.4.6 and 9.4.7.

### 2.6.3 Example: Decaying Axial-Vector State II

Let us now consider a slightly different example (that will nonetheless also prove to be useful in the subsequent chapters of this work): a generic decay of the form $A \to S\tilde{P}$ where $A$, $S$ and $\tilde{P}$ denote an axial-vector, a scalar and a pseudoscalar state, respectively, with the following interaction Lagrangian describing the decay of the neutral axial-vector component into neutral states:

$$\mathcal{L}_{AS\tilde{P}} \equiv A_{AS\tilde{P}}A^{\mu 0}S^0\partial_\mu\tilde{P}^0 + B_{AS\tilde{P}}A^{\mu 0}\tilde{P}^0\partial_\mu S^0. \tag{2.191}$$

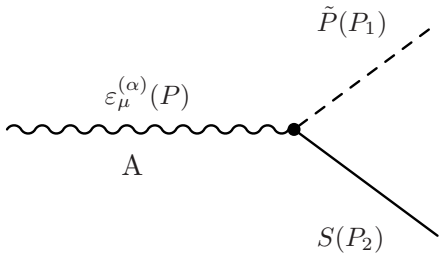


**Figure 2.4:** Decay process $A \to S\tilde{P}$.

As in the previous section, we denote the momenta of $A$, $\tilde{P}$ and $S$ as $P$, $P_1$ and $P_2$, respectively. Unlike the previous section, the decay process now involves only one vector state: $A$. Let us denote the corresponding polarisation vector as $\varepsilon_\mu^{(\alpha)}(P)$. Then, upon substitution $\partial^\mu \to iP_{1,2}^\mu$ for the decay products, we obtain the following Lorentz-invariant $AS\tilde{P}$ scattering amplitude $-i\mathcal{M}_{A\to S\tilde{P}}^{(\alpha)}$:

$$-i\mathcal{M}_{A\to S\tilde{P}}^{(\alpha)} = \varepsilon_\mu^{(\alpha)}(P) h_{AS\tilde{P}}^\mu = -\varepsilon_\mu^{(\alpha)}(P)\left(A_{AS\tilde{P}} P_1^\mu + B_{AS\tilde{P}} P_2^\mu\right) \tag{2.192}$$

with

$$h_{AS\tilde{P}}^\mu = -\left(A_{AS\tilde{P}} P_1^\mu + B_{AS\tilde{P}} P_2^\mu\right), \tag{2.193}$$

where $h_{AS\tilde{P}}^\mu$ denotes the $AS\tilde{P}$ vertex.

As in the previous section, calculation of the decay width will require us to calculate the square of the average decay amplitude. As apparent from Eq. (2.192), the scattering amplitude $-i\mathcal{M}_{A\to S\tilde{P}}^{(\alpha)}$ depends on the polarisation vector $\varepsilon_\mu^{(\alpha)}(P)$. Then the averaged squared amplitude $|-i\bar{\mathcal{M}}|^2$ is determined as follows:

$$\begin{aligned} -i\mathcal{M}_{A\to S\tilde{P}}^{(\alpha)} = \varepsilon_\mu^{(\alpha)}(P) h_{AS\tilde{P}}^\mu \Rightarrow \left|-i\bar{\mathcal{M}}_{A\to S\tilde{P}}\right|^2 &= \frac{1}{3}\sum_{\alpha=1}^{3}\left|-i\mathcal{M}_{A\to S\tilde{P}}^{(\alpha)}\right|^2 \\ &= \frac{1}{3}\sum_{\alpha,\beta=1}^{3} \varepsilon_\mu^{(\alpha)}(P) h_{AS\tilde{P}}^\mu \varepsilon_\nu^{(\alpha)}(P) h_{AS\tilde{P}}^{*\nu}. \end{aligned} \tag{2.194}$$

Let us denote the mass of the state $A$ as $m_A$. Then utilising Eq. (2.185) we obtain

$$|-i\bar{\mathcal{M}}_{A\to S\tilde{P}}|^2 = \frac{1}{3}\left(-g_{\mu\nu} + \frac{P_\mu P_\nu}{m_A^2}\right) h_{AS\tilde{P}}^\mu h_{AS\tilde{P}}^{*\nu} = \frac{1}{3}\left[-\left|h_{AS\tilde{P}}^\mu\right|^2 + \frac{\left|h_{AS\tilde{P}}^\mu P_\mu\right|^2}{m_A^2}\right]. \tag{2.195}$$

From Eq. (2.193) we obtain

$$\left|h_{AS\tilde{P}}^\mu\right|^2 = A_{AS\tilde{P}}^2 m_{\tilde{P}}^2 + B_{AS\tilde{P}}^2 m_S^2 + 2A_{AS\tilde{P}} B_{AS\tilde{P}} P_1 \cdot P_2, \tag{2.196}$$

where $m_{\tilde{P}}$ and $m_S$ denote the masses of $\tilde{P}$ and $S$, respectively. Our calculations are performed in the rest frame of the decaying particle, i.e., $P^\mu = (m_A, \mathbf{0})$. Consequently,

$$h_{AS\tilde{P}}^\mu P_\mu \equiv h_{AS\tilde{P}}^0 P_0 = h_{AS\tilde{P}}^0 m_A \overset{\text{Eq. (2.193)}}{=} -\left(A_{AS\tilde{P}} E_1 + B_{AS\tilde{P}} E_2\right) m_A \tag{2.197}$$

with $E_1 = \sqrt{k^2(m_A, m_S, m_{\tilde{P}}) + m_{\tilde{P}}^2}$, $E_2 = \sqrt{k^2(m_A, m_S, m_{\tilde{P}}) + m_S^2}$ and $k(m_A, m_S, m_{\tilde{P}})$ from Eq. (5.30). Inserting Eqs. (2.196) and (2.197) into Eq. (2.195) then yields

$$\begin{aligned} |-i\bar{\mathcal{M}}_{A\to S\tilde{P}}|^2 &= \frac{1}{3}\left[\left(A_{AS\tilde{P}} E_1 + B_{AS\tilde{P}} E_2\right)^2 - \left(A_{AS\tilde{P}}^2 m_{\tilde{P}}^2 + B_{AS\tilde{P}}^2 m_S^2 + 2A_{AS\tilde{P}} B_{AS\tilde{P}} P_1 \cdot P_2\right)\right] \\ &= \frac{1}{3}\left[\left(A_{AS\tilde{P}}^2 + B_{AS\tilde{P}}^2\right) k^2(m_A, m_S, m_{\tilde{P}}) + 2A_{AS\tilde{P}} B_{AS\tilde{P}}\left(E_1 E_2 - P_1 \cdot P_2\right)\right]. \end{aligned} \tag{2.198}$$

Given that $P_1^\mu = (E_1, \boldsymbol{k}(m_A, m_S, m_{\tilde{P}}))$ and $P_2^\mu = (E_2, -\boldsymbol{k}(m_A, m_S, m_{\tilde{P}}))$, we obtain $P_1 \cdot P_2 = E_1 E_2 + k^2(m_A, m_S, m_{\tilde{P}})$ or, from Eq. (2.198):

$$|-i\bar{\mathcal{M}}_{A\to S\tilde{P}}|^2 = \frac{1}{3}(A_{AS\tilde{P}} - B_{AS\tilde{P}})^2 k^2(m_A, m_S, m_{\tilde{P}}). \tag{2.199}$$

The formula for the decay width of the process $A \to S\tilde{P}$ may need to consider not only the decay $A^0 \to S^0\tilde{P}^0$ but also $A^0 \to S^\pm\tilde{P}^\mp$ (depending on isospin of the decay products); for this reason, we introduce an isospin factor $I$:

$$\Gamma_{A\to S\tilde{P}} = I\frac{k(m_A, m_S, m_{\tilde{P}})}{8\pi m_A^2}|-i\bar{\mathcal{M}}_{A\to S\tilde{P}}|^2 = I\frac{k^3(m_A, m_S, m_{\tilde{P}})}{24\pi m_A^2}(A_{AS\tilde{P}} - B_{AS\tilde{P}})^2. \tag{2.200}$$

### 2.6.4 Example: Decaying Scalar State

Let us consider the decay of a scalar state $S$ into two vector states $V$, i.e., $S \to V_1 V_2$. The interaction Lagrangian may be given in the following simple form:

$$\mathcal{L}_{SVV} \equiv A_{SVV} S V_{1\mu}^0 V_2^{\mu 0}. \tag{2.201}$$

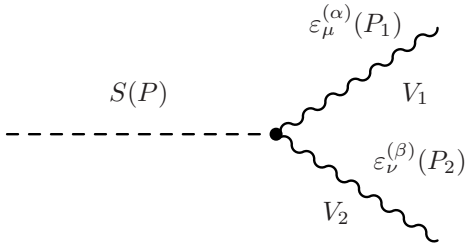


**Figure 2.5:** Decay process $S \to V_1 V_2$.

Our calculation of the decay width has to consider polarisations of the two vector states. We denote the momenta of $S$, $V_1$ and $V_2$ as $P$, $P_1$ and $P_2$, respectively, while the polarisation vectors are denoted as $\varepsilon_\mu^{(\alpha)}(P_1)$ and $\varepsilon_\nu^{(\beta)}(P_2)$. Then, upon substituting $\partial^\mu \to iP_{1,2}^\mu$ for the decay products, we obtain the following Lorentz-invariant $AS\tilde{P}$ scattering amplitude $-i\mathcal{M}_{A\to S\tilde{P}}^{(\alpha)}$:

$$-i\mathcal{M}_{S\to V_1V_2}^{(\alpha,\beta)} = \varepsilon_\mu^{(\alpha)}(P_1)\varepsilon_\nu^{(\beta)}(P_2)h_{SVV}^{\mu\nu} = i\varepsilon_\mu^{(\alpha)}(P_1)\varepsilon_\nu^{(\beta)}(P_2)A_{SVV}g^{\mu\nu} \tag{2.202}$$

with

$$h_{SVV}^{\mu\nu} = iA_{SVV}g^{\mu\nu}, \tag{2.203}$$

where $h_{SVV}^{\mu\nu}$ denotes the $SVV$ vertex.

The averaged squared amplitude $|-i\bar{\mathcal{M}}|^2$ is determined as follows:

$$-i\mathcal{M}^{(\alpha,\beta)}_{S\to V_1V_2} = \varepsilon^{(\alpha)}_\mu(P_1)\varepsilon^{(\beta)}_\nu(P_2)h^{\mu\nu}_{SVV} \Rightarrow \left|-i\bar{\mathcal{M}}_{S\to V_1V_2}\right|^2 = \frac{1}{3}\sum_{\alpha,\beta=1}^{3}\left|-i\mathcal{M}^{(\alpha,\beta)}_{S\to V_1V_2}\right|^2$$
$$= \frac{1}{3}\sum_{\alpha,\beta=1}^{3}\varepsilon^{(\alpha)}_\mu(P_1)\varepsilon^{(\beta)}_\nu(P_2)h^{\mu\nu}_{SVV}\varepsilon^{(\alpha)}_\kappa(P_1)\varepsilon^{(\beta)}_\lambda(P_2)h^{*\kappa\lambda}_{SVV}. \tag{2.204}$$

Equation (2.185) then yields the same expression as the one presented in Eq. (2.186):

$$|-i\bar{\mathcal{M}}_{S\to V_1V_2}|^2 = \frac{1}{3}\left[|h^{\mu\nu}_{SVV}|^2 - \frac{\left|h^{\mu\nu}_{SVV}P_{1\mu}\right|^2}{m^2_{V_1}} - \frac{\left|h^{\mu\nu}_{SVV}P_{2\nu}\right|^2}{m^2_{V_2}} + \frac{\left|h^{\mu\nu}_{SVV}P_{1\mu}P_{2\nu}\right|^2}{m^2_{V_1}m^2_{V_2}}\right]. \tag{2.205}$$

From Eq. (2.185) we obtain $h^{\mu\nu}_{SVV}P_{1\mu} = iA_{SVV}P_1^\nu$, $h^{\mu\nu}_{SVV}P_{2\nu} = iA_{SVV}P_2^\mu$ and $h^{\mu\nu}_{SVV}P_{1\mu}P_{2\nu} = iA_{SVV}P_1\cdot P_2$ and consequently

$$|-i\bar{\mathcal{M}}_{S\to V_1V_2}|^2 = \frac{1}{3}\left[4 - \frac{P_1^2}{m^2_{V_1}} - \frac{P_2^2}{m^2_{V_2}} + \frac{(P_1\cdot P_2)^2}{m^2_{V_1}m^2_{V_2}}\right]A^2_{SVV}. \tag{2.206}$$

For on-shell states, $P^2_{1,2} = m^2_{V_{1,2}}$ and Eq. (2.206) reduces to

$$|-i\bar{\mathcal{M}}_{S\to V_1V_2}|^2 = \frac{1}{3}\left[2 + \frac{(P_1\cdot P_2)^2}{m^2_{V_1}m^2_{V_2}}\right]A^2_{SVV} = \frac{1}{3}\left[2 + \frac{(m_S^2 - m^2_{V_1} - m^2_{V_2})^2}{4m^2_{V_1}m^2_{V_2}}\right]A^2_{SVV}. \tag{2.207}$$

The decay width is consequently

$$\Gamma_{S\to V_1V_2} = I\frac{k(m_S, m_{V_1}, m_{V_2})}{8\pi m_S^2}|-i\bar{\mathcal{M}}_{S\to V_1V_2}|^2 \tag{2.208}$$

with $k(m_S, m_{V_1}, m_{V_2})$ from Eq. (5.30); we have considered an isospin factor $I$ in case the vector particles are not isosinglets (then the contribution of the charged modes to the full decay width would also have to be considered).

Suppose now that the two vector states were unstable themselves and decayed into pseudoscalars: $V_1 \to \tilde{P}_1\tilde{P}_2$ and $V_2 \to \tilde{P}_3\tilde{P}_4$. Calculation of the decay width for the process $S \to V_1V_2 \to \tilde{P}_1\tilde{P}_2\tilde{P}_3\tilde{P}_4$ requires integration over the spectral functions of the two vector resonances, Eq. (2.189). The decay width then reads

$$\Gamma_{S\to V_1V_2\to\tilde{P}_1\tilde{P}_2\tilde{P}_3\tilde{P}_4} = \int\limits_{m_{\tilde{P}_1}+m_{\tilde{P}_2}}^{m_S} \mathrm{d}x_{V_1} \int\limits_{m_{\tilde{P}_3}+m_{\tilde{P}_4}}^{m_S-x_{V_1}} \mathrm{d}x_{V_2}\, I\frac{k(m_S, x_{V_1}, x_{V_2})}{8\pi m_S^2}\, d_V(x_{V_1})d_V(x_{V_2})|-i\bar{\mathcal{M}}_{S\to V_1V_2}|^2. \tag{2.209}$$

# 3. Review of Scalar Isosinglets

The scalar isosinglet mesons have been an extremely interesting topic of investigation from both theoretical and experimental standpoints for decades. Their features have often been ambiguous due to large background and various decay channels. This chapter is a brief review of the knowledge about scalar isosinglet mesons, what we think we know about them and how our understanding of these resonances has developed in experimental work over the last decades. It will contain a dedicated section regarding the putative new $f_0(1790)$ resonance which is of particular importance for this work because it is very close to, and may interfere with, the already established $f_0(1710)$ state – and the latter is of utmost importance for our calculations in the three-flavour version of our model.

## 3.1 The $f_0(600)$ Resonance

The $f_0(600)$ state (or $\sigma$; in older articles: $\epsilon$ or $\eta_{0+}$) has a long and troubled history. The existence of this state was suggested in linear sigma models approximately a decade before it was first discovered, see, e.g., Ref. [48]. The state was introduced theoretically as the putative chiral partner of the pion; however, it was shown to be highly non-trivial to ascertain experimentally.

The earliest versions of the linear sigma model incorporated only the sigma and the pion. The pion is a well-established $\bar{q}q$ state and consequently its chiral partner also had to be a quarkonium. The naive expectation was that the mass splitting between the pion and its chiral partner would not be large, or at least that the mass of the $\sigma$ state would be in the interval below 1 GeV, with a predominant decay into pions ($\sim 100\%$). For this reason, many experimental collaborations have looked closely into $\pi\pi$ scattering amplitudes up to 1 GeV (see below) in order to ascertain if an $I(J^{PC}) = 0(0^{++})$ signal could be found. Note, however, that the theoretical $\bar{q}q$ scalar state possesses the intrinsic angular momentum $L = 1$ as well as the relative spin of the quarks $S = 1$. For this reason one could also easily expect the state to be in the region above 1 GeV. This is contrary to the expectation of the first version of the $\sigma$ models. Additionally, four decades ago Gasiorowicz and Geffen suggested how to introduce vectors ($\rho$, $\omega$) and axial-vectors ($a_1$, $f_1$) into linear sigma models utilising the chiral symmetry [49]. (The latter article is also important because it suggested the existence of an axial-vector triplet, known nowadays as $a_1$, almost 10 years before the particle was first established reliably in the $\rho\pi$ final state produced in $K^-p$ reactions [50].) It was subsequently demonstrated that the inclusion of (axial-)vectors requires us to assign the scalar-isoscalar state present in the $\sigma$ models to a resonance above, rather than below, 1 GeV [51, 52, 53, 54, 55, 56, 57]. Experimental data available nowadays seem to strongly favour this assignment, particularly in view of the fact that the pure non-strange scalar state is expected to mix with a pure-strange and a glueball scalar state leading to experimental observation of three scalar states in the mutual vicinity: these could possibly be the established resonances $f_0(1370)$, $f_0(1500)$ and $f_0(1710)$ [10]. (See below for a review of these resonances.) This implies that scalar states below 1 GeV, including the $f_0(600)$ resonance, cannot be of $\bar{q}q$ structure. The mentioned theoretical ambiguity regarding the structure of this light scalar state is, however, not the only problem related to $f_0(600)$ – the data on this resonance suggest that its mass and width

are of comparable magnitude, rendering also the experimental search for this state rather difficult.

Before we proceed with a discussion of the experimental evidence for $f_0(600)$, let us summarise the reasons why the hadronic physics requires the existence of a light scalar meson:

- It is the putative chiral partner of the pion in the sigma models; the vacuum expectation value of the $\sigma$ state is used as means of modelling spontaneous chiral symmetry breaking [48]. Therefore, the existence of the $\sigma$ meson [expected to possess a mass $< 1$ GeV in the plain sigma models without (axial-)vectors] is a natural consequence of the existence of the pion and of the chiral symmetry (and the breaking of this symmetry).

- As already indicated, subsequent calculations suggested that the scalar $\bar{q}q$ state present in sigma models cannot correspond to a resonance below 1 GeV but rather to a state above 1 GeV. However, if we act on the assumption of the possible existence of tetraquark ($\bar{q}\bar{q}qq$) states [58], then the search for a light scalar state is nonetheless justified: it may possess a tetraquark structure.

- The Nambu–Jona-Lasinio model [28] requires the existence of a light scalar-isoscalar meson with mass $2m_q$ where $m_q$ denotes the constituent-quark mass; the vacuum expectation value of the scalar state is again utilised to model the spontaneous breaking of the chiral symmetry.

- Nucleon-nucleon scattering is expected to occur with exchange of a light scalar meson [59]; $f_0(980)$ cannot fulfill this role as it strongly couples to kaons although it was established as a resonance long before $f_0(600)$, see Sec. 3.2, and $f_0(1370)$ is too heavy to influence the nucleon scattering at low energies.

- It is required for a correct description of $\pi\pi$ scattering data, see below.

Experimental evidence for the existence of the $f_0(600)$ resonance stems from analyses of $\pi\pi$ scattering amplitudes. This is true historically as well as nowadays; however, given the notoriously large decay width of the state and the limited statistics of the first experiments, the first data on $\pi\pi$ scattering provided us only with hints rather than definitive proofs of the existence of this particle.
In 1973, $\pi\pi$ phase shifts were measured at CERN where pions were scattered off protons: a pion beam was targeted at a 50 cm long liquid-hydrogen target inducing the reaction $\pi^- p \to \pi^+\pi^- n$ at 17.2 GeV, with 300000 events reconstructed [60]. The results of Ref. [60] were later combined with results obtained from the same $\pi^- p$ reaction induced by targeting pions on butanol ($C_4H_9OH$) [61]. A broad enhancement in the $\pi\pi$ $S$-wave was observed but no definitive conclusions were possible. In 1976, the Particle Data Group (PDG) removed this state from their listing. The next decade saw $pp \to pp\pi^+\pi^-$ data suggesting a broad $S$-wave enhancement in the $\pi\pi$ scattering below 1 GeV [62] but still without definitive conclusions regarding the existence of $f_0(600)$. The resonance was reinstated by the PDG in 1996 after theoretical results amassed suggesting the existence of the state: the 1993 review of $\pi\pi$ and $KK$ scattering data in Ref. [63] found a pole with a mass of $(506\pm10)$ MeV and a width of $(494\pm5)$ MeV; a model of $\pi\pi \to \pi\pi$ and $\pi\pi \to KK$ scattering with crossing symmetry and unitarity found the data to require a light scalar meson [64] and a model-independent analysis of $\pi\pi$ scattering data below the $KK$ threshold in Ref. [65]

found a pole with a mass of $(553.3 \pm 0.5)$ MeV and a width of $(242.6 \pm 1.2)$ MeV (see also Ref. [66]).
Contrarily, high-statistics data from $\bar{p}p$ annihilation [67, 68] did not yield a clear $f_0(600)$ signal; additionally, there were no conclusive results from central $pp$ collisions either, although a broad enhancement below 1 GeV was observed [69].

However, subsequent experimental results did suggest the existence of a signal attributed to $f_0(600)$. The E791 Collaboration at Fermilab [70] used a sample of $2 \cdot 10^{10}$ events from the $\pi^-$-nucleon reaction at 500 GeV to produce charm ($D$) mesons; $1172 \pm 61$ events $D \to \pi^-\pi^+\pi^+$ were induced and strong evidence of a scalar resonance with a mass of $478^{+24}_{-23} \pm 17$ MeV and a decay width of $324^{+42}_{-40} \pm 21$ MeV was found in the $\pi\pi$ channel using a Dalitz plot. Similarly, the CLEO Collaboration [71] produced 780000 $DD$ pairs from reaction $e^+e^- \to \psi(3770) \to D^+D^-$; various analysis methods were used and a definitive contribution of $f_0(600)\pi^+$ in the decay channel $D \to \pi^-\pi^+\pi^+$ was observed (branching ratio $\sim 50\%$). Additionally, the BES II Collaboration produced 58 million $J/\psi$ events from electron-positron annihilation and various decay channels involving pions and kaons were analysed (see the following subsections). We note here that a broad $f_0(600)$ peak was observed in the decay channel $J/\psi \to \omega\pi^+\pi^-$ for which the pole mass was determined as $(541 \pm 39)$ MeV and the decay width as $(504 \pm 84)$ MeV [72]. Thus, the analyses found a very broad resonance with a mass of $\sim 500$ MeV and a comparable decay width.

On the other hand, the theoretical search for this state is confronted with various problems. As already mentioned, $f_0(600)$ is very broad. It is one of rare meson resonances where the decay width $\Gamma$ is virtually the same as the mass; this renders an extrapolation of the pole position from the $\pi\pi$ scattering data highly non-trivial as the pole is very distant from the real axis. The resonance may easily be distorted by background effects and by interference with other scalar isosinglets. For this reason, a parametrisation of $f_0(600)$ in terms of a Breit-Wigner distribution [see Eq. (2.175)] has to be performed with great care (if at all). Nonetheless, it is possible to determine the pole position of the resonance utilising Roy equations [73] with crossing symmetry, analyticity and unitarity. This allows one to demonstrate unambiguously that $f_0(600)$ is a genuine resonance – e.g., in the work of Leutwyler *et al.* [41], a resonance pole was found at $m_{f_0(600)} - i\Gamma_{f_0(600)}/2 = (441^{+16}_{-8} - i272^{+9}_{-12.5})$ MeV. Similarly, Peláez *et al.* [42] have found $m_{f_0(600)} - i\Gamma_{f_0(600)}/2 = (461^{+14.5}_{-15.5} - i255 \pm 16)$ MeV.
These results were obtained from analyses of $\pi\pi$ scattering data with the pions produced from kaon decays. Let us therefore briefly review kaon decays in the following. Kaons are produced by targeting protons onto a metal (such as beryllium). Two types of charged-kaon decays are relevant here – the exclusive decays into pions: $K^\pm \to \pi^\pm\pi^0\pi^0$ and $K^\pm \to \pi^\pm\pi^+\pi^-$ ($K_{3\pi}$ decays; branching ratio $\sim 10^{-2}$ [10]) and the semileptonic decays $K^+ \to \pi^+\pi^-e^+\nu$ (and hermitian conjugate for $K^-$). The latter ones are referred to as $K_{e4}$ decays; they belong to the so-called rare kaon decays because of the small branching ratio ($\sim 10^{-5}$ [10]). Note, however, that they also possess a much cleaner environment than $K_{3\pi}$ decays where pion rescattering may induce an increased error in the scattering amplitude. First measurements of the $K_{e4}$ decays were performed in 1977 [74] with a number of events several order of magnitudes smaller than the latest measurements performed at CERN by the NA48/2 Collaboration in 2003 and 2004 [43]. Note that the pion scattering data allow for determination of $\pi\pi$ scattering lengths, see Refs. [41, 42] and Sections 5.2.8 and 9.5 in this work. We will show in the mentioned sections that the pion scattering lengths

require the existence of a light scalar state [i.e., $f_0(600)$] as otherwise their proper description is not possible. However, the broader phenomenology will disfavour a $\bar{q}q$ structure of this resonance.

We note that the PDG lists $f_0(600)$ as having a mass of (400 – 1200) MeV and a width of (600 – 1000) MeV [10]. Let us also note that $\kappa$ [or $K_0^\star(800)$], the strange counterpart of $f_0(600)$, has similarly also been subject of a prolonged debate about its existence with some analyses finding a corresponding pole [75] while others do not [76]. The fact that $m_\kappa \simeq \Gamma_\kappa$ renders it extremely important not to fit the $\kappa$ meson with a Breit-Wigner distribution of a constant width; such fits can easily fail to detect this state. There is, however, a scalar kaon in the region above 1 GeV as well, the existence of which appears to be confirmed: this state, denoted as $K_0^\star(1430)$, is found in the $K\pi$ channel (see Ref. [10] and references therein).

### 3.2 The $f_0(980)$ Resonance

This resonance is close to the kaon-kaon threshold rendering an experimental analysis somewhat difficult, with different collaborations and reviews obtaining at times very different results. For the same reason, the structure of the resonance is not clear: it may be interpreted as a quarkonium [77, 78, 79], as a $\bar{q}^2q^2$ state [58, 80, 81, 82, 83, 84], as a $KK$ bound state [85, 86, 87, 88], as a glueball [89] or even as an $\eta\eta$ bound state [90]. One of the most suitable of ways to ascertain the $f_0(980)$ structure is utilising the decay $f_0(980) \to \gamma\gamma$. The PDG cite world-average value is $\Gamma_{f_0(980)\to\gamma\gamma} = 0.29^{+0.07}_{-0.06}$ keV. Various approaches have been utilised to calculate this decay width: a relativistic nonstrange-quark model obtained values between 1.3 keV and 1.8 keV [77]; assuming a $KK$ structure yielded values between 0.2 keV and 0.6 keV [85] and assuming a strange-quarkonium structure of the resonance resulted in values $\sim$ 0.3 keV [78]. Thus the only assignment that appears to be excluded is the one where the resonance is a non-strange quarkonium.
The work presented here contains only quarkonium states; the only possible interpretation of $f_0(980)$ within our model could be as a $\bar{q}q$ state. In the $U(3) \times U(3)$ version of our model, it is not possible to interpret $f_0(980)$ as a $\bar{q}q$ state within our Fit I, Chapter 9 (the decay width would be several times too large), and it is strongly disfavoured as a $\bar{q}q$ state within Fit II, Chapter 11 [see in particular the short note on $f_0(980)$ at the end of Sec. 11.1.2].

The earliest evidence for $f_0(980)$ came from Berkeley in 1972 [91]. (There were even earlier data from $\bar{p}p \to \pi^+\pi^-\omega$ at Saclay in 1969 where the analysis required an $S$-wave isoscalar structure at $\sim$ 940 MeV [92]; however, no kaon events were considered.) A pion beam of 7.1 GeV was targeted at protons (in a hydrogen bubble chamber) and reactions $\pi^+p \to \pi^+\pi^-\Delta^{++}$ (32100 events) and $\pi^+p \to K^+K^-\Delta^{++}$ (682 events) were observed. The $\pi\pi$ system was found to exhibit a rapid drop in the cross-section in the energy region between 950 MeV and 980 MeV (i.e., close to the $KK$ threshold: $2m_{K^\pm} = 987.4$ MeV [10]). This effect occurred due to strong coupling of the $\pi\pi$ and $KK$ channels upon opening of the kaon threshold. Subsequent partial-wave analysis of both the pion and kaon scattering data yielded a pole at $(997 \pm 6)$ MeV; the pole width was $(54 \pm 16)$ MeV. [Incidentally, the same analysis also found a pole at 660 MeV and the width of 640 MeV, corresponding to the nowadays $f_0(600)$ meson, but the pole was not stable in all parametrisations due to lack of data below 550 MeV.]
CERN-Munich data from 1973 confirmed a strong $S$-wave enhancement at approximately 1 GeV

from the one-pion-exchange (OPE) reaction $\pi^- p \to \pi^+\pi^- n$ at 17.2 GeV [93]. Subsequent data from $\pi^- p \to \pi^+\pi^- n$ and $K^+K^- n$ taken at Rutherford Laboratory in Chilton, England, also produced a sharp drop in the $\pi^+\pi^-$ spectrum close to the $KK$ threshold, assigning this signal to a $J^P = 0^+$ resonance with pole mass of $(987 \pm 7)$ MeV and pole width of $(48 \pm 14)$ MeV [94]. Further publications regarding $f_0(980)$ are listed in Ref. [95]; let us, however, discuss here studies of the resonance performed by several collaborations:

- *WA76 / WA102.* Data were gathered using the CERN Omega Spectrometer in reactions $pp \to p_f(\pi^+\pi^-)p_s$, $pp \to p_f(\pi^0\pi^0)p_s$, $pp \to p_f(K^+K^-)p_s$ and $pp \to p_f(\bar{K}^0_S K^0_S)p_s$ at 85 GeV and at 300 GeV and in reaction $\pi^+ p \to \pi^+_f \pi^+\pi^- p_s$ at 85 GeV (subscripts $f$ and $s$ denote the fastest and slowest particles in the laboratory frame, respectively). The $f_0(980)$ resonance was identified in both pion and kaon final states; the coupling of the resonance to kaons ($g_K$) was found to be dominant in comparison to the pion coupling ($g_\pi$): $g_K/g_\pi = 2.0 \pm 0.9$ [96]. A pole mass of $(1001 \pm 2)$ MeV and a pole width of $(72 \pm 8)$ were determined. Note, however, that care is needed when interpreting these results, as a relativistic form of the Breit-Wigner distribution was utilised to analyse data, with no dispersive corrections (that are important due to the effects of the $KK$-threshold opening). In 1999, data from a higher-resolution reaction $pp \to p_f(K^+K^-)p_s$ and $pp \to p_f(\bar{K}^0_S K^0_S)p_s$ at 450 GeV indicated a Breit-Wigner mass of $(985 \pm 10)$ MeV and a width of $(65 \pm 20)$ MeV, with interference effects of $f_0(1500)$ and $f_0(1710)$ included [97]. A similar analysis was performed for $pp \to p_f(\pi^+\pi^-)p_s$, also at 450 GeV [98] allowing for a combined analysis to be performed in both pion and kaon channels [99]. Both the T-matrix formalism [100] and the K-matrix formalism [101] were used. Results were obtained regarding four scalar resonances: $f_0(980)$, $f_0(1370)$, $f_0(1500)$ and $f_0(1710)$. For $f_0(980)$, the obtained mean values were $m_{f_0(980)} = (987 \pm 6 \pm 6)$ MeV and $\Gamma_{f_0(1500)} = (96 \pm 24 \pm 16)$ MeV. The $f_0(980)$ coupling to kaons was found to be approximately two times larger than the coupling to pions.

- *Crystal Barrel.* The $f_0(980)$ resonance appeared in high-statistics data produced by 16.8 million $\bar{p}p$ collisions at CERN-LEAR (Low Energy Antiproton Ring) and analysed in 1995. From these collisions, 712000 events for $\bar{p}p \to 3\pi^0$ were selected [102]. The $f_0(980)$ resonance was reconstructed with a K-matrix approach and the values $m_{f_0(980)} = (994 \pm 5)$ MeV and $\Gamma_{f_0(980)} = (26 \pm 10)$ MeV were obtained. Subsequently, data were taken from reactions $\bar{p}p \to \pi^0\pi^0\pi^0$ (712000 events), $\bar{p}p \to \pi^0\pi^0\eta$ (280000 events) and $\bar{p}p \to \pi^0\eta\eta$ (198000 events) [67]. Data analysis was not conclusive in that different Riemann sheets in the T-matrix formalism yielded somewhat different pole masses [(938 - 996) MeV] and widths [(70 - 112) MeV]; nonetheless the existence of a pole (i.e., of a resonance) was ascertained.

- *GAMS.* Data were taken from the OPE reaction $\pi^- p \to \pi^0\pi^0 n \to (4\gamma)n$ at GAMS-IHEP (GAMS: Russian abbreviation for Hodoscope Automatic Multiphoton Spectrometer). A pion beam at 38 GeV was utilised to induce the reaction. A drop in the $\pi\pi$ cross section just below 1 GeV was observed allowing for a resonance with a mass of $(997 \pm 5)$ MeV and a width of $(48 \pm 10)$ MeV to be reconstructed [103]. The same experiment was later repeated at the CERN-SPS accelerator using the electromagnetic hodoscope calorimeter GAMS-4000 but with a pion beam of 100 GeV [104]. The results were similar to those of Ref. [103] although an optimal fit was found for a Breit-Wigner mass of $(960 \pm 10)$ MeV, i.e., below

the $KK$ threshold. The Collaboration also used two additional production mechanisms. The first involved targeting antiprotons at 450 GeV onto liquid hydrogen and inducing the reaction $\bar{p}p \to p_f(\pi^0\pi^0)p_s \to p_f(4\gamma)p_s$ at CERN-SPS. A Breit-Wigner fit was optimised at a mass of $(955 \pm 10)$ MeV and a width of $(69 \pm 15)$ MeV in Ref. [69]. The second involved the same reaction, however with protons at 450 GeV: $pp \to p_f(\pi^0\pi^0)p_s \to p_f(4\gamma)p_s$ [105]. A fit to data yielded $m_{f_0(980)} = (989 \pm 15)$ MeV and $\Gamma_{f_0(980)} = (65 \pm 25)$ MeV. Note that already GAMS data from Ref. [103] suggested an interesting feature of the $\pi^0\pi^0$ invariant mass spectrum where $f_0(980)$ was reconstructed: there was a dip in the spectrum (for lower momentum transfer of $\pi^-$ to the two neutral pions) as well as a peak (if higher momentum transfer was considered). This unusual feature of $f_0(980)$ was analysed in Ref. [106] where the observed alteration in the spectrum was suggested to occur due to an $a_1$ exchange contribution in the $\pi^- p$ amplitude that rises with momentum transfer.

- *CMD-2.* Data regarding $f_0(980)$ obtained by this Collaboration were result of studies of $\varphi(1020)$ radiative decays. To this end, 20 million $\varphi$ events were produced in the annihilation reaction $e^+e^- \to \pi^+\pi^-\gamma$ and observed by the Cryogenic Magnetic Detector CMD-2 in Novosibirsk. The $\varphi(1020)$ resonance was reconstructed in the $\pi^+\pi^-\gamma$ final state; isolating photons with energy below $\sim$ 100 MeV and assuming that the pions in this final state dominantly coupled to $f_0(980)$ yielded $m_{f_0(980)} = 975$ MeV. However, the resonance width was not determined from the mentioned annihilation process but rather held at 40 MeV [107]. The same process was subsequently repeated [108] with $\pi^0\pi^0\gamma$ and $\eta\pi^0\gamma$ final states. The lack of bremsstrahlung for the neutral final-state modes allowed for a better reconstruction of $f_0(980)$ in the $\pi^0\pi^0$ channel. Again, a dominant coupling of pions to $f_0(980)$ was assumed once the photons of energy below $\sim$ 100 MeV were isolated. The ensuing results reflected those of Ref. [107] in mass; the width was determined to be $(56 \pm 20 \pm 10)$ MeV. These results are, however, obtained within certain models – as discussed in Ref. [108]. Note that the annihilation process $e^+e^- \to \pi\pi\gamma$ (at 1020 MeV) was also used by the KLOE Collaboration in the "Frascati $\varphi$ factory", with results very similar to those of CMD-2 but unfortunately with no determination of the $f_0(980)$ width (see Ref. [109] and references therein).

- *Belle.* The Belle Collaboration at KEK (High Energy Accelerator Research Organization, located in Tsukuba, Japan) have used the annihilation process $e^+e^- \to e^+e^-\pi^+\pi^-$ at 10.58 GeV aquiring high-statistics data, see Ref. [110]. The $f_0(980)$ resonance was reconstructed in the $\pi^+\pi^-$ final state with $m_{f_0(980)} = 985.6^{+1.2+1.1}_{-1.5-1.6}$ MeV and $\Gamma_{f_0(980)\to\pi\pi} = 34.2^{+13.9+8.8}_{-11.8-2.5}$ MeV. The stated result for the decay width suffers from large errors (particularly at the upper boundary) and the reason is the possible interference of $e^+e^- \to e^+e^-\pi^+\pi^-$ events with dilepton events $e^+e^- \to \mu^+\mu^-$ yielding an increased uncertainty in data evaluation. Subsequent analysis of the same reaction with $\pi^0\pi^0$ final states [111] yielded $m_{f_0(980)} = 982.2 \pm 1.0^{+8.1}_{-8.0}$ MeV and $\Gamma_{f_0(980)\to\pi\pi} = 66.9 \pm 2.2^{+17.6}_{-12.5}$ MeV. The latter is very different from the value of Ref. [110] because differential cross-sections (in $S$, $D$, $G$ waves) were fitted rather than the total one. However, no consideration was given to the kaon decays of $f_0(980)$. A Breit-Wigner analysis was used in both cases.

The PDG estimates $m_{f_0(980)} = (980 \pm 10)$ MeV and $\Gamma_{f_0(980)} = (40 - 100)$ MeV [10].

### 3.3 The $f_0(1370)$ Resonance

The $f_0(1370)$ resonance decays predominantly into pions and is therefore a possible candidate for a non-strange quarkonium state. We will discuss this possibility from the viewpoint of our model in Fit II, Chapter 11. It is an established experimental fact that $f_0(1370)$ is a broad resonance with $\Gamma_{f_0(1370)} \sim (200 - 500)$ MeV [10]. Although the stated value of the decay width is not comparable to the mass of the resonance, there large width nonetheless needs to be considered with care when features of the resonance are analysed. One of the reasons for the large width arises from the fact that $f_0(1370)$ is reconstructed in various decay channels (see below) that may have different thresholds. For this reason, in this section we will prefer an analysis combining different sets of data, in various channels and by various collaborations. The resonance is mostly observed in $\bar{p}p$ annihilations, $\pi^- p$ scattering and $J/\psi$ decays (see below).
There are several reviews offering combined analyses of $f_0(1370)$ features [40, 63, 101, 112, 113, 114, 115, 116, 117, 118, 119]. They are important for at least two reasons. Firstly, they clearly demonstrate that $f_0(600)$ and $f_0(1370)$ are distinct resonances [63, 112, 113, 115]. Secondly, a broad resonance with various decay channels – such as $f_0(1370)$ – is bound to experience interference among different decay channels due to threshold openings. These have to be considered within comprehensive reviews combining different sets of production data (as performed, for example, in references that have already been stated). In this section, we will in particular emphasise results from a comprehensive review of $f_0(1370)$ by D. Bugg published in 2007 [40]. Nonetheless, let us first briefly summarise experimental data where a signal for $f_0(1370)$ was seen.

- *CERN.* A bubble-chamber experiment involving $\bar{p}p \to \pi^+\pi^-\pi^+\pi^-\pi^0$ (antiprotons at 1.2 GeV targeted at hydrogen at rest) was analysed in 1969. A possible $\rho\rho$ enhancement was claimed at 1.4 GeV [120].

- *Argonne.* Data were taken from 400000 events observed at the Argonne National Laboratory in 1976 from the reaction $\pi^- p$ producing neutrons and neutral pseudoscalar kaons [121]. Pions were scattered off a 7.5 cm-long liquid-hydrogen target, with ensuing photons (originating from the kaon decays) detected from scintillation counters in a hodoscope. An enhancement with $\Gamma \sim 80$ MeV was observed at approximately 1.25 GeV but with $I = 1$ . Subsequent data from higher statistics (110000 events in $\pi^- p \to nK^-K^+$ and 50000 events in $\pi^+ n \to pK^-K^+$) confirmed the enhancement, but found it to be rather broad ($\Gamma \sim 150$ MeV, at $\sim 1.3$ GeV) and with $I = 0$ [122]; see also Ref. [123].

- *BNL.* Data from 15000 events on $\pi^- p \to \bar{K}^0_S K^0_S n$ taken at Brookhaven National Laboratory suggested a resonance with a mass of $\sim 1463$ MeV and a width of $\Gamma \sim 118$ MeV (but with large errors for the width) [124].

- *Crystal Barrel.* The earliest evidence for $f_0(1370)$ by the Crystal Barrel Collaboration was published in 1992 from $\eta\eta$ final states [125]. Data were obtained from the reaction $\bar{p}p \to \eta\eta\pi^0 \to 6\gamma$, where the antiprotons were stopped by a liquid-hydrogen target at the centre of the Crystal Barrel detector. In this way, $\bar{p}p$ annihilation states were limited to $S$ and $P$ waves allowing for a better reconstruction of putative scalar resonances. The Crystal Barrel itself was in essence comprised of a magnetic detector with a CsI calorimeter used to detect photons. An optimised fit suggested the existence of a scalar resonance with a mass

of 1430 MeV and a decay width of 250 MeV. The same Collaboration also analysed data from $\bar{p}p \to \pi^+\pi^- 3\pi^0 \to \rho^+\rho^-\pi^0$ (antiprotons at 200 MeV stopped in a 4 cm long liquid-hydrogen target at the centre of the detector); a strong signal with a mass of $(1374 \pm 38)$ MeV and a width of $(375 \pm 61)$ MeV was reconstructed in both $\rho^+\rho^-$ and $\sigma\sigma$ channels [126]. Subsequent analysis of data from $\bar{p}p \to 3\pi^0$ and $\bar{p}p \to \eta\eta\pi^0$ found both $f_0(1370)$ and $f_0(1500)$ [114, 127, 128]. High-statistics data from reactions $\bar{p}p \to 3\pi^0$ (712000 events), $\bar{p}p \to \eta\eta\pi^0$ (280000 events) and $\bar{p}p \to \eta\pi^0\pi^0$ (198000 events) were analysed in Refs. [67, 129]. They yielded not only evidence for $f_0(1370)$ and $f_0(1500)$ but also for the non-strange isotriplet member of the scalar nonet above 1 GeV, the $a_0(1450)$ resonance, found in the $\eta\pi^0\pi^0$ final state [130]. Finally, a simultaneous fit [116] of the Crystal Barrel $\bar{p}p$ data with CERN-Munich data regarding $\pi^- p \to \pi^-\pi^+ n$ [93] with BNL analyses from Refs. [124, 131] and Argonne results from Refs. [123, 132] determined that $\pi\pi$ scattering data above 1 GeV require the presence of $f_0(1370)$.

- *Rome-Syracuse.* A review of earlier data in Ref. [133] suggested a resonance with a mass of $(1386 \pm 10 \pm 28)$ MeV and a width of $(310 \pm 17 \pm 47)$ MeV.

- *OBELIX.* The Collaboration utilised reactions induced by antineutrons; they were produced by the charge-exchange reaction $\bar{p}p \to \bar{n}n$ in a 15 cm long liquid-hydrogen target inside the OBELIX spectrometer at CERN-LEAR [134]. The ensuing beam produced reactions $\bar{n}p \to \pi^+\pi^-\pi^+$ and $\bar{n}p \to \pi^+\pi^-\pi^+\pi^-\pi^+$. A scalar state with a mass of $(1345 \pm 12)$ MeV and width of $(398 \pm 26)$ MeV was reconstructed.

- *Belle.* Recently, the Belle Collaboration have claimed observation of a signal consistent with $f_0(1370)$ from $B$ meson decays produced in $e^+e^-$ collisions: $e^+e^- \to \Upsilon \to \bar{B}_S^0 B_S^0$, $\bar{B}_S^0 B_S^*$ and $\bar{B}_S^* B_S^*$ (with $B_S^* \to \gamma B_S^0$) and $B_S^0 \to J/\psi f_0(1370) \to J/\psi\pi^+\pi^-$. The signal was observed at $1405 \pm 15^{+1}_{-7}$ MeV; the width was $54 \pm 33^{+14}_{-3}$ MeV [135]. However, no interference with the nearby scalar states was considered due to low statistics, although the observation of a signal for $f_0(980)$ was also claimed.

However, there are also claims disputing the existence of $f_0(1370)$. It has been claimed that $f_0(1370)$ could be merely a broad background in the energy region up to 1.5 GeV interfering with $f_0(1500)$ and producing a peak at 1370 MeV [136]. Additionally, $f_0(1370)$ was not unambiguously identified in the CERN-Munich data of Ref. [93] and might even, with $f_0(600)$, represent a single state - the scalar glueball [137]; see also Ref. [138].
This work will not follow the assertions of the stated references for several reasons:

- It is highly unlikely that $f_0(600)$ and $f_0(1370)$ merely represent two manifestations of a single state; features of $f_0(600)$ have been discussed in Sec. 3.1 where we have noted that $\pi\pi$ scattering data unambiguously require a light scalar state corresponding to a pole in the $\pi\pi$ scattering amplitude. For this reason alone, $f_0(600)$ is a state distinct from other resonances, including $f_0(1370)$. [We have already noted at the beginning of this section that Refs. [63, 112, 113, 115] also demonstrate that $f_0(600)$ and $f_0(1370)$ are distinct. The same is shown as well in Ref. [40] in a simultaneous fit of Crystal Barrel data on $\bar{p}p$ and BES II data from $J/\psi$ decays, see below.]

- The mentioned CERN-Munich data have to be refitted simultaneously with data that have higher statistics if one would like to make a more elaborate statement regarding scalar

resonances. This has actually been performed in Ref. [138] where, for example, Argonne data on $KK$ scattering from Ref. [123] (discussed above) were considered. The Argonne data possess the largest statistics to date for the $KK$ channel ($\sim 10^5$ events), as noted in Ref. [138]; however, there are even larger statistics in the $\pi\pi$ channel obtained by Crystal Barrel from $\bar{p}p$ reactions ($\sim 7 \cdot 10^5$ events in $\pi^0\pi^0$; $\sim 3 \cdot 10^5$ events in $\eta\eta$) [67, 129]. Reference [138] does not consider the Crystal Barrel data, although they appear to be the most definitive ones regarding $f_0(1370)$. For this reason, the ensuing conclusion disputing the existence of $f_0(1370)$ is rather doubtful. The mentioned data from CERN-Munich and Argonne (and also from BNL [124, 131]) were considered in Ref. [116]. As discussed above, the combined fit required the presence of $f_0(1370)$ with a mass of $(1300 \pm 15)$ MeV and a full width of $(230 \pm 15)$ MeV.

- The issue whether $f_0(1370)$ is actually merely a broad background in the energy region above 1 GeV was discussed in some detail in Ref. [40] where it was found to be a genuine resonance. The stated publication contains various interesting statements regarding $f_0(1370)$ and, as a final part of this section, we will discuss the most important ones.

Five sets of data have been simultaneously fitted in Ref. [40]: Crystal Barrel data on $\bar{p}p \to 3\pi^0$ at rest in liquid [129] and gaseous hydrogen [101]; Crystal Barrel data on $\bar{p}p \to \eta\eta\pi^0$ at rest in liquid [125, 127, 139] and gaseous hydrogen [101] and also BES II data on $J/\psi \to \varphi\pi^+\pi^-$ [140]. The last set of data actually contains a peak at 1.35 GeV, contributed to interference of $f_0(1370)$, $f_0(1500)$ and $f_2(1270)$; the corresponding data can be refitted with and without $f_0(1370)$. The main conclusions from the combined fit are:

- Crystal Barrel data on $\bar{p}p \to 3\pi^0$ require $f_0(1370)$ as a $32\sigma$ signal in liquid-hydrogen $\bar{p}p$ reactions ($\sigma$: standard deviation) and as a $33\sigma$ signal in gaseous-hydrogen $\bar{p}p$ reactions.

- Crystal Barrel data on $\bar{p}p \to \eta\eta\pi^0$ require $f_0(1370)$ as a $17\sigma$ signal in liquid-hydrogen $\bar{p}p$ reactions and as an $8\sigma$ signal in gaseous-hydrogen $\bar{p}p$ reactions.

- BES II data on $J/\psi \to \varphi\pi^+\pi^-$ require $f_0(1370)$ as an $8\sigma$ signal.

- It is not possible to simulate $f_0(1370)$ as a high-tail representation of $f_0(600)$ neither in the $\pi\pi$ nor in the $\eta\eta$ channels, as the ensuing $\chi^2$ fit is noticeably worse than in the case where $f_0(1370)$ is included as a separate resonance.

- If one fits the $S$-wave $\pi\pi$ scattering amplitude between 1.1 GeV and 1.46 GeV [putative mass range of $f_0(1370)$] without assuming a Breit-Wigner form (i.e., freely in bins of $\pi\pi$ invariant mass), then a resonance form of the fitted amplitude is still obtained. The resonance is labelled as $f_0(1370)$.

- CERN-Munich data [93] can be fitted slightly better with $f_0(1370)$ than without this state but are not definitive in this regard.

- Due to lack of experimental data on $\pi\pi \to 4\pi$, it is only possible to constrain $\Gamma_{f_0(1370)\to\pi\pi}/\Gamma_{f_0(1370)\to 4\pi}$ rather than the two decay widths by themselves ($\Gamma$ refers to the Breit-Wigner width). The $2\pi$ line-shape of $f_0(1370)$ can then be fitted with a range of values for both $\Gamma_{f_0(1370)\to\pi\pi}$ and $\Gamma_{f_0(1370)\to 4\pi}$. The Breit-Wigner width in the $2\pi$ channel optimises the fit

at $\Gamma_{f_0(1370)\to\pi\pi} = 325$ MeV and implies $\Gamma_{f_0(1370)\to 4\pi} = (54 \pm 2 \pm 5)$ MeV with $m_{f_0(1370)} = (1309 \pm 1 \pm 15)$ MeV. Note, however, that the values of the $2\pi$ and $4\pi$ decay widths are strongly dependent on the value of $m_{f_0(1370)}$ at which they are determined. The reason is that the $4\pi$ phase space increases rapidly above approximately 1.35 GeV (see the next point).

- The quantitative features (mass/width) of $f_0(1370)$ are strongly dependent on the energy range considered. Up to approximately 1.35 GeV, the $2\pi$ decay channel of $f_0(1370)$ is dominant; thereafter, a rapid rise in the $4\pi$ phase space and cross-section occurs and thus the $4\pi$ decay channel becomes dominant and the $2\pi$ contribution decreases rapidly. For this reason, a proper dispersive analysis of $\pi\pi$ scattering in the energy region relevant for $f_0(1370)$ has to consider contributions from both $2\pi$ and $4\pi$ channels but also the $s$-dependence of these channels ($s$: pion invariant mass). This in turn implies that $f_0(1370)$ has *two pion peaks*. The peak in the $2\pi$ channel is at 1282 MeV and possesses a full width at half maximum (FWHM) of 207 MeV. The resonance mass at the centre of the FWHM interval is 1269 MeV. (It does not coincide with the peak mass because the line shape is not symmetric due to the opening of the $4\pi$ phase space.) The $4\pi$ peak is shifted by approximately 50 MeV: the peak is at 1331 MeV and possesses a FWHM of 273 MeV (these results are in reasonable agreement with $4\pi$ analyses of Refs. [126, 133, 134]). The resonance mass at the centre of the FWHM interval is 1377 MeV – it is thus shifted by more than 100 MeV in comparison with the $2\pi$ channel. We emphasise therefore that care is needed when one quotes a value of a $f_0(1370)$ decay width: the mass of the resonance always has to be specified as well.
  Despite exhibiting the mentioned two peaks, $f_0(1370)$ is still a single resonance for at least two reasons:

  - A combined analysis of both $2\pi$ and $4\pi$ channels yields only one pole. Depending on the sheet considered, the pole position varies between 1292 MeV and 1309 MeV (close to the $2\pi$ peak because the $s$-dependence in the $2\pi$ channel is smaller than in the $4\pi$ channel). The pole width is at average $\sim 181$ MeV.
  - Additionally, finding two distinct but near scalar resonances [$\sim$ (50 - 100) MeV mass difference], one in the $2\pi$ channel and one in the $4\pi$ channel, would appear to violate the well-known level repulsion of states with the same quantum numbers. Indeed such proximate resonances with the same quantum numbers are only expected if they possess orthogonal wave functions. This can obviously not be the case if two hypothetical states were both reconstructed from pions. Conversely, an example where this may occur is given by the pair of resonances $f_0(1710)$ – reconstructed predominantly in kaon final states – and $f_0(1790)$, reconstructed predominantly in pion final states (see Sections 3.5 and 3.6). There is another similar example: the $f_2(1565)$ resonance. It possesses a small-intensity peak in the $\pi\pi$ channel at 1565 MeV and a larger-intensity peak in the $\omega\omega$ channel at 1660 MeV; however, a dispersive analysis similar to that performed in Ref. [40] still yields a single pole at 1598 MeV [141].

The PDG nonetheless accumulate all available data on $f_0(1370)$ estimating $m_{f_0(1370)} = (1200$ - $1500)$ MeV and $\Gamma_{f_0(1370)} = (200$ - $500)$ MeV [10].

### 3.4 The $f_0(1500)$ Resonance

The discovery of the $f_0(1500)$ resonance originated in search for the scalar glueball state. This resonance is found mostly in pion final states from nucleon-nucleon (or antinucleon-nucleon) and pion-nucleon scattering processes. If such processes produce four pions, then $f_0(1500)$ is reconstructed from $\rho\rho$ final states in the $2(\pi^+\pi^-)$ channel and from $\sigma\sigma$ final states in the $2(\pi^+\pi^-)$ or $2(\pi^0\pi^0)$ channels. The resonance is therefore at least partly reconstructed in channels containing a double Pomeron exchange rendering the state a glueball candidate [142]. Our results from the $U(2) \times U(2)$ version of the model will confirm this assertion, see Chapter 12.

The $f_0(1500)$ resonance was first observed by the Columbia-Syracuse Collaboration in 1982 [143]. A 76-cm bubble chamber at BNL-Columbia containing deuterium at rest was exposed to antiprotons of various energies yielding the reactions $\bar{p} + p \to \pi^0 f_0(1500) \to 3\pi^0$ and $\bar{p} + n \to \pi^- f_0(1500) \to \pi^-\pi^+\pi^-$. The mass of the resonance was $(1525 \pm 5)$ MeV; the decay width was $(101 \pm 13)$ MeV. The new scalar, found in the pion channel, was determined to be virtually degenerate in mass with the already-known tensor state $f_2^{'}(1525)$, produced predominantly in the kaon channels in the same annihilation process. The state was swiftly confirmed by the GAMS data (obtained from $\pi^- p$ and $\pi^- n$ annihilation at IHEP) in the subsequent few years [144, 145], with mass values typically $(50-100)$ MeV larger than the value reported by Columbia-Syracuse. Note that the GAMS Collaboration typically utilised Breit-Wigner fits, known to shift in different sets of data due to interference of $f_0(1500)$ with the nearby states $f_0(1370)$ and $f_0(1710)$. (The same is true for data from $\pi^-\text{Be} \to \eta\eta'\pi^-\text{Be}$ [146] and $\pi^-\text{Be} \to \eta\eta\pi^-\text{Be}$ [147] from the Vertex Spectrometer VES, also at IHEP.) Later GAMS publications considered interference effects with $f_0(1370)$ [104, 105] and $f_0(1710)$ [148]. In Ref. [105], GAMS data from the reaction $pp \to p_f(\pi^0\pi^0)p_s \to p_f(4\gamma)p_s$ were utilised. The photons were detected by the Hodoscope Automatic Multiphoton Spectrometer (the Russian abbreviation for which is, as already indicated, GAMS), momenta of $p_f$ were measured by a magnetic spectrometer with gas chambers while momenta of $p_s$ were measured by a recoil proton detector.

- *WA76, WA91 and WA102.* A range of data regarding $f_0(1500)$ were presented by the WA76, WA91 and WA102 Collaborations using the CERN Omega Spectrometer. In 1989, data from the reaction $pp \to p_f(\pi^+\pi^-\pi^+\pi^-)p_s$ at 300 GeV were analysed confirming a scalar state with a mass of (1449±4) MeV and a width of (78±18) MeV from a Breit-Wigner fit [149]. The same reaction and the same analysis method were used in the subsequent years [150]. A five-time increase in statistics allowed for a range of resonances between 1.2 GeV and 2.0 GeV to be observed by the WA102 Collaboration. This included a $J^{PC} = 0^{++}$ peak at 1.45 GeV, found to be a superposition of two scalar resonances, $f_0(1370)$ and $f_0(1500)$ [151]. Subsequently, data from reactions $pp \to p_f(K^+K^-)p_s$ and $pp \to p_f(\bar{K}^0_S K^0_S)p_s$ [97] and $pp \to p_f(\pi^+\pi^-)p_s$ [98] allowed for a combined analysis to be performed in both pion and kaon channels [99]. Both the T-matrix formalism and the K-matrix formalism were used to obtain results regarding four scalar resonances: $f_0(980)$, $f_0(1370)$, $f_0(1500)$ and $f_0(1710)$. For $f_0(1500)$, the mean obtained values were $m_{f_0(1500)} = (1502 \pm 12 \pm 10)$ MeV and $\Gamma_{f_0(1500)} = (98 \pm 18 \pm 16)$ MeV. The best WA102 data stem from an analysis of $pp \to p_f(\pi^0\pi^0\pi^0\pi^0)p_s$, $pp \to p_f(\pi^0\pi^0\pi^+\pi^-)p_s$ and $pp \to p_f(\pi^+\pi^-\pi^+\pi^-)p_s$ (at 450 GeV) because they allowed for a study of both $\sigma\sigma$ and $\rho\rho$ contributions to scalars above 1 GeV. Both decay channels were observed for $f_0(1500)$ with $m_{f_0(1500)} = (1511 \pm 9)$ MeV and

$\Gamma_{f_0(1500)} = (102 \pm 18)$ MeV [152]. Additionally, data from $pp \to p_f(\eta\eta)p_s$ production (identified via $\eta \to \gamma\gamma$ and $\eta \to \pi^+\pi^-\pi^0$) also allowed for $f_0(1500)$ to be reconstructed [153], with a pole position virtually the same as in Ref. [152].

- *Crystal Barrel.* The earliest evidence for $f_0(1500)$ by the Crystal Barrel Collaboration at CERN-LEAR was published in 1992 from $\eta\eta$ final states [125]. Data were obtained from the reaction $\bar{p}p \to \eta\eta\pi^0 \to 6\gamma$ involving antiprotons stopped in liquid hydrogen. Data analysis in Ref. [125] suggested $m_{f_0(1500)} = (1560 \pm 25)$ MeV and $\Gamma_{f_0(1500)} = (245 \pm 50)$ MeV from a Breit-Wigner fit but no interference with the nearby scalar states was considered. Further analyses of $\bar{p}p \to \pi^0\pi^0\pi^0$ and $\bar{p}p \to \eta\eta\pi^0$ [127] as well as $\bar{p}p \to \eta\eta'\pi^0$ [154] confirmed the state [with the latter reaction having a small branching ratio to $f_0(1500)$ due to the phase-space suppression]. Data with highest statistics were analysed in 1995; they included 16.8 million $\bar{p}p$ collisions. From these collisions, 712000 events for $\bar{p}p \to 3\pi^0$ were selected, see Ref. [102]. The $f_0(1500)$ resonance was reconstructed with $m_{f_0(1500)} = (1500 \pm 15)$ MeV and $\Gamma_{f_0(1500)} = (120 \pm 25)$ MeV. Additionally, 198000 events for $\bar{p}p \to \eta\eta\pi^0$ were selected yielding $m_{f_0(1500)} = (1505 \pm 15)$ MeV and $\Gamma_{f_0(1500)} = (120 \pm 30)$ MeV [139]. The Collaboration also utilised the $\bar{p}p$ annihilation to study $4\pi^0$ decay channel of $f_0(1500)$ via $\bar{p}p \to 5\pi^0$ in 1996 [68]. This channel is nowadays known to represent approximately 50% of the $f_0(1500)$ decays [10]. In Ref. [68], an enhancement in the $4\pi$ scalar channel was observed at 1505 MeV; the width was 169 MeV. In subsequent work, an additional production channel was used by the Collaboration: $\bar{p}d \to \pi^- 4\pi^0 p$; in this way, data evaluation was simplified as only one combination of four pions had to be considered (unlike in $\bar{p}p \to 5\pi^0$ where four-pion states could be reconstructed in five different ways from the five pions) [155]. Results were nonetheless consistent with Ref. [68]. Note that the Collaboration has also observed subdominant $f_0(1500)$ decays into kaons from $\bar{p}p \to K_L^0 K_L^0 \pi^0$ [156] and $\bar{p}p \to K^+K^-\pi^0$ [157], suggesting a small contribution of $\bar{s}s$ to $f_0(1500)$.

- *OBELIX.* Data taken from the reaction $\bar{p}p \to \pi^+\pi^-\pi^0$ at CERN-LEAR were analysed in 1997 [158]. Three scalar poles were found in a K-matrix formalism: $f_0(980)$, $f_0(1370)$ and $f_0(1500)$, with $m_{f_0(1500)} = (1449 \pm 20)$ MeV and $\Gamma_{f_0(1500)} = (114 \pm 30)$ MeV. It was necessary to include $f_0(1500)$ in particular into the fit as the $\chi$/d.o.f. increased from 1.53 to 1.71 if $f_0(1500)$ was omitted. The existence of the resonance was subsequently confirmed by data from $\bar{n}p \to \pi^+\pi^+\pi^-$ [159].

The PDG cites a world-average mass $m_{f_0(1500)} = (1505 \pm 6)$ MeV and decay width $\Gamma_{f_0(1710)} = (109 \pm 7)$ MeV [10].

### 3.5 The $f_0(1710)$ Resonance

The $f_0(1710)$ resonance is of importance for this work because it decays predominantly into kaons (see below); thus experimental data suggest that it may be a $\bar{s}s$ state. This is confirmed by our findings in Fit II, Sec. 11. Other approaches suggest that $f_0(1710)$ may possess a large glueball component [160]; however, this may be in doubt due to the latest ZEUS results that do not exclude coupling of $f_0(1710)$ to photons (see below as well). Experimentally, $f_0(1710)$ is reconstructed in $\pi^- p$ and $e^- p$ scatterings and $J/\psi$ decays.

The earliest evidence for the $f_0(1710)$ resonance was obtained from the decay $J/\psi \to \gamma\eta\eta$ at the SLAC Crystal Ball detector from $e^+e^-$ annihilation and published in 1982 [161]. A resonance with a mass of $(1640 \pm 50)$ MeV and a decay width of $220^{+100}_{-70}$ MeV was found. The resonance was determined to have positive charge-conjugation quantum number ($C = +1$) because it was produced in a radiative $J/\psi$ decay. Given that it was reconstructed from two pseudoscalar final states, it could only have even spin and parity (i.e., $J^P = 0^+$, $2^+$,...) and the initial data analysis in Ref. [161] preferred $J = 2$ rather than $J = 0$ [but the nearby spin-two state $f_2'(1525)$ was omitted from the analysis].
Confirmation of the new resonance was published several months later by the Brookhaven National Laboratory from data on $\pi^- p \to \bar{K}^0_S K^0_S n$ [162]. Discovery of a resonance with mass of $(1730 \pm 10 \pm 20)$ MeV was claimed; the value of the decay width was later determined as $200^{+156}_{-9}$ MeV [124]. An isoscalar resonance of similar mass [$(1650 \pm 50)$ MeV] and decay width [$(200 \pm 100)$ MeV] was found by the MARK II Collaboration at SLAC in 1982 from $J/\psi \to \gamma\rho^0\rho^0$ [163]. Afterwards, $J/\psi$ decays into etas were used by the Crystal Ball Collaboration at SLAC to reconstruct the resonance, see Ref. [164], confirmed soon thereafter by Ref. [165] (but with no $J^P$ determination).
First DM2 data about this state were published in 1987 [166] citing a resonance at approximately 1.7 GeV (width: approximately 140 MeV). Further analysis yielded a mass $(1707 \pm 10)$ MeV and a width $(166.4 \pm 33.2)$ MeV in 1988 [167]. The two sets of data were obtained from $J/\psi$ radiative decays into pions and kaons, respectively. However, no $J^P$ determination was possible due to a low signal-to-background ratio. The same issue prevented a determination of $J^P$ in a further set of data ($J/\psi \to \varphi\pi^+\pi^-$, $\varphi K^+K^-$, $\varphi\bar{K}^0_S K^0_S$, $\omega K^+K^-$, $\omega\bar{K}^0_S K^0_S$, $\varphi\bar{K}K^\star$ and $\varphi\bar{p}p$; only decays into kaons were relevant) [168].
There were several publications claiming this resonance to possess $J = 2$ rather than $J = 0$ (see Ref. [169, 170] in addition to Ref. [161]). However, more recent data suggest that the resonance is spin-zero:

- *GAMS.* Experiments regarding $\eta\eta$ final states, performed at the GAMS-IHEP proton synchrotron from $\pi^- p \to \eta\eta n \to (4\gamma)n$ reactions, suggested a mass of $(1755 \pm 8)$ MeV and a width $< 50$ MeV in 1986 [171]. In 1992, an improved version of the same experiment, considering also reactions $\pi^- p \to \eta\eta n^* \to (4\gamma)n\pi^0$ and $\pi^- p \to \eta\eta n^* \to (4\gamma)n\pi^0\pi^0$ (where $n^*$ denotes an excited neutron), allowed for analysis of new data combined with the old 1986 data. The Collaboration obtained a mass of $(1744 \pm 15)$ MeV and a width $< 80$ MeV at 90% CL [172]. The resonance was found to possess $J = 0$ already in 1986; the 1992 data suggested that it does not decay into $\eta\eta'$ or $\pi^0\pi^0$. A Breit-Wigner fit of GAMS data yielded mass of $(1670 \pm 20)$ MeV and width $(260 \pm 50)$ MeV in 2005 [148].

- *MARK-III.* In 1986 and 1992 the MARK-III Collaboration at SLAC [173] published results regarding pion production from decays $e^+e^- \to J/\psi \to \gamma\pi^+\pi^-\pi^+\pi^-$ and $e^+e^- \to J/\psi \to \gamma\pi^+\pi^0\pi^-\pi^0$ claiming the discovery of two pseudoscalar $\rho\rho$ states at 1.55 and 1.8 GeV. Similar results were published in 1989 by the DM2 Collaboration at DCI-Orsay [174] where the discovery of three $\eta$-like states in the region between 1.4 GeV and 2.2 GeV was claimed (see also results by the E760 Collaboration at Fermilab published in 1993 [175]). The MARK-III and DM2 Collaborations made use only of $^3S_1$ $\pi\pi$ final states ($\rho$). A re-analysis of MARK-III data was performed in 1995 by the Crystal Barrel Collaboration [176]; here, scalar $^3P_0$ $\pi\pi$ final states ($\sigma$) were considered in addition to the vector $^3S_1$ states. A

different picture emerged: no pseudoscalar peak was found (there was a $0^-$ signal over the entire energy range between 1.6 GeV and 2.4 GeV but no clear resonance); inclusion of the $\sigma$-like $\pi\pi$ final states yielded a new scalar resonance, denoted as $f_0(1750)$ with $m_{f_0(1750)} = (1750 \pm 15)$ MeV and $\Gamma_{f_0(1750)} = (160 \pm 40)$ MeV. The resonance was found to decay predominantly into $\sigma$ mesons; decay into $\rho$ states was found to be approximately 4.5 times less probable. The mass of this resonance is close to the PDG-preferred value $m_{f_0(1710)} = (1720 \pm 6)$ MeV but nonetheless appears to be too large when compared to the value of $m_{f_0(1710)}$ accepted nowadays. Thus the mentioned MARK-III result may be viewed as evidence that there exists a scalar resonance between 1.7 GeV and 1.8 GeV; however, it may also be viewed as superposition of two distinct states: $f_0(1710)$ and $f_0(1790)$, with evidence for the latter state discussed in the next section.

- *BES.* Results consistent with the MARK-III reanalysis of Ref. [176] were obtained by the BES Collaboration at BEPC (Beijing Electron Positron Collider) in 2000 [177] where an $I(J^{PC}) = 0(0^{++})$ resonance labelled as $f_0(1740)$ with $m_{f_0(1740)} = 1740^{+30}_{-25}$ MeV and $\Gamma_{f_0(1740)} = 120^{+50}_{-40}$ MeV was found. This result was again obtained in the decay channel $e^+e^- \to J/\psi \to \gamma\pi^+\pi^-\pi^+\pi^-$. Note, however, that these data involved no kaon decays of $J/\psi$. Subsequently, the same collaboration performed an analysis of a larger number of $J/\psi$ decay channels: $J/\psi \to \gamma K^+K^-$, $\omega K^+K^-$ and $\varphi K^+K^-$ as well as $J/\psi \to \gamma\pi^+\pi^-\pi^+\pi^-$, $\omega\pi^+\pi^-\pi^+\pi^-$ and $\varphi\pi^+\pi^-$ [178]. The kaon channels allowed for reconstruction of the $f_0(1710)$ resonance [referred to as $f_0(1710 \pm 20)$] while the pion channels suggested the existence of a separate $f_0(1760 \pm 20)$ resonance. Thus a resonance with a mass distinct from $f_0(1710)$ appeared to have been found; it was also produced in different decay channels [i.e., those involving pions whereas the $f_0(1710)$ resonance was reconstructed predominantly in kaon final states]. This new resonance was later denoted as $f_0(1790)$, see next section.

- *BES II.* An upgrade of BEPC allowed for 58M of $J/\psi$ events to be collected at BES II. In 2003, $f_0(1710)$ was confirmed as a $J^P = 0^+$ resonance reconstructed in kaon final states from $J/\psi \to \gamma K^+K^-$ and $\gamma\bar{K}^0_S K^0_S$ with $m_{f_0(1710)} = 1740 \pm 4^{+10}_{-25}$ MeV and $\Gamma_{f_0(1710)} = 166^{+5+15}_{-8-10}$ MeV [179]. These results were confirmed in 2004 from $J/\psi \to \omega K^+K^-$ [180]. Additional evidence for the existence of $f_0(1710)$ was presented in Ref. [181] from the $\chi_{c0} \to \pi^+\pi^-K^+K^-$ decay; however, this analysis also suggested the existence of a further scalar state between 1.7 GeV and 1.8 GeV, referred to as $f_0(1790)$.

- *WA102.* Experiments involving $pp$ collisions at 450 GeV were performed by the WA102 Collaboration. Final states were reconstructed from reactions $pp \to p_f(K^+K^-)p_s$ and $pp \to p_f(\bar{K}^0_S K^0_S)p_s$ (subscripts $f$ and $s$ denote the fastest and slowest protons in the laboratory frame, respectively). Results for the $f_0(1710)$ resonance suggested $m_{f_0(1710)} = (1730 \pm 15)$ MeV and $\Gamma_{f_0(1710)} = (100 \pm 25)$ MeV [97]. The same experiment also allowed for resonances in the pion final states to be looked for [98]. The corresponding reaction $pp \to p_f(\pi^+\pi^-)p_s$ allowed for the reconstruction of $f_0(980)$, $f_0(1370)$ and $f_0(1500)$ but the fit of $f_0(1710)$ was conspicuously worse than in $pp \to p_f(K^+K^-)p_s$. The two stated publications presented results of respective Breit-Wigner fits. A coupled-channel analysis of both pion and kaon final states yielded a pole at $m_{f_0(1710)} = (1727 \pm 12 \pm 11)$ MeV and $\Gamma_{f_0(1710)} = (126 \pm 16 \pm 18)$ MeV [99]. Note that a subsequent $T$-matrix analysis [153] of $pp \to p_f(\eta\eta)p_s$ production data (identified via $\eta \to \gamma\gamma$ and $\eta \to \pi^+\pi^-\pi^0$) yielded results very close to those of Ref.

[99]. Note also that all the mentioned results implied $J^P = 0^+$ for $f_0(1710)$.

- *ZEUS.* Electrons at 27.5 GeV were collided with protons at 820 GeV and 920 GeV at the HERA storage ring in Hamburg (DESY) during the 1996-2000 running period. Reactions were observed using the ZEUS detector and $\bar{K}^0_S K^0_S$ final states were studied. The $f_0(1710)$ was observed from a $5\sigma$ $J^P = 0^+$ signal yielding $m_{f_0(1710)} = (1701 \pm 5^{+9}_{-2})$ MeV and $\Gamma_{f_0(1710)} = (100 \pm 24^{+7}_{-22})$ MeV [182]. However, the Collaboration was not able to exclude the coupling of $f_0(1710)$ to photons, implying that this resonance is not a certain candidate for a predominantly glueball state. Indeed calculations in our model prefer $f_0(1710)$ to be predominantly strange quarkonium, as we will discuss in Sec. 9.

The PDG cites a world-average mass $m_{f_0(1710)} = (1720 \pm 6)$ MeV and a decay width $\Gamma_{f_0(1710)} = (135 \pm 8)$ MeV [10]. A more detailed discussion of the $f_0(1710)$ decay channels can be found in Sec. 3.7.

### 3.6 The Peculiar Case of $f_0(1790)$

Our results in Fit II, Chapter 10, will suggest the existence of an $I(J^{PC}) = 0(0^{++})$, predominantly $\bar{s}s$ state in the energy region of approximately 1.6 - 1.7 GeV. Assignment of this state to an experimentally established resonance will depend on decay patterns of our model state; however, experimental results regarding the $I(J^{PC}) = 0(0^{++})$ channel in this energy region are far from clear [although admittedly the issue is less ambiguous than in the case of $f_0(600)$]. The reason is that the existence of two distinct resonances is claimed within an energy interval of only 100 MeV: in addition to $f_0(1710)$, the BES II Collaboration [140] have claimed that a state labelled as $f_0(1790)$ also exists. In the following we will discuss data regarding this resonance; if $f_0(1790)$ does exist, then the disentanglement of data regarding this state from those regarding the close-by state $f_0(1710)$ in experimental observations becomes imperative, as entangled data are bound to lead to results that could certainly be described as peculiar (or at least such that they should not be used in models and theories). Note that data sets regarding $f_0(1790)$ – described in the following – provide us with a rather straightforward tool to distinguish this resonance from $f_0(1710)$: the $f_0(1790)$ resonance decays predominantly into pions and only marginally into kaons. For $f_0(1710)$, the opposite is true. Thus a careful analysis of experimental data should be able to discriminate between these two states. [Additionally, the feature of predominantly decaying into pions and the mass difference to $f_0(1370)$ qualify $f_0(1790)$ as a putative radial excitation of $f_0(1370)$.]

Experimental evidence for $f_0(1790)$ reads as follows:

- *MARK-III / Crystal Barrel.* In the previous section we have already discussed the reanalysis of MARK-III data performed in 1995 by the Crystal Barrel Collaboration [176]. We have indicated that a careful analysis of the mentioned data yields a scalar resonance denoted as $f_0(1750)$ with $m_{f_0(1750)} = (1750 \pm 15)$ MeV and $\Gamma_{f_0(1750)} = (160 \pm 40)$ MeV. However, the mass of this resonance appears to be too large to describe $f_0(1710)$ alone; it appears more probable that the mentioned data actually yield a superposition of the $f_0(1710)$ resonance (the existence of which may be regarded as proven) with a putative new resonance (the existence of which would require more experimental data, discussed in

the following). Therefore, the central value of the mass of this resonance may indicate a superposition of a state denoted nowadays as $f_0(1790)$ with $f_0(1710)$.

- *Crystal Barrel.* The Crystal Barrel Collaboration also published analysis of data from the reaction $\bar{p}p \to \eta\eta\pi^0$ in 1999 [183]. An $8\sigma$ signal was found; the resonance was referred to as $f_0(1770)$ with $m_{f_0(1770)} = (1770 \pm 12)$ MeV and $\Gamma_{f_0(1750)} = (220 \pm 40)$ MeV.

- *BES.* As mentioned in the previous section, in 2000 the BES Collaboration claimed the existence of a resonance denoted as $f_0(1760 \pm 20)$, found to be distinct from the $f_0(1710)$ state [178]. Factors of distinction involved not only the mass but also production channels: $f_0(1710)$ appeared in the $J/\psi \to \gamma K^+K^-$, $\omega K^+K^-$ and $\varphi K^+K^-$ channels while the $f_0(1760 \pm 20)$ was reconstructed in $J/\psi \to \gamma\pi^+\pi^-\pi^+\pi^-$, $\omega\pi^+\pi^-\pi^+\pi^-$ and $\varphi\pi^+\pi^-$. More conclusive evidence for a second resonance between 1.7 and 1.8 GeV was obtained by the BES II Collaboration (see below). Note that already in 1996 the BES Collaboration claimed the existence of a scalar resonance with a mass of $1781 \pm 8^{+10}_{-31}$ MeV and a width of $85 \pm 24^{+22}_{-19}$ MeV that appeared to correspond well to a resonance at 1.79 GeV [i.e., to the putative $f_0(1790)$ resonance] but was, however, found in the $J/\psi \to \gamma K^+K^-$ channel only [184]. Thus results of Ref. [184] did not include $J/\psi$ decays in the pion channels and possible interference effects with kaons; therefore they need to be considered with care.

- *BES II – $J/\psi$.* An upgrade of BEPC allowed for 58M of $J/\psi$ events to be collected at BES II. A clear $f_0(1790)$ peak corresponding to a $15\sigma$ signal was observed in the $J/\psi \to \varphi\pi^+\pi^-$ decay [140] yielding $m_{f_0(1790)} = 1790^{+40}_{-30}$ MeV and $\Gamma_{f_0(1790)} = 270^{+60}_{-30}$ MeV. This is the best available set of data on $f_0(1790)$. Conversely, the $f_0(1710)$ resonance was observed in the $J/\psi \to \varphi K^+K^-$ channel confirming this resonance as decaying predominantly into kaons [$m_{f_0(1710)}$ and $\Gamma_{f_0(1710)}$ were fixed to the PDG values]. An additional reason for the assertion that there exist two scalar states in the region between 1.7 GeV and 1.8 GeV was presented in Ref. [140]. As already mentioned, a fit of the $J/\psi \to \varphi\pi^+\pi^-$ data allows for determination of the $f_0(1790)$ mass and width. Let us assume that $f_0(1710)$ and $f_0(1790)$ actually represent the same resonance and let us denote this resonance as $\tilde{f}_0$ – i.e., let $\tilde{f}_0$ be the only $I(J^{PC}) = 0(0^{++})$ resonance between 1.7 GeV and 1.8 GeV. We can then remove (artificially) the $f_0(1710)$ resonance from the $J/\psi \to \varphi K^+K^-$ data. This yields the branching ratio $\Gamma_{\tilde{f}_0\to\pi\pi}/\Gamma_{\tilde{f}_0\to KK} = 1.82 \pm 0.33$ (in addition to a poorer fit). However, according to Ref. [180] the same ratio for a scalar state between 1.7 GeV and 1.8 GeV should possess a value $< 0.11$, obtained from different production channels: $J/\psi \to \omega\pi^+\pi^-$ and $J/\psi \to \omega K^+K^-$. A single resonance must possess the same value of a branching ratio in all production channels – in our case regardless whether it is produced in $J/\psi \to \varphi\pi^+\pi^-$ and $J/\psi \to \varphi K^+K^-$ or in $J/\psi \to \omega\pi^+\pi^-$ and $J/\psi \to \omega K^+K^-$. For the case of the assumed single scalar resonance $\tilde{f}_0$ between 1.7 GeV and 1.8 GeV this is obviously not true: the branching ratios differ by at least a factor of 17. Therefore, there must exist two distinct resonances.

- *BES II – $\chi_{c0}$.* Additional confirmation of the $f_0(1790)$ state can be found in Ref. [181] from a BES II analysis of the $\chi_{c0} \to \pi^+\pi^-K^+K^-$ decay; see also Ref. [185].

Thus there appears to be sufficient evidence for existence of a sixth isoscalar resonance below 1.9 GeV, $f_0(1790)$, in addition to $f_0(600)$, $f_0(980)$, $f_0(1370)$, $f_0(1500)$ and $f_0(1710)$. The relative

vicinity of $f_0(1790)$ to $f_0(1710)$ makes it imperative to consider carefully and, if necessary, to disentangle published results regarding both resonances. We illustrate this point in the following section where the partial decay widths of $f_0(1710)$ are determined.

### 3.7 Consequences for the $f_0(1710)$ Decay Channels

Considering the experimental ambiguities discussed in the previous section, let us now discuss numerical values regarding the $f_0(1710)$ decay channels. The PDG [10] lists five decay channels for this resonance: $f_0(1710) \to KK$, $\pi\pi$, $\eta\eta$, $\gamma\gamma$ and $\omega\omega$. The existence of the decay $f_0(1710) \to \omega\omega$ was determined only recently by the BES II Collaboration in 2006 [186]. No precise determination of the branching ratio was possible because the decay was reconstructed from the reaction $J/\psi \to \gamma\omega\omega$, yielding a strong pseudoscalar contribution and rather weak scalar and tensor contributions. There is no published value of the corresponding $\Gamma_{f_0(1710)\to\omega\omega}$ that is expected to be small. The latter is also true for $\Gamma_{f_0(1710)\to\gamma\gamma}$. We therefore consider only the first three decays: into kaons, pions and etas:

$$\begin{aligned}\Gamma_{f_0(1710)} &\equiv \Gamma_{f_0(1710)\to KK} + \Gamma_{f_0(1710)\to\pi\pi} + \Gamma_{f_0(1710)\to\eta\eta} \\ &= \Gamma_{f_0(1710)\to\pi\pi}\left[1 + \frac{\Gamma_{f_0(1710)\to KK}}{\Gamma_{f_0(1710)\to\pi\pi}} + \frac{\Gamma_{f_0(1710)\to\eta\eta}}{\Gamma_{f_0(1710)\to\pi\pi}}\right]. \end{aligned} \tag{3.1}$$

In the next three subsections we will calculate decay widths of $f_0(1710)$ in various channels using the experimentally known ratios $\Gamma_{f_0(1710)\to\pi\pi}/\Gamma_{f_0(1710)\to KK}$ and $\Gamma_{f_0(1710)\to\eta\eta}/\Gamma_{f_0(1710)\to KK}$. In Section 3.7.1 we discuss implications of data on $f_0(1710)$ preferred by the PDG; they include $\Gamma_{f_0(1710)\to\pi\pi}/\Gamma_{f_0(1710)\to KK} = 0.41^{+0.11}_{-0.17}$ from the BES II Collaboration [187] as well as the ratio $\Gamma_{f_0(1710)\to\eta\eta}/\Gamma_{f_0(1710)\to KK} = 0.48 \pm 0.15$ from the WA102 Collaboration [153] (the latter experiments performed at CERN Omega Spectrometer). Subsection 3.7.2 contains analogous calculation with the alternative BES II ratio $\Gamma_{f_0(1710)\to\pi\pi}/\Gamma_{f_0(1710)\to KK} < 0.11$ [180] (not used by the PDG) but retaining the WA102 ratio $\Gamma_{f_0(1710)\to\eta\eta}/\Gamma_{f_0(1710)\to KK} = 0.48 \pm 0.15$. In Subsection 3.7.3 we use only the WA102 ratios $\Gamma_{f_0(1710)\to\pi\pi}/\Gamma_{f_0(1710)\to KK} = 0.2 \pm 0.024 \pm 0.036$ [99] and $\Gamma_{f_0(1710)\to\eta\eta}/\Gamma_{f_0(1710)\to KK} = 0.48 \pm 0.15$.
Note that there are also corresponding results from a combined fit in Ref. [188] that, however, do not constrain the $2\pi/2K$ ratio very well: $\Gamma_{f_0(1710)\to\pi\pi}/\Gamma_{f_0(1710)\to KK} = 5.8^{+9.1}_{-5.5}$. Additionally, there are older data from the WA76 Collaboration at CERN [96] reading $\Gamma_{f_0(1710)\to\pi\pi}/\Gamma_{f_0(1710)\to KK} = 0.39 \pm 0.14$; these are qualitatively consistent with results of Ref. [99] and therefore omitted from our discussion.

#### 3.7.1 The $f_0(1710)$ Decay Widths from Data Preferred by the PDG

As already mentioned, the BES II [187] ratio cited by the PDG reads $\Gamma_{f_0(1710)\to\pi\pi}/\Gamma_{f_0(1710)\to KK} \equiv \Gamma^{\rm PDG}_{f_0(1710)\to\pi\pi}/\Gamma^{\rm PDG}_{f_0(1710)\to KK} = 0.41^{+0.11}_{-0.17}$. Two comments are in order for this result. Firstly, data used to extract the stated ratio ($J/\psi \to \gamma\pi^+\pi^-$ and $\gamma\pi^0\pi^0$) suffer from a large background in the $\pi^+\pi^-$ channel (of approximately 50%). This raises doubts about the reliability of the ratio. Additionally, the ratio was obtained for a scalar resonance with a mass of $1765^{+4}_{-3}$ MeV and width of $(145 \pm 8 \pm 69)$ MeV. Although the resonance may be assigned to $f_0(1710)$ (due to the value of its width; the mass is too large), the mass of the resonance appears to suggest that it could also

be a superposition of $f_0(1710)$ and $f_0(1790)$ rather than representing only a signal for $f_0(1710)$. This possibility was also discussed by the Collaboration itself [187]. Therefore, the stated ratio for $\Gamma_{f_0(1710)\to\pi\pi}/\Gamma_{f_0(1710)\to KK}$ has to be regarded with care. Indeed we will also consider alternative values of the $\Gamma_{f_0(1710)\to\pi\pi}/\Gamma_{f_0(1710)\to KK}$ ratio, such as for example a more reliable result of $\Gamma_{f_0(1710)\to\pi\pi}/\Gamma_{f_0(1710)\to KK} < 0.11$ from Ref. [180], also by the BES II Collaboration (see Subsection 3.7.2).

Despite the mentioned drawbacks, let us discuss the consequences of $\Gamma_{f_0(1710)\to\pi\pi}/\Gamma_{f_0(1710)\to KK} \equiv \Gamma^{\rm PDG}_{f_0(1710)\to\pi\pi}/\Gamma^{\rm PDG}_{f_0(1710)\to KK} = 0.41^{+0.11}_{-0.17}$. The inverse ratio $\Gamma_{f_0(1710)\to KK}/\Gamma_{f_0(1710)\to\pi\pi}$ has the central value of 2.44. The error value $\Delta(\Gamma_{f_0(1710)\to KK}/\Gamma_{f_0(1710)\to\pi\pi})$ is obtained from

$$\frac{\Gamma_{f_0(1710)\to KK}}{\Gamma_{f_0(1710)\to\pi\pi}} \equiv \frac{1}{\frac{\Gamma_{f_0(1710)\to\pi\pi}}{\Gamma_{f_0(1710)\to KK}}} \Rightarrow \Delta\frac{\Gamma_{f_0(1710)\to KK}}{\Gamma_{f_0(1710)\to\pi\pi}} = \left| -\frac{\Delta\frac{\Gamma_{f_0(1710)\to\pi\pi}}{\Gamma_{f_0(1710)\to KK}}}{\left[\frac{\Gamma_{f_0(1710)\to\pi\pi}}{\Gamma_{f_0(1710)\to KK}}\right]^2} \right|$$
$$\Rightarrow \Delta\frac{\Gamma_{f_0(1710)\to KK}}{\Gamma_{f_0(1710)\to\pi\pi}} = ^{+0.65}_{-1.01} . \tag{3.2}$$

Thus, in total:

$$\frac{\Gamma_{f_0(1710)\to KK}}{\Gamma_{f_0(1710)\to\pi\pi}} \equiv \frac{\Gamma^{\rm PDG}_{f_0(1710)\to KK}}{\Gamma^{\rm PDG}_{f_0(1710)\to\pi\pi}} = 2.44^{+0.65}_{-1.01}. \tag{3.3}$$

The PDG also uses the ratio $\Gamma_{f_0(1710)\to\eta\eta}/\Gamma_{f_0(1710)\to KK} = 0.48 \pm 0.15$, published originally by the WA102 Collaboration in 2000 [153]. Then we obtain for the central value of the ratio $\Gamma_{f_0(1710)\to\eta\eta}/\Gamma_{f_0(1710)\to\pi\pi}$

$$\overline{\frac{\Gamma_{f_0(1710)\to\eta\eta}}{\Gamma_{f_0(1710)\to\pi\pi}}} = \overline{\frac{\Gamma_{f_0(1710)\to\eta\eta}}{\Gamma_{f_0(1710)\to KK}}} \overline{\frac{1}{\frac{\Gamma_{f_0(1710)\to\pi\pi}}{\Gamma_{f_0(1710)\to KK}}}} = \frac{0.48}{0.41} = 1.17. \tag{3.4}$$

(Note that the line above the observable denotes the central value.) Additionally,

$$\frac{\Gamma_{f_0(1710)\to\eta\eta}}{\Gamma_{f_0(1710)\to\pi\pi}} = \frac{\Gamma_{f_0(1710)\to\eta\eta}}{\Gamma_{f_0(1710)\to KK}} \frac{\Gamma_{f_0(1710)\to KK}}{\Gamma_{f_0(1710)\to\pi\pi}}$$
$$\Rightarrow \Delta\frac{\Gamma_{f_0(1710)\to\eta\eta}}{\Gamma_{f_0(1710)\to\pi\pi}} = \sqrt{\left[\frac{\Gamma_{f_0(1710)\to\eta\eta}}{\Gamma_{f_0(1710)\to KK}}\,\Delta\frac{\Gamma_{f_0(1710)\to KK}}{\Gamma_{f_0(1710)\to\pi\pi}}\right]^2 + \left[\frac{\Gamma_{f_0(1710)\to KK}}{\Gamma_{f_0(1710)\to\pi\pi}}\,\Delta\frac{\Gamma_{f_0(1710)\to\eta\eta}}{\Gamma_{f_0(1710)\to KK}}\right]^2} \tag{3.5}$$

and consequently from Eq. (3.2):

$$\frac{\Gamma_{f_0(1710)\to\eta\eta}}{\Gamma_{f_0(1710)\to\pi\pi}} \equiv \frac{\Gamma^{\rm PDG}_{f_0(1710)\to\eta\eta}}{\Gamma^{\rm PDG}_{f_0(1710)\to\pi\pi}} = 1.17^{+0.48}_{-0.61}. \tag{3.6}$$

From Eq. (3.1) we obtain

$$\Gamma_{f_0(1710)\to\pi\pi} = \frac{\Gamma_{f_0(1710)}}{1 + \frac{\Gamma_{f_0(1710)\to KK}}{\Gamma_{f_0(1710)\to\pi\pi}} + \frac{\Gamma_{f_0(1710)\to\eta\eta}}{\Gamma_{f_0(1710)\to\pi\pi}}} \tag{3.7}$$

and thus, given that $\Gamma_{f_0(1710)} = (135 \pm 8)$ MeV [10], Eqs. (3.3) and (3.6) yield the central value $\overline{\Gamma}_{f_0(1710)\to\pi\pi} = 29.28$ MeV. The corresponding error value $\Delta\Gamma_{f_0(1710)\to\pi\pi}$ is obtained from Eq. (3.7) as follows:

$$\Delta\Gamma_{f_0(1710)\to\pi\pi} = \left\{ \left[ \frac{\Delta\Gamma_{f_0(1710)}}{1 + \frac{\Gamma_{f_0(1710)\to KK}}{\Gamma_{f_0(1710)\to\pi\pi}} + \frac{\Gamma_{f_0(1710)\to\eta\eta}}{\Gamma_{f_0(1710)\to\pi\pi}}} \right]^2 + \left\{ \frac{\Gamma_{f_0(1710)}\ \Delta\frac{\Gamma_{f_0(1710)\to\eta\eta}}{\Gamma_{f_0(1710)\to\pi\pi}}}{\left[1 + \frac{\Gamma_{f_0(1710)\to KK}}{\Gamma_{f_0(1710)\to\pi\pi}} + \frac{\Gamma_{f_0(1710)\to\eta\eta}}{\Gamma_{f_0(1710)\to\pi\pi}}\right]^2} \right\}^2 + \left\{ \frac{\Gamma_{f_0(1710)}\ \Delta\frac{\Gamma_{f_0(1710)\to KK}}{\Gamma_{f_0(1710)\to\pi\pi}}}{\left[1 + \frac{\Gamma_{f_0(1710)\to KK}}{\Gamma_{f_0(1710)\to\pi\pi}} + \frac{\Gamma_{f_0(1710)\to\eta\eta}}{\Gamma_{f_0(1710)\to\pi\pi}}\right]^2} \right\}^2 \right\}^{\frac{1}{2}} \tag{3.8}$$

Equations (3.3), (3.6) and (3.8) yield

$$\Delta\Gamma_{f_0(1710)\to\pi\pi} = ^{+5.42}_{-7.69}\ \text{MeV}. \tag{3.9}$$

Thus,

$$\Gamma_{f_0(1710)\to\pi\pi} \equiv \Gamma^{\text{PDG}}_{f_0(1710)\to\pi\pi} = 29.28^{+5.42}_{-7.69}\ \text{MeV}. \tag{3.10}$$

We obtain from Eqs. (3.3) and (3.10) for $\Gamma_{f_0(1710)\to KK}$:

$$\overline{\Gamma}_{f_0(1710)\to KK} = \frac{\overline{\Gamma_{f_0(1710)\to KK}}}{\Gamma_{f_0(1710)\to\pi\pi}} \overline{\Gamma}_{f_0(1710)\to\pi\pi} \tag{3.11}$$

$$\Rightarrow \overline{\Gamma}_{f_0(1710)\to KK} = 71.44\ \text{MeV}. \tag{3.12}$$

Error values $\Delta\Gamma_{f_0(1710)\to KK}$ are obtained from

$$\Delta\Gamma_{f_0(1710)\to KK} = \left[ \left( \Gamma_{f_0(1710)\to\pi\pi}\ \Delta\frac{\Gamma_{f_0(1710)\to KK}}{\Gamma_{f_0(1710)\to\pi\pi}} \right)^2 + \left( \frac{\Gamma_{f_0(1710)\to KK}}{\Gamma_{f_0(1710)\to\pi\pi}}\ \Delta\Gamma_{f_0(1710)\to\pi\pi} \right)^2 \right]^{\frac{1}{2}} \tag{3.13}$$

$$\Rightarrow \Delta\Gamma_{f_0(1710)\to KK} = ^{+23.18}_{-35.02}\ \text{MeV}. \tag{3.14}$$

Thus in total:

$$\Gamma_{f_0(1710)\to KK} \equiv \Gamma^{\text{PDG}}_{f_0(1710)\to KK} = 71.44^{+23.18}_{-35.02}\ \text{MeV}. \tag{3.15}$$

Analogously, in the $f_0(1710) \to \eta\eta$ channel we obtain from Eqs. (3.6) and (3.10):

$$\overline{\Gamma}_{f_0(1710)\to\eta\eta} = \frac{\overline{\Gamma_{f_0(1710)\to\eta\eta}}}{\Gamma_{f_0(1710)\to\pi\pi}} \overline{\Gamma}_{f_0(1710)\to\pi\pi} \tag{3.16}$$

$$\Rightarrow \overline{\Gamma}_{f_0(1710)\to\eta\eta} = 34.26\ \text{MeV}. \tag{3.17}$$

while the error values $\Delta\Gamma_{f_0(1710)\to\eta\eta}$ are obtained from

$$\Delta\Gamma_{f_0(1710)\to\eta\eta} = \left[\left(\Gamma_{f_0(1710)\to\pi\pi}\ \Delta\frac{\Gamma_{f_0(1710)\to\eta\eta}}{\Gamma_{f_0(1710)\to\pi\pi}}\right)^2 + \left(\frac{\Gamma_{f_0(1710)\to\eta\eta}}{\Gamma_{f_0(1710)\to\pi\pi}}\ \Delta\Gamma_{f_0(1710)\to\pi\pi}\right)^2\right]^{\frac{1}{2}} \tag{3.18}$$

$$\Rightarrow \Delta\Gamma_{f_0(1710)\to KK} = ^{+15.42}_{-20.0}\ \text{MeV}. \tag{3.19}$$

Therefore,

$$\Gamma_{f_0(1710)\to\eta\eta} \equiv \Gamma^{\text{PDG}}_{f_0(1710)\to\eta\eta} = 34.26^{+15.42}_{-20.0}\ \text{MeV}. \tag{3.20}$$

### 3.7.2 The $f_0(1710)$ Decay Widths from Alternative BES II Data

Results for $\Gamma_{f_0(1710)\to\pi\pi}$, $\Gamma_{f_0(1710)\to KK}$ and $\Gamma_{f_0(1710)\to\eta\eta}$, stated respectively in Eqs. (3.10), (3.15) and (3.20), depend among others on the result $\Gamma_{f_0(1710)\to\pi\pi}/\Gamma_{f_0(1710)\to KK} = 0.41^{+0.11}_{-0.17}$ from Ref. [187], the reliability of which was discussed at the beginning of Sec. 3.7.1. In this subsection we discuss implications of an alternative (and more reliable) BES II result:

$$\frac{\Gamma_{f_0(1710)\to\pi\pi}}{\Gamma_{f_0(1710)\to KK}} \equiv \frac{\Gamma^{\text{BES II}}_{f_0(1710)\to\pi\pi}}{\Gamma^{\text{BES II}}_{f_0(1710)\to KK}} < 0.11. \tag{3.21}$$

This result implies

$$\frac{\Gamma_{f_0(1710)\to KK}}{\Gamma_{f_0(1710)\to\pi\pi}} \equiv \frac{\Gamma^{\text{BES II}}_{f_0(1710)\to KK}}{\Gamma^{\text{BES II}}_{f_0(1710)\to\pi\pi}} > 9.09. \tag{3.22}$$

From $\Gamma_{f_0(1710)\to\eta\eta}/\Gamma_{f_0(1710)\to KK} = 0.48$ [153] we obtain

$$\frac{\Gamma_{f_0(1710)\to\eta\eta}}{\Gamma_{f_0(1710)\to\pi\pi}} \equiv \frac{\Gamma^{\text{BES II}}_{f_0(1710)\to\eta\eta}}{\Gamma^{\text{BES II}}_{f_0(1710)\to\pi\pi}} = \frac{\Gamma_{f_0(1710)\to\eta\eta}}{\Gamma_{f_0(1710)\to KK}}\frac{1}{\frac{\Gamma_{f_0(1710)\to\pi\pi}}{\Gamma_{f_0(1710)\to KK}}} > \frac{0.48}{0.11} = 4.36. \tag{3.23}$$

We will restrain from calculating errors because the ratio $\Gamma_{f_0(1710)\to\pi\pi}/\Gamma_{f_0(1710)\to KK} < 0.11$ provides us only with an upper boundary and no error information. The condition (3.23) implies

$$\frac{\Gamma_{f_0(1710)\to\pi\pi}}{\Gamma_{f_0(1710)\to\eta\eta}} \equiv \frac{\Gamma^{\text{BES II}}_{f_0(1710)\to\pi\pi}}{\Gamma^{\text{BES II}}_{f_0(1710)\to\eta\eta}} < 0.23. \tag{3.24}$$

From conditions (3.7), (3.22) and (3.23) we obtain

$$\Gamma_{f_0(1710)\to\pi\pi} \equiv \Gamma^{\text{BES II}}_{f_0(1710)\to\pi\pi} < 9.34\ \text{MeV}. \tag{3.25}$$

Note that a similar calculation of an interval for $\Gamma_{f_0(1710)\to KK}$ would yield

$$\Gamma_{f_0(1710)\to KK} = \frac{\Gamma_{f_0(1710)\to KK}}{\Gamma_{f_0(1710)\to\pi\pi}}\Gamma_{f_0(1710)\to\pi\pi}; \tag{3.26}$$

then constraining $\Gamma_{f_0(1710)\to KK}$ is not possible because condition (3.22) determines the lower boundary for $\Gamma_{f_0(1710)\to KK}/\Gamma_{f_0(1710)\to\pi\pi}$ and, contrarily, condition (3.25) suggests the upper boundary for $\Gamma_{f_0(1710)\to\pi\pi}$. For analogous reasons, a calculation of $\Gamma_{f_0(1710)\to\eta\eta}$ is also not possible. However, given that $\Gamma_{f_0(1710)} \equiv \Gamma_{f_0(1710)\to KK} + \Gamma_{f_0(1710)\to\pi\pi} + \Gamma_{f_0(1710)\to\eta\eta}$, the condition (3.25) leads to $125.66\ \text{MeV} < \Gamma_{f_0(1710)\to KK} + \Gamma_{f_0(1710)\to\eta\eta} < 135\ \text{MeV} \equiv \Gamma_{f_0(1710)}$.

### 3.7.3 The $f_0(1710)$ Decay Widths from WA102 Data

The WA102 result [99]

$$\frac{\Gamma_{f_0(1710)\to\pi\pi}}{\Gamma_{f_0(1710)\to KK}} \equiv \frac{\Gamma^{\rm WA102}_{f_0(1710)\to\pi\pi}}{\Gamma^{\rm WA102}_{f_0(1710)\to KK}} = 0.2 \pm 0.024 \pm 0.036 \equiv 0.2 \pm 0.06 \tag{3.27}$$

implies that the central value of the inverse ratio $\Gamma_{f_0(1710)\to KK}/\Gamma_{f_0(1710)\to\pi\pi}$ is 5.0. Corresponding error values are calculated using the first line of Eq. (3.2):

$$\Delta\frac{\Gamma_{f_0(1710)\to KK}}{\Gamma_{f_0(1710)\to\pi\pi}} = 1.5. \tag{3.28}$$

Thus in total we obtain

$$\frac{\Gamma_{f_0(1710)\to KK}}{\Gamma_{f_0(1710)\to\pi\pi}} \equiv \frac{\Gamma^{\rm WA102}_{f_0(1710)\to KK}}{\Gamma^{\rm WA102}_{f_0(1710)\to\pi\pi}} = 5.0 \pm 1.5. \tag{3.29}$$

From $\Gamma_{f_0(1710)\to\eta\eta}/\Gamma_{f_0(1710)\to KK} = 0.48 \pm 0.15$ [153] we obtain

$$\frac{\overline{\Gamma_{f_0(1710)\to\eta\eta}}}{\Gamma_{f_0(1710)\to\pi\pi}} = \frac{\overline{\Gamma_{f_0(1710)\to\eta\eta}}}{\Gamma_{f_0(1710)\to KK}}\frac{1}{\frac{\Gamma_{f_0(1710)\to\pi\pi}}{\Gamma_{f_0(1710)\to KK}}} = \frac{0.48}{0.2} = 2.4. \tag{3.30}$$

Then Eq. (3.5) yields

$$\frac{\Gamma_{f_0(1710)\to\eta\eta}}{\Gamma_{f_0(1710)\to\pi\pi}} \equiv \frac{\Gamma^{\rm WA102}_{f_0(1710)\to\eta\eta}}{\Gamma^{\rm WA102}_{f_0(1710)\to\pi\pi}} = 2.4 \pm 1.04. \tag{3.31}$$

Given that $\Gamma_{f_0(1710)} = (135 \pm 8)$ MeV, we obtain the central value $\overline{\Gamma}_{f_0(1710)\to\pi\pi} = 16.1$ MeV from Eq. (3.7). The error is calculated from Eq. (3.7); we obtain $\Delta\Gamma_{f_0(1710)\to\pi\pi} = 3.6$ MeV. Thus in total

$$\Gamma_{f_0(1710)\to\pi\pi} \equiv \Gamma^{\rm WA102}_{f_0(1710)\to\pi\pi} = (16.1 \pm 3.6)\ \text{MeV}. \tag{3.32}$$

Equations (3.11), (3.29) and (3.32) yield $\overline{\Gamma}_{f_0(1710)\to KK} = 80.5$ MeV whereas from Eq. (3.13) we obtain $\Delta\Gamma_{f_0(1710)\to KK} = 30.1$ MeV. In total:

$$\Gamma_{f_0(1710)\to KK} \equiv \Gamma^{\rm WA102}_{f_0(1710)\to KK} = (80.5 \pm 30.1)\ \text{MeV}. \tag{3.33}$$

Finally, from Eqs. (3.16), (3.31) and (3.32) we obtain $\overline{\Gamma}_{f_0(1710)\to\eta\eta} = 38.6$ MeV while Eq. (3.18) yields $\Delta\Gamma_{f_0(1710)\to\eta\eta} = 18.8$ MeV. In total:

$$\Gamma_{f_0(1710)\to\eta\eta} \equiv \Gamma^{\rm WA102}_{f_0(1710)\to\eta\eta} = (38.6 \pm 18.8)\ \text{MeV}. \tag{3.34}$$

We note from Eq. (3.32) that $\Gamma_{f_0(1710)\to\pi\pi}$ is approximately by a factor of two smaller in the WA102 data than in the combined BES II/WA102 data that lead to $\Gamma_{f_0(1710)\to\pi\pi} = 29.28^{+5.42}_{-7.69}$ MeV, Eq. (3.10). This is due to the difference of the $\Gamma_{f_0(1710)\to\pi\pi}/\Gamma_{f_0(1710)\to KK}$ ratios from Refs. [99] and [187].

Therefore, we are now in possession of three distinct sets of data regarding decay widths of $f_0(1710)$: those preferred by the PDG [Eqs. (3.3), (3.6), (3.10), (3.15) and (3.20)], those from BES II, not used by the PDG [Eqs. (3.21) - (3.25)] and those from WA102 [Eqs. (3.27), (3.29), (3.31), (3.32), (3.33) and (3.34)]. We will discuss implications of these results for our model in Sec. 11.1.3.

# 4. Construction of a Meson Model

## 4.1 General Remarks

We have seen in Chapter 2 that QCD possesses an exact $SU(3)_c$ local gauge symmetry (the colour symmetry) and an approximate global $U(N_f)_R \times U(N_f)_L$ symmetry for $N_f$ massless quark flavours (the chiral symmetry). For sufficiently low temperature and density, quarks and gluons are confined inside colourless hadrons [i.e., $SU(3)_c$ invariant configurations]. Thus, it is the chiral symmetry which predominantly determines hadronic interactions in the low-energy region. However, QCD is strongly non-perturbative in the low-energy region as is evident from the running coupling $g^2(\mu)$, Eq. (2.86). Thus, in the non-perturbative regime, effective theories and models based on the features of the QCD Lagrangian are utilised.
Effective field theories which contain hadrons as degrees of freedom rather than quarks and gluons have been developed along two lines which differ in the way in which chiral symmetry is realised: linear [48] and non-linear [189]. In the non-linear realisation, the so-called non-linear sigma model, the scalar states are integrated out, leaving the pseudoscalar states as the only degrees of the freedom. On the other hand, in the linear representation of the symmetry, the so-called linear sigma model, both the scalar and pseudoscalar degrees of freedom are present.
In this work, we consider the linear representation of chiral symmetry. Let us discuss the reasons.

- *Chiral partners.* The linear sigma model contains not only pseudoscalar states but also their so-called *chiral partners* from the onset. The definition of the chiral partners requires us to introduce a quantum number denoted as $G$-parity [next to the parity $P$ (2.61) and charge conjugation $C$ (2.64)]. To this end, consider a special case of the flavour transformation (here exemplary for two flavours)

$$q_f = \begin{pmatrix} u \\ d \end{pmatrix} \longrightarrow q_f' = U_2 \begin{pmatrix} u \\ d \end{pmatrix},$$

where $U_2 = \exp(i\pi t_2)$. Then the $G$-parity operator is defined as $G = C \cdot U_2$ with the value of the corresponding quantum number calculated from [190]

$$G = (-1)^{L+S+I} \tag{4.1}$$

where $I$ denotes the isospin. [Remember Eqs. (2.94) and (2.95) for the parity $P$ and the charge conjugation $C$.] The $G$-parity is defined in such a way that it possesses true eigenvectors, e.g., for pions

$$G\,|\pi^0\rangle = -|\pi^0\rangle, \tag{4.2}$$
$$G\,|\pi^+\rangle = -|\pi^+\rangle, \tag{4.3}$$
$$G\,|\pi^-\rangle = -|\pi^-\rangle, \tag{4.4}$$

unlike the charge conjugation that, per definition, flips the charge of the state concerned:

$$C\,|\pi^+\rangle = -|\pi^-\rangle, \tag{4.5}$$
$$C\,|\pi^-\rangle = -|\pi^+\rangle. \tag{4.6}$$

Note that the $G$-parity is also conserved under strong interactions. [It is slightly broken, e.g., in the decay $\omega(782) \to \pi^+\pi^-$ – the branching ratio is $\sim 1.53\%$ [10].]
Then we define the chiral partners as states that have the same quantum numbers with the exception of parity and $G$-parity – for example, the scalar states sigma and pion are chiral partners, see Eqs. (2.110) and (2.111). The particular version of the model constructed in this work will in addition also include vector mesons and their chiral partners, the axial-vectors. For example, the vector state $\rho$ and the axial-vector state $a_1$ are chiral partners [see Eqs. (2.112) and (2.113)]. Thus the existence of the chiral partners is a consequence of an exactly realised QCD chiral symmetry (see Sec. 2.5).

- *Extensions.* The linear sigma model can be extended straightforwardly to a larger number of flavours. This chapter will see the construction of a sigma model with two quark flavours (light quarks $u$ and $d$). The extension of the model to three flavours ($u$, $d$, $s$) will be presented in Chapters 6 – 11. The model can also be extended to four flavours ($u$, $d$, $s$, $c$) to account for the abundant meson spectrum around 2 GeV [191]. The extension of the model to include a scalar glueball state will be presented in Chapter 12. The model presented in this work contains mesons up to spin 1. It can, however, also be extended to include tensor mesons [192]. Additionally, the model can be extended to include a pseudoscalar glueball [191, 193], tetraquarks, i.e., $\bar{q}\bar{q}qq$ mesons [194] and the nucleon and its chiral partner [59, 195].

- *Non-zero temperatures and densities.* Although this thesis will be concerned with meson phenomenology in vacuum, the model can be readily extended to $T \neq 0 \neq \mu$ to study the chiral phase transition, the critical point of QCD or matter at finite densities [37, 194, 196, 197, 198].

A model based on QCD must, of course, implement features of the QCD Lagrangian demonstrated in Chapter 2. Let us summarise these features now.

- *Colour symmetry.* The $SU(3)_c$ gauge symmetry is one of the basic features of QCD. It is an exact symmetry of the QCD Lagrangian (see Sec. 2.2). In accordance with the confinement hypothesis, all the states in our model have to be colour-neutral. As we will be working with $\bar{q}q$ meson states, the confinement will be trivially fulfilled. Note, however, that the model will contain no order parameter for deconfinement.

- *Chiral symmetry.* As we have discussed in Sec. 2.5, the QCD Lagrangian with $N_f$ quark flavours possesses a $U(N_f)_L \times U(N_f)_R$ chiral symmetry. This symmetry is exact in the limit of vanishing quark masses and it has to be considered in any field theory or model based on QCD.

- *Spontaneous breaking of the chiral symmetry.* Experimental data in vacuum (and at sufficiently low temperatures and densities of matter) demonstrate that the chiral $U(N_f)_L \times U(N_f)_R \equiv U(1)_V \times U(1)_A \times SU(N_f)_V \times SU(N_f)_A$ symmetry is broken spontaneously by a

non-vanishing expectation value of the quark condensate (2.114): $\langle\bar{q}q\rangle = \langle\bar{q}_R q_L + \bar{q}_L q_R\rangle \neq 0$. As we have seen in Sec. 2.5, this symmetry breaking leads to the emergence of $N_f^2 - 1$ pseudoscalar Goldstone bosons. The scalar states representing the chiral partners of the Goldstone bosons remain massive. For $N_f = 2$, the three lightest meson states, the pions, are identified with these Goldstone bosons of QCD. They will be present as explicit degrees of freedom in our model (together with scalar, vector and axial-vector states).

- *Chiral anomaly.* As we have seen in Sec. 2.3, the $U(N_f)_L \times U(N_f)_R$ symmetry is broken by quantum effects to $U(1)_V \times SU(N_f)_V \times SU(N_f)_A$ [the $U(1)_A$ anomaly (2.60)]. The chiral-anomaly term will allow us to generate the splitting of mass between the pions and the $\eta$ meson (as well as $\eta'$ in Chapter 6).

- *Explicit breaking of the chiral symmetry.* The explicit breaking of the axial symmetry $SU(N_f)_A$ is due to non-zero quark masses. The vector symmetry $SU(N_f)_V$ is broken by non-zero, non-degenerate quark masses. Our model will therefore contain terms proportional to quark masses to implement this symmetry-breaking mechanism.

- $CPT$. QCD also possesses discrete symmetries such as charge conjugation ($C$), parity ($P$) and time reversal ($T$) symmetry ($CPT$), which are to a very good precision separately conserved by strong interactions. We have demonstrated in Sec. 2.4 that the $CP$-invariance is a feature of the QCD Lagrangian; therefore, according to the famous $CPT$ theorem (see Ref. [199] and references therein), QCD is also $T$-invariant. This fact offers further constraints in the construction of effective models of QCD as all the terms in such models have to be $CPT$ invariant.

In Chapter 5 we will study the $N_f = 2$ version of a linear sigma model which contains scalar ($\sigma_N$, $\boldsymbol{a}_0$) and pseudoscalar ($\eta_N$, $\boldsymbol{\pi}$), and in addition also vector ($\omega_N$, $\boldsymbol{\rho}$) and axial-vector ($f_{1N}$, $\boldsymbol{a}_1$) degrees of freedom. Usually, such models are constructed under the requirement of local chiral invariance $U(N_f)_R \times U(N_f)_L$, with the exception of the vector meson mass term which renders the local symmetry a global one [49, 53]. In a slight abuse of terminology, we will refer to these models as locally chirally invariant models in the following.
As shown in Refs. [49, 52, 53, 54, 57, 200], the locally invariant linear sigma model fails to simultaneously describe meson decay widths and pion-pion scattering lengths in vacuum. As outlined in Ref. [52], there are at least two ways to solve this issue. One way is to utilise a model in which the (up to the vector meson mass term) local invariance of the theory is retained while higher-order terms are added to the Lagrangian [49, 53, 200]. The second way which is pursued here is the following: we construct a **linear sigma model with *global* chiral invariance** containing all terms up to naive scaling dimension four [47], see also Ref. [201]. (Note that the chiral symmetry of the QCD Lagrangian is also a global one.) The global invariance allows for additional terms to appear in our Lagrangian in comparison to the locally invariant case presented, e.g., in Ref. [37]. (We remark that, introducing a dilaton field, one can argue [59, 202, 203] that chirally invariant terms of higher order than scaling dimension four should be absent. The consequences of the dilaton-field introduction will be discussed in Chapter 12.)
We have to distinguish between two possible assignments for the scalar fields $\sigma_N = (\bar{u}u + \bar{d}d)/\sqrt{2}$ and $a_0^0 = (\bar{u}u - \bar{d}d)/\sqrt{2}$:

- They may be identified with $f_0(600)$ and $a_0(980)$ which are members of a nonet that in addition consists of $f_0(980)$ and $K_0^\star(800)$.

- They may be identified with $f_0(1370)$ and $a_0(1450)$ which are members of a multiplet that also consists of $f_0(1500)$, $f_0(1710)$, and $K_0^\star(1430)$, where the additional scalar-isoscalar state emerges from the admixture of a glueball field [204, 205, 206, 207].

In the second assignment, scalar mesons below 1 GeV are not (predominantly) quark-antiquark states. Their spectroscopic wave functions might contain a dominant tetraquark or mesonic molecular contribution [58, 208, 209, 210, 211]. The correct assignment of the scalar quark-antiquark fields of the model to physical resonances is not only important as a contribution to the ongoing debate about the nature of these resonances, but it is also vital for a study of the properties of hadrons at nonzero temperature and density, where the chiral partner of the pion plays a crucial role [194].
It is important to stress that the theoretical $\sigma_N$ and $a_0$ fields entering the linear sigma model describe pure quark-antiquark states, just as all the other fields. This property can be easily proven by using well-known large-$N_c$ results (see Sec. 4.3 and Ref. [21]): the mass and the decay widths of both $\sigma_N$ and $a_0$ fields scale in the model as $N_c^0$ and $N_c^{-1}$, respectively.

## 4.2 The Lagrangian with Global Chiral Symmetry

In this section we conduct the construction of a linear sigma model with vector and axial-vector mesons in two flavours. The model is constructed based on the requirements from the QCD Lagrangian discussed in the previous section. This chapter will discuss the model construction in the meson sector; for a discussion regarding the model construction, e.g., in the nucleon sector, see Ref. [212].

We first note that all the states in our model will be hadrons, i.e., colour-neutral. Thus the confinement hypothesis and the $SU(3)_c$ colour symmetry of the QCD will be fulfilled per construction. Note, however, that the model parameters will depend on the number of colours ($N_c$), as discussed in Sec. 4.3.

The basic step in the construction of our model is the definition of the meson matrix

$$\Phi_{ij} \equiv \sqrt{2}\bar{q}_{j,R}q_{i,L}. \tag{4.7}$$

The equivalence sign in Eq. (4.7) states merely that $\Phi_{ij}$ and $\bar{q}_{j,R}q_{i,L}$ transform in the same manner under the (left-handed and right-handed) chiral groups. It is not to be comprehended as the statement that $\Phi_{ij}$ contains perturbative $\bar{q}q$ pairs as the matrix $\Phi_{ij}$ is a non-perturbative object. The reason is that the perturbative (*bare*) quarks are non-perturbatively modified in vacuum due to their strong interaction and the interaction with gluons. The ensuing non-perturbative (or constituent) quarks are then, in a good approximation, elements of the matrix $\Phi_{ij}$. It is actually possible to connect $\Phi_{ij}$ with the perturbative currents $\bar{q}_{j,R}q_{i,L}$ by rendering $\Phi_{ij}$ non-local:

$$\Phi_{ij} \equiv \sqrt{2}\int \mathrm{d}^4y\, \bar{q}_{j,R}\left(x+\frac{y}{2}\right) q_{i,L}\left(x-\frac{y}{2}\right) f(y) \tag{4.8}$$

where $f(y)$ denotes a non-perturbative vertex function and the perturbative limit is, of course, obtained by setting $f(y) = \delta(y)$. It is clear from Eq. (4.8) that the global flavour transformations are the same for the non-perturbative object $\Phi_{ij}$ and the perturbative quarks. Considering our

discussion in the previous section regarding the chiral symmetry and its breaking mechanisms, it is clear that the transformation behaviour of the objects in our model will be pivotal for the model construction. Thus given our interest in the transformation behaviour only, it is then sufficient to start with the equivalence $\Phi_{ij} \equiv \sqrt{2}\bar{q}_{j,R}q_{i,L}$.
Considering transformation properties of the quarks (2.32) and (2.33), we obtain immediately that the matrix $\Phi$ transforms as

$$\Phi \to U_L \Phi U_R^\dagger. \tag{4.9}$$

From Eqs. (4.7) and (2.19) we obtain

$$\begin{aligned}\Phi_{ij} &\equiv \sqrt{2}\bar{q}_{j,R}q_{i,L} = \sqrt{2}\bar{q}_j\mathcal{P}_L\mathcal{P}_L q_i = \sqrt{2}\bar{q}_j\mathcal{P}_L q_i \\ &= \frac{1}{\sqrt{2}}\left(\bar{q}_j q_i - \bar{q}_j\gamma^5 q_i\right) = \frac{1}{\sqrt{2}}\left(\bar{q}_j q_i + i\bar{q}_j i\gamma^5 q_i\right).\end{aligned} \tag{4.10}$$

Then comparing to Eqs. (2.96) and (2.100) we recognise the scalar current

$$S_{ij} \equiv \frac{1}{\sqrt{2}}\bar{q}_j q_i \tag{4.11}$$

and the pseudoscalar current

$$P_{ij} \equiv \frac{1}{\sqrt{2}}\bar{q}_j i\gamma^5 q_i. \tag{4.12}$$

In other words,

$$\Phi = S + iP. \tag{4.13}$$

Thus our matrix $\Phi$ is a combination of scalar and pseudoscalar currents. Additionally, the matrices $S$ and $P$ are hermitian and therefore they can be decomposed in terms of generators $t^a$ of a unitary group $U(N_f)$ with $a = 0, ..., N_f^2 - 1$:

$$S = S^a t^a, \tag{4.14}$$

$$P = P^a t^a, \tag{4.15}$$

where

$$S^a \equiv \sqrt{2}\bar{q}t^a q, \tag{4.16}$$

$$P^a \equiv \sqrt{2}\bar{q}i\gamma^5 t^a q. \tag{4.17}$$

As a first step toward the model construction, we consider only terms that implement the chiral symmetry exactly (note again that the symmetry is exact in the QCD Lagrangian as well up to the axial anomaly that is of quantum nature):

$$\mathcal{L}_{\text{sym.}} = \text{Tr}[(\partial^\mu\Phi)^\dagger(\partial_\mu\Phi)] - m_0^2\text{Tr}(\Phi^\dagger\Phi) - \lambda_1[\text{Tr}(\Phi^\dagger\Phi)]^2 - \lambda_2\text{Tr}(\Phi^\dagger\Phi)^2. \tag{4.18}$$

The Lagrangian in Eq. (4.18) is invariant under the transformation (4.9). This is the original version of the sigma model containing only scalar and pseudoscalar degrees of freedom. Note

that $\mathcal{L}_{\text{sym.}}$ contains only terms up to order four in the naive scaling dimension. Higher-order terms are usually discarded to preserve renormalisability of the model. However, the model is not valid up to arbitrary large scales (it is valid only up to the energy of the heaviest resonance incorporated into the model). For this reason, we consider an alternative criterion allowing us to constrain the order of terms considered in the Lagrangian. The criterion is the dilatation invariance rather than renormalisability. The dilatation invariance of the QCD Lagrangian has already been discussed in Sec. 2.4. In the language of our model where only composite states rather than partons are present, once a dilaton field $G$ has been included then only terms with dimensionless couplings are allowed in the Lagrangian in order that, in the chiral limit, the trace anomaly in the model is generated in the same manner as in the QCD Lagrangian [202, 203]; see also Chapter 12. Then terms of the form

$$\alpha[\text{Tr}(\Phi^\dagger\Phi)]^6 \tag{4.19}$$

are disallowed because the coupling $\alpha$ would possess dimension $[E^{-2}]$. The coupling $\alpha$ could actually be rendered dimensionless by modifying the mentioned term as

$$\frac{\alpha}{G^2}[\text{Tr}(\Phi^\dagger\Phi)]^6 \tag{4.20}$$

that would, however, lead to a singularity for $G \to 0$. Therefore, in the following, we will only consider terms up to order four in the fields.

The validity of our model is determined by the energy of the heaviest state present in the model. In Chapter 3, we will discuss the features of the physical scalar resonances that can in principle be assigned to the scalar states present in our model. These resonances possess energies up to $\sim 1.8$ GeV – thus they belong to an energy region where a multitude of vector and axial-vector states is experimentally established as well [10]. Additionally, (pseudo)scalars are known to interact with (axial-)vectors [10] and thus any realistic model of QCD should in principle contain as many as possible of all the mentioned states. For this reason, we need to extend the Lagrangian in Eq. (4.18) to include the (axial-)vector degrees of freedom. Indeed we will see in Sec. 5.3.2 that the inclusion of (axial-)vectors into our model necessitates the interpretation of scalars above (rather than below) 1 GeV as $\bar{q}q$ states.
We construct the vector and axial-vector matrices analogously to those in Eqs. (4.11) and (4.12). We first define the right-handed matrix

$$\begin{aligned} R^\mu_{ij} &\equiv \sqrt{2}\bar{q}_{j,R}\gamma^\mu q_{i,R} \overset{\text{Eq. (2.29)}}{=} \sqrt{2}q_j^\dagger\mathcal{P}_R\gamma^0\gamma^\mu\mathcal{P}_R q_i \overset{\text{Eq. (2.19)}}{=} \sqrt{2}q_j^\dagger\frac{1+\gamma_5}{2}\gamma^0\gamma^\mu\frac{1+\gamma_5}{2}q_i \\ &= \frac{\sqrt{2}}{4}(q_j^\dagger\gamma^0\gamma^\mu q_i + q_j^\dagger\gamma_5\gamma^0\gamma^\mu q_i + q_j^\dagger\gamma^0\gamma^\mu\gamma_5 q_i + q_j^\dagger\gamma_5\gamma^0\gamma^\mu\gamma_5 q_i) \\ &\overset{\text{Eq. (2.26)}}{=} \frac{1}{\sqrt{2}}\left(\bar{q}_j\gamma^\mu q_i - \bar{q}_j\gamma^5\gamma^\mu q_i\right) \end{aligned} \tag{4.21}$$

and the left-handed matrix

$$L^\mu_{ij} \equiv \sqrt{2}\bar{q}_{j,L}\gamma^\mu q_{i,L} = \frac{1}{\sqrt{2}}\left(\bar{q}_j\gamma^\mu q_i + \bar{q}_j\gamma^5\gamma^\mu q_i\right). \tag{4.22}$$

As in the case of currents from the QCD Lagrangian, we define

$$R^\mu = V^\mu - A^\mu, \tag{4.23}$$
$$L^\mu = V^\mu + A^\mu \tag{4.24}$$

and thus

$$V^\mu_{ij} \equiv \frac{1}{\sqrt{2}}\bar{q}_j\gamma^\mu q_i,\ A^\mu_{ij} \equiv \frac{1}{\sqrt{2}}\bar{q}_j\gamma^\mu\gamma^5 q_i \tag{4.25}$$

or, upon decomposition in terms of the $U(N_f)$ generators,

$$V^\mu = V^{\mu a}t^a, \tag{4.26}$$
$$A^\mu = A^{\mu a}t^a, \tag{4.27}$$

where

$$V^{\mu a} \equiv \sqrt{2}\bar{q}\gamma^\mu t^a q, \tag{4.28}$$
$$A^{\mu a} \equiv \sqrt{2}\bar{q}\gamma^\mu\gamma^5 t^a q. \tag{4.29}$$

With Eqs. (4.21), (4.22), (2.32) and (2.33), we obtain immediately that $R^\mu$ and $L^\mu$ transform as

$$R^\mu \to U_R R^\mu U_R^\dagger \tag{4.30}$$

and

$$L^\mu \to U_L L^\mu U_L^\dagger. \tag{4.31}$$

Let us define the right-handed field-strength tensor $R^{\mu\nu}$ and the left-handed field strength tensor $L^{\mu\nu}$ as

$$R^{\mu\nu} = \partial^\mu R^\nu - \partial^\nu R^\mu, \tag{4.32}$$
$$L^{\mu\nu} = \partial^\mu L^\nu - \partial^\nu L^\mu. \tag{4.33}$$

Then considering the transformation properties (4.9), (4.30) and (4.31) we can construct further chirally invariant terms containing both (pseudo)scalars and (axial-)vectors, up to order four in the fields:

$$\begin{aligned}
\mathcal{L}_{\text{sym.},1} = &-\frac{1}{4}\text{Tr}(L^2_{\mu\nu} + R^2_{\mu\nu}) + \text{Tr}\left[\frac{m_1^2}{2}(L^2_\mu + R^2_\mu)\right] \\
&+ i\frac{g_2}{2}(\text{Tr}\{L_{\mu\nu}[L^\mu, L^\nu]\} + \text{Tr}\{R_{\mu\nu}[R^\mu, R^\nu]\}) \\
&+ \frac{h_1}{2}\text{Tr}(\Phi^\dagger\Phi)\text{Tr}[(L^\mu)^2 + (R^\mu)^2] + h_2\text{Tr}[|L^\mu\Phi|^2 + |\Phi R^\mu|^2] + 2h_3\text{Tr}(\Phi R_\mu \Phi^\dagger L^\mu) \\
&+ g_3[\text{Tr}(L_\mu L_\nu L^\mu L^\nu) + \text{Tr}(R_\mu R_\nu R^\mu R^\nu)] + g_4[\text{Tr}\,(L_\mu L^\mu L_\nu L^\nu) + \text{Tr}\,(R_\mu R^\mu R_\nu R^\nu)] \\
&+ g_5\text{Tr}\,(L_\mu L^\mu)\ \text{Tr}\,(R_\nu R^\nu) + g_6[\text{Tr}(L_\mu L^\mu)\,\text{Tr}(L_\nu L^\nu) + \text{Tr}(R_\mu R^\mu)\,\text{Tr}(R_\nu R^\nu)].
\end{aligned} \tag{4.34}$$

The explicit symmetry breaking has to be modelled separately in the (pseudo)scalar and (axial-)vector channels. In the (pseudo)scalar sector we introduce the term

$$\mathcal{L}_{\text{ESB}} = \text{Tr}[H(\Phi + \Phi^\dagger)], \tag{4.35}$$

where

$$H = \text{diag}\left[h_0^1, h_0^2, ...h_0^{N_f}\right] \tag{4.36}$$

and $h_0^n$ is proportional to the mass of the $n^{\text{th}}$ quark flavour. Similarly, in the (axial-)vector channel we introduce the term

$$\mathcal{L}_{\text{ESB, 1}} = \text{Tr}\left[\Delta(L_\mu^2 + R_\mu^2)\right], \tag{4.37}$$

where

$$\Delta = \text{diag}\left[\delta_u, \delta_d, \delta_s...\right] \sim \text{diag}\left[m_u^2, m_d^2, m_s^2...\right]. \tag{4.38}$$

The chiral anomaly is usually modelled as [213]

$$\mathcal{L}_{\text{anomaly}} = c(\det\Phi + \det\Phi^\dagger) \tag{4.39}$$

because the determinant is invariant under $SU(N_f)_L \times SU(N_f)_R$ but not under $U(1)_A$. Note, however, that the chiral anomaly can also be modelled as

$$\mathcal{L}_{\text{anomaly, 1}} = c_1(\det\Phi - \det\Phi^\dagger)^2. \tag{4.40}$$

We will discuss the implications of the two anomaly terms in Sec. 6.4; only the term (4.39) will be used in the two-flavour version of our model (see Chapter 5).

Finally, for the modelling of the spontaneous breaking of the chiral symmetry, let us consider the (pseudo)scalar Lagrangian (4.18) along the axis $\Phi = \sigma_N t^0$:

$$\mathcal{V}_{\text{sym.}}(\sigma_N) = m_0^2\sigma_N^2 + (\lambda_1 + \lambda_2)\sigma_N^4. \tag{4.41}$$

The minimum $\sigma_N^{(0)} \neq 0$ for $m_0^2 < 0$. This implies spontaneous symmetry breaking because the vacuum is no longer symmetric under the axial transformation. Note that the scalar isosinglet state is the only one that can condense in the vacuum because that state is the only with the same quantum numbers as the vacuum ($J$, $P$, $C$ and $I$).

Then utilising the Lagrangians of Eqs. (4.18), (4.34), (4.35), (4.37) and (4.39) we construct the following meson Lagrangian for an arbitrary number of flavours $N_f$ and colours $N_c$:

$$\begin{aligned}
\mathcal{L} = {} & \text{Tr}[(D^\mu\Phi)^\dagger(D^\mu\Phi)] - m_0^2\text{Tr}(\Phi^\dagger\Phi) - \lambda_1[\text{Tr}(\Phi^\dagger\Phi)]^2 - \lambda_2\text{Tr}(\Phi^\dagger\Phi)^2 \\
& - \frac{1}{4}\text{Tr}(L_{\mu\nu}^2 + R_{\mu\nu}^2) + \text{Tr}\left[\left(\frac{m_1^2}{2} + \Delta\right)(L_\mu^2 + R_\mu^2)\right] + \text{Tr}[H(\Phi + \Phi^\dagger)] \\
& + c(\det\Phi + \det\Phi^\dagger) + i\frac{g_2}{2}(\text{Tr}\{L_{\mu\nu}[L^\mu, L^\nu]\} + \text{Tr}\{R_{\mu\nu}[R^\mu, R^\nu]\}) \\
& + \frac{h_1}{2}\text{Tr}(\Phi^\dagger\Phi)\text{Tr}[(L^\mu)^2 + (R^\mu)^2] + h_2\text{Tr}[|L^\mu\Phi|^2 + |\Phi R^\mu|^2] + 2h_3\text{Tr}(\Phi R_\mu\Phi^\dagger L^\mu) \\
& + g_3[\text{Tr}(L_\mu L_\nu L^\mu L^\nu) + \text{Tr}(R_\mu R_\nu R^\mu R^\nu)] + g_4[\text{Tr}\,(L_\mu L^\mu L_\nu L^\nu) + \text{Tr}\,(R_\mu R^\mu R_\nu R^\nu)] \\
& + g_5\text{Tr}\,(L_\mu L^\mu)\ \text{Tr}\,(R_\nu R^\nu) + g_6[\text{Tr}(L_\mu L^\mu)\,\text{Tr}(L_\nu L^\nu) + \text{Tr}(R_\mu R^\mu)\,\text{Tr}(R_\nu R^\nu)],
\end{aligned} \tag{4.42}$$

where

$$D^\mu \Phi = \partial^\mu \Phi - i g_1 (L^\mu \Phi - \Phi R^\mu). \tag{4.43}$$

The Lagrangian is invariant under $P$ and $C$ transformations. The (pseudo)scalar matrix $\Phi$ transforms under parity as

$$\Phi(t, \boldsymbol{x}) \xrightarrow{P} \Phi^\dagger(t, -\boldsymbol{x}). \tag{4.44}$$

This is due to Eq. (2.61) and the definition of $\Phi$, Eq. (2.61):

$$\begin{aligned}
\Phi_{ij}(t, \boldsymbol{x}) &\equiv \sqrt{2} \bar{q}_{j,R}(t, \boldsymbol{x}) q_{i,L}(t, \boldsymbol{x}) = \sqrt{2} q^\dagger_{j,R}(t, \boldsymbol{x}) \gamma^0 q_{i,L}(t, \boldsymbol{x}) \overset{\text{Eq. (2.29)}}{=} \sqrt{2} q^\dagger_j(t, \boldsymbol{x}) \mathcal{P}_R \gamma^0 \mathcal{P}_L q_i(t, \boldsymbol{x}) \\
&\xrightarrow{P} \sqrt{2} q^\dagger_j(t, -\boldsymbol{x}) \gamma^0 \mathcal{P}_R \gamma^0 \mathcal{P}_L \gamma^0 q_i(t, -\boldsymbol{x}) \overset{\text{Eq. (2.26)}}{=} \sqrt{2} q^\dagger_j(t, -\boldsymbol{x}) \mathcal{P}_L \gamma^0 \gamma^0 \gamma^0 \mathcal{P}_R q_i(t, -\boldsymbol{x}) \\
&= \sqrt{2} q^\dagger_{j,L}(t, -\boldsymbol{x}) \gamma^0 q_{i,R}(t, -\boldsymbol{x}) = \left[ \sqrt{2} q^\dagger_{j,L}(t, -\boldsymbol{x}) \gamma^0 q_{i,R}(t, -\boldsymbol{x}) \right]^\dagger \equiv \Phi^\dagger_{ij}(t, -\boldsymbol{x}).
\end{aligned} \tag{4.45}$$

Parity transforms the left-handed matrix $L^\mu$ into the right-handed matrix $R^\mu$ and vice versa:

$$R^\mu(t, \boldsymbol{x}) \xrightarrow{P} g^{\mu\nu} L_\nu(t, -\boldsymbol{x}), \tag{4.46}$$

$$L^\mu(t, \boldsymbol{x}) \xrightarrow{P} g^{\mu\nu} R_\nu(t, -\boldsymbol{x}), \tag{4.47}$$

due to Eq. (2.61) and the definitions (4.21) and (4.22):

$$\begin{aligned}
R^\mu_{ij} &\equiv \sqrt{2} \bar{q}_{j,R}(t, \boldsymbol{x}) \gamma^\mu q_{i,R}(t, \boldsymbol{x}) = \sqrt{2} q^\dagger_{j,R}(t, \boldsymbol{x}) \gamma^0 \gamma^\mu q_{i,R}(t, \boldsymbol{x}) \overset{\text{Eq. (2.29)}}{=} \sqrt{2} q^\dagger_j(t, \boldsymbol{x}) \mathcal{P}_R \gamma^0 \gamma^\mu \mathcal{P}_R q_i(t, \boldsymbol{x}) \\
&\xrightarrow{P} \sqrt{2} q^\dagger_j(t, -\boldsymbol{x}) \gamma^0 \mathcal{P}_R \gamma^0 \gamma^\mu \mathcal{P}_R \gamma^0 q_i(t, -\boldsymbol{x}) \overset{\text{Eq. (2.26)}}{=} \sqrt{2} q^\dagger_j(t, -\boldsymbol{x}) \mathcal{P}_L \gamma^0 \gamma^0 \gamma^\mu \gamma^0 \mathcal{P}_L q_i(t, -\boldsymbol{x}) \\
&= \sqrt{2} q^\dagger_{j,L}(t, -\boldsymbol{x}) \gamma^\mu \gamma^0 q_{i,L}(t, -\boldsymbol{x}) \overset{\text{Eq. (2.24)}}{=} \begin{cases} \bar{q}_{j,L}(t, -\boldsymbol{x}) \gamma^0 q_{i,L}(t, -\boldsymbol{x}) \text{ for } \mu = 0, \\ -\bar{q}_{j,L}(t, -\boldsymbol{x}) \gamma^k q_{i,L}(t, -\boldsymbol{x}) \text{ for } \mu = k \in \{1, 2, 3\} \end{cases}
\end{aligned} \tag{4.48}$$

and analogously for $L^\mu$.
The matrix $\Phi$ transforms under charge conjugation as

$$\Phi \xrightarrow{C} \Phi^t. \tag{4.49}$$

The proof is analogous to the calculation in Eq. (2.93). Similarly, the left-handed matrix $L^\mu$ and the right-handed matrix $R^\mu$ transform as:

$$R_\mu \xrightarrow{C} -L^t_\mu, \tag{4.50}$$

$$L_\mu \xrightarrow{C} R^t_\mu. \tag{4.51}$$

Then it is straightforward to demonstrate that all terms in the Lagrangian (4.42) fulfill $P$-invariance as well as $C$-invariance; given that the model is Lorentz-invariant, it is consequently also $T$-invariant [199].
Before we discuss the $N_f = 2$ and $N_f = 3$ applications of the Lagrangian (4.42), let us discuss the large-$N_c$ dependence of the model parameters.

### 4.3 Large-$N_c$ Behaviour of Model Parameters

It is important to determine the large-$N_c$ dependence of the model parameters for two reasons:

- It allows us to estimate the relative magnitudes of parameters (different parameters will possess different large-$N_c$ scaling because they may be associated to different vertices). In this way, parameters shown to be suppressed in comparison with other parameters may be set to zero.

- It enables us to prove that the states present in our model (up to the dilaton field introduced in Chapter 12) are indeed $\bar{q}q$ states. This is essential because the goal of this work is to study whether experimentally ascertained meson states can be interpreted as quarkonia. Such a study is, of course, only possible if the theoretical framework presented in this work already contains $\bar{q}q$ states that are to be assigned to physical states – and the success of the assignment is determined by comparison with experimental data.

The large-$N_c$ dependence of the parameters in Lagrangian (4.42) is [21]:

$$\begin{aligned} g_1,\, g_2 &\propto N_c^{-1/2}, \\ \lambda_2,\, h_2,\, h_3,\, g_3,\, g_4 &\propto N_c^{-1}, \\ \lambda_1,\, h_1,\, g_5,\, g_6 &\propto N_c^{-2}, \\ m_0^2,\, m_1^2,\, \delta_{u,d,s\ldots} &\propto N_c^0, \\ c &\propto N_c^{-N_f/2}, \\ h_0^i &\propto N_c^{1/2}. \end{aligned} \tag{4.52}$$

Let us remember that a vertex of $n$ quark-antiquark mesons scales as $N_c^{-(n-2)/2}$. As a consequence, the parameters $g_1$, $g_2$ scale as $N_c^{-1/2}$, because they are associated with a three-point vertex of quark-antiquark vector fields (of the kind $\rho^3$). This has already been discussed in Sec. 2.4, see Eq. (2.86).
Similarly, the parameters $\lambda_2$, $h_2$, $h_3$ scale as $N_c^{-1}$, because they are associated with quartic terms such as $\pi^4$ and $\pi^2\rho^2$. The parameters $\lambda_1$, $h_1$ also describe quartic interactions, but are further suppressed by a factor $1/N_c$ because of the trace structure of the corresponding terms in the Lagrangian. The quantities $m_0^2$, $m_1^2$ are bare-mass terms and therefore scale as $N_c^0$. Note that our mass terms will be proportional to the square of the pion and kaon decay constants $f_\pi$ and $f_K$ [see Eqs. (5.14) – (5.19) in the $N_f = 2$ case and Eqs. (6.32) – (6.45) in the $N_f = 3$ case]. Consequently, $f_\pi$ and $f_K$ have to scale as $N_c^{1/2}$.
The suppression of the parameter $c$ depends on the number of flavours and colours considered. The axial anomaly is suppressed in the large-$N_c$ limit. Note that $c$ possesses a dimension for $N_f \neq 4$. This is an exception to the rule illustrated via term (4.19) where we have discussed that only dimensionless couplings should appear in the Lagrangian. This is, however, not problematic because the chiral anomaly also stems from the gauge sector of the QCD Lagrangian, see Eq. (2.60). [Note that the chiral anomaly can also be modelled using an alternative term: $c_1(\det\Phi - \det\Phi^\dagger)^2$, see Eq. (6.1) and Sec. 6.4. In this case, $c_1 \propto N_c^{-N_f}$ holds.]

Note that without any assumptions about the fields, we immediately obtain that their masses scale as $N_c^0$ and their decay widths as $N_c^{-1}$, as we shall see in Chapters 5 – 11. Therefore, they must also correspond to quark-antiquark degrees of freedom.

# 5. Two-Flavour Linear Sigma Model

Having constructed a generic Lagrangian containing meson fields for an arbitrary number of flavours and colours, let us now discuss the implications of the Lagrangian for the case of two flavours (and, of course, three colours).

## 5.1 The $N_f = 2$ Lagrangian

The globally invariant $U(2)_L \times U(2)_R$ Lagrangian possesses the same structure as the one in Eq. (4.42):

$$\begin{aligned}
\mathcal{L} &= \mathrm{Tr}[(D^\mu\Phi)^\dagger(D^\mu\Phi)] - m_0^2\mathrm{Tr}(\Phi^\dagger\Phi) - \lambda_1[\mathrm{Tr}(\Phi^\dagger\Phi)]^2 - \lambda_2\mathrm{Tr}(\Phi^\dagger\Phi)^2 \\
&- \frac{1}{4}\mathrm{Tr}(L_{\mu\nu}^2 + R_{\mu\nu}^2) + \mathrm{Tr}\left[\left(\frac{m_1^2}{2} + \Delta\right)(L_\mu^2 + R_\mu^2)\right] + \mathrm{Tr}[H(\Phi + \Phi^\dagger)] \\
&+ c(\det\Phi + \det\Phi^\dagger) + i\frac{g_2}{2}(\mathrm{Tr}\{L_{\mu\nu}[L^\mu, L^\nu]\} + \mathrm{Tr}\{R_{\mu\nu}[R^\mu, R^\nu]\}) \\
&+ \frac{h_1}{2}\mathrm{Tr}(\Phi^\dagger\Phi)\mathrm{Tr}[(L^\mu)^2 + (R^\mu)^2] + h_2\mathrm{Tr}[|L^\mu\Phi|^2 + |\Phi R^\mu|^2] + 2h_3\mathrm{Tr}(\Phi R_\mu\Phi^\dagger L^\mu) \\
&+ g_3[\mathrm{Tr}(L_\mu L_\nu L^\mu L^\nu) + \mathrm{Tr}(R_\mu R_\nu R^\mu R^\nu)] + g_4[\mathrm{Tr}\,(L_\mu L^\mu L_\nu L^\nu) + \mathrm{Tr}\,(R_\mu R^\mu R_\nu R^\nu)] \\
&+ g_5\mathrm{Tr}\,(L_\mu L^\mu)\ \mathrm{Tr}\,(R_\nu R^\nu) + g_6[\mathrm{Tr}(L_\mu L^\mu)\,\mathrm{Tr}(L_\nu L^\nu) + \mathrm{Tr}(R_\mu R^\mu)\,\mathrm{Tr}(R_\nu R^\nu)]. \qquad (5.1)
\end{aligned}$$

In Eq. (5.1),

$$\Phi = (\sigma_N + i\eta_N)\,t^0 + (\boldsymbol{a}_0 + i\boldsymbol{\pi})\cdot\boldsymbol{t} \qquad (5.2)$$

contains scalar and pseudoscalar mesons, where $t^0$, $\boldsymbol{t}$ are the generators of $U(2)$ in the fundamental representation and $\eta_N$ denotes the non-strange content of the $\eta$ meson (more details will be given in Sec. 7.1). Vector and axial-vector mesons are contained in the left-handed and right-handed vector fields:

$$L^\mu = (\omega_N^\mu + f_{1N}^\mu)\,t^0 + (\boldsymbol{\rho}^\mu + \boldsymbol{a}_1^\mu)\cdot\boldsymbol{t}, \qquad (5.3)$$

$$R^\mu = (\omega_N^\mu - f_{1N}^\mu)\,t^0 + (\boldsymbol{\rho}^\mu - \boldsymbol{a}_1^\mu)\cdot\boldsymbol{t}, \qquad (5.4)$$

respectively. The covariant derivative

$$D^\mu\Phi = \partial^\mu\Phi - ig_1(L^\mu\Phi - \Phi R^\mu) - ieA^\mu[t^3, \Phi] \qquad (5.5)$$

couples scalar and pseudoscalar degrees of freedom to vector and axial-vector ones as well as to the electromagnetic field $A^\mu$. [The derivative leads to a kinetic term invariant under $U(2)_L \times U(2)_R$ and will allow us to calculate the decay width $\Gamma_{a_1\to\pi\gamma}$ in Eq. (5.75). For this reason it contains $A^\mu$, unlike the derivative in Eq. (4.43).] The left-handed and right-handed field strength tensors (again with $A^\mu$)

$$L^{\mu\nu} = \partial^\mu L^\nu - ieA^\mu[t^3, L^\nu] - \left\{\partial^\nu L^\mu - ieA^\nu[t^3, L^\mu]\right\}, \qquad (5.6)$$

$$R^{\mu\nu} = \partial^\mu R^\nu - ieA^\mu[t^3, R^\nu] - \left\{\partial^\nu R^\mu - ieA^\nu[t^3, R^\mu]\right\}, \qquad (5.7)$$

respectively, couple vector and axial-vector mesons to the electromagnetic field $A^\mu$. Explicit breaking of the global symmetry is described by the term $\mathrm{Tr}[H(\Phi+\Phi^\dagger)] \equiv h_{0N}\sigma$ ($h_{0N} = const.$) in the (pseudo)scalar sector and by the term $\mathrm{Tr}\left[\Delta(L_\mu^2 + R_\mu^2)\right]$ in the (axial-)vector channels, with $\Delta = diag(\delta_N, \delta_N)$ and $\delta_N \sim m_{u,d}^2$. The chiral anomaly is described by the term $c\,(\det\Phi + \det\Phi^\dagger)$, see Sec. 4.2. (Note that a slightly different form of the chiral-anomaly term will be utilised in Sec. 6.4.)

In the pseudoscalar and (axial-)vector sectors the identification of mesons with particles listed in Ref. [10] is straightforward, as already indicated in Eqs. (5.2) and (5.3)-(5.4): the fields $\boldsymbol{\pi}$ and $\eta_N$ correspond to the pion and the $SU(2)$ counterpart of the $\eta$ meson, $\eta_N \equiv (\bar{u}u + \bar{d}d)/\sqrt{2}$, with a mass of about 700 MeV. This value can be obtained by "unmixing" the physical $\eta$ and $\eta'$ mesons, which also contain $\bar{s}s$ contributions. The fields $\omega^\mu$ and $\boldsymbol{\rho}^\mu$ represent the $\omega(782)$ and $\rho(770)$ vector mesons, respectively, while the fields $f_{1N}^\mu$ and $\boldsymbol{a_1}^\mu$ represent the $f_1(1285)$ and $a_1(1260)$ axial-vector mesons, respectively. (In principle, the physical $\omega$ and $f_1$ states also contain $\bar{s}s$ contributions, however their admixture is negligibly small.) Unfortunately, the identification of the $\sigma_N$ and $\boldsymbol{a}_0$ fields is controversial, the possibilities being the pairs $\{f_0(600), a_0(980)\}$ and $\{f_0(1370), a_0(1450)\}$. As already mentioned, we will refer to these two assignments as Scenarios I and II, respectively. We discuss the implications of these two scenarios in the following.

The inclusion of (axial-)vector mesons in effective models of QCD has been done also in other ways than the one presented here. Vector and axial-vector mesons have been included in chiral perturbation theory in Ref. [214]. While the mathematical expressions for the interaction terms turn out to be similar to our results, in our linear approach the number of parameters is smaller. In Ref. [215] the so-called hidden gauge formalism is used to introduce vector mesons, and subsequently axial-vector mesons, into a chiral Lagrangian with a nonlinear realization of chiral symmetry. In this case the number of parameters is smaller. This approach is closely related to the locally chirally invariant models [49, 53] (also called massive Yang-Mills approaches). We refer also to Ref. [216], where a comparative analysis of effective chiral Lagrangians for spin-1 mesons is presented.

One may raise the question whether vector meson dominance (VMD) is still respected in the globally invariant linear sigma model (5.1). As outlined in Ref. [217], there are two ways to realize VMD in a linear sigma model. The standard version of VMD was introduced by Sakurai [218] and considers vector mesons as Yang-Mills gauge fields [24]; see also Ref. [54]. The gauge symmetry is explicitly broken by the vector meson masses. Another realization of VMD was first explored by Lurie [219] whose theory contained a Lagrangian which was globally invariant. It is interesting to note that Lurie's Lagrangian contained direct couplings of the photon to pions and $\rho$ mesons, as well as a $\rho$-$\pi$ coupling. It was shown in Ref. [217] that the two representations of VMD are equivalent if the $\rho$-$\pi$ coupling $g_{\rho\pi\pi}$ equals the photon-$\rho$ coupling $g_\rho$ (the so-called "universal limit"). It was also shown that, if the underlying theory is globally invariant, the pion form factor at threshold $F_\pi(q^2 = 0) = 1$ for *any* value of the above mentioned couplings. On the other hand, in Sakurai's theory $F_\pi(q^2 = 0) \neq 1$ unless one demands $g_{\rho\pi\pi} \stackrel{!}{=} g_\rho$, or other parameters are adjusted in such a way that $F_\pi(q^2 = 0) = 1$. In other words, for *any* globally invariant model, and thus also for ours, one has the liberty of choosing different values for the photon-$\rho$ and $\rho$-$\pi$ couplings, without violating VMD.

### 5.1.1 Tree-Level Masses

The Lagrangian (5.1) contains 16 parameters. However, the parameters $g_k$ with $k = 3, ..., 6$ are not relevant for the results presented here; additionally, the explicit symmetry breaking in the non-strange sector is negligible because the quark masses are small – therefore, we set $\delta_N = 0$. Then the number of undetermined parameters decreases to eleven:

$$m_0,\ \lambda_1,\ \lambda_2,\ m_1,\ g_1,\ g_2,\ c,\ h_{0N},\ h_1,\ h_2,\ h_3. \tag{5.8}$$

The squared tree-level masses of the mesons in our model contain a contribution arising from spontaneous symmetry breaking, proportional to $\phi_N^2$. The value $\phi_N$ is the vacuum expectation value of the $\sigma_N$ field and coincides with the minimum of the potential that follows from Eq. (5.1). The $\sigma_N$ field is the only field with the quantum numbers of the vacuum, $J^{PC} = 0^{++}$, i.e., the condensation of which does not lead to the breaking of parity, charge conjugation, and Lorentz invariance. The potential for the $\sigma_N$ field reads explicitly

$$V(\sigma_N) = \frac{1}{2}(m_0^2 - c)\sigma_N^2 + \frac{1}{4}\left(\lambda_1 + \frac{\lambda_2}{2}\right)\sigma_N^4 - h_{0N}\sigma_N, \tag{5.9}$$

and its minimum is determined by

$$0 = \left(\frac{\mathrm{d}V}{\mathrm{d}\sigma_N}\right)_{\sigma_N=\phi_N} = \left[m_0^2 - c + \left(\lambda_1 + \frac{\lambda_2}{2}\right)\phi_N^2\right]\phi_N - h_{0N}. \tag{5.10}$$

Spontaneous symmetry breaking corresponds to the case when the potential $V(\phi_N)$ assumes its minimum for a non-vanishing value $\sigma_N = \phi_N \neq 0$. In order to determine the fluctuation of the $\sigma_N$ field around the new vacuum, one shifts it by its vacuum expectation value $\phi_N \neq 0$, $\sigma_N \to \sigma_N + \phi_N$. The shift leads also to $\eta_N$-$f_1$ and $\boldsymbol{\pi}$-$\boldsymbol{a}_1$ mixing terms and thus to non-diagonal elements in the scattering matrix:

$$-g_1\phi_N(f_{1N}^\mu\partial_\mu\eta_N + \boldsymbol{a}_1^\mu\cdot\partial_\mu\boldsymbol{\pi}). \tag{5.11}$$

These terms are removed from the Lagrangian by shifting the $f_1$ and $\boldsymbol{a}_1$ fields as follows [220]:

$$\begin{aligned} &f_{1N}^\mu \to f_{1N}^\mu + Z_{\eta_N} w_{f_{1N}}\partial^\mu\eta_N,\ \ \boldsymbol{a}_1^\mu \to \boldsymbol{a}_1^\mu + Z_\pi w_{a_1}\partial^\mu\boldsymbol{\pi}, \\ &\eta_N \to Z_{\eta_N}\eta_N,\ \ \boldsymbol{\pi} \to Z_\pi\boldsymbol{\pi}, \end{aligned} \tag{5.12}$$

where we defined the quantities

$$w_{f_{1N}} = w_{a_1} = \frac{g_1\phi_N}{m_{a_1}^2},\quad Z_{\eta_N} = Z_\pi = \left(1 - \frac{g_1^2\phi_N^2}{m_{a_1}^2}\right)^{-1/2}. \tag{5.13}$$

More details on these calculations can be found in Ref. [220]; alternatively, see the analogous calculation performed in the $N_f = 3$ case later in this work (see Chapters 6 - 11). Note that the field renormalisation of $\eta_N$ and $\boldsymbol{\pi}$ guarantees the canonical normalisation of the kinetic terms. This is necessary in order to interpret the Fourier components of the properly normalized one-meson states as creation or annihilation operators [49]. Once the shift $\sigma_N \to \sigma_N + \phi_N$ and the transformations (5.12) have been performed, the mass terms of the mesons in the Lagrangian

(5.1) read:

$$m_{\sigma_N}^2 = m_0^2 - c + 3\left(\lambda_1 + \frac{\lambda_2}{2}\right)\phi_N^2, \tag{5.14}$$

$$m_{\eta_N}^2 = Z^2\left[m_0^2 + c + \left(\lambda_1 + \frac{\lambda_2}{2}\right)\phi_N^2\right] = m_\pi^2 + 2cZ_\pi^2, \tag{5.15}$$

$$m_{a_0}^2 = m_0^2 + c + \left(\lambda_1 + 3\frac{\lambda_2}{2}\right)\phi_N^2, \tag{5.16}$$

$$m_\pi^2 = Z^2\left[m_0^2 - c + \left(\lambda_1 + \frac{\lambda_2}{2}\right)\phi_N^2\right] \overset{(5.10)}{=} \frac{Z_\pi^2 h_{0N}}{\phi_N}, \tag{5.17}$$

$$m_{\omega_N}^2 = m_\rho^2 = m_1^2 + \frac{\phi_N^2}{2}(h_1 + h_2 + h_3), \tag{5.18}$$

$$m_{f_{1N}}^2 = m_{a_1}^2 = m_1^2 + g_1^2\phi_N^2 + \frac{\phi_N^2}{2}(h_1 + h_2 - h_3). \tag{5.19}$$

Note that the $\rho$ and $\omega_N$ masses as well as the $f_{1N}$ and $a_1$ masses are degenerate. In Sec. 5.6 we show the Lagrangian in the form when all shifts have been explicitly performed. From Eqs. (5.18) and (5.19) we obtain:

$$m_{a_1}^2 = m_\rho^2 + g_1^2\phi_N^2 - h_3\phi_N^2. \tag{5.20}$$

The pion decay constant $f_\pi$ is determined from the axial current,

$$J_{A_\mu}^a = \frac{\phi_N}{Z}\partial_\mu\pi^a + \ldots \equiv f_\pi\partial_\mu\pi^a + \ldots \quad \to \quad \phi_N = Zf_\pi. \tag{5.21}$$

Note that the photon coupling entailed in Eqs. (5.5), (5.6) and (5.7) yields the correct coupling of photons to pions as the corresponding term from the Lagrangian (5.1) reads

$$\begin{aligned}
\mathcal{L}_{\gamma\pi\pi} &= eZ_\pi^2(1 - g_1 w_{a_1}\phi_N)A^\mu\left(\pi^1\partial_\mu\pi^2 - \pi^2\partial_\mu\pi^1\right) \\
&\overset{w_{a_1}=g_1\phi_N/m_{a_1}^2}{=} eZ_\pi^2\frac{m_{a_1}^2 - (g_1\phi_N)^2}{m_{a_1}^2}A^\mu\left(\pi^1\partial_\mu\pi^2 - \pi^2\partial_\mu\pi^1\right) \\
&\equiv eZ_\pi^2 Z_\pi^{-2}A^\mu\left(\pi^1\partial_\mu\pi^2 - \pi^2\partial_\mu\pi^1\right) = eA^\mu\left(\pi^1\partial_\mu\pi^2 - \pi^2\partial_\mu\pi^1\right) \\
&= ieA^\mu(\pi^-\partial_\mu\pi^+ - \pi^+\partial_\mu\pi^-),
\end{aligned} \tag{5.22}$$

where in the last line we have substituted $\pi^1 = (\pi^+ + \pi^-)/\sqrt{2}$ and $\pi^2 = i(\pi^+ - \pi^-)/\sqrt{2}$. The photon-pion coupling is thus equal to the elementary electric charge $e = \sqrt{4\pi\alpha}$ where $\alpha$ denotes the fine-structure constant $\alpha = 1/137.035999679(94)$ in vacuum [10].

We note that the phenomenology of low-lying axial-vector mesons is also considered in approaches where the Bethe-Salpeter equation is used to unitarise the scattering of vector and pseudoscalar mesons – see, e.g., Ref. [221]. Here, the Bethe-Salpeter kernel is given by the lowest-order effective Lagrangian. This leads to the dynamical generation of resonances, one of which has a pole mass of 1011 MeV and is consequently assigned to the $a_1(1260)$ meson. This unitarised approach is used in Ref. [222] to study the large-$N_c$ behaviour of the dynamically generated resonances, with the conclusion that the $a_1(1260)$ resonance is not a genuine quark-antiquark state.
However, it was shown in Ref. [202] that, while unitarising the chiral Lagrangian by means of a Bethe-Salpeter study allows one to find poles in the complex plane and identify them with

physical resonances, it does not necessarily allow one to make a conclusion about the structure of those resonances in the large-$N_c$ limit. In order to be able to draw correct conclusions, a Bethe-Salpeter study requires at least one additional term of higher order not included in the Lagrangian of Refs. [221, 222]. Alternatively, the Inverse Amplitude Method of Ref. [83] can be used.

A very similar approach to the one in Refs. [221, 222] was also used in Ref. [223] where a very good fit to the $\tau$ decay data from the ALEPH collaboration [224] was obtained by fine-tuning the subtraction point of a loop diagram. Note, however, that detuning the subtraction point by 5% will spoil the agreement with experimental data. Alternately, these data may be described by approaches with the $a_1(1260)$ meson as an explicit degree of freedom, such as the one in Ref. [47], where $a_1(1260)$ is a quark-antiquark state and where the experimental $a_1(1260)$ spectral function is fitted very well. In Ref. [47], $m_{a_1(1260)} \simeq 1150$ MeV and a full width $\Gamma_{a_1(1260)} \simeq 410$ MeV are obtained. Note that our results, as will be shown later, give very good results on the $a_1(1260)$ phenomenology, for example in the $a_1(1260) \to \pi\gamma$ and $a_1(1260) \to \rho\pi$ decay channels, see Sec. 5.3.3.

For the following discussion, it is interesting to note that the $\rho$ meson mass can be split into two contributions:

$$m_\rho^2 = m_1^2 + \frac{\phi_N^2}{2}(h_1 + h_2 + h_3). \tag{5.23}$$

Without further assumptions, it is not possible to relate the quantity $m_1^2$ to microscopic condensates of QCD. However, invoking dilatation invariance, the term $m_1^2 \mathrm{Tr}[(L^\mu)^2 + (R^\mu)^2]/2$ in Eq. (5.1) arises from a term $aG^2\mathrm{Tr}[(L^\mu)^2+(R^\mu)^2]/2$ where $G$ is the dilaton field and $a$ a dimensionless constant [see Eq. (12.5) and Chapter 12]. Upon shifting the dilatation field by $G \to G_0 + G$, with $G_0$ being the gluon condensate, one obtains the term in our Lagrangian upon identifying $m_1^2 = aG_0^2$. Thus, the quantity $m_\rho^2$ in Eq. (5.23) is expressed as a sum of a term which is directly proportional to the gluon condensate $G_0$, and a term which is directly proportional to the chiral condensate $\phi_N^2$.

We shall require that none of the two contributions be negative: in fact, a negative $m_1^2 = aG_0^2$ would imply that the system is unstable when $\phi_N \to 0$; a negative $\phi_N^2(h_1 + h_2 + h_3)/2$ would imply that spontaneous chiral symmetry breaking decreases the $\rho$ mass. This is clearly unnatural because the breaking of chiral symmetry generates a sizable effective mass for the light quarks, which is expected to positively contribute to the meson masses. This positive contribution is a feature of all known models (such as the Nambu–Jona-Lasinio model and constituent quark approaches). Indeed, in an important class of hadronic models (see Ref. [225] and refs. therein) the only and obviously positive contribution to the $\rho$ mass is proportional to $\phi_N^2$ (i.e., $m_1 = 0$).

In the vacuum, the very occurrence of chiral symmetry breaking can be also traced back to the interaction with the dilaton field: in fact, the quantity $-m_0^2\mathrm{Tr}(\Phi^\dagger\Phi)$, where $m_0^2 < 0$, arises from a dilatation-invariant interaction term of the form $bG^2\mathrm{Tr}(\Phi^\dagger\Phi)$ upon the identification $m_0^2 = bG_0^2$ [see Eq. (12.5)]. This property also implies that the chiral condensate $\phi_N$ is proportional to the gluon condensate $G_0$, $\phi_N \sim G_0$. This means that the vacuum expression in Eq. (5.23) can be rewritten in the form $m_\rho^2 \sim \phi_N^2$, which resembles the KSFR relation [226]. However, the quantities $G_0$ are $\phi_N$ may vary independently from each other at nonzero temperature and density, thus generating a nontrivial behaviour of $m_\rho^2$.

### 5.1.2 Equivalent Set of Parameters

Instead of the eleven parameters in Eq. (5.8), it is technically simpler to use the following, equivalent set of eleven parameters in the expressions for the physical quantities:

$$m_\pi,\, m_{\sigma_N},\, m_{a_0},\, m_{\eta_N},\, m_\rho,\, m_{a_1},\, Z_\pi,\, \phi_N,\, g_2,\, h_1,\, h_2. \tag{5.24}$$

The quantities $m_\pi$, $m_\rho$, $m_{a_1}$ are taken as the mean values of the masses of the $\pi$, $\rho$, and $a_1$ meson, respectively, as given by the PDG [10]: $m_\pi = 139.57$ MeV, $m_\rho = 775.49$ MeV, and $m_{a_1} = 1230$ MeV. While $m_\pi$ and $m_\rho$ are measured to very good precision, this is not the case for $m_{a_1}$. The mass value given above is referred to as an "educated guess" by the PDG [10]. Therefore, we shall also consider a smaller value, as suggested e.g. by the results of Ref. [47]. We shall see that, although the overall picture remains qualitatively unchanged, the description of the decay width of $a_1$ into $\rho\pi$ can be substantially improved.
As outlined in Ref. [57], the mass of the $\eta_N$ meson can be calculated using the mixing of strange and non-strange contributions in the physical fields $\eta$ and $\eta'(958)$:

$$\eta = \eta_N \cos\varphi_\eta + \eta_S \sin\varphi_\eta,\; \eta' = -\eta_N \sin\varphi_\eta + \eta_S \cos\varphi_\eta, \tag{5.25}$$

where $\eta_S$ is a pure $\bar{s}s$ state and $\varphi_\eta \simeq -36°$ [227]. (A detailed discussion of the $\eta_N$-$\eta_S$ mixing will be presented in Sec. 7.1, i.e., in the $N_f = 3$ version of our model where the pure-strange field $\eta_S$ will be included as an explicit degree of freedom.) In this way, we obtain the value $m_{\eta_N} = 716$ MeV. Given the well-known uncertainty of the value of $\varphi_\eta$, one could also consider other values, e.g., $\varphi_\eta = -41.4°$, as published by the KLOE Collaboration [228]. In this case, $m_{\eta_N} = 755$ MeV. The variation of the $\eta_N$ mass does not change the results significantly.
The quantities $\phi_N$ and $Z_\pi$ are linked to the pion decay constant as $\phi_N/Z_\pi = f_\pi = 92.4$ MeV. Therefore, the following six quantities remain as free parameters:

$$m_{\sigma_N},\, m_{a_0},\, Z_\pi,\, g_2,\, h_1,\, h_2. \tag{5.26}$$

The masses $m_{\sigma_N}$ and $m_{a_0}$ depend on the scenario adopted for the scalar mesons.
At the end of this subsection we report three useful formulas which link the parameters $g_1$, $h_3$, and $m_1$ of the original set (5.8) to the second set of parameters (5.24) [see also Eq. (5.13)]:

$$g_1 = g_1(Z_\pi) = \frac{m_{a_1}}{Z_\pi f_\pi}\sqrt{1 - \frac{1}{Z_\pi^2}}, \tag{5.27}$$

$$h_3 = h_3(Z_\pi) = \frac{m_{a_1}^2}{Z_\pi^2 f_\pi^2}\left(\frac{m_\rho^2}{m_{a_1}^2} - \frac{1}{Z_\pi^2}\right), \tag{5.28}$$

$$m_1^2 = m_1^2(Z_\pi, h_1, h_2) = \frac{1}{2}\left[m_\rho^2 + m_{a_1}^2 - Z_\pi^2 f_\pi^2\left(g_1^2 + h_1 + h_2\right)\right]. \tag{5.29}$$

## 5.2 Decay Widths and $\pi\pi$ Scattering Lengths

In this section, we calculate the formulas for the decay widths and the $\pi\pi$ scattering lengths and specify their dependence on the parameters $m_\sigma$, $m_{a_0}$, $Z_\pi$, $g_2$, $h_1$, and $h_2$. Using the scaling behaviour (4.52) we obtain that all strong decays and scattering lengths scale as $N_c^{-1}$, as expected. The decay widths are calculated from the interaction part of the Lagrangian (5.1).

For future use we introduce the momentum function

$$k(m_a, m_b, m_c) = \frac{1}{2m_a}\sqrt{m_a^4 - 2m_a^2\,(m_b^2 + m_c^2) + (m_b^2 - m_c^2)^2}\theta(m_a - m_b - m_c). \tag{5.30}$$

In the decay process $a \to b+c$, with masses $m_a$, $m_b$, $m_c$, respectively, the quantity $k(m_a, m_b, m_c)$ represents the modulus of the three-momentum of the outgoing particles $b$ and $c$ in the rest frame of the decaying particle $a$. The theta function ensures that the decay width vanishes below threshold.

### 5.2.1 Decay Width $\rho \to \pi\pi$

The $\rho\pi\pi$ interaction Lagrangian obtained from Eq. (5.1) reads

$$\mathcal{L}_{\rho\pi\pi} = A_{\rho\pi\pi}\,(\partial_\mu \boldsymbol{\pi}) \cdot (\boldsymbol{\rho}^\mu \times \boldsymbol{\pi}) + B_{\rho\pi\pi}\,(\partial_\mu \boldsymbol{\rho}_\nu) \cdot (\partial^\mu \boldsymbol{\pi} \times \partial^\nu \boldsymbol{\pi})\,. \tag{5.31}$$

with the following coefficients

$$A_{\rho\pi\pi} = Z_\pi^2\,[g_1(1 - g_1 w_{a_1}\phi_N) + h_3 w_{a_1}\phi_N] \equiv Z_\pi^2 g_1 \frac{m_\rho^2}{m_{a_1}^2}, \tag{5.32}$$

$$B_{\rho\pi\pi} = -Z_\pi^2 g_2 w_{a_1}^2. \tag{5.33}$$

Let us consider the decay of $\rho^0$ only; the decays of the charged states are calculated analogously and possess the same values because of the isospin symmetry that is manifest in our model. The third $\rho$ component possesses the following interaction Lagrangian

$$\mathcal{L}_{\rho^0\pi\pi} = iA_{\rho\pi\pi}\rho_\mu^0\left(\pi^-\partial^\mu\pi^+ - \pi^+\partial^\mu\pi^-\right) + iB_{\rho\pi\pi}\partial_\nu\rho_\mu^0\left(\partial^\nu\pi^-\partial^\mu\pi^+ - \partial^\nu\pi^+\partial^\mu\pi^-\right). \tag{5.34}$$

Let us denote the momenta of $\rho$, $\pi^+$ and $\pi^-$ as $P$, $P_1$ and $P_2$, respectively. The $\rho$ meson is a vector state for which we have to consider the polarisation vector labelled as $\varepsilon_\mu^{(\alpha)}(P)$.

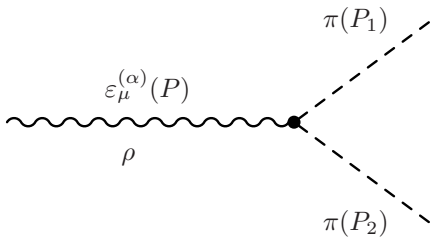


**Figure 5.1:** Decay process $\rho \to \pi\pi$.

Then, upon substituting $\partial^\mu \to -iP^\mu$ for the decaying particle and $\partial^\mu \to iP_{1,2}^\mu$ for the decay products, we obtain the following Lorentz-invariant $\rho\pi\pi$ scattering amplitude $-i\mathcal{M}_{\rho^0\to\pi\pi}^{(\alpha)}$ from the Lagrangian (5.34):

$$-i\mathcal{M}_{\rho^0\to\pi\pi}^{(\alpha)} = \varepsilon_\mu^{(\alpha)}(P)h_{\rho\pi\pi}^\mu = \varepsilon_\mu^{(\alpha)}(P)[A_{\rho\pi\pi}(P_2^\mu - P_1^\mu) + B_{\rho\pi\pi}P_\nu(P_2^\mu P_1^\nu - P_1^\mu P_2^\nu)], \tag{5.35}$$

where

$$h_{\rho\pi\pi}^\mu = A_{\rho\pi\pi}(P_2^\mu - P_1^\mu) + B_{\rho\pi\pi}P_\nu(P_2^\mu P_1^\nu - P_1^\mu P_2^\nu). \tag{5.36}$$

denotes the $\rho\pi\pi$ vertex.
The vertex can be transformed in the following way:

$$h^{\mu}_{\rho\pi\pi} = A_{\rho\pi\pi}(P_2^{\mu} - P_1^{\mu}) + B_{\rho\pi\pi}P_{\nu}(P_2^{\mu}P_1^{\nu} - P_1^{\mu}P_2^{\nu}) = A_{\rho\pi\pi}(P_2^{\mu} - P_1^{\mu}) + B_{\rho\pi\pi}\frac{m_{\rho}^2}{2}(P_2^{\mu} - P_1^{\mu})$$
$$= \left(A_{\rho\pi\pi} + B_{\rho\pi\pi}\frac{m_{\rho}^2}{2}\right)(P_2^{\mu} - P_1^{\mu}), \tag{5.37}$$

where the equality $P_{\mu}P_1^{\mu} = P_{\mu}P_2^{\mu} = m_{\rho}^2/2$ was used. The calculation of the decay width will require the determination of the square of the scattering amplitude. Given that the scattering amplitude in Eq. (5.35) depends on the polarisation vector $\varepsilon_{\mu}^{(\alpha)}(P)$, it is necessary to calculate the average of the amplitude for all values of $\varepsilon_{\mu}^{(\alpha)}(P)$. For a general scattering amplitude $-i\mathcal{M}^{(\alpha)} = \varepsilon_{\mu}^{(\alpha)}(P)h^{\mu}$ of a process containing one vector state with mass $m$, the calculation reads as follows:

$$-i\mathcal{M}^{(\alpha)} = \varepsilon_{\mu}^{(\alpha)}(P)h^{\mu} \Rightarrow |-i\bar{\mathcal{M}}|^2 = \frac{1}{3}\sum_{\alpha=1}^{3}|-i\mathcal{M}^{(\alpha)}|^2 = \frac{1}{3}\sum_{\alpha=1}^{3}\varepsilon_{\mu}^{(\alpha)}(P)h^{\mu}\varepsilon_{\nu}^{(\alpha)}(P)h^{\nu}$$
$$= \frac{1}{3}\sum_{\alpha=1}^{3}\varepsilon_{\mu}^{(\alpha)}(P)\varepsilon_{\nu}^{(\alpha)}(P)h^{\mu}h^{\nu} = \frac{1}{3}\left(-g_{\mu\nu} + \frac{P_{\mu}P_{\nu}}{m^2}\right)h^{\mu}h^{\nu} = \frac{1}{3}\left[-(h^{\mu})^2 + \frac{(P_{\mu}h^{\mu})^2}{m^2}\right], \tag{5.38}$$

where, in the second line of Eq. (5.38), we have used

$$\sum_{\alpha=1}^{3}\varepsilon_{\mu}^{(\alpha)}(P)\varepsilon_{\nu}^{(\alpha)}(P) = -g_{\mu\nu} + \frac{P_{\mu}P_{\nu}}{m^2}. \tag{5.39}$$

Equation (5.38) contains the metric tensor $g_{\mu\nu} = \mathrm{diag}(1, -1 - 1, -1)$. Note that, if the vector particle decays, then $P_{\mu} = (P_0, \mathbf{0})$ in the rest frame of the decaying particle and thus

$$\frac{(P_{\mu}h^{\mu})^2}{m^2} \equiv \frac{(P_0h^0)^2}{m^2} = \frac{m^2(h^0)^2}{m^2} = (h^0)^2. \tag{5.40}$$

It is clear that in our case $h^0_{\rho\pi\pi} = 0$, see Eq. (5.37). Therefore we only have to determine $(h^{\mu}_{\rho\pi\pi})^2$:

$$(h^{\mu}_{\rho\pi\pi})^2 = \left(A_{\rho\pi\pi} + B_{\rho\pi\pi}\frac{m_{\rho}^2}{2}\right)^2\left(m_{\pi}^2 + m_{\pi}^2 - 2P_1P_2\right) = \left(A_{\rho\pi\pi} + B_{\rho\pi\pi}\frac{m_{\rho}^2}{2}\right)^2\left(4m_{\pi}^2 - m_{\rho}^2\right). \tag{5.41}$$

Inserting Eq. (5.41) into Eq. (5.38) yields

$$|-i\bar{\mathcal{M}}_{\rho^0\to\pi\pi}|^2 = \frac{1}{3}\left(A_{\rho\pi\pi} + B_{\rho\pi\pi}\frac{m_{\rho}^2}{2}\right)^2\left(4m_{\pi}^2 - m_{\rho}^2\right)$$
$$= \frac{4}{3}\left(A_{\rho\pi\pi} + B_{\rho\pi\pi}\frac{m_{\rho}^2}{2}\right)^2 k^2(m_{\rho}, m_{\pi}, m_{\pi}), \tag{5.42}$$

where in the second line we have used Eq. (5.30).
Finally, the full decay width reads

$$\Gamma_{\rho\to\pi\pi} = \frac{k(m_\rho, m_\pi, m_\pi)}{8\pi m_\rho^2} |-i\bar{\mathcal{M}}_{\rho^0\to\pi\pi}| = \frac{k^3(m_\rho, m_\pi, m_\pi)}{6\pi m_\rho^2} \left( A_{\rho\pi\pi} + B_{\rho\pi\pi} \frac{m_\rho^2}{2} \right)^2 . \tag{5.43}$$

Note that the formula presented in Eq. (5.43) can be transformed further using Eqs. (5.30), (5.32) and (5.33); we make explicit the dependence of the decay width on the parameters $Z_\pi$ and $g_2$:

$$\Gamma_{\rho\to\pi\pi}(Z_\pi, g_2) = \frac{m_\rho^5}{48\pi m_{a_1}^4} \left[ 1 - \left( \frac{2m_\pi}{m_\rho} \right)^2 \right]^{3/2} \left[ g_1 Z_\pi^2 + \left( 1 - Z_\pi^2 \right) \frac{g_2}{2} \right]^2 . \tag{5.44}$$

The experimental value is $\Gamma^{\text{exp}}_{\rho\to\pi\pi} = (149.1 \pm 0.8)$ MeV [10]. The small experimental error can be neglected and the central value is used as a further constraint allowing us to fix the parameter $g_2$ as function of $Z_\pi$:

$$g_2 = g_2(Z_\pi) = \frac{2}{Z_\pi^2 - 1} \left( g_1 Z_\pi^2 \pm \frac{4m_{a_1}^2}{m_\rho} \sqrt{\frac{3\pi\Gamma^{\text{exp}}_{\rho\to\pi\pi}}{(m_\rho^2 - 4m_\pi^2)^{3/2}}} \right) . \tag{5.45}$$

Note that all input values in Eq. (5.45) are experimentally known [10]. The parameter $g_1 = g_1(Z_\pi)$ is fixed via Eq. (5.27).
As apparent from Eq. (5.45), two solutions for $g_2$ are obtained. The solution with the positive sign in front of the square root may be neglected because it leads to unphysically large values for the $a_1 \to \rho\pi$ decay width, which is another quantity predicted by our study that also depends on $g_2$ [see Eq. (5.95)]. For example, the value $Z_\pi = 1.6$ (see below) would lead to $g_2 \cong 40$ which in turn would give $\Gamma_{a_1\to\rho\pi} \cong 14$ GeV – clearly an unphysically large value. Therefore, we will take the solution for $g_2$ with the negative sign in front of the square root. In this case, reasonable values for both $g_2$ (see Table 5.1) and $\Gamma_{a_1\to\rho\pi}$ (see Sec. 5.2.7) are obtained.

### 5.2.2 Decay Width $f_1(1285) \to a_0\pi$

The $f_{1N}a_0\pi$ interaction Lagrangian from Eq. (5.1) reads

$$\mathcal{L}_{f_{1N}a_0\pi} = A_{f_{1N}a_0\pi} f_{1N}^\mu \left( \partial_\mu \boldsymbol{\pi} \cdot \boldsymbol{a}_0 \right) + B_{f_{1N}a_0\pi} f_{1N}^\mu \left( \partial_\mu \boldsymbol{a}_0 \cdot \boldsymbol{\pi} \right) \tag{5.46}$$

with the following coefficients:

$$A_{f_{1N}a_0\pi} = Z_\pi g_1 (2 g_1 w_{a_1} \phi_N - 1) + Z_\pi w_{a_1} (h_2 - h_3) \phi_N , \tag{5.47}$$

$$B_{f_{1N}a_0\pi} = Z_\pi g_1 . \tag{5.48}$$

The decay width of an axial-vector into a scalar and a pseudoscalar has already been considered in Sec. 2.6.3; the obtained formula for the decay width from Eq. (2.200) can be used here with $I = 3$:

$$\Gamma_{f_{1N}\to a_0\pi} = \frac{k^3(m_{f_{1N}}, m_{a_0}, m_\pi)}{8\pi m_{f_{1N}}^2} (A_{f_{1N}a_0\pi} - B_{f_{1N}a_0\pi})^2 . \tag{5.49}$$

Using Eqs. (5.30), (5.47) and (5.48), Eq. (5.49) can be transformed as follows (we make explicit the dependence on $Z_\pi$ and $h_2$):

$$\Gamma_{f_{1N}\to a_0\pi}(m_{a_0}, Z_\pi, h_2) = \frac{g_1^2 Z_\pi^2}{2\pi} \frac{k^3(m_{f_{1N}}, m_{a_0}, m_\pi)}{m_{f_{1N}}^2 m_{a_1}^4} \left[ m_\rho^2 - \frac{1}{2}(h_2 + h_3)\phi_N^2 \right]^2 . \tag{5.50}$$

There is a subtle point to comment on here. When the quark-antiquark $a_0$ state of our model is identified as the $a_0(980)$ meson of the PDG compilation (Scenario I, Sec. 5.3), then this decay width can be used to fix the parameter $h_2$ as function of $Z_\pi$, $h_2 \equiv h_2(Z_\pi)$, by using the corresponding experimental value $\Gamma^{\rm exp}_{f_{1N}\to a_0\pi} = (8.748 \pm 2.097)$ MeV [10].

$$h_2 = h_2(Z_\pi) = \frac{2}{\phi_N^2} \left( m_\rho^2 - \frac{h_3}{2}\phi_N^2 \pm \frac{m_{f_{1N}} m_{a_0}^2}{g_1 Z_\pi} \sqrt{\frac{2\pi \Gamma^{\rm exp}_{f_{1N}\to a_0\pi}}{k^3(m_{f_{1N}}, m_{a_0}, m_\pi)}} \right) . \tag{5.51}$$

Again, there are two solutions, just as in the case of the parameter $g_2$. How strongly the somewhat uncertain experimental value of $\Gamma_{f_{1N}\to a_0\pi}$ influences the possible values of $h_2$, depends on the choice of the sign in front of the square root in Eq. (5.51). Varying $\Gamma_{f_{1N}\to a_0\pi}$ within its experimental range of uncertainty changes the value of $h_2$ by an average of 25% if the negative sign is chosen, but the same variation of $\Gamma_{f_{1N}\to a_0\pi}$ changes $h_2$ by an average of only 6% if the positive sign is considered. This is due to the fact that the solution with the positive square root sign yields larger values of $h_2 \sim 80$, while the solution with the negative sign leads to $h_2 \sim 20$. The absolute change of $h_2$ is the same in both cases. Our calculations have shown that using the negative sign in front of the square root yields a too small value of the $\eta$-$\eta'$ mixing angle $\varphi \cong -9°$. This follows by inserting $h_2$ into Eq. (5.65) so that it is removed as a degree of freedom (i.e., replaced by $Z_\pi$) and calculating the mixing angle $\varphi_\eta$ from Eq. (5.59) using the experimental value of the $a_0 \to \eta\pi$ decay amplitude from Ref. [114]. For this reason, we only use the positive sign in front of the square root in Eq. (5.51), i.e., the constraint leading to higher values of $h_2$. Then $\varphi_\eta \cong -41.8°$ is obtained, in very good agreement with the central value quoted by the KLOE collaboration [228], $\varphi_\eta \cong -41.4°$ (see also Sec. 5.3.1).
It may be interesting to note that only the (disregarded) lower value of $h_2$ leads to the expected behaviour of the parameter $h_1$ which [according to Eq. (4.52)] should be large-$N_c$ suppressed: the lower value of $h_2$ yields $h_1 = 1.8$ whereas the higher value of $h_2$ yields $h_1 = -68$ (see Table 5.1).
Note that if the quark-antiquark $a_0$ meson of our model is identified as the $a_0(1450)$ meson of the PDG compilation (Scenario II, Sec. 5.4) then the described procedure of replacing $h_2$ by $Z_\pi$ using Eq. (5.51) is no longer applicable because the decay $f_{1N} \to a_0\pi$ is kinematically not allowed and its counterpart $a_0 \to f_{1N}\pi$ has not been measured.

### 5.2.3 Decay Width $\sigma_N \to \pi\pi$

The interaction Lagrangian of the scalar state $\sigma_N$ with the pions from Eq. (5.1) reads:

$$\mathcal{L}_{\sigma_N\pi\pi} = A_{\sigma_N\pi\pi}\sigma_N \boldsymbol{\pi}^2 + B_{\sigma_N\pi\pi}\sigma_N \partial_\mu \boldsymbol{\pi}^2 + C_{\sigma_N\pi\pi}\sigma_N \boldsymbol{\pi}\Box\boldsymbol{\pi} \tag{5.52}$$

with

$$A_{\sigma_N\pi\pi} = -\left(\lambda_1 + \frac{\lambda_2}{2}\right) Z_\pi^2 \phi_N, \tag{5.53}$$

$$B_{\sigma_N\pi\pi} = -2g_1 Z_\pi^2 w_{a_1} + \left(g_1^2 + \frac{h_1+h_2-h_3}{2}\right) Z_\pi^2 w_{a_1}^2 \phi_N, \tag{5.54}$$

$$C_{\sigma_N\pi\pi} = -g_1 Z_\pi^2 w_{a_1}. \tag{5.55}$$

The corresponding decay amplitude reads

$$-i\mathcal{M}_{\sigma_N\to\pi\pi}(m_{\sigma_N}) = i\left(A_{\sigma_N\pi\pi} - B_{\sigma_N\pi\pi}\frac{m_{\sigma_N}^2 - 2m_\pi^2}{2} - C_{\sigma_N\pi\pi}m_\pi^2\right) \tag{5.56}$$

and, consequently, summing over all decay channels $\sigma_{1,2} \to \pi^0\pi^0, \pi^\pm\pi^\mp$ we obtain the following formula for the decay width $\Gamma_{\sigma_N\to\pi\pi}$:

$$\Gamma_{\sigma_N\to\pi\pi} = \frac{3k(m_{\sigma_N}, m_\pi, m_\pi)}{4\pi m_{\sigma_N}^2} |-i\mathcal{M}_{\sigma_N\to\pi\pi}(m_{\sigma_N})|^2. \tag{5.57}$$

Note that, using Eqs. (5.30) and (5.53) - (5.55), we can transform Eq. (5.57) as follows (we make explicit the dependence on free parameters):

$$\Gamma_{\sigma_N\to\pi\pi}(m_{\sigma_N}, Z_\pi, h_1, h_2) = \frac{3}{32\pi m_{\sigma_N}}\sqrt{1-\left(\frac{2m_\pi}{m_{\sigma_N}}\right)^2}\left\{\frac{m_{\sigma_N}^2 - m_\pi^2}{Z_\pi f_\pi}\right.$$
$$\left. -\frac{g_1^2 Z_\pi^3 f_\pi}{m_{a_1}^4}\left[m_\rho^2 - \frac{\phi_N^2}{2}(h_1+h_2+h_3)\right](m_{\sigma_N}^2 - 2\,m_\pi^2)\right\}^2. \tag{5.58}$$

It is apparent from Eqs. (4.52) that the sigma decay width decreases as the number of colors $N_c$ increases. Thus, the sigma field in our model is a $\bar{q}q$ state [83]. In Scenario I, Sec. 5.3, we have assigned the $\sigma_N$ field as $f_0(600)$, correspondingly we are working with the assumption that $f_0(600)$ [as well as $a_0(980)$] is a $\bar{q}q$ state. In Scenario II, Sec. 5.4, the same assumption is valid for the $f_0(1370)$ and $a_0(1450)$ states.

Note that in Eq. (9.27) the first term in braces arises from the scalar $\sigma_N\pi\pi$ vertex, while the second term comes from the coupling of the $\sigma_N$ to the $a_1$, which becomes a derivatively coupled pion after the shift (5.12). Because of the different signs, these two terms interfere destructively. As the decay width of a light $\sigma_N$ meson into two pions can be very well reproduced in the linear sigma model without vector mesons (corresponding to the case $g_1 \to 0$), this interference prevents obtaining a reasonable value for this decay width in the present model *with (axial-)vector mesons*, see Sec. 5.3.2. This problem does not occur for a heavy $\sigma_N$ meson, see Sec. 5.4.2 and Ref. [55].

### 5.2.4 Decay Amplitudes $a_0 \to \eta\pi$ and $a_0 \to \eta'\pi$

Our $N_f = 2$ Lagrangian (5.1) contains the unphysical field $\eta_N$. However, by making use of Eq. (7.23) and invoking the OZI rule, it is possible to calculate the decay amplitude for the physical process $a_0 \to \eta\pi$ as

$$-i\mathcal{M}_{a_0\eta\pi} = \cos\varphi(-i\mathcal{M}_{a_0\eta_N\pi}). \tag{5.59}$$

The following $a_0^0\eta_N\pi^0$ interaction Lagrangian is obtained from Eq. (5.1):

$$\mathcal{L}_{a_0\eta_N\pi} = A_{a_0\eta_N\pi}\boldsymbol{a_0}\cdot\eta_N\boldsymbol{\pi} + B_{a_0\eta_N\pi}\boldsymbol{a_0}\cdot\partial_\mu\eta_N\partial^\mu\boldsymbol{\pi} + C_{a_0\eta_N\pi}\partial_\mu\boldsymbol{a_0}\cdot(\boldsymbol{\pi}\partial^\mu\eta_N + \eta_N\partial^\mu\boldsymbol{\pi}) \tag{5.60}$$

with

$$A_{a_0\eta_N\pi} = -\lambda_2 Z_\pi^2\phi_N, \tag{5.61}$$

$$\begin{aligned} B_{a_0\eta_N\pi} &= 2g_1 Z_\pi^2 w_{a_1}(g_1 w_{a_1}\phi_N - 1) + (Z_\pi w_{a_1})^2(h_2 - h_3)\phi_N \\ &\equiv -2\frac{g_1^2\phi_N}{m_{a_1}^2}\left[1 - \frac{1}{2}\frac{Z_\pi^4 f_\pi^2}{m_{a_1}^2}(h_2 - h_3)\right], \end{aligned} \tag{5.62}$$

$$C_{a_0\eta_N\pi} = g_1 w_{a_1} Z_\pi^2. \tag{5.63}$$

As in Sec. 5.2.3, we obtain

$$-i\mathcal{M}_{a_0^0\to\eta_N\pi^0} = i\left(A_{a_0\eta_N\pi} - B_{a_0\eta_N\pi}\frac{m_{a_0}^2 - m_\eta^2 - m_\pi^2}{2} + C_{a_0\eta_N\pi}m_{a_0}^2\right) \tag{5.64}$$

Using Eqs. (5.30) and (5.61) - (5.63), Eq. (5.64) can be transformed in the following way:

$$\begin{aligned} -i\mathcal{M}_{a_0^0\to\eta_N\pi^0}(m_{a_0}, Z, h_2) = \frac{i}{Z_\pi f_\pi}\Big\{&m_{\eta_N}^2 - m_{a_0}^2 \\ &+ \left(1 - \frac{1}{Z_\pi^2}\right)\left[1 - \frac{1}{2}\frac{Z_\pi^2\phi_N^2}{m_{a_1}^2}(h_2 - h_3)\right](m_{a_0}^2 - m_\pi^2 - m_\eta^2)\Big\}. \end{aligned} \tag{5.65}$$

Note that Eqs. (5.64) and (5.65) contain the unmixed mass $m_{\eta_N}$ which enters when expressing the coupling constants in terms of the parameters (5.24), as well as the physical mass $m_\eta = 547.8$ MeV. The latter arises because the derivative couplings in the Lagrangian lead to the appearance of scalar invariants formed from the four-momenta of the particles emerging from the decay, which can be expressed in terms of the physical (invariant) masses.
The decay width $\Gamma_{a_0\to\eta\pi}$ follows from Eq. (5.59) by including a phase space factor:

$$\Gamma_{a_0\to\eta\pi}(m_{a_0}, Z_\pi, h_2) = \frac{k(m_{a_0}, m_\eta, m_\pi)}{8\pi m_{a_0}^2}\left|-i\mathcal{M}_{a_0^0\to\eta_N\pi^0}(m_{a_0}, Z_\pi, h_2)\right|^2. \tag{5.66}$$

In the case of Scenario I (Sec. 5.3), in which $a_0 \equiv a_0(980)$, we shall compare the decay amplitude $-i\mathcal{M}_{a_0^0\to\eta_N\pi^0}$, Eq. (5.59), with the corresponding experimental value deduced from Crystal Barrel data: $-i\mathcal{M}^{\rm exp}_{a_0^0\to\eta\pi^0} = (3330 \pm 150)$ MeV [114]. This is preferable to the use of the decay width quoted by the PDG [10] for $a_0(980)$, which refers to the mean peak width, an unreliable quantity due to the closeness of the kaon-kaon threshold.
In the case of Scenario II (Sec. 5.4), in which $a_0 \equiv a_0(1450)$, it is also possible to calculate the decay width $a_0(1450) \to \eta'\pi$, using the OZI rule. The amplitude $-i\mathcal{M}_{a_0\eta'\pi}(m_{a_0}, Z_\pi, h_2)$ is obtained following the same steps as in the previous case, Eq. (5.65):

$$\begin{aligned} -i\mathcal{M}_{a_0\eta'\pi}(m_{a_0}, Z_\pi, h_2) = -i\frac{\sin\varphi}{Z_\pi f_\pi}\Big\{&m_{\eta_N}^2 - m_{a_0}^2 \\ &+ \left(1 - \frac{1}{Z_\pi^2}\right)\left[1 - \frac{1}{2}\frac{Z_\pi^2\phi_N^2}{m_{a_1}^2}(h_2 - h_3)\right](m_{a_0}^2 - m_\pi^2 - m_{\eta'}^2)\Big\}, \end{aligned} \tag{5.67}$$

where the difference compared to Eqs. (5.59) and (5.65) is the prefactor $-\sin\varphi$ and the physical $\eta'$ mass $m_{\eta'} = 958$ MeV. The corresponding decay width reads:

$$\Gamma_{a_0(1450)\to\eta'\pi}(m_{a_0}, Z_\pi, h_2) = \frac{k(m_{a_0}, m_{\eta'}, m_\pi)}{8\pi m_{a_0}^2} \left|-i\mathcal{M}_{a_0\eta'\pi}(m_{a_0}, Z_\pi, h_2)\right|^2 . \tag{5.68}$$

### 5.2.5 Decay Width $a_1(1260) \to \pi\gamma$

The $a_1\pi\gamma$ interaction Lagrangian from Eq. (5.1) reads

$$\mathcal{L}_{a_1\pi\gamma} = eJ_\mu A^\mu, \tag{5.69}$$

where $A^\mu$ denotes the photon field and $J_\mu$ the $a_1$-$\pi$ current of the form

$$J_\mu = -iB_{a_1\pi\gamma}\left(a_{1\mu}^+\pi^- - a_{1\mu}^-\pi^+\right) - iC_{a_1\pi\gamma}\left(a_{1\mu\nu}^+\partial^\nu\pi^- - a_{1\mu\nu}^-\partial^\nu\pi^+\right) \tag{5.70}$$

with

$$B_{a_1\pi\gamma} = g_1 Z_\pi^2 f_\pi, \tag{5.71}$$

$$C_{a_1\pi\gamma} = Z_\pi w_{a_1} = g_1\frac{Z_\pi^2 f_\pi}{m_{a_1}^2} \equiv \frac{B_{a_1\pi\gamma}}{m_{a_1}^2} \tag{5.72}$$

and $a_{1\mu\nu}^\pm = \partial_\mu a_{1\nu}^\pm - \partial_\nu a_{1\mu}^\pm$. The calculation of $\Gamma_{a_1\to\pi\gamma}$ is performed analogously to the generic one presented in Sec. 2.6.2; considering that the photon has no mass and denoting the momenta of $a_1$, $\pi$ and $\gamma$ respectively as $P$, $P_1$ and $P_2$, we obtain

$$\Gamma_{a_1\to\pi\gamma} = e^2\frac{k(m_{a_1}, m_\pi, 0)}{24\pi m_{a_1}^2}\left|3B_{a_1\pi\gamma}^2 + C_{a_1\pi\gamma}^2\left[m_{a_1}^2 m_\pi^2 + 2(P\cdot P_1)^2\right] - 6B_{a_1\pi\gamma}C_{a_1\pi\gamma}(P\cdot P_1)\right| . \tag{5.73}$$

From $P = (m_{a_1}, \mathbf{0})$ and $P_1 = (E_1, \boldsymbol{k}(m_{a_1}, m_\pi, 0))$ we obtain $P\cdot P_1 = m_{a_1}\sqrt{k^2(m_{a_1}, m_\pi, 0) + m_\pi^2}$ $= (m_{a_1}^2 + m_\pi^2)/2$ using Eq. (5.30). Additionally, we can substitute $B_{a_1\pi\gamma}$ in Eq. (5.73) by $C_{a_1\pi\gamma}$ using Eq. (5.72) and transform Eq. (5.73) as follows:

$$\begin{aligned}
\Gamma_{a_1\to\pi\gamma} &= e^2\frac{k(m_{a_1}, m_\pi, 0)}{24\pi m_{a_1}^2}\left|3C_{a_1\pi\gamma}^2 m_{a_1}^4 + \frac{1}{2}C_{a_1\pi\gamma}^2(m_{a_1}^4 + m_\pi^4 + 4m_{a_1}^2 m_\pi^2)\right. \\
&\quad \left. - 3C_{a_1\pi\gamma}^2 m_{a_1}^2(m_{a_1}^2 + m_\pi^2)\right| \\
&= e^2 C_{a_1\pi\gamma}^2 m_{a_1}^2\frac{k(m_{a_1}, m_\pi, 0)}{24\pi}\left|\frac{1}{2}\left(\frac{m_\pi}{m_{a_1}}\right)^4 - \left(\frac{m_\pi}{m_{a_1}}\right)^2 + \frac{1}{2}\right| \\
&\overset{\text{Eq. (5.72)}}{=} e^2 g_1^2\frac{Z_\pi^4 f_\pi^2}{m_{a_1}^2}\frac{k(m_{a_1}, m_\pi, 0)}{24\pi}\left|\frac{1}{2}\left(\frac{m_\pi}{m_{a_1}}\right)^4 - \left(\frac{m_\pi}{m_{a_1}}\right)^2 + \frac{1}{2}\right| \\
&\overset{\text{Eq. (5.30)}}{=} \frac{e^2 g_1^2 Z_\pi^4 f_\pi^2}{48\pi m_{a_1}}\left[1 - \left(\frac{m_\pi}{m_{a_1}}\right)^2\right]\left|\frac{1}{2}\left(\frac{m_\pi}{m_{a_1}}\right)^4 - \left(\frac{m_\pi}{m_{a_1}}\right)^2 + \frac{1}{2}\right| \\
&\overset{\text{Eq. (5.27)}}{=} \frac{e^2(Z_\pi^2 - 1)m_{a_1}}{48\pi}\left[1 - \left(\frac{m_\pi}{m_{a_1}}\right)^2\right]\left|\frac{1}{2}\left(\frac{m_\pi}{m_{a_1}}\right)^4 - \left(\frac{m_\pi}{m_{a_1}}\right)^2 + \frac{1}{2}\right|
\end{aligned} \tag{5.74}$$

or in other words

$$\Gamma_{a_1\to\pi\gamma}(Z_\pi) = \frac{e^2}{96\pi}\,(Z_\pi^2-1)\,m_{a_1}\left[1-\left(\frac{m_\pi}{m_{a_1}}\right)^2\right]^3. \tag{5.75}$$

Note that the $a_1 \to \pi\gamma$ decay width depends only on the renormalisation constant $Z_\pi$, explicitly denoted in Eq. (5.75). In fact, it is generated via the $a_1$-$\pi$ mixing and vanishes in the limit $Z_\pi \to 1$. [A similar mechanism for this decay is described in Ref. [214].] The fact that we include photons following the second realisation of VMD described in Ref. [217] renders this process possible in our model. Inverting Eq. (5.75) we obtain

$$\begin{aligned} Z_\pi^2 &= 1+\frac{96\pi\Gamma_{a_1\to\pi\gamma}}{e^2 m_{a_1}\left[1-\left(\frac{m_\pi}{m_{a_1}}\right)^2\right]^3} \\ \Rightarrow Z_\pi &= \sqrt{1+\frac{96\pi\Gamma_{a_1\to\pi\gamma}}{e^2 m_{a_1}\left[1-\left(\frac{m_\pi}{m_{a_1}}\right)^2\right]^3}}. \end{aligned} \tag{5.76}$$

The first line of Eq. (5.76) yields in principle two opposite-sign solutions. We work, however, only with the positive-sign renormalisation.
Using $\Gamma^{\text{exp}}_{a_1\to\pi\gamma} = (0.640 \pm 0.246)$ MeV [10], one obtains $Z_\pi = 1.67 \pm 0.2$ from Eq. (5.76). Unfortunately, the experimental error for the quantity $\Gamma_{a_1\to\pi\gamma}$ is large. Given that almost all quantities of interest depend very strongly on $Z_\pi$, a better experimental knowledge of this decay would be useful to constrain $Z_\pi$. In the study of Scenario I, Sec. 5.3, this decay width will be part of a $\chi^2$ analysis, but still represents the main constraint for $Z_\pi$.

### 5.2.6 Decay Width $a_1(1260) \to \sigma_N\pi$

The interaction Lagrangian obtained from Eq. (5.1) reads

$$\mathcal{L}_{a_1\sigma_N\pi} = A_{a_1\sigma_N\pi}\boldsymbol{a}_{1\mu}\cdot\sigma_N\partial^\mu\boldsymbol{\pi} + B_{a_1\sigma_N\pi}\boldsymbol{a}_{1\mu}\cdot\boldsymbol{\pi}\partial^\mu\sigma_N \tag{5.77}$$

with the following coefficients:

$$A_{a_1\sigma_N\pi} = Z_\pi\left[g_1(-1+2g_1 w_{a_1}\phi_N) + (h_1+h_2-h_3)w_{a_1}\phi_N\right], \tag{5.78}$$

$$B_{a_1\sigma_N\pi} = g_1 Z_\pi. \tag{5.79}$$

As in Sec. 2.6.3 we obtain

$$\Gamma_{a_1\to\sigma_N\pi} = \frac{k^3(m_{a_1},m_{\sigma_N},m_\pi)}{24\pi m_{a_1}^2}(A_{a_1\sigma_N\pi}-B_{a_1\sigma_N\pi})^2, \tag{5.80}$$

where we have set the isospin factor $I = 1$ in Eq. (2.200). Equation (5.80) can be further transformed using Eqs. (5.30), (5.78) and (5.79):

$$\Gamma_{a_1\to\sigma_N\pi} \equiv \Gamma_{a_1\to\sigma_N\pi}(m_{\sigma_N},Z_\pi,h_1,h_2) = \frac{k^3(m_{a_1},m_{\sigma_N},m_\pi)}{6\pi m_{a_1}^6} g_1^2 Z_\pi^2\left[m_\rho^2 - \frac{\phi_N^2}{2}(h_1+h_2+h_3)\right]^2. \tag{5.81}$$

### 5.2.7 Decay Width $a_1(1260) \to \rho\pi$

We obtain the following $a_1\rho\pi$ interaction Lagrangian from Eq. (5.1):

$$\begin{aligned}\mathcal{L}_{a_1\rho\pi} &= A_{a_1\rho\pi}\boldsymbol{a}_{1\mu}\cdot(\boldsymbol{\pi}\times\boldsymbol{\rho}^{\mu}) + B_{a_1\rho\pi}\boldsymbol{a}_{1\mu}\cdot[(\partial^{\mu}\boldsymbol{\rho}^{\nu}-\partial^{\nu}\boldsymbol{\rho}^{\mu})\times\partial_{\nu}\boldsymbol{\pi}] \\ &+ C_{a_1\rho\pi}(\partial_{\nu}\boldsymbol{a}_{1\mu}-\partial_{\mu}\boldsymbol{a}_{1\nu})\cdot(\boldsymbol{\rho}^{\mu}\times\partial^{\nu}\boldsymbol{\pi})\end{aligned} \tag{5.82}$$

with the following coefficients:

$$A_{a_1\rho\pi} = Z_{\pi}(g_1^2 - h_3)\phi_N, \tag{5.83}$$

$$B_{a_1\rho\pi} = Z_{\pi}g_2 w_{a_1}, \tag{5.84}$$

$$C_{a_1\rho\pi} = Z_{\pi}g_2 w_{a_1}. \tag{5.85}$$

Let us isolate the interaction Lagrangian of the neutral $a_1$ component from Eq. (5.82):

$$\begin{aligned}\mathcal{L}_{a_1^0\rho\pi} &= -iA_{a_1\rho\pi}a_{1\mu}^0(\rho^{\mu-}\pi^+ - \rho^{\mu+}\pi^-) \\ &- iB_{a_1\rho\pi}a_{1\mu}^0[(\partial^{\nu}\rho^{\mu-}-\partial^{\mu}\rho^{\nu-})\partial_{\nu}\pi^+ - \left(\partial^{\nu}\rho^{\mu+}-\partial^{\mu}\rho^{\nu+}\right)\partial_{\nu}\pi^-] \\ &- iC_{a_1\rho\pi}(\partial_{\nu}a_{1\mu}^0-\partial_{\mu}a_{1\nu}^0)(\partial^{\nu}\pi^-\rho^{\mu+}-\partial^{\nu}\pi^+\rho^{\mu-}).\end{aligned} \tag{5.86}$$

Let us for the beginning consider the decay $a_1^0 \to \rho^-\pi^+$ only:

$$\begin{aligned}\mathcal{L}_{a_1^0\rho^-\pi^+} &= -iA_{a_1\rho\pi}a_{1\mu}^0\rho^{\mu-}\pi^+ - iB_{a_1\rho\pi}a_{1\mu}^0(\partial^{\nu}\rho^{\mu-}-\partial^{\mu}\rho^{\nu-})\partial_{\nu}\pi^+ \\ &+ iC_{a_1\rho\pi}(\partial_{\nu}a_{1\mu}^0-\partial_{\mu}a_{1\nu}^0)\partial^{\nu}\pi^+\rho^{\mu-} \\ &= -iA_{a_1\rho\pi}a_{1\mu}^0\rho^{\mu-}\pi^+ - iB_{a_1\rho\pi}a_{1\mu}^0(\partial^{\nu}\rho^{\mu-}-\partial^{\mu}\rho^{\nu-})\partial_{\nu}\pi^+ \\ &- iC_{a_1\rho\pi}\partial_{\nu}a_{1\mu}^0(\partial^{\mu}\pi^+\rho^{\nu-}-\partial^{\nu}\pi^+\rho^{\mu-}).\end{aligned} \tag{5.87}$$

Let us denote the momenta of $a_1$, $\rho$ and $\pi$ as $P$, $P_1$ and $P_2$. Our decay process involves two vector states: $a_1$ and $\rho$. For this reason we have to consider the corresponding polarisation vectors labelled as $\varepsilon_{\mu}^{(\alpha)}(P)$ for $a_1$ and $\varepsilon_{\nu}^{(\beta)}(P_1)$ for $\rho$. Then, upon substituting $\partial^{\mu} \to -iP^{\mu}$ for the decaying particle and $\partial^{\mu} \to iP_{1,2}^{\mu}$ for the decay products, we obtain the following Lorentz-invariant $a_1\rho\pi$ scattering amplitude $-i\mathcal{M}_{a_1^0\to\rho^-\pi^+}^{(\alpha,\beta)}$:

$$\begin{aligned}-i\mathcal{M}_{a_1^0\to\rho^-\pi^+}^{(\alpha,\beta)} &= \varepsilon_{\mu}^{(\alpha)}(P)\varepsilon_{\nu}^{(\beta)}(P_1)h_{a_1\rho\pi}^{\mu\nu} = \varepsilon_{\mu}^{(\alpha)}(P)\varepsilon_{\nu}^{(\beta)}(P_1) \\ &\times\{A_{a_1\rho\pi}g^{\mu\nu} + B_{a_1\rho\pi}\left[P_1^{\mu}P_2^{\nu} - (P_1\cdot P_2)g^{\mu\nu}\right] \\ &+C_{a_1\rho\pi}\left[P_2^{\mu}P^{\nu} - (P\cdot P_2)g^{\mu\nu}\right]\}\end{aligned} \tag{5.88}$$

with

$$h_{a_1\rho\pi}^{\mu\nu} = A_{a_1\rho\pi}g^{\mu\nu} + B_{a_1\rho\pi}\left[P_1^{\mu}P_2^{\nu} - (P_1\cdot P_2)g^{\mu\nu}\right] + C_{a_1\rho\pi}\left[P_2^{\mu}P^{\nu} - (P\cdot P_2)g^{\mu\nu}\right], \tag{5.89}$$

where $h_{a_1\rho\pi}^{\mu\nu}$ denotes the $a_1\rho\pi$ vertex [more precisely, this is only the $a_1\rho^-\pi^+$ vertex but, as evident from Eq. (5.86), it is the same as the $a_1\rho^+\pi^-$ vertex up to a sign that is of no importance for

the calculation of the decay width]. Given that $B_{a_1\rho\pi} = C_{a_1\rho\pi}$ [see Eqs. (5.84) and (5.85)], we observe that the vertex of Eq. (5.89) possesses exactly the same form as the one presented in Eq. (2.182). Consequently, we can utilise results from Sec. 2.6.2 where the generic decay of an axial-vector into a vector and a pseudoscalar was presented. The squared averaged decay amplitude for the decay $a_1 \to \rho\pi$ then reads

$$|-i\bar{\mathcal{M}}_{a_1^0\to\rho^-\pi^+}|^2 = \frac{1}{3}\left[\left|h^{\mu\nu}_{a_1\rho\pi}\right|^2 - \frac{\left|h^{\mu\nu}_{a_1\rho\pi}P_\mu\right|^2}{m_{a_1}^2} - \frac{\left|h^{\mu\nu}_{a_1\rho\pi}P_{1\nu}\right|^2}{m_\rho^2} + \frac{\left|h^{\mu\nu}_{a_1\rho\pi}P_\mu P_{1\nu}\right|^2}{m_\rho^2 m_{a_1}^2}\right]. \tag{5.90}$$

Using the identities $P_1\cdot P_2 = (m_{a_1}^2 - m_\rho^2 - m_\pi^2)/2$, $P\cdot P_1 = m_{a_1}E_1$ and $P\cdot P_2 = m_{a_1}E_2$, we can now calculate the four contributions to $|-i\bar{\mathcal{M}}_{a_1^0\to\rho^-\pi^+}|^2$ in Eq. (5.90):

$$\begin{aligned}
\left|h^{\mu\nu}_{a_1\rho\pi}\right|^2 &= 4A_{a_1\rho\pi}^2 + B_{a_1\rho\pi}^2[m_\pi^2 m_\rho^2 + 2(P_1\cdot P_2)^2] + C_{a_1\rho\pi}^2[m_\pi^2 m_{a_1}^2 + 2(P\cdot P_2)^2] \\
&\quad - 6A_{a_1\rho\pi}B_{a_1\rho\pi}(P_1\cdot P_2) - 6A_{a_1\rho\pi}C_{a_1\rho\pi}(P\cdot P_2) + 6B_{a_1\rho\pi}C_{a_1\rho\pi}(P_1\cdot P_2)(P\cdot P_2) \\
&\overset{\text{Eqs. (5.83) - (5.85)}}{\equiv} Z_\pi^4 f_\pi^2\left\{4(g_1^2-h_3)^2 + \frac{g_1^2g_2^2}{m_{a_1}^4}\left[m_{a_1}^4 + m_\pi^4 + m_\rho^4 + m_\pi^2 m_\rho^2\right.\right. \\
&\quad + \left. m_{a_1}^2(m_\pi^2 - 2m_\rho^2) + 3(m_{a_1}^2 - m_\rho^2 - m_\pi^2)m_{a_1}E_2\right] \\
&\quad - \left.3\,\frac{g_1g_2(g_1^2-h_3)}{m_{a_1}^2}\left(m_{a_1}^2 - m_\rho^2 - m_\pi^2 + 2m_{a_1}E_2\right)\right\},
\end{aligned} \tag{5.91}$$

$$\begin{aligned}
\left|h^{\mu\nu}_{a_1\rho\pi}P_\mu\right|^2 &= A_{a_1\rho\pi}^2 m_\rho^2 + C_{a_1\rho\pi}^2\left[(P\cdot P_1)^2 m_\pi^2 + (P\cdot P_2)^2 m_\rho^2 - 2(P\cdot P_1)(P\cdot P_2)(P_1\cdot P_2)\right] \\
&\quad + 2A_{a_1\rho\pi}C_{a_1\rho\pi}\left[(P\cdot P_1)(P_1\cdot P_2) - (P\cdot P_2)m_\rho^2\right] \\
&\overset{\text{Eqs. (5.83) - (5.85)}}{\equiv} Z_\pi^4 f_\pi^2\left\{(g_1^2-h_3)^2 m_{a_1}^2 + \frac{g_1^2g_2^2}{4m_{a_1}^4}\left[(m_{a_1}^2 - m_\pi^2)^2(m_{a_1}^2 + m_\pi^2 - 2m_\rho^2)\right.\right. \\
&\quad + \left.(m_\pi^2 + m_{a_1}^2)m_\rho^4 - 4(m_{a_1}^2 - m_\rho^2 - m_\pi^2)m_{a_1}^2 E_1E_2\right] \\
&\quad + \left.\frac{g_1g_2(g_1^2-h_3)}{m_{a_1}^2}[2m_{a_1}^2E_1E_2 - (m_{a_1}^2 - m_\rho^2 - m_\pi^2)m_{a_1}^2]\right\},
\end{aligned} \tag{5.92}$$

$$\begin{aligned}
\left|h^{\mu\nu}_{a_1\rho\pi}P_{1\nu}\right|^2 &= A_{a_1\rho\pi}^2 m_{a_1}^2 + B_{a_1\rho\pi}^2\left[(P\cdot P_1)^2 m_\pi^2 + (P_1\cdot P_2)^2 m_{a_1}^2 - 2(P\cdot P_1)(P\cdot P_2)(P_1\cdot P_2)\right] \\
&\quad + 2A_{a_1\rho\pi}B_{a_1\rho\pi}\left[(P\cdot P_1)(P\cdot P_2) - (P_1\cdot P_2)m_{a_1}^2\right] \\
&\overset{\text{Eqs. (5.83) - (5.85)}}{\equiv} Z_\pi^4 f_\pi^2\left\{(g_1^2-h_3)^2 m_\rho^2 + \frac{g_1^2g_2^2}{4m_{a_1}^4}\left[(m_\pi^2 - m_\rho^2)^2(m_\pi^2 + m_\rho^2 - 2m_{a_1}^2)\right.\right. \\
&\quad + \left.(m_\pi^2 + m_\rho^2)m_{a_1}^4 - 4(m_{a_1}^2 - m_\rho^2 - m_\pi^2)m_{a_1}^2 E_1E_2\right] \\
&\quad + \left.\frac{g_1g_2(g_1^2-h_3)}{m_{a_1}^2}\left[(m_{a_1}^2 - m_\pi^2)m_{a_1}E_1 - 2m_{a_1}m_\rho^2\left(E_2 + \frac{E_1}{2}\right)\right]\right\},
\end{aligned} \tag{5.93}$$

$$\left|h^{\mu\nu}_{a_1\rho\pi}P_\mu P_{1\nu}\right|^2 = \left[A_{a_1\rho\pi}(P\cdot P_1)\right]^2 \overset{\text{Eqs. (5.83) - (5.85)}}{\equiv} (g_1^2-h_3)^2 Z_\pi^4 f_\pi^2 m_{a_1}^2 E_1^2 \tag{5.94}$$

with $E_1 = \sqrt{k^2(m_{a_1}, m_\rho, m_\pi) + m_\rho^2}$ and $E_2^2 = \sqrt{k^2(m_{a_1}, m_\rho, m_\pi) + m_\pi^2}$.

The formula for the decay width $\Gamma_{a_1\to\rho\pi}$ is the same as the one presented in Eq. (2.187), multiplied by a factor of two in order to consider the two decay channels $a_1^0 \to \rho^-\pi^+$ and $a_1^0 \to \rho^+\pi^-$ from Eq. (5.86):

$$\Gamma_{a_1\to\rho\pi} = \frac{k(m_{a_1}, m_\rho, m_\pi)}{4\pi m_{a_1}^2} |-i\bar{\mathcal{M}}_{a_1^0\to\rho^-\pi^+}|^2 \tag{5.95}$$

with $|-i\bar{\mathcal{M}}_{a_1^0\to\rho^-\pi^+}|^2$ from Eq. (5.90), i.e., Eqs. (5.91) - (5.94).

### 5.2.8 Tree-Level Scattering Lengths

The calculation of the tree-level $\pi\pi$ scattering lengths has been described in detail in Ref. [220]; in this section we will repeat the main points.

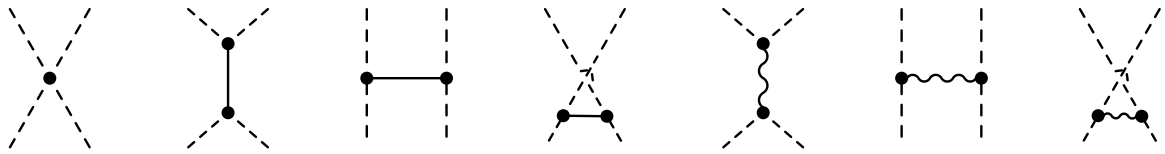

**Figure 5.2:** Diagrams contributing to the $\pi\pi$ scattering lengths. The dashed lines denote the pions, the solid lines denote the intermediate scalar meson whereas the wavy lines denote the intermediate vector state.

The scattering lengths are calculated from three contributions: the "pure" $\pi\pi$ (contact) scattering, $\pi\pi$ scattering via the virtual $\sigma_N$ meson ($s$, $t$, $u$ channels; $s$, $t$, $u$ denote the Mandelstam variables) and $\pi\pi$ scattering via the virtual $\rho$ meson (also $s$, $t$, $u$ channels). Consequently, the corresponding scattering Lagrangian consists of a term containing $4\pi$ vertices ($\mathcal{L}_{4\pi}$) and terms describing interactions of pions with $\sigma_N$ [depicted in $\mathcal{L}_{\sigma_N\pi\pi}$, Eq. (5.52)] and interactions of pions with $\rho$ [depicted in $\mathcal{L}_{\rho\pi\pi}$, Eq. (5.31)]:

$$\mathcal{L}_{\pi\pi} = \mathcal{L}_{4\pi} + \mathcal{L}_{\sigma_N\pi\pi} + \mathcal{L}_{\rho\pi\pi}, \tag{5.96}$$

where the following form of $\mathcal{L}_{4\pi}$ is obtained from the Lagrangian (5.1):

$$\begin{aligned}\mathcal{L}_{4\pi} = &-\frac{1}{4}(\lambda_1 + \frac{\lambda_2}{2}) Z_\pi^4 (\boldsymbol{\pi}^2)^2 + \frac{1}{2}(g_1^2 - h_3) w_{a_1}^2 Z_\pi^4 (\partial_\mu \boldsymbol{\pi}\cdot\boldsymbol{\pi})^2 \\ &+ \frac{1}{4}(h_1 + h_2 + h_3) w_{a_1}^2 Z_\pi^4 \boldsymbol{\pi}^2 (\partial_\mu \boldsymbol{\pi})^2.\end{aligned} \tag{5.97}$$

Note that Eq. (5.96) may also contain contributions proportional to $[(\partial^\mu\boldsymbol{\pi})\times(\partial^\nu\boldsymbol{\pi})]^2$ from the $g_{3,4}$ terms in the Lagrangian (5.1). However, we do not consider these terms because all our calculations will be at threshold where the terms with only pion derivatives do not contribute. Let us denote the incoming pions with labels $a$ and $b$ and the outgoing pions with labels $c$ and $d$. The $\pi\pi$ scattering amplitude $\mathcal{M}_{\pi\pi}(s,t,u)$ obtained from the Lagrangian (5.96) then has three contributions, one for the $s$, $t$ and $u$ channels, respectively:

$$\mathcal{M}_{\pi\pi}(s,t,u) = i\delta^{ab}\delta^{cd}A(s,t,u) + i\delta^{ac}\delta^{bd}A(t,u,s) + i\delta^{ad}\delta^{bc}A(u,s,t), \tag{5.98}$$

where

$$A(s,t,u) = (g_1^2 - h_3) Z_\pi^4 w_{a_1}^2 s - 2\left(\lambda_1 + \frac{\lambda_2}{2}\right) Z_\pi^4 - (h_1+h_2+h_3) Z_\pi^4 w_{a_1}^2 (s - 2m_\pi^2)$$
$$- [-2m_\pi^2 C_{\sigma_N \pi\pi} + B_{\sigma_N \pi\pi}(2m_\pi^2 - s) + 2A_{\sigma_N \pi\pi}]^2 \frac{1}{s - m_{\sigma_N}^2}$$
$$+ \left(A_{\rho\pi\pi} + B_{\rho\pi\pi}\frac{t}{2}\right)^2 \frac{u-s}{t - m_\rho^2} + \left(A_{\rho\pi\pi} + B_{\rho\pi\pi}\frac{u}{2}\right)^2 \frac{t-s}{u - m_\rho^2}, \tag{5.99}$$

$$A(t,u,s) = (g_1^2 - h_3) Z_\pi^4 w_{a_1}^2 t - 2\left(\lambda_1 + \frac{\lambda_2}{2}\right) Z_\pi^4 - (h_1+h_2+h_3) Z_\pi^4 w_{a_1}^2 (t - 2m_\pi^2)$$
$$- [-2m_\pi^2 C_{\sigma_N \pi\pi} + B_{\sigma_N \pi\pi}(2m_\pi^2 - t) + 2A_{\sigma_N \pi\pi}]^2 \frac{1}{t - m_{\sigma_N}^2}$$
$$+ \left(A_{\rho\pi\pi} + B_{\rho\pi\pi}\frac{s}{2}\right)^2 \frac{u-t}{s - m_\rho^2} + \left(A_{\rho\pi\pi} + B_{\rho\pi\pi}\frac{u}{2}\right)^2 \frac{s-t}{u - m_\rho^2}, \tag{5.100}$$

$$A(u,s,t) = (g_1^2 - h_3) Z_\pi^4 w_{a_1}^2 u - 2\left(\lambda_1 + \frac{\lambda_2}{2}\right) Z_\pi^4 - (h_1+h_2+h_3) Z_\pi^4 w_{a_1}^2 (u - 2m_\pi^2)$$
$$- [-2m_\pi^2 C_{\sigma_N \pi\pi} + B_{\sigma_N \pi\pi}(2m_\pi^2 - u) + 2A_{\sigma_N \pi\pi}]^2 \frac{1}{u - m_{\sigma_N}^2}$$
$$+ \left(A_{\rho\pi\pi} + B_{\rho\pi\pi}\frac{s}{2}\right)^2 \frac{t-u}{s - m_\rho^2} + \left(A_{\rho\pi\pi} + B_{\rho\pi\pi}\frac{t}{2}\right)^2 \frac{s-u}{t - m_\rho^2} \tag{5.101}$$

with $A_{\sigma_N\pi\pi}$, $B_{\sigma_N\pi\pi}$, $C_{\sigma_N\pi\pi}$, $A_{\rho\pi\pi}$ and $B_{\rho\pi\pi}$ respectively from Eqs. (5.53), (5.54), (5.55), (5.32) and (5.33). Note that the scattering amplitude $\mathcal{M}_{\pi\pi}$ vanishes at threshold: $\mathcal{M}_{\pi\pi}(0,0,0) = 0$ [220].

We can now calculate the three contributions to the scattering amplitude at threshold ($\boldsymbol{p}_\pi = 0 \Rightarrow P_\pi^2 = m_\pi^2$ and thus $s \equiv 4P_\pi^2 = 4m_\pi^2$, $t = 0$, $u = 0$). Let us first substitute the coefficient $A_{\rho\pi\pi}$ in Eqs. (5.99) - (5.101) using Eq. (5.32); note that, at threshold, there is no contribution from the terms $\sim B_{\rho\pi\pi}$. We then obtain

$$A(s,t,u)|_{s=4m_\pi^2} = 4g_1^2 Z_\pi^4 w_{a_1}^2 m_\pi^2 - 2\left(\lambda_1 + \frac{\lambda_2}{2}\right) Z_\pi^4 - 2(h_1+h_2+3h_3) Z_\pi^4 w_{a_1}^2 m_\pi^2$$
$$- 4[(B_{\sigma_N\pi\pi} + C_{\sigma_N\pi\pi})m_\pi^2 - A_{\sigma_N\pi\pi}]^2 \frac{1}{4m_\pi^2 - m_{\sigma_N}^2}$$
$$+ 8[g_1 Z_\pi^2 (1 - g_1 w_{a_1}\phi_N) + h_3 Z_\pi^2 w_{a_1}\phi_N]^2 \frac{m_\pi^2}{m_\rho^2}, \tag{5.102}$$

$$A(t,u,s)|_{s=4m_\pi^2} = -2\left(\lambda_1 + \frac{\lambda_2}{2}\right) Z_\pi^4 + 2(h_1+h_2+h_3) Z_\pi^4 w_{a_1}^2 m_\pi^2 - 4g_1^2 Z_\pi^4 \frac{m_\pi^2 m_\rho^2}{m_{a_1}^4}$$
$$+ 4[(B_{\sigma_N\pi\pi} - C_{\sigma_N\pi\pi})m_\pi^2 + A_{\sigma_N\pi\pi}]^2 \frac{1}{m_{\sigma_N}^2} \tag{5.103}$$

and

$$A(u,s,t)|_{s=4m_\pi^2} = A(t,u,s)|_{s=4m_\pi^2}. \tag{5.104}$$

The scattering amplitude $T^0$ for zero isospin is obtained from [229]

$$T^0|_{s=4m_\pi^2} = 3A(s,t,u)|_{s=4m_\pi^2} + A(t,u,s)|_{s=4m_\pi^2} + A(u,s,t)|_{s=4m_\pi^2}. \tag{5.105}$$

Additionally, the interdependence of $T^0$ and the $S$-wave, isospin-zero $\pi\pi$ scattering length $a_0^0$ is, at threshold, given by the following formula [see Ref. [220], Eq. (4.30)]:

$$a_0^0|_{s=4m_\pi^2} = \frac{1}{32\pi} T^0|_{s=4m_\pi^2}. \tag{5.106}$$

Inserting Eqs. (5.102) - (5.104) into Eq. (5.105) and substituting $T^0|_{s=4m_\pi^2}$ in Eq. (5.106) yields (in units of $m_\pi^{-1}$):

$$\begin{aligned} a_0^0|_{s=4m_\pi^2} = \frac{1}{32\pi}\Bigg\{ & 12(g_1^2 - h_3) Z_\pi^4 w_{a_1}^2 m_\pi^2 - 10\left(\lambda_1 + \frac{\lambda_2}{2}\right) Z_\pi^4 - 2(h_1+h_2+h_3) Z_\pi^4 w_{a_1}^2 m_\pi^2 \\ & + 12[(B_{\sigma_N\pi\pi} + C_{\sigma_N\pi\pi}) m_\pi^2 - A_{\sigma_N\pi\pi}]^2 \frac{1}{m_{\sigma_N}^2 - 4m_\pi^2} \\ & + 8[(B_{\sigma_N\pi\pi} - C_{\sigma_N\pi\pi}) m_\pi^2 + A_{\sigma_N\pi\pi}]^2 \frac{1}{m_{\sigma_N}^2} + 16 g_1^2 Z_\pi^4 \frac{m_\pi^2 m_\rho^2}{m_{a_1}^4} \Bigg\}. \end{aligned} \tag{5.107}$$

Upon substitution of $A_{\sigma_N\pi\pi}$, $B_{\sigma_N\pi\pi}$ and $C_{\sigma_N\pi\pi}$, respectively, from Eqs. (5.53), (5.54) and (5.55), we obtain the following formula for the scattering length:

$$\begin{aligned} a_0^0|_{s=4m_\pi^2} \equiv a_0^0|_{s=4m_\pi^2}(Z_\pi, m_{\sigma_N}, h_1) = \frac{1}{4\pi}\Bigg( & 2g_1^2 Z_\pi^4 \frac{m_\pi^2}{m_{a_1}^4}\left\{ m_\rho^2 + \frac{\phi_N^2}{16}[12g_1^2 - 2(h_1+h_2) - 14h_3] \right\} \\ & - \frac{3}{2}\left\{ g_1^2 Z_\pi^2 \phi_N \frac{m_\pi^2}{m_{a_1}^4}\left[ 2m_{a_1}^2 + m_\rho^2 - \frac{\phi_N^2}{2}(h_1+h_2+h_3) \right] - \frac{Z_\pi^2 m_{\sigma_N}^2 - m_\pi^2}{2\phi_N} \right\}^2 \frac{1}{4m_\pi^2 - m_{\sigma_N}^2} \\ & + \left\{ g_1^2 Z^2 \phi_N \frac{m_\pi^2}{m_{a_1}^4}\left[ m_\rho^2 - \frac{\phi_N^2}{2}(h_1+h_2+h_3) \right] + \frac{Z_\pi^2 m_{\sigma_N}^2 - m_\pi^2}{2\phi_N} \right\}^2 \frac{1}{m_{\sigma_N}^2} \Bigg) \\ & - \frac{5}{8}\frac{Z_\pi^2 m_{\sigma_N}^2 - m_\pi^2}{f_\pi^2}. \end{aligned} \tag{5.108}$$

We use the value $a_0^{0\,\mathrm{exp}} = 0.218 \pm 0.020$ in accordance with the data from the NA48/2 collaboration [43].

Given that $T^1 = A(t,u,s) - A(u,s,t)$ [229], we obtain $T^1 = 0$ at threshold because of $A(u,s,t)|_{s=4m_\pi^2} = A(t,u,s)|_{s=4m_\pi^2}$ [see Eq. (5.104)]. Therefore,

$$a_0^1|_{s=4m_\pi^2} = 0. \tag{5.109}$$

The $S$-wave, isospin-two $\pi\pi$ scattering length is obtained from the corresponding $I = 2$ scattering amplitude $T^2$ given by [229]

$$T^2|_{s=4m_\pi^2} = A(t,u,s)|_{s=4m_\pi^2} + A(u,s,t)|_{s=4m_\pi^2} \overset{\text{Eq. (5.104)}}{\equiv} 2A(t,u,s)|_{s=4m_\pi^2}. \tag{5.110}$$

Analogously to Eq. (5.106),

$$32\pi a_0^2|_{s=4m_\pi^2} \equiv T^2|_{s=4m_\pi^2} \tag{5.111}$$

or

$$16\pi a_0^2|_{s=4m_\pi^2} \equiv A(t,u,s)|_{s=4m_\pi^2}\,, \tag{5.112}$$

implying

$$a_0^2|_{s=4m_\pi^2} \equiv \frac{1}{16\pi} A(t,u,s)|_{s=4m_\pi^2}\,. \tag{5.113}$$

Then inserting Eqs. (5.53), (5.54), (5.55) and (5.103) into Eq. (5.113) we obtain:

$$\begin{aligned} a_0^2|_{s=4m_\pi^2} \equiv a_0^2|_{s=4m_\pi^2}(Z_\pi, m_{\sigma_N}, h_1) = -\frac{1}{4\pi}\Bigg( & g_1^2 Z_\pi^4 \frac{m_\pi^2}{m_{a_1}^4}\left[m_\rho^2 - \frac{\phi_N^2}{2}(h_1+h_2+h_3)\right] \\ & - \left\{ g_1^2 Z_\pi^2 \phi_N \frac{m_\pi^2}{m_{a_1}^4}\left[m_\rho^2 - \frac{\phi_N^2}{2}(h_1+h_2+h_3)\right] + \frac{Z_\pi^2 m_{\sigma_N}^2 - m_\pi^2}{2\phi_N}\right\}^2 \frac{1}{m_{\sigma_N}^2} + \frac{Z_\pi^2 m_{\sigma_N}^2 - m_\pi^2}{4f_\pi^2}\Bigg)\,. \end{aligned} \tag{5.114}$$

The experimental result for $a_0^2$ from the NA48/2 collaboration is $a_0^{2\,\mathrm{exp}} = -0.0457 \pm 0.0125$ [43]. Note that the $\pi\pi$ scattering lengths were also studied away from threshold in Ref. [230], in a model quite similar to ours. We will discuss the scattering lengths also within the extended $U(3) \times U(3)$ version of our model in Sec. 9.5.

## 5.3 Scenario I: Light Scalar Quarkonia

We can now discuss two different interpretations of the scalar mesons. Sections 5.3.1 - 5.3.4 describe the results obtained when $f_0(600)$ and $a_0(980)$ are interpreted as scalar quarkonia (Scenario I). Then, in Sec. 5.4, we discuss the results obtained when $f_0(1370)$ and $a_0(1450)$ are interpreted as scalar quarkonia (Scenario II).

### 5.3.1 Fit procedure

As a first step we utilise the central value of the experimental result $\Gamma^{\mathrm{exp}}_{\rho\to\pi\pi} = 149.1$ MeV [10] in order to express the parameter $g_2$ as a function of $Z_\pi$ via Eq. (5.45). Moreover, we fix the mass $m_{a_0} = 980$ MeV [10] and we also use the central value $\Gamma_{f_{1N}\to a_0\pi}(Z_\pi, h_2) = 8.748$ MeV to express $h_2$ as a function of $Z_\pi$. The results are practically unaffected by the 6% uncertainty in $h_2$ originating from the uncertainty in $\Gamma_{f_{1N}\to a_0\pi}$, see Eq. (5.51).
As a result, the set of free parameters in Eq. (5.26) is further reduced to three parameters:

$$Z_\pi,\ m_{\sigma_N},\ h_1. \tag{5.115}$$

Note that in this scenario the field $\sigma_N$ is identified with the resonance $f_0(600)$, but the experimental uncertainty on its mass is so large that it does not allow us to fix $m_{\sigma_N}$. We therefore keep $m_{\sigma_N}$ as a free parameter.
We now determine the parameters $Z_\pi$, $h_1$, and $m_{\sigma_N}$ using known data on the $a_1 \to \pi\gamma$ decay width (5.75) and on the $\pi\pi$ scattering lengths $a_0^0$ and $a_0^2$ reported in Eqs. (5.108) and (5.114). This is a system of three equations with three variables and can be solved uniquely. We make

use of the $\chi^2$ method in order to determine not only the central values for our parameters but also their error intervals:

$$\chi^2(Z_\pi, m_{\sigma_N}, h_1) = \left( \frac{\Gamma_{a_1\to\pi\gamma}(Z_\pi) - \Gamma^{\rm exp}_{a_1\to\pi\gamma}}{\triangle\Gamma^{\rm exp}_{\rm decay}} \right)^2 + \sum_{i\in\{0,2\}} \left( \frac{a_0^i(Z_\pi, m_{\sigma_N}, h_1) - a_0^{i,\ {\rm exp}}}{\triangle a_0^{i,\ {\rm exp}}} \right)^2 . \quad (5.116)$$

The errors for the model parameters are calculated as the square roots of the diagonal elements of the inverted Hessian matrix obtained from $\chi^2(Z_\pi, m_{\sigma_N}, h_1)$. The minimal value is obtained for $\chi^2 = 0$, as expected given that the parameters are determined from a uniquely solvable system of equations. The values of the parameters are as follows:

$$Z_\pi = 1.67 \pm 0.2\,,\ m_{\sigma_N} = (332 \pm 456)\ {\rm MeV}\,,\ h_1 = -68 \pm 338. \quad (5.117)$$

Clearly, the error intervals for $m_{\sigma_N}$ and $h_1$ are very large. Fortunately, it is possible to constrain the $h_1$ error interval as follows. As evident from Eq. (5.18), $m_\rho^2$ contains two contributions – the bare mass term $m_1^2$ and the quark condensate contribution ($\sim \phi_N^2$). The contribution of the quark condensate is special for the globally invariant sigma model; in the locally invariant model $m_\rho$ is always equal to $m_1$ [37]. Each of these contributions should have at most the value of 775.49 MeV ($= m_\rho$) because otherwise either the bare mass or the quark condensate contribution to the rho mass would be negative, which appears to be unphysical. A plot of the function $m_1 = m_1(Z_\pi, h_1, h_2(Z_\pi))$, see Eq. (5.29), for the central values of $Z_\pi = 1.67$ and $\Gamma^{\rm exp}_{f_{1N}\to a_0\pi} = 8.748$ MeV is shown in Fig. 5.3.

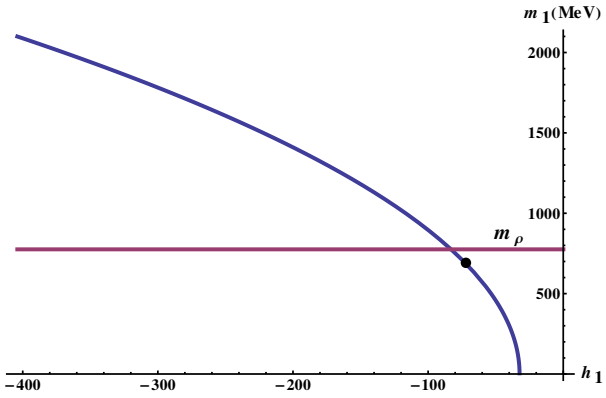


**Figure 5.3:** $m_1$ as function of $h_1$, constrained at the central value of $Z_\pi = 1.67$. The black dot marks the position of central values $h_1 = -68$ and $m_1 = 652$ MeV.

Note that varying the value of $\Gamma^{\rm exp}_{f_{1N}\to a_0\pi}$ within its experimental boundaries would only very slightly change $h_1$ by $\pm 4$ and this parameter is thus unaffected by the experimental error for $\Gamma^{\rm exp}_{f_{1N}\to a_0\pi}$. If the value of $m_1$ were known exactly, then Eq. (5.29) would allow us to constrain $h_1$ via $Z_\pi$. However, given that at this point we can only state that $0 \le m_1 \le m_\rho$, for each $Z_\pi$ one may consider all values of $h_1$ between two boundaries, one obtained from the condition $m_1(Z_\pi, h_1, h_2(Z_\pi)) \equiv 0$ and another obtained from the condition $m_1(Z_\pi, h_1, h_2(Z_\pi)) \equiv m_\rho$. For example, using the central value of $Z_\pi = 1.67$, we obtain $-83 \le h_1 \le -32$. The lower boundary follows from $m_1 \equiv m_\rho$ and the upper boundary from $m_1 \equiv 0$, see Fig. 5.3. Note that the

central value $h_1 = -68$ from Eq. (5.117) corresponds to $m_1 = 652$ MeV. If the minimal value of $Z_\pi = 1.47$ is used, then $h_1 = -112$ is obtained from $m_1 \equiv m_\rho$ and $h_1 = -46$ from $m_1 \equiv 0$. Thus, $-112 \leq h_1 \leq -46$ for $Z_\pi = 1.47$. Analogously, $-64 \leq h_1 \leq -24$ is obtained for the maximal value $Z_\pi = 1.87$.
Clearly, each lower boundary for $h_1$ is equivalent to $m_1 \equiv m_\rho$ and each upper boundary for $h_1$ is equivalent to $m_1 \equiv 0$. Thus, in the following we will only state the values of $Z_\pi$ and $m_1$; $h_1$ can always be calculated using Eq. (5.29). In this way, the dependence of our results on $m_1$ and thus on the origin of the $\rho$ mass will be exhibited.
The value of $m_{\sigma_N}$ can be constrained in a way similar to $h_1$ using the scattering length $a_0^0$; the scattering length $a_0^2$ possesses a rather large error interval making it unsuitable to constrain $m_{\sigma_N}$. Figure 5.4 shows the different values for $a_0^0$ and $a_0^2$ depending on the choice of $Z_\pi$ and $m_1$.

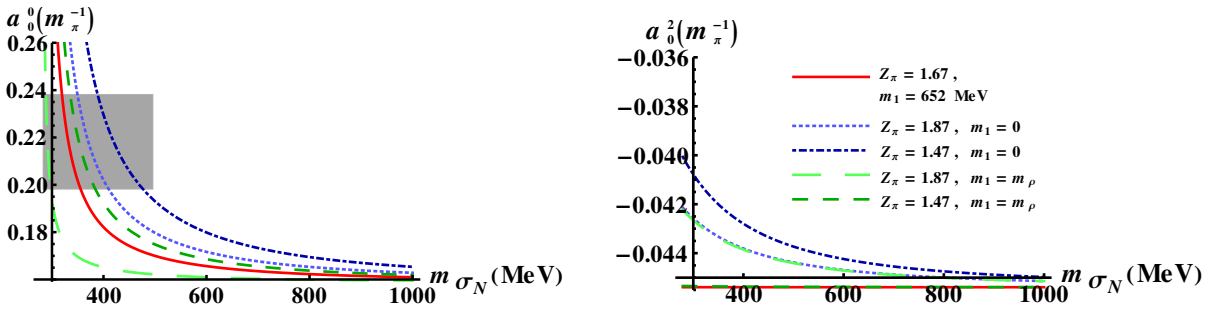


**Figure 5.4:** Scattering lengths $a_0^0$ and $a_0^2$ as function of $m_{\sigma_N}$ (the shaded band corresponds to the NA48/2 value of $a_0^0$; no error interval is shown for $a_0^2$ due to the large interval size [43]).

It is obvious that the value of $a_0^0$ is only consistent with the NA48/2 value [43] if $m_{\sigma_N}$ is in the interval [288, 477] MeV, i.e., $m_{\sigma_N} = 332^{+145}_{-44}$ MeV. This value for $m_{\sigma_N}$ follows if the parameters $Z$ and $m_1$ are varied within the allowed boundaries. If we only consider the $a_0^0$ curve that is obtained for the central values of $Z$ and $m_1$, a much more constrained value of $m_{\sigma_N} = 332^{+24}_{-13}$ MeV follows from Fig. 5.4. We will be working with the broader interval of $m_{\sigma_N}$. Even then, constraining $m_1$ to the interval $[0, m_\rho]$, the error bars for $m_{\sigma_N}$ are reduced by at least a factor of three in comparison to the result (5.117) following from the $\chi^2$ calculation.
We summarise our results for the parameters $Z$ and $m_{\sigma_N}$:

$$Z_\pi = 1.67 \pm 0.2\,, \; m_{\sigma_N} = 332^{+145}_{-44} \text{ MeV}. \tag{5.118}$$

The central values of all parameters of the original set (5.8) are given in Table 5.1. They follow from the $\chi^2$ fit $(m_{\sigma_N}, h_1)$, via decay width constraints $(h_2, g_2)$, and from Eqs. (5.14) - (5.19) and (5.27) - (5.28). The central values of $Z_\pi$, $m_{\sigma_N}$ and $h_1$, Eq. (5.117), have been used to calculate all other parameters. We neglect the errors, apart from those of $m_1$, which in this scenario vary in a large range.

Note that the values of $a_0^2$ depend strongly on the choice of the parameters $Z_\pi$ and $m_1$. Whereas for the central values of $Z_\pi$ and $m_1$ this scattering length is constant and has the value $a_0^2 = -0.0454$, its value increases if $Z_\pi$ and $m_1$ are considered at their respective boundaries, see Fig. 5.4.

| *Parameter* | $m_{\sigma_N}$ | $h_1$ | $h_2$ | $h_3$ |
|---|---|---|---|---|
| *Value* | 332 MeV | -68 | 80 | 2.4 |
| *Parameter* | $g_1$ | $g_2$ | $m_0$ | $m_1$ |
| *Value* | 6.4 | 3.1 | 210 MeV | $652^{+123}_{-652}$ MeV |
| *Parameter* | $\lambda_1$ | $\lambda_2$ | $c$ | $h_{0N}$ |
| *Value* | -14 | 33 | 88744 MeV$^2$ | $1 \cdot 10^6$ MeV$^3$ |

**Table 5.1:** Central values of parameters for Scenario I.

The value of $Z_\pi$ alone allows us to calculate certain decay widths in the model. For example, as a consistency check we obtain $\Gamma_{a_1\to\pi\gamma} = 0.640^{+0.261}_{-0.231}$ MeV which is in good agreement with the experimental result. Also, given that the $a_0 \to \eta_N\pi$ decay amplitude only depends on $Z_\pi$, it is possible to calculate the value of this amplitude, Eq. (5.65). For $Z_\pi = 1.67$, we obtain the value of 3939 MeV for the decay amplitude $a_0 \to \eta\pi$ involving the physical $\eta$ field if the $\eta$-$\eta'$ mixing angle of $\varphi_\eta = -36°$ [227] is taken. The Crystal Barrel Collaboration [114] obtained 3330 MeV and hence there is an approximate discrepancy of 20%. If the KLOE Collaboration [228] value of $\varphi_\eta = -41.4°$ is considered, then the value of $A_{a_0\to\eta\pi} = 3373$ MeV follows – in perfect agreement with the Crystal Barrel value. From this we conclude that this scenario prefers a relatively large value of the $\eta$-$\eta'$ mixing angle. In fact, if we use the Crystal Barrel value $A^{\rm exp}_{a_0\to\eta\pi} = 3330$ MeV as input, we would predict $\varphi_\eta = -41.8°$ for the central value of $Z_\pi$ as well as $\varphi_\eta = -42.3°$ and $\varphi_\eta = -41.6°$ for the highest and lowest values of $Z_\pi$, respectively, i.e., $\varphi_\eta = -41.8°^{+0.2°}_{-0.5°}$. This is in excellent agreement with the KLOE collaboration result $\varphi_\eta = -41.4° \pm 0.5°$ but also with the results from approaches using the Bethe-Salpeter formalism, such as the one in Ref. [231].

### 5.3.2 Decay Width $\sigma_N \to \pi\pi$

The sigma decay width $\Gamma_{\sigma_N\to\pi\pi}$ depends on all three parameters $Z_\pi$, $m_1$ (originally $h_1$), and $m_{\sigma_N}$. In Fig. 5.5 we show the dependence of this decay width on the sigma mass for fixed values of $Z_\pi$ and $m_1$, varying the latter within their respective boundaries.

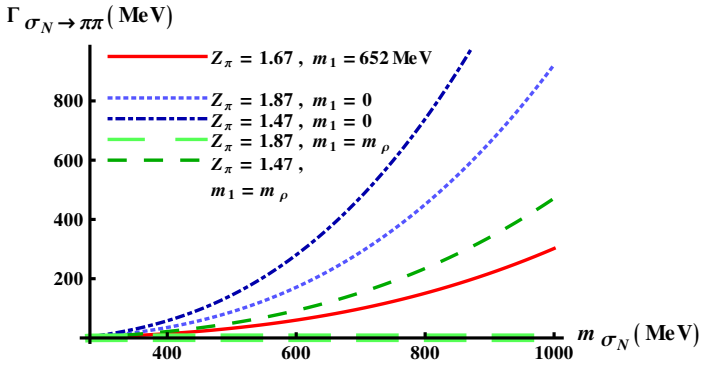


**Figure 5.5:** $\Gamma_{\sigma_N\to\pi\pi}$ as function of $m_{\sigma_N}$ for different values of $Z_\pi$ and $m_1$. The PDG [10] notes $\Gamma_{\sigma_N} = (600 - 1000)$ MeV; the results from the chiral perturbation theory suggest $\Gamma_{\sigma_N} = 544$ MeV [41] and $\Gamma_{\sigma_N} = 510$ MeV [42].

Generally, the values that we obtain are too small when compared to the PDG data [10] and to other calculations of the sigma meson decay width, such as the one performed by Leutwyler *et*

*al.* [41] who found $\Gamma_{\sigma_N\to\pi\pi}/2 = 272^{+9}_{-12.5}$ MeV and Peláez *et al.* [42] who found $\Gamma_{\sigma_N\to\pi\pi}/2 = (255 \pm 16)$ MeV. The largest values for the decay width that we were able to obtain within our model are for the case when $Z_\pi$ is as small as possible, $Z_\pi = 1.47$, and $m_1 = 0$, i.e., when the $\rho$ mass is solely generated by the quark condensate. As seen above, for this case the scattering lengths allow a maximum value $m_{\sigma_N} = 477$ MeV, for which $\Gamma_{\sigma_N\to\pi\pi} \cong 145$ MeV. In all other cases, the decay width is even smaller. However, as will be discussed in Sec. 5.3.3, the case $m_1 = 0$ leads to the unphysically small value $\Gamma_{a_1\to\sigma_N\pi} \simeq 0$ and should therefore not be taken too seriously. As apparent from Fig. 5.4, excluding small values of $m_1$ would require smaller values for $m_{\sigma_N}$ in order to be consistent with the scattering lengths. According to Fig. 5.5, however, this in turn leads to even smaller values for the decay width.
Hence, we conclude that the isoscalar meson in our model cannot be $f_0(600)$, thus excluding that this resonance is predominantly a $\bar{q}q$ state and the chiral partner of the pion. Then the interpretation of the isospin-one state $a_0(980)$ as a (predominantly) quarkonium state is also excluded. The only choice is to consider Scenario II, see Sec. 5.4, i.e., to interpret the scalar states above 1 GeV, $f_0(1370)$ and $a_0(1450)$, as being predominantly quarkonia. If the decay width of $f_0(1370)$ could be described by the model, this would be a very strong indication that these higher-lying states can be indeed interpreted as (predominantly) $\bar{q}q$ states. Note that very similar results about the nature of the light scalar mesons were also found using different approaches: from an analysis of the meson behaviour in the large-$N_c$ limit in Refs. [83] and [232] as well as from lattice studies, such as those in Refs. [233].
We remark that the cause for preventing a reasonable fit of the light sigma decay width is the interference term arising from the vector mesons in Eq. (9.27). In the unphysical case without vector meson degrees of freedom, a simultaneous fit of the decay width and the scattering lengths is possible, see Fig. 5.6 and Ref. [55].

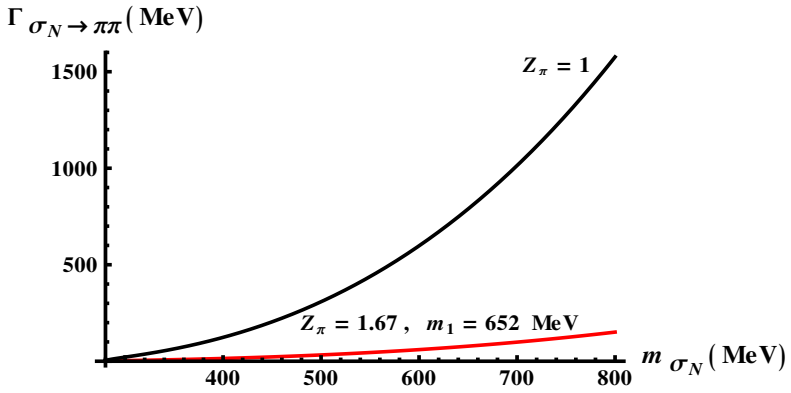


**Figure 5.6:** $\Gamma_{\sigma_N\to\pi\pi}$ as function of $m_{\sigma_N}$ in the case without (axial-)vectors (upper line, corresponds to $Z_\pi = 1$) and in the case with (axial-)vectors (lower line, exemplary for the central values of $Z_\pi$ and $m_1$). A strong suppression of $\Gamma_{\sigma_N}$ is observed upon inclusion of the (axial-)vectors into the model.

### 5.3.3 Decays of the $a_1(1260)$ Meson

We first consider the decay width $\Gamma_{a_1\to\rho\pi}$. For a given $m_{a_1}$, this decay width depends only on $Z_\pi$. The PDG quotes a rather large band of values, $\Gamma^{(\mathrm{exp})}_{a_1\to\rho\pi} = (250 - 600)$ MeV. For $m_{a_1} = 1230$ MeV, our fit of meson properties yields $Z_\pi = 1.67 \pm 0.2$. The ensuing region is shown as shaded

area in Fig. 5.7. For $m_{a_1} = 1230$ MeV, $\Gamma_{a_1\to\rho\pi}$ decreases from 2.4 GeV to 353 MeV, if $Z_\pi$ varies from 1.47 to 1.87.

We also observe from Fig. 5.7 that the range of values for $Z_\pi$, which give values for $\Gamma_{a_1\to\rho\pi}$ consistent with the experimental error band, becomes larger if one considers smaller masses for the $a_1$ meson. We have taken $m_{a_1} = 1180$ MeV and $m_{a_1} = 1130$ MeV, the latter being similar to the values used in Refs. [47] and [234]. Repeating our calculations, we obtain a new range of possible values for $Z_\pi$, $Z_\pi \simeq 1.69 \pm 0.2$ for $m_{a_1} = 1180$ MeV and $Z_\pi \simeq 1.71 \pm 0.2$ for $m_{a_1} = 1130$ MeV. For the respective central values of $Z_\pi$ we then compute $\Gamma_{a_1\to\rho\pi}^{m_{a_1}=1180\ \mathrm{MeV}} = 483$ MeV ($Z_\pi^{m_{a_1}=1180\,\mathrm{MeV}} = 1.69$) and $\Gamma_{a_1\to\rho\pi}^{m_{a_1}=1130\ \mathrm{MeV}} = 226$ MeV ($Z_\pi^{m_{a_1}=1130\,\mathrm{MeV}} = 1.71$), in good agreement with experimental data. All other results remain valid when $m_{a_1}$ is decreased by about 100 MeV. Most notably, the $f_0(600)$ decay width remains too small.

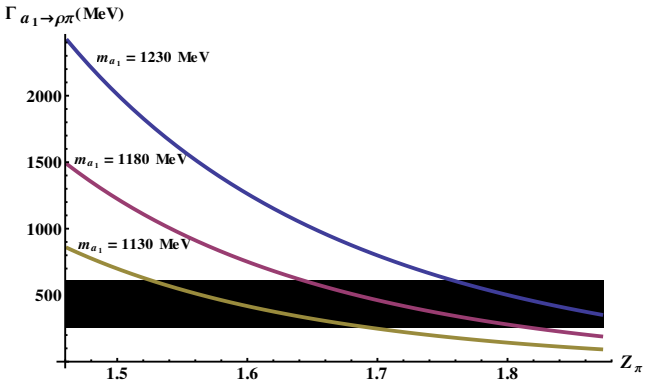


**Figure 5.7:** $\Gamma_{a_1\to\rho\pi}$ for different values of $m_{a_1}$. The shaded area corresponds to the possible values of $\Gamma_{a_1\to\rho\pi}$ as stated by the PDG.

We also consider the $a_1 \to \sigma_N\pi$ decay width. Experimental data on this decay channel [10] are inconclusive. The value $\Gamma_{a_1\to\sigma_N\pi} = 56$ MeV is obtained for the central values of $Z_\pi$, $m_1$, $m_{\sigma_N}$ and $\Gamma_{f_{1N}\to a_0\pi}$ (which was used to constrain $h_2$ via $Z_\pi$). Taking the limit $m_1 = 0$ pulls the value of $\Gamma_{a_1\to\sigma_N\pi}$ down to practically zero, regardless of whether $Z_\pi = Z_{\pi\,\mathrm{min}}$ or $Z_\pi = Z_{\pi\,\mathrm{max}}$. This is an indication that the $m_1 = 0$ limit, where $m_\rho$ is completely generated from the quark condensate, cannot be physical. Note that the case $Z_\pi = Z_{\pi\,\mathrm{max}} = 1.87$ and $m_1 \equiv m_\rho$, i.e., where the quark condensate contribution to the $\rho$ mass vanishes, leads to a rather large value of $\Gamma_{a_1\to\sigma_N\pi}$, e.g., for the central value of $m_{\sigma_N} = 332$ MeV the value of $\Gamma_{a_1\to\sigma_N\pi} = 120$ MeV follows. Interestingly, this picture persists even if lower values of $m_{a_1}$ are considered. Improving experimental data for this decay channel would allow us to further constrain our parameters.

### 5.3.4 The Case of Isospin-Exact Scattering Lengths

So far, the values of the scattering lengths used in our fit, $a_0^0 = 0.218 \pm 0.020$ and $a_0^2 = -0.0457 \pm 0.0125$ [43], account for the small explicit breaking of isospin symmetry due to the difference of the up and down quark masses. However, in our model the isospin symmetry is exact. Thus, one should rather use the isospin-exact values $a_0^{0\,(\mathrm{I})} = 0.244 \pm 0.020$ and $a_0^{2\,(\mathrm{I})} = -0.0385 \pm 0.0125$ [235]. In this section we will briefly show that the conclusions reached so far remain qualitatively unchanged if the isospin-exact values for the scattering lengths are considered.

Performing the $\chi^2$ fit, Eq. (5.116), with $\Gamma_{a_1\to\pi\gamma}$, $a_0^{0\,(\mathrm{I})}$ and $a_0^{2\,(\mathrm{I})}$ as experimental input yields $Z_\pi = 1.67 \pm 0.2$ – unchanged in comparison with the previous case ($Z_\pi$ is largely determined by $\Gamma_{a_1\to\pi\gamma}$ which is the same in both $\chi^2$ calculations), $h_1 = -116 \pm 70$, and $m_{\sigma_N} = (284 \pm 16)$ MeV. Note that in this case the errors are much smaller than previously. The reason is that the mean value of $m_{\sigma_N}$ is almost on top of the two-pion decay threshold and thus leads to an artificially small error band. For such small values of $m_{\sigma_N}$ the decay width $\Gamma_{\sigma_N\to\pi\pi}$ is at least an order of magnitude smaller than the physical value, but even for values of $m_{\sigma_N}$ up to 500 MeV (not supported by our error analysis) the decay width never exceeds 150 MeV, see Fig. 5.5.

## 5.4 Scenario II: Scalar Quarkonia above 1 GeV

A possible way to resolve the problem of the unphysically small two-pion decay width of the sigma meson is to identify the fields $\sigma_N$ and $a_0$ of the model with the resonances $f_0(1370)$ and $a_0(1450)$, respectively. Thus, the scalar quarkonium states are assigned to the energy region above 1 GeV. In the following we investigate the consequences of this assignment. However, the analysis cannot be conclusive for various reasons:

- The glueball field is missing. Many studies find that its role in the mass region at about 1.5 GeV is crucial, since it mixes with the other scalar resonances. Indeed, we will extend the $N_f = 2$ model in Chapter 12 to include the dilaton field representing the scalar glueball; however, the ensuing result about the structure of $f_0(1370)$ as a $\bar{q}q$ state (see Sec. 5.4.2) will remain unchanged.
- The light scalar mesons below 1 GeV, such as $f_0(600)$ and $a_0(980)$, are not included as elementary fields in our model. The question is if they can be dynamically generated from the pseudoscalar fields already present in our model by solving a Bethe-Salpeter equation. If not, they should be introduced as additional elementary fields from the very beginning [see also the discussion in Ref. [202]].
- Due to absence of the resonance $f_0(600)$, the $\pi\pi$ scattering length $a_0^0$ cannot be correctly described at tree-level: whereas $a_0^2$ stays always within the experimental error band, $a_0^0$ clearly requires a light scalar meson for a proper description of experimental data because a large value of $m_{\sigma_N}$ drives this quantity to the Weinberg limit ($\simeq 0.159$ [236]) which is outside the experimental error band (see Fig. 5.4).

Despite these drawbacks, we turn to a quantitative analysis of this scenario.

### 5.4.1 Decays of the $a_0(1450)$ Meson

As in Scenario I, the parameter $g_2$ can be expressed as a function of $Z_\pi$ by using the $\rho \to \pi\pi$ decay width (5.44). However, the parameter $h_2$ can no longer be fixed by the $f_{1N} \to a_0\pi$ decay width: the $a_0$ meson is now identified with the $a_0(1450)$ resonance listed in Ref. [10], with a central mass of $m_{a_0} = 1474$ MeV, and thus $f_{1N}$ is too light to decay into $a_0$ and $\pi$. One would be able to determine $h_2$ from the (energetically allowed) decay $a_0(1450) \to f_{1N}\pi$, but the corresponding decay width is not experimentally known.
Instead of performing a global fit, it is more convenient to proceed step by step and calculate the parameters $Z_\pi$, $h_1$, $h_2$ explicitly. We vary $m_{\sigma_N} \equiv m_{f_0(1370)}$ within the experimentally known error band [10] and check if our result for $\Gamma_{f_0(1370)\to\pi\pi}$ is in agreement with experimental data.

We first determine $Z_\pi$ from $a_1 \to \pi\gamma$, Eq. (5.76), and obtain $Z_\pi = 1.67 \pm 0.21$. We then immediately conclude that the $a_1 \to \rho\pi$ decay width, Eq. (5.95), will remain the same as in Scenario I because this decay width depends on $Z_\pi$ (which is virtually the same in both scenarios) and $g_2$ [which is fixed via $\Gamma_{\rho\to\pi\pi}$, Eq. (5.45), in both scenarios].
The parameter $h_1$, being large-$N_c$ suppressed, will be set to zero in the present study. We then only have to determine the parameter $h_2$. This is done by fitting the total decay width of the $a_0(1450)$ meson to its experimental value [10],

$$\Gamma_{a_0(1450)}(Z_\pi, h_2) = \Gamma_{a_0\to\pi\eta} + \Gamma_{a_0\to\pi\eta'} + \Gamma_{a_0\to KK} + \Gamma_{a_0\to\omega_N\pi\pi} \equiv \Gamma^{\rm exp}_{a_0(1450)} = (265 \pm 13)\ \text{MeV}. \tag{5.119}$$

Although kaons have not yet been included into the calculations, we can easily evaluate the decay into $KK$ by using flavour symmetry

$$\Gamma_{a_0(1450)\to KK}(Z_\pi, h_2) = 2\,\frac{k(m_{a_0}, m_K, m_K)}{8\pi m_{a_0}^2} |-i\bar{\mathcal{M}}_{a_0(1450)\to KK}(Z_\pi, h_2)|^2, \tag{5.120}$$

$$\begin{aligned} -i\bar{\mathcal{M}}_{a_0(1450)\to KK}(Z_\pi, h_2) = \frac{i}{2Z_\pi f_\pi}\Bigg\{ & m_{\eta_N}^2 - m_{a_0}^2 + \left(1 - \frac{1}{Z_\pi^2}\right) \\ & \times \left[1 - \frac{1}{2}\frac{Z_\pi^2\phi_N^2}{m_{a_1}^2}(h_2 - h_3)\right](m_{a_0}^2 - 2m_K^2)\Bigg\}. \end{aligned} \tag{5.121}$$

The remaining, experimentally poorly known decay width $\Gamma_{a_0(1450)\to\omega_N\pi\pi}$ can be calculated from the sequential decay $a_0 \to \omega_N\rho \to \omega_N\pi\pi$. Note that the first decay step requires the $\rho$ to be slightly below its mass shell, since $m_{a_0} < m_\rho + m_{\omega_N}$. We denote the off-shell mass of the $\rho$ meson by $x_\rho$. From the Lagrangian (6.1) we obtain the following $a_0\omega_N\rho$ interaction Lagrangian:

$$\mathcal{L}_{a_0\omega_N\rho} = (h_2 + h_3)\phi_N \boldsymbol{a}_0 \cdot \omega_{N\mu}\boldsymbol{\rho}^\mu. \tag{5.122}$$

The generic calculation of the decay width of a scalar state $S$ into two vector states $V_{1,2}$ has already been presented in Sec. 2.6.4. We identify the state $V_2$ in the decay amplitude (2.206) with our off-shell $\rho$ meson; the vertex from the Lagrangian (5.122) reads $h^{\mu\nu}_{a_0\omega_N\rho} = i(h_2+h_3)\phi_N g^{\mu\nu}$ and consequently we obtain from Eq. (2.208):

$$\begin{aligned} \Gamma_{a_0(1450)\to\omega_N\rho}(x_\rho) = & \frac{k(m_{a_0}, m_{\omega_N}, x_\rho)}{8\pi m_{a_0}^2}(h_2 + h_3)^2 Z_\pi^2 f_\pi^2 \\ & \times \left[3 - \frac{x_\rho^2}{m_\rho^2} + \frac{(m_{a_0}^2 - x_\rho^2 - m_{\omega_N}^2)^2}{4m_{\omega_N}^2 m_\rho^2}\right] \end{aligned} \tag{5.123}$$

with $I = 3$ used in the formula presented in Eq. (2.208).
The full decay width $\Gamma_{a_0(1450)\to\omega_N\pi\pi}$ is then obtained from Eq. (2.209):

$$\Gamma_{a_0(1450)\to\omega_N\pi\pi} = \int_0^\infty \mathrm{d}x_\rho\, \Gamma_{a_0\to\omega_N\rho}(x_\rho)\, d_\rho(x_\rho), \tag{5.124}$$

where $d_\rho(x_\rho)$ is the mass distribution of the $\rho$ meson, which is taken to be of relativistic Breit-Wigner form [see Eq. (2.175)]:

$$d_\rho(x_\rho) = N_\rho \frac{x_\rho^2 \Gamma^{\rm exp}_{\rho\to\pi\pi}}{(x_\rho^2 - m_\rho^2)^2 + (x_\rho \Gamma^{\rm exp}_{\rho\to\pi\pi})^2}\,\theta(x_\rho - 2m_\pi), \tag{5.125}$$

where $\Gamma^{\rm exp}_{\rho\to\pi\pi} = 149.1$ MeV and $m_\rho = 775.49$ MeV [10]. [As demonstrated in Eq. (2.174), one should in general use the theoretical quantity $\Gamma_{\rho\to\pi\pi}(x_\rho)$ instead of $\Gamma^{\rm exp}_{\rho\to\pi\pi}$, see Refs. [46, 237]. This is, however, numerically irrelevant in the following.] The normalisation constant $N_\rho$ is chosen such that

$$\int_0^\infty \mathrm{d}x_\rho \, d_\rho(x_\rho) = 1, \tag{5.126}$$

in agreement with the interpretation of $\mathrm{d}x_\rho \, d_\rho(x_\rho)$ as the probability that the off-shell $\rho$ meson has a mass between $x_\rho$ and $x_\rho + \mathrm{d}x_\rho$.

Inserting Eqs. (5.66), (5.68), (5.120) and (5.124) into Eq. (5.119), we can express $h_2$ as a function of $Z_\pi$, analogously to Eq. (5.45) where $g_2$ was expressed as a function of $Z_\pi$. Similarly to that case, we obtain two bands for $h_2$, $-115 \leq h_2 \leq -20$ and $-25 \leq h_2 \leq 10$, the width of the bands corresponding to the uncertainty in determining $Z_\pi$, $Z_\pi = 1.67 \pm 0.21$. Both bands for $h_2$ remain practically unchanged if the 5% experimental uncertainty of $\Gamma^{\rm exp}_{a_0(1450)}$ is taken into account and thus we only use the mean value 265 MeV in the following. Since $h_1$ is assumed to be zero, Eq. (5.29) allows to express $m_1$ as a function of $Z_\pi$, $m_1 = m_1(Z_\pi, h_1 = 0, h_2(Z_\pi))$ (we neglect the experimental uncertainties of $m_\rho$, $m_{a_1}$, and $f_\pi$). The result is shown in Fig. 5.8. The first band of (lower) $h_2$ values should be discarded because it leads to $m_1 > m_\rho$. The second set of (higher) values leads to $m_1 < m_\rho$ only if the lower boundary for $Z_\pi$ is 1.60 rather than 1.46. Thus, we shall use the set of larger $h_2$ values and take the constraint $m_1 < m_\rho$ into account by restricting the values for $Z_\pi$ to the range $Z_\pi = 1.67^{+0.21}_{-0.07}$. As can be seen from Fig. 5.8, this sets a lower boundary for the value of $m_1$, $m_1 \geq 580$ MeV. Thus, in this scenario we obtain $m_1 = 720^{+55}_{-140}$ MeV.

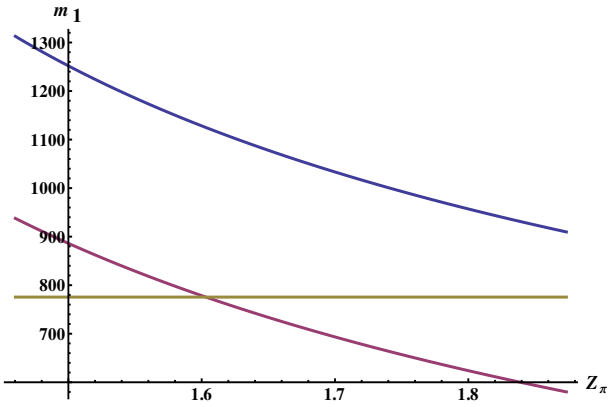


**Figure 5.8:** Dependence of $m_1$ on $Z_\pi$. The upper curve corresponds to the lower set of $h_2$ values and the lower curve to the higher set of $h_2$ values. The horizontal line corresponds to $m_\rho$.

The values for the other parameters can be found in Table 5.2 (only central values are shown with the exception of $m_1$ where the corresponding uncertainties are stated as well).

Note that $\lambda_1 \ll \lambda_2$, in agreement with the expectations from the large-$N_c$ limit, Eq. (4.52). The value of $m_1 = 720$ MeV is sizable and constitutes a dominant contribution to the $\rho$ mass. This implies that non-quark contributions, for instance a gluon condensate, play a decisive role in the $\rho$ mass generation.

As a final step, we study the ratios $\Gamma_{a_0(1450)\to\eta'\pi}/\Gamma_{a_0(1450)\to\eta\pi}$ and $\Gamma_{a_0(1450)\to K\overline{K}}/\Gamma_{a_0(1450)\to\eta\pi}$.

| *Parameter* | $h_1$ | $h_2$ | $h_3$ | $g_1$ |
|---|---|---|---|---|
| *Value* | 0 | 4.7 | 2.4 | 6.4 |
| *Parameter* | $g_2$ | $m_0^2$ | $m_1$ | $\lambda_1$ |
| *Value* | 3.1 | -811987 MeV$^2$ | $720^{+55}_{-140}$ MeV | -3.6 |
| *Parameter* | $\lambda_2$ | $c$ | $h_{0N}$ | |
| *Value* | 84 | 88747 MeV$^2$ | $1 \cdot 10^6$ MeV$^3$ | |

**Table 5.2:** Central values of the parameters for Scenario II.

Their experimental values read [10]

$$\frac{\Gamma^{\rm exp}_{a_0(1450)\to\eta'\pi}}{\Gamma^{\rm exp}_{a_0(1450)\to\eta\pi}} = 0.35 \pm 0.16, \tag{5.127}$$

$$\frac{\Gamma^{\rm exp}_{a_0(1450)\to K\overline{K}}}{\Gamma^{\rm exp}_{a_0(1450)\to\eta\pi}} = 0.88 \pm 0.23. \tag{5.128}$$

Using the central value $Z_\pi = 1.67$ and $\varphi_\eta = -36^\circ$ for the $\eta$-$\eta'$ mixing angle, we obtain $\Gamma_{a_0(1450)\to\eta'\pi}/\Gamma_{a_0(1450)\to\eta\pi} = 1.0$ and $\Gamma_{a_0(1450)\to K\overline{K}}/\Gamma_{a_0(1450)\to\eta\pi} = 0.96$. The latter is in very good agreement with the experiment, the former a factor of two larger. Note, however, that according to Eqs. (5.59) and (5.67) the value of the ratio $\Gamma_{a_0(1450)\to\eta'\pi}/\Gamma_{a_0(1450)\to\eta\pi}$ is proportional to $\sin^2\varphi_\eta/\cos^2\varphi_\eta$. If a lower value of the angle is considered, e.g., $\varphi_\eta = -30^\circ$, then we obtain $\Gamma_{a_0(1450)\to\eta'\pi}/\Gamma_{a_0(1450)\to\eta\pi} = 0.58$ for the central value of $Z_\pi$ and the central value of $\Gamma_{a_0(1450)}$ in Eq. (5.119). Taking $Z_\pi = Z_{\pi\,\rm max}$ and the upper boundary $\Gamma^{\rm exp}_{a_0(1450)} = 278$ MeV results in $\Gamma_{a_0(1450)\to\eta'\pi}/\Gamma_{a_0(1450)\to\eta\pi} = 0.48$, i.e., in agreement with the experimental value. Therefore, our results in this scenario favour a smaller value of $\varphi_\eta$ than the one suggested by the KLOE Collaboration [228].

It is possible to calculate the decay width $\Gamma_{a_0(1450)\to\omega_N\pi\pi}$ using Eq. (5.124). We have obtained a very small value $\Gamma_{a_0(1450)\to\omega_N\pi\pi} = 0.1$ MeV. From Eq. (5.66) we obtain $\Gamma_{a_0(1450)\to\eta\pi} = 89.5$ MeV, such that the ratio $\Gamma_{a_0(1450)\to\omega_N\pi\pi}/\Gamma_{a_0(1450)\to\eta\pi} = 0.0012$, in contrast to the results of Ref. [238].

### 5.4.2 Decays of the $f_0(1370)$ Meson

It is now possible to calculate the width for the $f_0(1370) \to \pi\pi$ decay using Eq. (9.27). The decay width depends on the $f_0(1370)$ mass, $Z_\pi$, $h_1$, and $h_2$ which is expressed via $Z_\pi$ using Eq. (5.119). The values of the latter three are listed in Table 5.2. In Fig. 5.9 we show the decay width as a function of the mass of $f_0(1370)$.

Assuming that the two-pion decay dominates the total decay width (true up to a mass of 1350 MeV, see Sec. 3.3), we observe a good agreement with the experimental values. The values of the decay width are $\sim 100$ MeV larger than those of Ref. [40] but this is not surprising as the current version of the model contains no strange degrees of freedom (they are discussed in Chapters 9 and 11) and no glueball (discussed in Chapter 12). We will see in the mentioned chapters that the currently missing contributions to the decay width will reduce the upper boundary on $m_{f_0(1370)}$. Nevertheless, the correspondence with the experiment is a lot better in this scenario where we have identified $f_0(1370)$ rather than $f_0(600)$ as the (predominantly) isoscalar $\bar{q}q$ state. Note that

this result has been obtained using the decay width of the $a_0(1450)$ meson (in order to express $h_2$ via $Z_\pi$) which is also assumed to be a scalar $\bar{q}q$ state in this scenario.
It is remarkable that vector mesons are crucial to obtain realistic values for the decay width of $f_0(1370)$: without vector mesons, the decay width is $\sim 10$ GeV and thus much too large. This is why Scenario II has not been considered in the standard linear sigma model.

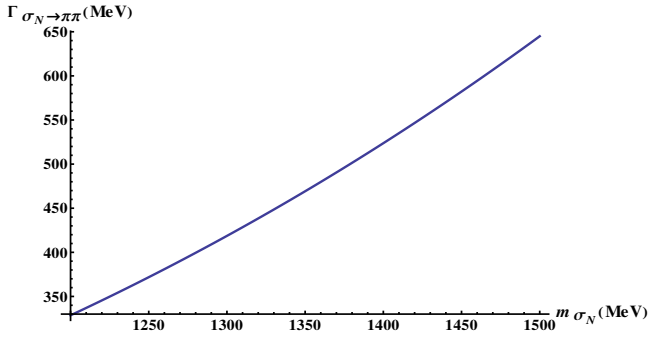


**Figure 5.9:** Dependence of the $\sigma_N \equiv f_0(1370)$ decay width on $m_{\sigma_N}$. The experimental value of the width is expected to be in the range (1200-1500) MeV [10].

The four-body decay $f_0(1370) \to 4\pi$ can also be studied. Similarly to the $a_0(1450) \to \omega_N \rho$ decay, we view $f_0(1370) \to 4\pi$ as a sequential decay of the form $f_0(1370) \to \rho\rho \to 4\pi$. The Lagrangian (6.1) leads to

$$\mathcal{L}_{\sigma\rho\rho} = \frac{1}{2}(h_1 + h_2 + h_3)\phi_N \sigma_N \boldsymbol{\rho}_\mu^2 \tag{5.129}$$

and repeating the calculation of Sec. 2.6.4 we obtain

$$\begin{aligned}\Gamma_{f_0(1370)\to\rho\rho}(x_{1\rho}, x_{2\rho}) = &\frac{3}{16\pi}\frac{k(m_{f_0}, x_{1\rho}, x_{2\rho})}{m_{f_0}^2}(h_1 + h_2 + h_3)^2 \\ &\times Z_\pi^2 f_\pi^2 \left[4 - \frac{x_{1\rho}^2 + x_{2\rho}^2}{m_\rho^2} + \frac{(m_{f_0}^2 - x_{1\rho}^2 - x_{2\rho}^2)^2}{4m_\rho^4}\right],\end{aligned} \tag{5.130}$$

where $x_{1\rho}$ and $x_{2\rho}$ are the off-shell masses of the $\rho$ mesons. The decay width $\Gamma_{f_0\to 4\pi}$ is then given by

$$\Gamma_{f_0(1370)\to 4\pi} = \int_0^\infty \int_0^\infty \mathrm{d}x_{1\rho}\, \mathrm{d}x_{2\rho}\, \Gamma_{f_0(1370)\to\rho\rho}(x_{1\rho}, x_{2\rho}) d_\rho(x_{1\rho})\, d_\rho(x_{2\rho}), \tag{5.131}$$

with $\Gamma_{f_0(1370)\to\rho\rho}(x_{1\rho}, x_{2\rho})$ from Eq. (5.130) and $d_\rho(x_\rho)$ from Eq. (5.125).
Using the previous values for the parameters we obtain that the $\rho\rho$ contribution for the decay is small: $\Gamma_{f_0(1370)\to\rho\rho\to 4\pi} \simeq 10 \pm 10$ MeV. (The error comes from varying $Z_\pi$ between 1.6 and 1.88.) Reference [40] quotes 54 MeV for the total $4\pi$ decay width at $\sim 1300$ MeV. Since Ref. [239] ascertains that about 26% of the total $4\pi$ decay width originates from the $\rho\rho$ decay channel, our result is qualitatively consistent with these findings.

## 5.5 Conclusions from the Two-Flavour Version of the Model

In this chapter we have presented the two-flavour version of the generic Lagrangian with vector mesons and global chiral invariance introduced in Chapter 4. This Lagrangian describes mesons

as pure quarkonium states. As shown in Sec. 5.3, the resulting low-energy phenomenology is in general in good agreement with experimental data – with one exception: the model fails to correctly describe the $f_0(600) \to \pi\pi$ decay width. This led us to conclude that $f_0(600)$ and $a_0(980)$ cannot be predominantly $\bar{q}q$ states.

Assigning the scalar fields $\sigma_N$ and $a_0$ of the model to the $f_0(1370)$ and $a_0(1450)$ resonances, respectively, improves the results for the decay widths considerably. We have obtained $\Gamma_{f_0(1370)\to\pi\pi} \simeq$ (300-500) MeV for $m_{f_0(1370)} =$ (1200-1400) MeV (see Fig. 5.9). Thus, the scenario in which the scalar states above 1 GeV, $f_0(1370)$ and $a_0(1450)$, are considered to be (predominantly) $\bar{q}q$ states appears to be favoured over the assignment in which $f_0(600)$ and $a_0(980)$ are considered (predominantly) $\bar{q}q$ states. However, a more detailed study of this scenario is necessary, because a glueball state with the same quantum numbers mixes with the quarkonium states. This allows to include the experimentally well-known resonance $f_0(1500)$ into the study.

Of course, interpreting $f_0(1370)$ and $a_0(1450)$ as $\bar{q}q$ states leads to question about the nature of $f_0(600)$ and $a_0(980)$. Their presence is necessary for the correct description of $\pi\pi$ scattering lengths that differ from experiment for too large values of the isoscalar mass (see Sec. 5.3.1). We distinguish two possibilities: $(i)$ They can arise as (quasi-)molecular states. This is possible if the attraction in the $\pi\pi$ and $KK$ channels is large enough. In order to prove this, one should solve the corresponding Bethe-Salpeter equation in the framework of Scenario II. In this case $f_0(600)$ and $a_0(980)$ can be classified as genuinely dynamically generated states and should not appear in the Lagrangian, see the discussion in Ref. [202]. If, however, the attraction is not sufficient to generate the two resonances $f_0(600)$ and $a_0(980)$ we are led to the alternative possibility that $(ii)$ these two scalar states must be incorporated into the model as additional tetraquark states [194]. In this case they shall appear from the very beginning in the Lagrangian and should not be considered as dynamically generated states. Of course, the isoscalar tetraquark, quarkonium, and glueball will mix to produce $f_0(600)$, $f_0(1370)$, and $f_0(1500)$, and the isovector tetraquark and quarkonium will mix to produce $a_0(980)$ and $a_0(1450)$.

An extension of the model to $N_f = 3$ will be performed in the next chapters. One reason is that much more data are available for the strange mesons, which constitute an important test for the validity of our approach. In addition, an extremely important question arising from the results presented so far will be addressed: whether the conclusions reached at $N_f = 2$ [in particular that $f_0(1370)$ rather than $f_0(600)$ is a $\bar{q}q$ state] hold in the more general three-flavour case.

## 5.6 The Full $N_f = 2$ Lagrangian

This is the final form of the Lagrangian (5.1) that is obtained after the shifts (5.12) and the renormalisation of the pseudoscalar wave functions; $\rho^{\mu\nu} \equiv \partial^\mu \rho^\nu - \partial^\nu \rho^\mu$; $a_1^{\mu\nu} \equiv \partial^\mu a_1^\nu - \partial^\nu a_1^\mu$; $(\boldsymbol{A})_3$ marks the third component of the vector $\boldsymbol{A}$. Note that the term $\mathcal{L}_4$ contains the (axial-)vector four-point vertices [the terms $\sim g_{3,4,5,6}$ in the Lagrangian (5.1)]. We do not give the explicit form of $\mathcal{L}_4$ because it is not relevant for the results that are presented here.

$$\begin{aligned}\mathcal{L} = &\frac{1}{2}\left(\partial^\mu \sigma_N + g_1 Z_\pi\, \boldsymbol{\pi}\cdot\boldsymbol{a}_1^\mu + g_1 w_{a_1} Z_\pi^2\, \partial^\mu \boldsymbol{\pi}\cdot\boldsymbol{\pi} + g_1 Z_\pi \eta_N f_1^\mu + g_1 w_{a_1} Z_\pi^2 \eta_N\, \partial^\mu \eta_N\right)^2 \\ &- \frac{1}{2}\left[m_0^2 - c + 3\left(\lambda_1 + \frac{\lambda_2}{2}\right)\phi_N^2\right]\sigma_N^2\end{aligned}$$

$$
\begin{aligned}
&+\frac{1}{2}\left(Z_\pi\partial^\mu\boldsymbol{\pi}+g_1Z_\pi\boldsymbol{\rho}^\mu\times\boldsymbol{\pi}-g_1f_{1N}^\mu\boldsymbol{a}_0-g_1w_{a_1}Z_\pi\partial^\mu\eta_N\boldsymbol{a}_0-g_1\sigma_N\boldsymbol{a}_1^\mu-g_1w_{a_1}Z_\pi\sigma_N\partial^\mu\boldsymbol{\pi}\right)^2\\
&+\frac{1}{2}\left(Z_\pi\partial^\mu\eta_N-g_1\sigma_Nf_{1N}^\mu-g_1w_{a_1}Z_\pi\sigma_N\partial^\mu\eta_N-g_1\,\boldsymbol{a}_1^\mu\cdot\boldsymbol{a}_0-g_1w_{a_1}Z_\pi\,\partial^\mu\boldsymbol{\pi}\cdot\boldsymbol{a}_0\right)^2\\
&-\frac{1}{2}\left[m_0^2-c+\left(\lambda_1+\frac{\lambda_2}{2}\right)\phi_N^2\right]Z_\pi^2\boldsymbol{\pi}^2-\frac{1}{2}\left[m_0^2+c+\left(\lambda_1+\frac{\lambda_2}{2}\right)\phi_N^2\right]Z_\pi^2\eta_N^2\\
&+\frac{1}{2}\left[\partial^\mu\boldsymbol{a}_0+g_1\boldsymbol{\rho}^\mu\times\boldsymbol{a}_0+g_1Z_\pi f_{1N}^\mu\boldsymbol{\pi}+g_1w_{a_1}Z_\pi^2\boldsymbol{\pi}\partial^\mu\eta_N+g_1Z_\pi\eta_N\,\boldsymbol{a}_1^\mu+g_1w_{a_1}Z_\pi^2\eta_{\,N}\partial^\mu\boldsymbol{\pi}\right]^2\\
&-\frac{1}{2}\left[m_0^2+c+\left(\lambda_1+\frac{3}{2}\lambda_2\right)\phi_N^2\right]\boldsymbol{a}_0^2-\frac{\lambda_2}{2}[(\sigma_N\boldsymbol{a}_0+Z_\pi^2\eta_N\,\boldsymbol{\pi})^2+Z_\pi^2\boldsymbol{a}_0^2\boldsymbol{\pi}^2-Z_\pi^2(\boldsymbol{a}_0\cdot\boldsymbol{\pi})^2]\\
&-\frac{1}{4}\left(\lambda_1+\frac{\lambda_2}{2}\right)(\sigma_N^2+\boldsymbol{a}_0^2+Z_\pi^2\eta_N^2+Z_\pi^2\boldsymbol{\pi}^2)^2-\left(\lambda_1+\frac{\lambda_2}{2}\right)\phi_N\sigma_N\,(\sigma_N^2+\boldsymbol{a}_0^2+Z_\pi^2\eta_N^2+Z_\pi^2\boldsymbol{\pi}^2)\\
&-\lambda_2\phi_N\boldsymbol{a}_0\cdot(\sigma_N\boldsymbol{a}_0+Z_\pi^2\eta_N\,\boldsymbol{\pi})-\frac{1}{4}\,(\partial^\mu\omega_N^\nu-\partial^\nu\omega_N^\mu)^2+\frac{m_1^2}{2}\,(\omega_N^\mu)^2\\
&-\frac{1}{4}\left[\partial^\mu\boldsymbol{\rho}^\nu-\partial^\nu\boldsymbol{\rho}^\mu+g_2\boldsymbol{\rho}^\mu\times\boldsymbol{\rho}^\nu+g_2\boldsymbol{a}_1^\mu\times\boldsymbol{a}_1^\nu+g_2w_{a_1}Z_\pi\partial^\mu\boldsymbol{\pi}\times\boldsymbol{a}_1^\nu+g_2w_{a_1}Z_\pi\boldsymbol{a}_1^\mu\times\partial^\nu\boldsymbol{\pi}\right.\\
&\left.+\,g_2w_{a_1}^2Z_\pi^2(\partial^\mu\boldsymbol{\pi}\,)\times(\partial^\nu\boldsymbol{\pi})\right]^2\\
&+\frac{m_1^2}{2}(\boldsymbol{\rho}^\mu)^2-\frac{1}{4}\,(\partial^\mu f_{1N}^\nu-\partial^\nu f_{1N}^\mu)^2+\frac{m_1^2+g_1^2\phi_N^2}{2}\,(f_{1N}^\mu)^2+\frac{m_1^2+g_1^2\phi_N^2}{2}\,(\boldsymbol{a}_1^\mu)^2\\
&-\frac{1}{4}\left[\partial^\mu\boldsymbol{a}_1^\nu-\partial^\nu\boldsymbol{a}_1^\mu+g_2\boldsymbol{\rho}^\mu\times\boldsymbol{a}_1^\nu+g_2w_{a_1}Z_\pi\boldsymbol{\rho}^\mu\times\partial^\nu\boldsymbol{\pi}+g_2\boldsymbol{a}_1^\mu\times\boldsymbol{\rho}^\nu+g_2w_{a_1}Z_\pi(\partial^\mu\boldsymbol{\pi})\times\boldsymbol{\rho}^\nu\right]^2\\
&-g_1^2\,\phi_N\,\boldsymbol{a}_{1\mu}\cdot[\boldsymbol{\rho}^\mu\times Z_\pi\boldsymbol{\pi}-f_{1N}^\mu\boldsymbol{a}_0-w_{a_1}Z_\pi\boldsymbol{a}_0\,\partial^\mu\eta_N]\\
&-g_1^2w_{a_1}Z_\pi\,\phi_N\,\partial_\mu\boldsymbol{\pi}\cdot\,[Z_\pi\boldsymbol{\rho}^\mu\times\boldsymbol{\pi}-f_{1N}^\mu\boldsymbol{a}_0-w_{a_1}Z_\pi\partial^\mu\eta_N\,\boldsymbol{a}_0]\\
&+g_1^2\,\phi_Nf_{1N\mu}\,(\boldsymbol{a}_1^\mu\cdot\boldsymbol{a}_0+w_{a_1}Z_\pi\partial^\mu\boldsymbol{\pi}\cdot\boldsymbol{a}_0)\\
&+g_1^2w_{a_1}Z_\pi\,\phi_N\,\partial_\mu\eta_N\,(\boldsymbol{a}_1^\mu\cdot\boldsymbol{a}_0+w_{a_1}Z_\pi\partial^\mu\boldsymbol{\pi}\cdot\boldsymbol{a}_0)\\
&+g_1^2\,\phi_N\,\sigma_N\,[(f_{1N}^\mu)^2+2w_{a_1}Z_\pi f_{1N\,\mu}\partial^\mu\eta_N+w_{a_1}^2Z_\pi^2(\partial^\mu\eta_N)^2]\\
&+g_1^2\,\phi_N\,\sigma_N\,[(\boldsymbol{a}_1^\mu)^2+2w_{a_1}Z_\pi\boldsymbol{a}_{1\mu}\cdot\partial^\mu\boldsymbol{\pi}+w_{a_1}^2Z_\pi^2(\partial^\mu\boldsymbol{\pi})^2]\\
&-\frac{1}{2}\,\frac{g_1^2\phi_N^2}{m_{a_1}^2}\,Z_\pi^2\,(\partial_\mu\eta_N\partial^\mu\eta_N+\partial_\mu\boldsymbol{\pi}\cdot\partial^\mu\boldsymbol{\pi})\\
&+eA_\mu\{(\boldsymbol{a}_0\times\partial^\mu\boldsymbol{a}_0)_3+Z_\pi^2(\boldsymbol{\pi}\times\partial^\mu\boldsymbol{\pi})_3-4(\boldsymbol{\rho}^{\mu\nu}\times\boldsymbol{\rho}_\nu)_3-4[(\boldsymbol{a}_{1\nu}+Z_\pi w_{a_1}\partial_\nu\boldsymbol{\pi})\times\boldsymbol{a}_1^{\mu\nu}]_3\\
&+g_1\{2Z_\pi(f_{1N}^\mu+Z_\pi w_{a_1}\partial^\mu\eta_N)(\boldsymbol{a}_0\times\boldsymbol{\pi})_3+Z_\pi(\sigma_N+\phi_N)[(\boldsymbol{a}_1^\mu+Z_\pi w_{a_1}\partial^\mu\boldsymbol{\pi})\times\boldsymbol{\pi}]_3\\
&+\eta_N[\boldsymbol{a}_0\times(\boldsymbol{a}_1^\mu+Z_\pi w_{a_1}\partial^\mu\boldsymbol{\pi})]_3-a_0^3(a_0^1\rho^{\mu1}+a_0^2\rho^{\mu2})-Z_\pi^2\pi^3(\pi^1\rho^{\mu1}+\pi^2\rho^{\mu2})\\
&+\rho^{\mu3}[(a_0^1)^2+(a_0^2)^2+Z_\pi^2(\pi^1)^2+Z_\pi^2(\pi^2)^2]\}\\
&+4g_2\{[\boldsymbol{\rho}_\nu^2+\boldsymbol{a}_{1\nu}^2+Z_\pi^2w_{a_1}^2\,(\partial_\nu\boldsymbol{\pi})^2+Z_\pi w_{a_1}\boldsymbol{a}_{1\nu}\cdot\partial^\nu\boldsymbol{\pi}]\rho^{\mu3}\\
&+2\boldsymbol{\rho}_\nu\cdot(\boldsymbol{a}_1^\nu+Z_\pi w_{a_1}\partial^\nu\boldsymbol{\pi})\times(a_1^{\mu3}+Z_\pi w_{a_1}\partial^\mu\pi^3)\\
&-(\boldsymbol{\rho}_\nu\cdot\boldsymbol{\rho}^\mu+\boldsymbol{a}_{1\nu}\cdot\boldsymbol{a}_1^\mu+Z_\pi w_{a_1}\boldsymbol{a}_{1\nu}\cdot\partial^\mu\boldsymbol{\pi}+Z_\pi w_{a_1}\boldsymbol{a}_1^\mu\cdot\partial_\nu\boldsymbol{\pi}+Z_\pi^2w_{a_1}^2\partial_\nu\boldsymbol{\pi}\cdot\partial^\mu\boldsymbol{\pi})\rho^{\nu3}\\
&-(\boldsymbol{\rho}^\mu\cdot\boldsymbol{a}_{1\nu}+\boldsymbol{a}_1^\mu\cdot\boldsymbol{\rho}_\nu+Z_\pi w_{a_1}\boldsymbol{\rho}^\mu\cdot\partial_\nu\boldsymbol{\pi}+Z_\pi w_{a_1}\boldsymbol{\rho}_\nu\cdot\partial^\mu\boldsymbol{\pi})a_1^{\nu3}\}\}\\
&+\frac{e^2}{2}A_\mu A^\mu[(a_0^1)^2+(a_0^2)^2+Z_\pi^2(\pi^1)^2+Z_\pi^2(\pi^2)^2+4(\rho^{\nu1})^2+4(\rho^{\nu2})^2\\
&+4(a_{1\nu}^1+Z_\pi w_{a_1}\partial_\nu\pi^1)^2+4(a_{1\nu}^2+Z_\pi w_{a_1}\partial_\nu\pi^2)^2]\\
&-2e^2A_\mu A_\nu[\rho^{\mu1}\rho^{\nu1}+\rho^{\mu2}\rho^{\nu2}+(a_1^{\mu1}+Z_\pi w_{a_1}\partial^\mu\pi^1)(a_1^{\nu1}+Z_\pi w_{a_1}\partial^\nu\pi^1)\\
&+(a_1^{\mu2}+Z_\pi w_{a_1}\partial^\mu\pi^2)(a_1^{\nu2}+Z_\pi w_{a_1}\partial^\nu\pi^2)]+\mathcal{L}_{h_{1,2,3}}+\mathcal{L}_4
\end{aligned}
\tag{5.132}
$$

$$
\begin{aligned}
\mathcal{L}_{h_{1,2,3}} = & \left(\frac{h_1}{4}+\frac{h_2}{4}+\frac{h_3}{4}\right)\left(\sigma_N^2+2\phi_N\sigma_N+Z_\pi^2\eta_N^2+\boldsymbol{a}_0^2+Z_\pi^2\boldsymbol{\pi}^2\right)\left(\omega_{N\mu}^2+\boldsymbol{\rho}_\mu^2\right) \\
& + \left(\frac{h_1}{4}+\frac{h_2}{4}-\frac{h_3}{4}\right)\left(\sigma_N^2+2\phi_N\sigma_N+Z_\pi^2\eta_N^2+\boldsymbol{a}_0^2+Z_\pi^2\boldsymbol{\pi}^2\right)\{f_{1N\mu}^2+\boldsymbol{a}_{1\mu}^2 \\
& + Z_\pi^2 w_{a_1}^2[(\partial_\mu\eta_N)^2+(\partial_\mu\boldsymbol{\pi})^2]+2Z_\pi w_{a_1}(f_{1N\mu}\partial^\mu\eta_N+\boldsymbol{a}_{1\mu}\cdot\partial^\mu\boldsymbol{\pi})\} \\
& + \left(\frac{h_1}{4}+\frac{h_2}{4}+\frac{h_3}{4}\right)\phi_N^2(\omega_{N\mu}^2+\boldsymbol{\rho}_\mu^2)+\left(\frac{h_1}{4}+\frac{h_2}{4}-\frac{h_3}{4}\right)\phi_N^2(f_{1N\mu}^2+\boldsymbol{a}_{1\mu}^2) \\
& + (h_2+h_3)\omega_{N\mu}[(\sigma_N+\phi_N)\boldsymbol{a}_0+Z_\pi^2\eta_N\boldsymbol{\pi}]\cdot\boldsymbol{\rho}^\mu \\
& + (h_2-h_3)[(\sigma_N+\phi_N)\boldsymbol{a}_0+Z_\pi^2\eta_N\boldsymbol{\pi}]\cdot[f_{1N\mu}\boldsymbol{a}_1^\mu \\
& + Z_\pi w_{a_1}(\boldsymbol{a}_{1\mu}\partial^\mu\eta_N+f_{1N\mu}\partial^\mu\boldsymbol{\pi})+Z_\pi^2 w_{a_1}^2(\partial_\mu\eta_N)(\partial^\mu\boldsymbol{\pi})] \\
& + (h_2+h_3)Z_\pi(\boldsymbol{a}_0\times\boldsymbol{\pi})\cdot(\omega_{N\mu}\boldsymbol{a}_1^\mu+Z_\pi w_{a_1}\omega_{N\mu}\partial^\mu\boldsymbol{\pi}) \\
& + (h_2-h_3)Z_\pi(\boldsymbol{a}_0\times\boldsymbol{\pi})\cdot(f_{1N\mu}\boldsymbol{\rho}^\mu+Z_\pi w_{a_1}\boldsymbol{\rho}_\mu\partial^\mu\eta_N) \\
& + h_3 Z_\pi[\eta_N\boldsymbol{a}_0-(\sigma_N+\phi_N)\boldsymbol{\pi}]\cdot[\boldsymbol{\rho}_\mu\times(\boldsymbol{a}_1^\mu+Z_\pi w_{a_1}\partial^\mu\boldsymbol{\pi})] \\
& - \frac{h_3}{2}\{(\boldsymbol{a}_0\times\boldsymbol{\rho}^\mu)^2-[\boldsymbol{a}_0\times(\boldsymbol{a}_1^\mu+Z_\pi w_{a_1}\partial^\mu\boldsymbol{\pi})]^2+Z_\pi^2(\boldsymbol{\pi}\times\boldsymbol{\rho}^\mu)^2 \\
& - Z_\pi^2[\boldsymbol{\pi}\times(\boldsymbol{a}_1^\mu+Z_\pi w_{a_1}\partial^\mu\boldsymbol{\pi})]^2\}
\end{aligned}
\tag{5.133}
$$

# 6. Three-Flavour Linear Sigma Model

In this chapter we discuss the application of the generic Lagrangian from Chapter 4 to three flavours: scalar, pseudoscalar, vector and axial-vector strange mesons are added to the model.

## 6.1 The $N_f = 3$ Lagrangian

The globally invariant $U(3)_L \times U(3)_R$ Lagrangian possesses the same structure as the one in Eq. (4.42) up to the chiral-anomaly term $c_1$ (see discussion in Sec. 6.4):

$$\begin{aligned}
\mathcal{L} &= \mathrm{Tr}[(D_\mu\Phi)^\dagger(D_\mu\Phi)] - m_0^2\mathrm{Tr}(\Phi^\dagger\Phi) - \lambda_1[\mathrm{Tr}(\Phi^\dagger\Phi)]^2 - \lambda_2\mathrm{Tr}(\Phi^\dagger\Phi)^2 \\
&- \frac{1}{4}\mathrm{Tr}(L_{\mu\nu}^2 + R_{\mu\nu}^2) + \mathrm{Tr}\left[\left(\frac{m_1^2}{2} + \Delta\right)(L_\mu^2 + R_\mu^2)\right] + \mathrm{Tr}[H(\Phi + \Phi^\dagger)] \\
&+ c_1(\det\Phi - \det\Phi^\dagger)^2 + i\frac{g_2}{2}(\mathrm{Tr}\{L_{\mu\nu}[L^\mu, L^\nu]\} + \mathrm{Tr}\{R_{\mu\nu}[R^\mu, R^\nu]\}) \\
&+ \frac{h_1}{2}\mathrm{Tr}(\Phi^\dagger\Phi)\mathrm{Tr}(L_\mu^2 + R_\mu^2) + h_2\mathrm{Tr}[|L_\mu\Phi|^2 + |\Phi R_\mu|^2] + 2h_3\mathrm{Tr}(L_\mu\Phi R^\mu\Phi^\dagger). \\
&+ g_3[\mathrm{Tr}(L_\mu L_\nu L^\mu L^\nu) + \mathrm{Tr}(R_\mu R_\nu R^\mu R^\nu)] + g_4[\mathrm{Tr}\,(L_\mu L^\mu L_\nu L^\nu) + \mathrm{Tr}\,(R_\mu R^\mu R_\nu R^\nu)] \\
&+ g_5\mathrm{Tr}\,(L_\mu L^\mu)\ \mathrm{Tr}\,(R_\nu R^\nu) + g_6[\mathrm{Tr}(L_\mu L^\mu)\,\mathrm{Tr}(L_\nu L^\nu) + \mathrm{Tr}(R_\mu R^\mu)\,\mathrm{Tr}(R_\nu R^\nu)].
\end{aligned} \tag{6.1}$$

In the three-flavour case, it is more convenient to write the (pseudo)scalar and (axial-)vector matrices explicitly straightaway rather than implicitly in terms of the $U(3)$ group generators. The scalar states present in the $U(3)_L \times U(3)_R$ version of the model are [see Eq. (4.11)]:

$$S = \frac{1}{\sqrt{2}}\begin{pmatrix} \frac{\sigma_N + a_0^0}{\sqrt{2}} & a_0^+ & K_S^+ \\ a_0^- & \frac{\sigma_N - a_0^0}{\sqrt{2}} & K_S^0 \\ K_S^- & \bar{K}_S^0 & \sigma_S \end{pmatrix} \tag{6.2}$$

and the pseudoscalar states are [see Eq. (4.12)]:

$$P = \frac{1}{\sqrt{2}}\begin{pmatrix} \frac{\eta_N + \pi^0}{\sqrt{2}} & \pi^+ & K^+ \\ \pi^- & \frac{\eta_N - \pi^0}{\sqrt{2}} & K^0 \\ K^- & \bar{K}^0 & \eta_S \end{pmatrix}. \tag{6.3}$$

Consequently, the $\Phi$ matrix from Eq. (4.7) now reads

$$\Phi = S + iP = \frac{1}{\sqrt{2}}\begin{pmatrix} \frac{(\sigma_N + a_0^0) + i(\eta_N + \pi^0)}{\sqrt{2}} & a_0^+ + i\pi^+ & K_S^+ + iK^+ \\ a_0^- + i\pi^- & \frac{(\sigma_N - a_0^0) + i(\eta_N - \pi^0)}{\sqrt{2}} & K_S^0 + iK^0 \\ K_S^- + iK^- & \bar{K}_S^0 + i\bar{K}^0 & \sigma_S + i\eta_S \end{pmatrix} \tag{6.4}$$

and the adjoint matrix $\Phi^\dagger$ is

$$\Phi^\dagger = \frac{1}{\sqrt{2}}\begin{pmatrix} \frac{(\sigma_N + a_0^0) - i(\eta_N + \pi^0)}{\sqrt{2}} & a_0^+ - i\pi^+ & K_S^+ - iK^+ \\ a_0^- - i\pi^- & \frac{(\sigma_N - a_0^0) - i(\eta_N - \pi^0)}{\sqrt{2}} & K_S^0 - iK^0 \\ K_S^- - iK^- & \bar{K}_S^0 - i\bar{K}^0 & \sigma_S - i\eta_S \end{pmatrix}. \tag{6.5}$$

(Note again that, in this work, $K_S^0$ does not denote the short-lived pseudoscalar kaon but a neutral scalar kaon.)

The matrix containing vectors is [see Eq. (4.26)]:

$$V^\mu = \frac{1}{\sqrt{2}} \begin{pmatrix} \frac{\omega_N^\mu + \rho^{\mu 0}}{\sqrt{2}} & \rho^{\mu +} & K^{\star \mu +} \\ \rho^{\mu -} & \frac{\omega_N^\mu - \rho^{\mu 0}}{\sqrt{2}} & K^{\star \mu 0} \\ K^{\star \mu -} & \bar{K}^{\star \mu 0} & \omega_S^\mu \end{pmatrix} \tag{6.6}$$

whereas the matrix containing axial-vectors is [see Eq. (4.27)]:

$$A = \frac{1}{\sqrt{2}} \begin{pmatrix} \frac{f_{1N}^\mu + a_1^{\mu 0}}{\sqrt{2}} & a_1^{\mu +} & K_1^{\mu +} \\ a_1^{\mu -} & \frac{f_{1N}^\mu - a_1^{\mu 0}}{\sqrt{2}} & K_1^{\mu 0} \\ K_1^{\mu -} & \bar{K}_1^{\mu 0} & f_{1S}^\mu \end{pmatrix}. \tag{6.7}$$

The matrices from Eqs. (6.6) and (6.7) are combined into a right-handed structure just as in Eq. (4.23):

$$R^\mu = \frac{1}{\sqrt{2}} \begin{pmatrix} \frac{\omega_N^\mu + \rho^{\mu 0}}{\sqrt{2}} - \frac{f_{1N}^\mu + a_1^{\mu 0}}{\sqrt{2}} & \rho^{\mu +} - a_1^{\mu +} & K^{\star \mu +} - K_1^{\mu +} \\ \rho^{\mu -} - a_1^{\mu -} & \frac{\omega_N^\mu - \rho^{\mu 0}}{\sqrt{2}} - \frac{f_{1N}^\mu - a_1^{\mu 0}}{\sqrt{2}} & K^{\star \mu 0} - K_1^{\mu 0} \\ K^{\star \mu -} - K_1^{\mu -} & \bar{K}^{\star \mu 0} - \bar{K}_1^{\mu 0} & \omega_S^\mu - f_{1S}^\mu \end{pmatrix} \tag{6.8}$$

and into a left-handed structure just as in Eq. (4.24):

$$L^\mu = \frac{1}{\sqrt{2}} \begin{pmatrix} \frac{\omega_N^\mu + \rho^{\mu 0}}{\sqrt{2}} + \frac{f_{1N}^\mu + a_1^{\mu 0}}{\sqrt{2}} & \rho^{\mu +} + a_1^{\mu +} & K^{\star \mu +} + K_1^{\mu +} \\ \rho^{\mu -} + a_1^{\mu -} & \frac{\omega_N^\mu - \rho^{\mu 0}}{\sqrt{2}} + \frac{f_{1N}^\mu - a_1^{\mu 0}}{\sqrt{2}} & K^{\star \mu 0} + K_1^{\mu 0} \\ K^{\star \mu -} + K_1^{\mu -} & \bar{K}^{\star \mu 0} + \bar{K}_1^{\mu 0} & \omega_S^\mu + f_{1S}^\mu \end{pmatrix}. \tag{6.9}$$

The covariant derivative is defined in accordance with Eq. (4.43):

$$D^\mu \Phi = \partial^\mu \Phi - i g_1 (L^\mu \Phi - \Phi R^\mu) \tag{6.10}$$

couples scalar and pseudoscalar degrees of freedom to vector and axial-vector ones and, unlike the one in Eq. (5.5), it contains no photon field $A^\mu$. The reason is that this and the subsequent chapters will be dedicated to meson decays into other mesons only; the only exception will be the decay $a_1 \to \pi\gamma$ but the $a_1 \pi \gamma$ Lagrangian in the $N_f = 3$ case would be exactly the same as the one presented in Eq. (5.69) for $N_f = 2$ and thus we do not need to recalculate it in this version of the model.

The left-handed and right-handed field strength tensors are defined just as in Eqs. (4.32) and (4.33):

$$L^{\mu\nu} = \partial^\mu L^\nu - \partial^\nu L^\mu, \tag{6.11a}$$

$$R^{\mu\nu} = \partial^\mu R^\nu - \partial^\nu R^\mu. \tag{6.11b}$$

Explicit breaking of the global symmetry in the (pseudo)scalar channel is described by the term $\mathrm{Tr}[H(\Phi + \Phi^\dagger)]$, see Eq. (4.35), and in the (axial-)vector channel by the term $\mathrm{Tr}\left[\Delta(L_\mu^2 + R_\mu^2)\right]$, see Eq. (4.37), where

$$H = \begin{pmatrix} \frac{h_{0N}}{2} & 0 & 0 \\ 0 & \frac{h_{0N}}{2} & 0 \\ 0 & 0 & \frac{h_{0S}}{\sqrt{2}} \end{pmatrix}, \tag{6.12}$$

$$\Delta = \begin{pmatrix} \delta_N & 0 & 0 \\ 0 & \delta_N & 0 \\ 0 & 0 & \delta_S \end{pmatrix}. \tag{6.13}$$

As in Chapter 5, the spontaneous breaking of the chiral symmetry will be implemented by condensing scalar isosinglet states – in the case of $N_f = 3$, there are two such states [see Eq. (6.2)]: $\sigma_N \equiv (\bar{u}u + \bar{d}d)/\sqrt{2}$ and $\sigma_N \equiv \bar{s}s$. Let us denote their respective condensates as $\phi_N$ and $\phi_S$. The relations between $\phi_{N,S}$ and the pion decay constant $f_\pi$ as well as the kaon decay constant $f_K$ are determined analogously to Eq. (5.21)]:

$$\phi_N = Z_\pi f_\pi, \tag{6.14a}$$

$$\phi_S = \frac{Z_K f_K}{\sqrt{2}}, \tag{6.14b}$$

where $f_\pi = 92.4$ MeV and $f_K = 155.5/\sqrt{2}$ MeV [10]. Then the chiral condensates $\phi_N$ and $\phi_S$ lead to the following mixing terms in the Lagrangian (6.1):

$$\begin{aligned} &- g_1\phi_N(f_{1N}^\mu\partial_\mu\eta_N + \boldsymbol{a}_1^\mu\cdot\partial_\mu\boldsymbol{\pi}) - \sqrt{2}g_1\phi_S f_{1S}^\mu\partial_\mu\eta_S \\ &- \left(\frac{g_1}{\sqrt{2}}\phi_S + \frac{g_1}{2}\phi_N\right)\left(K_1^{\mu 0}\partial_\mu\bar{K}^0 + K_1^{\mu +}\partial_\mu K^- + \text{h.c.}\right) \text{ and} \\ &+ \left(i\frac{g_1}{\sqrt{2}}\phi_S - i\frac{g_1}{2}\phi_N\right)\left(\bar{K}^{\star\mu 0}\partial_\mu K_S^0 + K^{\star\mu -}\partial_\mu K_S^+\right) \\ &+ \left(-i\frac{g_1}{\sqrt{2}}\phi_S + i\frac{g_1}{2}\phi_N\right)\left(K^{\star\mu 0}\partial_\mu\bar{K}_S^0 + K^{\star\mu +}\partial_\mu K_S^-\right). \end{aligned} \tag{6.15}$$

The first term in the first line of Eq. (6.15) corresponds exactly to the term (5.11) obtained in the $N_f = 2$ case; the other contributions are new. Note that, in the $N_f = 3$ case, the mixing between the pseudoscalars and the axial-vectors is accompanied by the vector-scalar mixing of the fields $K^\star$ and $K_S$. The corresponding coupling is imaginary but this is not problematic as the Lagrangian is nonetheless hermitian, i.e., real.

The mixing terms (6.15) are removed by the following suitable shifts of the (axial-)vector states:

$$f_{1N}^\mu \to f_{1N}^\mu + w_{f_{1N}}\partial^\mu\eta_N, \tag{6.16}$$

$$\boldsymbol{a}_1^\mu \to \boldsymbol{a}_1^\mu + w_{a_1}\partial^\mu\boldsymbol{\pi}, \tag{6.17}$$

$$f_{1S}^\mu \to f_{1S}^\mu + w_{f_{1S}}\partial^\mu\eta_S, \tag{6.18}$$

$$K_1^{\mu 0} \to K_1^{\mu 0} + w_{K_1}\partial^\mu K^0 \,(\text{and h.c.}), \tag{6.19}$$

$$K^{\star\mu 0} \to K^{\star\mu 0} + w_{K^\star}\partial^\mu K_S^0, \tag{6.20}$$

$$K^{\star\mu +} \to K^{\star\mu +} + w_{K^\star}\partial^\mu K_S^+, \tag{6.21}$$

$$\bar{K}^{\star\mu 0} \to \bar{K}^{\star\mu 0} + w_{K^\star}^*\partial^\mu\bar{K}_S^0, \tag{6.22}$$

$$K^{\star\mu -} \to K^{\star\mu -} + w_{K^\star}^*\partial^\mu K_S^-. \tag{6.23}$$

The shifts (6.16) and (6.17) correspond to the one performed in the $N_f = 2$ case (5.12). The quantities $w_{f_{1N}}$, $w_{a_1}$, $w_{f_{1S}}$, $w_{K_1}$ and $w_{K^\star}$ are calculated from the condition that the mixing terms (6.15) vanish once the shifts of the (axial-)vectors have been implemented:

$$\begin{aligned}
&\left[-g_1\phi_N + \left(g_1^2 + \frac{h_1}{2} + \frac{h_2}{2} - \frac{h_3}{2}\right) w_{f_{1N}}\phi_N^2 + (m_1^2 + 2\delta_N) w_{f_{1N}} + \frac{h_1}{2} w_{f_{1N}}\phi_S^2\right] \\
&\times \left(f_{1N}^\mu \partial_\mu \eta_N + \boldsymbol{a}_1^\mu \cdot \partial_\mu \boldsymbol{\pi}\right) \stackrel{!}{=} 0, \qquad (6.24) \\
&\left[-\sqrt{2} g_1 \phi_S + \left(2g_1^2 + \frac{h_1}{2} + h_2 - h_3\right) w_{f_{1S}}\phi_S^2 + (m_1^2 + 2\delta_S) w_{f_{1S}} + \frac{h_1}{2} w_{f_{1S}}\phi_N^2\right] f_{1S}^\mu \partial_\mu \eta_S \stackrel{!}{=} 0, \qquad (6.25) \\
&\left[-\frac{g_1}{\sqrt{2}}\phi_S + \frac{g_1^2 - h_3}{\sqrt{2}} w_{K_1}\phi_N\phi_S + \frac{g_1^2 + h_1 + h_2}{2} w_{K_1}\phi_S^2 + (m_1^2 + \delta_N + \delta_S) w_{K_1} - \frac{g_1}{2}\phi_N \right. \\
&\left. + \left(\frac{g_1^2}{4} + \frac{h_1}{2} + \frac{h_2}{4}\right) w_{K_1}\phi_N^2\right] \left(K_1^{\mu 0}\partial_\mu \bar{K}^0 + K_1^{\mu +}\partial_\mu K^- + \text{h.c.}\right) \stackrel{!}{=} 0, \qquad (6.26) \\
&\left[i\frac{g_1}{\sqrt{2}}\phi_S + \frac{h_3 - g_1^2}{\sqrt{2}} w_{K^\star}\phi_N\phi_S + \frac{g_1^2 + h_1 + h_2}{2} w_{K^\star}\phi_S^2 + (m_1^2 + \delta_N + \delta_S) w_{K^\star} - i\frac{g_1}{2}\phi_N \right. \\
&\left. + \left(\frac{g_1^2}{4} + \frac{h_1}{2} + \frac{h_2}{4}\right) w_{K^\star}\phi_N^2\right] \left(\bar{K}^{\star\mu 0}\partial_\mu K_S^0 + K^{\star\mu -}\partial_\mu K_S^+\right) \stackrel{!}{=} 0, \\
+ &\left[-i\frac{g_1}{\sqrt{2}}\phi_S + \frac{h_3 - g_1^2}{\sqrt{2}} w_{K^\star}^*\phi_N\phi_S + \frac{g_1^2 + h_1 + h_2}{2} w_{K^\star}^*\phi_S^2 + (m_1^2 + \delta_N + \delta_S) w_{K^\star}^* + i\frac{g_1}{2}\phi_N \right. \\
&\left. + \left(\frac{g_1^2}{4} + \frac{h_1}{2} + \frac{h_2}{4}\right) w_{K^\star}^*\phi_N^2\right] \left(K^{\star\mu 0}\partial_\mu \bar{K}_S^0 + K^{\star\mu +}\partial_\mu K_S^-\right) \stackrel{!}{=} 0. \qquad (6.27)
\end{aligned}$$

Equation (6.24) corresponds exactly to the $f_{1N}^\mu$-$\partial_\mu \eta_N$ and $\boldsymbol{a}_1^\mu$-$\partial_\mu \boldsymbol{\pi}$ mixing terms obtained upon the stated shifts in the $N_f = 2$ case. Equations (6.24) – (6.27) are fulfilled only if we define:

$$w_{f_{1N}} = w_{a_1} = \frac{g_1\phi_N}{m_{a_1}^2}, \qquad (6.28)$$

$$w_{f_{1S}} = \frac{\sqrt{2} g_1 \phi_S}{m_{f_{1S}}^2}, \qquad (6.29)$$

$$w_{K_1} = \frac{g_1(\phi_N + \sqrt{2}\phi_S)}{2m_{K_1}^2}, \qquad (6.30)$$

$$w_{K^\star} = i\frac{g_1(\phi_N - \sqrt{2}\phi_S)}{2m_{K^\star}^2}. \qquad (6.31)$$

The definitions (6.28) – (6.31) require the knowledge of the following mass terms obtained from the Lagrangian (6.1):

$$m_{\sigma_N}^2 = m_0^2 + 3\left(\lambda_1 + \frac{\lambda_2}{2}\right)\phi_N^2 + \lambda_1\phi_S^2, \qquad (6.32)$$

$$m_{\eta_N}^2 = Z_\pi^2\left[m_0^2 + \left(\lambda_1 + \frac{\lambda_2}{2}\right)\phi_N^2 + \lambda_1\phi_S^2 + c_1\phi_N^2\phi_S^2\right] \equiv m_\pi^2 + c_1 Z_\pi^2 \phi_N^2 \phi_S^2, \qquad (6.33)$$

$$m_{a_0}^2 = m_0^2 + \left(\lambda_1 + 3\frac{\lambda_2}{2}\right)\phi_N^2 + \lambda_1\phi_S^2, \tag{6.34}$$

$$m_\pi^2 = Z_\pi^2\left[m_0^2 + \left(\lambda_1 + \frac{\lambda_2}{2}\right)\phi_N^2 + \lambda_1\phi_S^2\right] \equiv \frac{Z_\pi^2 h_{0N}}{\phi_N}, \tag{6.35}$$

$$m_{\sigma_S}^2 = m_0^2 + \lambda_1\phi_N^2 + 3(\lambda_1+\lambda_2)\phi_S^2, \tag{6.36}$$

$$m_{\eta_S}^2 = Z_{\eta_S}^2\left[m_0^2 + \lambda_1\phi_N^2 + (\lambda_1+\lambda_2)\phi_S^2 + c_1\frac{\phi_N^4}{4}\right] = \frac{Z_{\eta_S}^2 h_{0S}}{\phi_S}, \tag{6.37}$$

$$m_{K_S}^2 = Z_{K_S}^2\left[m_0^2 + \left(\lambda_1 + \frac{\lambda_2}{2}\right)\phi_N^2 \ + \frac{\lambda_2}{\sqrt{2}}\phi_N\phi_S + (\lambda_1+\lambda_2)\phi_S^2\right], \tag{6.38}$$

$$m_K^2 = Z_K^2\left[m_0^2 + \left(\lambda_1 + \frac{\lambda_2}{2}\right)\phi_N^2 \ - \frac{\lambda_2}{\sqrt{2}}\phi_N\phi_S + (\lambda_1+\lambda_2)\phi_S^2\right], \tag{6.39}$$

$$m_{\omega_N}^2 = m_\rho^2 = m_1^2 + 2\delta_N + \frac{\phi_N^2}{2}(h_1+h_2+h_3) + \frac{h_1}{2}\phi_S^2, \tag{6.40}$$

$$m_{f_{1N}}^2 = m_{a_1}^2 = m_1^2 + 2\delta_N + g_1^2\phi_N^2 + \frac{\phi_N^2}{2}(h_1+h_2-h_3) + \frac{h_1}{2}\phi_S^2, \tag{6.41}$$

$$m_{\omega_S}^2 = m_1^2 + 2\delta_S + \frac{h_1}{2}\phi_N^2 + \phi_S^2\left(\frac{h_1}{2} + h_2 + h_3\right), \tag{6.42}$$

$$m_{f_{1S}}^2 = m_1^2 + 2\delta_S + \frac{h_1}{2}\phi_N^2 + 2g_1^2\phi_S^2 + \phi_S^2\left(\frac{h_1}{2} + h_2 - h_3\right), \tag{6.43}$$

$$m_{K^\star}^2 = m_1^2 + \delta_N + \delta_S + \frac{\phi_N^2}{2}\left(\frac{g_1^2}{2} + h_1 + \frac{h_2}{2}\right) + \frac{1}{\sqrt{2}}\phi_N\phi_S(h_3 - g_1^2) + \frac{\phi_S^2}{2}\left(g_1^2 + h_1 + h_2\right), \tag{6.44}$$

$$m_{K_1}^2 = m_1^2 + \delta_N + \delta_S + \frac{\phi_N^2}{2}\left(\frac{g_1^2}{2} + h_1 + \frac{h_2}{2}\right) + \frac{1}{\sqrt{2}}\phi_N\phi_S(g_1^2 - h_3) + \frac{\phi_S^2}{2}\left(g_1^2 + h_1 + h_2\right), \tag{6.45}$$

with the renormalisation factors ensuring the canonical normalisation of the $\eta_{N,S}$, $\boldsymbol{\pi}$ and $K_S$ wave functions

$$Z_\pi \equiv Z_{\eta_N} = \frac{m_{a_1}}{\sqrt{m_{a_1}^2 - g_1^2\phi_N^2}} \text{ (just as before)}, \tag{6.46}$$

$$Z_K = \frac{2m_{K_1}}{\sqrt{4m_{K_1}^2 - g_1^2(\phi_N + \sqrt{2}\phi_S)^2}}, \tag{6.47}$$

$$Z_{\eta_S} = \frac{m_{f_{1S}}}{\sqrt{m_{f_{1S}}^2 - 2g_1^2\phi_S^2}}, \tag{6.48}$$

$$Z_{K_S} = \frac{2m_{K^\star}}{\sqrt{4m_{K^\star}^2 - g_1^2(\phi_N - \sqrt{2}\phi_S)^2}}. \tag{6.49}$$

It is obvious from Eqs. (6.46) - (6.49) that all the renormalisation coefficients will have values larger than 1.

Note that the right-hand sides of Eqs. (6.35) and (6.37) are obtained by minimising the potential $\mathcal{V}(\phi_N, \phi_S)$ present in the Lagrangian (6.1). The potential reads:

$$\mathcal{V}(\phi_N,\phi_S) = \frac{1}{2}m_0^2(\phi_N^2+\phi_S^2) + \frac{\lambda_1}{4}(\phi_N^4 + 2\phi_N^2\phi_S^2 + \phi_S^4) + \frac{\lambda_2}{4}\left(\frac{\phi_N^4}{2} + \phi_S^4\right) - h_{0N}\phi_N - h_{0S}\phi_S \tag{6.50}$$

and, consequently, the first derivatives of the potential $\mathcal{V}(\phi_N, \phi_S)$ from the above Eq. (6.50) are

$$\frac{\partial \mathcal{V}(\phi_N, \phi_S)}{\partial \phi_N} = [m_0^2 + \lambda_1(\phi_N^2 + \phi_S^2)]\phi_N + \frac{\lambda_2}{2}\phi_N^3 - h_{0N}, \tag{6.51}$$

$$\frac{\partial \mathcal{V}(\phi_N, \phi_S)}{\partial \phi_S} = [m_0^2 + \lambda_1(\phi_N^2 + \phi_S^2)]\phi_S + \lambda_2\phi_S^3 - h_{0S}. \tag{6.52}$$

Then we obtain

$$\frac{\partial \mathcal{V}(\phi_N, \phi_S)}{\partial \phi_N} \stackrel{!}{=} 0 \Leftrightarrow h_{0N} = m_0^2 + \lambda_1(\phi_N^2 + \phi_S^2)]\phi_N + \frac{\lambda_2}{2}\phi_N^3, \tag{6.53}$$

$$\frac{\partial \mathcal{V}(\phi_N, \phi_S)}{\partial \phi_S} \stackrel{!}{=} 0 \Leftrightarrow h_{0S} = m_0^2 + \lambda_1(\phi_N^2 + \phi_S^2)]\phi_S + \lambda_2\phi_S^3. \tag{6.54}$$

and the right-hand side of Eqs. (6.35) and (6.37) ensue.
Note also that from Eq. (6.46) we obtain the $g_1 = g_1(Z_\pi)$ dependence, just as in Eq. (5.27):

$$g_1 = g_1(Z_\pi) = \frac{m_{a_1}}{Z_\pi f_\pi}\sqrt{1 - \frac{1}{Z_\pi^2}} \tag{6.55}$$

and also from Eqs. (6.40) and (6.41):

$$h_3 = h_3(Z_\pi) = \frac{m_{a_1}^2}{Z_\pi^2 f_\pi^2}\left(\frac{m_\rho^2}{m_{a_1}^2} - \frac{1}{Z_\pi^2}\right). \tag{6.56}$$

Utilising Eq. (6.55) we can transform Eq. (6.28) as follows:

$$w_{a_1} = \frac{\frac{m_{a_1}}{Z_\pi f_\pi}\sqrt{1 - \frac{1}{Z_\pi^2}}\phi_N}{m_{a_1}^2} = \frac{\sqrt{1 - \frac{1}{Z_\pi^2}}}{m_{a_1}} = \frac{\sqrt{Z_\pi^2 - 1}}{Z_\pi m_{a_1}}. \tag{6.57}$$

Additionally, from Eqs. (6.47), (6.48) and (6.49) we obtain

$$g_1 = g_1(Z_\pi, Z_K) = \frac{2m_{K_1}}{Z_\pi f_\pi + Z_K f_K}\sqrt{1 - \frac{1}{Z_K^2}}, \tag{6.58}$$

$$g_1 = g_1(Z_K, Z_{\eta_S}) = \frac{m_{f_{1S}}}{Z_K f_K}\sqrt{1 - \frac{1}{Z_{\eta_S}^2}}, \tag{6.59}$$

$$g_1 = g_1(Z_\pi, Z_{K_S}) = \frac{2m_{K^\star}}{Z_\pi f_\pi - Z_K f_K}\sqrt{1 - \frac{1}{Z_{K_S}^2}}. \tag{6.60}$$

Then analogously to Eq. (6.57) we obtain from Eqs. (6.30) and (6.58):

$$w_{K_1} = \frac{\frac{2m_{K_1}}{Z_\pi f_\pi + Z_K f_K}\sqrt{1 - \frac{1}{Z_K^2}}(\phi_N + \sqrt{2}\phi_S)}{2m_{K_1}^2} = \frac{\sqrt{1 - \frac{1}{Z_K^2}}}{m_{K_1}} = \frac{\sqrt{Z_K^2 - 1}}{Z_K m_{K_1}}. \tag{6.61}$$

It is very important to stress that Eq. (6.47) is not the only equation regarding $Z_K$. From Eqs. (6.42) and (6.43) we obtain

$$m_{f_{1S}}^2 - m_{\omega_S}^2 = 2[g_1^2(Z_\pi) - h_3(Z_\pi)]\phi_S^2 \stackrel{\phi_S = \frac{1}{\sqrt{2}}Z_K f_K}{=} [g_1^2(Z_\pi) - h_3(Z_\pi)]Z_K^2 f_K^2$$

$$\Rightarrow Z_K = \frac{1}{f_K}\sqrt{\frac{m_{f_{1S}}^2 - m_{\omega_S}^2}{g_1^2(Z_\pi) - h_3(Z_\pi)}} \tag{6.62}$$

with $g_1(Z_\pi)$ and $h_3(Z_\pi)$ from Eqs. (6.55) and (6.56), respectively. Also, from Eqs. (6.44) and (6.45) we obtain

$$m_{K_1}^2 - m_{K_\star}^2 = \sqrt{2}\phi_N\phi_S[g_1^2(Z_\pi) - h_3(Z_\pi)] \overset{\phi_S=\frac{1}{\sqrt{2}}Z_K f_K, \phi_N = Z_\pi f_\pi}{\equiv} Z_\pi f_\pi Z_K f_K[g_1^2(Z_\pi) - h_3(Z_\pi)]$$
$$\Rightarrow Z_K = \frac{m_{K_1}^2 - m_{K_\star}^2}{Z_\pi f_\pi f_K[g_1^2(Z_\pi) - h_3(Z_\pi)]}. \tag{6.63}$$

Therefore, in order to be consistent, the values of $Z_K$ have to simultaneously fulfill three equations: (6.47), which is the definition of $Z_K$; (6.62) and (6.63). This will represent a very strong constraint on the values of the parameters in the Lagrangian (6.1).
We also emphasise that the explicit form of the Lagrangian (6.1) is an extremely complicated function due to the abundance of terms permitted by the global $U(3)_L \times U(3)_R$ symmetry [increased further by the eight shifts (6.16) – (6.23)] and also because of the large number of fields from both non-strange and strange sectors. For this reason, the evaluation of the Lagrangian and the extrapolation of vertices necessary for the calculation of decay widths in this chapter as well as Chapters 7 – 11 have been performed using a computer algorithm (available from the author upon request).

Most model parameters can be calculated from the meson mass terms (6.32) – (6.45). However, using only mass terms as means of parameter calculation would leave some important parameters undetermined, such as, e.g., $g_2$ [that strongly influences the (axial-)vector phenomenology, see below]. For this reason, our parameter calculation will use some decay widths as well, but only as few as necessary to determine the model parameters. All other decay widths will then be calculated as a consequence, thus raising the predictive power of the model.
Before we determine the parameters we first need to assign the fields from our model to the physical ones.

## 6.2 Assigning the Fields

The model contains four nonets: scalar (6.2), pseudoscalar (6.3), vector (6.6) and axial-vector (6.7) containing both non-strange and strange states. If we consider isospin multiplets as single degrees of freedom, then there are sixteen resonances that can be described by the model: $\sigma_N$, $\sigma_S$, $\boldsymbol{a}_0$, $K_S$ (scalar); $\eta_N$, $\eta_S$, $\boldsymbol{\pi}$, $K$ (pseudoscalar); $\omega_N^\mu$, $\omega_S^\mu$, $\boldsymbol{\rho}^\mu$, $K^{\star\mu}$ (vector) and $f_{1N}^\mu$, $f_{1S}^\mu$, $\boldsymbol{a}_1^\mu$, $K_1$ (axial-vector). All of the states present in the model possess the $\bar{q}q$ structure, for the same reasons as those presented in Sec. 4.3.
As in Ref. [52], in the non-strange sector we assign the fields $\boldsymbol{\pi}$ and $\eta_N$ to the pion and the $SU(2)$ counterpart of the $\eta$ meson, $\eta_N \equiv (\bar{u}u + \bar{d}d)/\sqrt{2}$. The fields $\omega_N^\mu$ and $\boldsymbol{\rho}^\mu$ represent the $\omega(782)$ and $\rho(770)$ vector mesons, respectively, and the fields $f_{1N}^\mu$ and $\boldsymbol{a}_1^\mu$ represent the $f_1(1285)$ and $a_1(1260)$ mesons, respectively. In the strange sector, we assign the $K$ fields to the kaons; the $\eta_S$ field is the strange contribution to the physical $\eta$ and $\eta'$ fields; the $\omega_S$, $f_{1S}$, $K^\star$ and $K_1$ fields correspond to the $\phi(1020)$, $f_1(1420)$, $K^\star(892)$, and $K_1(1270)$ mesons, respectively.
Unfortunately, the assignment of the scalar fields is substantially less clear. Experimental data presented in Chapter 3 suggest the existence of six scalar-isoscalar states below 1.8 GeV: $f_0(600)$, $f_0(980)$, $f_0(1370)$, $f_0(1500)$, $f_0(1710)$ and $f_0(1790)$. Our model contains the pure non-strange isoscalar $\sigma_N$, the pure strange isoscalar $\sigma_S$ and the scalar kaon $K_S$. We will see in the subsequent

chapters that our model yields mixing of $\sigma_N$ and $\sigma_S$ producing a predominantly non-strange state, labelled as $\sigma_1$, and a predominantly strange state, labelled as $\sigma_2$. Assigning $\sigma_1$ and $\sigma_2$ to physical states will be the primary focus of Chapters 9 and 11. Therefore, a conclusive assignment of the latter states is not possible at this point.
Similarly, the isospin triplet $\boldsymbol{a}_0$ can be assigned to different physical resonances, although in this case there are only two candidate states: $a_0(980)$ and $a_0(1450)$. An analogous statement holds for the scalar kaon $K_S$ that can be assigned to the resonances $K_0^\star(800)$ or $K_0^\star(1430)$. In the following chapters we will therefore consider two possibilities for assignments of scalar fields performing two fits:

- *Fit I*, where $\boldsymbol{a}_0$ is assigned to $a_0(980)$ and $K_S$ to $K_0^\star(800)$ (Chapters 8 and 9) – we assign our scalar states to resonances below 1 GeV.
- *Fit II*, where $\boldsymbol{a}_0$ is assigned to $a_0(1450)$ and $K_S$ to $K_0^\star(1430)$ (Chapters 10 and 11) – we assign our scalar states to resonances above 1 GeV.

Note that Fit I implies that $a_0(980)$ is a non-strange $\bar{q}q$ state and that $K_0^\star(800)$ is a strange $\bar{q}q$ state. Conversely, Fit II implies that $a_0(1450)$ is a non-strange $\bar{q}q$ state and that $K_0^\star(1430)$ is a strange $\bar{q}q$ state. Given the large number of the $f_0$ resonances, it will not be possible to assign $\sigma_1$ and $\sigma_2$ *ab initio* in the two fits; the assignment of these two states will depend on the fit results. However, some remarks regarding the model parameters are in order before the calculations can proceed.

### 6.3 General Discussion of the Model Parameters

The model contains 18 parameters:

$$m_0^2,\, m_1^2,\, c_1,\, \delta_N,\, \delta_S,\, g_1,\, g_2,\, g_3,\, g_4,\, g_5,\, g_6,\, h_{0N},\, h_{0S},\, h_1,\, h_2,\, h_3,\, \lambda_1,\, \lambda_2. \tag{6.64}$$

Let us make following observations regarding the model parameters:

- The parameters $h_{0N}$ and $h_{0S}$ model the explicit breaking of the chiral symmetry (ESB) in the (pseudo)scalar sector via the term $\mathrm{Tr}[H(\Phi+\Phi^\dagger)]$ in the Lagrangian (6.1); they are calculated using the extremum equations (6.51) and (6.52) of the potential $\mathcal{V}(\phi_N,\phi_S)$ or, equivalently, from the mass terms of the pion, Eq. (6.35), and of $\eta_S$, the strange counterpart of the $\eta$ meson [see Eq. (6.37)]. We can then conclude that the masses of $\boldsymbol{\pi}$ and $\eta_S$ are generated by ESB. Given that $h_{0N}$ and $h_{0S}$ are determined uniquely from Eqs. (6.35) and (6.37), we are then left with 16 free parameters.
- The parameters $\delta_N$ and $\delta_S$ model the explicit symmetry breaking in the vector and axial-vector channels. The ESB stems from the non-vanishing quark masses and therefore we employ the correspondence $\delta_N \propto m_{u,d}^2$ and $\delta_S \propto m_s^2$. Given that $m_{u,d} \ll m_s$, we will set $\delta_N = 0$ throughout this work; $\delta_S$ will be determined by the fit of (axial-)vector masses. Consequently, the number of free parameters is decreased to 15.
- Our fit will make use of all scalar mass terms except $m_{\sigma_N}$ and $m_{\sigma_S}$ due to the well-known ambiguities regarding the phenomenology of scalar mesons (see Chapter 3). However, the mass terms that will be used in the fit only contain the linear combination $m_0^2+\lambda_1(\phi_N^2+\phi_S^2)$

rather than the parameters $m_0^2$ and $\lambda_1$ (that only appear separately in $m_{\sigma_N}$ and $m_{\sigma_S}$). Nonetheless, the knowledge of the mentioned linear combination will allow us to express the parameter $\lambda_1$ via the bare-mass parameter $m_0^2$. Consequently, the number of free parameters is decreased to 14.

- Similarly, the (axial-)vector mass terms [Eqs. (6.40) - (6.45)] allow only for the linear combination $m_1^2 + h_1(\phi_N^2 + \phi_S^2)/2$ rather than the parameters $m_1^2$ and $h_1$ separately to be determined. Given that the parameter $h_1$ is suppressed in the limit of a large number of colours (large-$N_c$ limit, see discussion in Sec. 4.3), we will set $h_1 = 0$ throughout this work. Thus the number of unknown parameters is decreased to 13. [Note that the parameter $\lambda_1$ is also large-$N_c$ suppressed and could also in principle be set to zero; however we do not set $\lambda_1 = 0$ as in that case there would be no mixing between $\sigma_N$ and $\sigma_S$, see Eq. (9.16). Nonetheless, the mixing between the two pure $\sigma$ states is shown to be small in Sec. 9.1.3 (see Fig. 9.4) – this is in line with expectations because the mixing is governed by a large-$N_c$ suppressed parameter.]

- The parameter $g_2$ is determined by the decay width $\Gamma_{\rho\to\pi\pi}$, see Eq. (5.45). Additionally, the parameters $g_3$, $g_4$, $g_5$ and $g_6$ do not influence any of the decays to be discussed in this work and are therefore also left out from the fit. Thus the number of unknown parameters is decreased to eight.

- The parameter $c_1$ can be substituted by the $\eta$-$\eta'$ mixing angle $\varphi_\eta$, as we will see in Sec. 7.1, Eq. (7.24). The value of the mixing angle $\varphi_\eta$ can be determined in a way that the masses of $\eta$ and $\eta'$ are as close to the physical masses as possible. That in turn implies that the value of the parameter $c_1$ is determined uniquely by $m_\eta$ and $m_{\eta'}$ – and therefore, $c_1$ is not a free parameter in the model.

- It is obvious from Eqs. (6.55) - (6.60) that the parameters $g_1$ and $h_3$ can be substituted by a pair of renormalisation coefficients. In principle, any pair of coefficients can be used; however, given that the coefficients $Z_\pi$ and $Z_K$ appear respectively in the chiral condensates $\phi_N$ and $\phi_S$ (that, in turn, influence all observables in this work), it is convenient to substitute $g_1$ and $h_3$ by $Z_\pi$ and $Z_K$. The coefficients $Z_{\eta_S}$ and $Z_{K_S}$ can be calculated from Eqs. (6.48) and (6.49).

We are therefore left with six parameters: $Z_\pi$, $Z_K$, $m_1^2$, $h_2$, $\delta_S$ and $\lambda_2$ and one parameter combination: $m_0^2 + \lambda_1(\phi_N^2 + \phi_S^2)$. Before we turn to the calculation of the parameters, let us briefly discuss the chiral-anomaly term in the Lagrangian (6.1) and the large-$N_c$ behaviour of the model parameters.

## 6.4 Modelling the Chiral Anomaly

We turn now to the chiral-anomaly term present in our Lagrangian (6.1). The goal of this subsection is to clarify how different ways of chiral-anomaly modelling influence the mass terms; the mass terms in turn represent a crucial part of the fit that will enable us to determine model parameters.

The term $c_1(\det\Phi - \det\Phi^\dagger)^2$ in the Lagrangian (6.1) describes the chiral anomaly of QCD as was first discussed by Veneziano and Witten in 1979 [240]. We will refer to this chiral-anomaly term as the VW term in the following. The term has been subject of further calculations in Ref. [241]. However, this is not the only way to model the chiral anomaly; an alternative had been discussed in 1971 by Kobayashi, Kondo and Maskawa [242]. This alternative term has the form $c(\det\Phi + \det\Phi^\dagger)$ as described by 't Hooft [213]; see also Ref. [243]. We will refer to this term as the Kobayashi-Kondo-Maskawa-'t Hooft (KKMH) term in the following. Although the two terms model the same (chiral) anomaly of QCD, there are some notable differences between the two terms.

- The Veneziano-Witten term is of order $\mathcal{O}(6)$ in the naive scaling of fields whereas the KKMH term is of order $\mathcal{O}(3)$ in fields. We have stated in Sec. 4.2 (see also Chapter 12) that, in principle, our Lagrangian only allows for terms up to order $\mathcal{O}(4)$ in fields so that the dilatation invariance is satisfied. However, the chirally anomalous terms do not need to fulfill this invariance and therefore one can choose either of the two terms, or both, or even additional terms compatible with the anomaly.

- The Veneziano-Witten term of the chiral anomaly influences only the phenomenology of the pseudoscalar singlets ($\eta_N$ and $\eta_S$, i.e., $\eta$ and $\eta'$). The contribution can be inferred from Eqs. (6.33), (6.37) and (7.5):

$$(m^2_{\eta_N})^{\mathrm{VW}} \equiv m^2_{\eta_N} \sim c_1 Z^2_\pi \phi^2_N \phi^2_S, \tag{6.65}$$

$$(m^2_{\eta_S})^{\mathrm{VW}} \equiv m^2_{\eta_S} \sim c_1 Z^2_{\eta_S} \frac{\phi^4_N}{4}, \tag{6.66}$$

$$\mathcal{L}_{\eta_N\eta_S} = -c_1 \frac{Z_{\eta_S} Z_\pi}{2} \phi^3_N \phi_S \eta_N \eta_S. \tag{6.67}$$

  Additionally, we can see from Eq. (6.33) that the chiral anomaly is responsible for the mass splitting between the pseudoscalar isotriplet $\boldsymbol{\pi}$ and its SU(2) counterpart, the isosinglet $\eta_N$. Contrarily, the KKMH term influences phenomenology of other scalar mesons as well [244]. The (pseudo)scalar mass terms and other relevant parts of the Lagrangian are in this case as follows:

$$(m^2_{\sigma_N})^{\mathrm{KKMH}} = m_0^2 + 3\left(\lambda_1 + \frac{\lambda_2}{2}\right)\phi^2_N + \lambda_1\phi^2_S - \frac{c}{\sqrt{2}}\phi_S, \tag{6.68}$$

$$(m^2_{\eta_N})^{\mathrm{KKMH}} = Z^2_\pi\left[m_0^2 + \left(\lambda_1 + \frac{\lambda_2}{2}\right)\phi^2_N + \lambda_1\phi^2_S + \frac{c}{\sqrt{2}}\phi_S\right] \equiv (m^2_\pi)^{\mathrm{KKMH}} + \sqrt{2}cZ^2_\pi\phi_S, \tag{6.69}$$

$$(m^2_{a_0})^{\mathrm{KKMH}} = m_0^2 + \left(\lambda_1 + 3\frac{\lambda_2}{2}\right)\phi^2_N + \lambda_1\phi^2_S + \frac{c}{\sqrt{2}}\phi_S, \tag{6.70}$$

$$(m^2_\pi)^{\mathrm{KKMH}} = Z^2_\pi\left[m_0^2 + \left(\lambda_1 + \frac{\lambda_2}{2}\right)\phi^2_N + \lambda_1\phi^2_S - \frac{c}{\sqrt{2}}\phi_S\right] \equiv \frac{Z^2_\pi h_{0N}}{\phi_N}, \tag{6.71}$$

$$(m^2_{\sigma_S})^{\mathrm{KKMH}} = m_0^2 + \lambda_1\phi^2_N + 3(\lambda_1+\lambda_2)\phi^2_S, \tag{6.72}$$

$$(m^2_{\eta_S})^{\mathrm{KKMH}} = Z^2_{\eta_S}[m_0^2 + \lambda_1\phi^2_N + (\lambda_1+\lambda_2)\phi^2_S] = \frac{Z^2_{\eta_S}}{\phi_S}(h_{0S} + \frac{c}{2\sqrt{2}}\phi^2_N), \tag{6.73}$$

$$(m_{K_S}^2)^{\rm KKMH} = Z_{K_S}^2\left[m_0^2 + \left(\lambda_1 + \frac{\lambda_2}{2}\right)\phi_N^2 \ + \frac{\lambda_2}{\sqrt{2}}\phi_N\phi_S + (\lambda_1+\lambda_2)\phi_S^2 + \frac{c}{2}\phi_N\right], \tag{6.74}$$

$$(m_K^2)^{\rm KKMH} = Z_K^2\left[m_0^2 + \left(\lambda_1 + \frac{\lambda_2}{2}\right)\phi_N^2 \ - \frac{\lambda_2}{\sqrt{2}}\phi_N\phi_S + (\lambda_1+\lambda_2)\phi_S^2 - \frac{c}{2}\phi_N\right], \tag{6.75}$$

$$\mathcal{L}_{\eta_N\eta_S}^{\rm KKMH} = -c\frac{Z_\pi Z_{\eta_S}}{\sqrt{2}}\phi_N\eta_N\eta_S, \tag{6.76}$$

$$\mathcal{L}_{\sigma_N\sigma_S}^{\rm KKMH} \sim \frac{c}{\sqrt{2}}\phi_N\sigma_N\sigma_S, \tag{6.77}$$

$$\mathcal{V}(\phi_N,\phi_S)^{\rm KKMH} \sim -\frac{c}{2\sqrt{2}}\phi_N^2\phi_S. \tag{6.78}$$

From Eqs. (6.68) - (6.75) we can see that the KKMH term influences all scalars and pseudoscalars except for $\bar{s}s$ states (and analogously to the case of the Veneziano-Witten term, it induces the mass splitting between $\boldsymbol{\pi}$ and $\eta_N$); the contributions from the KKMH term have the same magnitude but opposite sign for pairs of states with the same parity but different isospin ($\sigma_N$-$a_0$ and $\eta_N$-$\pi$) or with the same isospin but different parity ($K_S$-$K$). Additionally, the KKMH term influences not only the $\eta_N$-$\eta_S$ mixing but also the mixing of $\sigma_N$ and $\sigma_S$. Note that the contribution to the potential $\mathcal{V}(\phi_N,\phi_S)$, Eq. (6.78), does not change the conditions regarding the spontaneous symmetry breaking, i.e., the potential with this contribution still yields Eqs. (9.4) and (9.15).

Although one might assume that the results regarding phenomenology to be presented in this work will differ depending on the choice of the chiral-anomaly term, this is not the case for the following reasons: (*i*) for the $\eta_N$-$\eta_S$ mixing, the constants $c$ and $c_1$ are mutually dependent, as obvious from a comparison of Eqs. (6.78) and (6.67):

$$c\frac{\phi_N}{\sqrt{2}} \equiv c_1\frac{\phi_N^3\phi_S}{2} \Leftrightarrow c \equiv c_1\frac{\phi_N^2\phi_S}{\sqrt{2}}; \tag{6.79}$$

(*ii*) Eqs. (9.4) and (9.15) regarding the correct implementation of the spontaneous breaking of the chiral symmetry are not affected by the lack of presence of the chiral-anomaly term in the potential and (*iii*) for the $\sigma_N$-$\sigma_S$ mixing, the full mixing term is the sum of Eqs. (9.16) and (6.77): $\mathcal{L}_{\sigma_N\sigma_S}^{\rm KKMH} = (c/\sqrt{2} - 2\lambda_1\phi_N)\phi_S\sigma_N\sigma_S$; the parameter $\lambda_1$ cannot be calculated but only constrained from the linear combination $m_0^2 + \lambda_1(\phi_N^2+\phi_S^2)$ and therefore the value of $\lambda_1$ can always be adjusted in such a way that it absorbs the contribution from the parameter $c$ to the mixing: for this reason, the results regarding the $\sigma_N$-$\sigma_S$ mixing are unaffected by our choice of chiral-anomaly term. Of course, this may not be true for all the decays that could in principle be calculated from our Lagrangian. The reason is that the contributions of the full $c$ and $c_1$ terms to the Lagrangian would not be the same (although both describe the same anomaly); we nonetheless note that the chiral anomaly does not influence any other decays that will be presented in this work other than those already mentioned. Then for reason of simplicity we will be using the VW term in the $N_f = 3$ version of our model. Note that this form of the chiral-anomaly term allows us to incorporate a pseudoscalar glueball field $\tilde{G}$ into our model in a very simple way: the term $i\tilde{c}\tilde{G}(\det\Phi - \det\Phi^\dagger)$ couples our (pseudo)scalar fields to $\tilde{G}$ with a single constant $\tilde{c}$.

# 7. The Fit Structure

As already mentioned, there are six free parameters: $Z_\pi$, $Z_K$, $m_1^2$, $h_2$, $\delta_S$ and $\lambda_2$ and one parameter combination: $m_0^2 + \lambda_1(\phi_N^2 + \phi_S^2)$ that need to be determined from our fit. Let us note at the beginning that these parameters can be combined into three groups: (*i*) parameters influencing only (pseudo)scalar phenomenology: $m_0^2 + \lambda_1(\phi_N^2 + \phi_S^2)$ and $\lambda_2$; (*ii*) parameters influencing only (axial-)vector phenomenology: $m_1^2$, $h_2$ and $\delta_S$ and (*iii*) parameters appearing in Lagrangian terms relevant for the phenomenology of both (pseudo)scalars and (axial-)vectors: $Z_\pi$ and $Z_K$. If there were no parameters from the group (*iii*), then the other parameters would neatly split into two independent groups thus noticeably simplifying the fit; however, the presence of the renormalisation coefficients $Z_\pi$ and $Z_K$ complicates the search for a fit considerably. The following observables enter the fit:

- In the (pseudo)scalar sector, we consider all mass terms except for $m_{\sigma_N}$ and $m_{\sigma_S}$. We do not consider the $\sigma$ masses because the data regarding the $I(J^{PC}) = 0(0^{++})$ states is poor [10], especially in the region under 1 GeV. Therefore, six mass terms enter the fit, i.e., Eqs. (6.33) - (6.35) and (6.37) - (6.39). Note that we first have to implement the mixing of the pure non-strange state $\eta_N$ and the pure strange state $\eta_S$ that will allow us to calculate $m_\eta$ and $m_{\eta'}$. Note also that the inclusion of $m_{a_0}$ into the fit forces us to consider two different assignments of the isotriplet scalar state [given that the experimental data ascertain the existence of two $I(J^{PC}) = 1(0^{++})$ states, $a_0(980)$ and $a_0(1450)$]. This in turn means that we will have to consider two different fits, each containing an assignment of the $\boldsymbol{a}_0$ state in our model to the physical state in the region under 1 GeV (referred to as Fit I in the following) or above 1 GeV (referred to as Fit II in the following). Note that the scalar kaon state $K_S$ present in the model can also be assigned to a physical state in two different ways: although the PDG confirmes the existence of only one meson with quantum numbers $I(J^P) = 1/2(0^+)$, the $K_0^\star(1430)$ state, we will nonetheless also work with $K_0^\star(800)$ or $\kappa$ in our Fit I. This is necessary as otherwise a scalar isotriplet from the region under 1 GeV [$a_0(980)$] would enter the same fit as the scalar kaon from the region above 1 GeV [$K_0^\star(1430)$] which would be counter-intuitive because it would imply a large mass splitting ($\simeq 400$ MeV) between a non-strange meson and a kaon whereas one would expect the mass splitting to be $\simeq 100$ MeV, i.e., close to the strange-quark mass.

- In the (axial-)vector channel, we consider all mass terms that follow from the Lagrangian (6.1), i.e., Eqs. (6.40) - (6.45).

- Our result regarding the decay $a_1 \to \pi\gamma$ from the $N_f = 2$ version of the model is still valid as the corresponding interaction Lagrangian remains the same once the $U(3) \times U(3)$ version of the model is considered. We have seen in Sec. 5.2.5 that this decay width depends only on $Z_\pi$ but does not constrain $Z_\pi$ very well due to lack of precise experimental data. Still, the fit to be performed in the following sections should also take this constraint into account (by producing $Z_\pi$ within the limits provided by $\Gamma_{a_1\to\pi\gamma}$). Note that in principle $Z_\pi$ can also be determined from $\tau$-lepton decays [245]. However, the model presented in this work neglects weak interactions and, for this reason, only $\Gamma_{a_1\to\pi\gamma}$ will be used.

- Each of the two fits to be performed will have a decay width that only depends on $h_2$. In the case of Fit I, this will be the decay width $\Gamma_{f_{1N}\to a_0(980)\pi}$ and in the case of Fit II, this will be the total decay width of $a_0(1450)$. This is analogous to Scenarios I and II in the $U(2)\times U(2)$ version of the model.

- We have already noted that there are three formulas for the renormalisation coefficient $Z_K$: Eqs. (6.47), (6.62) and (6.63). These equations have to be pairwise the same:

$$\frac{2m_{K_1}}{\sqrt{4m_{K_1}^2 - g_1^2(\phi_N+\sqrt{2}\phi_S)^2}} \stackrel{!}{=} \frac{1}{f_K}\sqrt{\frac{m_{f_{1S}}^2 - m_{\omega_S}^2}{g_1^2 - h_3}}, \tag{7.1}$$

$$\frac{2m_{K_1}}{\sqrt{4m_{K_1}^2 - g_1^2(\phi_N+\sqrt{2}\phi_S)^2}} \stackrel{!}{=} \frac{m_{K_1}^2 - m_{K^\star}^2}{Z_\pi f_\pi f_K(g_1^2 - h_3)}. \tag{7.2}$$

  However, each of the Eqs. (7.1), (7.2) contains mass terms ($m_{K^\star}$, $m_{\omega_S}$, $m_{K_1}$, $m_{f_{1S}}$) that are not mere numbers but also themselves functions of the parameters $Z_\pi$, $Z_K$, $m_1^2$, $h_2$ and $\delta_S$ [see Eqs. (6.44), (6.42), (6.45) and (6.43)]. Additionally, the equations also contain parameters $g_1$ and $h_3$ [see Eqs. (6.55) and (6.56)] that depend on $m_\rho$ and $m_{a_1}$, with the latter two themselves mass terms depending on the parameters $Z_\pi$, $Z_K$, $m_1^2$ and $h_2$. Note also that the parameters $g_1$ and $h_3$ enter all of the mass terms mentioned.

  Therefore, Eqs. (7.1) and (7.2) actually represent a system of implicit equations for the fit parameters:

$$\begin{aligned}&\frac{2m_{K_1}[Z_\pi, Z_K, m_1^2, h_2, \delta_S]}{\sqrt{4m_{K_1}^2[Z_\pi, Z_K, m_1^2, h_2, \delta_S] - g_1^2[Z_\pi, Z_K, m_1^2, h_2](\phi_N[Z_\pi]+\sqrt{2}\phi_S[Z_K])^2}}\\ &\stackrel{!}{=} \frac{1}{f_K}\sqrt{\frac{m_{f_{1S}}^2[Z_\pi, Z_K, m_1^2, h_2, \delta_S] - m_{\omega_S}^2[Z_\pi, Z_K, m_1^2, h_2, \delta_S]}{g_1^2[Z_\pi, Z_K, m_1^2, h_2] - h_3[Z_\pi, Z_K, m_1^2, h_2]}},\end{aligned} \tag{7.3}$$

$$\begin{aligned}&\frac{2m_{K_1}[Z_\pi, Z_K, m_1^2, h_2, \delta_S]}{\sqrt{4m_{K_1}^2[Z_\pi, Z_K, m_1^2, h_2, \delta_S] - g_1^2[Z_\pi, Z_K, m_1^2, h_2](\phi_N[Z_\pi]+\sqrt{2}\phi_S[Z_K])^2}}\\ &\stackrel{!}{=} \frac{m_{K_1}^2[Z_\pi, Z_K, m_1^2, h_2, \delta_S] - m_{K^\star}^2[Z_\pi, Z_K, m_1^2, h_2, \delta_S]}{Z_\pi f_\pi f_K(g_1^2[Z_\pi, Z_K, m_1^2, h_2] - h_3[Z_\pi, Z_K, m_1^2, h_2])}.\end{aligned} \tag{7.4}$$

  Equations (7.3) and (7.4) have to be considered as well, and represent an additional, strong constraint in the fit.

*We therefore have 16 equations for seven unknowns [$Z_\pi$, $Z_K$, $m_1^2$, $h_2$, $\delta_S$, $\lambda_2$ and $m_0^2+\lambda_1(\phi_N^2+\phi_S^2)$].*

Before we perform the fits, it is necessary to discuss the issue of the $\eta$-$\eta'$ mixing in the model given that the corresponding masses enter the fit (and also determine the value of the parameter $c_1$, as we have already mentioned).

## 7.1 Mixing of $\eta$ and $\eta'$

The pure non-strange and strange fields $\eta_N$ and $\eta_S$ mix in the Lagrangian (6.1):

$$\mathcal{L}_{\eta_N\eta_S} = -c_1\frac{Z_{\eta_S}Z_\pi}{2}\phi_N^3\phi_S\eta_N\eta_S. \tag{7.5}$$

The full $\eta_N$-$\eta_S$ interaction Lagrangian has the form

$$\mathcal{L}_{\eta_N\eta_S,\,\text{full}} = \frac{1}{2}(\partial_\mu\eta_N)^2 + \frac{1}{2}(\partial_\mu\eta_S)^2 - \frac{1}{2}m_{\eta_N}^2{\eta_N}^2 - \frac{1}{2}m_{\eta_S}^2{\eta_S}^2 + z_\eta\eta_N\eta_S, \tag{7.6}$$

where $z_\eta$ is the mixing term of pure states $\eta_N \equiv (\bar{u}u - \bar{d}d)/\sqrt{2}$ and $\eta_S \equiv \bar{s}s$.
Comparing Eqs. (7.5) and (7.6) we see that in the case of our model Lagrangian the mixing term $z_\eta$ is

$$z_\eta = -c_1\frac{Z_{\eta_S}Z_\pi}{2}\phi_N^3\phi_S. \tag{7.7}$$

However, the mixing between the pure states $\eta_N$ and $\eta_S$ can be equivalently expressed as the mixing between the octet state

$$\eta_8 = \sqrt{\frac{1}{6}}(\bar{u}u + \bar{d}d - 2\bar{s}s) \equiv \sqrt{\frac{1}{3}}\eta_N - \sqrt{\frac{2}{3}}\eta_S \tag{7.8}$$

and the singlet state

$$\eta_0 = \sqrt{\frac{1}{3}}(\bar{u}u + \bar{d}d + \bar{s}s) \equiv \sqrt{\frac{2}{3}}\eta_N + \sqrt{\frac{1}{3}}\eta_S. \tag{7.9}$$

We determine the physical states $\eta$ and $\eta'$ as mixture of the octet and singlet states with a mixing angle $\varphi_P$:

$$\begin{pmatrix}\eta\\ \eta'\end{pmatrix} = \begin{pmatrix}\cos\varphi_P & -\sin\varphi_P\\ \sin\varphi_P & \cos\varphi_P\end{pmatrix}\begin{pmatrix}\eta_8\\ \eta_0\end{pmatrix} \tag{7.10}$$

or, using Eqs. (7.8) and (7.9),

$$\begin{pmatrix}\eta\\ \eta'\end{pmatrix} = \begin{pmatrix}\cos\varphi_P & -\sin\varphi_P\\ \sin\varphi_P & \cos\varphi_P\end{pmatrix}\begin{pmatrix}\sqrt{\frac{1}{3}} & -\sqrt{\frac{2}{3}}\\ \sqrt{\frac{2}{3}} & \sqrt{\frac{1}{3}}\end{pmatrix}\begin{pmatrix}\eta_8\\ \eta_0\end{pmatrix}. \tag{7.11}$$

If we introduce $\arcsin(\sqrt{2/3}) = 54.7456^\circ \equiv \varphi_I$, then the trigonometric addition formulas lead to

$$\begin{pmatrix}\eta\\ \eta'\end{pmatrix} = \begin{pmatrix}\cos(\varphi_P+\varphi_I) & -\sin(\varphi_P+\varphi_I)\\ \sin(\varphi_P+\varphi_I) & \cos(\varphi_P+\varphi_I)\end{pmatrix}\begin{pmatrix}\eta_N\\ \eta_S\end{pmatrix}. \tag{7.12}$$

Defining the $\eta$-$\eta'$ mixing angle $\varphi_\eta$

$$\varphi_\eta = -(\varphi_P + \varphi_I), \tag{7.13}$$

we obtain

$$\begin{pmatrix}\eta\\ \eta'\end{pmatrix} = \begin{pmatrix}\cos\varphi_\eta & \sin\varphi_\eta\\ -\sin\varphi_\eta & \cos\varphi_\eta\end{pmatrix}\begin{pmatrix}\eta_N\\ \eta_S\end{pmatrix} \tag{7.14}$$

or in other words

$$\eta = \cos\varphi_\eta\eta_N + \sin\varphi_\eta\eta_S, \tag{7.15}$$

$$\eta' = -\sin\varphi_\eta\eta_N + \cos\varphi_\eta\eta_S. \tag{7.16}$$

The interaction Lagrangian, Eq. (7.6), contains only pure states $\eta_N$ and $\eta_S$. Inverting Eqs. (7.15) and (7.16)

$$\eta_N = \cos\varphi_\eta \eta - \sin\varphi_\eta \eta', \tag{7.17}$$
$$\eta_S = \sin\varphi_\eta \eta + \cos\varphi_\eta \eta', \tag{7.18}$$

and substituting $\eta_N$ and $\eta_S$ by $\eta$ and $\eta'$ in Eq. (7.6) we obtain

$$\begin{aligned}
\mathcal{L}_{\eta\eta'} &= \frac{1}{2}[(\partial_\mu\eta)^2(\cos\varphi_\eta)^2 + (\partial_\mu\eta')^2(\sin\varphi_\eta)^2 - \sin(2\varphi_\eta)\partial_\mu\eta\partial^\mu\eta'] \\
&+ \frac{1}{2}[(\partial_\mu\eta)^2(\sin\varphi_\eta)^2 + (\partial_\mu\eta')^2(\cos\varphi_\eta)^2 + \sin(2\varphi_\eta)\partial_\mu\eta\partial^\mu\eta'] \\
&- \frac{1}{2}m_{\eta_N}^2[\eta^2(\cos\varphi_\eta)^2 + (\eta')^2(\sin\varphi_\eta)^2 - \sin(2\varphi_\eta)\eta\eta'] \\
&- \frac{1}{2}m_{\eta_S}^2[\eta^2(\sin\varphi_\eta)^2 + (\eta')^2(\cos\varphi_\eta)^2 + \sin(2\varphi_\eta)\eta\eta'] \\
&+ z_\eta\{[\eta^2 - (\eta')^2]\sin\varphi_\eta\cos\varphi_\eta + \cos(2\varphi_\eta)\eta\eta'\} \\
&= \frac{1}{2}(\partial_\mu\eta)^2 + \frac{1}{2}(\partial_\mu\eta')^2 - \frac{1}{2}[m_{\eta_N}^2(\cos\varphi_\eta)^2 + m_{\eta_S}^2(\sin\varphi_\eta)^2 - z_\eta\sin(2\varphi_\eta)]\eta^2 \\
&- \frac{1}{2}[m_{\eta_N}^2(\sin\varphi_\eta)^2 + m_{\eta_S}^2(\cos\varphi_\eta)^2 + z_\eta\sin(2\varphi_\eta)](\eta')^2 \\
&- \frac{1}{2}[(m_{\eta_S}^2 - m_{\eta_N}^2)\sin(2\varphi_\eta) - 2z_\eta\cos(2\varphi_\eta)]\eta\eta'.
\end{aligned} \tag{7.19}$$

From Eq. (7.19) we obtain the following relations for $m_\eta$ and $m_{\eta'}$ in terms of the pure non-strange and strange mass terms $m_{\eta_N}$ and $m_{\eta_S}$ [with the latter known from Eqs. (6.33) and (6.37), respectively]:

$$m_\eta^2 = m_{\eta_N}^2\cos^2\varphi_\eta + m_{\eta_S}^2\sin^2\varphi_\eta - z_\eta\sin(2\varphi_\eta), \tag{7.20}$$
$$m_{\eta'}^2 = m_{\eta_N}^2\sin^2\varphi_\eta + m_{\eta_S}^2\cos^2\varphi_\eta + z_\eta\sin(2\varphi_\eta). \tag{7.21}$$

Additionally, assigning our fields $\eta$ and $\eta'$ to physical (asymptotic) states requires that the Lagrangian $\mathcal{L}_{\eta\eta'}$ does not contain any $\eta$-$\eta'$ mixing terms and thus from Eq. (7.19) we obtain

$$z_\eta \stackrel{!}{=} (m_{\eta_S}^2 - m_{\eta_N}^2)\tan(2\varphi_\eta)/2. \tag{7.22}$$

consequently, from Eqs. (7.7) and (7.22) we obtain

$$(m_{\eta_S}^2 - m_{\eta_N}^2)\tan(2\varphi_\eta) = -c_1 Z_{\eta_S} Z_\pi \phi_N^3 \phi_S. \tag{7.23}$$

Given that $m_{\eta_N}$ and $m_{\eta_S}$ depend on $c_1$ [see Eqs. (6.33) and (6.37)], we obtain from Eq. (7.23) that

$$\begin{aligned}
&\left\{Z_{\eta_S}^2\left[m_0^2 + \lambda_1\phi_N^2 + (\lambda_1+\lambda_2)\phi_S^2 + c_1\frac{\phi_N^4}{4}\right] - Z_\pi^2\left[m_0^2 + \left(\lambda_1 + \frac{\lambda_2}{2}\right)\phi_N^2 + \lambda_1\phi_S^2 + c_1\phi_N^2\phi_S^2\right]\right\} \\
&\times\tan(2\varphi_\eta) = -c_1 Z_{\eta_S} Z_\pi \phi_N^3\phi_S \\
&\Leftrightarrow \left\{(Z_{\eta_S}^2 - Z_\pi^2)[m_0^2 + \lambda_1(\phi_N^2+\phi_S^2)] + \lambda_2\left(Z_{\eta_S}^2\phi_S^2 - \frac{Z_\pi^2}{2}\phi_N^2\right) + c_1\left(\frac{Z_{\eta_S}^2}{4}\phi_N^2 - Z_\pi^2\phi_S^2\right)\phi_N^2\right\} \\
&\times\tan(2\varphi_\eta) = -c_1 Z_{\eta_S} Z_\pi\phi_N^3\phi_S \\
&\Leftrightarrow c_1 = \frac{4(Z_\pi^2 - Z_{\eta_S}^2)[m_0^2 + \lambda_1(\phi_N^2+\phi_S^2)] + 2\lambda_2\left(Z_\pi^2\phi_N^2 - 2Z_{\eta_S}^2\phi_S^2\right)}{\left(Z_{\eta_S}^2\phi_N^2 - 4Z_\pi^2\phi_S^2\right)\phi_N^2\tan(2\varphi_\eta) + 4Z_{\eta_S}Z_\pi\phi_N^3\phi_S}\tan(2\varphi_\eta).
\end{aligned} \tag{7.24}$$

Using Eq. (7.24) it is possible to calculate $c_1$ from the $\eta$-$\eta'$ mixing angle $\varphi_\eta$ (and vice versa) if the other parameters are known. We will choose $\varphi_\eta$ such that our results for $m_{\eta_N}$ and $m_{\eta_S}$ are as close as possible to their experimental values; then $c_1$ is no longer a free parameter, as already mentioned in the general discussion of the fit.

## 8. Fit I: Scalars below 1 GeV

Seven unknowns [$Z_\pi$, $Z_K$, $m_1^2$, $h_2$, $\delta_S$, $\lambda_2$ and $m_0^2+\lambda_1(\phi_N^2+\phi_S^2)$] enter the fit together with 16 equations: for $m_\pi$, $m_K$, $m_{K_S}\equiv m_{K_0^\star(800)\equiv\kappa}$, $m_{a_0}\equiv m_{a_0(980)}$, $m_\eta$, $m_{\eta'}$ [the latter two via Eqs. (7.20) and (7.21) from $m_{\eta_N}$ and $m_{\eta_S}$], $m_\rho$, $m_{K^\star}$, $m_{\omega_S}$, $m_{a_1}$, $m_{K_1}$, $m_{f_{1S}}$, $\Gamma_{a_1\to\pi\gamma}$, $\Gamma_{f_{1N}\to a_0(980)\pi}$ (Fit I) or $\Gamma_{a_0(1450)}$ (Fit II) as well as Eqs. (7.3) and (7.4). Explicitly, the fit results should satisfy the following equations (experimental central values from the PDG [10]; at this point we disregard the experimental uncertainties):

$$Z_\pi^2\left[m_0^2+\lambda_1(\phi_N^2+\phi_S^2)+\frac{\lambda_2}{2}\phi_N^2\right]=(139.57\text{ MeV})^2\equiv m_\pi^2, \tag{8.1}$$

$$Z_K^2\left[m_0^2+\lambda_1(\phi_N^2+\phi_S^2)+\lambda_2\left(\frac{\phi_N^2}{2}-\frac{\phi_N\phi_S}{\sqrt{2}}+\phi_S^2\right)\right]=(493.677\text{ MeV})^2\equiv m_K^2, \tag{8.2}$$

$$Z_{K_S}^2\left[m_0^2+\lambda_1(\phi_N^2+\phi_S^2)+\lambda_2\left(\frac{\phi_N^2}{2}+\frac{\phi_N\phi_S}{\sqrt{2}}+\phi_S^2\right)\right]=(676\text{ MeV})^2\equiv m_\kappa^2, \tag{8.3}$$

$$m_0^2+\lambda_1(\phi_N^2+\phi_S^2)+\frac{3}{2}\lambda_2\phi_N^2=(980\text{ MeV})^2\equiv m_{a_0(980)}^2, \tag{8.4}$$

$$\begin{aligned}&Z_\pi^2\left[m_0^2+\lambda_1(\phi_N^2+\phi_S^2)+\frac{\lambda_2}{2}\phi_N^2+c_1\phi_N^2\phi_S^2\right]\cos^2\varphi_\eta\\&+Z_{\eta_S}^2\left[m_0^2+\lambda_1(\phi_N^2+\phi_S^2)+\lambda_2\phi_S^2+c_1\frac{\phi_N^4}{4}\right]\sin^2\varphi_\eta\\&+c_1\frac{Z_{\eta_S}Z_\pi}{2}\phi_N^3\phi_S\sin(2\varphi_\eta)=(547.853\text{ MeV})^2\equiv m_\eta^2,\end{aligned} \tag{8.5}$$

$$\begin{aligned}&Z_\pi^2\left[m_0^2+\lambda_1(\phi_N^2+\phi_S^2)+\frac{\lambda_2}{2}\phi_N^2+c_1\phi_N^2\phi_S^2\right]\sin^2\varphi_\eta\\&+Z_{\eta_S}^2\left[m_0^2+\lambda_1(\phi_N^2+\phi_S^2)+\lambda_2\phi_S^2+c_1\frac{\phi_N^4}{4}\right]\cos^2\varphi_\eta\\&-c_1\frac{Z_{\eta_S}Z_\pi}{2}\phi_N^3\phi_S\sin(2\varphi_\eta)=(957.78\text{ MeV})^2\equiv m_{\eta'}^2,\end{aligned} \tag{8.6}$$

$$m_1^2+(h_2+h_3)\frac{\phi_N^2}{2}=(775.49\text{ MeV})^2\equiv m_\rho^2, \tag{8.7}$$

$$m_1^2+g_1^2\phi_N^2+(h_2-h_3)\frac{\phi_N^2}{2}=(1230\text{ MeV})^2\equiv m_{a_1}^2, \tag{8.8}$$

$$m_1^2+\delta_S+\left(g_1^2+h_2\right)\frac{\phi_N^2}{4}+\frac{1}{\sqrt{2}}(h_3-g_1^2)\phi_N\phi_S+\left(g_1^2+h_2\right)\frac{\phi_S^2}{2}=(891.66\text{ MeV})^2\equiv m_{K^\star}^2, \tag{8.9}$$

$$m_1^2+\delta_S+\left(g_1^2+h_2\right)\frac{\phi_N^2}{4}+\frac{1}{\sqrt{2}}(g_1^2-h_3)\phi_N\phi_S+\left(g_1^2+h_2\right)\frac{\phi_S^2}{2}=(1272\text{ MeV})^2\equiv m_{K_1}^2, \tag{8.10}$$

$$m_1^2+2\delta_S+(h_2+h_3)\,\phi_S^2=(1019.455\text{ MeV})^2\equiv m_{\omega_S}^2, \tag{8.11}$$

$$m_1^2+2\delta_S+2g_1^2\phi_S^2+(h_2-h_3)\,\phi_S^2=(1426.4\text{ MeV})^2\equiv m_{f_{1S}}^2, \tag{8.12}$$

$$\frac{e^2}{96\pi}(Z_\pi^2-1)m_{a_1}\left[1-\left(\frac{m_\pi}{m_{a_1}}\right)^2\right]^3=0.640\text{ MeV}\equiv\Gamma_{a_1\to\pi\gamma}, \tag{8.13}$$

$$\frac{g_1^2 Z_\pi^2}{16\pi}\frac{[m_{f_{1N}}^4 - 2m_{f_{1N}}^2\,(m_{a_0}^2+m_\pi^2) + (m_{a_0}^2-m_\pi^2)^2]^{3/2}}{m_{f_{1N}}^5 m_{a_1}^4}$$
$$\times\left[m_\rho^2 - \frac{1}{2}(h_2+h_3)\phi_N^2\right]^2 = 8.748\ \text{MeV} \equiv \Gamma_{f_{1N}\to a_0(980)\pi}, \tag{8.14}$$

and additionally the $Z_K$ Eqs. (7.3) and (7.4). We have set $h_1 = 0 = \delta_N$; note that $c_1 = c_1(\varphi_\eta)$ by Eq. (7.24) and that we also use $\phi_N = Z_\pi f_\pi$ ($f_\pi = 92.4$ MeV), $\phi_S = Z_K f_K/\sqrt{2}$ ($f_K = 155.5/\sqrt{2}$ MeV), $g_1$ from Eq. (6.55), $h_3$ from Eq. (6.56), $Z_{K_S}$ from Eq. (6.49) and $Z_{\eta_S}$ from Eq. (6.48). Note also that the mass terms present in Eqs. (6.55), (6.56), (6.49) and (6.48) are themselves functions of the parameters stated at the beginning of this section.
Therefore, a comment is necessary before we proceed with the parameter determination. Equations (8.1) - (8.14), (7.3) and (7.4) could in principle be subject of a $\chi^2$ fit analogous to the one performed in the $N_f = 2$ version of our model, see Sec. 5.3. However, the $N_f = 3$ version of the model requires us to consider a significantly larger number of equations and parameters. For this reason, a $\chi^2$ fit in $N_f = 3$ is extremely complicated to perform numerically, not least because the large number of input equations would imply an extremely large number of local minima that would have to be considered. In addition, the minima strongly depend on the initial conditions of the parameters. To circumvent the technical issues that a $\chi^2$ fit would bring about, we will use an iterative procedure (described below) rather than a fit to determine the parameters of the model. The procedure does not allow for errors to be determined (this would be possible in a fit) but nonetheless the parameters determined in this way can in turn be used as initial conditions in a $\chi^2$ fit ascertaining that a global minimum has been found. Such a $\chi^2$ fit is currently under development [246] and it appears to assign small errors to our parameters (of the order of several percent). Thus all results presented in this and the subsequent chapters 9 – 11 should be considered as possessing an error $\lesssim 10\%$. Then we can refer to the parameter determinations in the stated chapters as "Fit I" and "Fit II".

The parameter values can be found iteratively in the following four steps:

- *Step 1: $Z_\pi$, $Z_K$, (pseudo)scalar parameters.* Solve the first four equations in the fit [Eqs. (8.1) - (8.4)] and determine $Z_\pi$ and $Z_K$ (among others).
- *Step 2: (axial-)vector masses.* Constrain the values of $m_\rho$, $m_{a_1}$, $m_{K^\star}$, $m_{\omega_S}$, $m_{K_1}$ and $m_{f_{1S}}$ via the $Z_K$ Eqs. (7.3) and (7.4).
- *Step 3: (axial-)vector parameters.* Calculate $h_2$, $m_1^2$ and $\delta_S$ from the mass values determined in Step 2.
- *Step 4: $\eta$-$\eta'$ mixing angle $\varphi_\eta$.* Calculate $\varphi_\eta$ from $m_\eta$ and $m_{\eta'}$; additionally, $c_1$ is calculated from Eq. (7.24).

*Step 1.* Let us note that the first four equations entering the fit, i.e., Eqs. (8.1) - (8.4) contain four variables: $Z_\pi$, $Z_K$, $\lambda_2$, $m_0^2 + \lambda_1(\phi_N^2 + \phi_S^2)$ if we assign certain values to $m_{a_1}$ and $m_{K^\star}$ (e.g., $m_{a_1} = 1230$ MeV and $m_{K^\star} = 891.66$ MeV [10]) in order for $Z_{K_S}$ to be calculated [subsequently, it is possible to choose (axial-)vector parameters in the mass terms for $m_{a_1}$ and $m_{K^\star}$ – see Eqs. (8.8) and (8.9) – in such a way that the values assigned are correct]. Note, however, that the starting values of $m_{a_1}$ and $m_{K^\star}$ are not strongly constrained because $Z_{K_S}$ changes by approximately 0.1%

if $m_{a_1}$ and $m_{K^\star}$ are varied, see Fig. 8.1. Indeed, experimental data allow for a rather large interval in particular of $m_{a_1}$ because $a_1(1260)$ is a very broad resonance, with $\Gamma_{a_1(1260)} = (250 - 600)$ MeV [10].

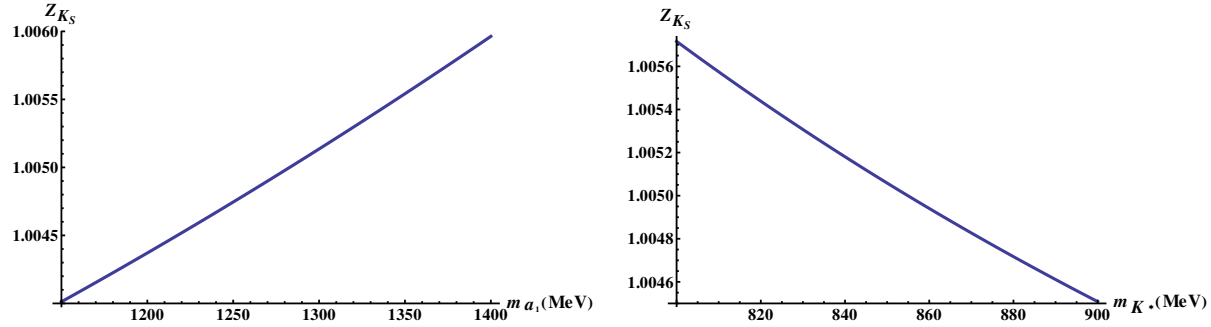


**Figure 8.1:** Dependence of the renormalisation coefficient $Z_{K_S}$ on $m_{a_1}$ (left panel) and $m_{K^\star}$ (right panel).

We thus obtain a system of four equations with four unknowns. This equation system can be solved exactly with a numerical analysis yielding the following parameter values:

$$\begin{aligned} Z_\pi &= 0.31, \\ Z_K &= 0.51, \\ \lambda_2 &= 931, \\ m_0^2 + \lambda_1(\phi_N^2 + \phi_S^2) &= -172665 \text{ MeV}^2. \end{aligned}$$

Unfortunately, the stated solutions cannot be used because that would imply $Z_\pi < 1$ and $Z_K < 1$ that cannot be true due to the definitions of $Z_\pi$, Eq. (6.46), and $Z_K$, Eq. (6.47) as otherwise one would have to allow either for imaginary scalar-vector coupling $g_1$ in the Lagrangian (6.1) or for imaginary condensates $\phi_{N,S}$. Therefore, we have to consider other (approximate) solutions of Eqs. (8.1) - (8.4). A numerical analysis leads to the parameter values shown in Table 8.1.

| Parameter | Value | Observable | Value [MeV] |
|---|---|---|---|
| $Z_\pi$ | 1.38 | $m_\pi$ | 138.04 |
| $Z_K$ | 1.39 | $m_K$ | 490.84 |
| $\lambda_2$ | 58.5 | $m_{a_0(980)}$ | 978 |
| $m_0^2 + \lambda_1(\phi_N^2 + \phi_S^2)$ | $-463425$ MeV$^2$ | $m_\kappa$ | 1129 |

**Table 8.1:** Best solutions of Eqs. (8.1) - (8.4) under the conditions $Z_\pi \overset{!}{>} 1$, $Z_K \overset{!}{>} 1$.

The parameters produce an excellent agreement with all input masses except $m_\kappa$ where the value from the fit is almost by a factor of two larger than the PDG value $m_\kappa^{\text{exp}} = (676 \pm 40)$ MeV. However, we note that the $\kappa$ resonance is very broad [$\Gamma_\kappa^{\text{exp}} = (548 \pm 24)$ MeV] and therefore we will, for the moment, disregard the large mass difference between the fit result and the PDG value. Additionally, $\Gamma_{a_1 \to \pi\gamma} = 0.322$ MeV is obtained from the parameter values in Table 8.1, slightly smaller than the lower boundary on this decay width cited by the PDG to be 0.394 MeV.

*Step 2.* Let us now turn to the parameters in (axial-)vector mass terms. The most convenient way to proceed is to first determine the values of vector and axial-vector masses that lead to

the pairwise equality of the three $Z_K$ formulas, Eqs. (7.3) and (7.4). Note that the calculation involving Eqs. (7.3) and (7.4) requires knowledge of $Z_\pi$ and $Z_K$ (see Table 8.1) and also of $m_\rho$, $m_{a_1}$, $m_{K^\star}$, $m_{\omega_S}$, $m_{K_1}$ and $m_{f_{1S}}$. We start with the PDG values of all masses except $m_{a_1}$ (as already mentioned, the variation of $m_{a_1}$ is experimentally allowed by the large decay width of this resonance and it does not lead to an inconsistency with the determination of scalar parameters in Table 8.1). We then look for conditions under which the pairwise equality of the three $Z_K$ formulas can be obtained. Unfortunately, the mentioned equality does not exist for the PDG values of masses. We therefore alternate all the mass values (holding all masses except $m_{a_1}$ as close as possible to their respective experimental values) until the pairwise equality of the three $Z_K$ formulas has been reached. In this way we obtain (axial-)vector masses as follows:

$$m_{a_1} = 1396 \text{ MeV}, \, m_\rho = 775.49 \text{ MeV}, \, m_{K^\star} = 832.53 \text{ MeV},$$
$$m_{\omega_S} = 870.35 \text{ MeV}, \, m_{K_1} = 1520 \text{ MeV}, \, m_{f_{1S}} = 1643.4 \text{ MeV}.$$

*Step 3.* Once the values of the (axial-)vector masses are known, then the (axial-)vector fit parameters are determined in such a way that the mass values determined by the three $Z_K$ formulas are reproduced. Note, however, that this does not require for many parameters to be calculated: $h_2$ is already known from $\Gamma_{f_{1N}\to a_0(980)\pi}$; $g_1$ and $h_3$ are determined from $m_\rho$ and $m_{a_1}$ [see Eqs. (6.55) and (6.56)] and consequently we need to calculate only the values of $m_1^2$ and $\delta_S$. As already mentioned in Sec. 7, it is possible to calculate the parameter $h_2$ via $\Gamma_{f_{1N}\to a_0(980)\pi}$, Eq. (8.14). In Scenario I of the two-flavour version of the model (Sec. 5.3) we have seen that in this way two sets of $h_2$ values arise, a set of relatively lower and a set of relatively higher values, see Eq. (5.51). We have also seen that the set of relatively lower $h_2$ values does not yield a correct value of the $a_0(980) \to \eta\pi$ decay amplitude. Therefore, we are also in this case naturally inclined to use the set of higher $h_2$ values, i.e., $h_2 \sim 80$. However, the only way to obtain a fit in this case is to allow for negative values of $m_1^2$ and $\delta_S$ (see Table 8.2). However, such a fit could not be considered physical as it would imply an imaginary vector meson mass in the chirally restored phase.

| Parameter | Value |
|---|---|
| $m_1^2$ | $-697^2$ MeV$^2$ |
| $\delta_S$ | $-404^2$ MeV$^2$ |
| $h_2$ | 161 |

**Table 8.2:** (Axial-)vector parameters from Eqs. (8.7) - (8.12) using the higher set of $h_2$ values from Eq. (8.14). The parameter $h_2$ has a rather large value due to the large value of $m_{a_1}$, constrained from the $Z_K$ formulas (7.3) and (7.4).

For these reasons, we have to use the smaller set of $h_2$ values [and later ascertain whether it is still possible to obtain a correct value of the $a_0(980) \to \eta\pi$ decay amplitude, see Sec. 9.2]. In this case, the fit yields positive values of $m_1^2$ and $\delta_S$.

*Step 4.* Using Eqs. (7.20) and (7.21) we can calculate the $\eta$-$\eta'$ mixing angle $\varphi_\eta$ under the conditions that $m_\eta$ and $m_{\eta'}$ are as close as possible to their respective experimental values. Additionally, we also require $\varphi_\eta <| \, 45^\circ \, |$ as otherwise we would have the (counter-intuitive) ordering $m_{\eta_S} < m_{\eta_N}$. Under the latter condition it is actually not possible to exactly obtain the

| Parameter | Value |
|---|---|
| $m_1^2$ | $697^2$ MeV$^2$ |
| $\delta_S$ | $229^2$ MeV$^2$ |
| $h_2$ | 40.6 |

**Table 8.3:** (Axial-)vector parameters from Eqs. (8.7) - (8.12) using the lower set of $h_2$ values from Eq. (8.14).

experimental value of $m_\eta$ but rather a slightly lower one: $m_\eta = 517.13$ MeV. We obtain also $m_{\eta'} = 957.78$ MeV $\equiv m_{\eta'}^{\rm exp}$ with $\varphi_\eta = -42°$; Eq. (7.24) yields $c_1 = 0.0015$ MeV$^{-2}$.
Table 8.4 shows results for all parameters from Fit I.

| Parameter | Value | Parameter | Value |
|---|---|---|---|
| $Z_\pi$ | 1.38 | $g_1$, Eq. (6.55) | 7.54 |
| $Z_K$ | 1.39 | $g_2$, Eq. (5.45) | $-11.2$ |
| $\lambda_2$ | 58.5 | $h_3$, Eq. (6.56) | $-26.3$ |
| $m_0^2 + \lambda_1(\phi_N^2 + \phi_S^2)$ | $-463425$ MeV$^2$ | $h_{0N}$, Eq. (6.35) | $1.279 \cdot 10^6$ MeV$^3$ |
| $m_1$ | 697 MeV | $h_{0S}$, Eq. (6.37) | $3.443 \cdot 10^7$ MeV$^3$ |
| $\delta_S$ | $229^2$ MeV$^2$ | $h_1$ | 0 |
| $h_2$ | 40.6 | $\delta_N$ | 0 |
| $c_1$ | 0.0015 MeV$^{-2}$ | $g_{3,4,5,6}$ | 0 |

**Table 8.4:** Best values of parameters from Fit I (experimental are uncertainties omitted).

Table 8.5 shows the results for all observables from Fit I. Note that the implemented iterative calculation of the parameters does not allow for an error determination and thus we also do not cite experimental errors in Table 8.5. Additionally, some mass values (e.g., $m_\pi$ and $m_K$) are known very precisely (up to several decimals), i.e., the corresponding errors are very small. Our model does not aim to reproduce these mass values to such a high precision – it suffices to reproduce the experimental masses sufficiently closely. Then our results for some masses [such as $m_{a_0(980)}$] will be within errors, others will not ($m_\pi$ and $m_K$) but they will still be sufficiently close to the experimental result (within several MeV) rendering them acceptable.
Nonetheless, the proximity of our results to the experiment is actually not accomplished very well at this point (because the underlying assumption of scalar $\bar{q}q$ states below 1 GeV is generally disfavoured by our model, see below) – we will see that the correspondence of our results with the data is significantly improved once the scalar $\bar{q}q$ states are assumed to be above 1 GeV, see Table 10.3.
We observe from Table 8.5 that, in addition to a rather large value of $m_\kappa$, the fit also yields too large values of $m_{a_1}$ and $m_{f_{1S}}$. The $a_1(1260)$ resonance is very broad: $\Gamma^{\rm exp}_{a_1(1260)} = (250 - 600)$ MeV [10] and thus the discrepancy between our and the experimental results is not too serious; however, the $f_1(1420) \equiv f_{1S}$ resonance is much narrower [$\Gamma^{\rm exp}_{f_1(1420)} = (54.9 \pm 2.6)$ MeV] and therefore, in this case, the discrepancy with the experimental value is rather large. The same holds for the $\omega_S \equiv \varphi(1020)$ resonance, a sharp peak with a width of $4.26 \pm 0.04$ MeV [10] and also for $K^\star(892)$, although for the latter resonance the discrepancy with the experimental mass is of the order of the decay width, i.e., $(50.8 \pm 0.9)$ MeV. Note that the discrepancy between the fit value and experimental result is also very large for our $K_1$ resonance; however, this can

| Observable | Our Value [MeV] | Experimental Value [MeV] |
|---|---|---|
| $m_\pi$ | 138.04 | 139.57 |
| $m_K$ | 490.84 | 493.68 |
| $m_{a_0(980)}$ | 978.27 | 980 |
| $m_\kappa$ | 1128.7 | 676 |
| $m_\eta$ | 517.13 | 547.85 |
| $m_{\eta'}$ | 957.78 | 957.78 |
| $m_\rho$ | 775.49 | 775.49 |
| $m_{a_1}$ | 1396 | 1230 |
| $m_{K^\star}$ | 832.53 | 891.66 |
| $m_{\omega_S}$ | 870.35 | 1019.46 |
| $m_{K_1}$ | 1520 | 1272 |
| $m_{f_{1S}}$ | 1643.4 | 1426.4 |
| $\Gamma_{a_1\to\pi\gamma}$ | 0.369 | 0.640 |
| $\Gamma_{f_{1N}\to a_0(980)\pi}$ | 8.748 | 8.748 |

**Table 8.5:** Observables from Fit I.

be amended by assigning the $K_1$ state in the model to the $K_1(1400)$ resonance rather than to $K_1(1270)$. Data regarding the former resonance suggest $m_{K_1(1400)} = (1403 \pm 7)$ MeV and $\Gamma_{K_1(1400)} = (174 \pm 13)$ MeV and then the discrepancy between our value $m_{K_1} = 1520$ MeV and the experimental result is smaller than the value of the $K_1(1400)$ decay width. [Note, however, that the stated correspondence to $K_1(1400)$ is actually in itself problematic because axial-vector kaons are expected to mix, see Sec. 10.3. The mixing of the $K_1$ states is well-established [10, 247, 248, 249, 250, 251]; thus the absence of the mixing within Fit I represents another discrepancy with experiment.]
Note that the results also imply $m_1 = 697$ MeV, i.e., non-quark contributions are favoured to play a decisive role in the $\rho$ mass generation.

# 9. Implications of Fit I

Despite some discrepancies between results stemming from the fit and experimental data, we will proceed with calculations of hadronic decay widths in scalar and axial-vector channels (as these channels possess the most ambiguities regarding not only the decay widths but also regarding the structure of resonances).

## 9.1 Phenomenology in the $I(J^{PC}) = 0(0^{++})$ Channel

As apparent from Eqs. (6.32) and (6.36), the masses of the strange and non-strange sigma fields, $m_{\sigma_N}$ and $m_{\sigma_S}$, depend on $m_0^2 + 3\lambda_1\phi_N^2 + \lambda_1\phi_S^2$ and $m_0^2 + \lambda_1\phi_N^2 + 3\lambda_1\phi_S^2$, respectively, and thus cannot be calculated with the knowledge of the parameter combination $m_0^2 + \lambda_1(\phi_N^2 + \phi_S^2)$ stated in Table 8.4. However, if the linear combination $m_0^2 + \lambda_1(\phi_N^2 + \phi_S^2)$ is known, then the parameter $\lambda_1$ can be expressed in terms of the mass parameter $m_0^2$ (given that $Z_\pi$ and $Z_K$ are also known). Nonetheless, this is not satisfactory because it does not allow us to constrain the masses and decay widths of the two $I(J^{PC}) = 0(0^{++})$ resonances present in the model. In the next two subsections we will therefore derive a constraint on $m_0^2$ and $\lambda_1$, using the spontaneous breaking of chiral symmetry. We will discuss conditions under which the vacuum potential $\mathcal{V}(\phi_N, \phi_S)$ arising from the Lagrangian (6.1) allows for the Spontaneous Symmetry Breaking (SSB) to occur while having the correct behaviour in the limit of large values of condensates $\phi_N$ and $\phi_S$ ($\lim_{\phi_{N,S}\to\infty} \mathcal{V}(\phi_N, \phi_S) \to \infty$).

### 9.1.1 A Necessary Condition for the Spontaneous Symmetry Breaking

Calculating the elements of the Hesse matrix from the potential $\mathcal{V}(\phi_N, \phi_S)$ with respect to the condensates $\phi_N$ and $\phi_S$ yields:

$$\frac{\partial^2\mathcal{V}(\phi_N,\phi_S)}{\partial\phi_N^2} = m_0^2 + \lambda_1(3\phi_N^2 + \phi_S^2) + \frac{3}{2}\lambda_2\phi_N^2, \tag{9.1}$$

$$\frac{\partial^2\mathcal{V}(\phi_N,\phi_S)}{\partial\phi_S^2} = m_0^2 + \lambda_1\phi_N^2 + 3(\lambda_1 + \lambda_2)\phi_S^2, \tag{9.2}$$

$$\frac{\partial^2\mathcal{V}(\phi_N,\phi_S)}{\partial\phi_N\partial\phi_S} = 2\lambda_1\phi_N\phi_S. \tag{9.3}$$

From Eqs. (9.1) - (9.2) we obtain the following form of the Hesse matrix in the limit $\phi_N = \phi_S = 0$:

$$H(m_0^2) = \begin{pmatrix} m_0^2 & 0 \\ 0 & m_0^2 \end{pmatrix}$$

and the vacuum is unstable only if the Hesse matrix has negative eigenvalues or in other words

$$m_0^2 \overset{!}{<} 0. \tag{9.4}$$

This is a necessary condition for the Spontaneous Symmetry Breaking to occur. However, we still need to ascertain whether the potential $\mathcal{V}(\phi_N, \phi_S)$ from Eq. (6.50) has the right behaviour in the limit $\phi_{N,S} \to \infty$. This will be verified in the following subsection.

### 9.1.2 A Condition for $\lambda_{1,2}$ from SSB

Let us isolate the quartic terms from the potential $\mathcal{V}(\phi_N, \phi_S)$, Eq. (6.50), in the following expression $\mathcal{V}_4(\phi_N, \phi_S)$:

$$\mathcal{V}_4(\phi_N, \phi_S) = \frac{\lambda_1}{4}(\phi_N^4 + 2\phi_N^2\phi_S^2 + \phi_S^4) + \frac{\lambda_2}{4}\left(\frac{\phi_N^4}{2} + \phi_S^4\right). \tag{9.5}$$

The quadratic terms in the potential $\mathcal{V}(\phi_N, \phi_S)$ represent a negative-sign contribution due to the condition $m_0^2 \overset{!}{<} 0$. Thus, a correct implementation of the Spontaneous Symmetry Breaking requires that the quartic term $\mathcal{V}_4(\phi_N, \phi_S)$ is a positive-sign contribution to $\mathcal{V}(\phi_N, \phi_S)$ because otherwise the potential $\mathcal{V}(\phi_N, \phi_S)$ would not exhibit minima. Let us now define the variables $x_\sigma \equiv \phi_N^2$ and $y_\sigma \equiv \phi_S^2$, bringing $\mathcal{V}_4(\phi_N, \phi_S)$, Eq. (9.5), to the following form:

$$\mathcal{V}_4(\phi_N, \phi_S) = \frac{2\lambda_1 + \lambda_2}{8}x_\sigma^2 + \frac{\lambda_1 + \lambda_2}{4}y_\sigma^2 + \frac{\lambda_1}{2}x_\sigma y_\sigma \qquad (x_\sigma \geq 0, y_\sigma \geq 0). \tag{9.6}$$

Obviously the conditions $2\lambda_1 + \lambda_2 \overset{!}{>} 0 \wedge \lambda_1 + \lambda_2 \overset{!}{>} 0$ have to be satisfied. In other words:

$$\lambda_1 \overset{!}{>} -\frac{\lambda_2}{2} \text{ for } \lambda_2 > 0 \tag{9.7}$$

$$\lambda_1 \overset{!}{>} -\lambda_2 \text{ for } \lambda_2 < 0. \tag{9.8}$$

Additionally, we have to ascertain that $\mathcal{V}_4(\phi_N, \phi_S)$ is a positive-sign contribution to $\mathcal{V}(\phi_N, \phi_S)$ in all directions of the condensates. In order to verify that this is fulfilled, we set $y_\sigma \equiv \eta_\sigma x_\sigma$ ($\eta_\sigma \geq 0$) yielding the following form of $\mathcal{V}_4(\phi_N, \phi_S)$:

$$\mathcal{V}_4(\phi_N, \phi_S) = a_\sigma x_\sigma^2 + b_\sigma \eta_\sigma^2 x_\sigma^2 + c_\sigma \eta_\sigma x_\sigma^2 \equiv f_\sigma(\eta_\sigma) x_\sigma^2 \tag{9.9}$$

with $a_\sigma \equiv (2\lambda_1 + \lambda_2)/8 \overset{!}{>} 0$, $b_\sigma \equiv (\lambda_1 + \lambda_2)/4 \overset{!}{>} 0$, $c_\sigma \equiv \lambda_1/2$ and $f_\sigma(\eta_\sigma) \equiv b_\sigma \eta_\sigma^2 + c_\sigma \eta_\sigma + a_\sigma \overset{!}{>} 0$. The latter can be written in the following way:

$$f_\sigma(\eta_\sigma) \equiv b_\sigma \left(\eta_\sigma + \frac{c_\sigma}{2b_\sigma}\right)^2 + \left(a_\sigma - \frac{c_\sigma^2}{4b_\sigma}\right). \tag{9.10}$$

Thus, additionally to the already stated condition $b_\sigma \overset{!}{>} 0$ we also need to ascertain that $a_\sigma - \frac{c_\sigma^2}{4b_\sigma} \overset{!}{>} 0$ in order for $f_\sigma(\eta_\sigma) \overset{!}{>} 0$ to be fulfilled. Consequently, we obtain

$$a_\sigma > \frac{c_\sigma^2}{4b_\sigma} \Rightarrow c_\sigma < 2\sqrt{a_\sigma b_\sigma} \tag{9.11}$$

or in other words

$$\frac{\lambda_1}{2} < 2\sqrt{\frac{(2\lambda_1 + \lambda_2)(\lambda_1 + \lambda_2)}{32}} = \frac{1}{2}\sqrt{\left(\lambda_1 + \frac{\lambda_2}{2}\right)(\lambda_1 + \lambda_2)} \Leftrightarrow \lambda_1 < \sqrt{\left(\lambda_1 + \frac{\lambda_2}{2}\right)(\lambda_1 + \lambda_2)}. \tag{9.12}$$

The square root on the right-hand side of inequality (9.12) is well defined due to the already stated conditions (9.7) and (9.8). For $\lambda_1 < 0$, only the condition (9.7), i.e., $\lambda_1 \overset{!}{>} -\lambda_2/2$ and $\lambda_2 > 0$ can be fulfilled. Consequently,

$$\frac{-\lambda_2}{2} < \lambda_1 < 0 \text{ and } \lambda_2 > 0. \tag{9.13}$$

For $\lambda_1 > 0$, the square of the inequality (9.12) yields

$$\lambda_1^2 < \lambda_1^2 + \frac{3}{2}\lambda_1\lambda_2 + \frac{\lambda_2^2}{2} \Leftrightarrow 0 < \lambda_2(3\lambda_1 + \lambda_2) \Leftrightarrow \begin{cases} \lambda_2 < 0 \wedge \lambda_1 < -\lambda_2/3 \\ \text{[contradiction to } \lambda_1 \overset{!}{>} -\lambda_2 \\ \text{from condition (9.8)]} \\ \lambda_2 > 0 \wedge \lambda_1 > -\lambda_2/3 \\ \text{(fulfilled per definition because } \lambda_1 > 0). \end{cases} \tag{9.14}$$

Combining both conditions (9.13) and (9.14) yields

$$\lambda_2 > 0 \text{ and } \lambda_1 > \frac{-\lambda_2}{2}. \tag{9.15}$$

The conditions (9.4) and (9.15) will be used in the following calculation of the decay widths in the scalar meson sector.

### 9.1.3 Scalar Isosinglet Masses

The Lagrangian (6.1) yields mixing between the $\sigma_N$ and $\sigma_S$ fields with the mixing term given by

$$\mathcal{L}_{\sigma_N\sigma_S} = -2\lambda_1\phi_N\phi_S\sigma_N\sigma_S. \tag{9.16}$$

The full $\sigma_N$-$\sigma_S$ interaction Lagrangian has the form

$$\mathcal{L}_{\sigma_N\sigma_S,\,\text{full}} = \frac{1}{2}(\partial_\mu\sigma_N)^2 + \frac{1}{2}(\partial_\mu\sigma_S)^2 - \frac{1}{2}m_{\sigma_N}^2{\sigma_N}^2 - \frac{1}{2}m_{\sigma_S}^2{\sigma_S}^2 + z_\sigma\sigma_N\sigma_S, \tag{9.17}$$

where $z_\sigma$ is the mixing term of the pure states $\sigma_N \equiv (\bar{u}u + \bar{d}d)/\sqrt{2}$ and $\sigma_S \equiv \bar{s}s$.
The mixing between the states $\sigma_N$ and $\sigma_S$ yields two fields, denoted henceforth as $\sigma_1$ and $\sigma_2$ [analogously to Eq. 7.10]:

$$\begin{pmatrix} \sigma_1 \\ \sigma_2 \end{pmatrix} = \begin{pmatrix} \cos\varphi_\sigma & \sin\varphi_\sigma \\ -\sin\varphi_\sigma & \cos\varphi_\sigma \end{pmatrix} \begin{pmatrix} \sigma_N \\ \sigma_S \end{pmatrix}. \tag{9.18}$$

At this point, it is not possible to assign the fields $\sigma_1$ and $\sigma_2$ (considered to be physical just as the resonances $\eta$ and $\eta'$ in Sec. 7.1). The reason is that the experimental data suggest a larger number of physical resonances in the scalar isosinglet channel than can be accommodated within the model (as discussed in Chapter 3). We will therefore calculate masses and decay widths of the resonances $\sigma_1$ and $\sigma_2$; the resonances will then be assigned to physical states depending on the results regarding the $\sigma_{1,2}$ masses and decay widths.
We can calculate the masses of the mixed sigma states, $m_{\sigma_1}$ and $m_{\sigma_2}$, and the $\sigma_N$-$\sigma_S$ mixing angle $\varphi_\sigma$ analogously to the calculations concerning $m_\eta$, $m_{\eta'}$ and $\varphi_\eta$ in Eqs. (7.20) - (7.23). We obtain

$$m_{\sigma_1}^2 = m_{\sigma_N}^2\cos^2\varphi_\sigma + m_{\sigma_S}^2\sin^2\varphi_\sigma - z_\sigma\sin(2\varphi_\sigma), \tag{9.19}$$

$$m_{\sigma_2}^2 = m_{\sigma_N}^2\sin^2\varphi_\sigma + m_{\sigma_S}^2\cos^2\varphi_\sigma + z_\sigma\sin(2\varphi_\sigma) \tag{9.20}$$

with $m_{\sigma_N}$ from Eq. (6.32), $m_{\sigma_S}$ from Eq. (6.36) and the mixing term

$$z_\sigma \overset{!}{=} (m_{\sigma_S}^2 - m_{\sigma_N}^2)\tan(2\varphi_\sigma)/2. \tag{9.21}$$

Consequently, from Eqs. (9.16) and (9.21) we obtain

$$(m_{\sigma_S}^2 - m_{\sigma_N}^2)\tan(2\varphi_\sigma) = -4\lambda_1\phi_N\phi_S \tag{9.22}$$

or, in other words,

$$\begin{aligned}\varphi_\sigma &= -\frac{1}{2}\arctan\left(\frac{4\lambda_1\phi_N\phi_S}{m_{\sigma_S}^2 - m_{\sigma_N}^2}\right) \\ &\overset{\text{Eqs. (6.32), (6.36)}}{=} \frac{1}{2}\arctan\left[\frac{8\lambda_1\phi_N\phi_S}{(4\lambda_1+3\lambda_2)\phi_N^2 - (4\lambda_1+6\lambda_2)\phi_S^2}\right],\end{aligned} \tag{9.23}$$

with $\lambda_1$ constrained via $m_0^2 + \lambda_1(\phi_N^2 + \phi_S^2) = -463425$ MeV$^2$.
Using the parameter combination $m_0^2 + \lambda_1(\phi_N^2 + \phi_S^2)$ allows us to remove $\lambda_1$ from the mixing term (9.16) as well as from the mass terms (6.32) and (6.36). The parameter $\lambda_1$ then fulfills the condition (9.15), as is evident from Fig. 9.1.

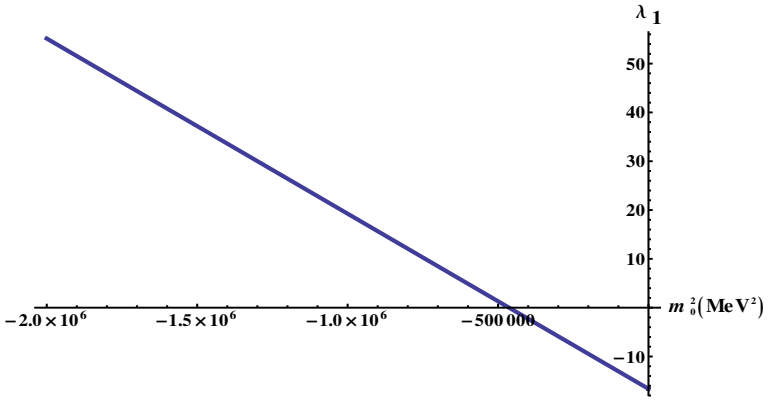


**Figure 9.1:** Dependence of parameter $\lambda_1$ on $m_0^2$ from Fit I. The condition (9.15), i.e., $\lambda_1 > -\lambda_2/2$, is apparently fulfilled for all values of $m_0^2 < 0$.

This leads to the dependence of $m_{\sigma_1}$ and $m_{\sigma_2}$, Eqs. (9.19) and (9.20), on $m_0^2$ only. The dependence is depicted in Fig. 9.2, with $m_0^2 \leq 0$ in accordance with Eq. (9.4).
We conclude immediately from Fig. 9.2 that the values of $m_{\sigma_1}$ and $m_{\sigma_2}$ vary over wide intervals, respectively, and that it is therefore not possible to assign the mixed states $\sigma_1$ and $\sigma_2$ to physical states using only the masses of the mixed states. Note also that, at $m_0^2 \simeq -2.413 \cdot 10^6$ MeV$^2$, $m_{\sigma_N}$ becomes larger than $m_{\sigma_S}$, $\varphi_\sigma = 45°$ (see Fig. 9.3) and thus $\sigma_1$ and $\sigma_2$ interchange places. Therefore, $m_0^2 = -2.413 \cdot 10^6$ MeV$^2$ represents the lower limit for $m_0^2$ and thus, together with Eq. (9.4), we obtain

$$-2.413 \cdot 10^6 \text{ MeV}^2 \leq m_0^2 \leq 0. \tag{9.24}$$

From the previous inequality we obtain the following boundaries for $m_{\sigma_{1,2}}$:

$$456 \text{ MeV} \leq m_{\sigma_1} \leq 1139 \text{ MeV}, \tag{9.25}$$

$$1187 \text{ MeV} \leq m_{\sigma_2} \leq 2268 \text{ MeV}. \tag{9.26}$$

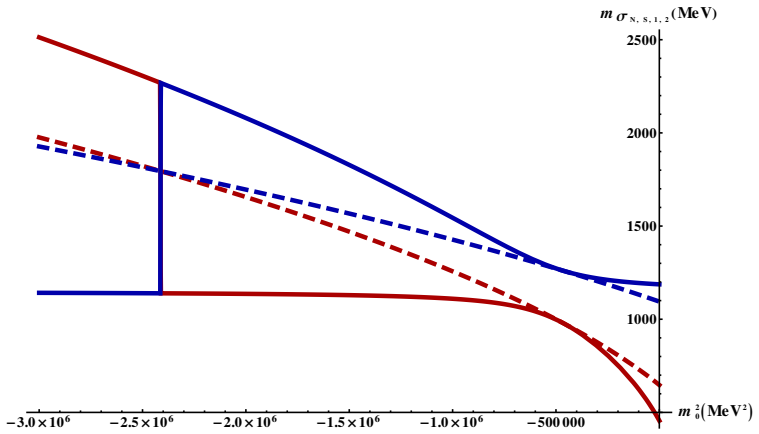


**Figure 9.2:** Dependence of $m_{\sigma_1}$ (full lower curve), $m_{\sigma_2}$ (full upper curve), $m_{\sigma_N}$ (dashed lower curve) and $m_{\sigma_S}$ (dashed upper curve) on $m_0^2$ under the condition $m_0^2 < 0$.

Considering the mass values, $\sigma_1$ may correspond either to $f_0(600)$ or $f_0(980)$ and $\sigma_2$ may correspond to $f_0(1370)$, $f_0(1500)$ or $f_0(1710)$. [We do not consider the as yet unconfirmed states $f_0(2020)$, $f_0(2100)$ and $f_0(2200)$ although they could also come within the $m_{\sigma_2}$ range. Note also our comments in Sec. 3.6 regarding the $f_0(1790)$ resonance that decays predominantly into pions and appears to be a radial excitation of $f_0(1370)$ – therefore it cannot correspond to our state $\sigma_2$ that is predominantly strange, as we will see in the following.] Therefore, a mere calculation of scalar masses does not allow us to assign the scalar states $\sigma_1$ and $\sigma_2$ to physical resonances. To resolve this ambiguity, we will calculate various decay widths of the states $\sigma_1$ and $\sigma_2$; comparison of the decay widths with experimental data [10] will allow for a definitive statement regarding the assignment of our theoretical states to the physical ones.

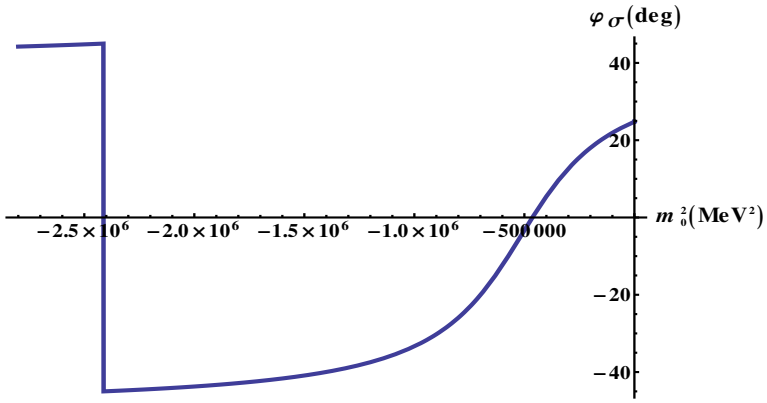


**Figure 9.3:** Dependence of the $\sigma_N$-$\sigma_S$ mixing angle $\varphi_\sigma$ on $m_0^2$, Eq. (9.23).

Nonetheless, from the variation of the $\sigma_N$ - $\sigma_S$ mixing angle $\varphi_\sigma$ we can conclude that the $\sigma_1$ field is predominantly non-strange and the $\sigma_2$ field is predominantly composed of strange quarks, see Fig. 9.4. Note that the two diagrams on Fig. 9.4 were obtained from two simultaneous, implicit plots of $\varphi_\sigma(\lambda_1)$, Eq. (9.23), and $m_{\sigma_{1,2}}[\varphi_\sigma(\lambda_1)]$, Eqs. (9.19) and (9.20), with $m_0^2 + \lambda_1(\phi_N^2 + \phi_S^2) = -463425$ MeV$^2$ and $m_0^2$ from inequality (9.24).

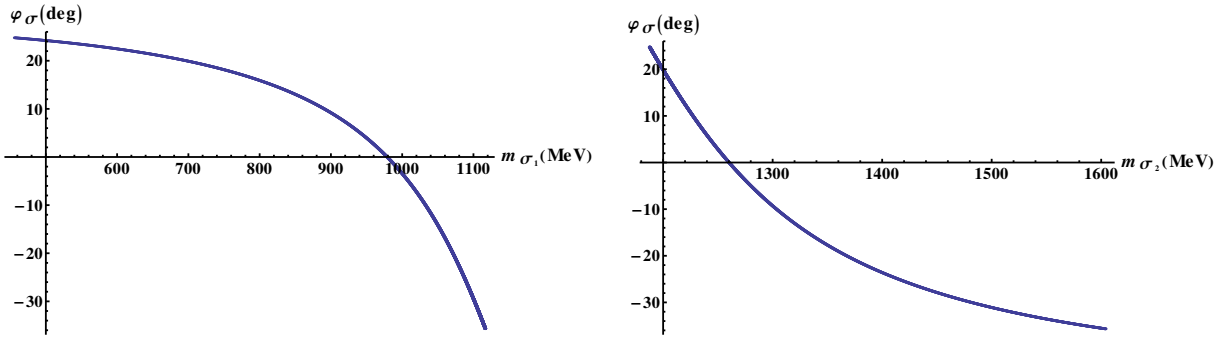


**Figure 9.4:** The $\sigma_N$-$\sigma_S$ mixing angle $\varphi_\sigma$ as function of $m_{\sigma_{1,2}}$.

We illustrate the contribution of $m_{\sigma_N}$ to $m_{\sigma_1}$ and of $m_{\sigma_S}$ to $m_{\sigma_2}$ in Fig. 9.5. The contributions expectedly decrease with $m_{\sigma_{1,2}}$ because the mixing angle approaches $-45$ (see Fig. 9.4) where $\sigma_1$ and $\sigma_2$ interchange places.

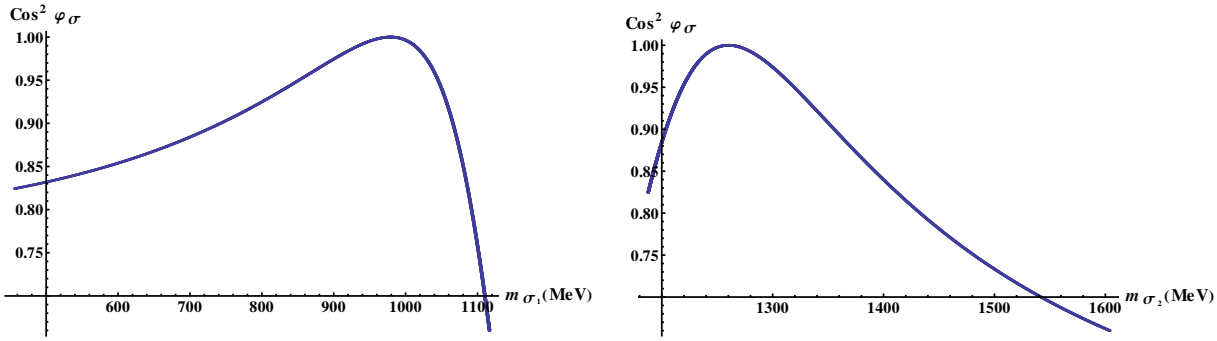


**Figure 9.5:** Contribution of the pure non-strange field $\sigma_N$ to $\sigma_1$ (left panel) and of the pure strange field $\sigma_S$ to $\sigma_2$ (right panel), respectively in dependence on $m_{\sigma_1}$ and $m_{\sigma_2}$.

### 9.1.4 Decay Width $\sigma_{1,2} \to \pi\pi$

The Lagrangian (6.1) contains the pure states $\sigma_N$ and $\sigma_S$; the interaction Lagrangian of these states with the pions reads:

$$\begin{aligned}\mathcal{L}_{\sigma\pi\pi} &= A_{\sigma_N\pi\pi}\sigma_N[(\pi^0)^2 + 2\pi^+\pi^-] + B_{\sigma_N\pi\pi}\sigma_N[(\partial_\mu\pi^0)^2 + 2\partial_\mu\pi^+\partial^\mu\pi^-] \\ &+ C_{\sigma_N\pi\pi}\sigma_N(\pi^0\Box\pi^0 + \pi^+\Box\pi^- + \pi^-\Box\pi^+) \\ &+ A_{\sigma_S\pi\pi}\sigma_S[(\pi^0)^2 + 2\pi^+\pi^-] + B_{\sigma_S\pi\pi}\sigma_S[(\partial_\mu\pi^0)^2 + 2\partial_\mu\pi^+\partial^\mu\pi^-] \qquad (9.27)\end{aligned}$$

with

$$A_{\sigma_N\pi\pi} = -\left(\lambda_1 + \frac{\lambda_2}{2}\right) Z_\pi^2 \phi_N, \tag{9.28}$$

$$B_{\sigma_N\pi\pi} = -2g_1 Z_\pi^2 w_{a_1} + \left(g_1^2 + \frac{h_1+h_2-h_3}{2}\right) Z_\pi^2 w_{a_1}^2 \phi_N, \tag{9.29}$$

$$C_{\sigma_N\pi\pi} = -g_1 Z_\pi^2 w_{a_1}, \tag{9.30}$$

$$A_{\sigma_S\pi\pi} = -\lambda_1 Z_\pi^2 \phi_S, \tag{9.31}$$

$$B_{\sigma_S\pi\pi} = \frac{h_1}{2} Z_\pi^2 w_{a_1}^2 \phi_S. \tag{9.32}$$

Note that the term $B_{\sigma_N\pi\pi}$, Eq. (9.29), can be further transformed as follows:

$$\begin{aligned} B_{\sigma_N\pi\pi} &\overset{\text{Eq. (6.28)}}{=} Z_\pi^2 \frac{g_1^2\phi_N}{m_{a_1}^2}\left(-2 + \frac{g_1^2\phi_N^2}{m_{a_1}^2} + \frac{h_1+h_2-h_3}{2}\frac{\phi_N^2}{m_{a_1}^2}\right) \\ &= Z_\pi^2 \frac{g_1^2\phi_N}{m_{a_1}^4}\left(-2m_{a_1}^2 + g_1^2\phi_N^2 + \frac{h_1+h_2-h_3}{2}\phi_N^2\right) \\ &\overset{\text{Eq. (6.41)}}{=} Z_\pi^2 \frac{g_1^2\phi_N}{m_{a_1}^4}\left(-2m_{a_1}^2 + m_{a_1}^2 - m_1^2 - \frac{h_1}{2}\phi_S^2 - 2\delta_N\right) \equiv -Z_\pi^2 \frac{g_1^2\phi_N}{m_{a_1}^4}\left(m_{a_1}^2 + m_1^2\right), \end{aligned} \tag{9.33}$$

as $h_1 = 0 = \delta_N$. Note also that the decay of the pure strange state $\sigma_S$ into pions is driven by the large-$N_c$ suppressed couplings $\lambda_1$ and $h_1$, see Eq. (4.52).

At this point it is necessary to disentangle the pure states $\sigma_N$ and $\sigma_S$ that do not represent asymptotic states in the $\sigma\pi\pi$ Lagrangian (9.27). To obtain decay widths of the physical, mixed states $\sigma_1$ and $\sigma_2$, we have to consider the full Lagrangian containing the $\sigma$ fields [$\mathcal{L}_{\sigma_N\sigma_S,\,\text{full}}$ from Eq. (9.17)]:

$$\begin{aligned} \mathcal{L}_{\sigma\pi\pi,\,\text{full}} &= \mathcal{L}_{\sigma_N\sigma_S,\,\text{full}} + \mathcal{L}_{\sigma\pi\pi} \\ &= \frac{1}{2}(\partial_\mu\sigma_N)^2 + \frac{1}{2}(\partial_\mu\sigma_S)^2 - \frac{1}{2}m_{\sigma_N}^2 - \frac{1}{2}m_{\sigma_S}^2 + z_\sigma\sigma_N\sigma_S \\ &+ A_{\sigma_N\pi\pi}\sigma_N[(\pi^0)^2 + 2\pi^+\pi^-] + B_{\sigma_N\pi\pi}\sigma_N[(\partial_\mu\pi^0)^2 + 2\partial_\mu\pi^+\partial^\mu\pi^-] \\ &+ C_{\sigma_N\pi\pi}\sigma_N(\pi^0\Box\pi^0 + \pi^+\Box\pi^- + \pi^-\Box\pi^+) \\ &+ A_{\sigma_S\pi\pi}\sigma_S[(\pi^0)^2 + 2\pi^+\pi^-] + B_{\sigma_S\pi\pi}\sigma_S[(\partial_\mu\pi^0)^2 + 2\partial_\mu\pi^+\partial^\mu\pi^-]. \end{aligned} \tag{9.34}$$

Let us now insert the inverted Eq. (9.18) into Eq. (9.34); analogously to Eq. (7.6) we obtain:

$$\begin{aligned} \mathcal{L}_{\sigma\pi\pi,\,\text{full}} &= \frac{1}{2}[(\partial_\mu\sigma_1)^2(\cos\varphi_\sigma)^2 + (\partial_\mu\sigma_2)^2(\sin\varphi_\sigma)^2] \\ &+ \frac{1}{2}[(\partial_\mu\sigma_1)^2(\sin\varphi_\sigma)^2 + (\partial_\mu\sigma_2)^2(\cos\varphi_\sigma)^2] \\ &- \frac{1}{2}m_{\sigma_N}^2[\sigma_1^2(\cos\varphi_\sigma)^2 + \sigma_2^2(\sin\varphi_\eta)^2 - \sin(2\varphi_\sigma)\sigma_1\sigma_2] \\ &- \frac{1}{2}m_{\sigma_S}^2[\sigma_1^2(\sin\varphi_\sigma)^2 + \sigma_2^2(\cos\varphi_\sigma)^2 + \sin(2\varphi_\sigma)\sigma_1\sigma_2] \\ &+ z_\sigma[(\sigma_1^2 - \sigma_2^2)\sin\varphi_\sigma\cos\varphi_\sigma + \cos(2\varphi_\sigma)\sigma_1\sigma_2] \\ &+ (A_{\sigma_N\pi\pi}\cos\varphi_\sigma + A_{\sigma_S\pi\pi}\sin\varphi_\sigma)\sigma_1[(\pi^0)^2 + 2\pi^+\pi^-] \end{aligned}$$

$$
\begin{aligned}
&+ (B_{\sigma_N\pi\pi}\cos\varphi_\sigma + B_{\sigma_S\pi\pi}\sin\varphi_\sigma)\sigma_1[(\partial_\mu\pi^0)^2 + 2\partial_\mu\pi^+\partial^\mu\pi^-] \\
&+ C_{\sigma_N\pi\pi}\cos\varphi_\sigma\sigma_1(\pi^0\Box\pi^0 + \pi^+\Box\pi^- + \pi^-\Box\pi^+) \\
&+ (A_{\sigma_S\pi\pi}\cos\varphi_\sigma - A_{\sigma_N\pi\pi}\sin\varphi_\sigma)\sigma_2[(\pi^0)^2 + 2\pi^+\pi^-] \\
&+ (B_{\sigma_S\pi\pi}\cos\varphi_\sigma - B_{\sigma_N\pi\pi}\sin\varphi_\sigma)\sigma_2[(\partial_\mu\pi^0)^2 + 2\partial_\mu\pi^+\partial^\mu\pi^-] \\
&- C_{\sigma_N\pi\pi}\sin\varphi_\sigma\sigma_2(\pi^0\Box\pi^0 + \pi^+\Box\pi^- + \pi^-\Box\pi^+) \\
&= \frac{1}{2}(\partial_\mu\sigma_1)^2 + \frac{1}{2}(\partial_\mu\sigma_2)^2 - \frac{1}{2}[m^2_{\sigma_N}(\cos\varphi_\sigma)^2 + m^2_{\sigma_S}(\sin\varphi_\sigma)^2 - z_\sigma\sin(2\varphi_\sigma)]\sigma_1^2 \\
&- \frac{1}{2}[m^2_{\sigma_N}(\sin\varphi_\sigma)^2 + m^2_{\sigma_S}(\cos\varphi_\sigma)^2 + z_\sigma\sin(2\varphi_\sigma)]\sigma_2^2 \\
&- \frac{1}{2}[(m^2_{\sigma_S} - m^2_{\sigma_N})\sin(2\varphi_\sigma) - 2z_\sigma\cos(2\varphi_\sigma)]\sigma_1\sigma_2 \\
&+ (A_{\sigma_N\pi\pi}\cos\varphi_\sigma + A_{\sigma_S\pi\pi}\sin\varphi_\sigma)\sigma_1[(\pi^0)^2 + 2\pi^+\pi^-] \\
&+ (B_{\sigma_N\pi\pi}\cos\varphi_\sigma + B_{\sigma_S\pi\pi}\sin\varphi_\sigma)\sigma_1[(\partial_\mu\pi^0)^2 + 2\partial_\mu\pi^+\partial^\mu\pi^-] \\
&+ C_{\sigma_N\pi\pi}\cos\varphi_\sigma\sigma_1(\pi^0\Box\pi^0 + \pi^+\Box\pi^- + \pi^-\Box\pi^+) \\
&+ (A_{\sigma_S\pi\pi}\cos\varphi_\sigma - A_{\sigma_N\pi\pi}\sin\varphi_\sigma)\sigma_2[(\pi^0)^2 + 2\pi^+\pi^-] \\
&+ (B_{\sigma_S\pi\pi}\cos\varphi_\sigma - B_{\sigma_N\pi\pi}\sin\varphi_\sigma)\sigma_2[(\partial_\mu\pi^0)^2 + 2\partial_\mu\pi^+\partial^\mu\pi^-] \\
&- C_{\sigma_N\pi\pi}\sin\varphi_\sigma\sigma_2(\pi^0\Box\pi^0 + \pi^+\Box\pi^- + \pi^-\Box\pi^+). \qquad (9.35)
\end{aligned}
$$

From Eq. (9.35) we then retrieve the already known Eqs. (9.19) and (9.20) for $m^2_{\sigma_{1,2}}$ as well as the condition (9.21) for $z_\sigma$ ascertaining that there is no mixing between the physical states $\sigma_1$ and $\sigma_2$. Let us now write the Lagrangian (9.35) in the following form:

$$
\begin{aligned}
\mathcal{L}_{\sigma\pi\pi,\,\text{full}} &= \frac{1}{2}(\partial_\mu\sigma_1)^2 - \frac{1}{2}m^2_{\sigma_1}\sigma_1^2 \\
&+ (A_{\sigma_N\pi\pi}\cos\varphi_\sigma + A_{\sigma_S\pi\pi}\sin\varphi_\sigma)\sigma_1[(\pi^0)^2 + 2\pi^+\pi^-] \\
&+ (B_{\sigma_N\pi\pi}\cos\varphi_\sigma + B_{\sigma_S\pi\pi}\sin\varphi_\sigma)\sigma_1[(\partial_\mu\pi^0)^2 + 2\partial_\mu\pi^+\partial^\mu\pi^-] \\
&+ C_{\sigma_N\pi\pi}\cos\varphi_\sigma\sigma_1(\pi^0\Box\pi^0 + \pi^+\Box\pi^- + \pi^-\Box\pi^+) \\
&+ \frac{1}{2}(\partial_\mu\sigma_2)^2 - \frac{1}{2}m^2_{\sigma_2}\sigma_2^2 \\
&+ (A_{\sigma_S\pi\pi}\cos\varphi_\sigma - A_{\sigma_N\pi\pi}\sin\varphi_\sigma)\sigma_2[(\pi^0)^2 + 2\pi^+\pi^-] \\
&+ (B_{\sigma_S\pi\pi}\cos\varphi_\sigma - B_{\sigma_N\pi\pi}\sin\varphi_\sigma)\sigma_2[(\partial_\mu\pi^0)^2 + 2\partial_\mu\pi^+\partial^\mu\pi^-] \\
&- C_{\sigma_N\pi\pi}\sin\varphi_\sigma\sigma_2(\pi^0\Box\pi^0 + \pi^+\Box\pi^- + \pi^-\Box\pi^+). \qquad (9.36)
\end{aligned}
$$

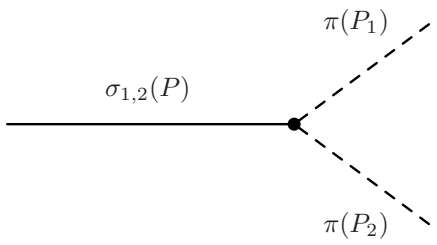


**Figure 9.6:** Decay process $\sigma_{1,2} \to \pi\pi$.

The decay amplitudes of the mixed states read

$$
\begin{aligned}
-i\mathcal{M}_{\sigma_1\to\pi\pi}(m_{\sigma_1}) = i\Bigg\{&\cos\varphi_\sigma\left[A_{\sigma_N\pi\pi} - B_{\sigma_N\pi\pi}\frac{m_{\sigma_1}^2-2m_\pi^2}{2} - C_{\sigma_N\pi\pi}m_\pi^2\right]\\
&+\sin\varphi_\sigma\left[A_{\sigma_S\pi\pi} - B_{\sigma_S\pi\pi}\frac{m_{\sigma_1}^2-2m_\pi^2}{2}\right]\Bigg\}\\
= i\Bigg\{&\cos\varphi_\sigma\left[A_{\sigma_N\pi\pi} - \frac{B_{\sigma_N\pi\pi}}{2}m_{\sigma_1}^2 + (B_{\sigma_N\pi\pi}-C_{\sigma_N\pi\pi})m_\pi^2\right]\\
&+\sin\varphi_\sigma\left[A_{\sigma_S\pi\pi} - B_{\sigma_S\pi\pi}\frac{m_{\sigma_1}^2-2m_\pi^2}{2}\right]\Bigg\}
\end{aligned}
\tag{9.37}
$$

and

$$
\begin{aligned}
-i\mathcal{M}_{\sigma_2\to\pi\pi}(m_{\sigma_2}) = i\Bigg\{&\cos\varphi_\sigma\left[A_{\sigma_S\pi\pi} - B_{\sigma_S\pi\pi}\frac{m_{\sigma_2}^2-2m_\pi^2}{2}\right]\\
&-\sin\varphi_\sigma\left[A_{\sigma_N\pi\pi} - \frac{B_{\sigma_N\pi\pi}}{2}m_{\sigma_2}^2 + (B_{\sigma_N\pi\pi}-C_{\sigma_N\pi\pi})m_\pi^2\right]\Bigg\}.
\end{aligned}
\tag{9.38}
$$

Summing over all decay channels $\sigma_{1,2}\to\pi^0\pi^0,\pi^\pm\pi^\mp$ we obtain the following formulas for the decay widths $\Gamma_{\sigma_{1,2}\to\pi\pi}$:

$$\Gamma_{\sigma_1\to\pi\pi} = \frac{3k(m_{\sigma_1},m_\pi,m_\pi)}{4\pi m_{\sigma_1}^2}|-i\mathcal{M}_{\sigma_1\to\pi\pi}(m_{\sigma_1})|^2, \tag{9.39}$$

$$\Gamma_{\sigma_2\to\pi\pi} = \frac{3k(m_{\sigma_2},m_\pi,m_\pi)}{4\pi m_{\sigma_2}^2}|-i\mathcal{M}_{\sigma_2\to\pi\pi}(m_{\sigma_2})|^2. \tag{9.40}$$

We have considered an isospin factor of 6 in the above Eqs. (9.39) and (9.40). The Lagrangian (9.36) provides us with an additional factor of $2^2=4$ in $\Gamma_{\sigma_{1,2}\to\pi\pi}$ respectively from the charged ($\pi^\pm\pi^\mp$) and neutral ($\pi^0\pi^0$) modes, i.e., in total with a factor of 8. However, there is a symmetrisation factor of $1/\sqrt{2}$ that also has to be considered for the neutral modes; therefore, their contribution to $\Gamma_{\sigma_{1,2}\to\pi\pi}$ is actually not $2^2$ but rather $(2/\sqrt{2})^2=2$ that together with the charged-mode contribution $2^2=4$ yields a total isospin factor of 6.

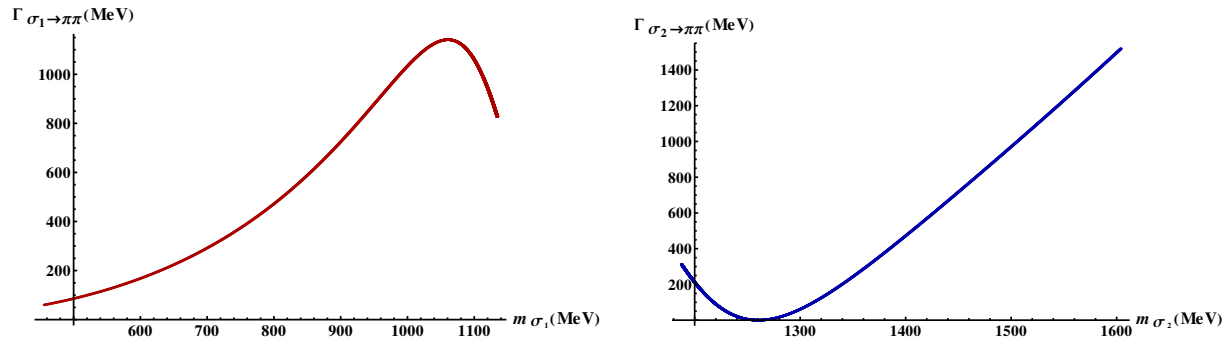


**Figure 9.7:** $\Gamma_{\sigma_1\to\pi\pi}$ and $\Gamma_{\sigma_2\to\pi\pi}$ as functions of $m_{\sigma_1}$ and $m_{\sigma_2}$, respectively.

A plot of the two decay widths is presented in Fig. 9.7. We conclude from the left panel of Fig. 9.7 that our state $\sigma_1$ possesses the best correspondence with the $f_0(600)$ resonance. For example, setting $m_{\sigma_1} = 800$ MeV yields $\Gamma_{\sigma_1\to\pi\pi} = 473.5$ MeV. From the right panel of Fig. 9.7 we note that $\Gamma_{\sigma_2\to\pi\pi}$ increases very rapidly with $m_{\sigma_2}$ and therefore the best values are obtained for $m_{\sigma_2} \simeq 1300$ MeV. If we consider data from Ref. [40], then our results are fairly close to the results from this review: Ref. [40] cites the value of 325 MeV at $m_{f_0(1370)} = (1309 \pm 1 \pm 15)$ MeV from an $f_0(1370)$ Breit-Wigner fit and we obtain $\Gamma_{\sigma_2\to\pi\pi} = 325$ MeV at $m_{\sigma_2} = 1368$ MeV; Ref. [40] cites the value of 207 MeV for the full width at one-half maximum (FWHM) with the peak in the decay channel $f_0(1370) \to \pi\pi$ at $m_{f_0(1370)} = 1282$ MeV – we obtain $\Gamma_{\sigma_2\to\pi\pi} = 207$ MeV at $m_{\sigma_2} = 1341$ MeV and at $m_{\sigma_2} = 1200$ MeV. Let us, however, emphasise that these results suggest $f_0(1370)$ to be predominantly a $\bar{s}s$ state as we can see from Fig. 9.5. Concretely, results suggest that $f_0(1370)$ is 88% a $\bar{s}s$ state at $m_{\sigma_2} = 1368$ MeV, 92% a $\bar{s}s$ state at $m_{\sigma_2} = 1341$ MeV and 89% a $\bar{s}s$ state at $m_{\sigma_2} = 1200$ MeV. Note that we do not assign error values to our masses because the errors in our model are determined by errors of experimental data used for our calculations and no errors were assigned to $\Gamma_{f_0(1370)\to\pi\pi}$ in Ref. [40].

As evident from Fig. 9.7, $\Gamma_{\sigma_2\to\pi\pi} = 0$ for $m_{\sigma_2} = 1260$ MeV, corresponding to $m_0^2 = -463425$ MeV$^2$ and thus $m_{\sigma_1} = 978$ MeV (see Fig. 9.2). The reason is that, due to the constraint $m_0^2 + \lambda_1(\phi_N^2 + \phi_S^2) = -463425$ MeV$^2$ (see Table 8.4), we obtain $\lambda_1 = 0$ for $m_0^2 = -463425$ MeV$^2$; consequently, according to Eq. (9.23), one also obtains that the $\sigma_N$ - $\sigma_S$ mixing angle $\varphi_\sigma = 0$. Thus $\sigma_N$ and $\sigma_S$ decouple at this point. Usually, this would merely imply that the $2\pi$ decay amplitude $\mathcal{M}_{\sigma_2\to\pi\pi}(m_{\sigma_2})$, Eq. (9.38), of the (now pure-strange) state $\sigma_2 \equiv \sigma_S$ would become suppressed but it would not necessarily vanish. It could still be non-zero by large-$N_c$ suppressed parameters, in our case $\lambda_1$ and $h_1$ that appear in $A_{\sigma_S\pi\pi}$ and $B_{\sigma_S\pi\pi}$ [Eqs. (9.31) and (9.32), respectively]. However, we have set $h_1 \equiv 0$ throughout our calculations (see Table 8.4) and, as we have just discussed, $\lambda_1$ also vanishes at this point. For this reason, $A_{\sigma_S\pi\pi} = 0 = B_{\sigma_S\pi\pi}$ and consequently also $\mathcal{M}_{\sigma_2\to\pi\pi} = 0$. Therefore, $\Gamma_{\sigma_2\to\pi\pi} = 0$. Note that setting $h_1 \neq 0$ would not alter the fact that $\Gamma_{\sigma_2\to\pi\pi}$ vanishes for a certain value of $m_{\sigma_2}$. The reason is the relative minus sign of the two terms in $\mathcal{M}_{\sigma_2\to\pi\pi}$ [see Eq. (9.38)], allowing for a value of $\varphi_\sigma$ to be found where they exactly cancel out.

### 9.1.5 Decay Width $\sigma_{1,2} \to KK$

The interaction Lagrangian of the pure states $\sigma_N$ and $\sigma_S$ with the kaons, Eq. (6.1), reads:

$$
\begin{aligned}
\mathcal{L}_{\sigma KK} &= A_{\sigma_N KK}\sigma_N(K^0\bar{K}^0 + K^-K^+) + B_{\sigma_N KK}\sigma_N(\partial_\mu K^0\partial^\mu\bar{K}^0 + \partial_\mu K^-\partial^\mu K^+) \\
&+ C_{\sigma_N KK}\partial_\mu\sigma_N(K^0\partial^\mu\bar{K}^0 + \bar{K}^0\partial^\mu K^0 + K^-\partial^\mu K^+ + K^+\partial^\mu K^-) \\
&+ A_{\sigma_S KK}\sigma_S(K^0\bar{K}^0 + K^-K^+) + B_{\sigma_S KK}\sigma_S(\partial_\mu K^0\partial^\mu\bar{K}^0 + \partial_\mu K^-\partial^\mu K^+) \\
&+ C_{\sigma_S KK}\partial_\mu\sigma_S(K^0\partial^\mu\bar{K}^0 + \bar{K}^0\partial^\mu K^0 + K^-\partial^\mu K^+ + K^+\partial^\mu K^-) \\
&= A_{\sigma_N KK}\sigma_N(K^0\bar{K}^0 + K^-K^+) + (B_{\sigma_N KK} - 2C_{\sigma_N KK})\sigma_N(\partial_\mu K^0\partial^\mu\bar{K}^0 + \partial_\mu K^-\partial^\mu K^+) \\
&- C_{\sigma_N KK}\sigma_N(K^0\Box\bar{K}^0 + \bar{K}^0\Box K^0 + K^-\Box K^+ + K^+\Box K^-) \\
&+ A_{\sigma_S KK}\sigma_S(K^0\bar{K}^0 + K^-K^+) + (B_{\sigma_S KK} - 2C_{\sigma_S KK})\sigma_S(\partial_\mu K^0\partial^\mu\bar{K}^0 + \partial_\mu K^-\partial^\mu K^+) \\
&- C_{\sigma_S KK}\sigma_S(K^0\Box\bar{K}^0 + \bar{K}^0\Box K^0 + K^-\Box K^+ + K^+\Box K^-) \qquad (9.41)
\end{aligned}
$$

with

$$A_{\sigma_N KK} = \frac{Z_K^2}{\sqrt{2}}[\lambda_2(\phi_S - \sqrt{2}\phi_N) - 2\sqrt{2}\lambda_1\phi_N], \tag{9.42}$$

$$B_{\sigma_N KK} = \frac{g_1}{2}Z_K^2 w_{K_1}[-2 + g_1 w_{K_1}(\phi_N + \sqrt{2}\phi_S)] + \frac{Z_K^2}{2}w_{K_1}^2[(2h_1 + h_2)\phi_N - \sqrt{2}h_3\phi_S], \tag{9.43}$$

$$C_{\sigma_N KK} = \frac{g_1}{2}Z_K^2 w_{K_1}, \tag{9.44}$$

$$A_{\sigma_S KK} = \frac{Z_K^2}{\sqrt{2}}[\lambda_2(\phi_N - 2\sqrt{2}\phi_S) - 2\sqrt{2}\lambda_1\phi_S], \tag{9.45}$$

$$B_{\sigma_S KK} = \frac{\sqrt{2}}{2}Z_K^2 g_1 w_{K_1}[-2 + g_1 w_{K_1}(\phi_N + \sqrt{2}\phi_S)] + \frac{Z_K^2}{\sqrt{2}}w_{K_1}^2[\sqrt{2}(h_1 + h_2)\phi_S - h_3\phi_N], \tag{9.46}$$

$$C_{\sigma_S KK} = \frac{\sqrt{2}}{2}Z_K^2 g_1 w_{K_1} \equiv \sqrt{2}C_{\sigma_N KK}. \tag{9.47}$$

Let us consider only the $\sigma_{1,2} \to K^0\bar{K}^0$ decay channel ($\sigma_{1,2} \to K^+K^-$ will give the same contribution to the full decay width due to the isospin symmetry). As in Eq. (9.34) we obtain from Eqs. (9.17) and (9.41)

$$\begin{aligned}
\mathcal{L}_{\sigma KK,\,\text{full}} &= \mathcal{L}_{\sigma_N\sigma_S,\,\text{full}} + \mathcal{L}_{\sigma KK} \\
&= \frac{1}{2}(\partial_\mu\sigma_N)^2 + \frac{1}{2}(\partial_\mu\sigma_S)^2 - \frac{1}{2}m_{\sigma_N}^2 - \frac{1}{2}m_{\sigma_S}^2 + z_\sigma\sigma_N\sigma_S \\
&+ A_{\sigma_N KK}\sigma_N K^0\bar{K}^0 + (B_{\sigma_N KK} - 2C_{\sigma_N KK})\sigma_N\partial_\mu K^0\partial^\mu\bar{K}^0 \\
&- C_{\sigma_N KK}\sigma_N(K^0\Box\bar{K}^0 + \bar{K}^0\Box K^0) \\
&+ A_{\sigma_S KK}\sigma_S K^0\bar{K}^0 + (B_{\sigma_S KK} - 2C_{\sigma_S KK})\sigma_S\partial_\mu K^0\partial^\mu\bar{K}^0 \\
&- C_{\sigma_S KK}\sigma_S(K^0\Box\bar{K}^0 + \bar{K}^0\Box K^0).
\end{aligned} \tag{9.48}$$

Inserting the inverted Eq. (9.18) into Eq. (9.48), identifying $m_{\sigma_{1,2}}^2$ from Eqs. (9.19) and (9.20) and $z_\sigma$ from Eq. (9.21) and rearranging parameters as in Eq. (9.35) leads to

$$\begin{aligned}
\mathcal{L}_{\sigma KK,\,\text{full}} &= \frac{1}{2}(\partial_\mu\sigma_1)^2 - \frac{1}{2}m_{\sigma_1}^2\sigma_1^2 \\
&+ (A_{\sigma_N KK}\cos\varphi_\sigma + A_{\sigma_S KK}\sin\varphi_\sigma)\sigma_1 K^0\bar{K}^0 \\
&+ [(B_{\sigma_N KK} - 2C_{\sigma_N KK})\cos\varphi_\sigma + (B_{\sigma_S KK} - 2C_{\sigma_S KK})\sin\varphi_\sigma]\sigma_1\partial_\mu K^0\partial^\mu\bar{K}^0 \\
&- (C_{\sigma_N KK}\cos\varphi_\sigma + C_{\sigma_S KK}\sin\varphi_\sigma)\sigma_1(K^0\Box\bar{K}^0 + \bar{K}^0\Box K^0) \\
&+ \frac{1}{2}(\partial_\mu\sigma_2)^2 - \frac{1}{2}m_{\sigma_2}^2\sigma_2^2 \\
&+ (A_{\sigma_S KK}\cos\varphi_\sigma - A_{\sigma_N KK}\sin\varphi_\sigma)\sigma_2 K^0\bar{K}^0 \\
&+ [(B_{\sigma_S KK} - 2C_{\sigma_S KK})\cos\varphi_\sigma - (B_{\sigma_N KK} - 2C_{\sigma_N KK})\sin\varphi_\sigma]\sigma_2\partial_\mu K^0\partial^\mu\bar{K}^0 \\
&- (C_{\sigma_S KK}\cos\varphi_\sigma - C_{\sigma_N KK}\sin\varphi_\sigma)\sigma_2(K^0\Box\bar{K}^0 + \bar{K}^0\Box K^0).
\end{aligned} \tag{9.49}$$

Let us denote the momenta of the two kaons as $P_1$ and $P_2$. Energy conservation on the vertex implies $P = P_1 + P_2$, where $P$ denotes the momentum of $\sigma_1$ or $\sigma_2$; given that our particles are on-shell, we obtain

$$P_1 \cdot P_2 = \frac{P^2 - P_1^2 - P_2^2}{2} \equiv \frac{m_{\sigma_1}^2 - 2m_K^2}{2}. \tag{9.50}$$

Then the decay amplitudes of the mixed states $\sigma_{1,2}$ read

$$\begin{aligned}
-i\mathcal{M}_{\sigma_1 \to K^0 \bar{K}^0}(m_{\sigma_1}) &= i \left\{ \cos\varphi_\sigma \left[ A_{\sigma_N KK} - (B_{\sigma_N KK} - 2C_{\sigma_N KK}) P_1 \cdot P_2 + 2C_{\sigma_N KK} m_K^2 \right] \right. \\
&\left. + \sin\varphi_\sigma \left[ A_{\sigma_S KK} - (B_{\sigma_S KK} - 2C_{\sigma_S KK}) \frac{m_{\sigma_1}^2 - 2m_K^2}{2} + 2C_{\sigma_S KK} m_K^2 \right] \right\} \\
&= i \left\{ \cos\varphi_\sigma \left[ A_{\sigma_N KK} - (B_{\sigma_N KK} - 2C_{\sigma_N KK}) \frac{m_{\sigma_1}^2 - 2m_K^2}{2} + 2C_{\sigma_N KK} m_K^2 \right] \right. \\
&\left. + \sin\varphi_\sigma \left[ A_{\sigma_S KK} - (B_{\sigma_S KK} - 2C_{\sigma_S KK}) \frac{m_{\sigma_1}^2 - 2m_K^2}{2} + 2C_{\sigma_S KK} m_K^2 \right] \right\}
\end{aligned} \tag{9.51}$$

and

$$\begin{aligned}
-i\mathcal{M}_{\sigma_2 \to K^0 \bar{K}^0}(m_{\sigma_2}) &= i \left\{ \cos\varphi_\sigma \left[ A_{\sigma_S KK} - (B_{\sigma_S KK} - 2C_{\sigma_S KK}) \frac{m_{\sigma_2}^2 - 2m_K^2}{2} + 2C_{\sigma_S KK} m_K^2 \right] \right. \\
&\left. - \sin\varphi_\sigma \left[ A_{\sigma_N KK} - (B_{\sigma_N KK} - 2C_{\sigma_N KK}) \frac{m_{\sigma_2}^2 - 2m_K^2}{2} + 2C_{\sigma_N KK} m_K^2 \right] \right\}.
\end{aligned} \tag{9.52}$$

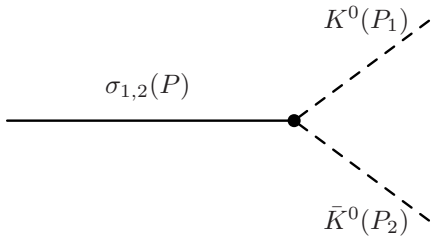


**Figure 9.8:** Decay process $\sigma_{1,2} \to K^0 \bar{K}^0$.

Finally, taking into account all contributions to the decay widths of the mixed states $\sigma_{1,2}$, i.e., $\sigma_{1,2} \to K^0 \bar{K}^0 + K^- K^+$, we obtain

$$\Gamma_{\sigma_1 \to KK} = \frac{k(m_{\sigma_1}, m_K, m_K)}{4\pi m_{\sigma_1}^2} | - i\mathcal{M}_{\sigma_1 \to K^0 \bar{K}^0}(m_{\sigma_1})|^2, \tag{9.53}$$

$$\Gamma_{\sigma_2 \to KK} = \frac{k(m_{\sigma_2}, m_K, m_K)}{4\pi m_{\sigma_2}^2} | - i\mathcal{M}_{\sigma_2 \to K^0 \bar{K}^0}(m_{\sigma_2})|^2. \tag{9.54}$$

The decay widths are depicted in Fig. 9.9. The kaon-kaon threshold opens at 981.7 MeV, see Table 8.5. Therefore, the decay $\sigma_1 \to KK$ is phase-space suppressed. Nonetheless, these results

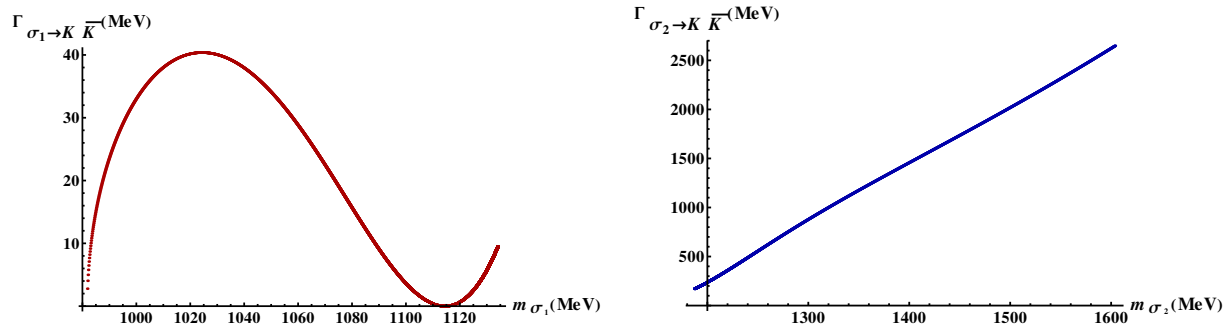


**Figure 9.9:** $\Gamma_{\sigma_1 \to KK}$ and $\Gamma_{\sigma_2 \to KK}$ as functions of $m_{\sigma_1}$ and $m_{\sigma_2}$, respectively.

suggest that $\sigma_1 \equiv f_0(600)$ also decays into kaons above the threshold, which is in principle possible but has not been observed [10]. The results regarding $\sigma_1$ are actually more consistent with the decay $f_0(980) \to KK$ but an interpretation of $\sigma_1$ as $f_0(980)$ is not possible due to the results in the two-pion channel, see previous subsection 9.1.4 and Fig. 9.7. We can therefore conclude that a proper determination of $\Gamma_{\sigma_1 \to KK}$ is not possible if one only considers $\sigma_1$ – we have to consider results regarding $\sigma_2 \to KK$ as well.

The decay width $\Gamma_{\sigma_2 \to KK}$ rises rapidly with $m_{\sigma_2}$. The lowest value is $\Gamma_{\sigma_2 \to KK} = 171$ MeV at $m_{\sigma_2} = 1187$ MeV, a value consistent with experiment [124, 170, 253, 259, 260, 261]. Our analysis of the $\sigma_2 \to \pi\pi$ decay yielded three values of the $m_{\sigma_2}$ where the correspondence with the decay width $f_0(1370) \to \pi\pi$ was particularly good: $m_{\sigma_2} = 1200$ MeV, $m_{\sigma_2} = 1341$ MeV and $m_{\sigma_2} = 1368$ MeV. In the $\sigma_2 \to KK$ channel we obtain $\Gamma_{\sigma_2 \to KK} = 240$ MeV for $m_{\sigma_2} = 1200$ MeV, $\Gamma_{\sigma_2 \to KK} = 1125$ MeV for $m_{\sigma_2} = 1341$ MeV and $\Gamma_{\sigma_2 \to KK} = 1281$ MeV for $m_{\sigma_2} = 1368$ MeV. (The width rises to $\Gamma_{\sigma_2 \to KK} = 2021$ MeV for $m_{\sigma_2} = 1500$ MeV.) Thus, there is some discrepancy between the results in the $\sigma_2 \to \pi\pi$ and $\sigma_2 \to KK$ channels, unless one works with

$$m_{\sigma_2} = 1200 \text{ MeV}. \tag{9.55}$$

The latter mass implies $m_0^2 = -160233$ MeV from Eq. (9.20) leading to

$$m_{\sigma_1} = 705 \text{ MeV} \tag{9.56}$$

via Eq. (9.19). Consequently, $\Gamma_{\sigma_1 \equiv f_0(600) \to KK} = 0$ as $m_{\sigma_1}$ is below the kaon-kaon decay threshold, a result in accordance with experimental data and also consistent with the assignment $\sigma_1 \equiv f_0(600)$. Note that $m_{\sigma_1} = 705$ MeV also yields $\Gamma_{\sigma_1 \to \pi\pi} = 305$ MeV via Eq. (9.39).

We can also look into results regarding the ratio $\Gamma_{\sigma_2 \to KK}/\Gamma_{\sigma_2 \to \pi\pi}$, see Fig. 9.10. Experimental data about this ratio are by far inconclusive [99, 140, 188, 262]; we observe $\Gamma_{\sigma_2 \to KK}/\Gamma_{\sigma_2 \to \pi\pi} = 1.15$ at $m_{\sigma_2} = 1200$ MeV, larger than any set of experimental data reported so far. The reason is the relatively large decay width $\sigma_2 \to KK$; in fact, we observe from Fig. 9.10 that $\Gamma_{\sigma_2 \to \pi\pi} < \Gamma_{\sigma_2 \to KK}$ at all values of $m_{\sigma_2}$ except for the lowest ones ($\lesssim 1200$ MeV). This would imply that $f_0(1370)$ decays predominantly into kaons, as one would expect from a $\bar{s}s$ state, but it is clearly at odds with the data [10].

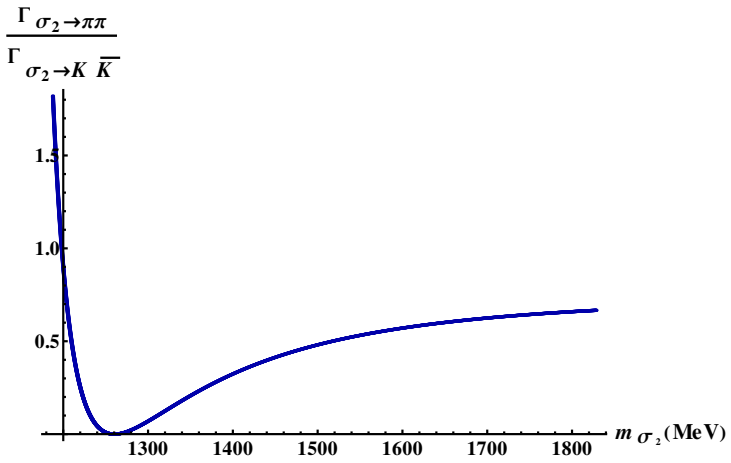


**Figure 9.10:** Ratio $\Gamma_{\sigma_2\to\pi\pi}/\Gamma_{\sigma_2\to KK}$ as function of $m_{\sigma_2}$.

### 9.1.6 Decay Width $\sigma_{1,2} \to \eta\eta$

The Lagrangian (6.1) contains only the pure fields $\sigma_{N,S}$ and $\eta_{N,S}$; the corresponding interaction Lagrangian reads:

$$\begin{aligned}
\mathcal{L}_{\sigma\eta_N\eta_S} = & -Z_\pi^2\phi_N\left(\lambda_1+\frac{\lambda_2}{2}+c_1\phi_S^2\right)\sigma_N\eta_N^2 - Z_{\eta_S}^2\phi_N\left(\lambda_1+\frac{c_1}{2}\phi_N^2\right)\sigma_N\eta_S^2 \\
& -\frac{3}{2}c_1 Z_\pi Z_{\eta_S}\phi_N^2\phi_S\sigma_N\eta_N\eta_S \\
& + Z_\pi^2 w_{a_1}\left[g_1(g_1 w_{a_1}\phi_N - 1) + \frac{\phi_N}{2}w_{a_1}(h_1+h_2-h_3)\right]\sigma_N(\partial_\mu\eta_N)^2 \\
& + \frac{h_1}{2}Z_{\eta_S}^2 w_{f_{1S}}^2\phi_N\sigma_N(\partial_\mu\eta_S)^2 + g_1 w_{a_1} Z_\pi^2\partial_\mu\sigma_N\partial^\mu\eta_N\eta_N \\
& -(\lambda_1+\lambda_2)Z_{\eta_S}^2\phi_S\sigma_S\eta_S^2 - Z_\pi^2\phi_S(\lambda_1+c_1\phi_N^2)\sigma_S\eta_N^2 - \frac{1}{2}c_1 Z_\pi Z_{\eta_S}\phi_N^3\sigma_S\eta_N\eta_S \\
& + Z_{\eta_S}^2 w_{f_{1S}}\left[\sqrt{2}g_1(\sqrt{2}g_1 w_{f_{1S}}\phi_S - 1) + w_{f_{1S}}\phi_S\left(\frac{h_1}{2}+h_2-h_3\right)\right]\sigma_S(\partial_\mu\eta_S)^2 \\
& + \frac{h_1}{2}Z_\pi^2 w_{a_1}^2\phi_S\sigma_S(\partial_\mu\eta_N)^2 + \sqrt{2}g_1 Z_{\eta_S}^2 w_{f_{1S}}\partial_\mu\sigma_S\partial^\mu\eta_S\eta_S. \qquad (9.57)
\end{aligned}$$

As in the case of $\mathcal{L}_{\sigma\pi\pi}$, Eq. (9.27), decays of the pure non-strange state $\sigma_N \to \eta_S\eta_S$ and of the pure strange state $\sigma_S \to \eta_N\eta_N$ are driven by the large-$N_c$ suppressed couplings $\lambda_1$ and $h_1$, see Eq. (4.52).

Note that the coupling of $\sigma_N$ to $(\partial_\mu\eta_N)^2$ in Eq. (9.57) can be transformed in the following way:

$$\begin{aligned}
& Z_\pi^2 w_{a_1}\left[g_1(g_1 w_{a_1}\phi_N - 1) + \frac{\phi_N}{2}w_{a_1}(h_1+h_2-h_3)\right] \\
& = Z_\pi^2 w_{a_1}\left\{w_{a_1}\left[g_1^2\phi_N + \frac{\phi_N}{2}(h_1+h_2-h_3)\right] - g_1\right\}
\end{aligned}$$

$$
\begin{aligned}
&\overset{\text{Eqs. (6.41)}}{=} Z_\pi^2 w_{a_1}\left(w_{a_1}\frac{m_{a_1}^2-m_1^2-\frac{h_1}{2}\phi_S^2-2\delta_N}{\phi_N}-g_1\right)\\
&\overset{\text{Eqs. (6.28)}}{=} -Z_\pi^2\frac{w_{a_1}^2}{\phi_N}\left(m_1^2+\frac{h_1}{2}\phi_S^2+2\delta_N\right),
\end{aligned}
\tag{9.58}
$$

where we have used $w_{a_1}m_{a_1}^2/\phi_N = g_1$, and that the coupling of $\sigma_S$ to $(\partial_\mu\eta_S)^2$ in Eq. (9.57) can be similarly transformed in the following way:

$$
\begin{aligned}
&Z_{\eta_S}^2 w_{f_{1S}}\left[\sqrt{2}g_1(\sqrt{2}g_1 w_{f_{1S}}\phi_S-1)+w_{f_{1S}}\phi_S\left(\frac{h_1}{2}+h_2-h_3\right)\right]\\
&= Z_{\eta_S}^2 w_{f_{1S}}\left\{w_{f_{1S}}\left[2g_1^2\phi_S+\phi_S\left(\frac{h_1}{2}+h_2-h_3\right)\right]-\sqrt{2}g_1\right\}\\
&\overset{\text{Eqs. (6.43)}}{=} Z_{\eta_S}^2 w_{f_{1S}}\left(w_{f_{1S}}\frac{m_{f_{1S}}^2-m_1^2-\frac{h_1}{2}\phi_N^2-2\delta_S}{\phi_S}-\sqrt{2}g_1\right)\\
&\overset{\text{Eqs. (6.29)}}{=} -Z_{\eta_S}^2\frac{w_{f_{1S}}^2}{\phi_S}\left(m_1^2+\frac{h_1}{2}\phi_N^2+2\delta_S\right),
\end{aligned}
\tag{9.59}
$$

where we have used $w_{f_{1S}}m_{f_{1S}}^2/(\sqrt{2}\phi_S) = g_1$. Substituting Eqs. (9.58) and (9.59) into Eq. (9.57) and additionally substituting $\eta_N$ and $\eta_S$ by $\eta$ and $\eta'$ according to Eqs. (7.17) and (7.18), we obtain the following form of the interaction Lagrangian:

$$
\begin{aligned}
\mathcal{L}_{\sigma\eta\eta} = {}& A_{\sigma_N\eta\eta}\sigma_N\eta^2 + B_{\sigma_N\eta\eta}\sigma_N(\partial_\mu\eta)^2 + C_{\sigma_N\eta\eta}\partial_\mu\sigma_N\partial^\mu\eta\eta\\
&+ A_{\sigma_S\eta\eta}\sigma_S\eta^2 + B_{\sigma_S\eta\eta}\sigma_S(\partial_\mu\eta)^2 + C_{\sigma_S\eta\eta}\partial_\mu\sigma_S\partial^\mu\eta\eta
\end{aligned}
\tag{9.60}
$$

with

$$
\begin{aligned}
A_{\sigma_N\eta\eta} &= -Z_\pi^2\phi_N\left(\lambda_1+\frac{\lambda_2}{2}+c_1\phi_S^2\right)\cos^2\varphi_\eta - Z_{\eta_S}^2\phi_N\left(\lambda_1+\frac{c_1}{2}\phi_N^2\right)\sin^2\varphi_\eta\\
&\quad -\frac{3}{4}c_1 Z_\pi Z_{\eta_S}\phi_N^2\phi_S\sin(2\varphi_\eta)\\
&= -\phi_N\left\{\lambda_1(Z_\pi^2\cos^2\varphi_\eta + Z_{\eta_S}^2\sin^2\varphi_\eta)+\frac{\lambda_2}{2}Z_\pi^2\cos^2\varphi_\eta\right.\\
&\quad \left.+c_1\left[\frac{Z_{\eta_S}^2}{2}\phi_N^2\sin^2\varphi_\eta + Z_\pi^2\phi_S^2\cos^2\varphi_\eta+\frac{3}{4}Z_\pi Z_{\eta_S}\phi_N\phi_S\sin(2\varphi_\eta)\right]\right\},
\end{aligned}
\tag{9.61}
$$

$$
B_{\sigma_N\eta\eta} = -Z_\pi^2\frac{w_{a_1}^2}{\phi_N}\left(m_1^2+\frac{h_1}{2}\phi_S^2+2\delta_N\right)\cos^2\varphi_\eta + \frac{h_1}{2}Z_{\eta_S}^2 w_{f_{1S}}^2\phi_N\sin^2\varphi_\eta,
\tag{9.62}
$$

$$
C_{\sigma_N\eta\eta} = g_1 w_{a_1} Z_\pi^2\cos^2\varphi_\eta,
\tag{9.63}
$$

$$
\begin{aligned}
A_{\sigma_S\eta\eta} &= -(\lambda_1+\lambda_2)Z_{\eta_S}^2\phi_S\sin^2\varphi_\eta - Z_\pi^2\phi_S(\lambda_1+c_1\phi_N^2)\cos^2\varphi_\eta - \frac{1}{4}c_1 Z_\pi Z_{\eta_S}\phi_N^3\sin(2\varphi_\eta)\\
&= -\lambda_1\phi_S(Z_{\eta_S}^2\sin^2\varphi_\eta + Z_\pi^2\cos^2\varphi_\eta) - Z_{\eta_S}^2\lambda_2\phi_S\sin^2\varphi_\eta\\
&\quad - Z_\pi c_1\phi_N\left[Z_\pi\phi_N\phi_S\cos^2\varphi_\eta+\frac{1}{4}Z_{\eta_S}\phi_N^2\sin(2\varphi_\eta)\right],
\end{aligned}
\tag{9.64}
$$

$$
B_{\sigma_S\eta\eta} = -Z_{\eta_S}^2\frac{w_{f_{1S}}^2}{\phi_S}\left(m_1^2+\frac{h_1}{2}\phi_N^2+2\delta_S\right)\sin^2\varphi_\eta + \frac{h_1}{2}Z_\pi^2 w_{a_1}^2\phi_S\cos^2\varphi_\eta,
\tag{9.65}
$$

$$C_{\sigma_S\eta\eta} = \sqrt{2} Z_{\eta_S}^2 g_1 w_{f_{1S}} \sin^2\varphi_\eta. \tag{9.66}$$

As in Eq. (9.34) we obtain from Eqs. (9.17) and (9.60)

$$\begin{aligned}
\mathcal{L}_{\sigma\eta\eta,\,\text{full}} &= \mathcal{L}_{\sigma_N\sigma_S,\,\text{full}} + \mathcal{L}_{\sigma\eta\eta} \\
&= \frac{1}{2}(\partial_\mu\sigma_N)^2 + \frac{1}{2}(\partial_\mu\sigma_S)^2 - \frac{1}{2}m_{\sigma_N}^2 - \frac{1}{2}m_{\sigma_S}^2 + z_\sigma\sigma_N\sigma_S \\
&+ A_{\sigma_N\eta\eta}\sigma_N\eta^2 + B_{\sigma_N\eta\eta}\sigma_N(\partial_\mu\eta)^2 + C_{\sigma_N\eta\eta}\partial_\mu\sigma_N\partial^\mu\eta\eta \\
&+ A_{\sigma_S\eta\eta}\sigma_S\eta^2 + B_{\sigma_S\eta\eta}\sigma_S(\partial_\mu\eta)^2 + C_{\sigma_S\eta\eta}\partial_\mu\sigma_S\partial^\mu\eta\eta.
\end{aligned} \tag{9.67}$$

Substituting $\sigma_{N,S}$ by $\sigma_{1,2}$ we obtain

$$\begin{aligned}
\mathcal{L}_{\sigma\eta\eta,\,\text{full}} &= \frac{1}{2}(\partial_\mu\sigma_1)^2 - \frac{1}{2}m_{\sigma_1}^2\sigma_1^2 \\
&+ (A_{\sigma_N\eta\eta}\cos\varphi_\sigma + A_{\sigma_S\eta\eta}\sin\varphi_\sigma)\sigma_1\eta^2 \\
&+ (B_{\sigma_N\eta\eta}\cos\varphi_\sigma + B_{\sigma_S\eta\eta}\sin\varphi_\sigma)\sigma_1(\partial_\mu\eta)^2 \\
&+ (C_{\sigma_N\eta\eta}\cos\varphi_\sigma + C_{\sigma_S\eta\eta}\sin\varphi_\sigma)\partial_\mu\sigma_1\partial^\mu\eta\eta \\
&+ \frac{1}{2}(\partial_\mu\sigma_2)^2 - \frac{1}{2}m_{\sigma_2}^2\sigma_2^2 \\
&+ (A_{\sigma_S\eta\eta}\cos\varphi_\sigma - A_{\sigma_N\eta\eta}\sin\varphi_\sigma)\sigma_2\eta^2 \\
&+ (B_{\sigma_S\eta\eta}\cos\varphi_\sigma - B_{\sigma_N\eta\eta}\sin\varphi_\sigma)\sigma_2(\partial_\mu\eta)^2 \\
&+ (C_{\sigma_S\eta\eta}\cos\varphi_\sigma - C_{\sigma_N\eta\eta}\sin\varphi_\sigma)\partial_\mu\sigma_2\partial^\mu\eta\eta.
\end{aligned} \tag{9.68}$$

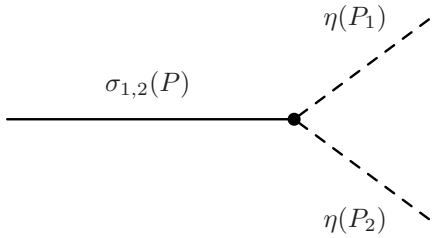


**Figure 9.11:** Decay process $\sigma_{1,2} \to \eta\eta$.

Let us set $P$ as momentum of $\sigma_1$ or $\sigma_2$ (depending on the decaying particle) and $P_1$ and $P_2$ as the momenta of the $\eta$ fields. Upon substituting $\partial^\mu \to -iP^\mu$ for the decaying particles and $\partial^\mu \to iP_{1,2}^\mu$ for the decay products, the decay amplitudes of the mixed states $\sigma_{1,2}$ read

$$\begin{aligned}
-i\mathcal{M}_{\sigma_1\to\eta\eta}(m_{\sigma_1}) = i\{&\cos\varphi_\sigma(A_{\sigma_N\eta\eta} - B_{\sigma_N\eta\eta}P_1\cdot P_2 + C_{\sigma_N\eta\eta}P\cdot P_1) \\
&+ \sin\varphi_\sigma\left[A_{\sigma_S\eta\eta} - B_{\sigma_S\eta\eta}\frac{m_{\sigma_1}^2 - 2m_\eta^2}{2} + C_{\sigma_S\eta\eta}\frac{m_{\sigma_1}^2}{2}\right]\Big\}
\end{aligned}$$

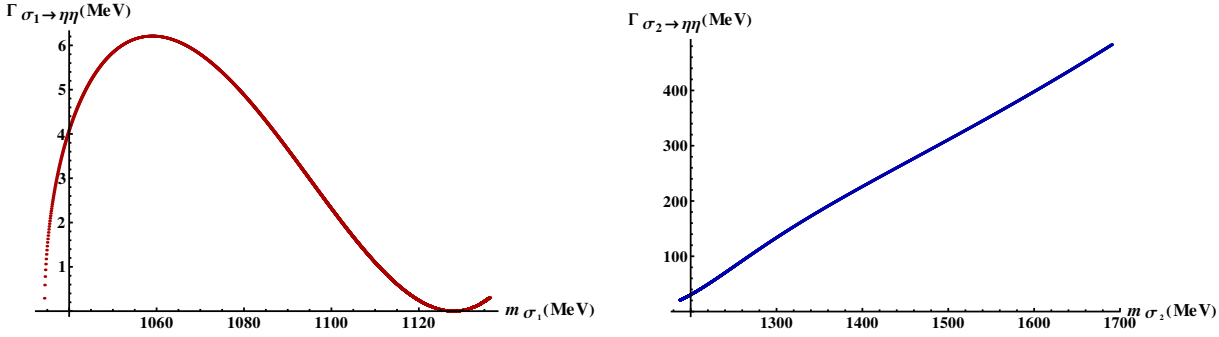


**Figure 9.12:** $\Gamma_{\sigma_1\to\eta\eta}$ and $\Gamma_{\sigma_2\to\eta\eta}$ as functions of $m_{\sigma_1}$ and $m_{\sigma_2}$, respectively.

$$= i\left\{\cos\varphi_\sigma\left[A_{\sigma_N\eta\eta} - B_{\sigma_N\eta\eta}\frac{m_{\sigma_1}^2 - 2m_\eta^2}{2} + C_{\sigma_N\eta\eta}\frac{m_{\sigma_1}^2}{2}\right]\right.$$
$$\left. + \sin\varphi_\sigma\left[A_{\sigma_S\eta\eta} - B_{\sigma_S\eta\eta}\frac{m_{\sigma_1}^2 - 2m_\eta^2}{2} + C_{\sigma_S\eta\eta}\frac{m_{\sigma_1}^2}{2}\right]\right\}, \tag{9.69}$$

$$-i\mathcal{M}_{\sigma_2\to\eta\eta}(m_{\sigma_2}) = i\left\{\cos\varphi_\sigma\left[A_{\sigma_S\eta\eta} - B_{\sigma_S\eta\eta}\frac{m_{\sigma_2}^2 - 2m_\eta^2}{2} + C_{\sigma_S\eta\eta}\frac{m_{\sigma_2}^2}{2}\right]\right.$$
$$\left. - \sin\varphi_\sigma\left[A_{\sigma_N\eta\eta} - B_{\sigma_N\eta\eta}\frac{m_{\sigma_2}^2 - 2m_\eta^2}{2} + C_{\sigma_N\eta\eta}\frac{m_{\sigma_2}^2}{2}\right]\right\}. \tag{9.70}$$

Finally, we obtain the following formulas for the decay widths:

$$\Gamma_{\sigma_1\to\eta\eta} = \frac{k(m_{\sigma_1}, m_\eta, m_\eta)}{8\pi m_{\sigma_1}^2}|-i\mathcal{M}_{\sigma_1\to\eta\eta}(m_{\sigma_1})|^2, \tag{9.71}$$

$$\Gamma_{\sigma_2\to\eta\eta} = \frac{k(m_{\sigma_2}, m_\eta, m_\eta)}{8\pi m_{\sigma_2}^2}|-i\mathcal{M}_{\sigma_2\to\eta\eta}(m_{\sigma_2})|^2. \tag{9.72}$$

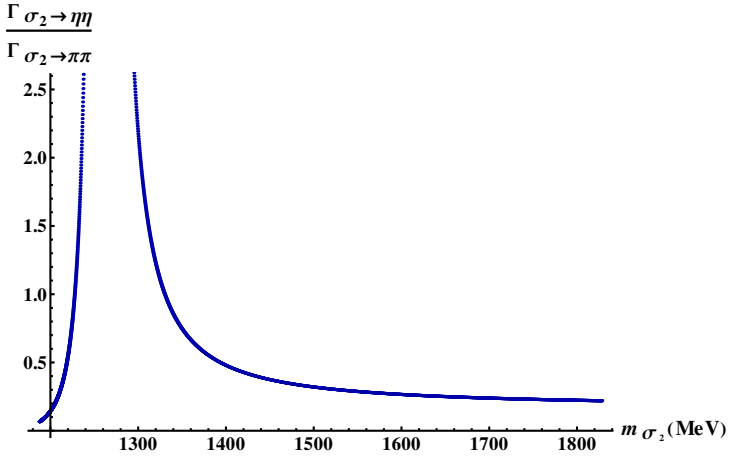


**Figure 9.13:** Ratio $\Gamma_{\sigma_2\to\eta\eta}/\Gamma_{\sigma_2\to\pi\pi}$ as function of $m_{\sigma_2}$.

The decay widths are shown diagrammatically in Fig. 9.12. As expected, $\Gamma_{\sigma_1\to\eta\eta}$ is suppressed due to a limited phase space for $\eta\eta$. We observe a strong increase of $\Gamma_{\sigma_2\to\eta\eta}$ over the $f_0(1370)$ mass interval (see the right panel in Fig. 9.12). Our results regarding the decay channels $\sigma_2 \to \pi\pi$ and $\sigma_2 \to KK$ favour $m_{\sigma_2} = 1200$ MeV for which we obtain $\Gamma_{\sigma_2\to\eta\eta} = 31$ MeV.

A plot of $\Gamma_{\sigma_2\to\eta\eta}/\Gamma_{\sigma_2\to\pi\pi}$ is shown in Fig. 9.13. There is a discontinuity in the ratio $\Gamma_{\sigma_2\to\eta\eta}/\Gamma_{\sigma_2\to\pi\pi}$ at the point $m_{\sigma_2} = 1260$ MeV; for $m_{\sigma_2} = 1200$ MeV we obtain $\Gamma_{\sigma_2\to\eta\eta}/\Gamma_{\sigma_2\to\pi\pi} = 0.15$, in accordance with the result $\Gamma_{f_0(1370)\to\eta\eta}/\Gamma_{f_0(1370)\to\pi\pi} = 0.19 \pm 0.07$ from Ref. [40]. We also observe that the $\sigma_2 \to KK$ channel is dominant in comparison with the $\sigma_2 \to \eta\eta$ channel, see Fig. 9.14, reaffirming the conclusion reached from the comparison of the decays $\sigma_2 \to KK$ and $\sigma_2 \to \eta\eta$ (see Fig. 9.10).

## 9.2 Decay Amplitude $a_0(980) \to \eta\pi$

We have seen in Sec. 8 that a calculation of the parameter $h_2$ via the decay width $\Gamma_{f_{1N}\to a_0(980)\pi}$, Eq. (8.14), yields two sets of values, a relatively lower and a relatively higher one. In the $U(2) \times U(2)$ version of the model, Sec. 5.2.2, the higher set of $h_2$ values was found to be preferred. Conversely, Fit I in Sec. 8 prefers lower values of $h_2$; in this section we discuss whether, in that case, it is still possible to obtain a correct value of the $a_0(980) \to \eta\pi$ decay amplitude.

The $a_0^0\eta\pi^0$ interaction Lagrangian reads

$$\mathcal{L}_{a_0\eta\pi} = A_{a_0\eta_N\pi}a_0^0\eta_N\pi^0 + B_{a_0\eta_N\pi}a_0^0\partial_\mu\eta_N\partial^\mu\pi^0 + C_{a_0\eta_N\pi}\partial_\mu a_0^0(\pi^0\partial^\mu\eta_N + \eta_N\partial^\mu\pi^0) + A_{a_0\eta_S\pi}a_0^0\eta_S\pi^0 \tag{9.73}$$

with

$$A_{a_0\eta_N\pi} = (-\lambda_2 + c_1\phi_S^2)Z_\pi^2\phi_N, \tag{9.74}$$

$$B_{a_0\eta_N\pi} = -2\frac{g_1^2\phi_N}{m_{a_1}^2}\left[1 - \frac{1}{2}\frac{Z_\pi^4 f_\pi^2}{m_{a_1}^2}(h_2 - h_3)\right], \tag{9.75}$$

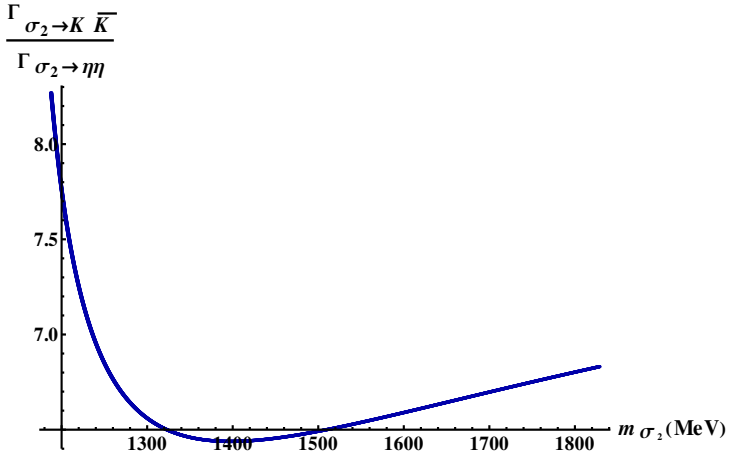


**Figure 9.14:** Ratio $\Gamma_{\sigma_2\to KK}/\Gamma_{\sigma_2\to\eta\eta}$ as function of $m_{\sigma_2}$.

$$C_{a_0\eta_N\pi} = g_1 w_{a_1} Z_\pi^2, \tag{9.76}$$

$$A_{a_0\eta_S\pi} = \frac{1}{2} c_1 Z_\pi Z_{\eta_S} \phi_N^2 \phi_S. \tag{9.77}$$

Substituting $\eta_N$ by $\eta\cos\varphi_\eta$ and $\eta_S$ by $\eta\sin\varphi_\eta$ [see Eqs. (7.17) and (7.18)] we obtain from the Lagrangian (9.73)

$$\begin{aligned}\mathcal{L}_{a_0\eta\pi} &= A_{a_0\eta_N\pi}\cos\varphi_\eta a_0^0\eta\pi^0 + B_{a_0\eta_N\pi}\cos\varphi_\eta a_0^0\partial_\mu\eta\partial^\mu\pi^0 \\ &+ C_{a_0\eta_N\pi}\cos\varphi_\eta\partial_\mu a_0^0(\pi^0\partial^\mu\eta + \eta\partial^\mu\pi^0) + A_{a_0\eta_S\pi}\sin\varphi_\eta a_0^0\eta\pi^0.\end{aligned} \tag{9.78}$$

Consequently, the decay amplitude $\mathcal{M}_{a_0^0\to\eta\pi^0}$ reads

$$\begin{aligned}-i\mathcal{M}_{a_0^0\to\eta\pi^0}(m_\eta) = i\Bigg\{&\cos\varphi_\eta\left[A_{a_0\eta_N\pi} - B_{a_0\eta_N\pi}\frac{m_{a_0}^2 - m_\eta^2 - m_\pi^2}{2} + C_{a_0\eta_N\pi}m_{a_0(980)}^2\right] \\ &+ \sin\varphi_\eta A_{a_0\eta_S\pi}\Bigg\}.\end{aligned} \tag{9.79}$$

Note that we can write $\mathcal{M}_{a_0^0\to\eta\pi^0}(m_\eta)$ also as

$$-i\mathcal{M}_{a_0^0\to\eta\pi^0}(m_\eta) = -i[\cos\varphi_\eta\mathcal{M}_{a_0^0\to\eta_N\pi^0}(m_\eta) + \sin\varphi_\eta\mathcal{M}_{a_0^0\to\eta_S\pi^0}(m_\eta)], \tag{9.80}$$

where

$$-i\mathcal{M}_{a_0^0\to\eta_N\pi^0}(m_\eta) = i\left[A_{a_0\eta_N\pi} - B_{a_0\eta_N\pi}\frac{m_{a_0}^2 - m_\eta^2 - m_\pi^2}{2} + C_{a_0\eta_N\pi}m_{a_0(980)}^2\right] \tag{9.81}$$

and

$$-i\mathcal{M}_{a_0^0\to\eta_S\pi^0}(m_\eta) = iA_{a_0\eta_S\pi}. \tag{9.82}$$

In Eqs. (9.81) and (9.82), $\mathcal{M}_{a_0^0\to\eta_N\pi^0}$ is obtained only from terms containing $\eta_N$ in Eq. (9.73) whereas $\mathcal{M}_{a_0^0\to\eta_S\pi^0}$ is obtained from the $a_0^0\eta_S\pi^0$ coupling in Eq. (9.73). Note also that $\mathcal{M}_{a_0^0\to\eta_N\pi^0}$ possesses an analogous form to Eq. (5.64).

All the parameters as well as $m_{a_0(980)}$, $m_\eta$ and $m_\pi$ are determined uniquely from the fit and can be found in Tables 8.4 and 8.5. Consequently, we obtain from Eq. (9.79)

$$|\,\mathcal{M}_{a_0^0(980)\to\eta\pi^0}(m_\eta)\,| = 3155\text{ MeV}. \tag{9.83}$$

The value is within experimental data stating $\mathcal{M}_{a_0\eta\pi}(m_\eta) = (3330 \pm 150)$ MeV [114]. Note that we have used $\varphi_\eta = -42°$, in accordance with results derived in *Step 4* of Sec. 8.

## 9.3 Decay Width $K_0^\star(800) \to K\pi$

In this section we turn to the phenomenology of the scalar kaon $K_S$, assigned to $K_0^\star(800)$, or $\kappa$, in Fit I. The scalar kaon is known to decay into $K\pi$ [10]. The corresponding interaction Lagrangian from Eq. (6.1) reads (we consider only the neutral component; the other ones possess analogous forms)

$$\mathcal{L}_{K_SK\pi} = A_{K_SK\pi}K_S^0(\bar{K}^0\pi^0 - \sqrt{2}K^-\pi^+) + B_{K_SK\pi}K_S^0(\partial_\mu\bar{K}^0\partial^\mu\pi^0 - \sqrt{2}\partial_\mu K^-\partial^\mu\pi^+)$$
$$+ C_{K_SK\pi}\partial_\mu K_S^0(\pi^0\partial^\mu\bar{K}^0 - \sqrt{2}\pi^+\partial_\mu K^-) + D_{K_SK\pi}\partial_\mu K_S^0(\bar{K}^0\partial^\mu\pi^0 - \sqrt{2}K^-\partial^\mu\pi^+) \quad (9.84)$$

with the following coefficients:

$$A_{K_SK\pi} = \frac{Z_\pi Z_K Z_{K_S}}{\sqrt{2}}\lambda_2\phi_S, \quad (9.85)$$

$$B_{K_SK\pi} = -\frac{Z_\pi Z_K Z_{K_S}}{4}w_{a_1}w_{K_1}\left[g_1^2(3\phi_N + \sqrt{2}\phi_S) - 2g_1\frac{w_{a_1} + w_{K_1}}{w_{a_1}w_{K_1}} + h_2(\phi_N + \sqrt{2}\phi_S) - 2h_3\phi_N\right], \quad (9.86)$$

$$C_{K_SK\pi} = \frac{Z_\pi Z_K Z_{K_S}}{4}[2g_1(\sqrt{2}ig_1w_{K^\star}w_{K_1}\phi_S - iw_{K^\star} - w_{K_1}) - 2\sqrt{2}ih_3w_{K^\star}w_{K_1}\phi_S], \quad (9.87)$$

$$D_{K_SK\pi} = -\frac{Z_\pi Z_K Z_{K_S}}{4}\{g_1[2w_{a_1} - 2iw_{K^\star} + ig_1w_{a_1}w_{K^\star}(3\phi_N - \sqrt{2}\phi_S)]$$
$$+ i(h_2 - 2h_3)w_{K^\star}w_{a_1}\phi_N - \sqrt{2}ih_2w_{K^\star}w_{a_1}\phi_S\}. \quad (9.88)$$

Note that the coefficients containing the imaginary unit are nonetheless real because $w_{K^\star}$, Eq. (6.31), is imaginary.

Let us focus on the decay $K_S^0 \to K^0\pi^0$ in the following. The contribution of the charged modes to the decay width is twice the contribution of the neutral modes, as apparent from Eq. (9.84). (We are changing the charge of the decay products in comparison to the one present in the interaction Lagrangian. The Lagrangian itself has to be charge-neutral and therefore contains particles and antiparticles simultaneously; however, decay products are charge-conjugated in the scattering matrix, see Sec. 2.6). It is then straightforward to calculate the decay amplitude ($P$, $P_1$ and $P_2$ denote momenta of $K_S$, kaon and pion, respectively, and we substitute $\partial^\mu \to -iP^\mu$ for the decaying particles and $\partial^\mu \to iP_{1,2}^\mu$ for the decay products):

$$-i\mathcal{M}_{K_S^0\to K^0\pi^0} = i(A_{K_SK\pi} - B_{K_SK\pi}P_1\cdot P_2 + C_{K_SK\pi}P\cdot P_1 + D_{K_SK\pi}P\cdot P_2). \quad (9.89)$$

Due to energy conservation on the vertex, $P = P_1 + P_2$; thus we obtain

$$-i\mathcal{M}_{K_S^0\to K^0\pi^0} = i[A_{K_SK\pi} - B_{K_SK\pi}P_1\cdot P_2 + C_{K_SK\pi}(P_1^2 + P_1\cdot P_2) + D_{K_SK\pi}(P_2^2 + P_1\cdot P_2)]. \quad (9.90)$$

Kaons and pions in the decay process are on-shell particles; therefore $P_1^2 = m_K^2$ and $P_2^2 = m_\pi^2$. Additionally, $P_1\cdot P_2 = (P^2 - P_1^2 - P_2^2)/2 \equiv (m_{K_S}^2 - m_K^2 - m_\pi^2)/2$. Therefore,

$$-i\mathcal{M}_{K_S^0\to K^0\pi^0} = i\left[A_{K_SK\pi} + (C_{K_SK\pi} + D_{K_SK\pi} - B_{K_SK\pi})\frac{m_{K_S}^2 - m_K^2 - m_\pi^2}{2}\right.$$
$$\left. + C_{K_SK\pi}m_K^2 + D_{K_SK\pi}m_\pi^2\right]. \quad (9.91)$$

The decay width $\Gamma_{K_S^0\to K\pi}$ then reads

$$\Gamma_{K_S^0\to K\pi} = 3\frac{k(m_{K_S}, m_K, m_\pi)}{8\pi m_{K_S}^2}|-i\mathcal{M}_{K_S^0\to K^0\pi^0}|^2. \quad (9.92)$$

Note that all parameters entering Eqs. (9.91) and (9.92) are known from Table 8.4; $Z_{K_S}$, $w_{a_1}$, $w_{K_1}$ and $w_{K^\star}$ are determined respectively from Eqs. (6.49), (6.28), (6.30) and (6.31). Then the value of $\Gamma_{K_S^0 \to K\pi}$ is determined uniquely:

$$\Gamma_{K_S^0 \to K\pi} = 490 \text{ MeV}. \tag{9.93}$$

The result is close to the value quoted by the PDG: $\Gamma_\kappa^{\text{exp}} = (548 \pm 24)$ MeV [10]. The $\kappa$ resonance is experimentally known to be broad and this finding is reproduced in our model. (Note, however, that our $m_{K_S}$ is approximately by a factor of two larger than $m_\kappa^{\text{exp}} = 676$ MeV, see Table 8.5 and Sec. 8.)

Let us also point out the remarkable influence of the diagonalisation shift, Eqs. (6.17) and (6.19) - (6.23), on this decay width: omitting the shift ($w_{a_1} = w_{K^\star} = w_{K_1} = 0$), i.e., ignoring mixing terms from Eq. (6.15), would yield $\Gamma_{K_0^\star(800) \to K\pi} \simeq 3$ GeV. Consequently, coefficients arising from the shift [Eqs. (9.86) - (9.88)] induce a destructive interference in the Lagrangian (9.84) decreasing the decay width by approximately a factor of 6.

## 9.4 Phenomenology of the Vector and Axial-Vector Mesons in Fit I

An important test of our Fit I derived in Sec. 8 is the phenomenology of the vector and axial-vector states. In the vector channel, the exact value of $\Gamma_{\rho \to \pi\pi} = 149.1$ MeV has already been implemented to determine the parameter $g_2$ (see Table 8.4). In principle our model also allows for the discussion of the phenomenology for the isosinglet vector state $\omega_S \equiv \varphi(1020)$. This state decays into kaons; our Fit I yields $m_{\omega_S} = 870.35$ MeV thus implying that no tree-level calculation of the decay width can be performed as $m_{\omega_S}$ is below the two-kaon threshold. Therefore, this state is not well described within Fit I. [Note that decays of the non-strange vector isosinglet $\omega_N$ cannot be calculated within the model because there are no corresponding vertices: $\omega_N$ always appears quadratically in the Lagrangian (6.1).] Therefore in this section we only need to consider the phenomenology of the $K^\star$ meson to complete the vector phenomenology (see subsection 9.4.5).

Fit I has also yielded $m_{f_{1S}} = 1643.4$ MeV, see Table 8.5. As discussed in Sec. 8, $m_{f_{1S}}$ is too large when compared to the experimental result $m_{f_1(1420)}^{\text{exp}} = (1426.4 \pm 0.9)$ MeV. The $f_{1S} \equiv f_1(1420)$ resonance decays predominantly into $K^\star K$ [10]. The corresponding decay width can be calculated within our model and it will represent an important test of Fit I because $f_1(1420)$ is a sharp resonance with $\Gamma_{f_1(1420)}^{\text{exp}} = (54.9 \pm 2.6)$ MeV, see subsection 9.4.6. The $K_1$ phenomenology is discussed in Sec. 9.4.7. We will, however, begin with the phenomenology of $a_1(1260)$. This state possesses a large decay width [$(250-600)$ MeV [10]] with a dominant $\rho\pi$ decay channel. From our model, $a_1(1260)$ is expected to be the chiral partner of the $\rho$ meson and to become degenerate with this state upon the chiral transition. However, one first needs to ascertain whether the $a_1(1260)$ phenomenology in vacuum can be described correctly from Fit I. This is discussed in the following subsections 9.4.1 and 9.4.2. The phenomenology of the axial-vector isosinglet $f_{1N} \equiv f_1(1285)$ is discussed subsequently in Sec. 9.4.4; as in the case of $f_1(1420)$, only the $K^\star K$ decay channel can be considered in our model.

### 9.4.1 Decay Width $a_1(1260) \to \rho\pi$ in Fit I

The interaction Lagrangian for the decay $a_1(1260) \to \rho\pi$ has the same form as in the $U(2) \times U(2)$ version of the model, Sec. 5.2.7. We can therefore make use of the same formula for $\Gamma_{a_1(1260)\to\rho\pi}$ as in Eq. (5.95). The decay width depends (among other parameters) on $g_2$; this parameter is fixed via the decay width $\Gamma_{\rho\to\pi\pi}$ [Eq. (5.45)] and given that our Fit I yields a relatively large value of $m_{a_1} = 1395.5$ MeV, see Table 8.5, then we obtain a value of $g_2 = -11.2$ for $\Gamma_{\rho\to\pi\pi} = 149.1$ MeV [10] (see Table 8.4). The large magnitude of this parameter influences $\Gamma_{a_1(1260)\to\rho\pi}$ in a very strong way: we obtain $\Gamma_{a_1(1260)\to\rho\pi} \simeq 13$ GeV for the stated value of $g_2$ and other parameters listed in Table 8.4. In fact, we would require $g_2 \gtrsim 10$ for $\Gamma_{a_1(1260)\to\rho\pi}$ to have values within the PDG interval $(250 - 600)$ MeV [10], see Fig. 9.15. Note that integrating over the $\rho$ spectral function, just as in Sec. 2.6.2, yields the decay width of $\sim 11$ GeV – again unphysically large.

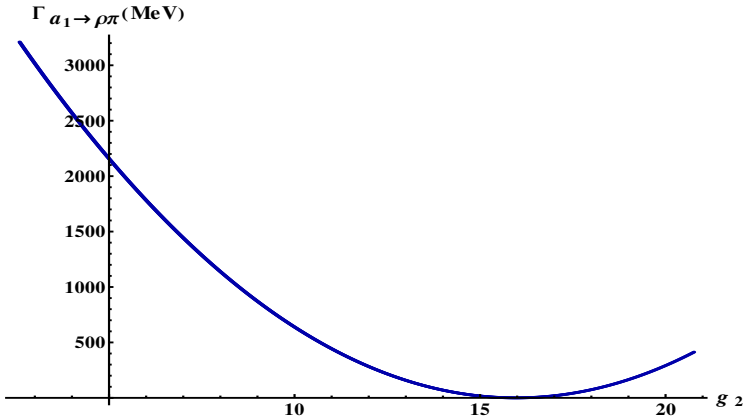


**Figure 9.15:** $\Gamma_{a_1(1260)\to\rho\pi}$ as function of $g_2$ in Fit I.

Our fit determines all parameter values uniquely and therefore we do not have a possibility to fine-tune $\Gamma_{a_1(1260)\to\rho\pi}$; the only exception arises by changing $\Gamma_{\rho\to\pi\pi}$ to increase $g_2$ and consequently decrease $\Gamma_{a_1(1260)\to\rho\pi}$ (note, however, that the experimental uncertainty regarding $\Gamma_{\rho\to\pi\pi}$ is actually very small: $\pm 0.8$ MeV [10]). Consequent changes in $\Gamma_{a_1(1260)\to\rho\pi}$ are depicted in Fig. 9.16.

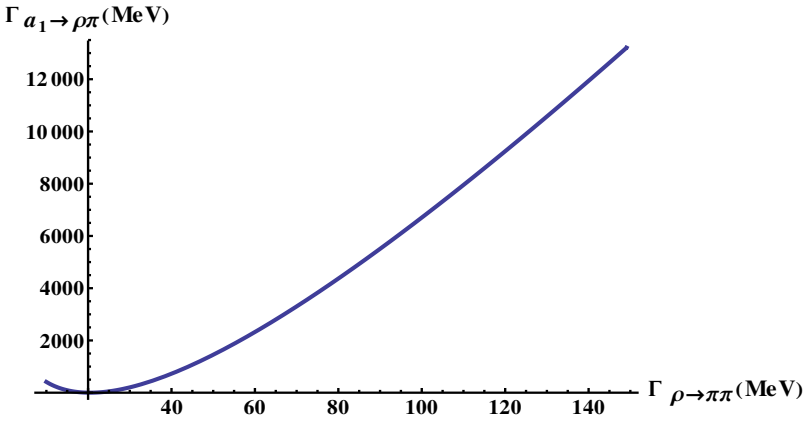


**Figure 9.16:** $\Gamma_{a_1(1260)\to\rho\pi}$ as function of $\Gamma_{\rho\to\pi\pi}$.

We can see from Fig. 9.16 that $\Gamma_{a_1(1260)\to\rho\pi} < 600$ MeV only if $\Gamma_{\rho\to\pi\pi} < 38$ MeV, more than 100 MeV smaller than the physical value of $\Gamma_{\rho\to\pi\pi} = 149.1$ MeV [10]. Alternatively, increasing $\Gamma_{\rho\to\pi\pi}$ also leads to a very strong increase of $\Gamma_{a_1(1260)\to\rho\pi}$ with $\Gamma_{a_1(1260)\to\rho\pi} > 1$ GeV already at $\Gamma_{\rho\to\pi\pi} \simeq 44$ MeV. Therefore, we observe a strong tension between the decays in the non-strange vector and axial-vector channels – it is not possible to obtain correct decay width values in both channels at the same time as either the decay $\rho \to \pi\pi$ is subdominant [and $\Gamma_{a_1(1260)\to\rho\pi}$ within the physical range] or the decay $\rho \to \pi\pi$ is correctly described but the channel $a_1(1260) \to \rho\pi$ is virtually dissolved in the continuum.

### 9.4.2 Decay Width $a_1(1260) \to f_0(600)\pi$ in Fit I

Unlike the case of the $a_1(1260) \to \rho\pi$ decay, the interaction Lagrangian for the process $a_1(1260) \to f_0(600)\pi$ with $f_0(600) \equiv \sigma_1$ is slightly different than in the $U(2) \times U(2)$ version of the model, Sec. 5.2.6:

$$\mathcal{L}_{a_1\sigma\pi} = A_{a_1\sigma_N\pi} a_1^{\mu 0} \sigma_N \partial_\mu \pi^0 + B_{a_1\sigma_N\pi} a_1^{\mu 0} \pi^0 \partial_\mu \sigma_N + A_{a_1\sigma_S\pi} a_1^{\mu 0} \sigma_S \partial_\mu \pi^0 \tag{9.94}$$

with the following coefficients:

$$A_{a_1\sigma_N\pi} = Z_\pi \left[ g_1(-1 + 2 g_1 w_{a_1} \phi_N) + (h_1 + h_2 - h_3) w_{a_1} \phi_N \right], \tag{9.95}$$

$$B_{a_1\sigma_N\pi} = g_1 Z_\pi, \tag{9.96}$$

$$A_{a_1\sigma_S\pi} = h_1 Z_\pi w_{a_1} \phi_S. \tag{9.97}$$

It is necessary to substitute the pure states $\sigma_N$ and $\sigma_S$ by the mixed states $\sigma_1$ and $\sigma_2$ in Eq. (9.94); we are considering only the decay $a_1(1260) \to \sigma_1\pi$ and thus it suffices to perform the substitutions $\sigma_N \to \cos\varphi_\sigma \sigma_1$ and $\sigma_S \to \sin\varphi_\sigma \sigma_2$:

$$\mathcal{L}_{a_1\sigma\pi} = (A_{a_1\sigma_N\pi} \cos\varphi_\sigma + A_{a_1\sigma_S\pi} \sin\varphi_\sigma) a_1^{\mu 0} \sigma_1 \partial_\mu \pi^0 + B_{a_1\sigma_N\pi} \cos\varphi_\sigma a_1^{\mu 0} \pi^0 \partial_\mu \sigma_1, \tag{9.98}$$

where $\varphi_\sigma$ is the $\sigma_N$-$\sigma_S$ mixing angle, Eq. (9.23). The interaction Lagrangian from Eq. (9.98) possesses an analogous form to the one presented in Eq. (2.191), with the latter describing a generic decay of an axial-vector state $A$ into a scalar $S$ and a pseudoscalar $\tilde{P}$. Thus we can use the generic formula for the decay width from Eq. (2.200) upon substituting $A \leftrightarrow a_1$, $S \leftrightarrow \sigma_1$, $\tilde{P} \leftrightarrow \pi$, $A_{AS\tilde{P}} \leftrightarrow A_{a_1\sigma_N\pi} \cos\varphi_\sigma + A_{a_1\sigma_S\pi} \sin\varphi_\sigma$ and $A_{AS\tilde{P}} \leftrightarrow B_{a_1\sigma_N\pi} \cos\varphi_\sigma$. We consequently obtain $\Gamma_{a_1(1260)\to\sigma_1\pi}$ as shown in Fig. 9.17.

We observe from Fig. 9.17 that $\Gamma_{a_1(1260)\to\sigma_1\pi}$ rapidly decreases with the available phase space. The exact value of $\Gamma_{a_1(1260)\to\sigma_1\pi}$ is therefore strongly dependent on $m_{\sigma_1}$; e.g., we obtain the result $\Gamma_{a_1(1260)\to\sigma_1\pi} = 21$ MeV for $m_{\sigma_1} = 705$ MeV [our best value of $m_{\sigma_1}$, see Eq. (9.56)]. Nonetheless, these results show $\Gamma_{a_1(1260)\to\sigma_1\pi}$ to be suppressed in comparison with $\Gamma_{a_1(1260)\to\rho\pi}$ and qualitatively similar to the values in Scenario I of the $U(2) \times U(2)$ version of the model.

### 9.4.3 Decay Width $a_1(1260) \to K^\star K \to KK\pi$ in Fit I

The corresponding interaction Lagrangian is a feature of the $U(3) \times U(3)$ version of the model. The Lagrangian reads

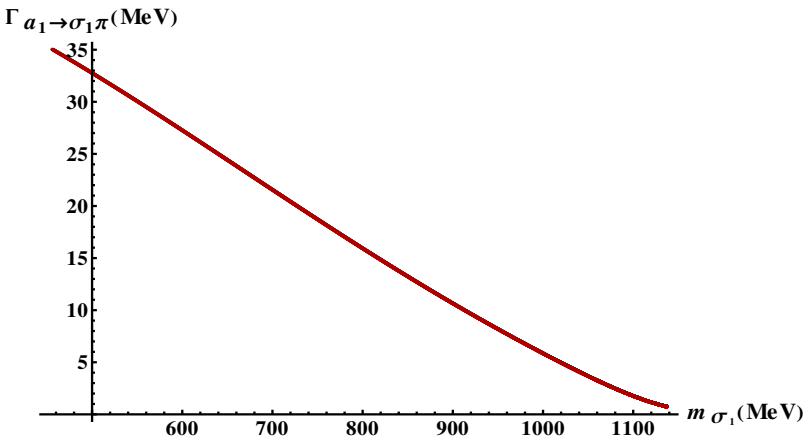


**Figure 9.17:** $\Gamma_{a_1(1260)\to\sigma_1\pi}$ as function of $m_{\sigma_1}$.

$$\begin{aligned}\mathcal{L}_{a_1K^\star K} &= A_{a_1K^\star K}a_1^{\mu 0}(K_\mu^{\star 0}\bar{K}^0 + K_\mu^{\star -}K^+) \\ &+ B^\mu_{a_1K^\star K}a_1^{\mu 0}[(\partial_\nu K_\mu^{\star 0} - \partial_\mu K_\nu^{\star 0})\partial^\nu \bar{K}^0 + (\partial_\nu K_\mu^{\star -} - \partial_\mu K_\nu^{\star -})\partial^\nu K^+] \\ &+ \partial^\nu a_1^{\mu 0}(K_\nu^{\star 0}\partial_\mu \bar{K}^0 - K_\mu^{\star 0}\partial_\nu \bar{K}^0 + K_\nu^{\star -}\partial_\mu K^+ - K_\mu^{\star -}\partial_\nu K^+)] + \text{h.c.}\end{aligned} \tag{9.99}$$

with the following coefficients:

$$A_{a_1K^\star K} = -\frac{i}{4}Z_K\left[g_1^2(3\phi_N - \sqrt{2}\phi_S) + h_2(\phi_N - \sqrt{2}\phi_S) - 2h_3\phi_N\right], \tag{9.100}$$

$$B_{a_1K^\star K} = -\frac{i}{2}Z_K g_2 w_{K_1}, \tag{9.101}$$

$$C_{a_1K^\star K} = -\frac{i}{2}Z_K g_2 w_{K_1}. \tag{9.102}$$

We can now consider results from Sec. 2.6.2 where a generic decay of an axial-vector into a vector and pseudoscalar was considered. The decay $a_1 \to \bar{K}^\star K$ is tree-level forbidden because $a_1$ is below the $K^\star K$ threshold. However, if an off-shell $K^\star$ state is considered then the ensuing decay $a_1 \to \bar{K}^\star K \to \bar{K}K\pi$ can be studied. We can therefore use Eq. (2.190) as formula for the decay width (the isospin factor is $I = 4$) and integrate over the $K^\star$ spectral function in Eq. (2.189). The value of the $K^\star$ decay width used in the spectral function is given further below, in Eq. (9.124). We obtain

$$\Gamma_{a_1\to\bar{K}^\star K\to\bar{K}K\pi} = 1.97 \text{ GeV}. \tag{9.103}$$

The decay is strongly enhanced for the same reasons as in the previousy discussed $a_1(1260)$ channels.

### 9.4.4 Decay Width $f_1(1285) \to K^\star K$ in Fit I

The $f_{1N} \equiv f_1(1285)$ meson is the non-strange axial-vector isosinglet state, i.e., the isospin-zero partner of the $a_1(1260)$ resonance. These two resonances are degenerate in our model [see Eq. (6.41)] given that the model implements the isospin symmetry exactly.

There are two decays of the $f_1(1285)$ resonance that can be calculated from the $U(3) \times U(3)$ version of our model: a decay involving non-strange states, $f_1(1285) \to a_0(980)\pi$, and a decay into kaons, $f_1(1285) \to \bar{K}^\star K$. The former decay width has already been utilised to calculate the parameter $h_2$ in Fit I, see Sec. 7 and Eq. (8.14); therefore, this decay width corresponds exactly to the experimental value $\Gamma_{f_1(1285)\to a_0(980)\pi} = 8.748$ MeV (see Table 8.5). The latter decay width is discussed in this section. The PDG actually lists the $f_1(1285) \to \bar{K}^\star K$ process as "not seen" although the three-body decay $f_1(1285) \to \bar{K}K\pi$ possesses a branching ratio of $(9.0 \pm 0.4)\%$; the full decay width of the resonance is $\Gamma_{f_1(1285)} = (24.3 \pm 1.1)$ MeV [10]. The stated three-body decay can, within our model, arise from the sequential decay $f_1(1285) \to \bar{K}^\star K \to \bar{K}K\pi$. Therefore, in this section, we discuss implications of the interaction Lagrangian for the $f_1(1285) \to \bar{K}^\star K$ decay.

The $f_{1N}K^\star K$ interaction Lagrangian from Eq. (6.1) reads

$$\begin{aligned}
\mathcal{L}_{f_{1N}K^\star K} &= A_{f_{1N}K^\star K} f_{1N}^\mu (K_\mu^{\star 0}\bar{K}^0 + K_\mu^{\star +}K^- - \bar{K}_\mu^{\star 0}K^0 - K_\mu^{\star -}K^+) \\
&+ B_{f_{1N}K^\star K} f_{1N}^\mu [(\partial_\nu K_\mu^{\star 0} - \partial_\mu K_\nu^{\star 0})\partial^\nu \bar{K}^0 + (\partial_\nu K_\mu^{\star +} - \partial_\mu K_\nu^{\star +})\partial^\nu K^- \\
&- (\partial_\nu \bar{K}_\mu^{\star 0} - \partial_\mu \bar{K}_\nu^{\star 0})\partial^\nu K^0 - (\partial_\nu K_\mu^{\star -} - \partial_\mu K_\nu^{\star -})\partial^\nu K^+] \\
&+ C_{f_{1N}K^\star K}\partial^\nu f_{1N}^\mu (K_\mu^{\star 0}\partial_\nu \bar{K}^0 - K_\nu^{\star 0}\partial_\mu \bar{K}^0 + K_\mu^{\star +}\partial_\nu K^- - K_\nu^{\star +}\partial_\mu K^- \\
&- \bar{K}_\mu^{\star 0}\partial_\nu K^0 + \bar{K}_\nu^{\star 0}\partial_\mu K^0 - K_\mu^{\star -}\partial_\nu K^+ + K_\nu^{\star -}\partial_\mu K^+)
\end{aligned} \tag{9.104}$$

with the following coefficients:

$$A_{f_{1N}K^\star K} = \frac{i}{4} Z_K \left[ g_1^2 (3\phi_N - \sqrt{2}\phi_S) + h_2(\phi_N - \sqrt{2}\phi_S) - 2h_3\phi_N \right], \tag{9.105}$$

$$B_{f_{1N}K^\star K} = \frac{i}{2} Z_K g_2 w_{K_1}, \tag{9.106}$$

$$C_{f_{1N}K^\star K} = -\frac{i}{2} Z_K g_2 w_{K_1}. \tag{9.107}$$

Let us now turn to the decay process $f_{1S} \to \bar{K}^{\star 0}K^0$ from Eq. (9.104); other decay processes from Eq. (9.104) will be considered by an appropriate isospin factor. Let us denote the momenta of $f_{1N}$, $\bar{K}_\mu^{\star 0}$ and $K^0$ as $P$, $P_1$ and $P_2$. The decay process involves two vector states: $f_{1N}$ and $K^\star$. We therefore have to consider the corresponding polarisation vectors labelled as $\varepsilon_\mu^{(\alpha)}(P)$ for $f_{1N}$ and $\varepsilon_\nu^{(\beta)}(P_1)$ for $K^\star$. Then, upon substituting $\partial^\mu \to -iP^\mu$ for the decaying particle and $\partial^\mu \to iP_{1,2}^\mu$ for the decay products, we obtain the following Lorentz-invariant $f_{1N}\bar{K}^{\star 0}K^0$ scattering amplitude $-i\mathcal{M}_{f_{1N}\to \bar{K}^{\star 0}K^0}^{(\alpha,\beta)}$:

$$\begin{aligned}
-i\mathcal{M}_{f_{1N}\to \bar{K}^{\star 0}K^0}^{(\alpha,\beta)} &= \varepsilon_\mu^{(\alpha)}(P)\varepsilon_\nu^{(\beta)}(P_1) h_{f_{1N}\bar{K}^{\star 0}K^0}^{\mu\nu} = i\varepsilon_\mu^{(\alpha)}(P)\varepsilon_\nu^{(\beta)}(P_1) \\
&\times \{A_{f_{1N}K^\star K} g^{\mu\nu} + [B_{f_{1N}K^\star K}(P_1^\mu P_2^\nu - (P_1 \cdot P_2)g^{\mu\nu}] \\
&+ C_{f_{1N}K^\star K}[(P \cdot P_2)g^{\mu\nu} - P_2^\mu P^\nu]\}
\end{aligned} \tag{9.108}$$

with

$$\begin{aligned}
h_{f_{1N}\bar{K}^{\star 0}K^0}^{\mu\nu} &= i\{A_{f_{1N}K^\star K} g^{\mu\nu} + [B_{f_{1N}K^\star K}(P_1^\mu P_2^\nu - (P_1 \cdot P_2)g^{\mu\nu}] \\
&+ C_{f_{1N}K^\star K}[(P \cdot P_2)g^{\mu\nu} - P_2^\mu P^\nu]\},
\end{aligned} \tag{9.109}$$

where $h^{\mu\nu}_{f_{1N}\bar{K}^{\star 0}K^0}$ denotes the $f_{1N}\bar{K}^{\star 0}K^0$ vertex. We observe that the form of the vertex in Eq. (9.109) is analogous to that of the $a_1\rho\pi$ vertex of Eq. (5.89). Therefore we can use the formulas for the $a_1(1260) \to \rho\pi$ decay amplitude and decay width to calculate $\Gamma_{f_{1S}\to\bar{K}^\star K}$ (naturally, upon substitution of corresponding coefficients: $A_{a_1\rho\pi} \to A_{f_{1N}K^\star K}$, $B_{a_1\rho\pi} \to B_{f_{1N}K^\star K}$, $C_{a_1\rho\pi} \to -C_{f_{1N}K^\star K}$); an isospin factor of four has to be considered to account for the decays $f_{1N} \to \bar{K}^{\star 0}K^0$, $\bar{K}^0K^{\star 0}$, $K^{\star +}K^-$ and $K^{\star -}K^+$. Note that all parameters entering the coefficients $A_{f_{1N}K^\star K}$, $B_{f_{1N}K^\star K}$ and $C_{f_{1N}K^\star K}$ in Eqs. (9.105) - (9.107) are known from Table 8.4; mass values can be found in Table 8.5.

The decay $f_{1N} \to \bar{K}^\star K$ is actually tree-level forbidden if one considers the physical masses of the three resonances concerned: $m^{\text{exp}}_{f_1(1285)} = (1281.8 \pm 0.6)$ MeV $< m^{\text{exp}}_{K^\star} + m^{\text{exp}}_K$ because $m^{\text{exp}}_{K^\star} = (891.66 \pm 0.26)$ MeV and $m^{\text{exp}}_K = (493.677 \pm 0.016)$ MeV. However, our Fit I yields $m_{a_1} = 1396$ MeV and given that (due to the isospin invariance of our model) $m_{f_{1N}} = m_{a_1}$, then the tree-level decay $f_{1N} \to \bar{K}^\star K$ is nonetheless kinematically allowed. The problem is that the value of the parameter $g_2 = -11.2$ possesses a rather large modulus that with all other parameter values leads to

$$\Gamma_{f_{1N}\to\bar{K}^\star K} = 2.15 \text{ GeV}. \tag{9.110}$$

A similar problem was present in Sec. 9.4.1; let us again try to remedy the issue by varying $\Gamma_{\rho\to\pi\pi}$ to decrease $g_2$.

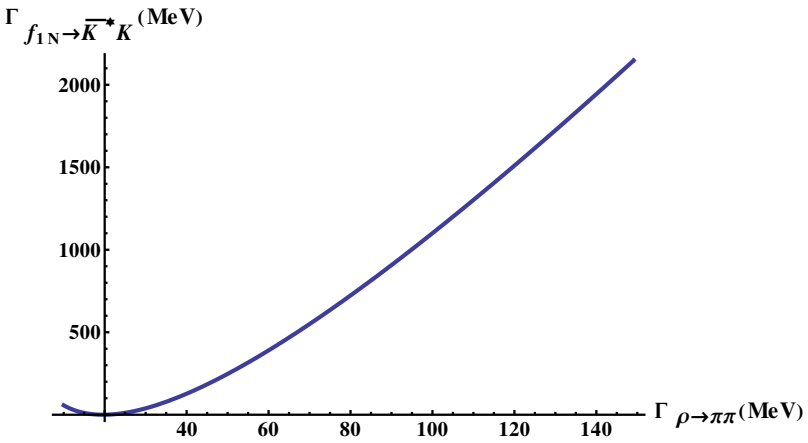


**Figure 9.18:** $\Gamma_{f_{1N}\equiv f_1(1285)\to\bar{K}^\star K}$ as function of $\Gamma_{\rho\to\pi\pi}$.

As apparent from Fig. 9.18, obtaining reasonable values of $\Gamma_{f_{1N}\to\bar{K}^\star K}$ (expected to be $\leq (2.2\pm0.1)$ MeV from the PDG branching ratio for $f_1(1285) \to \bar{K}K\pi$ stated at the beginning of this section) would require $\Gamma_{\rho\to\pi\pi} \simeq 20$ MeV, clearly at odds with experiment [10]. Note that the same holds if one integrates over the spectral function of the $K^\star$ meson (as in Sec. 2.6.2): we obtain $\Gamma_{f_{1N}\to\bar{K}^\star K\to\bar{K}K\pi} = 1.98$ GeV and, again, $\Gamma_{\rho\to\pi\pi} \overset{!}{\sim} 20$ MeV for $\Gamma_{f_{1N}\to\bar{K}^\star K\to\bar{K}K\pi} < 2$ MeV to be true. Thus Fit I yields kaon decay widths of the $f_1(1285)$ resonance that are three orders of magnitude larger than suggested by experimental data.

### 9.4.5 Decay Width $K^\star \to K\pi$ in Fit I

In this section we describe the phenomenology of the vector kaon $K^\star$, the strange counterpart of the $\boldsymbol{\rho}$ state present in our model. Our $K^\star$ state is assigned to $K^\star(892)$. This resonance decays to $\simeq 100\%$ into $K\pi$ [10].
The $K^{\star 0}K\pi$ interaction Lagrangian from Eq. (6.1) reads

$$\begin{aligned}\mathcal{L}_{K^\star K\pi} &= A_{K^\star K\pi}K^{\star 0}_\mu(\pi^0\partial^\mu\bar{K}^0 - \sqrt{2}\pi^+\partial^\mu K^-) + B_{K^\star K\pi}K^{\star 0}_\mu(\bar{K}^0\partial^\mu\pi^0 - \sqrt{2}K^-\partial^\mu\pi^+)\\ &+ C_{K^\star K\pi}\partial_\nu K^{\star 0}_\mu(\partial^\mu\bar{K}^0\partial^\nu\pi^0 - \sqrt{2}\partial^\mu K^-\partial^\nu\pi^+)\\ &+ C^*_{K^\star K\pi}\partial_\nu K^{\star 0}_\mu(\partial^\mu\pi^0\partial^\nu\bar{K}^0 - \sqrt{2}\partial^\mu\pi^+\partial^\nu K^-)\\ &+ A^*_{K^\star K\pi}\bar{K}^{\star 0}_\mu(\pi^0\partial^\mu K^0 - \sqrt{2}\pi^-\partial^\mu K^+) + B^*_{K^\star K\pi}\bar{K}^{\star 0}_\mu(K^0\partial^\mu\pi^0 - \sqrt{2}K^+\partial^\mu\pi^-)\\ &+ C^*_{K^\star K\pi}\partial_\nu\bar{K}^{\star 0}_\mu(\partial^\mu K^0\partial^\nu\pi^0 - \sqrt{2}\partial^\mu K^+\partial^\nu\pi^-)\\ &+ C_{K^\star K\pi}\partial_\nu\bar{K}^{\star 0}_\mu(\partial^\mu\pi^0\partial^\nu K^0 - \sqrt{2}\partial^\mu\pi^-\partial^\nu K^+)\end{aligned} \tag{9.111}$$

with the following coefficients:

$$A_{K^\star K\pi} = \frac{i}{2}Z_\pi Z_K\left[g_1(\sqrt{2}g_1 w_{K_1}\phi_S - 1) - \sqrt{2}h_3 w_{K_1}\phi_S\right], \tag{9.112}$$

$$B_{K^\star K\pi} = \frac{i}{4}Z_\pi Z_K\left[2g_1 + w_{a_1}(-3g_1^2 - h_2 + 2h_3)\phi_N + \sqrt{2}w_{a_1}(g_1^2 + h_2)\phi_S\right], \tag{9.113}$$

$$C_{K^\star K\pi} = \frac{i}{2}Z_\pi Z_K w_{a_1} w_{K_1} g_2. \tag{9.114}$$

The interaction Lagrangian containing $K^{\star\pm}$ is analogous to the Lagrangian presented in Eq. (9.111). Note that the Lagrangian in Eq. (9.111) contains not only the parameter combinations $A_{K^\star K\pi}$, $B_{K^\star K\pi}$ and $C_{K^\star K\pi}$ but also their complex conjugates. This is necessary to ascertain that the Lagrangian is hermitian; indeed we obtain $\mathcal{L}^\dagger_{K^\star K\pi} = \mathcal{L}_{K^\star K\pi}$ upon substituting $A_{K^\star K\pi} \to A^*_{K^\star K\pi}$, $B_{K^\star K\pi} \to B^*_{K^\star K\pi}$, $C_{K^\star K\pi} \to C^*_{K^\star K\pi}$, $K^{\star 0}_\mu \to \bar{K}^{\star 0}_\mu$, $K^0 \to \bar{K}^0$, $K^+ \to K^-$, $\pi^+ \to \pi^-$. In the following we will focus only on the decay $K^{\star 0} \to K\pi$; the corresponding decay of $\bar{K}^{\star 0}$ yields the same result due to isospin symmetry (as do the corresponding $K^{\star\pm}$ decays).
The calculation of $\Gamma_{K^{\star 0}\to K\pi}$ requires knowledge of decay widths in two distinct channels: $K^{\star 0} \to K^0\pi^0$ and $K^{\star 0} \to K^+\pi^-$. (Note the changed charges for the decay products, as in Sec. 9.3). As apparent from Eq. (9.111), these differ by a factor of two: $\Gamma_{K^{\star 0}\to K^+\pi^-} = 2\Gamma_{K^{\star 0}\to K^0\pi^0}$. Then $\Gamma_{K^{\star 0}\to K\pi} = 3\Gamma_{K^{\star 0}\to K^0\pi^0}$. Let us therefore calculate the decay width for the process $K^{\star 0} \to K^0\pi^0$. We denote the momenta of $K^\star$, $\pi$ and $K$ as $P$, $P_1$ and $P_2$, respectively. $K^\star_\mu$ is a vector state for which we have to consider the polarisation vector $\varepsilon^{(\alpha)}_\mu(P)$. Then, upon substituting $\partial^\mu \to -iP^\mu$ for the decaying particle and $\partial^\mu \to iP^\mu_{1,2}$ for the decay products, we obtain the following Lorentz-invariant $K^\star K\pi$ scattering amplitude $-i\mathcal{M}^{(\alpha)}_{K^{\star 0}\to K^0\pi^0}$ from the Lagrangian (9.111):

$$\begin{aligned}-i\mathcal{M}^{(\alpha)}_{K^{\star 0}\to K^0\pi^0} = \varepsilon^{(\alpha)}_\mu(P)h^\mu_{K^\star K\pi} = -\varepsilon^{(\alpha)}_\mu(P)\{&A_{K^\star K\pi}P_2^\mu + B_{K^\star K\pi}P_1^\mu + C_{K^\star K\pi}[P_2^\mu(P\cdot P_1)\\ &- P_1^\mu(P\cdot P_2)]\}\end{aligned} \tag{9.115}$$

with

$$h^\mu_{K^\star K\pi} = -\{A_{K^\star K\pi}P_2^\mu + B_{K^\star K\pi}P_1^\mu + C_{K^\star K\pi}[P_2^\mu(P\cdot P_1) - P_1^\mu(P\cdot P_2)]\}, \tag{9.116}$$

where $h^{\mu}_{K^\star K\pi}$ denotes the $K^\star K\pi$ vertex.

It will be necessary to determine the square of the scattering amplitude in order to calculate the decay width. Given that the scattering amplitude in Eq. (9.115) depends on the polarisation vector $\varepsilon^{(\alpha)}_{\mu}(P)$, it is necessary to calculate the average of the amplitude for all values of $\varepsilon^{(\alpha)}_{\mu}(P)$. This has already been performed in Sec. 5.2.1 for the decay $\rho \to \pi\pi$; we can calculate $|-i\bar{\mathcal{M}}_{K^{\star 0}\to K^0\pi^0}|^2$ in accordance with Eq. (5.38). We first calculate the squared vertex $(h^{\mu}_{K^\star K\pi})^2$ using Eq. (9.115):

$$\begin{aligned}(h^{\mu}_{K^\star K\pi})^2 &= A^2_{K^\star K\pi}m_K^2 + B^2_{K^\star K\pi}m_\pi^2 + C^2_{K^\star K\pi}[P_2^\mu(P\cdot P_1) - P_1^\mu(P\cdot P_2)]^2 \\ &+ 2A_{K^\star K\pi}B_{K^\star K\pi}P_1\cdot P_2 + 2A_{K^\star K\pi}C_{K^\star K\pi}[P\cdot P_1 m_K^2 - (P_1\cdot P_2)(P\cdot P_2)] \\ &+ 2B_{K^\star K\pi}C_{K^\star K\pi}[(P_1\cdot P_2)(P\cdot P_1) - P\cdot P_2 m_\pi^2]. \end{aligned} \tag{9.117}$$

Additionally, again from Eq. (9.115):

$$\begin{aligned}(h^{0}_{K^\star K\pi})^2 &= A^2_{K^\star K\pi}E_K^2 + B^2_{K^\star K\pi}E_\pi^2 + C^2_{K^\star K\pi}[E_K(P\cdot P_1) - E_\pi(P\cdot P_2)]^2 \\ &+ 2A_{K^\star K\pi}B_{K^\star K\pi}E_\pi E_K + 2A_{K^\star K\pi}C_{K^\star K\pi}[(P\cdot P_1)E_K^2 - E_\pi E_K(P\cdot P_2)] \\ &+ 2B_{K^\star K\pi}C_{K^\star K\pi}[E_\pi E_K(P\cdot P_1) - (P\cdot P_2)E_\pi^2]. \end{aligned} \tag{9.118}$$

From Eqs. (5.38), (9.117) and (9.118) we obtain

$$\begin{aligned}|-i\bar{\mathcal{M}}_{K^{\star 0}\to K^0\pi^0}|^2 &= \frac{1}{3}\{(A^2_{K^\star K\pi} + B^2_{K^\star K\pi})k^2(m_{K^\star}, m_K, m_\pi) \\ &+ C^2_{K^\star K\pi}\{k^2(m_{K^\star}, m_K, m_\pi)[(P\cdot P_1)^2 + (P\cdot P_2)^2] \\ &- 2(P\cdot P_1)(P\cdot P_2)(E_\pi E_K - P_1\cdot P_2)\} \\ &+ 2A_{K^\star K\pi}B_{K^\star K\pi}(E_\pi E_K - P_1\cdot P_2) \\ &+ 2A_{K^\star K\pi}C_{K^\star K\pi}[k^2(m_{K^\star}, m_K, m_\pi)P\cdot P_1 - (P\cdot P_2)(E_\pi E_K - P_1\cdot P_2)] \\ &+ 2B_{K^\star K\pi}C_{K^\star K\pi}[(P\cdot P_1)(E_\pi E_K - P_1\cdot P_2) - k^2(m_{K^\star}, m_K, m_\pi)(P\cdot P_2)]\} \\ &= \frac{1}{3}\{\{A^2_{K^\star K\pi} + B^2_{K^\star K\pi} + C^2_{K^\star K\pi}[(P\cdot P_1)^2 + (P\cdot P_2)^2] \\ &+ 2C_{K^\star K\pi}[A_{K^\star K\pi}(P\cdot P_1) - B_{K^\star K\pi}(P\cdot P_2)]\}k^2(m_{K^\star}, m_K, m_\pi) \\ &+ 2\{A_{K^\star K\pi}B_{K^\star K\pi} - C^2_{K^\star K\pi}(P\cdot P_1)(P\cdot P_2) + C_{K^\star K\pi}(B_{K^\star K\pi}P\cdot P_1 \\ &- A_{K^\star K\pi}P\cdot P_2)\}(E_\pi E_K - P_1\cdot P_2)\}. \end{aligned} \tag{9.119}$$

Note that Eq. (9.119) can also be written in a slightly different, but equivalent, manner. To this end, note that the vertex $h^{\mu}_{K^\star K\pi}$ from Eq. (9.116) can be transformed as

$$\begin{aligned}h^{\mu}_{K^\star K\pi} &= -[A_{K^\star K\pi}P_2^\mu + B_{K^\star K\pi}P_1^\mu + C_{K^\star K\pi}(m_{K^\star}E_\pi P_2^\mu - m_{K^\star}E_K P_1^\mu)] \\ &= -(B_{K^\star K\pi} - C_{K^\star K\pi}m_{K^\star}E_K)P_1^\mu - (A_{K^\star K\pi} + C_{K^\star K\pi}m_{K^\star}E_\pi)P_2^\mu. \end{aligned} \tag{9.120}$$

Inserting Eq. (9.120) into Eq. (5.38) yields

$$
\begin{aligned}
|-i\bar{\mathcal{M}}_{K^{\star 0}\to K^0\pi^0}|^2 = \frac{1}{3}\{&-[(B_{K^\star K\pi} - C_{K^\star K\pi} m_{K^\star} E_K) P_1^\mu + (A_{K^\star K\pi} + C_{K^\star K\pi} m_{K^\star} E_\pi) P_2^\mu]^2 \\
&+ \frac{1}{m_{K^\star}^2}[(B_{K^\star K\pi} - C_{K^\star K\pi} m_{K^\star} E_K) P_{1\mu} P^\mu \\
&+ (A_{K^\star K\pi} + C_{K^\star K\pi} m_{K^\star} E_\pi) P_{2\mu} P^\mu]^2\}. \qquad (9.121)
\end{aligned}
$$

Using $P_1 \cdot P = m_{K^\star} E_\pi$ and $P_2 \cdot P = m_{K^\star} E_K$ we obtain from Eq. (9.121)

$$
\begin{aligned}
|-i\bar{\mathcal{M}}_{K^{\star 0}\to K^0\pi^0}|^2 &= \frac{1}{3}[(B_{K^\star K\pi} - C_{K^\star K\pi} m_{K^\star} E_K)^2 + (A_{K^\star K\pi} + C_{K^\star K\pi} m_{K^\star} E_\pi)^2 \\
&- 2(A_{K^\star K\pi} + C_{K^\star K\pi} m_{K^\star} E_\pi)(B_{K^\star K\pi} - C_{K^\star K\pi} m_{K^\star} E_K)] k^2(m_{K^\star}, m_K, m_\pi) \\
&= \frac{1}{3}[A_{K^\star K\pi} - B_{K^\star K\pi} + C_{K^\star K\pi} m_{K^\star}(E_\pi + E_K)]^2 k^2(m_{K^\star}, m_K, m_\pi) \\
&= \frac{1}{3}(A_{K^\star K\pi} - B_{K^\star K\pi} + C_{K^\star K\pi} m_{K^\star}^2)^2 k^2(m_{K^\star}, m_K, m_\pi). \qquad (9.122)
\end{aligned}
$$

Using Eq. (9.122) – or, equivalently, Eq. (9.119) – we obtain the following formula for $\Gamma_{K^{\star 0}\to K^0\pi^0}$:

$$
\Gamma_{K^{\star 0}\to K\pi} = 3\frac{k(m_{K^\star}, m_K, m_\pi)}{8\pi m_{K^\star}^2}|-i\bar{\mathcal{M}}_{K^{\star 0}\to K^0\pi^0}|^2, \qquad (9.123)
$$

where we have used the already discussed equality $\Gamma_{K^{\star 0}\to K\pi} = 3\Gamma_{K^{\star 0}\to K^0\pi^0}$.

Note that all parameters entering Eq. (9.123), i.e., Eqs. (9.112) - (9.114) and (9.122), have been determined uniquely from our Fit I, see Table 8.4. Therefore we can calculate the value of the decay width immediately and obtain

$$
\Gamma_{K^{\star 0}\to K\pi} = 32.8 \text{ MeV}. \qquad (9.124)
$$

The experimental value reads $\Gamma^{\text{exp}}_{K^{\star 0}\to K\pi} = 46.2$ MeV [10]. Therefore, the value obtained within Fit I is by approximately 13 MeV (or 30%) too small.

### 9.4.6 Decay Width $f_1(1420) \to K^\star K$ in Fit I

The $f_1(1420) \equiv f_{1S}$ resonance represents a sharp peak in the $K^\star K$ channel with a mass of $m^{\text{exp}}_{f_1(1420)} = (1426.4 \pm 0.9)$ MeV and width $\Gamma^{\text{exp}}_{f_1(1420)} = (54.9 \pm 2.6)$ MeV [10]. (There are also other decay channels for this resonance but they are subdominant.) As discussed in Sec. 8, Fit I yields a rather large value of $m_{f_1(1420)} = 1643.4$ MeV, see Table 8.5. In this section we address the question whether a value of $\Gamma_{f_1(1420)}$ close to the experimental value $\Gamma^{\text{exp}}_{f_1(1420)}$ can be obtained, thus improving the $f_1(1420)$ phenomenology in Fit I.
The $f_{1S}K^\star K$ interaction Lagrangian from Eq. (6.1) reads

$$
\begin{aligned}
\mathcal{L}_{f_{1S}K^\star K} &= A_{f_{1S}K^\star K} f_{1S}^\mu (K_\mu^{\star 0}\bar{K}^0 + K_\mu^{\star +}K^- - \bar{K}_\mu^{\star 0}K^0 - K_\mu^{\star -}K^+) \\
&+ B_{f_{1S}K^\star K} f_{1S}^\mu [(\partial_\nu K_\mu^{\star 0} - \partial_\mu K_\nu^{\star 0})\partial^\nu \bar{K}^0 + (\partial_\nu K_\mu^{\star +} - \partial_\mu K_\nu^{\star +})\partial^\nu K^- \\
&- (\partial_\nu \bar{K}_\mu^{\star 0} - \partial_\mu \bar{K}_\nu^{\star 0})\partial^\nu K^0 - (\partial_\nu K_\mu^{\star -} - \partial_\mu K_\nu^{\star -})\partial^\nu K^+] \\
&+ C_{f_{1S}K^\star K}\partial^\nu f_{1S}^\mu (K_\mu^{\star 0}\partial_\nu \bar{K}^0 - K_\nu^{\star 0}\partial_\mu \bar{K}^0 + K_\mu^{\star +}\partial_\nu K^- - K_\nu^{\star +}\partial_\mu K^- \\
&- \bar{K}_\mu^{\star 0}\partial_\nu K^0 + \bar{K}_\nu^{\star 0}\partial_\mu K^0 - K_\mu^{\star -}\partial_\nu K^+ + K_\nu^{\star -}\partial_\mu K^+) \qquad (9.125)
\end{aligned}
$$

with

$$A_{f_{1S}K^\star K} = \frac{i}{4} Z_K \left[ g_1^2(\sqrt{2}\phi_N - 6\phi_S) + \sqrt{2} h_2(\phi_N - \sqrt{2}\phi_S) + 4h_3\phi_S \right], \tag{9.126}$$

$$B_{f_{1S}K^\star K} = -\frac{i}{\sqrt{2}} Z_K g_2 w_{K_1}, \tag{9.127}$$

$$C_{f_{1S}K^\star K} = \frac{i}{\sqrt{2}} Z_K g_2 w_{K_1}. \tag{9.128}$$

The Lagrangian (9.125) allows us to calculate the decay width for the process $f_{1S} \to \bar{K}^{\star 0} K^0$. Let us denote the momenta of $f_{1S}$, $\bar{K}^{\star 0}_\mu$ and $K^0$ as $P$, $P_1$ and $P_2$. Two vector states are involved in the decay process: $f_{1S}$ and $K^\star_\mu$. As in Sec. 9.4.4, we consider the corresponding polarisation vectors labelled as $\varepsilon^{(\alpha)}_\mu(P)$ for $f_{1S}$ and $\varepsilon^{(\beta)}_\nu(P_1)$ for $K^\star_\mu$. Then substituting $\partial^\mu \to -iP^\mu$ the for decaying particle and $\partial^\mu \to iP^\mu_{1,2}$ for the decay products, we obtain the following $f_{1S}\bar{K}^{\star 0}K^0$ scattering amplitude $-i\mathcal{M}^{(\alpha,\beta)}_{f_{1S}\to\bar{K}^{\star 0}K^0}$ from the Lagrangian (9.125):

$$\begin{aligned} -i\mathcal{M}^{(\alpha,\beta)}_{f_{1S}\to\bar{K}^{\star 0}K^0} &= \varepsilon^{(\alpha)}_\mu(P)\varepsilon^{(\beta)}_\nu(P_1) h^{\mu\nu}_{f_{1S}\bar{K}^{\star 0}K^0} = i\varepsilon^{(\alpha)}_\mu(P)\varepsilon^{(\beta)}_\nu(P_1) \\ &\quad \times \{A_{f_{1S}K^\star K} g^{\mu\nu} + [B_{f_{1S}K^\star K}(P_1^\mu P_2^\nu - (P_1\cdot P_2)g^{\mu\nu}] \\ &\quad + C_{f_{1S}K^\star K}[(P\cdot P_2)g^{\mu\nu} - P_2^\mu P^\nu]\} \end{aligned} \tag{9.129}$$

with

$$\begin{aligned} h^{\mu\nu}_{f_{1S}\bar{K}^{\star 0}K^0} &= i\{A_{f_{1S}K^\star K} g^{\mu\nu} + [B_{f_{1S}K^\star K}(P_1^\mu P_2^\nu - (P_1\cdot P_2)g^{\mu\nu}] \\ &\quad + C_{f_{1S}K^\star K}[(P\cdot P_2)g^{\mu\nu} - P_2^\mu P^\nu]\}, \end{aligned} \tag{9.130}$$

where $h^\mu_{f_{1S}\bar{K}^{\star 0}K^0}$ denotes the $f_{1S}\bar{K}^{\star 0}K^0$ vertex. The vertex in Eq. (9.130) is analogous to the $a_1\rho\pi$ vertex of Eq. (5.89). Therefore we can use the formulas for the $a_1(1260) \to \rho\pi$ decay amplitude and decay width to calculate $\Gamma_{f_{1S}\to\bar{K}^\star K}$. The corresponding coefficients in the two vertices have to be substituted: $A_{a_1\rho\pi} \to A_{f_{1S}K^\star K}$, $B_{a_1\rho\pi} \to B_{f_{1S}K^\star K}$, $C_{a_1\rho\pi} \to -C_{f_{1S}K^\star K}$ and an isospin factor of four has to be considered to account for the decays $f_{1S} \to \bar{K}^{\star 0}K^0$, $\bar{K}^0 K^{\star 0}$, $K^{\star +}K^-$ and $K^{\star -}K^+$. However, as in Sec. 9.4.4, the large modulus of the parameter $g_2 = -11.2$ (see Table 8.4) leads to

$$\Gamma_{f_{1S}\to\bar{K}^\star K} = 17.6 \text{ GeV}. \tag{9.131}$$

This value is in stark contrast to the one reported by the PDG: $\Gamma^{\text{exp}}_{f_1(1420)} = (54.9 \pm 2.6)$ MeV. Therefore Fit I, where the scalar meson states are assumed to be under 1 GeV, yields a very poor phenomenology of the strange axial-vector isosinglet: $m_{f_1(1420)} = 1643.4$ MeV is by approximately 200 MeV too large and $\Gamma_{f_{1S}\to\bar{K}^\star K} = 17.6$ GeV is unphysical (as it is two orders of magnitude too large). Note that we have obtained similarly large values of $\Gamma_{a_1(1260)\to\rho\pi} \approx 13$ GeV in Sec. 9.4.1 and of $\Gamma_{f_{1N}\to\bar{K}^\star K} \approx 2$ GeV in Sec. 9.4.4, again due to the large value of $g_2$.
Analogously to considerations in the mentioned sections, let us vary $\Gamma_{\rho\to\pi\pi}$ to examine the corresponding change of $\Gamma_{f_{1S}\to\bar{K}^\star K}$, as $\Gamma_{\rho\to\pi\pi}$ determines $g_2$ uniquely.
We observe from Fig. 9.19 that $\Gamma_{f_{1S}\to\bar{K}^\star K}$ corresponds to $\Gamma^{\text{exp}}_{f_1(1420)} = (54.9 \pm 2.6)$ MeV only if $\Gamma_{\rho\to\pi\pi} \sim 30$ MeV. Thus we would require $\Gamma_{\rho\to\pi\pi}$ that is approximately 120 MeV smaller than

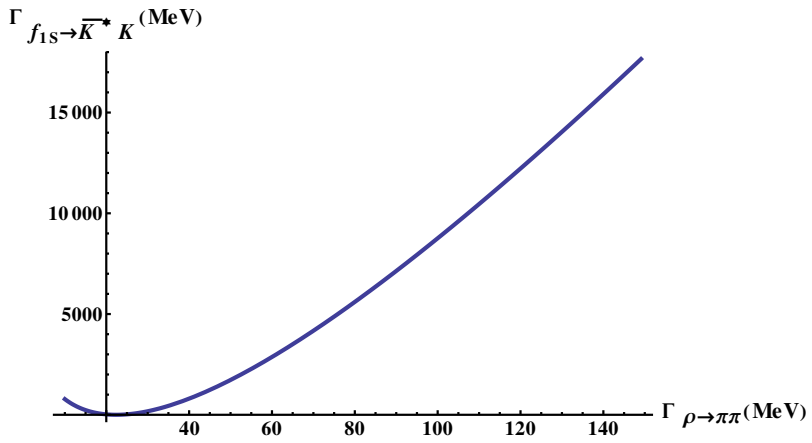


**Figure 9.19:** $\Gamma_{f_{1S}\equiv f_1(1420)\to\bar{K}^\star K}$ as function of $\Gamma_{\rho\to\pi\pi}$.

$\Gamma^{\rm exp}_{\rho\to\pi\pi}$. Consequently, there is tension between $\Gamma_{f_{1S}\to\bar{K}^\star K}$ and $\Gamma_{\rho\to\pi\pi}$ as it is not possible to obtain physical values simultaneously for both decay widths. This problem is analogous to the one described in Sec. 9.4.1 for $\Gamma_{a_1(1260)\to\rho\pi}$ and in Sec. 9.4.4 for $\Gamma_{f_{1N}\to\bar{K}^\star K}$ and represents an additional difficulty for Fit I.

### 9.4.7 $K_1$ Decays in Fit I

We have seen at the end of Sec. 8 that Fit I yields $m_{K_1} = 1520$ MeV, a value that is significantly larger than the mass of the resonance $K_1(1270)$ to which our $K_1$ state was assigned in Sec. 6.2. For this reason, we have reassigned our $K_1$ state to $K_1(1400)$ because the mass of this resonance $[m_{K_1(1400)} = (1403 \pm 7)$ MeV] corresponds better to the value of $m_{K_1}$ obtained from our Fit I. In this section we discuss whether it is possible to obtain a correct value for the decay width of the $K_1$ field [the experimental result reads $\Gamma_{K_1(1400)} = (174 \pm 13)$ MeV]. To this end, we will consider all hadronic decays of $K_1(1400)$ that can be calculated within our model: $K_1(1400) \to K^\star\pi$, $\rho K$ and $\omega K$.

We present the relevant interaction Lagrangians in a single equation:

$$
\begin{aligned}
\mathcal{L}_{K_1} &= A_{K_1K^\star\pi} K_1^{\mu 0}\left(\bar{K}_\mu^{\star 0}\pi^0 - \sqrt{2}K_\mu^{\star -}\pi^+\right) \\
&+ B_{K_1K^\star\pi}\left\{K_1^{\mu 0}\left[\left(\partial_\nu\bar{K}_\mu^{\star 0} - \partial_\mu\bar{K}_\nu^{\star 0}\right)\partial^\nu\pi^0 - \sqrt{2}\left(\partial_\nu K_\mu^{\star -} - \partial_\mu K_\nu^{\star -}\right)\partial^\nu\pi^+\right]\right. \\
&\left.+\partial^\nu K_1^{\mu 0}\left[\left(\bar{K}_\nu^{\star 0}\partial_\mu\pi^0 - \bar{K}_\mu^{\star 0}\partial_\nu\pi^0\right) - \sqrt{2}\left(K_\nu^{\star -}\partial_\mu\pi^+ - K_\mu^{\star -}\partial_\nu\pi^+\right)\right]\right\} \\
&+ A_{K_1\rho K} K_1^{\mu 0}\left(\rho_\mu^0\bar{K}^0 - \sqrt{2}\rho_\mu^+ K^-\right) \\
&+ B_{K_1\rho K}\left\{K_1^{\mu 0}\left[\left(\partial_\nu\rho_\mu^0 - \partial_\mu\rho_\nu^0\right)\partial^\nu\bar{K}^0 - \sqrt{2}\left(\partial_\nu\rho_\mu^+ - \partial_\mu\rho_\nu^+\right)\partial^\nu K^-\right]\right. \\
&\left.+\partial^\nu K_1^{\mu 0}\left[\left(\rho_\nu^0\partial_\mu\bar{K}^0 - \rho_\mu^0\partial_\nu\bar{K}^0\right) - \sqrt{2}\left(\rho_\nu^+\partial_\mu K^- - \rho_\mu^+\partial_\nu K^-\right)\right]\right\} \\
&+ A_{K_1\omega_N K} K_1^{\mu 0}\omega_{N\mu}\bar{K}^0 + B_{K_1\omega_N K}\left[K_1^{\mu 0}\left(\partial_\nu\omega_{N\mu} - \partial_\mu\omega_{N\nu}\right)\partial^\nu\bar{K}^0\right. \\
&\left.+\partial^\nu K_1^{\mu 0}\left(\omega_{N\nu}\partial_\mu\bar{K}^0 - \omega_{N\mu}\partial_\nu\bar{K}^0\right)\right]
\end{aligned}
\tag{9.132}
$$

with

$$A_{K_1K^\star\pi} = \frac{i}{\sqrt{2}} Z_\pi (h_3 - g_1^2)\phi_S, \tag{9.133}$$

$$B_{K_1K^\star\pi} = -\frac{i}{2} Z_\pi g_2 w_{a_1}, \tag{9.134}$$

$$A_{K_1\rho K} = \frac{i}{4} Z_K \left[ g_1^2(\phi_N + \sqrt{2}\phi_S) - h_2(\phi_N - \sqrt{2}\phi_S) - 2h_3\phi_N \right], \tag{9.135}$$

$$B_{K_1\rho K} = \frac{i}{2} Z_K g_2 w_{K_1}, \tag{9.136}$$

$$A_{K_1\omega_N K} = -\frac{i}{4} Z_K [g_1^2(\phi_N + \sqrt{2}\phi_S) - h_2(\phi_N - \sqrt{2}\phi_S) - 2h_3\phi_N], \tag{9.137}$$

$$B_{K_1\omega_N K} = -\frac{i}{2} Z_K g_2 w_{K_1}. \tag{9.138}$$

We observe from Eq. (9.132) that the interaction Lagrangians for the decay processes $K_1^0 \to K^{\star 0}\pi^0$, $K_1^0 \to \rho^0 K^0$ and $K_1^0 \to \omega_N K^0$ possess the same form:

$$\begin{aligned} \mathcal{L}_{K_1} &= A_{K_1} K_1^{\mu 0} V_\mu^0 \bar{P}^0 \\ &\quad + B_{K_1} \left[ K_1^{\mu 0} \left( \partial_\nu V_\mu^0 - \partial_\mu V_\nu^0 \right) \partial^\nu \bar{P}^0 + \partial^\nu K_1^{\mu 0} \left( V_\nu^0 \partial_\mu \bar{P}^0 - V_\mu^0 \partial_\nu \bar{P}^0 \right) \right], \end{aligned} \tag{9.139}$$

where $A_{K_1} = \{A_{K_1K^\star\pi}, A_{K_1\rho K}, A_{K_1\omega_N K}\}$, $B_{K_1} = \{B_{K_1K^\star\pi}, B_{K_1\rho K}, B_{K_1\omega_N K}\}$, $V_\mu = \{\bar{K}_\mu^\star, \rho_\mu, \omega_{N\mu}\}$ and $\bar{P} = \{\pi, \bar{K}\}$. Let us therefore consider a generic decay process of the form $K_1 \to V^0\bar{P}^0$ [if applicable, the contribution of the decays into charged modes to the full decay width will be larger by a factor of two than the contribution of the neutral modes, see Eq. (9.132)].
To this end, we denote the momenta of $K_1$, $V$ and $\bar{P}$ as $P$, $P_1$ and $P_2$, respectively. The stated decay process involves two vector states: $K_1$ and $V$. As in Sec. 2.6.2, we have to consider the corresponding polarisation vectors; let us denote them as $\varepsilon_\mu^{(\alpha)}(P)$ for $K_1$ and $\varepsilon_\nu^{(\beta)}(P_1)$ for $V$. Consequently, upon substituting $\partial^\mu \to -iP^\mu$ for the decaying particle and $\partial^\mu \to iP_{1,2}^\mu$ for the decay products, we obtain the following Lorentz-invariant $K_1V\bar{P}$ scattering amplitude $-i\mathcal{M}_{K_1\to V^0\bar{P}^0}^{(\alpha,\beta)}$:

$$\begin{aligned} -i\mathcal{M}_{K_1\to V^0\bar{P}^0}^{(\alpha,\beta)} &= \varepsilon_\mu^{(\alpha)}(P)\varepsilon_\nu^{(\beta)}(P_1) h_{K_1V\bar{P}}^{\mu\nu} = i\varepsilon_\mu^{(\alpha)}(P)\varepsilon_\nu^{(\beta)}(P_1) \\ &\quad \times A_{K_1} g^{\mu\nu} + B_{K_1} \left[ P_1^\mu P_2^\nu + P_2^\mu P^\nu - (P_1 \cdot P_2) g^{\mu\nu} - (P \cdot P_2) g^{\mu\nu} \right] \end{aligned} \tag{9.140}$$

with

$$h_{K_1V\bar{P}}^{\mu\nu} = i \left\{ A_{K_1} g^{\mu\nu} + B_{K_1} [P_1^\mu P_2^\nu + P_2^\mu P^\nu - (P_1 \cdot P_2) g^{\mu\nu} - (P \cdot P_2) g^{\mu\nu}] \right\}, \tag{9.141}$$

where $h_{K_1V\bar{P}}^{\mu\nu}$ denotes the $K_1V\bar{P}$ vertex.
The vertex of Eq. (9.141) corresponds to the vertex of Eq. (2.183). We can therefore utilise the decay width formula derived in Sec. 2.6.2 for a generic decay of an axial-vector state into a vector and a pseudoscalar state. Setting $A_{AV\tilde{P}} \equiv A_{K_1}$ and $B_{AV\tilde{P}} \equiv B_{K_1}$ in the Lagrangian (2.181) we obtain from Eq. (2.188)

$$\Gamma_{K_1\to V\bar{P}} = I \frac{k(m_{K_1}, m_V, m_{\bar{P}})}{8\pi m_{K_1}^2} | - i\bar{\mathcal{M}}_{K_1\to V^0\bar{P}^0}|^2 \tag{9.142}$$

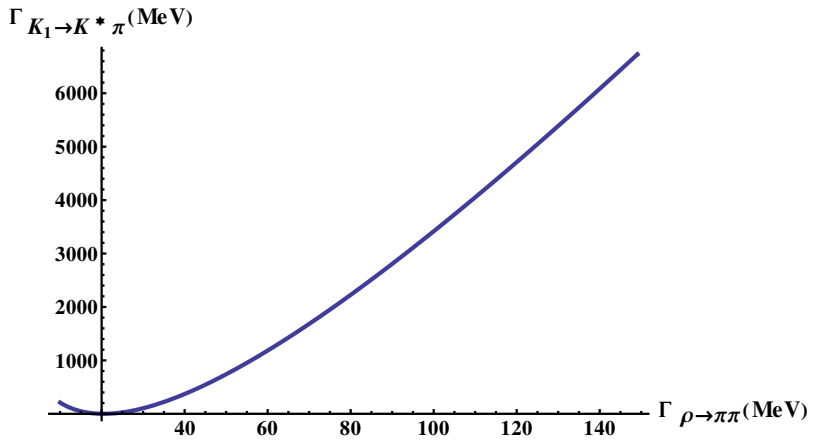


**Figure 9.20:** $\Gamma_{K_1\to K^\star\pi}$ as function of $\Gamma_{\rho\to\pi\pi}$.

with the isospin factor $I = 3$ for $K_1 \to K^\star\pi$ and $K_1 \to \rho K$ and $I = 1$ for $K_1 \to \omega K$ – as apparent from Eq. (9.132), the decay width into charged modes (if applicable) will be larger by a factor of two than the decay width into neutral modes.
We turn now to the discussion of results for the three decays in Eq. (9.132).

### Decay Width $K_1 \to K^\star\pi$

In this case we set $V^0 \equiv K^\star$ and $\bar{P} \equiv \pi$ in Eq. (9.142). Given that all parameters entering Eqs. (9.133) and (9.134) are known from Table 8.4, we consequently obtain the following value of the decay width

$$\Gamma_{K_1\to K^\star\pi} = 6.73 \text{ GeV}. \tag{9.143}$$

This decay width suffers from the same issues as the decay widths in Sections 9.4.1, 9.4.4 and 9.4.6: if we vary $\Gamma_{\rho\to\pi\pi}$ to ascertain whether $\Gamma_{K_1\to K^\star\pi}$ can be sufficiently decreased, then the dependence in Fig. 9.20 is obtained. It is apparent from Fig. 9.20 that $\Gamma_{\rho\to\pi\pi}$ would have to be decreased by approximately 120 MeV for $\Gamma_{K_1(1400)\to K^\star\pi} = (164 \pm 16)$ MeV [10] to be obtained. The value in Eq. (9.143) is thus by an order of magnitude too large.

### Decay Width $K_1 \to \rho K$

As in the case of $\Gamma_{K_1\to K^\star\pi}$, we use the parameter values from Table 8.4 to calculate the coefficients in Eqs. (9.135) and (9.136). Again, there is no freedom to adjust parameters as they are uniquely determined from the fit. We obtain from Eq. (9.142)

$$\Gamma_{K_1\to\rho K} = 4.77 \text{ GeV}. \tag{9.144}$$

This value is of the same order of magnitude as the one in Eq. (9.143), and equally unphysical. Additionally, the value in Eq. (9.144) cannot be sufficiently decreased to $\Gamma_{K_1(1400)\to\rho K} = (2.1 \pm 1.1)$ MeV [10] unless $\Gamma_{\rho\to\pi\pi} \simeq 25$ MeV, see Fig. 9.21. The value of Eq. (9.144) is thus by three orders of magnitude too large.

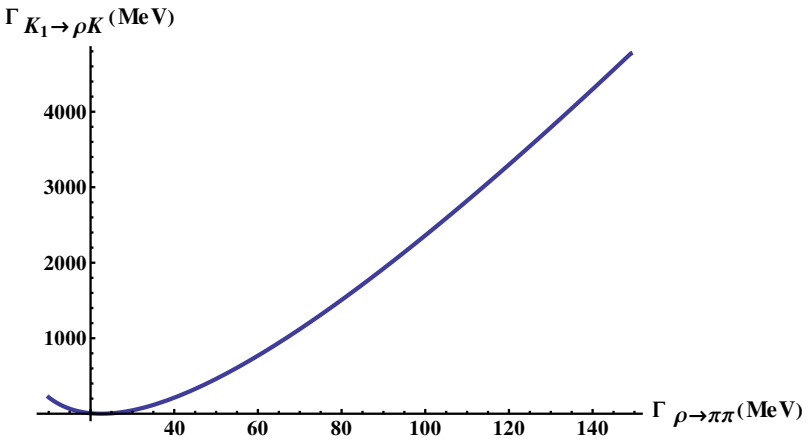


**Figure 9.21:** $\Gamma_{K_1\to\rho K}$ as function of $\Gamma_{\rho\to\pi\pi}$.

### Decay Width $K_1 \to \omega_N K$

Similarly to the previous two $K_1$ decays, we obtain from Eqs. (9.137), (9.138) and (9.142) and Table 8.4:

$$\Gamma_{K_1\to\omega_N K} = 1.59 \text{ GeV}. \tag{9.145}$$

This value is also dramatically larger than the physical value $\Gamma_{K_1(1400)\to\omega K} = (1.7 \pm 1.7)$ MeV [10]. The large value of $\Gamma_{K_1\to\omega_N K}$ is decreased to the physical value of the $K_1(1400)$ decay width in this channel only if $\Gamma_{\rho\to\pi\pi} \simeq 25$ MeV is considered, see Fig. 9.22. The value of Eq. (9.145) is thus by three orders of magnitude too large.

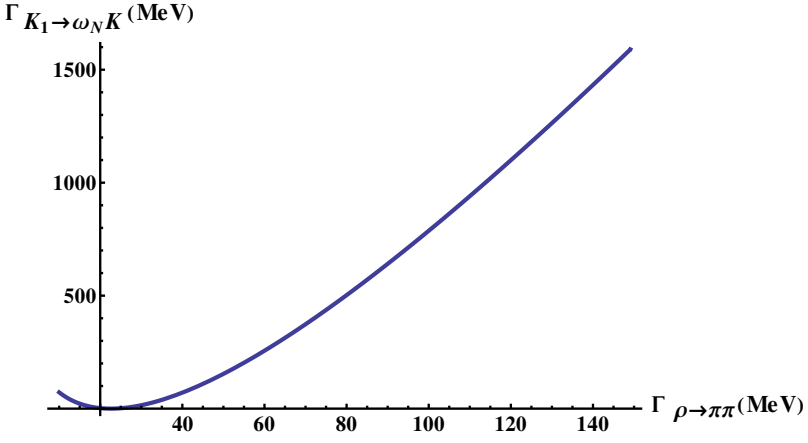


**Figure 9.22:** $\Gamma_{K_1\to\omega_N K}$ as function of $\Gamma_{\rho\to\pi\pi}$.

The $K_1$ phenomenology is therefore very poorly described in Fit I. Combined results of Eqs. (9.143), (9.144) and (9.145) suggest that the full decay width of the $K_1(1400)$ resonance should be $\sim 10$ GeV, two orders of magnitude larger than the experimental value $\Gamma_{K_1(1400)} = (174 \pm 13)$ MeV [10]. Such a resonance would then not be observable in the physical spectrum. These results are consequently another indication that the fit with the scalar states below 1 GeV is not

favoured.

Let us also note that the stated results for the decay widths $\Gamma_{K_1\to K^\star\pi}$, $\Gamma_{K_1\to\rho K}$ and $\Gamma_{K_1\to\omega K}$ would all require similar values of $\Gamma_{\rho\to\pi\pi}\sim(25-30)$ MeV. This in turn implies that $g_2\sim 14$ would be needed for the $K_1(1400)$ decays to be described properly, see Fig. 9.23. On the other hand, $g_2=-11.2$ used throughout this chapter is obtained under the condition that $\Gamma_{\rho\to\pi\pi}=149.1$ MeV $=\Gamma^{\rm exp}_{\rho\to\pi\pi}$. We thus have $g_2$ with the needed modulus, but the sign of $g_2$ leads to the mentioned bad results regarding the $K_1(1400)$ decay width.

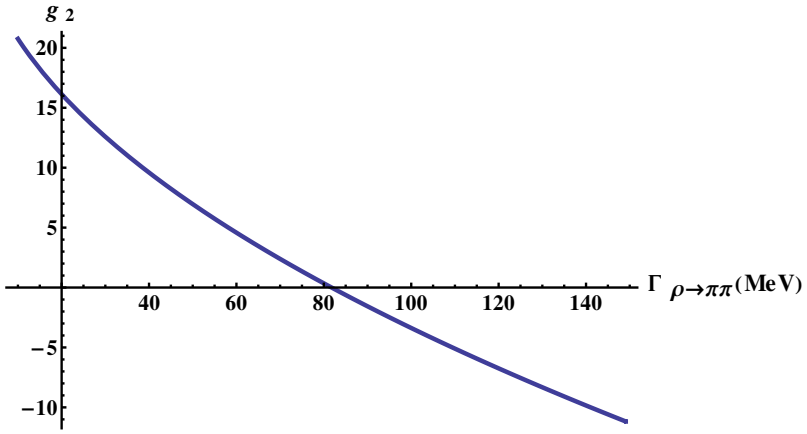


**Figure 9.23:** Parameter $g_2$ as function of $\Gamma_{\rho\to\pi\pi}$.

Let us nonetheless consider $\pi\pi$ scattering lengths as well, just as in Scenario I of the $U(2)\times U(2)$ version of the model.

## 9.5 Pion-Pion Scattering Lengths

In this section we calculate the $\pi\pi$ scattering lengths at threshold, analogously to the calculation already performed in the two-flavour version of the model (see Sec. 5.2.8). The main difference to the calculation in the two-flavour case lies in the fact that now the inclusion of an additional (pure strange) scalar isosinglet $\sigma_S$ generates an additional mixed (and predominantly strange) scalar isosinglet field ($\sigma_2$) that in principle also influences the $\pi\pi$ scattering. Note that an explicit calculation of the $\pi\pi$ scattering terms yields no further contributing terms other than those already mentioned here and in Sec. 5.2.8 – i.e., "pure" $\pi\pi$ scattering (contact scattering) and scattering via virtual $\sigma$ and $\rho$ mesons. The former are represented only by $\sigma_N$ in the two-flavour version of the model and by $\sigma_{1,2}$ in the current version of the model. Therefore, we have to modify the $\pi\pi$ scattering amplitude to include the contribution from the additional scalar field. This is implemented by considering the $\sigma\pi\pi$ Lagrangian $\mathcal{L}_{\sigma\pi\pi}$, Eq. (9.27), and substituting the pure fields $\sigma_{N,S}$ by the mixed fields $\sigma_{1,2}$. To this end, let us rewrite $\mathcal{L}_{\sigma\pi\pi}$ in the following way:

$$\begin{aligned}\mathcal{L}_{\sigma\pi\pi} &= (A_{\sigma_N\pi\pi}\cos\varphi_\sigma + A_{\sigma_S\pi\pi}\sin\varphi_\sigma)\sigma_1\boldsymbol{\pi}^2 + B_{\sigma_N\pi\pi}\cos\varphi_\sigma\sigma_1(\partial_\mu\boldsymbol{\pi})^2 + C_{\sigma_N\pi\pi}\cos\varphi_\sigma\sigma_1\boldsymbol{\pi}\cdot\Box\boldsymbol{\pi}\\ &+ (-A_{\sigma_N\pi\pi}\sin\varphi_\sigma + A_{\sigma_S\pi\pi}\cos\varphi_\sigma)\sigma_2\boldsymbol{\pi}^2 - B_{\sigma_N\pi\pi}\sin\varphi_\sigma\sigma_2(\partial_\mu\boldsymbol{\pi})^2 - C_{\sigma_N\pi\pi}\sin\varphi_\sigma\sigma_2\boldsymbol{\pi}\cdot\Box\boldsymbol{\pi}\end{aligned} \tag{9.146}$$

with $A_{\sigma_N\pi\pi}$, $B_{\sigma_N\pi\pi}$, $C_{\sigma_N\pi\pi}$ and $A_{\sigma_S\pi\pi}$ from Eqs. (9.28) - (9.31); for simplicity, we have also made use of $B_{\sigma_S\pi\pi} \sim h_1 = 0$, Eq. (9.32).

Then we obtain the following contribution from the the $\pi\pi\sigma$ vertex to the scattering amplitude $\mathcal{M}_{\pi\pi}$ (the calculation is analogous to the one described in Ref. [220]):

$$\begin{aligned}
\mathcal{M}_{\pi\pi}(s,t,u) \sim & -i\,\delta^{ab}\delta^{cd}[-2m_\pi^2 C_{\sigma_N\pi\pi}\cos\varphi_\sigma + B_{\sigma_N\pi\pi}\cos\varphi_\sigma(2m_\pi^2 - s) + 2(A_{\sigma_N\pi\pi}\cos\varphi_\sigma \\
& + A_{\sigma_S\pi\pi}\sin\varphi_\sigma)]^2 \frac{1}{s - m_{\sigma_1}^2} \\
& - i\,\delta^{ac}\delta^{bd}\,[-2m_\pi^2 C_{\sigma_N\pi\pi}\cos\varphi_\sigma + B_{\sigma_N\pi\pi}\cos\varphi_\sigma(2m_\pi^2 - t) + 2(A_{\sigma_N\pi\pi}\cos\varphi_\sigma \\
& + A_{\sigma_S\pi\pi}\sin\varphi_\sigma)]^2 \frac{1}{t - m_{\sigma_1}^2} \\
& - i\,\delta^{ad}\delta^{bc}[-2m_\pi^2 C_{\sigma_N\pi\pi}\cos\varphi_\sigma + B_{\sigma_N\pi\pi}\cos\varphi_\sigma(2m_\pi^2 - u) + 2(A_{\sigma_N\pi\pi}\cos\varphi_\sigma \\
& + A_{\sigma_S\pi\pi}\sin\varphi_\sigma)]^2 \frac{1}{u - m_{\sigma_1}^2} \\
& - i\,\delta^{ab}\delta^{cd}[2m_\pi^2 C_{\sigma_N\pi\pi}\sin\varphi_\sigma - B_{\sigma_N\pi\pi}\sin\varphi_\sigma(2m_\pi^2 - s) + 2(A_{\sigma_S\pi\pi}\cos\varphi_\sigma \\
& - A_{\sigma_N\pi\pi}\sin\varphi_\sigma)]^2 \frac{1}{s - m_{\sigma_2}^2} \\
& - i\,\delta^{ac}\delta^{bd}\,[2m_\pi^2 C_{\sigma_N\pi\pi}\sin\varphi_\sigma - B_{\sigma_N\pi\pi}\sin\varphi_\sigma(2m_\pi^2 - t) + 2(A_{\sigma_S\pi\pi}\cos\varphi_\sigma \\
& - A_{\sigma_N\pi\pi}\sin\varphi_\sigma)]^2 \frac{1}{t - m_{\sigma_2}^2} \\
& - i\,\delta^{ad}\delta^{bc}[2m_\pi^2 C_{\sigma_N\pi\pi}\sin\varphi_\sigma - B_{\sigma_N\pi\pi}\sin\varphi_\sigma(2m_\pi^2 - u) + 2(A_{\sigma_S\pi\pi}\cos\varphi_\sigma \\
& - A_{\sigma_N\pi\pi}\sin\varphi_\sigma)]^2 \frac{1}{u - m_{\sigma_2}^2}. \qquad (9.147)
\end{aligned}$$

Let us now rewrite the $\pi\pi$ scattering amplitude of Eqs. (5.98) in the following way [we substitute $A_{\rho\pi\pi}$ and $B_{\rho\pi\pi}$ present in Eqs. (5.99) - (5.101) by terms in Eqs. (5.32) and (5.33)]:

$$\begin{aligned}
\mathcal{M}_{\pi\pi}(s,t,u) = & i\delta^{ab}\delta^{cd}\left\{(g_1^2 - h_3)Z_\pi^4 w_{a_1}^2 s - 2\left(\lambda_1 + \frac{\lambda_2}{2}\right)Z_\pi^4 - (h_1 + h_2 + h_3)Z_\pi^4 w_{a_1}^2(s - 2m_\pi^2)\right. \\
& -[-2m_\pi^2 C_{\sigma_N\pi\pi}\cos\varphi_\sigma + B_{\sigma_N\pi\pi}\cos\varphi_\sigma(2m_\pi^2 - s) + 2(A_{\sigma_N\pi\pi}\cos\varphi_\sigma \\
& + A_{\sigma_S\pi\pi}\sin\varphi_\sigma)]^2 \frac{1}{s - m_{\sigma_1}^2} \\
& - [2m_\pi^2 C_{\sigma_N\pi\pi}\sin\varphi_\sigma - B_{\sigma_N\pi\pi}\sin\varphi_\sigma(2m_\pi^2 - s) + 2(A_{\sigma_S\pi\pi}\cos\varphi_\sigma \\
& - A_{\sigma_N\pi\pi}\sin\varphi_\sigma)]^2 \frac{1}{s - m_{\sigma_2}^2} \\
& + Z_\pi^4\left[g_1(1 - g_1 w_{a_1}\phi_N) + h_3 w_{a_1}\phi_N - g_2 w_{a_1}^2\frac{t}{2}\right]^2 \frac{u - s}{t - m_\rho^2} \\
& \left. + Z_\pi^4\left[g_1(1 - g_1 w_{a_1}\phi_N) + h_3 w_{a_1}\phi_N - g_2 w_{a_1}^2\frac{u}{2}\right]^2 \frac{t - s}{u - m_\rho^2}\right\} \\
& + i\delta^{ac}\delta^{bd}\left\{(g_1^2 - h_3)Z_\pi^4 w_{a_1}^2 t - 2\left(\lambda_1 + \frac{\lambda_2}{2}\right)Z_\pi^4 - (h_1 + h_2 + h_3)Z_\pi^4 w_{a_1}^2(t - 2m_\pi^2)\right.
\end{aligned}$$

$$
\begin{aligned}
&-[-2m_\pi^2 C_{\sigma_N\pi\pi}\cos\varphi_\sigma + B_{\sigma_N\pi\pi}\cos\varphi_\sigma(2m_\pi^2 - t) + 2(A_{\sigma_N\pi\pi}\cos\varphi_\sigma \\
&+A_{\sigma_S\pi\pi}\sin\varphi_\sigma)]^2\frac{1}{t-m_{\sigma_1}^2} \\
&-[2m_\pi^2 C_{\sigma_N\pi\pi}\sin\varphi_\sigma - B_{\sigma_N\pi\pi}\sin\varphi_\sigma(2m_\pi^2 - t) + 2(A_{\sigma_S\pi\pi}\cos\varphi_\sigma \\
&-A_{\sigma_N\pi\pi}\sin\varphi_\sigma)]^2\frac{1}{t-m_{\sigma_2}^2} \\
&+Z_\pi^4\left[g_1(1-g_1w_{a_1}\phi_N) + h_3 w_{a_1}\phi_N - g_2 w_{a_1}^2\frac{s}{2}\right]^2\ \frac{u-t}{s-m_\rho^2} \\
&+Z_\pi^4\left[g_1(1-g_1w_{a_1}\phi_N) + h_3 w_{a_1}\phi_N - g_2 w_{a_1}^2\frac{u}{2}\right]^2\ \frac{s-t}{u-m_\rho^2}\Bigg\} \\
&+\ i\,\delta^{ad}\delta^{bc}\left\{(g_1^2-h_3)Z_\pi^4 w_{a_1}^2 u - 2\left(\lambda_1+\frac{\lambda_2}{2}\right)Z_\pi^4 - (h_1+h_2+h_3)Z_\pi^4 w_{a_1}^2(u-2m_\pi^2)\right. \\
&-[-2m_\pi^2 C_{\sigma_N\pi\pi}\cos\varphi_\sigma + B_{\sigma_N\pi\pi}\cos\varphi_\sigma(2m_\pi^2 - u) + 2(A_{\sigma_N\pi\pi}\cos\varphi_\sigma \\
&+A_{\sigma_S\pi\pi}\sin\varphi_\sigma)]^2\frac{1}{u-m_{\sigma_1}^2} \\
&-[2m_\pi^2 C_{\sigma_N\pi\pi}\sin\varphi_\sigma - B_{\sigma_N\pi\pi}\sin\varphi_\sigma(2m_\pi^2 - u) + 2(A_{\sigma_S\pi\pi}\cos\varphi_\sigma \\
&-A_{\sigma_N\pi\pi}\sin\varphi_\sigma)]^2\frac{1}{u-m_{\sigma_2}^2} \\
&+Z_\pi^4\left[g_1(1-g_1w_{a_1}\phi_N) + h_3 w_{a_1}\phi_N - g_2 w_{a_1}^2\frac{s}{2}\right]^2\ \frac{t-u}{s-m_\rho^2} \\
&+Z_\pi^4\left[g_1(1-g_1w_{a_1}\phi_N) + h_3 w_{a_1}\phi_N - g_2 w_{a_1}^2\frac{t}{2}\right]^2\ \frac{s-u}{t-m_\rho^2}\Bigg\} \\
&\equiv i\delta^{ab}\delta^{cd}A(s,t,u) + i\delta^{ac}\delta^{bd}A(t,u,s) + \ i\,\delta^{ad}\delta^{bc}A(u,s,t).
\end{aligned}
\tag{9.148}
$$

We can now consider the three components of the scattering amplitude at threshold.

$$
\begin{aligned}
A(s,t,u)|_{s=4m_\pi^2} &= 4(g_1^2-h_3)Z_\pi^4 w_{a_1}^2 m_\pi^2 - 2\left(\lambda_1+\frac{\lambda_2}{2}\right)Z_\pi^4 - 2(h_1+h_2+h_3)Z_\pi^4 w_{a_1}^2 m_\pi^2 \\
&\quad - 4[(B_{\sigma_N\pi\pi}+C_{\sigma_N\pi\pi})m_\pi^2\cos\varphi_\sigma - (A_{\sigma_N\pi\pi}\cos\varphi_\sigma + A_{\sigma_S\pi\pi}\sin\varphi_\sigma)]^2\frac{1}{4m_\pi^2-m_{\sigma_1}^2} \\
&\quad - 4[(B_{\sigma_N\pi\pi}+C_{\sigma_N\pi\pi})m_\pi^2\sin\varphi_\sigma + (A_{\sigma_S\pi\pi}\cos\varphi_\sigma - A_{\sigma_N\pi\pi}\sin\varphi_\sigma)]^2\frac{1}{4m_\pi^2-m_{\sigma_2}^2} \\
&\quad + 8[g_1 Z_\pi^2(1-g_1w_{a_1}\phi_N) + h_3 Z_\pi^2 w_{a_1}\phi_N]^2\frac{m_\pi^2}{m_\rho^2}.
\end{aligned}
\tag{9.149}
$$

Using Eq. (6.28) we can transform the last line of Eq. (9.149) in the following way:

$$
\begin{aligned}
1 - g_1 w_{a_1}\phi_N = 1 - \frac{g_1^2\phi_N^2}{m_{a_1}^2} &= \frac{m_{a_1}^2 - g_1^2\phi_N^2}{m_{a_1}^2} \overset{\text{Eq. (6.46)}}{=} \frac{1}{Z_\pi^2} \\
&\Rightarrow g_1 Z_\pi^2(1-g_1w_{a_1}\phi_N) + h_3 Z_\pi^2 w_{a_1}\phi_N = g_1 + h_3 Z_\pi^2\frac{g_1\phi_N^2}{m_{a_1}^2} \\
&\overset{\text{Eq. (6.56)}}{=} g_1\left[1+\frac{1}{m_{a_1}^2}\left(m_\rho^2 - \frac{m_{a_1}^2}{Z_\pi^2}\right)Z_\pi^2\right] = g_1 Z_\pi^2\frac{m_\rho^2}{m_{a_1}^2}
\end{aligned}
\tag{9.150}
$$

and thus we obtain

$$\begin{aligned}A(s,t,u)|_{s=4m_\pi^2} &= 4(g_1^2-h_3)Z_\pi^4 w_{a_1}^2 m_\pi^2 - 2\left(\lambda_1+\frac{\lambda_2}{2}\right)Z_\pi^4 - 2(h_1+h_2+h_3)Z_\pi^4 w_{a_1}^2 m_\pi^2 \\ &- 4[(B_{\sigma_N\pi\pi}+C_{\sigma_N\pi\pi})m_\pi^2\cos\varphi_\sigma - (A_{\sigma_N\pi\pi}\cos\varphi_\sigma + A_{\sigma_S\pi\pi}\sin\varphi_\sigma)]^2\frac{1}{4m_\pi^2-m_{\sigma_1}^2} \\ &- 4[(B_{\sigma_N\pi\pi}+C_{\sigma_N\pi\pi})m_\pi^2\sin\varphi_\sigma + (A_{\sigma_S\pi\pi}\cos\varphi_\sigma - A_{\sigma_N\pi\pi}\sin\varphi_\sigma)]^2\frac{1}{4m_\pi^2-m_{\sigma_2}^2} \\ &+ 8g_1^2 Z_\pi^4\frac{m_\pi^2 m_\rho^2}{m_{a_1}^4}. \end{aligned} \tag{9.151}$$

We also obtain

$$\begin{aligned}A(t,u,s)|_{s=4m_\pi^2} &= -2\left(\lambda_1+\frac{\lambda_2}{2}\right)Z_\pi^4 + 2(h_1+h_2+h_3)Z_\pi^4 w_{a_1}^2 m_\pi^2 - 4g_1^2 Z_\pi^4\frac{m_\pi^2 m_\rho^2}{m_{a_1}^4} \\ &+ 4[(B_{\sigma_N\pi\pi}-C_{\sigma_N\pi\pi})m_\pi^2\cos\varphi_\sigma + (A_{\sigma_N\pi\pi}\cos\varphi_\sigma + A_{\sigma_S\pi\pi}\sin\varphi_\sigma)]^2\frac{1}{m_{\sigma_1}^2} \\ &+ 4[(C_{\sigma_N\pi\pi}-B_{\sigma_N\pi\pi})m_\pi^2\sin\varphi_\sigma + (A_{\sigma_S\pi\pi}\cos\varphi_\sigma - A_{\sigma_N\pi\pi}\sin\varphi_\sigma)]^2\frac{1}{m_{\sigma_2}^2} \end{aligned} \tag{9.152}$$

and

$$A(u,s,t)|_{s=4m_\pi^2} = A(t,u,s)|_{s=4m_\pi^2}. \tag{9.153}$$

We can now calculate the scattering lengths. We already know from Sec. 5.2.8 that

$$T^0|_{s=4m_\pi^2} \equiv 32\pi a_0^0|_{s=4m_\pi^2} = 3A(s,t,u)|_{s=4m_\pi^2} + A(t,u,s)|_{s=4m_\pi^2} + A(u,s,t)|_{s=4m_\pi^2}. \tag{9.154}$$

We then obtain

$$\begin{aligned}32\pi a_0^0|_{s=4m_\pi^2} &= 12(g_1^2-h_3)Z_\pi^4 w_{a_1}^2 m_\pi^2 - 10\left(\lambda_1+\frac{\lambda_2}{2}\right)Z_\pi^4 - 2(h_1+h_2+h_3)Z_\pi^4 w_{a_1}^2 m_\pi^2 \\ &+ 12[(B_{\sigma_N\pi\pi}+C_{\sigma_N\pi\pi})m_\pi^2\cos\varphi_\sigma - (A_{\sigma_N\pi\pi}\cos\varphi_\sigma + A_{\sigma_S\pi\pi}\sin\varphi_\sigma)]^2\frac{1}{m_{\sigma_1}^2-4m_\pi^2} \\ &+ 12[(B_{\sigma_N\pi\pi}+C_{\sigma_N\pi\pi})m_\pi^2\sin\varphi_\sigma + (A_{\sigma_S\pi\pi}\cos\varphi_\sigma - A_{\sigma_N\pi\pi}\sin\varphi_\sigma)]^2\frac{1}{m_{\sigma_2}^2-4m_\pi^2} \\ &+ 8[(B_{\sigma_N\pi\pi}-C_{\sigma_N\pi\pi})m_\pi^2\cos\varphi_\sigma + (A_{\sigma_N\pi\pi}\cos\varphi_\sigma + A_{\sigma_S\pi\pi}\sin\varphi_\sigma)]^2\frac{1}{m_{\sigma_1}^2} \\ &+ 8[(C_{\sigma_N\pi\pi}-B_{\sigma_N\pi\pi})m_\pi^2\sin\varphi_\sigma + (A_{\sigma_S\pi\pi}\cos\varphi_\sigma - A_{\sigma_N\pi\pi}\sin\varphi_\sigma)]^2\frac{1}{m_{\sigma_2}^2} \\ &+ 16g_1^2 Z_\pi^4\frac{m_\pi^2 m_\rho^2}{m_{a_1}^4}. \end{aligned} \tag{9.155}$$

Similarly to Eq. (9.33), let us note that the linear combination $B_{\sigma_N\pi\pi}+C_{\sigma_N\pi\pi}$ can be transformed

in the following way:

$$
\begin{aligned}
B_{\sigma_N\pi\pi} + C_{\sigma_N\pi\pi} &\overset{\text{Eq. (6.28)}}{=} Z_\pi^2 \frac{g_1^2\phi_N}{m_{a_1}^2}\left(-3 + \frac{g_1^2\phi_N^2}{m_{a_1}^2} + \frac{h_1+h_2-h_3}{2}\frac{\phi_N^2}{m_{a_1}^2}\right) \\
&= Z_\pi^2 \frac{g_1^2\phi_N}{m_{a_1}^4}\left(-3m_{a_1}^2 + g_1^2\phi_N^2 + \frac{h_1+h_2-h_3}{2}\phi_N^2\right) \\
&\overset{\text{Eq. (6.41)}}{=} Z_\pi^2 \frac{g_1^2\phi_N}{m_{a_1}^4}\left(-3m_{a_1}^2 + m_{a_1}^2 - m_1^2 - \frac{h_1}{2}\phi_S^2 - 2\delta_N\right) \equiv -Z_\pi^2 \frac{g_1^2\phi_N}{m_{a_1}^4}\left(2m_{a_1}^2 + m_1^2\right), \qquad (9.156)
\end{aligned}
$$

where we have used $h_1 = 0 = \delta_N$, and also that the linear combination $B_{\sigma_N\pi\pi} - C_{\sigma_N\pi\pi}$ can be written in this way:

$$
\begin{aligned}
B_{\sigma_N\pi\pi} - C_{\sigma_N\pi\pi} &\overset{\text{Eq. (6.28)}}{=} Z_\pi^2 \frac{g_1^2\phi_N}{m_{a_1}^2}\left(-1 + \frac{g_1^2\phi_N^2}{m_{a_1}^2} + \frac{h_1+h_2-h_3}{2}\frac{\phi_N^2}{m_{a_1}^2}\right) \\
&= Z_\pi^2 \frac{g_1^2\phi_N}{m_{a_1}^4}\left(-m_{a_1}^2 + g_1^2\phi_N^2 + \frac{h_1+h_2-h_3}{2}\phi_N^2\right) \\
&\overset{\text{Eq. (6.41)}}{=} Z_\pi^2 \frac{g_1^2\phi_N}{m_{a_1}^4}\left(-m_1^2 - \frac{h_1}{2}\phi_S^2 - 2\delta_N\right) \equiv -Z_\pi^2 \frac{g_1^2\phi_N}{m_{a_1}^4} m_1^2. \qquad (9.157)
\end{aligned}
$$

Then, using Eqs. (9.28), (9.31), (9.156) and (9.157), we obtain from Eq. (9.155):

$$
\begin{aligned}
32\pi a_0^0|_{s=4m_\pi^2} &= [12g_1^2 - 2(h_1+h_2) - 14h_3]Z_\pi^4 w_{a_1}^2 m_\pi^2 - 10\left(\lambda_1 + \frac{\lambda_2}{2}\right)Z_\pi^4 + 16g_1^2 Z_\pi^4 \frac{m_\pi^2 m_\rho^2}{m_{a_1}^4} \\
&+ 12Z_\pi^4\left[\frac{g_1^2\phi_N}{m_{a_1}^4}\left(2m_{a_1}^2 + m_1^2\right)m_\pi^2\cos\varphi_\sigma - \lambda_1(\phi_N\cos\varphi_\sigma + \phi_S\sin\varphi_\sigma)\right. \\
&\left. - \frac{\lambda_2}{2}\phi_N\cos\varphi_\sigma\right]^2 \frac{1}{m_{\sigma_1}^2 - 4m_\pi^2} \\
&+ 12Z_\pi^4\left[\frac{g_1^2\phi_N}{m_{a_1}^4}\left(2m_{a_1}^2 + m_1^2\right)m_\pi^2\sin\varphi_\sigma - \lambda_1(\phi_N\sin\varphi_\sigma - \phi_S\cos\varphi_\sigma)\right. \\
&\left. - \frac{\lambda_2}{2}\phi_N\sin\varphi_\sigma\right]^2 \frac{1}{m_{\sigma_2}^2 - 4m_\pi^2} \\
&+ 8Z_\pi^4\left[\frac{g_1^2\phi_N}{m_{a_1}^4} m_1^2 m_\pi^2\cos\varphi_\sigma + \lambda_1(\phi_N\cos\varphi_\sigma + \phi_S\sin\varphi_\sigma) + \frac{\lambda_2}{2}\phi_N\cos\varphi_\sigma\right]^2 \frac{1}{m_{\sigma_1}^2} \\
&+ 8Z_\pi^4\left[\frac{g_1^2\phi_N}{m_{a_1}^4} m_1^2 m_\pi^2\sin\varphi_\sigma + \lambda_1(\phi_N\sin\varphi_\sigma - \phi_S\cos\varphi_\sigma) + \frac{\lambda_2}{2}\phi_N\sin\varphi_\sigma\right]^2 \frac{1}{m_{\sigma_2}^2} \qquad (9.158)
\end{aligned}
$$

and finally the following formula for the $S$-wave, isospin-zero $\pi\pi$ scattering length $a_0^0$:

$$
\begin{aligned}
a_0^0|_{s=4m_\pi^2} &= \frac{Z_\pi^4}{\pi}\left\{\left[\frac{3}{8}g_1^2 - \frac{1}{16}(h_1+h_2) - \frac{7}{16}h_3\right]w_{a_1}^2 m_\pi^2 - \frac{5}{16}\left(\lambda_1 + \frac{\lambda_2}{2}\right) + \frac{1}{2}g_1^2 Z_\pi^4 \frac{m_\pi^2 m_\rho^2}{m_{a_1}^4}\right. \\
&+ \frac{3}{8}\left[\frac{g_1^2\phi_N}{m_{a_1}^4}\left(2m_{a_1}^2 + m_1^2\right)m_\pi^2\cos\varphi_\sigma - \lambda_1(\phi_N\cos\varphi_\sigma + \phi_S\sin\varphi_\sigma)\right. \\
&\left.\left. - \frac{\lambda_2}{2}\phi_N\cos\varphi_\sigma\right]^2 \frac{1}{m_{\sigma_1}^2 - 4m_\pi^2}\right.
\end{aligned}
$$

$$
\begin{aligned}
&+\frac{3}{8}\left[\frac{g_1^2\phi_N}{m_{a_1}^4}\left(2m_{a_1}^2+m_1^2\right)m_\pi^2\sin\varphi_\sigma-\lambda_1(\phi_N\sin\varphi_\sigma-\phi_S\cos\varphi_\sigma)\right.\\
&\left.-\frac{\lambda_2}{2}\phi_N\sin\varphi_\sigma\right]^2\frac{1}{m_{\sigma_2}^2-4m_\pi^2}\\
&+\frac{1}{4}\left[\frac{g_1^2\phi_N}{m_{a_1}^4}m_1^2m_\pi^2\cos\varphi_\sigma+\lambda_1(\phi_N\cos\varphi_\sigma+\phi_S\sin\varphi_\sigma)+\frac{\lambda_2}{2}\phi_N\cos\varphi_\sigma\right]^2\frac{1}{m_{\sigma_1}^2}\\
&+\frac{1}{4}\left[\frac{g_1^2\phi_N}{m_{a_1}^4}m_1^2m_\pi^2\sin\varphi_\sigma+\lambda_1(\phi_N\sin\varphi_\sigma-\phi_S\cos\varphi_\sigma)+\frac{\lambda_2}{2}\phi_N\sin\varphi_\sigma\right]^2\frac{1}{m_{\sigma_2}^2}\Bigg\}. \qquad (9.159)
\end{aligned}
$$

Given that $T^1=A(t,u,s)-A(u,s,t)$, we obtain $T^1=0$ at threshold because of $A(t,u,s)|_{s=4m_\pi^2}=A(u,s,t)|_{s=4m_\pi^2}$ [see Eq. (9.153)]. Therefore,

$$
a_0^1=0. \qquad (9.160)
$$

We now turn to the calculation of the $S$-wave, isospin-two $\pi\pi$ scattering length $a_0^2$. As already known from Sec. 5.2.8,

$$
T^2|_{s=4m_\pi^2}=A(t,u,s)|_{s=4m_\pi^2}+A(u,s,t)|_{s=4m_\pi^2} \qquad (9.161)
$$

or in other words

$$
T^2|_{s=4m_\pi^2}=2A(t,u,s)|_{s=4m_\pi^2} \qquad (9.162)
$$

because of Eq. (9.153). Given that

$$
32\pi a_0^2\equiv T^2|_{s=4m_\pi^2}, \qquad (9.163)
$$

we consequently obtain

$$
16\pi a_0^2\equiv A(t,u,s)|_{s=4m_\pi^2}. \qquad (9.164)
$$

Then substituting Eqs. (9.28), (9.31) and (9.157) into Eq. (9.152) implies

$$
\begin{aligned}
16\pi a_0^2=&-2\left(\lambda_1+\frac{\lambda_2}{2}\right)Z_\pi^4+2(h_1+h_2+h_3)Z_\pi^4w_{a_1}^2m_\pi^2-4g_1^2Z_\pi^4\frac{m_\pi^2m_\rho^2}{m_{a_1}^4}\\
&+4Z_\pi^4\left[\frac{g_1^2\phi_N}{m_{a_1}^4}m_1^2m_\pi^2\cos\varphi_\sigma+\lambda_1(\phi_N\cos\varphi_\sigma+\phi_S\sin\varphi_\sigma)+\frac{\lambda_2}{2}\phi_N\cos\varphi_\sigma\right]^2\frac{1}{m_{\sigma_1}^2}\\
&+4Z_\pi^4\left[\frac{g_1^2\phi_N}{m_{a_1}^4}m_1^2m_\pi^2\sin\varphi_\sigma+\lambda_1(\phi_N\sin\varphi_\sigma-\phi_S\cos\varphi_\sigma)+\frac{\lambda_2}{2}\phi_N\sin\varphi_\sigma\right]^2\frac{1}{m_{\sigma_2}^2}. \qquad (9.165)
\end{aligned}
$$

Finally, we obtain

$$
\begin{aligned}
a_0^2=&\frac{Z_\pi^4}{\pi}\left\{\frac{1}{8}(h_1+h_2+h_3)w_{a_1}^2m_\pi^2-\frac{1}{8}\left(\lambda_1+\frac{\lambda_2}{2}\right)-\frac{1}{4}g_1^2\frac{m_\pi^2m_\rho^2}{m_{a_1}^4}\right.\\
&+\frac{1}{4}\left[\frac{g_1^2\phi_N}{m_{a_1}^4}m_1^2m_\pi^2\cos\varphi_\sigma+\lambda_1(\phi_N\cos\varphi_\sigma+\phi_S\sin\varphi_\sigma)+\frac{\lambda_2}{2}\phi_N\cos\varphi_\sigma\right]^2\frac{1}{m_{\sigma_1}^2}\\
&\left.+\frac{1}{4}\left[\frac{g_1^2\phi_N}{m_{a_1}^4}m_1^2m_\pi^2\sin\varphi_\sigma+\lambda_1(\phi_N\sin\varphi_\sigma-\phi_S\cos\varphi_\sigma)+\frac{\lambda_2}{2}\phi_N\sin\varphi_\sigma\right]^2\frac{1}{m_{\sigma_2}^2}\right\}. \qquad (9.166)
\end{aligned}
$$

We observe from of Eqs. (9.159) and (9.166) that the $\pi\pi$ scattering lengths now depend on two scalar masses ($m_{\sigma_1}$ and $m_{\sigma_2}$) unlike in the two-flavour version of the model where the dependence was only on one scalar mass ($m_{\sigma_N}$). Both scattering lengths are depicted as functions of $m_{\sigma_1}$ in Fig. 9.24.

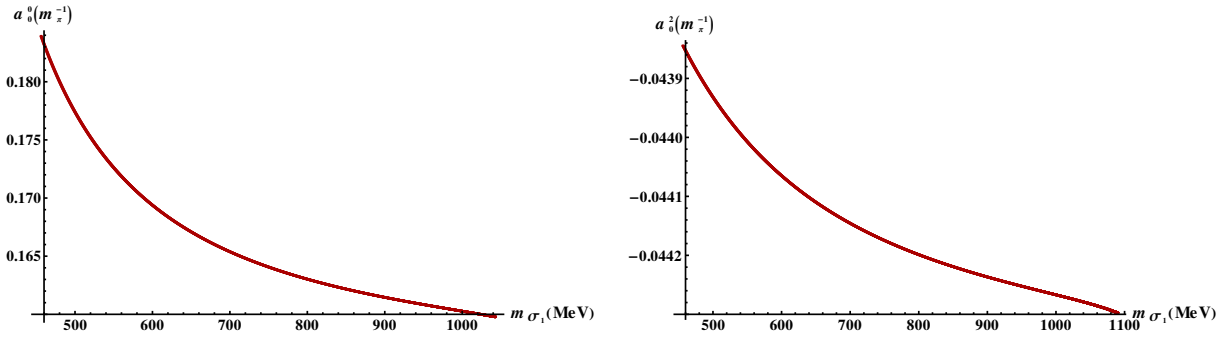


**Figure 9.24:** Pion-pion scattering lengths from Fit I. We do not indicate the NA48/2 error bands [43] because $a_0^0$ (left panel) is completely outside the NA48/2 interval $a_0^0 = 0.218 \pm 0.020$ and $a_0^2$ (left panel) is completely within the NA48/2 interval $a_0^2 = -0.0457 \pm 0.0125$. The latter is true because the NA48/2 result possesses large errors and our $a_0^2$ barely changes with $m_{\sigma_1}$.

We observe that the obtained values of the isospin-zero scattering length $a_0^0$ are smaller than those in Scenario I of the two-flavour model as well as those reported by the NA48/2 Collaboration [43]. The largest value of this scattering length is $a_0^0 = 0.184$, obtained for $m_{\sigma_1} = 456$ MeV [note that this is the smallest value of $m_{\sigma_1}$, determined by the condition $m_0^2 = 0$, see Eq. (9.25)]. The scattering length $a_0^2$ is within the NA48/2 results.

We can therefore conclude that, as in Scenario I of the two-flavour version of the model, it is not possible to obtain satisfying results for scattering lengths as well as scalar decay widths simultaneously: the decay widths $\Gamma_{\sigma_1\to\pi\pi}$ and $\Gamma_{\sigma_2\to\pi\pi}$ possess very good values respectively for $m_{\sigma_1} = 705$ MeV and $m_{\sigma_1} = 1200$ MeV [see Eqs. (9.56) and (9.55) and Fig. 9.7]; however, the same is not true for $a_0^0 = 0.165$ that is outside the NA48/2 interval reading $a_0^0 = 0.218 \pm 0.020$ although $a_0^2 = -0.0442$ is within the respective NA48/2 interval (that is, however, rather broad: $a_0^2 = -0.0457 \pm 0.0125$ [43]). Note that the discrepancy with the NA48/2 result becomes even larger if the isospin-exact values of $a_0^{0\,(\mathrm{I})} = 0.244 \pm 0.020$ and $a_0^{2\,(\mathrm{I})} = -0.0385 \pm 0.0125$ from Sec. 5.3.4 are considered. Therefore, our Fit I yields the reverse situation to that of Scenario I in the $U(2) \times U(2)$ version of the model where we were able to describe the scattering lengths correctly but the $\sigma_N$ decay width was too small. Nonetheless, it is apparent that the scattering lengths still require the existence of a light scalar meson as they saturate for large values of $m_{\sigma_1}$.

Note that it is possible to obtain the already-known results for the scattering lengths within the $N_f = 2$ model in Scenario I. Setting the $\sigma_N$-$\sigma_S$ mixing angle $\varphi_\sigma = 0$ and considering the limit $m_{\sigma_S} \to \infty$ leads to the diagrams already depicted in Scenario I of the two-flavour version of the model (see Fig. 5.4) once the parameter values have been adjusted to those from the stated scenario.

A different limit is obtained from our Fit I by artificially decoupling $\sigma_2$ (i.e., setting $m_{\sigma_2} \to \infty$) but still allowing for $m_{\sigma_1}$ and $\varphi_\sigma$ to change simultaneously with $m_0^2$ [see Eqs. (9.19) and (9.23)]. In this limit, $\varphi_\sigma$ is not fixed to zero. We observe that the correspondence of the scattering lengths to data is in this case very much spoiled. Acceptable values of $a_0^2$ are obtained only in a

small range of 960 MeV $\leq m_{\sigma_1} \leq$ 994 MeV while $a_0^0 < 0.161$ for all values of $m_{\sigma_1}$, see Fig. 9.25. In the case of $a_0^0$ with two scalar resonances, Fig. 9.24, the values of $a_0^0$ were relatively larger for relatively smaller values of $m_{\sigma_1}$ whereas here, in the one-resonance case, the dependence of scattering lengths on $m_{\sigma_1}$ gains a parabolic form and therefore peaks in a limited $m_{\sigma_1}$ interval. The scattering length $a_0^0$ then continues to decrease with decreasing $m_{\sigma_1}$ until the contribution of the pole term $1/(m_{\sigma_1}^2 - 4m_\pi^2)$ becomes sufficiently large and forces $a_0^0$ to rise again (this, however, happens only for $m_{\sigma_1} \simeq 300$ MeV, i.e., $m_0^2 > 0$, according to Fig. 9.2 – we do not represent this value of $m_{\sigma_1}$ in Fig. 9.25 and thus do not see an increase of $a_0^0$ there); $a_0^2$ possesses no pole at $\pi\pi$ threshold and therefore retains a parabolic form until $m_{\sigma_1} = 0$.

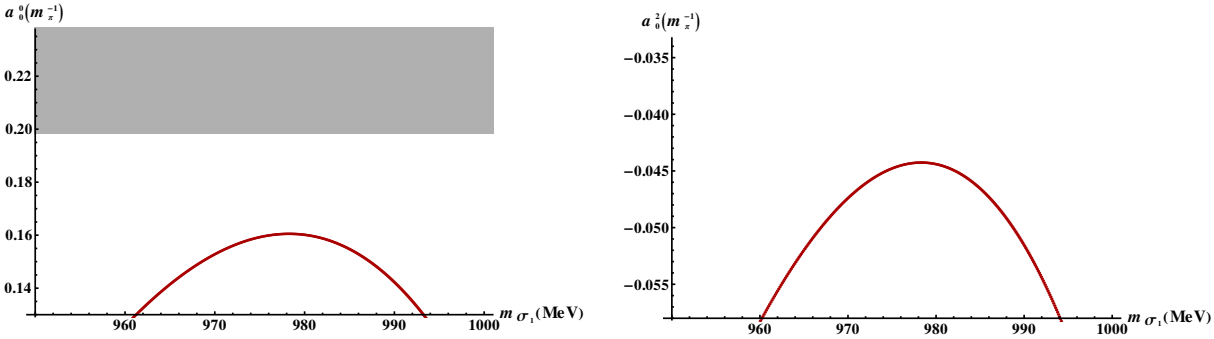


**Figure 9.25:** Scattering lengths $a_0^0$ and $a_0^2$ as functions of $m_{\sigma_1}$ in the limit $m_{\sigma_2} \to \infty$. The shaded area on the left panel represents the NA48/2 result regarding $a_0^0$ [43]; the entire right panel represents the $a_0^2$ interval from NA48/2.

We can thus conclude that artificially removing $\sigma_2$ from the $\pi\pi$ scattering worsens the correspondence with the NA48/2 results considerably although, given the relatively large values of $m_{\sigma_2}$ [see Eq. (9.26)], one would have expected that the contribution of $\sigma_2$ to the scattering lengths is suppressed. Nonetheless, the scattering lengths depend decisively on the scalar masses – as already mentioned, they saturate for large values of the masses (see Fig. 9.24). Our Fit II will be developed under the assumption that the scalar $I = 1/2$ and $I = 1$ states are above 1 GeV yielding $m_{\sigma_{1,2}} > 1$ GeV as well (see Sec. 11.1.1). Our combined analysis in Sec. 11.1.5 will subsequently yield $m_{\sigma_1}^{(\text{FIT II})} = 1310$ MeV and $m_{\sigma_2}^{(\text{FIT II})} = 1606$ MeV. This implies that there needs to be no calculation of scattering lengths in Fit II because the scattering lengths will be in their respective Weinberg limits [236]: $a_0^{0(\text{FIT II})} \simeq 0.158$, $a_0^{2(\text{FIT II})} \simeq -0.0448$.

## 9.6 Conclusions from Fit with Scalars below 1 GeV

In the previous sections we have addressed the question whether it is possible to obtain a reasonable phenomenology of mesons in vacuum under the assumption that scalar $\bar{q}q$ states possess energies below 1 GeV. To this end, we have looked for a fit (labelled Fit I) incorporating the masses of $\pi$, $K$, $\eta$, $\eta'$,$\rho$, $K^\star$, $\omega_S \equiv \varphi(1020)$, $a_1$, $K_1$, $f_{1S} \equiv f_1(1420)$, decay widths $\Gamma_{a_1 \to \pi\gamma}$ and $\Gamma_{f_{1N} \to a_0(980)\pi}$, as well as the masses of the scalar states $a_0$ and $K_S$ assigned to $a_0(980)$ and $K_0^\star(800) \equiv \kappa$, respectively. We have not included any scalar isosinglet masses into the fit in order to let these masses remain a prediction of the fit.

We summarise the main conclusions of the fit as follows:

- It is possible to find a fit; masses entering the fit are well described except
  - $m_\kappa = 1128.7$ MeV, almost by a factor of two larger than the corresponding PDG value [10] (but the $\kappa$ resonance is very broad),
  - $m_{a_1} = 1395.5$ MeV, approximately 170 MeV larger than the corresponding PDG value $m_{a_1}^{\mathrm{exp}} = 1230$ MeV [but the $a_1(1260)$ resonance is also broad and the PDG mass is only an educated guess],
  - $m_{K_1} = 1520$ MeV, approximately 250 MeV larger than the mass of $K_1(1270)$; however, assigning our $K_1$ field to the (broad) resonance $K_1(1400)$ yields the stated result for $m_{K_1}$ acceptable,
  - $m_{\omega_S} = 870.35$ MeV, approximately 150 MeV less than $m_{\varphi(1020)}^{\mathrm{exp}} = 1019.46$ MeV and $m_{f_{1S}} = 1643.4$ MeV, approximately 220 MeV larger than $m_{f_1(1420)}^{\mathrm{exp}} = 1426.4$ MeV – this in particular represents a problem because $\varphi(1020)$ and $f_1(1420)$ are rather sharp resonances.

  Additionally, $\Gamma_{a_1\to\pi\gamma} = 0.369$ MeV is outside the experimental interval $\Gamma_{a_1\to\pi\gamma}^{\mathrm{exp}} = 0.640 \pm 0.246$ MeV [10].

- It is not possible to assign the two mixed scalar isosinglets $\sigma_1$ (predominantly non-strange) and $\sigma_2$ (predominantly strange) to measured resonances if one considers only their masses because $m_{\sigma_1}$ and $m_{\sigma_2}$ vary in rather large intervals: 456 MeV $\leq m_{\sigma_1} \leq$ 1139 MeV and 1187 MeV $\leq m_{\sigma_2} \leq$ 2268 MeV. (Interval boundaries are determined by the conditions $m_0^2 < 0$ and $m_{\sigma_N} < m_{\sigma_S}$.) Therefore, an analysis of scalar decay widths is called for.

- We obtain satisfying results in the decay channels $\sigma_{1,2} \to \pi\pi$ and $\sigma_{1,2} \to KK$ if we set $m_{\sigma_1} = 705$ MeV and $m_{\sigma_2} = 1200$ MeV leading to $\Gamma_{\sigma_1\to\pi\pi} = 305$ MeV and $\Gamma_{\sigma_2\to\pi\pi} = 207$ MeV in the former and $\Gamma_{\sigma_1\to KK} = 0$ and $\Gamma_{\sigma_2\to KK} = 240$ MeV in the latter channel. This allows us to assign $\sigma_1$ to $f_0(600)$ and $\sigma_2$ to $f_0(1370)$; $\Gamma_{\sigma_2\to\pi\pi}$ was chosen such that it corresponds to $\Gamma_{f_0(1370)\to\pi\pi} = 207$ MeV from Ref. [40]. Consequently, we interpret $f_0(600)$ as a predominantly non-strange $\bar{q}q$ state while $f_0(1370)$ is interpreted as a predominantly strange quarkonium. The results also suggest, however, that $f_0(1370)$ should predominantly decay into kaons (as $\Gamma_{\sigma_2\to KK}/\Gamma_{\sigma_2\to\pi\pi} = 1.15$) – not surprising for a strange quarkonium but clearly at odds with experimental data [10].

- Satisfying results are obtained in the $\sigma_{1,2} \to \eta\eta$ decay channel: $m_{\sigma_1} = 705$ MeV yields $\Gamma_{\sigma_1\to\eta\eta} = 0$ (as expected) and $m_{\sigma_2} = 1200$ MeV yields $\Gamma_{\sigma_1\to\eta\eta} = 31$ MeV (also in line with expectations). Additionally, one obtains $\Gamma_{\sigma_2\to\eta\eta}/\Gamma_{\sigma_2\to\pi\pi} = 0.15$, in accordance with the result $\Gamma_{f_0(1370)\to\eta\eta}/\Gamma_{f_0(1370)\to\pi\pi} = 0.19 \pm 0.07$ from Ref. [40]. However, the ratio $\Gamma_{\sigma_2\to KK}/\Gamma_{\sigma_2\to\eta\eta} \gg 1$ again suggests that $f_0(1370)$ should decay predominantly into kaons, problematic from the experimental point of view.

- We obtain $\Gamma_{K_0^\star(800)\to K\pi} = 490$ MeV, a satisfying result predicting a broad scalar kaon resonance in accordance with the PDG data [10]. However, the mass of the resonance is $m_{K_0^\star(800)} = 1128.7$ MeV, and thus larger than $m_{K_0^\star(800)}^{\mathrm{exp}} = 676$ MeV by a factor of two.

- The decay amplitude $a_0(980) \to \eta\pi$ is within experimental data.
- For the scattering lengths, we obtain $a_0^0 < 0.184$ for all values of $m_{\sigma_1}$; $a_0^0$ is thus below NA48/2 results [43]. Contrarily, the scattering length $a_0^2$ is within the NA48/2 results (that, for this scattering length, possess rather large uncertainties). We can therefore conclude that Fit I does not allow for scattering lengths as well as scalar decay widths to be described simultaneously: although we obtain satisfying values for the decay widths $\Gamma_{\sigma_1\to\pi\pi}$ and $\Gamma_{\sigma_2\to\pi\pi}$, the same is not true for $a_0^0$. Nonetheless, the scattering lengths still require the existence of a light scalar meson because they saturate for large values of $m_{\sigma_1}$.
- Additionally, the phenomenology in the vector and axial-vector channels is not well described.
  - $\Gamma_{K^\star\to K\pi} = 32.8$ MeV whereas experimental data suggest $\Gamma^{\rm exp}_{K^\star\to K\pi} = 46.2$ MeV [10].
  - The decay width $\Gamma_{a_1(1260)\to\rho\pi}$ depends (among others) on the parameter $g_2$, fixed via $\Gamma_{\rho\to\pi\pi}$. A calculation of $\Gamma_{a_1(1260)\to\rho\pi}$ then yields values of more than 10 GeV if we set $\Gamma_{\rho\to\pi\pi} = 149.1$ MeV (as suggested by the PDG [10]). Alternatively, if one forces $\Gamma_{a_1(1260)\to\rho\pi} < 600$ MeV to comply with the data, then $\Gamma_{\rho\to\pi\pi} < 38$ MeV is obtained – a value that is approximately 100 MeV less than the experimental result. We also obtain $\Gamma_{a_1\to\bar{K}^\star K\to\bar{K}K\pi} = 1.97$ GeV.
  - Analogous statements are true for $f_1(1285)$ and $f_1(1420)$. Fit I yields $\Gamma_{f_1(1285)\to\bar{K}^\star K} \simeq 2.15$ GeV for $\Gamma_{\rho\to\pi\pi} = 149.1$ MeV; the physical value $\Gamma_{f_1(1285)\to\bar{K}^\star K} \lesssim 2$ MeV is obtained only for $\Gamma_{\rho\to\pi\pi} \sim 20$ MeV. The fit also yields $\Gamma_{f_1(1420)\to\bar{K}^\star K} \simeq 18$ GeV for $\Gamma_{\rho\to\pi\pi} = 149.1$ MeV with the physical value $\Gamma_{f_1(1420)\to\bar{K}^\star K} \simeq 54.9$ MeV obtained for $\Gamma_{\rho\to\pi\pi} \sim 27$ MeV.
  - The phenomenology of the $K_1(1400)$ meson is described as poorly as the $a_1(1260)$ phenomenology. Combined results in the decay channels $K_1(1400) \to K^\star\pi$, $\rho K$ and $\omega K$ suggest that the full decay width of the $K_1(1400)$ resonance should be $\sim 10$ GeV, two orders of magnitude larger than the experimental value $\Gamma_{K_1(1400)} = (174 \pm 13)$ MeV [10]. The decay widths $\Gamma_{K_1(1400)\to\rho K} = 4.77$ GeV and $\Gamma_{K_1(1400)\to\omega K} = 1.59$ GeV are three orders of magnitude larger than their respective experimental values $\Gamma^{\rm exp}_{K_1(1400)\to\rho K} = (2.1\pm1.1)$ MeV and $\Gamma^{\rm exp}_{K_1(1400)\to\omega K} = (1.7\pm1.7)$ MeV; $\Gamma_{K_1(1400)\to K^\star\pi} = 6.73$ GeV is an order of magnitude larger than $\Gamma^{\rm exp}_{K_1(1400)\to K^\star\pi} = (164 \pm 16)$ MeV. In fact, the only piece of $K_1(1400)$ experimental data correctly described in Fit I is represented by the fact that $K_1(1400) \to K^\star\pi$ is found to be the dominant decay channel of this resonance; all other results are not compatible with the data.

  Thus we cannot accommodate a correct (axial-)vector phenomenology within the fit: either $a_1(1260)$, $f_1(1285)$, $f_1(1420)$ and $K_1(1400)$ are too broad [$\sim (1-10)$ GeV] or the $\rho$ meson is too narrow ($\lesssim 40$ MeV).

Then the fit results, and thus the assumption of scalar $\bar{q}q$ states below 1 GeV, are extremely problematic.

# 10. Fit II: Scalars above 1 GeV

In this chapter we look for a fit of meson masses (labelled Fit II) assuming that scalar $\bar{q}q$ states have masses above 1 GeV and discuss the ensuing phenomenology. We will consequently be able to draw comparative conclusions with regard to results obtained from Fit I where, conversely, scalar $\bar{q}q$ states were assigned to resonances below 1 GeV.

The formal structure of Fit II is very similar to that of Fit I. We have already described in Sec. 6 how the initial set of 18 parameters in the Lagrangian (6.1) is reduced to seven unknowns: $Z_\pi$, $Z_K$, $m_1^2$, $h_2$, $\delta_S$, $\lambda_2$ and $m_0^2 + \lambda_1(\phi_N^2 + \phi_S^2)$. In order to implement Fit II, we make use of 16 equations: for $m_\pi$, $m_K$, $m_{K_S} \equiv m_{K_0^\star(1430)}$, $m_{a_0} \equiv m_{a_0(1450)}$, $m_\eta$, $m_{\eta'}$ [the latter two via Eqs. (7.20) and (7.21) from $m_{\eta_N}$ and $m_{\eta_S}$], $m_\rho$, $m_{K^\star}$, $m_{\omega_S}$, $m_{a_1}$, $m_{K_1}$, $m_{f_{1S}}$, $\Gamma_{a_1\to\pi\gamma}$ and $\Gamma_{a_0(1450)}$ as well as Eqs. (7.3) and (7.4), the latter two for $Z_K$. Thus, in this fit our fields $\boldsymbol{a}_0$ and $K_S$ are assigned respectively to $a_0(1450)$ and $K_0^\star(1430)$, i.e., to states above 1 GeV. Conversely, this means that now we are working with the assumption that $a_0(1450)$ and $K_0^\star(1430)$ are $\bar{q}q$ states. Consequently, in Fit II there are no states from our model that are assigned to the resonances $a_0(980)$ and $\kappa$; these resonances could be introduced into our model only as additional fields, such as, for example, tetraquarks [194]. Note that there may also exist mixing in the isotriplet channel between $a_0(980)$ and $a_0(1450)$. The mixing is, however, small [211] and can be neglected. As mentioned previously, Fit II will require knowledge of the full $a_0(1450)$ decay width. The corresponding formulas are discussed in the following section.

## 10.1 Full decay width of $a_0(1450)$

Experimental data [10] suggest that $a_0(1450)$ possesses six decay channels: into $\pi\eta$, $\pi\eta'$, $KK$, $\omega\pi\pi$, $a_0(980)\pi\pi$ and $\gamma\gamma$. The latter two are poorly known and suppressed; we therefore omit these two decay channels from our considerations. The remaining decay channels can be calculated directly from our model as follows:

- The decay width $\Gamma_{a_0(1450)\to\pi\eta}$ is obtained from the interaction Lagrangian (9.73) as described in Sec. 9.2 by assigning our $\boldsymbol{a}_0$ field to $a_0(1450)$. We use the following formula for the decay width:

$$\Gamma_{a_0^0(1450)\to\eta\pi^0} = \frac{k(m_{a_0(1450)}, m_\eta, m_\pi)}{8\pi m_{a_0(1450)}^2} |-i\mathcal{M}_{a_0^0(1450)\to\eta\pi^0}(m_\eta)|^2 \tag{10.1}$$

  with $\mathcal{M}_{a_0^0(1450)\to\eta\pi^0}(m_\eta)$ from Eq. (9.79).

- The decay width $\Gamma_{a_0(1450)\to\pi\eta'}$ is also obtained from the interaction Lagrangian (9.73). Analogously to Eq. (9.80) we obtain for the decay amplitude

$$-i\mathcal{M}_{a_0^0(1450)\to\eta'\pi^0}(m_{\eta'}) = -i[\cos\varphi_\eta \mathcal{M}_{a_0^0\to\eta_S\pi^0}(m_{\eta'}) - \sin\varphi_\eta \mathcal{M}_{a_0^0\to\eta_N\pi^0}(m_{\eta'})] \tag{10.2}$$

  with $\mathcal{M}_{a_0^0\to\eta_N\pi^0}$ and $\mathcal{M}_{a_0^0\to\eta_S\pi^0}$ respectively from Eqs. (9.81) and (9.82). Then the decay width is calculated as

$$\Gamma_{a_0^0(1450)\to\eta'\pi^0} = \frac{k(m_{a_0(1450)}, m_{\eta'}, m_\pi)}{8\pi m_{a_0(1450)}^2} |-i\mathcal{M}_{a_0^0(1450)\to\eta'\pi^0}(m_{\eta'})|^2. \tag{10.3}$$

- The $a_0^0 KK$ interaction Lagrangian obtained from Eq. (6.1) has the following form:

$$\begin{aligned}\mathcal{L}_{a_0 KK} = A_{a_0 KK} a_0^0 (K^0 \bar{K}^0 - K^- K^+) + B_{a_0 KK} a_0^0 (\partial_\mu K^0 \partial^\mu \bar{K}^0 - \partial_\mu K^- \partial^\mu K^+) \\ + C_{a_0 KK} \partial_\mu a_0^0 (K^0 \partial^\mu \bar{K}^0 + \bar{K}^0 \partial^\mu K^0 - K^- \partial^\mu K^+ - K^+ \partial^\mu K^-)\end{aligned} \tag{10.4}$$

with

$$A_{a_0 KK} = \frac{\sqrt{2}}{2} \lambda_2 Z_K^2 (\sqrt{2}\phi_N - \phi_S), \tag{10.5}$$

$$B_{a_0 KK} = Z_K^2 \left\{ g_1 w_{K_1} \left[ 1 - \frac{1}{2} g_1 w_{K_1} (\phi_N + \sqrt{2}\phi_S) \right] - \frac{w_{K_1}^2}{2} (h_2 \phi_N - \sqrt{2} h_3 \phi_S) \right\}, \tag{10.6}$$

$$C_{a_0 KK} = -\frac{g_1}{2} Z_K^2 w_{K_1}. \tag{10.7}$$

We observe that the Lagrangian in Eq. (10.4) possesses the same form as $\mathcal{L}_{\sigma KK}$ from Eq. (9.41). Therefore, analogously to the calculation performed in Sec. 9.1.5 we obtain

$$\Gamma_{a_0^0(1450) \to K\bar{K}} = \frac{k(m_{a_0(1450)}, m_K, m_K)}{4\pi m_{a_0(1450)}^2} | - i\mathcal{M}_{a_0^0(1450) \to K\bar{K}}|^2, \tag{10.8}$$

where we have considered an isospin factor of two for the decays $a_0^0(1450) \to K^0 \bar{K}^0$ and $a_0^0(1450) \to K^- K^+$. The decay amplitude $-i\mathcal{M}_{a_0^0(1450) \to K\bar{K}}$ reads

$$-i\mathcal{M}_{a_0^0(1450) \to K\bar{K}} = -i \left\{ A_{a_0 KK} - B_{a_0 KK} \left[ \frac{m_{a_0(1450)}^2}{2} - m_K^2 \right] + C_{a_0 KK} m_{a_0(1450)}^2 \right\}. \tag{10.9}$$

- The decay width $\Gamma_{a_0(1450) \to \omega\pi\pi}$ is calculated via the sequential decay $a_0(1450) \to \omega\rho \to \omega\pi\pi$. The interaction Lagrangian is already known from Scenario II of the two-flavour version of our model, Eq. (5.122); the formula for the decay width $\Gamma_{a_0(1450) \to \omega\rho \to \omega\pi\pi}$ is stated in Eq. (5.124).

- The full decay width of the $a_0(1450)$ resonance is obtained from Eqs. (10.1), (10.3), (10.8) and (5.124):

$$\Gamma_{a_0(1450)} = \Gamma_{a_0^0(1450) \to \eta\pi^0} + \Gamma_{a_0^0(1450) \to \eta'\pi^0} + \Gamma_{a_0^0(1450) \to K\bar{K}} + \Gamma_{a_0(1450) \to \omega\rho \to \omega\pi\pi}. \tag{10.10}$$

The experimental value of this decay width is $\Gamma_{a_0(1450)} = (265 \pm 13)$ MeV [10].

## 10.2 Implementation of Fit II

Analogously to our calculations in Sec. 8, we look for a fit satisfying the following equations (experimental central values from the PDG [10]; no consideration of experimental uncertainties at this point):

$$Z_\pi^2\left[m_0^2+\lambda_1(\phi_N^2+\phi_S^2)+\frac{\lambda_2}{2}\phi_N^2\right]=(139.57\text{ MeV})^2\equiv m_\pi^2, \tag{10.11}$$

$$Z_K^2\left[m_0^2+\lambda_1(\phi_N^2+\phi_S^2)+\lambda_2\left(\frac{\phi_N^2}{2}-\frac{\phi_N\phi_S}{\sqrt{2}}+\phi_S^2\right)\right]=(493.677\text{ MeV})^2\equiv m_K^2, \tag{10.12}$$

$$Z_{K_S}^2\left[m_0^2+\lambda_1(\phi_N^2+\phi_S^2)+\lambda_2\left(\frac{\phi_N^2}{2}+\frac{\phi_N\phi_S}{\sqrt{2}}+\phi_S^2\right)\right]=(1425\text{ MeV})^2\equiv m_{K_0^\star(1430)}^2, \tag{10.13}$$

$$m_0^2+\lambda_1(\phi_N^2+\phi_S^2)+\frac{3}{2}\lambda_2\phi_N^2=(1474\text{ MeV})^2\equiv m_{a_0(1450)}^2, \tag{10.14}$$

$$\begin{aligned}&Z_\pi^2\left[m_0^2+\lambda_1(\phi_N^2+\phi_S^2)+\frac{\lambda_2}{2}\phi_N^2+c_1\phi_N^2\phi_S^2\right]\cos^2\varphi_\eta\\&+Z_{\eta_S}^2\left[m_0^2+\lambda_1(\phi_N^2+\phi_S^2)+\lambda_2\phi_S^2+c_1\frac{\phi_N^4}{4}\right]\sin^2\varphi_\eta\\&+c_1\frac{Z_{\eta_S}Z_\pi}{2}\phi_N^3\phi_S\sin(2\varphi_\eta)=(547.853\text{ MeV})^2\equiv m_\eta^2,\end{aligned} \tag{10.15}$$

$$\begin{aligned}&Z_\pi^2\left[m_0^2+\lambda_1(\phi_N^2+\phi_S^2)+\frac{\lambda_2}{2}\phi_N^2+c_1\phi_N^2\phi_S^2\right]\sin^2\varphi_\eta\\&+Z_{\eta_S}^2\left[m_0^2+\lambda_1(\phi_N^2+\phi_S^2)+\lambda_2\phi_S^2+c_1\frac{\phi_N^4}{4}\right]\cos^2\varphi_\eta\\&-c_1\frac{Z_{\eta_S}Z_\pi}{2}\phi_N^3\phi_S\sin(2\varphi_\eta)=(957.78\text{ MeV})^2\equiv m_{\eta'}^2,\end{aligned} \tag{10.16}$$

$$m_1^2+(h_2+h_3)\frac{\phi_N^2}{2}=(775.49\text{ MeV})^2\equiv m_\rho^2, \tag{10.17}$$

$$m_1^2+g_1^2\phi_N^2+(h_2-h_3)\frac{\phi_N^2}{2}=(1230\text{ MeV})^2\equiv m_{a_1}^2, \tag{10.18}$$

$$m_1^2+\delta_S+\left(g_1^2+h_2\right)\frac{\phi_N^2}{4}+\frac{1}{\sqrt{2}}(h_3-g_1^2)\phi_N\phi_S+\left(g_1^2+h_2\right)\frac{\phi_S^2}{2}=(891.66\text{ MeV})^2\equiv m_{K^\star}^2, \tag{10.19}$$

$$m_1^2+\delta_S+\left(g_1^2+h_2\right)\frac{\phi_N^2}{4}+\frac{1}{\sqrt{2}}(g_1^2-h_3)\phi_N\phi_S+\left(g_1^2+h_2\right)\frac{\phi_S^2}{2}=(1272\text{ MeV})^2\equiv m_{K_1}^2, \tag{10.20}$$

$$m_1^2+2\delta_S+(h_2+h_3)\,\phi_S^2=(1019.455\text{ MeV})^2\equiv m_{\omega_S}^2, \tag{10.21}$$

$$m_1^2+2\delta_S+2g_1^2\phi_S^2+(h_2-h_3)\,\phi_S^2=(1426.4\text{ MeV})^2\equiv m_{f_{1S}}^2, \tag{10.22}$$

$$\frac{e^2}{96\pi}(Z_\pi^2-1)m_{a_1}\left[1-\left(\frac{m_\pi}{m_{a_1}}\right)^2\right]^3=0.640\text{ MeV}\equiv\Gamma_{a_1\to\pi\gamma}, \tag{10.23}$$

$$\Gamma_{a_0^0(1450)\to\eta\pi^0}+\Gamma_{a_0^0(1450)\to\eta'\pi^0}+\Gamma_{a_0^0(1450)\to K\bar{K}}+\Gamma_{a_0(1450)\to\rho\pi\to\omega\pi\pi}=265\text{ MeV}\equiv\Gamma_{a_0(1450)}, \tag{10.24}$$

as well as the $Z_K$ Eqs. (7.3) and (7.4). Note that also in this fit we set $h_1 = 0 = \delta_N$; that $c_1 = c_1(\varphi_\eta)$ from Eq. (7.24) and that we also use $\phi_N = Z_\pi f_\pi$ ($f_\pi = 92.4$ MeV), $\phi_S = Z_K f_K/\sqrt{2}$ ($f_K = 155.5/\sqrt{2}$ MeV), $g_1$ from Eq. (6.55), $h_3$ from Eq. (6.56), $Z_{K_S}$ from Eq. (6.49) and $Z_{\eta_S}$ from Eq. (6.48).

Now we can make use of the same four-step procedure described in Sec. 8 to ascertain whether an acceptable fit can be found.

*Step 1.* We first consider the first four equations entering the fit, i.e., Eqs. (10.11) - (10.14) that depend only on four variables: $Z_\pi$, $Z_K$, $\lambda_2$ and $m_0^2 + \lambda_1(\phi_N^2 + \phi_S^2)$. As in Fit I, we set $m_{a_1} = m_{a_1}^{\rm exp} = 1230$ MeV and $m_{K^\star} = m_{K^\star}^{\rm exp} = 891.66$ MeV [10] in order for the renormalisation coefficient $Z_{K_S}$ to be calculated. We again find that $Z_{K_S}$ changes only minutely with $m_{a_1}$ and $m_{K^\star}$ and therefore the exact values of these two masses are at this point not of great importance. We thus obtain a system of four equations (10.11) - (10.14) with four unknowns that can be solved exactly; we obtain the following parameter values:

$$\begin{aligned} Z_\pi &= 0.36 \\ Z_K &= 0.47 \\ \lambda_2 &= 1860 \\ m_0^2 + \lambda_1(\phi_N^2 + \phi_S^2) &= -856580 \text{ MeV}^2. \end{aligned}$$

Unfortunately, this set of solutions cannot be used further as it implies $Z_\pi < 1$ and $Z_K < 1$, a condition that by the definitions of these renormalisation coefficients [Eqs. (6.46) and (6.47)] cannot be fulfilled as otherwise either $g_1^2 < 0$ or $\phi_N^2 < 0$ [in Eq. (6.46)] and $(\phi_N + \sqrt{2}\phi_S)^2 < 0$ [in Eq. (6.47)] would have to be true. We do not consider an imaginary scalar-vector coupling $g_1$ or imaginary condensates $\phi_{N,S}$ – therefore, we have to work for alternative (approximate) solutions for Eqs. (10.11) - (10.14). We then obtain the parameter values shown in Table 10.1.

| Parameter | Value | Observable | Value [MeV] |
|---|---|---|---|
| $Z_\pi$ | 1.66 | $m_\pi$ | 138.65 |
| $Z_K$ | 1.515 | $m_K$ | 497.96 |
| $\lambda_2$ | 89.7 | $m_{a_0(1450)}$ | 1452 |
| $m_0^2 + \lambda_1(\phi_N^2 + \phi_S^2)$ | $-1044148$ MeV$^2$ | $m_{K_0^\star(1430)}$ | 1550 |

**Table 10.1:** Best solutions of Eqs. (10.11) - (10.14) under the conditions $Z_\pi \overset{!}{>} 1$, $Z_K \overset{!}{>} 1$.

The value of $m_{K_S}$ is larger than the PDG value due to the pattern of explicit symmetry breaking that in our model makes strange mesons approximately 100 MeV ($\simeq$ strange-quark mass) heavier than their non-strange counterparts. We also note that the $K_0^\star(1430)$ resonance is rather broad [$\Gamma_{K_0^\star(1430)}^{\rm exp} = (270 \pm 80)$ MeV] and therefore a deviation of 100 MeV exhibited by $m_{K_S}$ is not too large.
Additionally, $\Gamma_{a_1 \to \pi\gamma} = 0.628$ MeV is obtained from the parameter values in Table 10.1, within the interval $\Gamma_{a_1 \to \pi\gamma}^{\rm exp} = (0.640 \pm 0.246)$ MeV cited by the PDG [10]. This is in contrast to the corresponding result in Fit I where we obtained $\Gamma_{a_1 \to \pi\gamma} = 0.322$ MeV (see Table 8.1).

*Step 2.* We now look for values of $m_\rho$, $m_{a_1}$, $m_{K^\star}$, $m_{\omega_S}$, $m_{K_1}$ and $m_{f_{1S}}$ that lead to the pairwise equality of the three $Z_K$ formulas, Eqs. (7.3) and (7.4). We use the already known values of $Z_\pi$ and $Z_K$ from Table 10.1 and also the PDG values of all mentioned (axial-)vector masses except $m_{a_1}$ [because the value cited by the PDG is merely an educated guess and also because $a_1(1260)$ is a rather broad resonance]. As in Fit I, it is not possible to equate pairwise the $Z_K$ formulas in Eqs. (7.3) and (7.4) if we use the PDG values of the masses. A numerical analysis demonstrates that Eqs. (7.3) and (7.4) are fulfilled if the following mass values are used:

$$m_{a_1} = 1219 \text{ MeV}, \; m_\rho = 775.49 \text{ MeV}, \; m_{K^\star} = 916.52 \text{ MeV},$$
$$m_{\omega_S} = 1036.90 \text{ MeV}, \; m_{K_1} = 1343 \text{ MeV}, \; m_{f_{1S}} = 1457.0 \text{ MeV}. \tag{10.25}$$

*Steps 3 and 4.* The (axial-)vector fit parameters can now be determined in such a way that the mass values determined by the three $Z_K$ formulas are reproduced. The total decay width of $a_0(1450)$, Eq. (10.10), allow us in principle to determine the value of parameter $h_2$, if all other parameters entering Eq. (10.10) are known, i.e., if the parameters $Z_\pi$, $Z_K$, $\lambda_2$, $g_1$, $h_3$ and $c_1$ have been determined. The parameters $Z_\pi$, $Z_K$ and $\lambda_2$ are known from Table 10.1; $g_1$ and $h_3$ can be calculated from $m_\rho$ and $m_{a_1}$ via Eqs. (6.55) and (6.56). As already discussed in Chapter 6, the parameter $c_1$ influences only the phenomenology of $\eta$ and $\eta'$; these two fields appear in two of the $a_0(1450)$ decay channels and for that reason we first have to determine the value of $c_1$ before the value of $h_2$ can be calculated. This is performed using the mass terms for $\eta$ and $\eta'$, Eqs. (10.15) and (10.16). We substitute $c_1$ by $\varphi_\eta$, Eq. (7.24) and use the parameter values from Table 10.1 as well as the mass values from Eqs. (10.25). A subsequent analysis yields $m_\eta = 523.20$ MeV, $m_{\eta'} = 957.78$ MeV and consequently $\varphi_\eta = -43.9°$. Therefore, as in Fit I, it is possible to exactly obtain the experimental value of $m_{\eta'}$, but not of $m_\eta$, due to the condition that $\varphi_\eta <| 45° |$ which is necessary to ascertain $m_{\eta_N} < m_{\eta_S}$. (Enforcing $m_\eta = m_\eta^{\text{exp}}$ would require $\varphi_\eta >| 45° |$ and would spoil the result for $m_{\eta'}$.) Then Eq. (7.24) yields $c_1 = 0.00063$ MeV$^{-2}$.
Consequently, all parameters entering the formula for the full decay width of $a_0(1450)$, see Eq. (10.10), are known; we obtain $h_2 = -0.736$ from the condition $\Gamma_{a_0(1450)} = 265$ MeV. The value of $h_2$ is considerably smaller than in Fit I that yielded $h_2 = 40.6$. The best values of the two remaining parameter values ($m_1$ and $\delta_S$), obtained from the (axial-)vector mass formulas in Eqs. (6.40) - (6.45) and mass values in Eqs. (10.25), read $m_1 = 762$ MeV and $\delta_S = 485^2$ MeV$^2$.
Table 10.2 shows the cumulated results for all parameters from Fit II.

| Parameter | Value | Parameter | Value |
|---|---|---|---|
| $Z_\pi$ | 1.66 | $g_1$, Eq. (6.55) | 6.35 |
| $Z_K$ | 1.515 | $g_2$, Eq. (5.45) | 3.07 |
| $\lambda_2$ | 89.7 | $h_3$, Eq. (6.56) | 2.56 |
| $m_0^2 + \lambda_1(\phi_N^2 + \phi_S^2)$ | $-1044148$ MeV$^2$ | $h_{0N}$, Eq. (6.35) | $1.072 \cdot 10^6$ MeV$^3$ |
| $m_1$ | 762 MeV | $h_{0S}$, Eq. (6.37) | $3.388 \cdot 10^7$ MeV$^3$ |
| $\delta_S$ | $485^2$ MeV$^2$ | $h_1$ | 0 |
| $h_2$ | $-0.736$ | $\delta_N$ | 0 |
| $c_1$ | 0.00063 MeV$^{-2}$ | $g_{3,4,5,6}$ | 0 |

**Table 10.2:** Cumulated best values of parameters from Fit II.

Table 10.3 shows the cumulated results for all observables from Fit II. We observe that all mass values stemming from Fit II are within 3% of their respective experimental values, with three exceptions: $m_\eta$, $m_{K_0^\star(1430)}$ and $m_{K_1}$.

We have already noted that the value of $m_\eta$ reproduced by our fit cannot correspond exactly to the experimental value $m_\eta^{\text{exp}} = 547.85$ MeV as this would require $\varphi_\eta >| 45° |$ and thus also $m_{\eta_N} > m_{\eta_S}$. The values of $m_\eta$ and $m_{\eta'}$ present in Table 10.3 imply $\varphi_\eta = -43.9°$; it is therefore

| Observable | Our Value [MeV] | Experimental Value [MeV] |
|---|---|---|
| $m_\pi$ | 138.65 | 139.57 |
| $m_K$ | 497.96 | 493.68 |
| $m_{a_0(1450)}$ | 1452 | 1474 |
| $m_{K_0^\star(1430)}$ | 1550 | 1425 |
| $m_\eta$ | 523.20 | 547.85 |
| $m_{\eta'}$ | 957.78 | 957.78 |
| $m_\rho$ | 775.49 | 775.49 |
| $m_{a_1}$ | 1219 | 1230 |
| $m_{K^\star}$ | 916.52 | 891.66 |
| $m_{\omega_S}$ | 1036.90 | 1019.46 |
| $m_{K_1}$ | 1343 | 1272 |
| $m_{f_{1S}}$ | 1457.0 | 1426.4 |
| $\Gamma_{a_1\to\pi\gamma}$ | 0.622 | 0.640 |
| $\Gamma_{a_0(1450)}$ | 265 | 265 |

**Table 10.3:** Cumulated values of observables from Fit II (experimental uncertainties omitted).

possible to (marginally) decrease $\varphi_\eta$ to $-45°$ and obtain a slightly larger value of $m_\eta$ (but still smaller than $m_\eta^{\rm exp}$). Then, however, the result for $m_{\eta'}$ would be spoiled. We will therefore work with the values of $m_\eta$ and $m_{\eta'}$ as stated in Table 10.3.

We have also already noted that the value of $m_{K_0^\star(1430)}$ from Table 10.3 is larger than the corresponding PDG value due to the pattern of explicit symmetry breaking that in our model made $K_0^\star(1430)$ approximately 100 MeV ($\simeq$ strange-quark mass) heavier than its non-strange counterpart, $a_0(1450)$. The $K_0^\star(1430)$ resonance also possesses a decay width of approximately 270 MeV and therefore the stated deviation of $m_{K_0^\star(1430)}$ from experiment is acceptable.

We observe from Table 10.3 that the value of $m_{K_1}$ is approximately 70 MeV larger than $m_{K_1(1270)}$ = 1272 MeV [10]. It is, however, approximately, 60 MeV smaller than $m_{K_1(1400)}$ = 1403 MeV [10]. Both mentioned resonances are rather broad [$\Gamma_{K_1(1270)} = (90 \pm 20)$ MeV; $\Gamma_{K_1(1400)} = (174 \pm 13)$ MeV]. Therefore, the field $K_1$ from our model can in principle be assigned to either of them. However, a more plausible explanation is that our $K_1$ field is a mixture of the two physical fields $K_1(1270)$ and $K_1(1400)$ – or, in other words, that the physical resonances $K_1(1270)$ and $K_1(1400)$ are mixtures of the field $K_1$ from our model and an additional field currently not present in our model. We discuss this possibility in Sec. 10.3.

Finally, let us also note that Fit II yields a large value of $m_1$ = 762 MeV, just as Fit I. This implies that non-quark contributions are expected to play a strong role in the mass generation of the $\rho$ meson. However, Fit II also yields the decay width $\Gamma_{a_1\to\pi\gamma}$ within the experimental boundaries (unlike Fit I) and we observe additionally that the correspondence of our mass values to experiment is in Fit II decisively better than in Fit I (see Tables 8.5 and 10.3). We can thus conclude that the results obtained until now give Fit II precedence over Fit I.

### 10.3 Two $K_1$ Fields

We have seen in the previous section that Fit II implies $m_{K_1} = 1343$ MeV, a value that is virtually the median of $m_{K_1(1270)}$ and $m_{K_1(1400)}$. Thus our previous assignment of the $K_1$ field from the model to the $K_1(1270)$ resonance appears to be somewhat in doubt as $m_{K_1}$ deviates almost equally from both $m_{K_1(1270)}$ and $m_{K_1(1400)}$. In this section we propose an explanation for the value of $m_{K_1}$ obtained from Fit II [247, 248, 249, 250, 251, 252].
Let us postulate the existence of the following two nonets, labelled $A_1^\mu$ and $B_1^\mu$:

$$A_1^\mu = \frac{1}{\sqrt{2}} \begin{pmatrix} \frac{f_{1N,A}+a_1^0}{\sqrt{2}} & a_1^+ & K_{1,A}^+ \\ a_1^- & \frac{f_{1N,A}-a_1^0}{\sqrt{2}} & K_{1,A}^0 \\ K_{1,A}^- & \bar{K}_{1,A}^0 & f_{1S,A} \end{pmatrix}^\mu , B_1^\mu = \frac{1}{\sqrt{2}} \begin{pmatrix} \frac{f_{1N,B}+b_1^0}{\sqrt{2}} & b_1^+ & K_{1,B}^+ \\ b_1^- & \frac{f_{1N,B}-b_1^0}{\sqrt{2}} & K_{1,B}^0 \\ K_{1,B}^- & \bar{K}_{1,B}^0 & f_{1S,B} \end{pmatrix}^\mu . \tag{10.26}$$

Let us assign the field $a_1^\mu$ from $A_1^\mu$ to the $a_1(1260)$ resonance and the field $b_1^\mu$ from $B_1^\mu$ to the $b_1(1235)$ resonance. The $a_1(1260)$ meson is a $I(J^{PC}) = 1(1^{++})$ state whereas $b_1(1235)$ is a $I(J^{PC}) = 1(1^{+-})$ state. Thus the resonances possess different charge conjugation $C$.
Due to $P = (-1)^{L+1}$, where $P$ denotes parity and $L$ the orbital angular momentum, both resonances exhibit $L = 1$; however, the difference in $C$ implies $S = 1$ for $a_1(1260)$ and $S = 0$ for $b_1(1235)$, with $C = (-1)^{L+S}$ and $S$ denoting the spin. In the spectroscopic $^{2S+1}L_J$ notation ($J$: total angular momentum), our states are thus $P$-wave states: $a_1^\mu$ is a $^3P_1$ state while $b_1^\mu$ represents a $^1P_1$ state. Consequently, all states present in the nonet $A_1^\mu$ are $^3P_1$ states and all states present in the nonet $B_1^\mu$ are $^1P_1$ states. Thus the nonet $A_1^\mu$ contains axial-vectors while the nonet $B_1^\mu$ contains pseudovectors. We then assign the fields in the two nonets as follows: $f_{1N,A} \equiv f_1(1285)$, $f_{1S,A} \equiv f_1(1420)$, $f_{1N,B} \equiv h_1(1170)$, $f_{1S,B} \equiv h_1(1380)$. Let us not assign $K_{1,A}$ and $K_{1,B}$ for the moment.

It is possible to bring about the mixing of the two nonets using the explicit symmetry breaking in the axial-vector channel, modelled by the $\Delta$ matrix in Eq. (6.13). Indeed a calculation of the following term containing the commutator of $A_1^\mu$ and $B_1^\mu$

$$\mathrm{Tr}(\Delta[A_1, B_1]^\mu) \tag{10.27}$$

yields

$$\mathrm{Tr}(\Delta[A_1, B_1]^\mu) = \frac{1}{2}(\delta_S - \delta_N)(\bar{K}_{1\mu,A}^0 K_{1,B}^{\mu 0} - \bar{K}_{1\mu,B}^0 K_{1,A}^{\mu 0} + K_{1\mu,A}^- K_{1,B}^{\mu +} - K_{1\mu,A}^+ K_{1,B}^{\mu -}). \tag{10.28}$$

Note that the commutator $[A_1, B_1]$ is $CP$ invariant: $P$ invariance is trivially fulfilled due to $A_1 \xrightarrow{P} A_1$, $B_1 \xrightarrow{P} B_1$ while the $C$ transformation ($A_1 \xrightarrow{C} A_1^\mathrm{t}$, $B_1 \xrightarrow{C} -B_1^\mathrm{t}$) yields $\mathrm{Tr}(\Delta[A_1, B_1]^\mu) \xrightarrow{C} \mathrm{Tr}(\Delta(B_1^\mathrm{t} A_1^\mathrm{t} - A_1^\mathrm{t} B_1^\mathrm{t})^\mu) = \mathrm{Tr}(\Delta(A_1 B_1 - B_1 A_1)^\mathrm{t})^\mu = \mathrm{Tr}(\Delta[A_1, B_1]^\mu)$.

Therefore, the non-vanishing difference of quark masses $m_s^2 - m_u^2 \sim \delta_S - \delta_N$ induces mixing of the axial-vector nonet $A_1^\mu$ with the pseudovector nonet $B_1^\mu$. The term (10.27) yields mixing of the $K_1$ states; in other words, the $K_1$ fields from the two nonets mix due to explicit breaking of the chiral symmetry. Consequently, we assert that the physical fields $K_1(1270)$ and $K_1(1400)$ arise from the mixing of $K_{1,A}$ and $K_{1,B}$. The $K_1$ state from our Lagrangian (6.1) then corresponds to

$K_{1,A}$ whose $^1P_1$ counterpart is not present in the model. For this reason, it is not surprising that our model yields $m_{K_1}$ different from masses of both $K_1(1270)$ and $K_1(1400)$, see Table 10.3. Therefore, an extension of our model by a nonet of $^1P_1$ states may be a useful tool to further study kaon phenomenology. Such spin-orbit mixing has been considered, e.g., in Ref. [247] (see also Ref. [248]) where, within a non-relativistic constituent quark model, it was found that two mixing scenarios of the $K_{1,A}$ and $K_{1,B}$ states are possible: (*i*) $K_{1,A}$-$K_{1,B}$ mixing angle $\varphi_{K_1} \simeq 37°$, $m_{K_{1,A}} = 1322$ MeV and $m_{K_{1,B}} = 1356$ MeV; (*ii*) $\varphi_{K_1} = 45°$, $m_{K_{1,A}} = m_{K_{1,B}} = 1339$ MeV. As shown in Ref. [247], possibility (*ii*) would imply $m_{a_1} = m_{b_1} = 1211$ MeV, slightly at odds with experimental data citing $m_{b_1} = (1229.5 \pm 3.2)$ MeV [10] whereas possibility (*i*) yields $m_{a_1} = 1191$ MeV and $m_{b_1} = 1231$ MeV [and also $m_{K_1(1270)} = 1273$ MeV, $m_{K_1(1400)} = 1402$ MeV] and thus a better correspondence with experiment. Our model is of course different from that of Ref. [247]; however, the qualitative consistency of our (independently obtained) value $m_{K_1} = 1343$ MeV with the results of Ref. [247] seems to confirm the notion that $K_1(1270)$ and $K_1(1400)$ indeed arise from the mixing of $^1P_1$ and $^3P_1$ nonets.

Note that the inclusion and further study of the term (10.27) in our model would make the mixing of $K_{1,A}$ and $K_{1,B}$ an intrinsic property of the model; however, there are also alternative mixing mechanisms, not based on an analysis of mass eigenstates, such as mixing via decay channels as suggested in Ref. [249]. Additionally, a calculation of $\varphi_{K_1}$ from a QCD-like theory in Ref. [250] found $\varphi_{K_1} \simeq 35°$ to be preferred; for other analyses of $\varphi_{K_1}$, see Ref. [251]. It is possible to study mixing of other states from the two nonets as well, such as $f_{1N,A}$-$f_{1S,A}$ and $f_{1N,B}$-$f_{1S,A}$ mixings in Refs. [250, 252].

We will discuss the broader $K_1$ phenomenology (decay widths) further on, in Sec. 11.3.7.

# 11. Implications of Fit II

We now turn to the discussion of meson phenomenology that follows from Fit II. As in Fit I, we will devote particular attention to hadronic decay widths of scalar and axial-vector resonances as a matter of comparing results between Fits I and II but also because these resonances possess the most ambiguities regarding their structure and decay widths.

## 11.1 Phenomenology in the $I(J^{PC}) = 0(0^{++})$ Channel

In this section we discuss results regarding the masses and decay widths of the two scalar states $\sigma_1$ and $\sigma_2$. These states arise from mixing of the two pure states $\sigma_N$ and $\sigma_S$ present in Lagrangian (6.1). The mixing is described at the beginning of Sec. 9.1.3, see Eqs. (9.16) - (9.23). We note again that the mass terms $m_{\sigma_N}$ and $m_{\sigma_S}$ depend on $m_0^2 + 3\lambda_1\phi_N^2 + \lambda_1\phi_S^2$ and $m_0^2 + \lambda_1\phi_N^2 + 3\lambda_1\phi_S^2$, respectively, and thus cannot be calculated from the knowledge of the linear combination $m_0^2 + \lambda_1(\phi_N^2 + \phi_S^2)$ in Table 10.2. Therefore, as in Fit I, we express the parameter $\lambda_1$ in terms of the mass parameter $m_0^2$ using the mentioned linear combination. Additionally, the necessary condition for the spontaneous breaking of the chiral symmetry suggests $m_0^2 < 0$ [see inequality (9.4)]. We note at this point that, due to the latter condition, the parameter $\lambda_1$ obtained from Fit II fulfills the constraint (9.15), as apparent from Fig. 11.1.

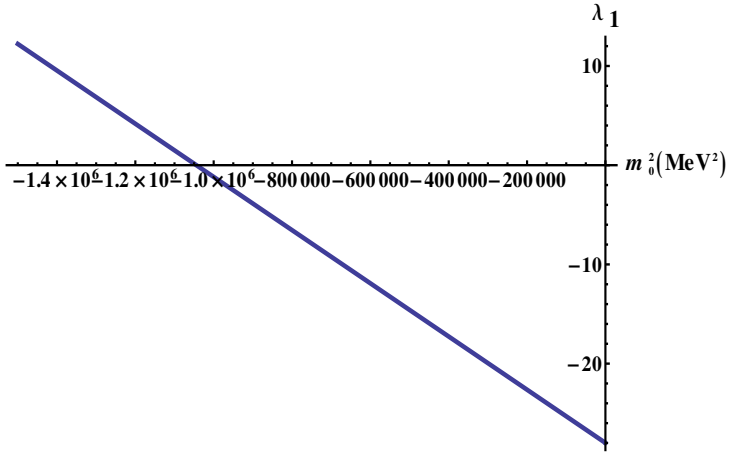


**Figure 11.1:** Dependence of parameter $\lambda_1$ on $m_0^2$ from Fit II. The condition (9.15), i.e., $\lambda_1 > -\lambda_2/2$, is fulfilled for all values of $m_0^2 < 0$, see Table 10.2.

Now we can turn to the calculation of $m_{\sigma_{1,2}}$ and $\sigma_{1,2}$ decay widths.

### 11.1.1 Scalar Isosinglet Masses

As described at the beginning of this section, we substitute $\lambda_1$ in Eqs. (9.19) and (9.20) by $m_0^2$ [from the linear combination $m_0^2 + \lambda_1(\phi_N^2 + \phi_S^2)$ in Table 10.2]. The ensuing dependence of $m_{\sigma_1}$ and $m_{\sigma_2}$ on $m_0^2$ is depicted in Fig. 11.2, with $m_0^2 \leq 0$ in accordance with Eq. (9.4).
As in Fit I, $m_{\sigma_1}$ and $m_{\sigma_2}$ vary over wide intervals. We note from Fig. 11.2 that $m_{\sigma_N}$ becomes

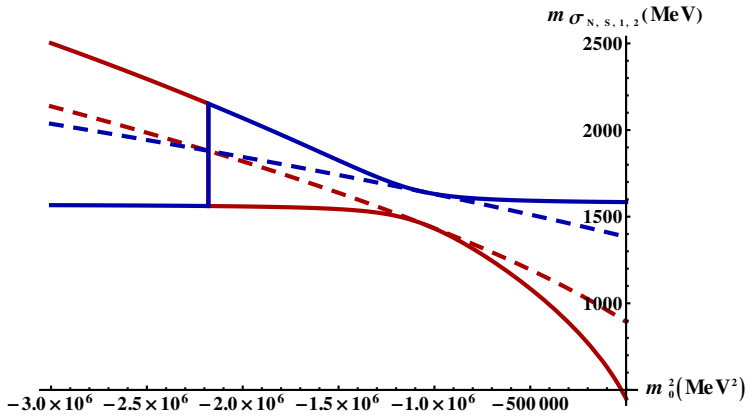


**Figure 11.2:** Dependence of $m_{\sigma_1}$ (full lower curve), $m_{\sigma_2}$ (full upper curve), $m_{\sigma_N}$ (dashed lower curve) and $m_{\sigma_S}$ (dashed upper curve) on $m_0^2$ under the condition $m_0^2 < 0$.

larger than $m_{\sigma_S}$ at $m_0^2 \simeq -2.179 \cdot 10^6$ MeV$^2$ at which point there is a jump of $\varphi_\sigma$ from $-45°$ to $45°$ (see Fig. 11.3).

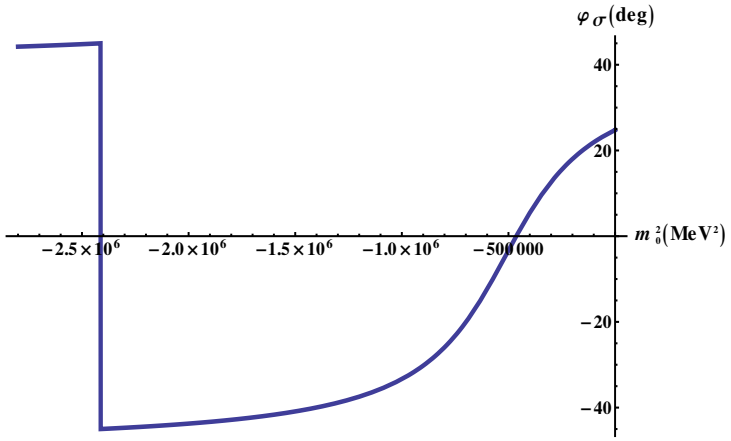


**Figure 11.3:** Dependence of the $\sigma_N$-$\sigma_S$ mixing angle $\varphi_\sigma$ on $m_0^2$, Eq. (9.23).

Therefore, $\sigma_1$ and $\sigma_2$ interchange places for $m_0^2 \simeq -2.179 \cdot 10^6$ MeV$^2$; we use this value of $m_0^2$ as an upper boundary for this parameter. Thus, together with Eq. (9.4), we obtain

$$-2.179 \cdot 10^6 \text{ MeV}^2 \leq m_0^2 \leq 0. \tag{11.1}$$

From the previous inequality we obtain the following boundaries for $m_{\sigma_{1,2}}$:

$$450 \text{ MeV} \leq m_{\sigma_1} \leq 1561 \text{ MeV}, \tag{11.2}$$

$$1584 \text{ MeV} \leq m_{\sigma_2} \leq 2152 \text{ MeV}. \tag{11.3}$$

The inequalities (11.2) and (11.3) suggest that the mixed state $\sigma_1$ may correspond to $f_0(600)$, $f_0(980)$, $f_0(1370)$ or $f_0(1500)$ whereas the only confirmed resonance within the range of $m_{\sigma_2}$ is $f_0(1710)$. [As in Fit I, we do not consider the states $f_0(1790)$, $f_0(2020)$, $f_0(2100)$ and $f_0(2200)$.] A definitive assignment of $\sigma_1$, and a confirmation whether $\sigma_2$ corresponds to $f_0(1710)$, require

a more detailed analysis of phenomenology in the scalar channel, performed in the following sections.
Nonetheless, from the variation of the $\sigma_N$ - $\sigma_S$ mixing angle $\varphi_\sigma$ we can conclude that $\sigma_1$ is predominantly a $\bar{n}n$ state and the $\sigma_2$ field is predominantly composed of strange quarks, see Fig. 11.4. Note that, as in Fit I, we obtain the two diagrams in Fig. 11.4 from two implicit plots: of $\varphi_\sigma(\lambda_1)$, Eq. (9.23), and $m_{\sigma_{1,2}}[\varphi_\sigma(\lambda_1)]$, Eqs. (9.19) and (9.20), with $m_0^2+\lambda_1(\phi_N^2+\phi_S^2) = -1044148$ MeV$^2$ from Table 10.2 and $m_0^2$ from the inequality (9.24).

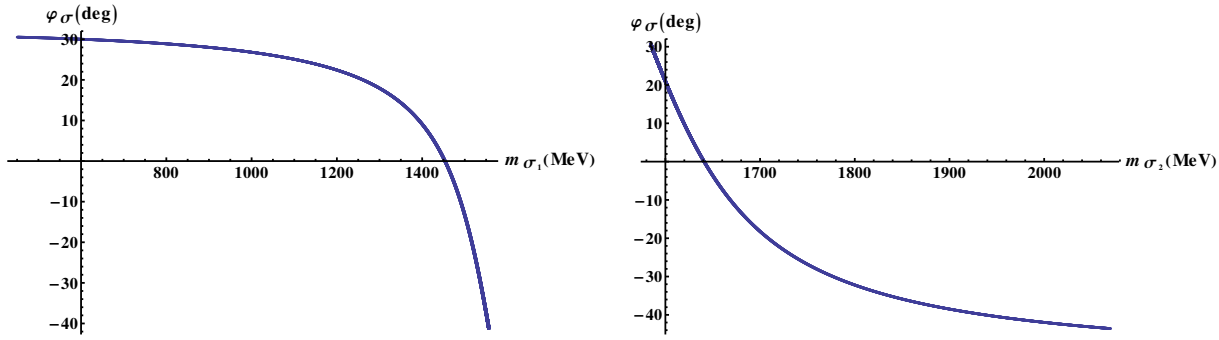


**Figure 11.4:** The $\sigma_N$-$\sigma_S$ mixing angle $\varphi_\sigma$ as function of $m_{\sigma_{1,2}}$.

Contribution of $m_{\sigma_N}$ to $m_{\sigma_1}$ and contribution of $m_{\sigma_S}$ to $m_{\sigma_2}$ are illustrated in Fig. 11.5.

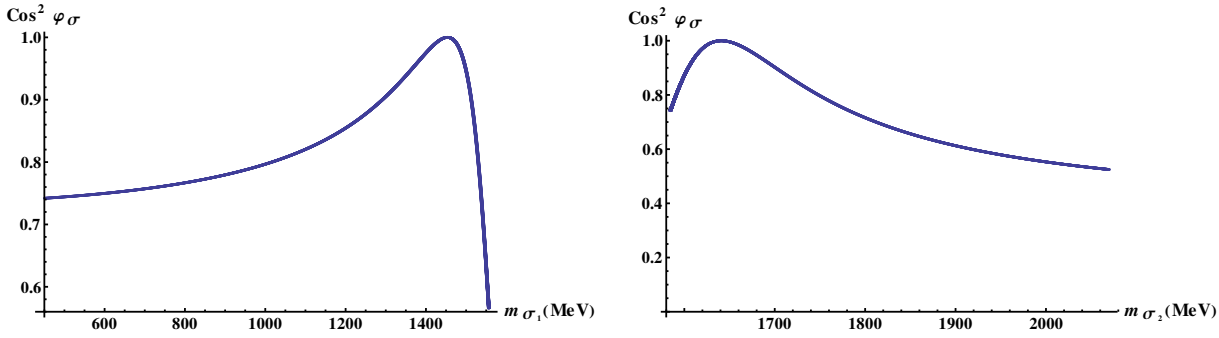


**Figure 11.5:** Contribution of the pure non-strange field $\sigma_N$ to $\sigma_1$ (left panel) and of the pure strange field $\sigma_S$ to $\sigma_2$ (right panel), respectively in dependence on $m_{\sigma_1}$ and $m_{\sigma_2}$.

Before we continue, let us make an important point: we observe from Fig. 11.2 that $m_{\sigma_1}$ and $m_{\sigma_2}$ are not independent. Thus, in the following, any determination of either of these masses (e.g., from a decay width) fixes the other mass to a certain value (and also determines values of all decay widths depending on this mass). This is true because the two masses are connected via the mass parameter $m_0^2$ (as also apparent from Fig. 11.2). We will be making use of this feature in the following sections.

### 11.1.2 Decay Width $\sigma_{1,2} \to \pi\pi$

In Sec. 9.1.4 we have already performed the calculation of the decay widths $\Gamma_{\sigma_1\to\pi\pi}$, Eq. (9.39), and $\Gamma_{\sigma_2\to\pi\pi}$, Eq. (9.40), from the $\sigma\pi\pi$ interaction Lagrangian (9.27). We can therefore immedi-

ately plot the two decay widths, see Fig. 11.6.

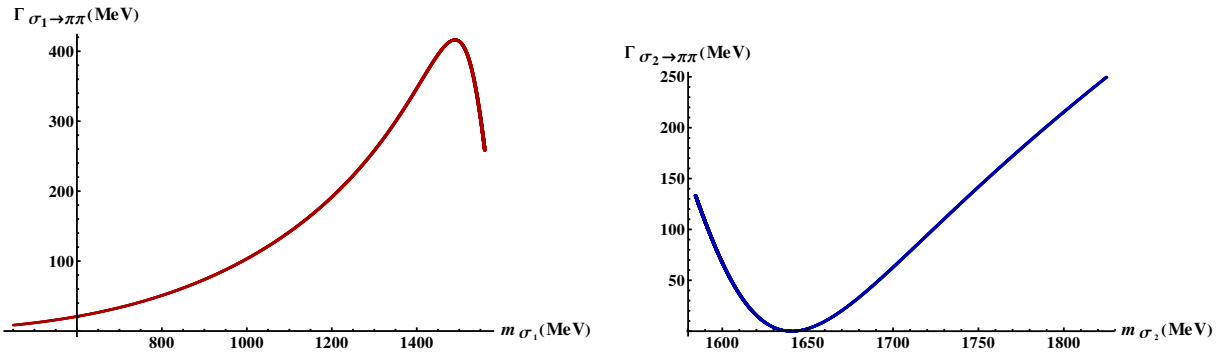


**Figure 11.6:** $\Gamma_{\sigma_1\to\pi\pi}$ and $\Gamma_{\sigma_2\to\pi\pi}$ as functions of $m_{\sigma_1}$ and $m_{\sigma_2}$, respectively.

From the left panel of Fig. 11.6 we can conclude that the state $\sigma_1$ appears to possess the best correspondence with the $f_0(1370)$ resonance. Clearly, $\Gamma_{\sigma_1\to\pi\pi}$ is too small in the mass region of $f_0(600)$, i.e., $m_{\sigma_2} \lesssim 800$ MeV. Therefore, an assignment of $\sigma_1$ to $f_0(600)$ based on the $2\pi$ decay channel is not possible. Additionally, $\sigma_1$ cannot correspond to the $f_0(1500)$ resonance either: we obtain $\Gamma_{\sigma_1\to\pi\pi} \simeq 400$ MeV at $m_{\sigma_1} \simeq 1500$ MeV, in stark contrast to experimental data [10] reading $\Gamma_{f_0(1500)\to\pi\pi} \simeq 30$ MeV.
Let us now ascertain whether there is indeed a good correspondence of our predominantly non-strange state $\sigma_1$ to $f_0(1370)$, and additionally of $\sigma_2$ to $f_0(1710)$ as suggested by $m_{\sigma_2}$, see discussion of Fig. 11.2. There are two strategies to this end: we can first determine $m_{\sigma_1}$ necessary to describe correctly $\Gamma_{f_0(1370)\to\pi\pi}$ from Ref. [40] (a comprehensive fit of several data sets used here because the PDG data [10] are not conclusive), then calculate $m_{\sigma_2}$ and $\Gamma_{\sigma_2\to\pi\pi}$ and compare these results with $m_{f_0(1710)}$ and $\Gamma_{f_0(1710)\to\pi\pi}$. Alternatively, we can first determine our result for $m_{\sigma_2}$ in such a way that $\Gamma_{\sigma_2\to\pi\pi}$ describes $\Gamma_{f_0(1710)\to\pi\pi}$ correctly and then calculate $m_{\sigma_1}$ and $\Gamma_{\sigma_1\to\pi\pi}$ and compare them with results for $m_{f_0(1370)}$ and $\Gamma_{f_0(1370)\to\pi\pi}$ from Ref. [40].

- Reference [40] cites the value of $\Gamma_{f_0(1370)} = 325$ MeV at $m_{f_0(1370)} = (1309 \pm 1 \pm 15)$ MeV from an $f_0(1370)$ Breit-Wigner fit and we obtain $\Gamma_{\sigma_1\to\pi\pi} = 325$ MeV at $m_{\sigma_1} = 1376$ MeV. Reference [40] also cites the value of 207 MeV for the full width at half maximum (FWHM) with the peak in the decay channel $f_0(1370) \to \pi\pi$ at $m_{f_0(1370)} = 1282$ MeV – we obtain $\Gamma_{\sigma_1\to\pi\pi} = 207$ MeV at $m_{\sigma_1} = 1225$ MeV. Our results are thus qualitatively consistent with results from Ref. [40]. As already noted, assigning a value to $m_{\sigma_1}$ implies also a certain value of $m_{\sigma_2}$. Consequently, $m_{\sigma_1} = 1376$ MeV leads to $m_{\sigma_2} = 1616$ MeV and to $\Gamma_{\sigma_2\to\pi\pi} = 22.6$ MeV whereas $m_{\sigma_1} = 1225$ MeV leads to $m_{\sigma_2} = 1599$ MeV and to $\Gamma_{\sigma_2\to\pi\pi} = 71.2$ MeV (see the right panel of Fig. 11.6). $\Gamma_{\sigma_2\to\pi\pi} = 22.6$ MeV is within the PDG-preferred interval of Eq. (3.10) reading $\Gamma_{f_0(1710)\to\pi\pi} = 29.28^{+5.42}_{-7.69}$ MeV; it is outside the BES II interval $\Gamma_{f_0(1710)\to\pi\pi} < 9.34$ MeV, Eq. (3.25) and also above the WA102 range $\Gamma_{f_0(1710)\to\pi\pi} = (16.1 \pm 3.6)$ MeV, see Eq. (3.32). $\Gamma_{\sigma_2\to\pi\pi} = 71.2$ MeV is outside all the mentioned intervals.

- Enforcing $\Gamma_{\sigma_2\to\pi\pi} = 29.28^{+5.42}_{-7.69}$ MeV $\equiv \Gamma^{\rm PDG}_{f_0(1710)\to\pi\pi}$ leads to two sets of solutions for $m_{\sigma_2}$ due to the parabolic form of $\Gamma_{\sigma_2\to\pi\pi}$, see Fig. 11.2. We obtain $(i)$ $m_{\sigma_2} = (1613 \mp 3)$ MeV and $(ii)$ $m_{\sigma_2} = 1677^{+4}_{-6}$ MeV. Both sets of results are below $m_{f_0(1710)} = (1720 \pm 6)$ MeV [10].

From results $(i)$ we obtain $m_{\sigma_1} = 1360^{-15}_{+19}$ MeV and $\Gamma_{\sigma_1\to\pi\pi} = 309^{-13}_{+19}$ MeV. From results $(ii)$ we obtain $m_{\sigma_1} = 1497^{+3}_{-5}$ MeV and $\Gamma_{\sigma_1\to\pi\pi} = (415 \mp 1)$ MeV. The second set of results would imply a dominant $2\pi$ decay of $f_0(1370)$ at approximately 1.5 GeV, at odds with experimental data [40] and therefore we will not consider it. The first set of results, however, can accommodate $\Gamma_{f_0(1370)} = 325$ MeV, although the corresponding mass $m_{\sigma_1} = 1360^{-15}_{+19}$ MeV is slightly larger than the one cited in Ref. [40]. Additionally, the first set of results describes $\Gamma_{f_0(1710)\to\pi\pi}$ correctly although the obtained mass interval $m_{\sigma_2} = (1613 \mp 3)$ MeV is approximately 100 MeV smaller than the PDG result $m_{f_0(1710)} = (1720 \pm 6)$ MeV.

Constraining $m_{\sigma_2}$ via $\Gamma^{\text{BES II}}_{f_0(1710)\to\pi\pi} < 9.34$ MeV, Eq. (3.25), yields 1624 MeV $\leq m_{\sigma_2} \leq$ 1659 MeV, 1411 MeV $\leq m_{\sigma_1} \leq$ 1480 MeV and 359 MeV $\leq \Gamma_{\sigma_1\to\pi\pi} \leq$ 415 MeV. These results imply a slightly too large value of $m_{\sigma_1}$ where the $2\pi$ channel is expected to be dominant for $f_0(1370)$ – Ref. [40] suggests the mass of approximately 1300 MeV, not 1400 MeV, where $f_0(1370)$ decays predominantly into $2\pi$ rather than $4\pi$.

We can also utilise $\Gamma^{\text{WA102}}_{f_0(1710)\to\pi\pi} = 16.1 \pm 3.6$ MeV, Eq. (3.32), to constrain $m_{\sigma_2}$. We obtain $(i)$ $m_{\sigma_2} = 1619^{-2}_{+3}$ MeV and $(ii)$ $m_{\sigma_2} = (1666 \pm 3)$ MeV. From results $(i)$ we obtain $m_{\sigma_1} = (1393 \mp 9)$ MeV and $\Gamma_{\sigma_1\to\pi\pi} = (341 \mp 9)$ MeV. From results $(ii)$ we obtain $m_{\sigma_1} = (1487 \pm 3)$ MeV and $\Gamma_{\sigma_1\to\pi\pi} = 416$ MeV. Results $(ii)$ would suggest a large contribution of the $2\pi$ channel to $f_0(1370)$ at $\simeq 1.49$ MeV and we therefore disregard them; results $(i)$ are then more acceptable but still above the range of $m_{\sigma_1} = 1360^{-15}_{+19}$ MeV and $\Gamma_{\sigma_1\to\pi\pi} = 309^{-13}_{+19}$ MeV, obtained from $\Gamma^{\text{PDG}}_{f_0(1710)\to\pi\pi}$. We thus prefer the latter result.

We conclude that results regarding the $2\pi$ decay channel allow for a correct description of the $f_0(1370)$ and $f_0(1710)$ decay widths, although the mass values could be improved. The latter point emphasises the need to include a glueball state into our model [203] because, if it is found at $\sim 1.5$ GeV, this state should induce a level repulsion shifting $m_{\sigma_1}$ downwards and $m_{\sigma_2}$ upwards – i.e., both masses being shifted in the directions favoured by the experiment.
The best results suggested by comparing $\Gamma_{\sigma_1\to\pi\pi}$ to $\Gamma_{f_0(1370)\to\pi\pi}$ and $\Gamma_{\sigma_2\to\pi\pi}$ to $\Gamma_{f_0(1710)\to\pi\pi}$ read $m_{\sigma_1} = 1360^{+16}_{-17}$ MeV, $\Gamma_{\sigma_1\to\pi\pi} = 309^{+16}_{-15}$ MeV, $m_{\sigma_2} = (1613 \pm 3)$ MeV and $\Gamma_{\sigma_2\to\pi\pi} = (29.3 \pm 6.5)$ MeV. These results justify the assignments $\sigma_1 \equiv f_0(1370)$ and $\sigma_2 \equiv f_0(1710)$; the assignments will also be confirmed in the subsequent sections (see below). The results also suggest that $f_0(1370)$ is $94.6^{-1.0}_{+1.4}\%$ a $\bar{n}n$ state and, conversely, that $f_0(1710)$ is $94.6^{-1.0}_{+1.4}\%$ a $\bar{s}s$ state.

As apparent from Fig. 11.6, $\Gamma_{\sigma_2\to\pi\pi} = 0$ for $m_{\sigma_2} = 1640$ MeV, corresponding to $m_0^2 = -1044148$ MeV$^2$ and thus $m_{\sigma_1} = 1452$ MeV (see Fig. 11.2). As already noted, the parameter $\lambda_1$ in our fit is determined only indirectly, from the linear combination $m_0^2 + \lambda_1(\phi_N^2 + \phi_S^2) = -1044148$ MeV$^2$ (see Table 10.2). Therefore, $\lambda_1 = 0$ for $m_0^2 = -1044148$ MeV$^2$; consequently, according to Eq. (9.23), one also obtains that the $\sigma_N$ - $\sigma_S$ mixing angle $\varphi_\sigma = 0$. Thus $\sigma_N$ and $\sigma_S$ decouple. As in Fit I, $\Gamma_{\sigma_2\to\pi\pi}$ then vanishes identically because $\lambda_1 = 0 = h_1$ (and only these large-$N_c$ suppressed parameters could bring about $\Gamma_{\sigma_2\to\pi\pi} \neq 0$). Setting $h_1 \neq 0$ would not alter $\Gamma_{\sigma_2\to\pi\pi} = 0$ for a certain value of $m_{\sigma_2}$ because of the relative minus sign of the two terms in $\mathcal{M}_{\sigma_2\to\pi\pi}$, Eq. (9.38). The relative sign difference still leads to a cancellation of the two terms in $\mathcal{M}_{\sigma_2\to\pi\pi}$ for a certain value of $\varphi_\sigma$.

Thus our Fit II prefers $f_0(1370)$ rather than $f_0(600)$ to be the non-strange quarkonium, just as Scenario II of the $U(2) \times U(2)$ version of our model.

*A note on $\sigma_{1,2} \to 4\pi$ decays.* We have also considered the sequential decay $\sigma_{1,2} \to \rho\rho \to 4\pi$ by integrating over the spectral functions of the two intermediate $\rho$ mesons, similarly to Sec. 5.4.2. The following Lagrangian obtained from Eq. (6.1) has been utilised:

$$\begin{aligned}\mathcal{L}_{\sigma\rho\rho} &= \frac{1}{2}(h_1+h_2+h_3)\phi_N\sigma_N\left[(\rho_\mu^0)^2+2\rho_\mu^+\rho_\mu^-\right]+\frac{1}{2}h_1\phi_S\sigma_S\left[(\rho_\mu^0)^2+2\rho_\mu^+\rho_\mu^-\right]\\ &= \frac{1}{2}\left[(h_1+h_2+h_3)\phi_N\cos\varphi_\sigma+h_1\phi_S\sin\varphi_\sigma\right]\sigma_1\left[(\rho_\mu^0)^2+2\rho_\mu^+\rho_\mu^-\right]\\ &+\frac{1}{2}\left[h_1\phi_S\cos\varphi_\sigma-(h_1+h_2+h_3)\phi_N\sin\varphi_\sigma\right]\sigma_2\left[(\rho_\mu^0)^2+2\rho_\mu^+\rho_\mu^-\right] \qquad (11.4)\end{aligned}$$

with the substitutions $\sigma_N \to \cos\varphi_\sigma\sigma_1$ and $\sigma_S \to \sin\varphi_\sigma\sigma_1$ that enable us to calculate decay width of $f_0(1370) \equiv \sigma_1$ and the substitutions $\sigma_N \to -\sin\varphi_\sigma\sigma_2$ and $\sigma_S \to \cos\varphi_\sigma\sigma_2$ that enable us to calculate decay width of $f_0(1710) \equiv \sigma_2$ [see Eq. (9.18)]. After the substitutions, the Lagrangian in Eq. (11.4) obtains an analogous form as the one in Eq. (5.129). For this reason it is subsequently possible to perform the mentioned integration over the $\rho$ spectral functions.
We then observe that results obtained from our $N_f = 3$ fit are by at least a factor of ten smaller than those obtained within the realm of Scenario II in the $U(2) \times U(2)$ version of the model. The reason is the different value of $h_2$: whereas in Scenario II of the two-flavour model this parameter had the value $\simeq 5$, our Fit I in the three-flavour model prefers the value of $h_2 \simeq 0$ scaling the $4\pi$ decay width of the scalar states downwards. We expect results in the $4\pi$ channel to improve considerably upon inclusion of the scalar glueball field into the $U(3) \times U(3)$ version of our model because we will see in Chapter 12 that the glueball-field coupling to the $4\pi$ channel is significantly stronger than the corresponding coupling of the non-strange quarkonium. The ensuing mixture of the pure glueball and the pure quarkonium should improve the decay width of the predominantly $\bar{n}n$ state in the $4\pi$ channel.

### A Putative Assignment of $\sigma_1$ to $f_0(980)$

Let us briefly discuss our $\sigma_1$ state in terms of $f_0(980)$, another resonance within the mass range of our $\sigma_1$ state. We note that $\Gamma_{\sigma_1\to\pi\pi} = 97$ MeV at $m_{\sigma_1} = 980$ MeV and that 94 MeV $\leq \Gamma_{\sigma_1\to\pi\pi} \leq$ 100 MeV for 970 MeV $\leq m_{\sigma_1} \leq 990$ MeV, with the latter mass interval corresponding to the lower and upper boundaries of $m_{f_0(980)}$. Given that the full decay width $\Gamma_{f_0(980)} = (40-100)$ MeV [10], there would appear to be some parallels between our $\sigma_1$ state and the $f_0(980)$ resonance. As noted in Sec. 3.2, this resonance is close to the kaon-kaon threshold; thus an experimental analysis is not always straightforward with different collaborations and reviews obtaining at times very different results [67, 95, 96, 97, 98, 99, 101, 102, 105, 113, 114, 115, 118, 119, 124, 158, 253]. We thus note that there is no universally accepted value of $\Gamma_{f_0(980)}$ that ranges between $\sim 14$ MeV [254] ($T$-matrix pole) and $(201 \pm 28)$ MeV [255], with the latter result model-dependent, broad due to inclusion of $KK$-threshold effects and not considering possible interference with the high-mass tail of $f_0(600)$. Additionally, even if the precise value of $\Gamma_{f_0(980)}$ were known, the branching ratio $\Gamma_{f_0(980)\to\pi\pi}/\Gamma_{f_0(980)}$ remains ambiguous.

The $f_0(980)$ resonance can actually also decay non-hadronically, into diphotons and dileptons; however, these decays are known to be suppressed [10] and therefore we can set $\Gamma_{f_0(980)} = \Gamma_{f_0(980)\to\pi\pi} + \Gamma_{f_0(980)\to KK}$ – consequently, $\Gamma_{f_0(980)\to\pi\pi}/\Gamma_{f_0(980)} \equiv \Gamma_{f_0(980)\to\pi\pi}/[\Gamma_{f_0(980)\to\pi\pi} +$

$\Gamma_{f_0(980)\to KK}$]. There are not many publications discussing both $\Gamma_{f_0(980)}$ and $\Gamma_{f_0(980)\to\pi\pi}$ / [$\Gamma_{f_0(980)\to\pi\pi} + \Gamma_{f_0(980)\to KK}$]. Recently, the BABAR Collaboration [256] has published results regarding the $f_0(980)$ phenomenology from the $B^\pm \to K^\pm K^\pm K^\mp$ decay obtaining $\Gamma_{f_0(980)\to\pi\pi}$ / [$\Gamma_{f_0(980)\to\pi\pi} + \Gamma_{f_0(980)\to KK}$] = $0.52 \pm 0.12$. Using $e^+e^-$ annihilation into kaons and pions and isolating hadronic intermediate states, the same Collaboration also found [257] $\Gamma^{(1)}_{f_0(980)} = (65 \pm 13)$ MeV from the $\varphi(1020)\pi^+\pi^-$ intermediate state and $\Gamma^{(2)}_{f_0(980)} = (81 \pm 21)$ MeV from the $\varphi(1020)\pi^0\pi^0$ intermediate state. The mentioned $f_0(980) \to \pi\pi$ branching ratio together with $\Gamma^{(1)}_{f_0(980)}$ suggests $\Gamma^{(1)}_{f_0(980)\to\pi\pi} \simeq (34 \pm 15)$ MeV whereas from $\Gamma^{(2)}_{f_0(980)}$ we obtain $\Gamma^{(2)}_{f_0(980)\to\pi\pi} \simeq (42 \pm 21)$ MeV. Both results are by approximately a factor of two smaller than our result $\Gamma_{\sigma_1\to\pi\pi} = 97$ MeV.
Additionally, a review in Ref. [258] found $\Gamma_{f_0(980)} \sim 25$ MeV and $\Gamma_{f_0(980)\to\pi\pi}/[\Gamma_{f_0(980)\to\pi\pi} + \Gamma_{f_0(980)\to KK}] = 0.68$ from a lowest-order chiral Lagrangian and unitarity. These results suggest $\Gamma_{f_0(980)\to\pi\pi} \sim 17$ MeV, substantially less than our results for $\Gamma_{\sigma_1\to\pi\pi}$. Therefore, our analysis does not favour $f_0(980)$ as a predominantly $\bar{q}q$ state. Note also that assigning $m_{\sigma_1}$ to the mass range between 970 MeV and 990 MeV would imply $m_{\sigma_2} \simeq 1590$ MeV (see Fig. 11.2) and thus $\Gamma_{\sigma_2\to\pi\pi} \simeq 100$ MeV (see the right panel of Fig. 11.6). Therefore, $\sigma_2 \equiv f_0(1710)$ would have to saturate in the $2\pi$ channel. This would clearly be at odds with data [10], and thus it represents an additional argument against interpreting $f_0(980)$ as a predominantly $\bar{q}q$ state within our model.

Nonetheless, it is possible that $f_0(980)$ may contain a quarkonium component [77, 78, 79]. Alternatively, this state can also be interpreted as a $\bar{q}^2q^2$ state, as a glueball, $KK$ bound state or even as an $\eta\eta$ bound state (see Sec. 3.2).

### 11.1.3 Decay Width $\sigma_{1,2} \to KK$

The interaction Lagrangian of the pure states $\sigma_{N,S}$ with the kaons has already been stated in Eq. (9.41). The corresponding decay widths $\Gamma_{\sigma_1\to KK}$ and $\Gamma_{\sigma_2\to KK}$ are given in Eqs. (9.53) and (9.54), respectively.
We can therefore turn directly to a discussion of the decay widths, depicted in Fig. 11.7.

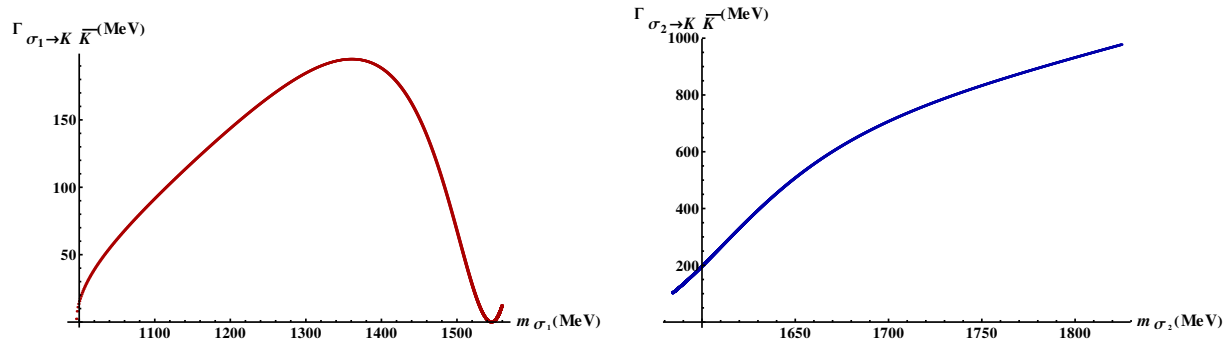


**Figure 11.7:** $\Gamma_{\sigma_1\to KK}$ and $\Gamma_{\sigma_2\to KK}$ as functions of $m_{\sigma_1}$ and $m_{\sigma_2}$, respectively.

From the left panel of Fig. 11.7 we observe that $\Gamma_{\sigma_1\to KK}$ is within the experimental results of Refs. [124, 170, 253, 259, 260, 261]. From the right panel of Fig. 11.7 we observe that $\Gamma_{\sigma_2\to KK}$ rises rapidly with $m_{\sigma_2}$. The PDG data suggest $\Gamma^{\text{PDG}}_{f_0(1710)\to KK} = 71.44^{+23.18}_{-35.02}$ MeV, Eq. (3.15);

note that this is the dominant decay channel of $f_0(1710)$ and thus the reason why, already from the experimental point of view, this resonance is a $\bar{s}s$ candidate. Due to the rapid growth of $\Gamma_{\sigma_2\to KK}$, an exact correspondence of our value with the central value of $\Gamma^{\rm PDG}_{f_0(1710)\to KK}$ would require $m_{\sigma_2} = 1578$ MeV. However, $m_{\sigma_2}$ would then be outside the interval (11.3) determined from the correct implementation of the spontaneous breaking of the chiral symmetry – we would require $m_0^2 > 0$ in contrast to condition (9.4). Due to condition (11.3), the lowest value of $m_{\sigma_2} = 1584$ MeV, for which we obtain $\Gamma_{\sigma_2\to KK} = 102.7$ MeV, is above the interval for $\Gamma^{\rm PDG}_{f_0(1710)\to KK}$. As in the $2\pi$ channel, our results again yield $m_{\sigma_2}$ that is by approximately 100 MeV smaller than $m_{f_0(1710)}$. Additionally, $m_{\sigma_2} = 1584$ MeV implies $m_{\sigma_1} = 450$ MeV (see Fig. 11.2), spoiling the correspondence of $\Gamma_{\sigma_1\to\pi\pi}$ to experiment (see Fig. 11.6). Note, however, that our results allow for the WA102 value $\Gamma^{\rm WA102}_{f_0(1710)\to KK} = (80.5 \pm 30.1)$ MeV to be described: considering 1584 MeV $\leq m_{\sigma_2} \leq$ 1586 MeV yields 103 MeV $\leq \Gamma_{\sigma_2\to KK} \leq$ 110.6 MeV; the $m_{\sigma_2}$ interval is small due to the steep rise of $\Gamma_{\sigma_2\to KK}$, see Fig. 11.7. The mentioned interval also implies 450 MeV $\leq m_{\sigma_1} \leq$ 688 MeV, again spoiling the correspondence of $\Gamma_{\sigma_1\to\pi\pi}$ to experiment as apparent from Fig. 11.6. Thus using $\Gamma_{f_0(1710)\to KK}$ does not allow us to constrain $m_{\sigma_1}$ and $m_{\sigma_2}$ very well.
Let us therefore look into the ratios $\Gamma_{\sigma_1\to KK}/\Gamma_{\sigma_1\to\pi\pi}$ and $\Gamma_{\sigma_2\to\pi\pi}/\Gamma_{\sigma_2\to KK}$, depicted in Fig. 11.8.

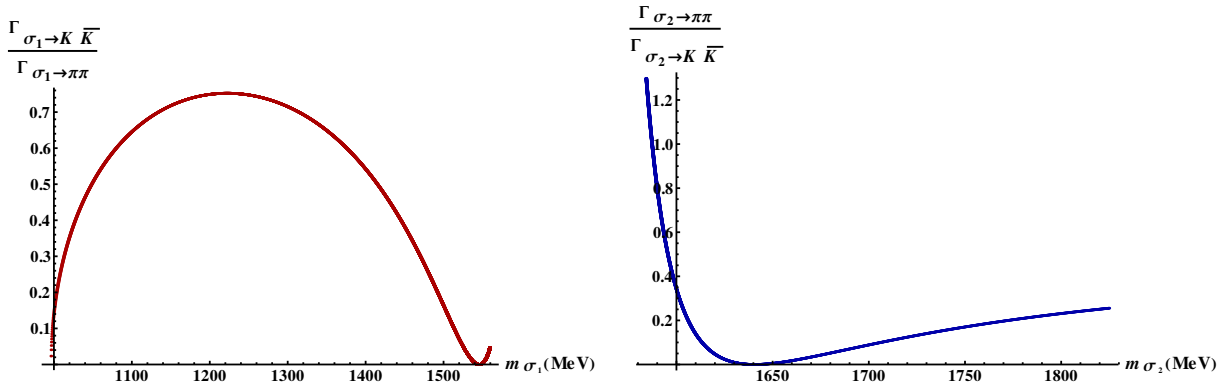


**Figure 11.8:** Left panel: ratio $\Gamma_{\sigma_1\to KK}/\Gamma_{\sigma_1\to\pi\pi}$ as function of $m_{\sigma_1}$. Right panel: ratio $\Gamma_{\sigma_2\to\pi\pi}/\Gamma_{\sigma_2\to KK}$ as function of $m_{\sigma_2}$.

Let us first discuss results for $\Gamma_{\sigma_1\to KK}/\Gamma_{\sigma_1\to\pi\pi}$ (left panel in Fig. 11.8). We observe that the ratio varies between 0.16 for $m_{\sigma_1} = 1500$ MeV and 0.75 for $m_{\sigma_1} = 1200$ MeV. Experimental data regarding this ratio are unfortunately inconclusive [10].

- In 2005, the BESII Collaboration [140] noted the ratio value of 0.08±0.08 from the hadronic decay of the $J/\psi$ meson ($J/\psi \to \varphi\pi^+\pi^-$ and $J/\psi \to \varphi K^+K^-$).
- In 2003, the OBELIX Collaboration [262] published a coupled-channel analysis of $\bar{p}p$ annihilation into light mesons with the result $\Gamma_{f_0(1370)\to KK}/\Gamma_{f_0(1370)\to\pi\pi} = 0.91 \pm 0.20$.
- A combined fit of Crystal Barrel, GAMS and BNL data performed by Anisovich, *et al.*, from 2002 found $\Gamma_{f_0(1370)\to KK}/\Gamma_{f_0(1370)\to\pi\pi} = 0.12 \pm 0.06$ [188].
- The WA102 Collaboration found in 1999 the ratio $\Gamma_{f_0(1370)\to KK}/\Gamma_{f_0(1370)\to\pi\pi} = 0.46 \pm 0.15 \pm 0.11$ [99].

Thus, the data vary over a large range of values. If we assign our $\sigma_1$ state to $f_0(1370)$ and vary $m_{\sigma_1}$ from 1200 MeV to 1500 MeV, then our results can be accommodated within all data sets. Clearly, more conclusive data would allow for more conclusive results regarding our theoretical predictions.

Regarding the ratio $\Gamma_{f_0(1710)\to\pi\pi}/\Gamma_{f_0(1710)\to KK}$, experimental results are rather ambiguous, as discussed in Sections 3.7.1, 3.7.2 and 3.7.3.

- From the PDG-preferred ratio $\Gamma^{\rm PDG}_{f_0(1710)\to\pi\pi}/\Gamma^{\rm PDG}_{f_0(1710)\to KK} = 0.41^{+0.11}_{-0.17}$ (see Sec. 3.7.1) we obtain $m_{\sigma_2} = 1598^{+6}_{-3}$ MeV. This result implies $\Gamma_{\sigma_2\to\pi\pi} = 75^{-21}_{+11}$ MeV from Eq. (9.40), too large when compared to data, see Eq. (3.10). Additionally, we obtain $m_{\sigma_1} = 1209^{+82}_{-56}$ MeV and $\Gamma_{\sigma_1\to\pi\pi} = 197^{+55}_{-30}$ MeV from Eq. (9.39). These results are within the boundaries cited in Ref. [40].

  Thus using $\Gamma^{\rm PDG}_{f_0(1710)\to\pi\pi}/\Gamma^{\rm PDG}_{f_0(1710)\to KK}$ constrains $m_{\sigma_2}$ in a way that does not allow us to describe simultaneously $\Gamma_{f_0(1710)\to\pi\pi}$ as well as $\Gamma_{f_0(1370)\to\pi\pi}$.
  Note that $\Gamma^{\rm PDG}_{f_0(1710)\to\pi\pi}/\Gamma^{\rm PDG}_{f_0(1710)\to KK}$ could also be described by the high-mass tail of $\Gamma_{\sigma_2\to\pi\pi}$ / $\Gamma_{\sigma_2\to KK}$ in Fig. 11.8; however, this would imply $m_{\sigma_2} \gtrsim 1800$ MeV leading to unphysically large values of $\Gamma_{\sigma_2\to KK}$, see Fig. 11.7.

- From the BES II ratio $\Gamma^{\rm BES\ II}_{f_0(1710)\to\pi\pi}/\Gamma^{\rm BES\ II}_{f_0(1710)\to KK} < 0.11$, Eq. (3.21), we obtain 1612 MeV $\leq m_{\sigma_2} \leq$ 1712 MeV. Given the parabolic form of $\Gamma_{\sigma_2\to\pi\pi}/\Gamma_{\sigma_2\to KK}$, let us separate the mentioned interval into two subintervals: $(i)$ 1612 MeV $\leq m_{\sigma_2} \leq$ 1640 MeV and $(ii)$ 1640 MeV $\leq m_{\sigma_2} \leq$ 1712 MeV with $m_{\sigma_2} = 1640$ MeV the point where the ratio vanishes (see Fig. 11.8). Interval $(i)$ yields 1356 MeV $\leq m_{\sigma_1} \leq$ 1452 MeV and 306 MeV $\leq \Gamma_{\sigma_1\to\pi\pi} \leq$ 398 MeV. Interval $(ii)$ yields 1452 MeV $\leq m_{\sigma_1} \leq$ 1517 MeV and 397 MeV $\leq \Gamma_{\sigma_1\to\pi\pi} \leq$ 416 MeV, see Fig. 11.6. As noted in Sec. 3.7.2, it is not possible to calculate $\Gamma_{f_0(1710)\to KK}$ from these data.

- The WA102 ratio $\Gamma^{\rm WA102}_{f_0(1710)\to\pi\pi}/\Gamma^{\rm WA102}_{f_0(1710)\to KK} = 0.2 \pm 0.06$, Eq. (3.27), also yields two intervals for $m_{\sigma_2}$: $(i)$ $m_{\sigma_2} = 1606^{-3}_{+4}$ MeV and $(ii)$ $m_{\sigma_2} = 1772^{+58}_{-42}$ MeV. We disregard the interval $(ii)$ because it leads to a very large value of $\Gamma_{\sigma_2\to KK}$, see Fig. 11.7. From interval $(i)$ we obtain $m_{\sigma_1} = 1310^{-29}_{+30}$ MeV and $\Gamma_{\sigma_1\to\pi\pi} = 267^{-50}_{+25}$ MeV. These results are consistent with the experimental values of Ref. [40].

In summary: it is not possible to constrain $m_{\sigma_2}$ via $\Gamma_{f_0(1710)\to KK}$ in a way that yields acceptable values of $\Gamma_{f_0(1710)\to\pi\pi}$ (because our values $\Gamma_{\sigma_2\to KK}$ increase rapidly with $m_{\sigma_2}$). However, utilising the ratio $\Gamma_{f_0(1710)\to\pi\pi}/\Gamma_{f_0(1710)\to KK}$ allows us to constrain $m_{\sigma_2}$ such that both $m_{\sigma_1}$ and $\Gamma_{\sigma_1\to\pi\pi}$ are within values published in Ref. [40]. This can be accomplished using either PDG-preferred or WA102 values for the mentioned ratio. Given the issues regarding $\Gamma^{\rm PDG}_{f_0(1710)\to\pi\pi}/\Gamma^{\rm PDG}_{f_0(1710)\to KK}$ discussed in Sec. 3.7.1, we prefer results obtained from $\Gamma^{\rm WA102}_{f_0(1710)\to\pi\pi}/\Gamma^{\rm WA102}_{f_0(1710)\to KK}$, i.e., $m_{\sigma_1} = 1310^{-29}_{+30}$ MeV, $m_{\sigma_2} = 1606^{-3}_{+4}$ MeV, $\Gamma_{\sigma_1\to\pi\pi} = 267^{-50}_{+25}$ MeV. Note that these results yield $\Gamma_{\sigma_2\to KK} \sim 200$ MeV [larger than experimental results but consistent with the notion of a predominant $2K$ decay channel of $f_0(1710)$] and also $\Gamma_{\sigma_2\to\pi\pi} = 47^{+9}_{-10}$ MeV [larger than the WA102 value of Eq. (3.32) but consistent with the notion of a subdominant $2\pi$ decay channel of $f_0(1710)$]. These combined results from the $2\pi$ and $2K$ channels suggest that $f_0(1370)$ is $(95.5 \pm 1.0)\%$ a $\bar{n}n$ state and that, conversely, that $f_0(1710)$ is $(95.5 \pm 1.0)\%$ a $\bar{s}s$ state.

### 11.1.4 Decay Width $\sigma_{1,2} \to \eta\eta$

We have already discussed the $\sigma\eta\eta$ interaction Lagrangian in Sec. 9.1.6, formulas for the decay widths $\Gamma_{\sigma_1\to\eta\eta}$ and $\Gamma_{\sigma_2\to\eta\eta}$ are stated in Eqs. (9.71) and (9.72), respectively.
The dependence of the decay widths on $m_{\sigma_{1,2}}$ is shown diagramatically in Fig. 11.9.

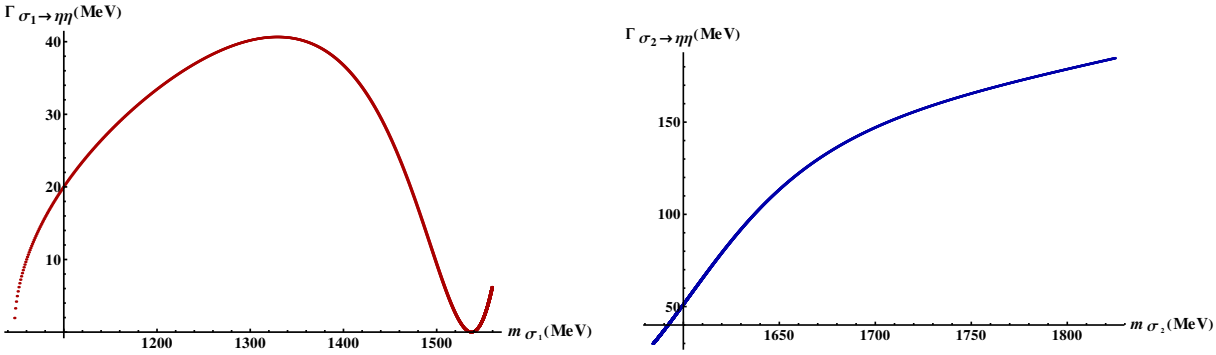


**Figure 11.9:** $\Gamma_{\sigma_1\to\eta\eta}$ and $\Gamma_{\sigma_2\to\eta\eta}$ as functions of $m_{\sigma_1}$ and $m_{\sigma_2}$ in Fit II.

We observe from the left panel of Fig. 11.9 that $\Gamma_{\sigma_1\to\eta\eta}$ is suppressed over the entire mass range of $\sigma_1$. Contrarily, $\Gamma_{\sigma_2\to\eta\eta}$ rises rapidly over the mass range of $\sigma_2$.
Experimental results regarding the decay $f_0(1370) \to \eta\eta$ are ambiguous; there are Crystal Barrel $\bar{p}p$ data [125] and GAMS $\pi^- p$ [145] suggesting a decay width of $\sim (250-300)$ MeV in this decay channel from Breit-Wigner fits. These are known, however, to be very sensitive to the opening of new channels (such as $4\pi$, see Sec. 3.3). For this reason, we will consider only the (more unambiguously determined) values of $\Gamma_{f_0(1710)\to\eta\eta}$ from Sec. 3.7.

Our discussion of $\Gamma_{\sigma_{1,2}\to\eta\eta}$ will be constrained by the following entries: $(i)$ the experimental result for $\Gamma_{f_0(1710)\to\eta\eta}$; $(ii)$ the condition $m_0^2 \leq 0$ from formula (9.4), necessary to utilise because the lower boundaries of $\Gamma_{f_0(1710)\to\eta\eta}$ from Sec. 3.7 may imply $m_{\sigma_2} < 1584$ MeV and thus $m_0^2 > 0$ [see condition (11.3)]; $(iii)$ given that the $\eta\eta$ channel represents a confirmed decay mode of $f_0(1370)$ [10] (although, as already mentioned, the corresponding decay width is by no means unambiguous), we also require that $m_{\sigma_1}$ is above the $\eta\eta$ threshold, i.e., $m_{\sigma_1} \geq 2m_\eta = 1046$ MeV with $m_\eta$ from Table 10.3. [Remember that $m_{\sigma_1}$ determines uniquely the values of $m_0^2$ and $m_{\sigma_2}$ from Fig. 11.2 or, equivalently, from Eqs. (9.19) - (9.23); $m_{\sigma_2}$ then allows for a determination of $\Gamma_{\sigma_2\to\eta\eta}$ from the right panel of Fig. 11.9, or, equivalently, from Eqs. (9.71) and (9.72).] The consequences of the stated three entries are as follows:

- The PDG-preferred result reads $\Gamma^{\text{PDG}}_{f_0(1710)\to\eta\eta} = 34.26^{+15.42}_{-20.0}$ MeV, see Eq. (3.20). It is not possible to accommodate the full experimental interval within our model as utilising the lower boundary of $\Gamma^{\text{PDG}}_{f_0(1710)\to\eta\eta}$ would violate the above condition $(ii)$. Then combining $\Gamma^{\text{PDG}}_{f_0(1710)\to\eta\eta} = 34.26^{+15.42}_{-20.0}$ MeV with condition $(ii)$ yields $m_{\sigma_2} = 1588^{+11}_{-4}$ MeV (the upper boundary for $m_{\sigma_2}$ was determined from the upper boundary of $\Gamma^{\text{PDG}}_{f_0(1710)\to\eta\eta}$) and, in turn, $\Gamma_{f_0(1710)\to\eta\eta} = 34.26^{+15.42}_{-4.41}$ MeV. However, condition $(iii)$, i.e., $m_{\sigma_1} \geq 1046$ MeV, implies $m_0^2 \leq -457456$ MeV$^2$ and thus $m_{\sigma_2} \geq 1591$ MeV. Combining the latter inequality with the interval $m_{\sigma_2} = 1588^{+11}_{-4}$ MeV yields 1591 MeV $\leq m_{\sigma_2} \leq 1599$ MeV and, consequently,

39.12 MeV $\leq \Gamma_{f_0(1710)\to\eta\eta} \leq$ 49.68 MeV. The latter two sets of inequalities also imply 1046 MeV $\leq m_{\sigma_1} \leq$ 1227 MeV (or 1200 MeV $\leq m_{\sigma_1} \leq$ 1227 MeV considering the PDG data [10]) and $0 \leq \Gamma_{\sigma_1 \equiv f_0(1370)\to\eta\eta} \leq$ 35.92 MeV. The $\eta\eta$ decay of $f_0(1370)$ is then suppressed in comparison with the $2\pi$ decay, see Sec. 11.1.2.

- There is another set of experimental data discussed in Sec. 3.7: $\Gamma^{\text{WA102}}_{f_0(1710)\to\eta\eta} = (38.6 \pm 18.8)$ MeV from Eq. (3.34). As in the case of the PDG-preferred data, we combine $\Gamma^{\text{WA102}}_{f_0(1710)\to\eta\eta} = (38.6 \pm 18.8)$ MeV with the above condition (*ii*) and obtain $m_{\sigma_2} = 1591^{+13}_{-7}$ MeV. Note that the lower boundary of $m_{\sigma_2} = 1594$ MeV implies $\Gamma_{f_0(1710)\to\eta\eta} = 29.8$ MeV hence modifying the WA102 result to $\Gamma_{f_0(1710)\to\eta\eta} = 38.6^{+18.8}_{-8.8}$ MeV. As already mentioned, condition (*iii*) implies $m_{\sigma_1} \geq 1046$ MeV, i.e., $m_0^2 \leq -457456$ MeV$^2$ and thus also $m_{\sigma_2} \geq 1591$ MeV. The latter inequality in conjunction with $m_{\sigma_2} = 1591^{+13}_{-7}$ MeV yields 1591 MeV $\leq m_{\sigma_2} \leq$ 1604 MeV and, consequently, 38.6 MeV $\leq \Gamma_{\sigma_2 \equiv f_0(1710)\to\eta\eta} \leq$ 56.6 MeV. The latter two sets of inequalities also imply 1046 MeV $\leq m_{\sigma_1} \leq$ 1289 MeV (i.e., 1200 MeV $\leq m_{\sigma_1} \leq$ 1289 MeV considering the PDG data [10]) and $0 \leq \Gamma_{\sigma_1 \equiv f_0(1370)\to\eta\eta} \leq$ 39.8 MeV. Therefore, $\Gamma_{f_0(1370)\to\eta\eta}$ is in this case slightly larger than in the case of the PDG-preferred data but still smaller than the $2\pi$ decay width discussed in Sec. 11.1.2.

Given the ambiguities in the BES II data utilised by the PDG (as discussed in Sec. 3.7.1), we prefer the results obtained from the WA102 data.

Let us now consider the ratios of the decay widths discussed so far. A plot of $\Gamma_{\sigma_1\to\eta\eta}/\Gamma_{\sigma_1\to\pi\pi}$ and $\Gamma_{\sigma_2\to\eta\eta}/\Gamma_{\sigma_2\to\pi\pi}$ is shown in Fig. 11.10.

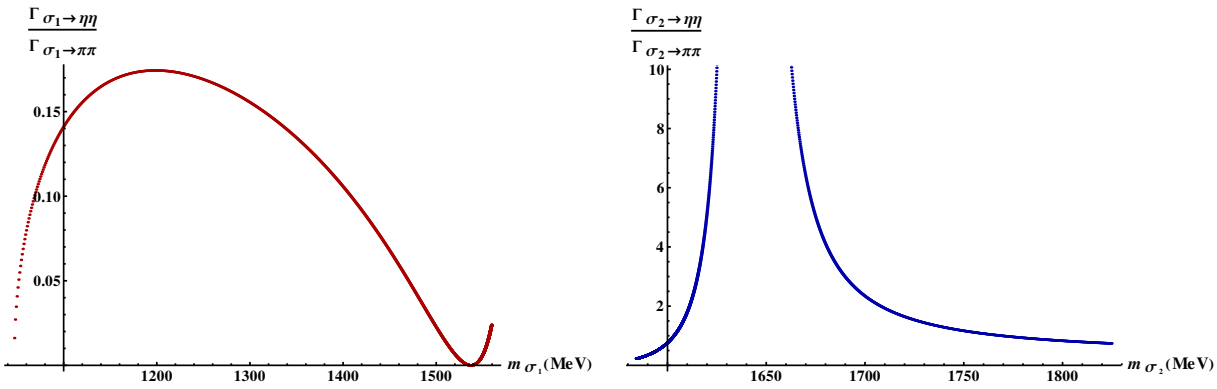


**Figure 11.10:** Ratios $\Gamma_{\sigma_1\to\eta\eta}/\Gamma_{\sigma_1\to\pi\pi}$ as function of $m_{\sigma_1}$ and $\Gamma_{\sigma_2\to\eta\eta}/\Gamma_{\sigma_2\to\pi\pi}$ as function of $m_{\sigma_2}$ in Fit II.

Our results for $\Gamma_{\sigma_1\to\eta\eta}/\Gamma_{\sigma_1\to\pi\pi}$ are within the ratio $\Gamma_{f_0(1370)\to\eta\eta}/\Gamma_{f_0(1370)\to\pi\pi} = 0.19 \pm 0.07$ [40] for a rather large mass interval: 1081 MeV $\leq m_{\sigma_1} \leq$ 1377 MeV. Due to the constraints regarding $m_{f_0(1370)}$ [10] we obtain 1200 MeV $\leq m_{\sigma_1} \leq$ 1377 MeV. Note that the largest value of the ratio obtained (and shown in Fig. 11.10) is 0.174, for $m_{\sigma_1} = 1200$ MeV.

Additionally, there are three sets of data regarding the ratio $\Gamma_{f_0(1710)\to\eta\eta}/\Gamma_{f_0(1710)\to\pi\pi}$ that need to be considered (see Sec. 3.7).

- Data preferred by the PDG suggest $\Gamma^{\rm PDG}_{f_0(1710)\to\eta\eta}/\Gamma^{\rm PDG}_{f_0(1710)\to\pi\pi} = 1.17^{+0.48}_{-0.61}$, Eq. (3.6). As apparent from Fig. 11.10, the stated ratio can be accommodated within our model for two sets of $m_{\sigma_2}$ values. The higher of these two sets ($m_{\sigma_2} \sim 1800$ MeV) is not considered because it would lead to very large values of the $2\pi$ and $2K$ decay widths for this resonance (see figures 11.6 and 11.7). For this reason, we consider the lower of the intervals reading $m_{\sigma_2} = 1605^{+4}_{-9}$ MeV. This value implies $m_{\sigma_1} = 1302^{+32}_{-102}$ MeV by Fig. 11.2, with the lower boundary limited to $m_{\sigma_1 \equiv f_0(1370)} = 1200$ MeV [10], and $0.14 \leq \Gamma_{\sigma_1\to\eta\eta}/\Gamma_{\sigma_1\to\pi\pi} \leq 0.17$, see Fig. 11.10.

- BES II data from condition (3.23) suggest $\Gamma^{\rm BES\ II}_{f_0(1710)\to\eta\eta}/\Gamma^{\rm BES\ II}_{f_0(1710)\to\pi\pi} > 4.36$. This ratio implies $m_{\sigma_2} > 1618$ MeV, $m_{\sigma_1} > 1389$ MeV (see Fig. 11.2) and $\Gamma_{\sigma_1\to\eta\eta}/\Gamma_{\sigma_1\to\pi\pi} < 0.11$, see Fig. 11.10 (we again disregard the high-mass tail of $m_{\sigma_2}$ that would also fulfill the stated ratio). The lower boundaries for $m_{\sigma_{1,2}}$ are incompatible with the best values in the $2\pi$ and $2K$ decay channels of $\sigma_{1,2}$, as discussed at the end of Sec. 11.1.3. The obtained ratio for $\Gamma_{\sigma_1\to\eta\eta}/\Gamma_{\sigma_1\to\pi\pi}$ is outside of the interval $\Gamma_{f_0(1370)\to\eta\eta}/\Gamma_{f_0(1370)\to\pi\pi} = 0.19 \pm 0.07$ suggested by Ref. [40]. For this reason, the BES II result regarding the ratio of $\Gamma_{f_0(1710)\to\eta\eta}/\Gamma_{f_0(1710)\to\pi\pi}$ is not supported by our model.

- WA102 data from Eq. (3.31) suggest $\Gamma^{\rm WA102}_{f_0(1710)\to\eta\eta}/\Gamma^{\rm WA102}_{f_0(1710)\to\pi\pi} = 2.4 \pm 1.04$. As apparent from Fig. 11.10, this ratio also implies two possible $m_{\sigma_2}$ intervals, a relatively lower one and a relatively higher one. The latter interval is disregarded because it would yield $m_{\sigma_2} \sim 1700$ MeV, a value that – although close to the experimental value of $m_{f_0(1710)} = 1720$ MeV – nonetheless yields very large values of $\Gamma_{\sigma_2\to\pi\pi}$ and $\Gamma_{\sigma_2\to KK}$, see figures 11.6 and 11.7. We therefore consider only the lower set of $m_{\sigma_2}$ values reading $m_{\sigma_2} = 1613^{+3}_{-6}$ MeV. This interval implies $m_{\sigma_1} = 1360^{+19}_{-43}$ MeV (see Fig. 11.2) and $0.12 \leq \Gamma_{\sigma_1\to\eta\eta}/\Gamma_{\sigma_1\to\pi\pi} \leq 0.15$, see Fig. 11.10. The latter ratio is within the interval $\Gamma_{f_0(1370)\to\eta\eta}/\Gamma_{f_0(1370)\to\pi\pi} = 0.19 \pm 0.07$ suggested by Ref. [40].

Let us now consider the ratio $\Gamma_{\sigma_{1,2}\to\eta\eta}/\Gamma_{\sigma_{1,2}\to KK}$ shown in Fig. 11.11. The corresponding ratio

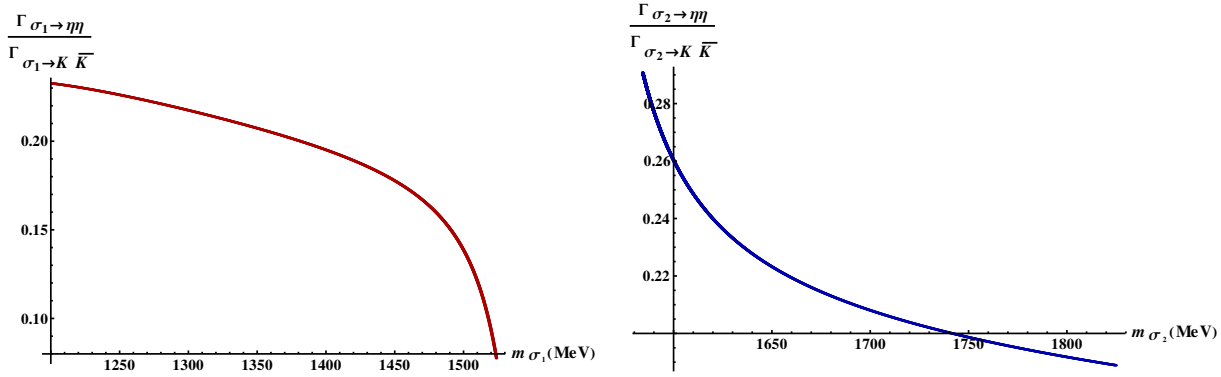


**Figure 11.11:** Ratios $\Gamma_{\sigma_1\to\eta\eta}/\Gamma_{\sigma_1\to KK}$ as function of $m_{\sigma_1}$ and $\Gamma_{\sigma_2\to\eta\eta}/\Gamma_{\sigma_2\to KK}$ as function of $m_{\sigma_2}$ in Fit II.

for $f_0(1710)$ has been determined by the WA102 Collaboration [153] with data from $pp$ collisions yielding $\Gamma_{f_0(1710)\to\eta\eta}/\Gamma_{f_0(1710)\to KK} = 0.48 \pm 0.15$ and in a combined-fit analysis of Ref. [188] where $\Gamma_{f_0(1710)\to\eta\eta}/\Gamma_{f_0(1710)\to KK} = 0.46^{+0.70}_{-0.38}$ was obtained. The results are obviously mutually

compatible; the PDG cites the WA102 result as the referential one. We observe, however, that the WA102 interval is outside the ratio on the right panel of Fig. 11.11 and that the result from Ref. [188] cannot be utilised to constrain $m_{\sigma_2}$ because the entire interval on the right panel of Fig. 11.11 is within the result $\Gamma_{f_0(1710)\to\eta\eta}/\Gamma_{f_0(1710)\to KK} = 0.46^{+0.70}_{-0.38}$. It is therefore not possible to utilise the ratio $\Gamma_{f_0(1710)\to\eta\eta}/\Gamma_{f_0(1710)\to KK}$ in order to constrain $m_{\sigma_2}$.

**Short Summary of Results**

Let us now summarise results obtained so far. The ratio $\Gamma^{\text{WA102}}_{f_0(1710)\to\pi\pi}/\Gamma^{\text{WA102}}_{f_0(1710)\to KK} = 0.2 \pm 0.06$ allows us to determine $m_{\sigma_2}$ and then observables for $\sigma_1$. We obtain $m_{\sigma_1} = 1310^{-29}_{+30}$ MeV, $m_{\sigma_2} = 1606^{-3}_{+4}$ MeV and $\Gamma_{\sigma_1\to\pi\pi} = 267^{-50}_{+25}$ MeV. The results for $\sigma_1$ are consistent with interpretation of this state as $f_0(1370)$. In particular $m_{\sigma_1}$ is consistent with the combined-fit value of $m_{f_0(1370)} = (1309 \pm 1 \pm 15)$ MeV from Ref. [40]; $\Gamma_{\sigma_1\to\pi\pi}$ is consistent with both the Breit-Wigner decay width and the FWHM value of Ref. [40]. The value of $m_{\sigma_2}$ is approximately 100 MeV smaller than $m_{f_0(1710)}$; however, a pure glueball state [that would very probably shift $m_{\sigma_2}$ in the direction of $m_{f_0(1710)}$] is not present in the $U(3) \times U(3)$ version of our model. Additionally, we observe that our state $\sigma_2$ possesses a strongly enhanced kaon decay, also consistent with the corresponding feature of $f_0(1710)$ although the absolute value of the decay width in this channel is too large. Additionally, $\Gamma_{\sigma_2\to\pi\pi} = 47^{+9}_{-10}$ MeV is larger than the value expected for the $f_0(1710)$ resonance; this may be a consequence of the missing glueball field that, if included, could modify decay amplitudes in such a way that $\Gamma_{\sigma_2\to\pi\pi}$ and $\Gamma_{\sigma_2\to KK}$ obtain values closer to those of $f_0(1710)$.

Additionally, the decay channel $\sigma_{1,2} \to \eta\eta$ is well accommodated within the model: our results for $\Gamma_{\sigma_2\equiv f_0(1710)\to\eta\eta}$ are within $\Gamma^{\text{WA102}}_{f_0(1710)\to\eta\eta} = (38.6 \pm 18.8)$ MeV if we set 1591 MeV $\leq m_{\sigma_2} \leq$ 1604 MeV. Then we obtain simultaneously 1200 MeV $\leq m_{\sigma_1} \leq$ 1289 MeV, $0 \leq \Gamma_{\sigma_1\equiv f_0(1370)\to\eta\eta} \leq 39.8$ MeV and 38.6 MeV $\leq \Gamma_{\sigma_2\equiv f_0(1710)\to\eta\eta} \leq$ 56.6 MeV. [$\Gamma_{\sigma_2\equiv f_0(1710)\to\eta\eta}$ does not correspond exactly to $\Gamma^{\text{WA102}}_{f_0(1710)\to\eta\eta}$ because we have required $m_{\sigma_1} \geq 2m_\eta$ hence constraining $m_0^2$ and consequently other observables as well.] Note, however, that the obtained $m_{\sigma_1}$ and $m_{\sigma_2}$ overlap with $m_{\sigma_1}$ and $m_{\sigma_2}$ determined from $\Gamma^{\text{WA102}}_{f_0(1710)\to\pi\pi}/\Gamma^{\text{WA102}}_{f_0(1710)\to KK}$ within errors.
Finally, it is not possible to constrain $m_{\sigma_{1,2}}$ and other observables from $\Gamma_{f_0(1710)\to\eta\eta}/\Gamma_{f_0(1710)\to KK}$; however, the opposite is true for $\Gamma_{f_0(1710)\to\eta\eta}/\Gamma_{f_0(1710)\to\pi\pi}$. We prefer the result of the WA102 Collaboration $\Gamma^{\text{WA102}}_{f_0(1710)\to\eta\eta}/\Gamma^{\text{WA102}}_{f_0(1710)\to\pi\pi} = 2.4 \pm 1.04$ because of reliability issues of an alternative, PDG-preferred ratio value (discussed at the beginning of Sec. 3.7.1). Utilising the stated WA102 interval we obtain $m_{\sigma_1} = 1360^{+19}_{-43}$ MeV, $m_{\sigma_2} = 1613^{+3}_{-6}$ MeV [suggesting that $f_0(1370)$ is $94.7^{+1.4}_{-3.0}\%$ a $\bar{n}n$ state and that, conversely, that $f_0(1710)$ is $94.7^{+1.4}_{-3.0}\%$ a $\bar{s}s$ state] and $0.12 \leq \Gamma_{\sigma_1\to\eta\eta}/\Gamma_{\sigma_1\to\pi\pi} \leq 0.15$. It is obvious that these results are also compatible with the previous two (within errors).

### 11.1.5 Combined Results in the Pion, Kaon and Eta Channels

Until now we have considered experimental information regarding the $\pi\pi$, $KK$ and $\eta\eta$ channels by exploring the possibility to describe each of these decay channels separately. However, the already noted compatibility of thus obtained results (within errors) prompts us to investigate whether similarly good results can be obtained considering a single observable. Let that observable be the ratio $\Gamma_{f_0(1710)\to\pi\pi}/\Gamma_{f_0(1710)\to KK}$ due to the importance of pion and kaon decays in

discriminating between predominantly non-strange and predominantly strange states. Utilising the WA102 result $\Gamma^{\rm WA102}_{f_0(1710)\to\pi\pi}/\Gamma^{\rm WA102}_{f_0(1710)\to KK} = 0.2 \pm 0.06$ [99] allows us to exactly determine the only parameter that we have varied until now: $m_0^2 = -791437^{+42287}_{-46053}$ MeV$^2$. (Note that until now the only conditions set upon $m_0^2$ were $m_0^2 \stackrel{!}{<} 0$ and that the values of this parameter must imply $m_{\sigma_N} < m_{\sigma_S}$). Then we obtain the following results [remember – our assignment is $\sigma_1 \equiv f_0(1370)$ and $\sigma_2 \equiv f_0(1710)$]:

- *Masses:* we obtain $m_{\sigma_1} = 1310^{-29}_{+30}$ MeV and $m_{\sigma_2} = 1606^{-3}_{+4}$ MeV. The former is virtually the same as the combined-fit Breit-Wigner mass in Ref. [40] where $m_{f_0(1370)} = (1309 \pm 1 \pm 15)$ MeV was obtained (our error results are dictated by uncertainties in $\Gamma^{\rm WA102}_{f_0(1710)\to\pi\pi}/\Gamma^{\rm WA102}_{f_0(1710)\to KK}$) and also very close to the $f_0(1370)$ peak mass in the $2\pi$ channel, found to be 1282 MeV in Ref. [40]. The latter is approximately 100 MeV smaller than $m_{f_0(1710)} = (1720 \pm 6)$ MeV because the glueball field has not been included in the current version of the model. This implies that $f_0(1370)$ is $91.2^{-1.7}_{+2.0}\%$ a $\bar{n}n$ state and that, conversely, $f_0(1710)$ is $91.2^{-1.7}_{+2.0}\%$ a $\bar{s}s$ state.

- *Pion decay channel:* we obtain $\Gamma_{\sigma_1\to\pi\pi} = 267^{-50}_{+25}$ MeV and $\Gamma_{\sigma_2\to\pi\pi} = 47^{+9}_{-10}$ MeV. The former is virtually a median of (and thus consistent with both) the Breit-Wigner decay width $\Gamma_{f_0(1370)\to\pi\pi} = 325$ MeV and the $f_0(1370)$ FWHM in the $2\pi$ channel, the value of which was determined as 207 MeV in Ref. [40]. The latter is too large when compared to the WA102 result in Eq. (3.32) but still demonstrates that the decay $f_0(1710) \to \pi\pi$ is suppressed in comparison with other decay modes (see below) – a fact that is in accordance with the data [10].

- *Kaon decay channel:* we obtain $\Gamma_{\sigma_1\to KK} = 188^{-9}_{+6}$ MeV and $\Gamma_{\sigma_2\to KK} = 237^{-20}_{+25}$ MeV. The two-kaon decay width for $f_0(1370)$ has not been determined unambiguously, but our result is consistent with experimental data in Refs. [124, 170, 253, 259, 260, 261]. We find $\Gamma_{f_0(1370)\to KK} < \Gamma_{f_0(1370)\to\pi\pi}$, consistent with the interpretation of $f_0(1370)$ as a predominantly non-strange $\bar{q}q$ state. $\Gamma_{\sigma_2\to KK}$ is larger than the WA102 data presented in Eq. (3.33); however, our results suggest nonetheless that $f_0(1710) \to KK$ is the most dominant decay channel for this resonance – in accordance with the data (see Sec. 3.7.3).

- *Eta decay channel:* we obtain $\Gamma_{\sigma_1\to\eta\eta} = (40 \mp 1)$ MeV and $\Gamma_{\sigma_2\to\eta\eta} = 60^{-4}_{+5}$ MeV. The former is lower than the values cited in Refs. [125, 145] but note that the cited publications did not consider in their Breit-Wigner fits that new decay channels may open over the broad $f_0(1370)$ decay interval. The latter is marginally (within errors) consistent with the value $\Gamma^{\rm WA102}_{f_0(1710)\to\eta\eta} = (38.6 \pm 18.8)$ MeV from Eq. (3.33).

- *Pion-kaon ratio:* $\Gamma_{\sigma_1\to\pi\pi}/\Gamma_{\sigma_1\to KK} = 1.42^{-0.05}_{+0.09}$ is consistent with the WA102 result stating $\Gamma_{f_0(1370)\to\pi\pi}/\Gamma_{f_0(1370)\to KK} = 2.17 \pm 1.23$ obtained from Ref. [99] and also qualitatively consistent with the result $\Gamma_{f_0(1370)\to\pi\pi}/\Gamma_{f_0(1370)\to KK} = 1.10 \pm 0.24$ obtained from the OBELIX data in Ref. [262].

- *The eta-pion ratios* read $\Gamma_{\sigma_1\to\eta\eta}/\Gamma_{\sigma_1\to\pi\pi} = 0.15 \pm 0.01$ and $\Gamma_{\sigma_2\to\eta\eta}/\Gamma_{\sigma_2\to\pi\pi} = 1.26^{-0.27}_{+0.52}$. The former is within the ratio $\Gamma_{f_0(1370)\to\eta\eta}/\Gamma_{f_0(1370)\to\pi\pi} = 0.19 \pm 0.07$ of Ref. [40]. The latter is corresponds almost completely to the WA102 ratio $\Gamma^{\rm WA102}_{f_0(1710)\to\eta\eta}/\Gamma^{\rm WA102}_{f_0(1710)\to\pi\pi} = 2.4 \pm 1.04$ from Eq. (3.31).

- *The eta-kaon ratios* read $\Gamma_{\sigma_1\to\eta\eta}/\Gamma_{\sigma_1\to KK} = 0.22 \pm 0.01$ and $\Gamma_{\sigma_2\to\eta\eta}/\Gamma_{\sigma_2\to KK} = 0.25 \pm 0.004$. To our knowledge, there are no experimental results for the ratio $\Gamma_{f_0(1370)\to\eta\eta}/\Gamma_{f_0(1370)\to KK}$. Our result for $\Gamma_{\sigma_1\equiv f_0(1370)\to\eta\eta}/\Gamma_{\sigma_1\equiv f_0(1370)\to KK}$ is hence a prediction. Our value of the ratio $\Gamma_{\sigma_2\to\eta\eta}/\Gamma_{\sigma_2\to KK}$ is completely within the combined-fit result of Ref. [188] reading $\Gamma_{f_0(1710)\to\eta\eta}/\Gamma_{f_0(1710)\to KK} = 0.46^{+0.70}_{-0.38}$ and within $2\sigma$ of the WA102 result where $\Gamma_{f_0(1710)\to\eta\eta}/\Gamma_{f_0(1710)\to KK} = 0.48 \pm 0.15$ was obtained [153].

For these reasons, the assumption of scalar $\bar{q}q$ states above 1 GeV is strongly preferred over the assumption that the same states are present below 1 GeV. Fit II describes non-strange scalars decisively better than Fit I (see Sec. 9.6). Additionally, results obtained in this section will allow us to explore three more decay channels of our $\sigma_1 \equiv f_0(1370)$ state: into $\eta\eta'$, $a_1(1260)\pi$, and $2\omega(782)$. Experimental information regarding these decays is scarce [10]; thus our results will have strong predictive power.

### 11.1.6 Decay Width $\sigma_{1,2} \to \eta\eta'$

The interaction Lagrangian for this decay has already been presented in Eq. (9.57). The Lagrangian contains the pure states $\sigma_{N,S}$ and $\eta_{N,S}$ and, as in Sec. 9.1.6, we will first introduce the fields $\eta$ and $\eta'$ in accordance with Eqs. (7.17) and (7.18). The Lagrangian in Eq. (9.57) then obtains the following form:

Substituting Eqs. (9.58) and (9.59) into Eq. (9.57) and additionally substituting $\eta_N$ and $\eta_S$ by $\eta$ and $\eta'$ according to Eqs. (7.17) and (7.18), we obtain the following form of the interaction Lagrangian:

$$\begin{aligned}\mathcal{L}_{\sigma\eta\eta'} &= A_{\sigma_N\eta\eta'}\sigma_N\eta\eta' + B_{\sigma_N\eta\eta'}\sigma_N(\partial_\mu\eta)(\partial^\mu\eta') + C_{\sigma_N\eta\eta'}\partial_\mu\sigma_N(\eta\partial^\mu\eta' + \eta'\partial^\mu\eta)\\ &+ A_{\sigma_S\eta\eta'}\sigma_S\eta\eta' + B_{\sigma_S\eta\eta'}\sigma_S(\partial_\mu\eta)(\partial^\mu\eta') + C_{\sigma_S\eta\eta'}\partial_\mu\sigma_S(\eta\partial^\mu\eta' + \eta'\partial^\mu\eta) \qquad (11.5)\end{aligned}$$

with

$$\begin{aligned}A_{\sigma_N\eta\eta'} &= Z_\pi^2\phi_N\left(\lambda_1 + \frac{\lambda_2}{2} + c_1\phi_S^2\right)\sin(2\varphi_\eta) - Z_{\eta_S}^2\phi_N\left(\lambda_1 + \frac{c_1}{2}\phi_N^2\right)\sin(2\varphi_\eta)\\ &- \frac{3}{2}c_1 Z_\pi Z_{\eta_S}\phi_N^2\phi_S\cos(2\varphi_\eta)\\ &= \phi_N\left\{\lambda_1(Z_\pi^2 - Z_{\eta_S}^2)\sin(2\varphi_\eta) + \frac{\lambda_2}{2}Z_\pi^2\sin(2\varphi_\eta)\right.\\ &\left.+c_1\left[\left(Z_\pi^2\phi_S^2 - \frac{Z_{\eta_S}^2}{2}\phi_N^2\right)\sin(2\varphi_\eta) - \frac{3}{2}Z_\pi Z_{\eta_S}\phi_N\phi_S\cos(2\varphi_\eta)\right]\right\}, \qquad (11.6)\\ B_{\sigma_N\eta\eta'} &= \left[Z_\pi^2\frac{w_{a_1}^2}{\phi_N}\left(m_1^2 + \frac{h_1}{2}\phi_S^2 + 2\delta_N\right) + \frac{h_1}{2}Z_{\eta_S}^2 w_{f_{1S}}^2\phi_N\right]\sin(2\varphi_\eta), \qquad (11.7)\end{aligned}$$

$$C_{\sigma_N\eta\eta'} = -\frac{g_1}{2} w_{a_1} Z_\pi^2 \sin(2\varphi_\eta), \tag{11.8}$$

$$\begin{aligned} A_{\sigma_S\eta\eta'} &= -(\lambda_1+\lambda_2) Z_{\eta_S}^2 \phi_S \sin(2\varphi_\eta) + Z_\pi^2 \phi_S (\lambda_1 + c_1\phi_N^2)\sin(2\varphi_\eta) - \frac{1}{2} c_1 Z_\pi Z_{\eta_S} \phi_N^3 \cos(2\varphi_\eta) \\ &= \phi_S \left\{ \left[\lambda_1 (Z_\pi^2 - Z_{\eta_S}^2) - \lambda_2 Z_{\eta_S}^2\right] \sin(2\varphi_\eta) + c_1 Z_\pi \phi_N^2 \left[ Z_\pi \sin(2\varphi_\eta) - \frac{Z_{\eta_S}}{2\phi_S} \phi_N \cos(2\varphi_\eta)\right]\right\}, \end{aligned} \tag{11.9}$$

$$B_{\sigma_S\eta\eta'} = \left[ -Z_{\eta_S}^2 \frac{w_{f_{1S}}^2}{\phi_S} \left( m_1^2 + \frac{h_1}{2}\phi_N^2 + 2\delta_S \right) - \frac{h_1}{2} Z_\pi^2 w_{a_1}^2 \phi_S \right] \sin(2\varphi_\eta), \tag{11.10}$$

$$C_{\sigma_S\eta\eta'} = \frac{\sqrt{2}}{2} Z_{\eta_S}^2 g_1 w_{f_{1S}} \sin(2\varphi_\eta). \tag{11.11}$$

As in Eq. (9.34) we obtain from Eqs. (9.17) and (11.5)

$$\begin{aligned} \mathcal{L}_{\sigma\eta\eta',\,\text{full}} &= \mathcal{L}_{\sigma_N\sigma_S,\,\text{full}} + \mathcal{L}_{\sigma\eta\eta'} \\ &= \frac{1}{2}(\partial_\mu\sigma_N)^2 + \frac{1}{2}(\partial_\mu\sigma_S)^2 - \frac{1}{2} m_{\sigma_N}^2 - \frac{1}{2} m_{\sigma_S}^2 + z_\sigma \sigma_N \sigma_S \\ &+ A_{\sigma_N\eta\eta'}\sigma_N\eta\eta' + B_{\sigma_N\eta\eta'}\sigma_N(\partial_\mu\eta)(\partial^\mu\eta') + C_{\sigma_N\eta\eta'}\partial_\mu\sigma_N(\eta\partial^\mu\eta' + \eta'\partial^\mu\eta) \\ &+ A_{\sigma_S\eta\eta'}\sigma_S\eta\eta' + B_{\sigma_S\eta\eta'}\sigma_S(\partial_\mu\eta)(\partial^\mu\eta') + C_{\sigma_S\eta\eta'}\partial_\mu\sigma_S(\eta\partial^\mu\eta' + \eta'\partial^\mu\eta). \end{aligned} \tag{11.12}$$

$\mathcal{L}_{\sigma\eta\eta',\,\text{full}}$ can be transformed in the following way:

$$\begin{aligned} \mathcal{L}_{\sigma\eta\eta,\,\text{full}} &= \frac{1}{2}(\partial_\mu\sigma_1)^2 - \frac{1}{2} m_{\sigma_1}^2 \sigma_1^2 \\ &+ (A_{\sigma_N\eta\eta'}\cos\varphi_\sigma + A_{\sigma_S\eta\eta'}\sin\varphi_\sigma)\sigma_1\eta\eta' \\ &+ (B_{\sigma_N\eta\eta'}\cos\varphi_\sigma + B_{\sigma_S\eta\eta'}\sin\varphi_\sigma)\sigma_1(\partial_\mu\eta)(\partial^\mu\eta') \\ &+ (C_{\sigma_N\eta\eta'}\cos\varphi_\sigma + C_{\sigma_S\eta\eta'}\sin\varphi_\sigma)\partial_\mu\sigma_1(\eta\partial^\mu\eta' + \eta'\partial^\mu\eta) \\ &+ \frac{1}{2}(\partial_\mu\sigma_2)^2 - \frac{1}{2} m_{\sigma_2}^2 \sigma_2^2 \\ &+ (A_{\sigma_S\eta\eta'}\cos\varphi_\sigma - A_{\sigma_N\eta\eta'}\sin\varphi_\sigma)\sigma_2\eta\eta' \\ &+ (B_{\sigma_S\eta\eta'}\cos\varphi_\sigma - B_{\sigma_N\eta\eta'}\sin\varphi_\sigma)\sigma_2(\partial_\mu\eta)(\partial^\mu\eta') \\ &+ (C_{\sigma_S\eta\eta'}\cos\varphi_\sigma - C_{\sigma_N\eta\eta'}\sin\varphi_\sigma)\partial_\mu\sigma_2(\eta\partial^\mu\eta' + \eta'\partial^\mu\eta). \end{aligned} \tag{11.13}$$

Let us set $P$ as the momentum of $\sigma_1$ or $\sigma_2$ (depending on the decaying particle) and $P_1$ and $P_2$ as the momenta of the $\eta$ and $\eta'$ fields, respectively. Upon substituting $\partial^\mu \to -iP^\mu$ for the decaying particles and $\partial^\mu \to iP_{1,2}^\mu$ for the decay products, the decay amplitudes of the mixed states $\sigma_{1,2}$ read

$$\begin{aligned} -i\mathcal{M}_{\sigma_1\to\eta\eta'}(m_{\sigma_1}) &= i\left\{\cos\varphi_\sigma (A_{\sigma_N\eta\eta'} - B_{\sigma_N\eta\eta'} P_1\cdot P_2 + C_{\sigma_N\eta\eta'} P\cdot(P_1+P_2)\right. \\ &\left. + \sin\varphi_\sigma \left[A_{\sigma_S\eta\eta'} - B_{\sigma_S\eta\eta'} P_1\cdot P_2 + C_{\sigma_S\eta\eta'} P\cdot(P_1+P_2)\right]\right\} \\ &= i\left\{\cos\varphi_\sigma \left[A_{\sigma_N\eta\eta'} - B_{\sigma_N\eta\eta'}\frac{m_{\sigma_1}^2 - m_\eta^2 - m_{\eta'}^2}{2} + C_{\sigma_N\eta\eta'} m_{\sigma_1}^2\right]\right. \\ &\left. + \sin\varphi_\sigma \left[A_{\sigma_S\eta\eta'} - B_{\sigma_S\eta\eta'}\frac{m_{\sigma_1}^2 - m_\eta^2 - m_{\eta'}^2}{2} + C_{\sigma_S\eta\eta'} m_{\sigma_1}^2\right]\right\}, \end{aligned} \tag{11.14}$$

$$-i\mathcal{M}_{\sigma_2\to\eta\eta'}(m_{\sigma_2}) = i\left\{\cos\varphi_\sigma\left[A_{\sigma_S\eta\eta'} - B_{\sigma_S\eta\eta'}\frac{m_{\sigma_2}^2 - m_\eta^2 - m_{\eta'}^2}{2} + C_{\sigma_S\eta\eta'}m_{\sigma_2}^2\right]\right.$$
$$\left. - \sin\varphi_\sigma\left[A_{\sigma_N\eta\eta'} - B_{\sigma_N\eta\eta'}\frac{m_{\sigma_2}^2 - m_\eta^2 - m_{\eta'}^2}{2} + C_{\sigma_N\eta\eta'}m_{\sigma_2}^2\right]\right\}. \tag{11.15}$$

Note that we have used the identity $P^2 = (P_1 + P_2)^2 \Leftrightarrow P_1 \cdot P_2 = (P^2 - P_1^2 - P_2^2)/2 = (m_{\sigma_1}^2 - m_\eta^2 - m_{\eta'}^2)/2$ in Eqs. (11.14) and (11.15).
Finally, we obtain the following decay widths formulas:

$$\Gamma_{\sigma_1\to\eta\eta'} = \frac{k(m_{\sigma_1}, m_\eta, m_{\eta'})}{8\pi m_{\sigma_1}^2}|-i\mathcal{M}_{\sigma_1\to\eta\eta'}(m_{\sigma_1})|^2, \tag{11.16}$$

$$\Gamma_{\sigma_2\to\eta\eta'} = \frac{k(m_{\sigma_2}, m_\eta, m_{\eta'})}{8\pi m_{\sigma_2}^2}|-i\mathcal{M}_{\sigma_2\to\eta\eta'}(m_{\sigma_2})|^2. \tag{11.17}$$

Note that the $\eta\eta'$ threshold in our model lies at 1481 MeV according to Table 10.3. For this reason, a non-vanishing value $\Gamma_{\sigma_1\to\eta\eta'}$ could only be obtained for correspondingly large $m_{\sigma_1}$ (that can actually be smaller than the threshold value if the state is sufficiently broad). Our model yields $m_{\sigma_1} = 1310^{-29}_{+30}$ MeV, see Sec. 11.1.5, and thus a value that does not allow for a tree-level $\sigma_1 \to \eta\eta'$ decay and renders an off-shell-$\sigma_1$ decay extremely suppressed.
The situation is quite different for $\sigma_2$. Constraining $\Gamma_{\sigma_2\to\eta\eta'}$ in Eq. (11.17) via $m_{\sigma_2} = 1606^{-3}_{+4}$ MeV (determined in Sec. 11.1.5) and using the parameters in Table 10.2 and masses in Table 10.3, we obtain

$$\Gamma_{\sigma_2\to\eta\eta'} = 41^{+4}_{-5}\text{ MeV}. \tag{11.18}$$

This result is a prediction because the PDG does not report an $\eta\eta'$ channel for $f_0(1710) \equiv \sigma_2$. Note, however, that results for the absolute values of the partial $f_0(1710)$ decay widths tend to be larger than experimental data (as discussed in Sec. 11.1.5); nonetheless, they also have correct relative magnitudes and for this reason we conclude that a non-vanishing value of $\Gamma_{f_0(1710)\to\eta\eta'}$ is expected, suppressed when compared to $f_0(1710) \to KK$ but of approximately equal magnitude as $f_0(1710) \to \pi\pi$ and $f_0(1710) \to \eta\eta$. Indeed using Eqs. (11.17) and (9.53) as well as $m_{\sigma_2} = 1606^{-3}_{+4}$ MeV we obtain

$$\Gamma_{\sigma_2\to\eta\eta'}/\Gamma_{\sigma_2\to KK} = 0.17^{+0.04}_{-0.03}, \tag{11.19}$$

using Eqs. (11.17) and (9.40) we obtain

$$\Gamma_{\sigma_2\to\eta\eta'}/\Gamma_{\sigma_2\to\pi\pi} = 0.86^{-0.06}_{+0.11}, \tag{11.20}$$

using Eqs. (11.17) and (9.72) we obtain

$$\Gamma_{\sigma_2\to\eta\eta'}/\Gamma_{\sigma_2\to\eta\eta} = 0.68 \pm 0.13. \tag{11.21}$$

There are no experimental results for these ratios – the results are pure predictions. We know from Sec. 11.1.5 that experimental ratios of scalar decay widths are better described in our model than absolute values of decay widths. For this reason, experimental measurements regarding $f_0(1710) \to \eta\eta'$ would be strongly appreciated and would represent a valuable test for our results in Eqs. (11.19) - (11.21).

### 11.1.7 Decay Width $\sigma_{1,2} \to a_1(1260)\pi \to \rho\pi\pi$

This decay width can be calculated from the same Lagrangian as the one stated in Eq. (9.94). However, the calculation of the decay width is in this case slightly different than the one presented in Sec. 2.6.3 because the $a_1(1260)$ spectral function has to be considered. Additionally, $a_1$ is no longer at rest (unlike the decaying axial-vector in Sec. 2.6.3). This has to be considered while the decay amplitude is calculated (see below).
The decay width is determined as follows. The pure states $\sigma_{N,S}$ in Eq. (9.94) need to be replaced by the physical states $\sigma_{1,2}$ according to the inverted Eq. (9.18):

$$\begin{aligned}
\mathcal{L}_{\sigma a_1\pi} &= A_{a_1\sigma_N\pi} a_1^{\mu 0}(\cos\varphi_\sigma\sigma_1 - \sin\varphi_\sigma\sigma_2)\partial_\mu\pi^0 + B_{a_1\sigma_N\pi} a_1^{\mu 0}\pi^0\partial_\mu(\cos\varphi_\sigma\sigma_1 - \sin\varphi_\sigma\sigma_2) \\
&+ A_{a_1\sigma_S\pi} a_1^{\mu 0}(\sin\varphi_\sigma\sigma_1 + \cos\varphi_\sigma\sigma_2)\partial_\mu\pi^0 \\
&= (A_{a_1\sigma_N\pi}\cos\varphi_\sigma + A_{a_1\sigma_S\pi}\sin\varphi_\sigma)\sigma_1 a_1^{\mu 0}\partial_\mu\pi^0 + B_{a_1\sigma_N\pi}\cos\varphi_\sigma a_1^{\mu 0}\pi^0\partial_\mu\sigma_1 \\
&+ (A_{a_1\sigma_S\pi}\cos\varphi_\sigma - A_{a_1\sigma_N\pi}\sin\varphi_\sigma)\sigma_2 a_1^{\mu 0}\partial_\mu\pi^0 - B_{a_1\sigma_N\pi}\sin\varphi_\sigma a_1^{\mu 0}\pi^0\partial_\mu\sigma_2 \\
&= A_{a_1\sigma_1\pi}\sigma_1 a_1^{\mu 0}\partial_\mu\pi^0 + B_{a_1\sigma_1\pi} a_1^{\mu 0}\pi^0\partial_\mu\sigma_1 \\
&+ A_{a_1\sigma_2\pi}\sigma_2 a_1^{\mu 0}\partial_\mu\pi^0 + B_{a_1\sigma_2\pi} a_1^{\mu 0}\pi^0\partial_\mu\sigma_2
\end{aligned} \tag{11.22}$$

with $A_{a_1\sigma_N\pi}$, $B_{a_1\sigma_N\pi}$ and $A_{a_1\sigma_S\pi}$ from Eqs. (9.95) - (9.97), $A_{a_1\sigma_1\pi} = A_{a_1\sigma_N\pi}\cos\varphi_\sigma + A_{a_1\sigma_S\pi}\sin\varphi_\sigma$, $B_{a_1\sigma_1\pi} = B_{a_1\sigma_N\pi}\cos\varphi_\sigma$, $A_{a_1\sigma_2\pi} = A_{a_1\sigma_S\pi}\cos\varphi_\sigma - A_{a_1\sigma_N\pi}\sin\varphi_\sigma$ and $B_{a_1\sigma_2\pi} = -B_{a_1\sigma_N\pi}\sin\varphi_\sigma$.
Let us consider only the decay $\sigma_1 \to a_1\pi$ in the following; the calculation of $\Gamma_{\sigma_2\to a_1\pi}$ is analogous. We denote the momenta of $\sigma_1$, $a_1$ and $\pi$ as $P$, $P_1$ and $P_2$, respectively. Then, upon substituting $\partial^\mu \to -iP^\mu$ for the decaying particle and $\partial^\mu \to iP_{1,2}^\mu$ for the decay products, we obtain the following Lorentz-invariant $\sigma_1 a_1\pi$ scattering amplitude $-i\mathcal{M}^{(\alpha)}_{\sigma_1\to a_1\pi}$:

$$-i\mathcal{M}^{(\alpha)}_{\sigma_1\to a_1\pi} = \varepsilon^{(\alpha)}_\mu(P_1)h^\mu_{\sigma_1 a_1\pi} = -\varepsilon^{(\alpha)}_\mu(P_1)\left(A_{\sigma_1 a_1\pi}P_2^\mu - B_{\sigma_1 a_1\pi}P^\mu\right), \tag{11.23}$$

where $\varepsilon^{(\alpha)}_\mu(P_1)$ denotes the polarisation tensor of $a_1$ and

$$h^\mu_{\sigma_1 a_1\pi} = -\left(A_{\sigma_1 a_1\pi}P_2^\mu - B_{\sigma_1 a_1\pi}P^\mu\right) \tag{11.24}$$

denotes the $\sigma_1 a_1\pi$ vertex.

It is now necessary to calculate the square of the averaged decay amplitude. This is performed analogously to Sec. 2.6.3:

$$\begin{aligned}
-i\mathcal{M}^{(\alpha)}_{\sigma_1\to a_1\pi} = \varepsilon^{(\alpha)}_\mu(P_1)h^\mu_{\sigma_1 a_1\pi} \Rightarrow \left|-i\bar{\mathcal{M}}_{\sigma_1\to a_1\pi}\right|^2 &= \frac{1}{3}\sum_{\alpha=1}^{3}\left|-i\mathcal{M}^{(\alpha)}_{\sigma_1\to a_1\pi}\right|^2 \\
&= \frac{1}{3}\sum_{\alpha,\beta=1}^{3}\varepsilon^{(\alpha)}_\mu(P_1)h^\mu_{\sigma_1 a_1\pi}\varepsilon^{(\alpha)}_\nu(P_1)h^{*\nu}_{\sigma_1 a_1\pi} \\
&\overset{\text{Eq. (2.195)}}{=} \frac{1}{3}\left[-\left|h^\mu_{\sigma_1 a_1\pi}\right|^2 + \frac{\left|h^\mu_{\sigma_1 a_1\pi}P_{1\mu}\right|^2}{m_{a_1}^2}\right].
\end{aligned} \tag{11.25}$$

Let us determine the two contributions to $\left|-i\bar{\mathcal{M}}_{\sigma_1\to a_1\pi}\right|^2$ in Eq. (11.25). The square of the vertex reads

$$\begin{aligned}\left|h^{\mu}_{\sigma_1 a_1 \pi}\right|^2 &= A^2_{\sigma_1 a_1 \pi} m_\pi^2 + B^2_{\sigma_1 a_1 \pi} m^2_{\sigma_1} - 2A_{\sigma_1 a_1 \pi} B_{\sigma_1 a_1 \pi} P \cdot P_2 \\ &= A^2_{\sigma_1 a_1 \pi} m_\pi^2 + B^2_{\sigma_1 a_1 \pi} m^2_{\sigma_1} - 2A_{\sigma_1 a_1 \pi} B_{\sigma_1 a_1 \pi} m_{\sigma_1} E_2(x_{a_1}). \end{aligned} \tag{11.26}$$

In the second line of Eq. (11.26) we have used $P \cdot P_2 = m_{\sigma_1} E_2(x_{a_1})$ with the pion energy $E_2(x_{a_1}) = \sqrt{k^2(m_{\sigma_1}, x_{a_1}, m_\pi) + m_\pi^2}$, $k(m_{\sigma_1}, x_{a_1}, m_\pi)$ from Eq. (5.30) and $x_{a_1}$ the running mass of the $a_1$ state.
The second term from Eq. (11.25) is calculated from

$$\left|h^{\mu}_{\sigma_1 a_1 \pi} P_{1\mu}\right|^2 = (A_{\sigma_1 a_1 \pi} P_1 \cdot P_2 - B_{\sigma_1 a_1 \pi} P \cdot P_1)^2 \tag{11.27}$$

and the equalities $P_1 \cdot P_2 = (m^2_{\sigma_1} - x^2_{a_1} - m^2_\pi)/2$ and $P \cdot P_1 = m_{\sigma_1} E_1(x_{a_1})$ with the $a_1$ energy $E_1(x_{a_1}) = \sqrt{k^2(m_{\sigma_1}, x_{a_1}, m_\pi) + x^2_{a_1}}$. Then we obtain

$$\begin{aligned}\left|h^{\mu}_{\sigma_1 a_1 \pi} P_{1\mu}\right|^2 &= A^2_{\sigma_1 a_1 \pi} \frac{(m^2_{\sigma_1} - x^2_{a_1} - m^2_\pi)^2}{4} + B^2_{\sigma_1 a_1 \pi} m^2_{\sigma_1} E_1^2(x_{a_1}) \\ &\quad - A_{\sigma_1 a_1 \pi} B_{\sigma_1 a_1 \pi} m_{\sigma_1} E_1(x_{a_1})(m^2_{\sigma_1} - x^2_{a_1} - m^2_\pi). \end{aligned} \tag{11.28}$$

Inserting Eqs. (11.26) and (11.28) into Eqs. (11.25) we obtain

$$\begin{aligned}\left|-i\bar{\mathcal{M}}_{\sigma_1 \to a_1 \pi}(x_{a_1})\right|^2 = \frac{1}{3}\Bigg\{ & A^2_{\sigma_1 a_1 \pi} \frac{(m^2_{\sigma_1} - x^2_{a_1} - m^2_\pi)^2 - 4m^2_{a_1} m^2_\pi}{4m^2_{a_1}} + B^2_{\sigma_1 a_1 \pi} m^2_{\sigma_1} \left[\frac{E_1^2(x_{a_1})}{m^2_{a_1}} - 1\right] \\ & - A_{\sigma_1 a_1 \pi} B_{\sigma_1 a_1 \pi} m_{\sigma_1} \left[\frac{E_1(x_{a_1})(m^2_{\sigma_1} - x^2_{a_1} - m^2_\pi)}{m^2_{a_1}} - 2E_2(x_{a_1})\right]\Bigg\}. \end{aligned} \tag{11.29}$$

The decay width needs to consider three possible decay channels: $\sigma_1 \to a_1^0 \pi^0$ and $\sigma_1 \to a_1^\pm \pi^\mp$. Then we obtain

$$\Gamma_{\sigma_1 \to a_1 \pi}(x_{a_1}) = \frac{3k(m_{\sigma_1}, x_{a_1}, m_\pi)}{8\pi m^2_{\sigma_1}} \left|-i\bar{\mathcal{M}}_{\sigma_1 \to a_1 \pi}(x_{a_1})\right|^2. \tag{11.30}$$

Additionally, we introduce the $a_1$ spectral function $d_{a_1}(x_{a_1})$ as in Sec. 2.6.2 assuming the decay width of $\Gamma^{\rm exp}_{a_1 \to \rho\pi} = 425$ MeV for $a_1(1260)$ – this is the mean value of the corresponding PDG interval reading $(250 - 600)$ MeV. Then we can determine the decay width $\Gamma_{\sigma_1 \to a_1 \pi \to \rho\pi\pi}$:

$$\Gamma_{\sigma_1 \to a_1 \pi \to \rho\pi\pi} = \int_0^\infty \mathrm{d}x_{a_1} \Gamma_{\sigma_1 \to a_1 \pi}(x_{a_1}) d_{a_1}(x_{a_1}), \tag{11.31}$$

where the spectral function reads

$$d_{a_1}(x_{a_1}) = N_{a_1} \frac{x^2_{a_1} \Gamma^{\rm exp}_{a_1 \to \rho\pi}}{(x^2_{a_1} - m^2_{a_1})^2 + (x_{a_1} \Gamma^{\rm exp}_{a_1 \to \rho\pi})^2} \theta(x_{a_1} - m_\rho - m_\pi) \tag{11.32}$$

with the constant $N_{a_1}$ determined such that $\int_0^\infty \mathrm{d}x_{a_1}\, d_{a_1}(x_{a_1}) = 1$. [We are using $\Gamma^{\rm exp}_{a_1 \to \rho\pi}$ in $d_{a_1}(x_{a_1})$ as a first approximation although in principle the fully parametrised $\Gamma_{a_1 \to \rho\pi}$ from our model should be used. The ensuing results are thus more of qualitative nature.]

Analogously, we obtain

$$\Gamma_{\sigma_2\to a_1\pi}(x_{a_1}) = \frac{3k(m_{\sigma_2}, x_{a_1}, m_\pi)}{8\pi m_{\sigma_2}^2} \left|-i\bar{\mathcal{M}}_{\sigma_2\to a_1\pi}(x_{a_1})\right|^2 . \tag{11.33}$$

and

$$\Gamma_{\sigma_2\to a_1\pi\to\rho\pi\pi} = \int_0^\infty \mathrm{d}x_{a_1}\Gamma_{\sigma_2\to a_1\pi}(x_{a_1})d_{a_1}(x_{a_1}). \tag{11.34}$$

We use the parameter values stated in Table 10.2 to determine the coefficients in Eq. (11.22). Mass values can be found in Table 10.2, except for $m_{\sigma_1} = 1310^{-29}_{+30}$ MeV and $m_{\sigma_2} = 1606^{-3}_{+4}$ MeV determined in Sec. 11.1.5. Then Eq. (11.31) yields

$$\Gamma_{\sigma_1\to a_1\pi\to\rho\pi\pi} = 12.7^{+5.8}_{-4.2}\ \text{MeV}. \tag{11.35}$$

Consequently, the decay channel $f_0(1370) \to a_1(1260)\pi \to \rho\pi\pi$ is strongly suppressed in our model. The PDG does not state a value for this decay width but rather notes the Crystal Barrel ratio $\Gamma_{f_0(1370)\to a_1(1260)\pi}/\Gamma_{f_0(1370)\to 4\pi} = 0.06 \pm 0.02$ [239]. Our results do not reproduce the stated ratio because the absence of the glueball field in our $U(3) \times U(3)$ model implies a very small $\Gamma_{f_0(1370)\to 4\pi}$ (see the note on $\sigma_{1,2} \to 4\pi$ decays in Sec. 11.1.2). Nonetheless, the results of Ref. [239] imply a suppressed decay of $f_0(1370)$ into $a_1(1260)$ and this is consistent with our finding. Additionally, from Eq. (11.34) we obtain

$$\Gamma_{\sigma_2\to a_1\pi\to\rho\pi\pi} = 15.2^{+2.6}_{-3.1}\ \text{MeV}. \tag{11.36}$$

Current PDG data do not suggest the existence of the decay channel $f_0(1710) \to a_1(1260)\pi \to \rho\pi\pi$ [10]; indeed we find it to be strongly suppressed in comparison to pion, kaon and eta decays of $f_0(1710)$. Nonetheless, our results imply that a small but definite signal should be observed for this resonance as well.

### 11.1.8 Decay Width $\sigma_2 \to \omega\omega$

The $\sigma\omega_N\omega_N$ interaction Lagrangian reads

$$\begin{aligned}\mathcal{L}_{\sigma\omega\omega} &= \frac{1}{2}(h_1+h_2+h_3)\phi_N\sigma_N(\omega_N^\mu)^2 + \frac{1}{2}h_1\phi_S\sigma_S(\omega_N^\mu)^2 \\ &= \frac{1}{2}\left[(h_1+h_2+h_3)\phi_N\cos\varphi_\sigma + h_1\phi_S\sin\varphi_\sigma\right]\sigma_1(\omega_N^\mu)^2 \\ &+ \frac{1}{2}\left[h_1\phi_S\sigma_S\cos\varphi_\sigma - (h_1+h_2+h_3)\phi_N\sin\varphi_\sigma\right]\sigma_2(\omega_N^\mu)^2\end{aligned} \tag{11.37}$$

with the substitutions $\sigma_N \to \cos\varphi_\sigma\sigma_1 - \sin\varphi_\sigma\sigma_2$ and $\sigma_S \to \sin\varphi_\sigma\sigma_1 + \cos\varphi_\sigma\sigma_2$. Let us remind ourselves of the assignment of the relevant fields: $\sigma_1 \equiv f_0(1370)$, $\sigma_2 \equiv f_0(1710)$, $\omega_N \equiv \omega(782) = \omega$. The state $\sigma_1$ is below the $\omega\omega$ threshold and, for that reason, we do not consider the corresponding decay. Conversely, the state $\sigma_2$ is above, but not far away from, the $\omega\omega$ threshold: $m_{\sigma_2} = 1606^{-3}_{+4}$ MeV (see Sec. 11.1.5). Nonetheless, the decay is kinematically possible. We have already considered the decay of a scalar state into two vectors in Sec. 2.6.4. We can modify the formula for the decay width obtained there for the purposes of this section:

$$\Gamma_{\sigma_2\to\omega_N\omega_N}(x_{\omega_N}) = \frac{k(m_{\sigma_2}, x_{\omega_N}, x_{\omega_N})}{16\pi m_{\sigma_2}^2}\left[(h_1+h_2+h_3)\phi_N\sin\varphi_\sigma - h_1\phi_S\cos\varphi_\sigma\right]^2 \times\left[1+\frac{(m_{\sigma_2}^2-2x_{\omega_N}^2)^2}{8m_{\omega_N}^4}\right] \tag{11.38}$$

with $x_{\omega_N}$ denoting the running $\omega$ mass and $k(m_{\sigma_1}, x_{a_1}, m_\pi)$ from Eq. (5.30). There are two ways to proceed with Eq. (11.38). It is possible to evaluate $\Gamma_{\sigma_2\to\omega\omega}$ at the point $x_{\omega_N} = m_{\omega_N} = 775.49$ MeV [$= m_\rho$ according to Eq. (6.40)]. The mass value stems from Table 10.3. Then using the parameter values from Table 10.2 we obtain the following result from Eq. (11.38):

$$\Gamma_{\sigma_2\to\omega_N\omega_N}(m_{\omega_N}) \simeq 0.02 \text{ MeV}. \tag{11.39}$$

Therefore the value is extremely small. The experimental situation regarding the decay $\sigma_2 \equiv f_0(1710) \to \omega\omega$ is uncertain: the existence of a weak signal was claimed only by the BES II Collaboration in $J/\psi \to \gamma\omega\omega$ decays but no values were cited for the partial decay width [186]. Our results are in qualitative agreement with the BES II result, and our model does not suggest a strong enhancement of $f_0(1710)$ in the $\omega\omega$ channel.
Equation (11.38) can also be used to consider the sequential decay $\sigma_2 \equiv f_0(1710) \to \omega\omega \to 6\pi$:

$$\Gamma_{\sigma_2\to\omega\omega\to 6\pi} = \int_0^\infty \mathrm{d}x_{\omega_N}\Gamma_{\sigma_2\to\omega_N\omega_N}(x_{\omega_N})d_{\omega_N}(x_{\omega_N}), \tag{11.40}$$

where $d_{\omega_N}(x_{\omega_N})$ denotes the spectral function of the $\omega_N$ state:

$$d_{\omega_N}(x_{\omega_N}) = N_{\omega_N}\frac{x_{\omega_N}^2\Gamma^{\text{exp}}_{\omega_N\to 3\pi}}{(x_{\omega_N}^2-m_{\omega_N}^2)^2+\left(x_{\omega_N}\Gamma^{\text{exp}}_{\omega_N\to 3\pi}\right)^2}\,\theta(x_{\omega_N}-3m_\pi) \tag{11.41}$$

with $\Gamma^{\text{exp}}_{\omega_N\to 3\pi} = 8.49$ MeV assuming, in excellent approximation, that $\omega(782)$ decays only into $3\pi$ [10] and $N_{\omega_N}$ determined such that $\int_0^\infty \mathrm{d}x_{\omega_N}\, d_{\omega_N}(x_{\omega_N}) = 1$. The $\omega(782)$ resonance is very narrow and therefore utilisation of $\Gamma^{\text{exp}}_{\omega_N\to 3\pi}$ (rather than a formula parametrised in our model) in $d_{\omega_N}(x_{\omega_N})$ is fully justified. Nonetheless, the result obtained is the same as the one in Eq. (11.39)

$$\Gamma_{\sigma_2\to\omega\omega\to 6\pi} \simeq 0.02 \text{ MeV}. \tag{11.42}$$

The reason is the narrowness of the $\omega(782)$ resonance. This result indicates that the $6\pi$ decay channel of $f_0(1710)$ is strongly suppressed if virtual $\omega$ states are considered. Note, however, that this decay channel might still arise from the more prominent $f_0(1710)$ decays into $KK$ and $\eta\eta$.

## 11.2 Decay Width $K_0^\star(1430) \to K\pi$

The $K_S K\pi$ interaction Lagrangian, Eq. (9.84), has already been discussed in Sec. 9.3. The scalar kaon field $K_S$ is reassigned to $K_0^\star(1430)$ in Fit II but the decay width formula for the process $K_S^0 \to K\pi$, presented in Eq. (9.92), is of course valid nonetheless. There are no free parameters – utilising parameter values from Table 10.2 and mass values from Table 10.3, $\Gamma_{K_S^0\to K\pi}$ is determined uniquely as

$$\Gamma_{K_S^0\to K\pi} = 263 \text{ MeV}. \tag{11.43}$$

The result is within the PDG value $\Gamma^{\rm exp}_{K_0^\star(1430)} = (270 \pm 80)$ MeV [10]. The stated PDG value actually depicts the full decay width of $K_0^\star(1430)$ but the resonance is known to decay almost exclusively to $K\pi$ [263]. Our result is therefore in excellent correspondence with experimental data and it justifies the assignment of $K_S$ to $K_0^\star(1430)$.
Let us, as in Sec. 9.3, point out the influence of the diagonalisation shift, Eqs. (6.17) and (6.19) - (6.23), on this decay width: omitting the shift ($w_{a_1} = w_{K^\star} = w_{K_1} = 0$) would yield $\Gamma_{K_0^\star(1430)\to K\pi} \simeq 12$ GeV. We thus conclude again that the coefficients arising from the shift [Eqs. (9.86) - (9.88)] induce a destructive interference in the Lagrangian (9.84) decreasing the decay width by two orders of magnitude. The necessity to perform the shift arises from the inclusion of vectors and axial-vectors into our model. Therefore $\Gamma_{K_S\to K\pi}$ demonstrates that a reasonable description of scalars requires that the (axial-)vectors be included into the model. We can note, of course, that decoupling of (axial-)vectors from our model would spoil the result for the decay width of the low-lying scalar kaon $\kappa$ as well (as described in Sec. 9.3) whereas, e.g., nonstrange-scalar decay widths would still be fine in this case. Nonetheless, it is clear that our scalar kaon (how ever it may be assigned) is only described properly if the (axial-)vectors are present in the model as well. We will discuss the phenomenology of the vectors and axial-vectors in the subsequent sections.

### 11.3 Phenomenology of Vector and Axial-Vector Mesons in Fit II

Vector and axial-vector states are extremely important for our model. They are known to decay into scalar and pseudoscalar states discussed so far [10] and their mixing with scalar and pseudoscalar degrees of freedom observed in Eq. (6.15) yields the diagonalisation shift of Eqs. (6.17) and (6.19) - (6.23) originating in new terms in our Lagrangian (6.1) that in turn influence the phenomenology of other states (but also of vectors and axial-vectors themselves).

Fit I showed considerable tension between the decay widths of $a_1(1260)$, $f_1(1285)$, $f_1(1420)$ and $K_1(1400)$ on the one side and $\Gamma_{\rho\to\pi\pi}$ on the other: either the axial-vectors were too broad [$\sim (1-10)$ GeV] or the $\rho$ meson was too narrow ($\lesssim 40$ MeV), see Sec. 9.6. Therefore, a major task in the following sections will be to ascertain whether this state of affairs is changed in Fit II where a fundamentally different assumption is implemented – that the scalar quarkonia are above 1 GeV.
In the vector channel, the exact value of $\Gamma_{\rho\to\pi\pi} = 149.1$ MeV has already been implemented to determine the parameter $g_2$ (see Table 10.2). Our model also allows for a calculation of the $2K$ decay width of the strange isosinglet vector state $\omega_S \equiv \varphi(1020)$. It was not possible to calculate $\Gamma_{\omega_S\to KK}$ because our Fit I implied $m_{\omega_S}^{\rm FIT\ I} = 870.35$ MeV – a value below the $2K$ threshold. Therefore, $\varphi(1020)$ was not well described within Fit I. This is not the case in Fit II that yields $m_{\omega_S} = 1036.90$ MeV $> 2m_K$, see Table 10.3. We will calculate $\Gamma_{\omega_S\to KK}$ in Sec. 11.3.3. We will also consider the phenomenology of the $K^\star$ meson in Sec. 11.3.4.
In the axial-vector channel, we will consider the phenomenology of both non-strange and strange isosinglets, $f_{1N} \equiv f_1(1285)$ in Sec. 11.3.5 and $f_{1S} \equiv f_1(1420)$ in Sec. 11.3.6 (only $K^\star K$ decay channel can be considered in our model for both resonances). Important considerations will regard the $a_1(1260)$ resonance, the putative chiral partner of the $\rho$ meson, in Sec. 11.3.1. Note that Fit II does not allow for $\Gamma_{a_1(1260)\to f_0(600)\pi}$ to be calculated because our $\sigma_1$ field has now been reassigned to $f_0(1370)$ whereas we determine the width for the sequential decay $a_1 \to \bar{K}^\star K \to$

$\bar{K}K\pi$ in Sec. 11.3.2. Note also that our $K_1$ field (the phenomenology of which is discussed in Sec. 11.3.7) no longer corresponds to $K_1(1400)$ as in Fit I because, in Fit II, it is found to be a member of an axial-vector nonet that in principle requires consideration of the mixing with the corresponding pseudovector nonet before phenomenology statements can be made [see Sec. 10.3 and Eq. (10.26)]. For this reason, our calculations in Sec. 11.3.7 will be more of informative nature.

### 11.3.1 Decay Width $a_1(1260) \to \rho\pi$ in Fit II

The interaction Lagrangian for the decay $a_1(1260) \to \rho\pi$ has the same form as in the $U(2)\times U(2)$ version of the model. We have considered the decay of an axial-vector state into a vector and a pseudoscalar in Sec. 2.6.2; utilising parameters in Table 10.2 allows us to calculate $\Gamma_{a_1\to\rho\pi}$ from Eq. (2.188) with $I = 2$:

$$\Gamma_{a_1\to\rho\pi} = 861 \text{ MeV}. \tag{11.44}$$

The result is outside the PDG value for the full width $\Gamma_{a_1(1260)} = (200 - 600)$ MeV but it is by more than an order of magnitude smaller than the corresponding result $\Gamma^{\text{FIT I}}_{a_1(1260)\to\rho\pi} \simeq 13$ GeV obtained from Fit I in Sec. 9.4.1. The decisive difference is the value of $g_2$: Fit II yields $g_2 = 3.07$ (Table 10.2) whereas Fit I implied $g_2 = -11.2$ (Table 8.4). $\Gamma_{a_1\to\rho\pi} < 600$ MeV would actually require $g_2 \gtrsim 4$ in Fit II, see Fig. 11.12, but the difference to $g_2 = 3.07$ is obviously not as large as in the case of Fit I where $g_2 \gtrsim 10$ was necessary but $g_2 = -11.2$ was obtained.

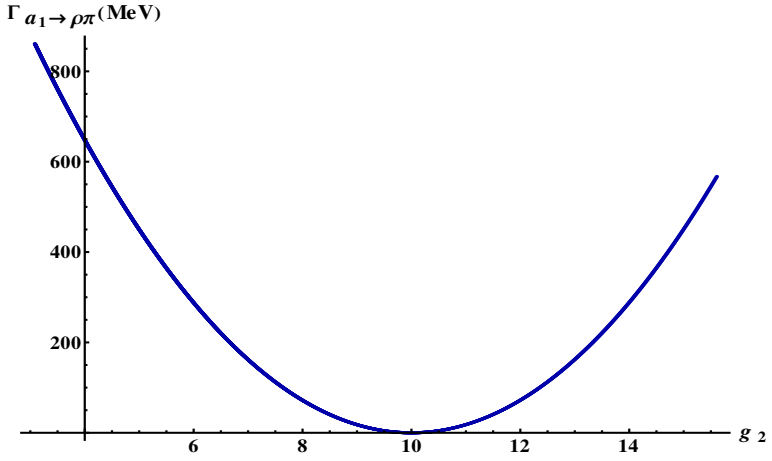


**Figure 11.12:** $\Gamma_{a_1\to\rho\pi}$ as a function of the parameter $g_2$ in Fit II.

Let us also consider, as in Sec. 9.4.1, how far $\Gamma_{\rho\to\pi\pi}$ (the decay width that determines $g_2$) would have to be changed to enable us to obtain reasonable values of $\Gamma_{a_1\to\rho\pi}$. The result is shown in Fig. 11.13.

We observe $a_1(1260)$ as a very broad resonance. We can see from Fig. 11.13 that values of $\Gamma_{a_1\to\rho\pi}$ within the PDG range are obtained if we set $\Gamma_{\rho\to\pi\pi}$ approximately 20 MeV lower than the PDG value. Smaller values of $\Gamma_{a_1\to\rho\pi}$ follow if $\Gamma_{\rho\to\pi\pi}$ is decreased further. We thus require $\Gamma_{\rho\to\pi\pi} \lesssim 130$ MeV for $\Gamma_{a_1\to\rho\pi} < 600$ MeV. The value of $\Gamma_{\rho\to\pi\pi}$ is somewhat smaller than $\Gamma^{\text{PDG}}_{\rho\to\pi\pi} = 149.1$ MeV [10]; nonetheless, this result is a strong improvement in comparison with $\Gamma_{\rho\to\pi\pi} \lesssim 38$ MeV in Fit I.

However, decreasing $\Gamma_{\rho\to\pi\pi}$ may not be the only possibility to decrease $\Gamma_{a_1\to\rho\pi}$. We could, for example, take into account the spectral function of the $\rho$ meson in order to obtain the decay width $a_1 \to \rho\pi \to 3\pi$. Note that, in this case, $g_2$ is not varied but rather fixed via on-shell values of $\Gamma_{\rho\to\pi\pi}$, $m_{a_1}$ and $m_\rho$ (i.e., $g_2 = 3.07$ as in Table 10.2). Integration over the $\rho$ spectral function, analogously to Sec. 2.6.2, yields

$$\Gamma_{a_1\to\rho\pi\to3\pi} = 706 \text{ MeV}. \tag{11.45}$$

$\Gamma_{a_1\to\rho\pi}$ is thus decreased by approximately 160 MeV once an off-shell $\rho$ meson is considered. Note that decreasing $\Gamma_{\rho\to\pi\pi}$ by only 10 MeV and re-integrating over the $\rho$ spectral function with the thus obtained $g_2 = 3.65$ leads to $\Gamma_{a_1\to\rho\pi} = 600$ MeV, corresponding to the upper boundary of the $a_1(1260)$ decay width as stated by the PDG.
Another possibility to decrease $\Gamma_{a_1\to\rho\pi}$ in Eq. (11.44) would be to introduce a form factor such as $\exp[-k^2(x_{a_1}, m_\rho, m_\pi)/\Lambda^2]$ to account for the finite range of strong interactions; $x_{a_1}$ denotes the off-shell mass of $a_1(1260)$ and $\Lambda$ is a cut-off with values between, e.g., 0.5 GeV and 1 GeV. However, introduction of form factors would need to be performed consistently throughout the model rather than *ad hoc* for a single decay width. For this reason, we will not utilise a form factor here, although we note that the trial value of $\Lambda \sim 0.5$ GeV allows for $\Gamma_{a_1\to\rho\pi} \sim 400$ MeV to be obtained once the decay width of Eq. (2.188) is modulated by the stated exponential and the $a_1(1260)$ spectral function. Modulating Eq. (2.188) with the spectral functions of both $\rho$ and $a_1(1260)$ as well as the stated form factor decreases the decay width $\Gamma_{a_1\to\rho\pi\to3\pi}$ even further, to $\sim 300$ MeV, for $\Lambda \sim 0.5$ GeV – to less than one half of the value presented in Eq. (11.45).
For these reasons, the value of the decay width in Eq. (11.44) is not too problematic not only because it is close the PDG decay width interval but also because, as we have seen, there exist means of decreasing it to the values preferred by the PDG.

### A Remark on the Decay Width $a_1(1260) \to f_0(1370)\pi$

It is not possible to calculate the decay width for the process $a_1(1260) \to f_0(600)\pi$ within Fit II. This was performed in Sec. 9.4.2, i.e., within Fit I, where our predominantly non-strange scalar $\sigma_1$ was assigned to the $f_0(600)$ resonance. This assignment is different in Fit II: $\sigma_1$ is identified with $f_0(1370)$. This allows us in principle to calculate $\Gamma_{a_1(1260)\to f_0(1370)\pi}$. However, this decay is forbidden for on-shell masses: utilising $m_{\sigma_1} = 1310^{-29}_{+30}$ MeV from Sec. 11.1.5 and

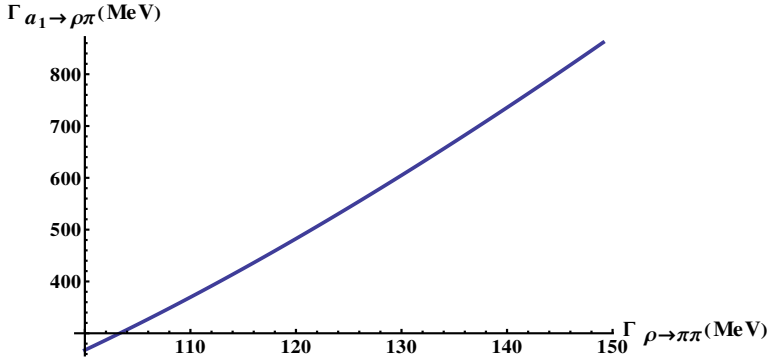


**Figure 11.13:** $\Gamma_{a_1(1260)\to\rho\pi}$ as function of $\Gamma_{\rho\to\pi\pi}$ in Fit II.

$m_\pi = 138.65$ MeV requires $m_{a_1} > 1419.65$ MeV. We obtained $m_{a_1} = 1219$ MeV in Table 10.3. Therefore, a non-vanishing value of $\Gamma_{a_1\to\sigma_1\pi}$ could only be obtained if a large $a_1(1260)$ decay width were considered in this decay channel such that the high-mass tail of $a_1$ would allow for the decay $a_1(1260) \to f_0(1370)\pi$ to occur. Performing a calculation analogous to the one in Sec. 2.6.3 to obtain the tree-level width for $a_1(1260) \to f_0(1370)\pi$ and integrating over the $a_1$ spectral function in Eq. (11.32) yields $\Gamma_{a_1(1260)\to f_0(1370)\pi} \simeq 0$. For this reason, we cannot confirm the existence of the $a_1(1260) \to f_0(1370)\pi$ decay mode. Indeed the only piece of experimental data asserting the existence of this decay channel [264] assumed the $f_0(1370)$ mass and width of 1186 and 350 MeV respectively. The assumed mass value is too small according to the PDG and also according to the review in Ref. [40]. Consequently, even experimental data regarding this decay seem to be uncertain. We thus conclude that the contribution of this decay channel to the $f_0(1370)$ width is negligible (if not zero).

### 11.3.2 Decay Width $a_1(1260) \to K^\star K \to KK\pi$ in Fit II

The corresponding interaction Lagrangian has already been stated in Eq. (9.99). As in Sec. 9.4.3, the decay $a_1 \to \bar{K}^\star K$ is tree-level forbidden because $a_1$ is below the $K^\star K$ threshold (see Table 10.3). However, if we consider an off-shell $K^\star$ state (just as in Sec. 2.6.2) then the ensuing decay $a_1 \to \bar{K}^\star K \to \bar{K}K\pi$ can be studied. We use Eq. (2.190) with an isospin factor $I = 4$ and integrate over the $K^\star$ spectral function in Eq. (2.189). The value of the $K^\star$ decay width is given further below, in Eq. (11.55). Equation (2.190) yields

$$\Gamma_{a_1\to\bar{K}^\star K\to\bar{K}K\pi} = 0.55 \text{ MeV}. \tag{11.46}$$

The above result is four orders of magnitude smaller than the one in Eq. (9.103) because of the different value of the parameter $g_2$ (as discussed in the previous sections) and also because $K^\star$ is a rather narrow resonance. We thus find that the kaon decay of the $a_1(1260)$ resonance is strongly suppressed. The value is below the branching ratio $\Gamma_{a_1(1260)\to\bar{K}^\star K}/\Gamma_{a_1(1260)} \lesssim 0.04$ (our estimate from Refs. [14, 264, 265]) and also below the result $\Gamma_{a_1(1260)\to\bar{K}^\star K}/\Gamma_{a_1(1260)} \lesssim (0.08 - 0.15)$ [266]. The reason is that we have actually considered a sequential decay ($a_1 \to \bar{K}^\star K \to \bar{K}K\pi$) rather than merely the tree-level decay $a_1 \to \bar{K}^\star K$ (although this decay will inevitably lead to $\bar{K}K\pi$ upon $\bar{K}^\star$ decay). Additionally, the full decay width of the $a_1(1260)$ state is ambiguous, $\Gamma_{a_1(1260)} = (250 - 600)$ MeV [10], and therefore an exact experimental value for a decay width such as $\Gamma_{a_1\to\bar{K}^\star K\to\bar{K}K\pi}$ cannot be trivially determined.

### 11.3.3 Decay Width $\varphi(1020) \to K^+K^-$ in Fit II

The $KK$ decay width of the $\omega_S \equiv \varphi(1020)$ state is specific within our model because it can only be calculated from Fit II. It was not possible to determine $\Gamma_{\omega_S\to KK}$ in the case of Fit I because, as apparent from Table 8.5, this fit yielded $m_{\omega_S}^{\text{FIT I}} = 870.35$ MeV – a value below the $2K$ threshold. Contrarily, Fit II yields $m_{\omega_S} = 1036.90$ MeV $> 2m_K$, see Table 10.3. The tree-level decay is therefore possible and the $\omega_S KK$ interaction Lagrangian reads

$$\begin{aligned}\mathcal{L}_{\omega_S KK} = {} & A_{\omega_S KK}\omega_S^\mu(\bar{K}^0\partial_\mu K^0 - K^0\partial_\mu\bar{K}^0 + K^-\partial_\mu K^+ - K^+\partial_\mu K^-) \\ & + B_{\omega_S KK}\partial^\nu\omega_S^\mu(\partial_\nu\bar{K}^0\partial_\mu K^0 - \partial_\nu K^0\partial_\mu\bar{K}^0 + \partial_\nu K^-\partial_\mu K^+ - \partial_\nu K^+\partial_\mu K^-)\end{aligned} \tag{11.47}$$

with

$$A_{\omega_S KK} = \frac{i}{2\sqrt{2}} Z_K^2 \left\{ -2g_1 + w_{K_1} \left[ g_1^2(\phi_N + \sqrt{2}\phi_S) + h_2(\phi_N - \sqrt{2}\phi_S) - 2\sqrt{2}h_3\phi_S \right] \right\}, \tag{11.48}$$

$$B_{\omega_S KK} = \frac{i}{\sqrt{2}} Z_K^2 g_2 w_{K_1}^2. \tag{11.49}$$

Note that the PDG data [10] cite the $\varphi(1020)$ decay width into charged as well as neutral kaon modes. They are not the same due to isospin violation [whereas our model is isospin-symmetric, as apparent, e.g., from Eq. (11.47)]. Our Fit II implemented $m_{K^\pm}$ [see Eq. (10.12)] and therefore we will in the following, for consistency, focus on the decay $\varphi(1020) \to K^+K^-$.
The calculation of $\Gamma_{\varphi(1020)\to K^+K^-}$ is analogous to the generic calculation described in Sec. 2.6.3. Equation (11.47) yields the following decay amplitude upon substituting $\partial^\mu \to -iP^\mu$ for the decaying particle and $\partial^\mu \to iP_{1,2}^\mu$ for the decay products:

$$-i\mathcal{M}^{(\alpha)}_{\omega_S\to K^+K^-} = \varepsilon_\mu^{(\alpha)}(P) h^\mu_{\omega_S KK} = -\varepsilon_\mu^{(\alpha)}(P) \left[ (A_{\omega_S KK} + B_{\omega_S KK} P\cdot P_1)(P_1^\mu - P_2^\mu) \right], \tag{11.50}$$

where the momenta of $\omega_S$, $K^+$ and $K^-$ are denoted as $P$, $P_1$ and $P_2$, respectively; $\varepsilon_\mu^{(\alpha)}(P)$ represents the polarisation vector of $\omega_S$ and the vertex $h^\mu_{\omega_S KK}$ reads

$$h^\mu_{\omega_S KK} = -(A_{\omega_S KK} + B_{\omega_S KK} P\cdot P_1)(P_1^\mu - P_2^\mu). \tag{11.51}$$

According to Eq. (2.195), there are two contributions to the averaged squared amplitude $|-i\bar{\mathcal{M}}_{\omega_S\to K^+K^-}|^2$ that involves a vector state: the first one is the squared vertex $\left|h^\mu_{\omega_S KK}\right|^2$ and the second one, $\left|h^\mu_{\omega_S KK} P_\mu\right|^2$, contains the vertex $h^\mu_{\omega_S KK}$ contracted with the vector-state momentum $P_\mu = (m_A, \mathbf{0})$. Consequently, $h^\mu_{\omega_S KK} P_\mu \equiv h^0_{\omega_S KK} P_0 = 0$ because $h^0_{\omega_S KK} = 0$, see Eq. (11.51). Therefore, only $\left|h^\mu_{\omega_S KK}\right|^2$ contributes to $|-i\bar{\mathcal{M}}_{\omega_S\to K^+K^-}|^2$:

$$\begin{aligned}
\left|-i\bar{\mathcal{M}}_{\omega_S\to K^+K^-}\right|^2 &= -\frac{1}{3}\left|h^\mu_{\omega_S KK}\right|^2 = -\frac{1}{3}(A_{\omega_S KK} + B_{\omega_S KK} P\cdot P_1)^2 (P_1^\mu - P_2^\mu)^2 \\
&= -\frac{2}{3}\left(A_{\omega_S KK} + B_{\omega_S KK}\frac{m_{\omega_S}^2}{2}\right)^2 (m_K^2 - P_1\cdot P_2) \\
&= \frac{1}{3}\left(A_{\omega_S KK} + B_{\omega_S KK}\frac{m_{\omega_S}^2}{2}\right)^2 (m_{\omega_S}^2 - 4m_K^2).
\end{aligned} \tag{11.52}$$

Then the decay width reads

$$\begin{aligned}
\Gamma_{\omega_S\to K^+K^-} &= \frac{k(m_{\omega_S}, m_K, m_K)}{8\pi m_{\omega_S}^2} |-i\bar{\mathcal{M}}_{\omega_S\to K^+K^-}|^2 \\
&= \frac{k(m_{\omega_S}, m_K, m_K)}{24\pi m_{\omega_S}^2}\left(A_{\omega_S KK} + B_{\omega_S KK}\frac{m_{\omega_S}^2}{2}\right)^2 (m_{\omega_S}^2 - 4m_K^2)
\end{aligned} \tag{11.53}$$

with $k(m_{\omega_S}, m_K, m_K)$ from Eq. (5.30). Using the parameter values from Table 10.2 to determine the coefficients in Eqs. (11.48) and (11.49) and the mass values from Table 10.3, Eq. (11.53) yields

$$\Gamma_{\omega_S \to K^+K^-} = 2.33 \text{ MeV}. \tag{11.54}$$

This value is slightly larger than the one suggested by the PDG data reading $\Gamma^{\text{exp}}_{\varphi(1020)\to K^+K^-} = (2.08 \pm 0.04)$ MeV. The reason is that our $m_{\omega_S} = 1036.90$ MeV is by approximately 20 MeV larger than $m_{\varphi(1020)} = 1019.46$ MeV [10]. Nonetheless, our chiral-model result is remarkably close to the experimental value; it represents an additional statement in favour of Fit II when compared to Fit I (with the latter not permitting for this decay width to be calculated at all, see introductory remarks in Sec. 9.4).

### 11.3.4 Decay Width $K^\star \to K\pi$ in Fit II

Phenomenology of the vector kaon $K^\star \equiv K^\star(892)$ has already been discussed within Fit I in Sec. 9.4.5. The value $\Gamma^{\text{FIT I}}_{K^{\star 0}\to K\pi} = 32.8$ MeV was obtained, see Eq. (9.124). The experimental value reads $\Gamma^{\text{exp}}_{K^\star \to K\pi} = 46.2$ MeV and the resonance decays to $\simeq 100\%$ into $K\pi$ [10]. Thus the value obtained in Fit I was by approximately 13 MeV (or 30%) smaller than the experimental result. The $K^{\star 0}K\pi$ interaction Lagrangian has been presented in Eq. (9.111). Repeating the calculation performed in Sec. 9.4.5 with the set of parameters from Table 10.2 and masses in Table 10.3 we obtain the following value in Fit II:

$$\Gamma_{K^{\star 0}\to K\pi} = 44.2 \text{ MeV}. \tag{11.55}$$

This result is only 2 MeV smaller than the stated experimental result. Correspondence with experiment is hence excellent: the assumption of scalar $\bar{q}q$ states above 1 GeV and the ensuing Fit II shift the value obtained in Fit I in the correct direction and allow us to describe the vector-kaon decay width almost exactly. This is a strong indication in favour of Fit II.

### 11.3.5 Decay Width $f_1(1285) \to K^\star K$ in Fit II

As stated in Sec. 9.4.4, there are two decay widths of the $f_{1N} \equiv f_1(1285)$ state that can be calculated from our model: $f_{1N} \to a_0\pi$ and $f_{1N} \to \bar{K}^\star K$. The former can only be considered within Fit I where the scalar states were assumed to be below 1 GeV [$a_0 \equiv \boldsymbol{a}_0(980)$]. In Fit II, the correspondence $a_0 \equiv \boldsymbol{a}_0(1450)$ holds and thus the decay width for the process $f_{1N} \to a_0\pi$ cannot be calculated (as it is kinematically forbidden). Note also that the decay $a_0(1450) \to f_1(1285)\pi$ has not been observed [10].

We then only need to consider the decay $f_1(1285) \to \bar{K}^\star K$, analogously to the calculations performed in Sec. 9.4.4. Let us again note that the PDG lists the $f_1(1285) \to \bar{K}^\star K$ process as "not seen" although the three-body decay $f_1(1285) \to \bar{K}K\pi$ possesses a branching ratio of $(9.0 \pm 0.4)\%$ whereas the full decay width of the resonance is $\Gamma_{f_1(1285)} = (24.3 \pm 1.1)$ MeV [10]. The $f_1(1285)$ decay into $\bar{K}^\star$ and $K$ is forbidden for the on-shell masses of the three particles considered, as apparent from experimental data and also from our mass values in Table 10.3. However, the three-body $\bar{K}K\pi$ decay can, within our model, arise from the sequential decay $f_1(1285) \to \bar{K}^\star K \to \bar{K}K\pi$. The latter decay was discussed in Sec. 9.4.4 within Fit I and the value $\Gamma_{f_{1N}\to\bar{K}^\star K\to\bar{K}K\pi} = 1.98$ GeV was obtained – three order of magnitude larger than the experimental limit $\Gamma_{f_{1N}\to\bar{K}^\star K\to\bar{K}K\pi} \leq (2.2 \pm 0.1)$ MeV expected from the mentioned branching

ratio for $f_1(1285) \to \bar{K}K\pi$ and the full $f_1(1285)$ decay width. In this section we discuss whether $\Gamma_{f_{1N}\to\bar{K}^\star K\to\bar{K}K\pi}$ is improved in Fit II.
To this end we need to repeat the calculations from Sec. 9.4.4 utilising the parameter set stated in Table 10.2. The $f_{1N}K^\star K$ interaction Lagrangian is stated in Eq. (9.104). We need to consider the $K^\star$ spectral function (because the decay is enabled by an off-shell $K^\star$ state), as described in Sec. 9.4.4. Consequently, we obtain

$$\Gamma_{f_{1N}\to\bar{K}^\star K\to\bar{K}K\pi} = 0.9 \text{ MeV}. \tag{11.56}$$

The value in Eq. (11.56) represents an improvement by three orders of magnitude compared to $\Gamma_{f_{1N}\to\bar{K}^\star K\to\bar{K}K\pi} = 1.98$ GeV obtained in Fit I. It is smaller than the PDG value $\Gamma_{f_1(1285)\to\bar{K}K\pi} = (2.2 \pm 0.1)$ MeV. Thus, at this point, we do not expect $\Gamma_{f_{1N}\to\bar{K}^\star K\to\bar{K}K\pi}$ to be the only contribution to $\Gamma_{f_{1N}\to\bar{K}K\pi}$ – for example, a direct three-body decay into $\bar{K}K\pi$ might also contribute to the total decay width in this channel. Nonetheless, from results presented until now we conclude that approximately 40% of the decay $f_1(1285) \to \bar{K}K\pi$ is generated via the sequential process $f_1(1285) \to \bar{K}^\star K \to \bar{K}K\pi$. This is contrary to the PDG conclusion stating that no such contribution exists. Note that the PDG conclusion is based on $\bar{p}p$ annihilation data from Ref. [267]; there are, however, newer data (but with limited statistics) from the L3 Collaboration [268] that suggest a non-vanishing contribution of $f_1(1285) \to \bar{K}^\star K \to \bar{K}K\pi$ to $f_1(1285) \to \bar{K}K\pi$. Our results seem to corroborate those of the L3 Collaboration.

$\Gamma_{f_{1N}\to\bar{K}^\star K\to\bar{K}K\pi}$ in Eq. (11.56) was obtained assuming $m_{f_{1N}} = 1219$ MeV $\equiv m_{a_1}$, see Eq. (6.41). Considering finite-width effects for the rather broad $a_1(1260)$ resonance (analogously to calculations in Ref. [46]) might, however, induce a mass splitting of $f_{1N}$ and $a_1$. Then $m_{f_{1N}} = m_{a_1}$ would no longer hold and Fig. 11.14 demonstrates the change of $\Gamma_{f_{1N}\to\bar{K}^\star K\to\bar{K}K\pi}$ if $m_{f_{1N}}$ is increased, e.g., to the experimental value $m_{f_1(1285)} = 1281.8$ MeV.

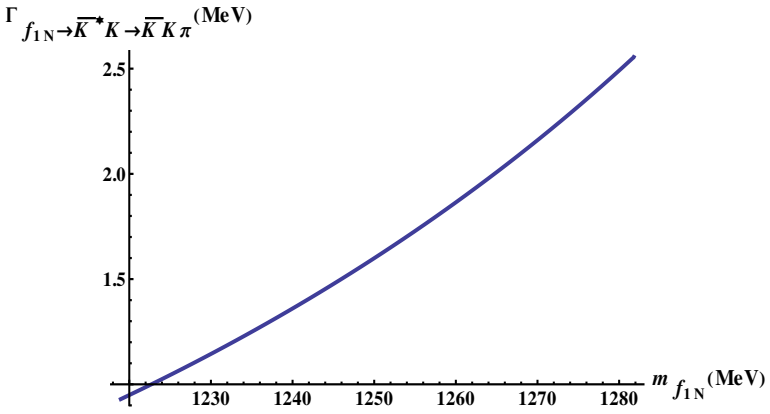


**Figure 11.14:** $\Gamma_{f_{1N}\to\bar{K}^\star K\to\bar{K}K\pi}$ as function of $m_{f_{1N}}$.

We observe that $\Gamma_{f_{1N}\to\bar{K}^\star K\to\bar{K}K\pi}$ is strongly dependent on $m_{f_{1N}}$ and increases by almost three times in the mass region of interest: from 0.9 MeV for $m_{f_{1N}} = 1219$ MeV to 2.6 MeV for $m_{f_{1N}} = m_{f_1(1285)} = 1281.8$ MeV. Therefore, varying $m_{f_{1N}}$ implies that the decay $f_1(1285) \to \bar{K}K\pi$ is completely saturated by the sequential decay $f_1(1285) \to \bar{K}^\star K \to \bar{K}K\pi$. It is actually possible to determine $m_{f_{1N}}$ such that $\Gamma_{f_{1N}\to\bar{K}K\pi}$ corresponds exactly to $\Gamma_{f_1(1285)\to\bar{K}K\pi} = (2.2 \pm 0.1)$ MeV.

As apparent from Fig. 11.14, this is realised for $m_{f_{1N}} = 1271^{+6}_{-7}$ MeV, in a very good agreement with $m_{f_1(1285)} = (1281.8 \pm 0.6)$ MeV.
We thus conclude that the $f_1(1285)$ phenomenology is decisively better described in Fit II than in Fit I.

### 11.3.6 Decay Width $f_1(1420) \to K^\star K$ in Fit II

Let us remind ourselves that the $f_1(1420)$ decays predominantly into $K^\star K$; the resonance possesses a mass of $m^{\rm exp}_{f_1(1420)} = (1426.4 \pm 0.9)$ MeV and width $\Gamma^{\rm exp}_{f_1(1420)} = (54.9 \pm 2.6)$ MeV [10]. We have seen in Sec. 9.4.6 that Fit I implies the $f_{1S} \equiv f_1(1420)$ resonance to be 17.6 GeV broad. Clearly, this result cannot be regarded as physical and in this section we discuss whether the stated large value of the decay width is decreased in Fit II. Additionally, we obtained $m_{f_1(1420)} = 1643.4$ MeV in Fit I (see Table 8.5). As apparent from Table 10.3, this value is decreased substantially to 1457 MeV within Fit II – the correspondence with the mentioned experimental value $m^{\rm exp}_{f_1(1420)}$ is therefore much better than in Fit I. In this section we discuss the phenomenology of $f_1(1420)$ within Fit II. Given the predominance of the decay into $K^\star K$, it suffices to discuss this decay channel only.
The calculation of the decay width is performed analogously to the one in Sec. 2.6.2. The $f_{1S}K^{\star 0}\bar{K}^0$ interaction Lagrangian presented in Eq. (9.125) is analogous to the one presented in Eq. (2.181); the same is true for the vertices in Eqs. (2.183) and (9.130). Consequently, we can utilise the generic formula for an axial-vector decay width presented in Eq. (2.188). Setting $I = 4$ to consider the decays $f_{1S} \to \bar{K}^{\star 0}K^0$, $\bar{K}^0 K^{\star 0}$, $K^{\star +}K^-$ and $K^{\star -}K^+$ we obtain

$$\Gamma_{f_{1S}\to\bar{K}^\star K} = 274 \text{ MeV}. \tag{11.57}$$

This value improves the Fit I value $\Gamma^{\rm FIT\ I}_{f_{1S}\to\bar{K}^\star K} = 17.6$ GeV by two orders of magnitude. Nonetheless, it is still larger than the one reported by the PDG: $\Gamma^{\rm exp}_{f_1(1420)} = (54.9 \pm 2.6)$ MeV. Therefore Fit II, where scalar meson states are assumed to be above 1 GeV, shifts $\Gamma_{f_{1S}\to\bar{K}^\star K}$ in the correct direction but does not yield the experimental result. We will see in the next section that the analogous problem persists in the $K_1$ phenomenology as well. The reason may be that the current form of our model does not implement mixing of our $1^{++}$ field [$\equiv f_{1N,A}$ in Eq. (10.26)] with the $C$-conjugated $1^{+-}$ partner [$\equiv f_{1N,B}$ in Eq. (10.26)]. Note that the value in Eq. (11.57) is decreased by approximately 40 MeV upon integration over the $K^\star$ spectral function. Thus the sequential decay $f_1(1420) \to \bar{K}^\star K \to \bar{K}K\pi$ appears to be dominant in the $f_1(1420) \to \bar{K}K\pi$ decay channel, just as in the case of the $f_1(1285)$ resonance.
Let us also note that the correct value of $\Gamma_{f_{1S}\to\bar{K}^\star K}$ can be obtained by decreasing $\Gamma_{\rho\to\pi\pi}$ to approximately 96 MeV (Fig. 11.15). However, this statement must be viewed with caution because, as already mentioned, the current form of the model lacks $f_{1N,A}$-$f_{1N,B}$ mixing upon which no decreasing of $\Gamma_{\rho\to\pi\pi}$ may be needed to obtain the correct value of $\Gamma_{f_{1S}\to\bar{K}^\star K}$.

### 11.3.7 $K_1$ Decays in Fit II

There are two important remarks regarding the $K_1$ phenomenology in Fit II. Firstly, our $K_1$ field can no longer *a priori* be assigned to a physical resonance because Fit II yields $m_{K_1} = 1343$ MeV, a value that is virtually the mass median of $K_1(1270)$ with $m_{K_1(1270)} = (1272 \pm 7)$ MeV and $K_1(1400)$ with $m_{K_1(1400)} = (1403 \pm 7)$ MeV. Indeed our discussion in Sec. 10.3 has suggested that the stated value of $m_{K_1}$ is an indication that a $1^{+-}$ nonet needs to be considered in our model

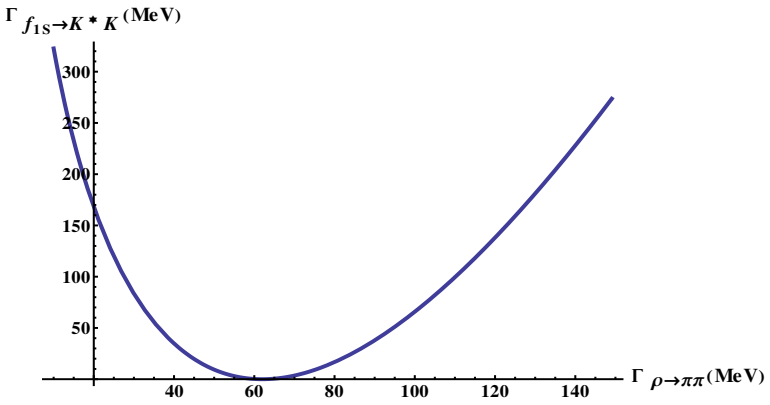


**Figure 11.15:** $\Gamma_{f_{1S}\equiv f_1(1420)\to \bar{K}^\star K}$ as function of $\Gamma_{\rho\to\pi\pi}$ in Fit II.

together with the (already present) $1^{++}$ nonet. The second remark is about results obtained in Fit I, Sec. 9.4.7. Three decay channels were considered: $K_1(1400) \to K^\star\pi$, $\rho K$ and $\omega K$. Each one of them was found to be more than 1 GeV broad; in fact, the sum of all partial decay widths in Eqs. (9.143), (9.144) and (9.145) suggests $\Gamma_{K_1(1400)} \sim 10$ GeV – a value that is two orders of magnitude larger than $\Gamma_{K_1(1400)} = (174 \pm 13)$ MeV [10].

In this section we discuss whether it is possible to amend the unphysically large values of the decay widths obtained in Sec. 9.4.7. A word of caution is nonetheless necessary: given the absence of the $1^{+-}$ nonet from the model and the consequent mass value of the $1^{++}$ field $m_{K_1} = 1343$ MeV corresponding to neither $K_1(1270)$ nor $K_1(1400)$, it cannot be expected that our results in this section will yield exact experimental values. However, we can still observe whether the results from Fit I are shifted in the correct direction by Fit II.

The interaction Lagrangian of the $K_1$ state with the already mentioned decay products has been presented in Eq. (9.132). The calculation of the decay widths proceeds exactly as described in Sec. 9.4.7; in this section we utilise parameter values from Table 10.2 and mass values from Table 10.3.

$$\Gamma_{K_1\to K^\star\pi} = 307 \text{ MeV}, \Gamma_{K_1\to\rho K} = 128 \text{ MeV}, \Gamma_{K_1\to\omega_N K} = 41 \text{ MeV}. \tag{11.58}$$

For comparison, Fit I yielded

$$\Gamma^{\text{FIT I}}_{K_1\to K^\star\pi} = 6.73 \text{ GeV}, \Gamma^{\text{FIT I}}_{K_1\to\rho K} = 4.77 \text{ GeV}, \Gamma^{\text{FIT I}}_{K_1\to\omega_N K} = 1.59 \text{ GeV}. \tag{11.59}$$

The sum of the decay widths in Eq. (11.58) suggests a full $K_1$ decay width of $\sim 480$ MeV, larger than both $\Gamma_{K_1(1400)} = (174 \pm 13)$ MeV and $\Gamma_{K_1(1270)} = (90 \pm 20)$ MeV but two orders of magnitude less than the value $\sim 10$ GeV obtained in Fit I. We observe that $\Gamma_{K_1\to K^\star\pi}$ and $\Gamma_{K_1\to\rho K}$ have been improved by an order of magnitude in comparison with Fit I; $\Gamma_{K_1\to\omega_N K}$ has been improved by two orders of magnitude. Thus we conclude that the values of the stated $K_1$ decay widths, while still not satisfactory, are nonetheless strongly improved in comparison with Fit I.

Note that all the mentioned decay widths could be improved if $\Gamma_{\rho\to\pi\pi}$ were decreased by $\sim 100$ MeV thus implying $g_2 \sim 10$. However, it is not necessary to include the corresponding diagrams

into this work because, as already stated, it is not possible to assign our $K_1$ field to a physical resonance. Nonetheless, we find Fit II to be favoured over Fit I.

### A Note on Decay $K_1 \to K f_0(1370)$

The decay into $K$ and $f_0(1370)$ has been observed for both $K_1(1270)$ and $K_1(1400)$; it can, in principle, be calculated from our model as the $K_1 K \sigma_{N,S}$ interaction Lagrangian obtained from Eq. (6.1) reads

$$\begin{aligned}\mathcal{L}_{K_1K\sigma} &= A_{K_1K\sigma_N} K_1^{\mu 0} \sigma_N \partial_\mu \bar{K}^0 + B_{K_1K\sigma_N} K_1^{\mu 0} \partial_\mu \sigma_N \bar{K}^0 \\ &+ A_{K_1K\sigma_S} K_1^{\mu 0} \sigma_S \partial_\mu \bar{K}^0 + B_{K_1K\sigma_S} K_1^{\mu 0} \partial_\mu \sigma_S \bar{K}^0 \end{aligned} \tag{11.60}$$

with

$$A_{K_1K\sigma_N} = \frac{Z_K}{2}\left\{ g_1 \left( -1 + g_1 w_{K_1} \phi_N + \sqrt{2} g_1 w_{K_1} \phi_S \right) + w_{K_1} \left[ (2h_1 + h_2)\, \phi_N - \sqrt{2} h_3 \phi_S \right] \right\}, \tag{11.61}$$

$$B_{K_1K\sigma_N} = \frac{g_1}{2} Z_K, \tag{11.62}$$

$$A_{K_1K\sigma_S} = \frac{Z_K}{\sqrt{2}}\left\{ g_1 \left( -1 + g_1 w_{K_1} \phi_N + \sqrt{2} g_1 w_{K_1} \phi_S \right) + w_{K_1} \left[ \sqrt{2}\, (h_1 + h_2)\, \phi_S - h_3 \phi_N \right] \right\}, \tag{11.63}$$

$$B_{K_1K\sigma_S} = \frac{g_1}{\sqrt{2}} Z_K. \tag{11.64}$$

Inserting the inverted Eq. (9.18) into Eq. (11.60) would allow us to determine the interaction Lagrangians for the processes $K_1 \to K\sigma_1$ and also $K_1 \to K\sigma_2$. However, the decay $K_1 \to K\sigma_2$ is kinematically forbidden due to the assignment of the fields $\sigma_1$ and $\sigma_2$ to $f_0(1370)$ and $f_0(1710)$, respectively. For this reason we only consider the part of the Lagrangian in Eq. (11.60) containing $\sigma_1$:

$$\begin{aligned}\mathcal{L}_{K_1K\sigma_1} &= (A_{K_1K\sigma_N} \cos\varphi_\sigma + A_{K_1K\sigma_S} \sin\varphi_\sigma) K_1^{\mu 0} \sigma_1 \partial_\mu \bar{K}^0 \\ &+ (B_{K_1K\sigma_N} \cos\varphi_\sigma + B_{K_1K\sigma_S} \sin\varphi_\sigma) K_1^{\mu 0} \bar{K}^0 \partial_\mu \sigma_1 \\ &\equiv A_{K_1K\sigma_1} K_1^{\mu 0} \sigma_1 \partial_\mu \bar{K}^0 + B_{K_1K\sigma_1} K_1^{\mu 0} \bar{K}^0 \partial_\mu \sigma_1 \end{aligned} \tag{11.65}$$

with $A_{K_1K\sigma_1} = A_{K_1K\sigma_N} \cos\varphi_\sigma + A_{K_1K\sigma_S} \sin\varphi_\sigma$ and $B_{K_1K\sigma_1} = B_{K_1K\sigma_N} \cos\varphi_\sigma + B_{K_1K\sigma_S} \sin\varphi_\sigma$. We note that the Lagrangian in Eq. (11.65) possesses the same form as the generic Lagrangian presented Sec. 2.6.3, Eq. (2.191). This allows us in principle to calculate the decay width $\Gamma_{K_1 \to K\sigma_1}$ from Eq. (2.200). However, such a calculation would only be possible for an off-shell $K_1$ state, i.e., an integration over the $K_1$ spectral function would be required. This is not feasible in the current form of the model because the absence of the $1^{+-}$ nonet still yields too large values of the $K_1$ decay width [see Eq. (11.58)]. Nonetheless, a discussion of the decay $K_1 \to K\sigma_1$ upon inclusion of the pseudovector nonet into our model would represent a valuable extension of this work.

### 11.4 Conclusions from Fit with Scalars above 1 GeV

The previous sections have addressed the question whether it is possible to obtain a reasonable phenomenology of mesons in vacuum under the assumption that scalar $\bar{q}q$ states possess energies above 1 GeV. This is the cardinal difference between the consequent fit (labelled as Fit II) and Fit I from Chapters 8 and 9 where, conversely, scalar $\bar{q}q$ states were assumed to be below 1 GeV. The parameters in Fit II were determined from the masses of $\pi$, $K$, $\eta$, $\eta'$,$\rho$, $K^\star$, $\omega_S \equiv \varphi(1020)$, $a_1$, $K_1$, $f_{1S} \equiv f_1(1420)$, decay widths $\Gamma_{a_1\to\pi\gamma}$ and $\Gamma_{a_0(1450)}$ as well as the masses of the scalar states $a_0$ and $K_S$ assigned to $a_0(1450)$ and $K_0^\star(1430)$, respectively. We have not included any scalar isosinglet masses into the fit in order to let these masses remain a prediction of the fit.

We summarise the main conclusions of Fit II as follows:

- It is possible to find a fit; unlike Fit I, all masses obtained from Fit II are within 3% of the respective experimental values except

  - $m_\eta = 523.20$ MeV, approximately 25 MeV ($\simeq 4.5\%$) smaller than $m_\eta^{\rm exp} = 547.85$ MeV due to the condition $m_{\eta_N} \overset{!}{<} m_{\eta_S}$ ($\eta_{N,S}$ are, respectively, pure-nonstrange and pure-strange contributions to the $\eta$ wave function),
  - $m_{K_0^\star(1430)} = 1550$ MeV, a value that is 125 MeV ($\simeq 8.8\%$) larger than the corresponding PDG value $m^{\rm exp}_{K_0^\star(1430)} = 1425$ MeV due to the pattern of explicit symmetry breaking in our model that always renders strange states approximately 100 MeV ($\simeq$ strange-quark mass) heavier than their corresponding non-strange counterparts [note, for example, that Fit II also yields $m_{a_0(1450)} = 1452$ MeV, approximately 100 MeV less than $m_{K_0^\star(1430)} = 1550$ MeV].

  In particular the narrow resonances $\varphi(1020)$ and $f_1(1420)$ are decisively better described in Fit II than in Fit I. They exhibited strong deviations from the experimental results in Fit I [$(150-200)$ MeV mass difference]. However, in Fit II, their masses differ by only $\simeq 2\%$ from the experimental values. Additionally, $\Gamma_{a_1\to\pi\gamma} = 0.622$ MeV is within the experimental interval $\Gamma^{\rm exp}_{a_1\to\pi\gamma} = 0.640 \pm 0.246$ MeV [10] and $\Gamma_{a_0(1450)} = 265$ MeV corresponds exactly to the experimental result.

- Fit II yields a somewhat unexpected result for the mass of the axial-vector kaon: $m_{K_1} = 1343$ MeV, a value representing virtually a mass-median of the two experimentally established axial-vector kaons, $K_1(1270)$ and $K_1(1400)$. Consequently, Fit II does not allow for the $K_1$ state in our model to be assigned to either of the two physical fields. This statement is compatible with our explanation of the stated value of $m_{K_1}$: our $K_1$ field is a member of a $1^{++}$ nonet that first mixes with a $1^{+-}$ (pseudovector) nonet and then leads to the physical fields $K_1(1270)$ and $K_1(1400)$. The $1^{+-}$ nonet is absent from the model presented in this work; however, inclusion of the nonet into the model is clearly demanded by our results, also because the full decay width $\Gamma_{K_1}$ corresponds to neither $\Gamma_{K_1(1270)}$ nor $\Gamma_{K_1(1400)}$. (See Sec. 10.3 for more details.)

- It is not possible to assign the two mixed isoscalar singlets $\sigma_{1,2}$ if one varies $m_0^2 < 0$ and requires $m_{\sigma_N} < m_{\sigma_S}$ because the ensuing intervals are rather large: 450 MeV $\leq m_{\sigma_1} \leq 1561$

MeV and 1584 MeV $\leq m_{\sigma_2} \leq$ 2152 MeV. Note, however, that $f_0(1710)$ is the only resonance confirmed by the PDG in the mass range of the predominantly strange field $\sigma_2$. Nonetheless, $m_{\sigma_2}$ varies too strongly for a definitive assignment of $\sigma_2$ to $f_0(1710)$ to be performed. Consequently, the assignment of the predominantly non-strange field $\sigma_1$ is, at this point, also uncertain.

- As indicated above, the ambiguity in the determination of $m_{\sigma_{1,2}}$ is caused by uncertainty in the determination of $m_0^2 < 0$. The $m_{\sigma_2}$ interval seems to suggest the correspondence $\sigma_2 \equiv f_0(1710)$. We therefore determine $m_0^2$ (with corresponding errors) from the experimentally known ratio $\Gamma_{f_0(1710)\to\pi\pi}(m_0^2)/\Gamma_{f_0(1710)\to KK}(m_0^2) = 0.2 \pm 0.06$ and test the ensuing phenomenology. [Note that the stated ratio did not enter Fit II because otherwise our results would have been inclined to a certain assignment of our scalar states. Note also that the stated ratio was obtained by the WA102 Collaboration and that it does not correspond to the one preferred by the PDG because the latter suffers from a large background and possible interference of $f_0(1710)$ with $f_0(1790)$, see Sections 3.6 and 3.7.1.] A large number of scalar-meson observables can consequently be determined using *only* the experimental ratio $\Gamma_{f_0(1710)\to\pi\pi}/\Gamma_{f_0(1710)\to KK} = 0.2 \pm 0.06$ as input:

  - *Masses:* we obtain $m_{\sigma_1} = 1310^{-29}_{+30}$ MeV and $m_{\sigma_2} = 1606^{-3}_{+4}$ MeV. The central value of $m_{\sigma_1}$ corresponds almost exactly to the combined-fit Breit-Wigner mass of Ref. [40] where $m_{f_0(1370)} = (1309 \pm 1 \pm 15)$ MeV was obtained and also to the $f_0(1370)$ peak mass in the $2\pi$ channel, found to be 1282 MeV in Ref. [40]. Additionally, we observe that $m_{\sigma_2}$ is $\sim 100$ MeV smaller than $m_{f_0(1710)} = (1720 \pm 6)$ MeV because the glueball field has not been included in the current version of the model. The mass values imply that $f_0(1370)$ is $91.2^{-1.7}_{+2.0}\%$ a $\bar{n}n$ state and that, conversely, $f_0(1710)$ is $91.2^{-1.7}_{+2.0}\%$ a $\bar{s}s$ state.
  - *Two-pion decays:* we obtain $\Gamma_{\sigma_1\to\pi\pi} = 267^{-50}_{+25}$ MeV and $\Gamma_{\sigma_2\to\pi\pi} = 47^{+9}_{-10}$ MeV. The former is consistent with the Breit-Wigner decay width $\Gamma_{f_0(1370)\to\pi\pi} = 325$ MeV and the $f_0(1370)$ full width at half-maximum in the $2\pi$ channel, the value of which was determined as 207 MeV in Ref. [40]. The latter is too large (see Sec. 3.7.3) but nonetheless demonstrates that $\Gamma_{f_0(1710)\to\pi\pi}$ is suppressed in comparison with $\Gamma_{f_0(1710)\to KK}$, in accordance with the PDG data [10].
  - *Two-kaon decays:* we obtain $\Gamma_{\sigma_1\to KK} = 188^{-9}_{+6}$ MeV and $\Gamma_{\sigma_2\to KK} = 237^{-20}_{+25}$ MeV. The former is consistent with results in Refs. [124, 170, 253, 259, 260, 261] and implies $\Gamma_{f_0(1370)\to KK} < \Gamma_{f_0(1370)\to\pi\pi}$, consistent with interpretation of $f_0(1370)$ as a predominantly $\bar{n}n$ state. $\Gamma_{\sigma_2\to KK}$ is larger than the corresponding experimental result $\sim 80$ MeV (see Sec. 3.7.3); however, it is also dominant in comparison with decay widths in other channels – consistent with the data [10].
  - *Two-eta decays:* we obtain $\Gamma_{\sigma_1\to\eta\eta} = (40 \mp 1)$ MeV and $\Gamma_{\sigma_2\to\eta\eta} = 60^{-4}_{+5}$ MeV. The former is lower than the values from Refs. [125, 145] that, however, did not consider the opening of new channels over the broad $f_0(1370)$ decay interval. The latter is marginally (within errors) consistent with the experimental result presented in Sec. 3.7.3. We also obtain $\Gamma_{\sigma_2\to\eta\eta'} = 41^{+4}_{-5}$ MeV; this result is a prediction.
  - *Decays with $a_1$:* we predict $\Gamma_{f_0(1370)\to a_1(1260)\pi\to\rho\pi\pi} = 12.7^{+5.8}_{-4.2}$ MeV and additionally $\Gamma_{f_0(1710)\to a_1(1260)\pi\to\rho\pi\pi} = 15.2^{+2.6}_{-3.1}$ MeV (strongly suppressed in comparison with other

decay channels of the two resonances).

- *The pion-kaon ratio* $\Gamma_{\sigma_1\to\pi\pi}/\Gamma_{\sigma_1\to KK} = 1.42^{-0.05}_{+0.09}$ is consistent with the WA102 result $\Gamma_{f_0(1370)\to\pi\pi}/\Gamma_{f_0(1370)\to KK} = 2.17 \pm 1.23$ [99].
- *The eta-pion ratios* read $\Gamma_{\sigma_1\to\eta\eta}/\Gamma_{\sigma_1\to\pi\pi} = 0.15\pm0.01$ and $\Gamma_{\sigma_2\to\eta\eta}/\Gamma_{\sigma_2\to\pi\pi} = 1.26^{-0.27}_{+0.52}$. The former is within the ratio $\Gamma_{f_0(1370)\to\eta\eta}/\Gamma_{f_0(1370)\to\pi\pi} = 0.19\pm0.07$ of Ref. [40]. The latter corresponds almost completely to the WA102 ratio $\Gamma^{\rm WA102}_{f_0(1710)\to\eta\eta}/\Gamma^{\rm WA102}_{f_0(1710)\to\pi\pi} = 2.4 \pm 1.04$, see Sec. 3.7.3.
- *The eta-kaon ratios* read $\Gamma_{\sigma_1\to\eta\eta}/\Gamma_{\sigma_1\to KK} = 0.22 \pm 0.01$ and $\Gamma_{\sigma_2\to\eta\eta}/\Gamma_{\sigma_2\to KK} = 0.25 \pm 0.004$. The former is purely a prediction. The latter is completely within the combined-fit result $\Gamma_{f_0(1710)\to\eta\eta}/\Gamma_{f_0(1710)\to KK} = 0.46^{+0.70}_{-0.38}$ [188] and within $2\sigma$ of the WA102 result $\Gamma_{f_0(1710)\to\eta\eta}/\Gamma_{f_0(1710)\to KK} = 0.48 \pm 0.15$ [153].
- *Ratios with $\eta'$:* our model predicts the values $\Gamma_{f_0(1710)\to\eta\eta'}/\Gamma_{f_0(1710)\to KK} = 0.17^{+0.04}_{-0.03}$, $\Gamma_{f_0(1710)\to\eta\eta'}/\Gamma_{f_0(1710)\to\pi\pi} = 0.86^{-0.06}_{+0.11}$ and $\Gamma_{f_0(1710)\to\eta\eta'}/\Gamma_{f_0(1710)\to\eta\eta} = 0.68 \pm 0.13$.
- *Decays with $\omega(782)$:* we predict $\Gamma_{f_0(1710)\to\omega\omega} \simeq 0.02$ MeV and $\Gamma_{f_0(1710)\to\omega\omega\to6\pi} \simeq 0.02$ MeV, thus virtually no $f_0(1710)$ decay in the $\omega\omega$ channel.

- We obtain $\Gamma_{K_0^\star(1430)\to K\pi} = 263$ MeV, within the PDG interval $\Gamma^{\rm exp}_{K_0^\star(1430)} = (270 \pm 80)$ MeV [10].

- The scattering lengths $a_0^{0,2}$ are saturated to their Weinberg limits $a_0^0 \simeq 0.158$, $a_0^2 \simeq -0.0448$ (see the end of Sec. 9.5) in Fit II. This implies the necessity to include the scalars below 1 GeV into our model – but they cannot be of $\bar{q}q$ structure.

- Additionally, the phenomenology in the vector and axial-vector channels is extremely improved in comparison with Fit I.

  - We obtain $\Gamma_{K^\star\to K\pi} = 44.2$ MeV, only 2 MeV less than the PDG result $\Gamma^{\rm exp}_{K^\star\to K\pi} = 46.2$ MeV [10]. Note that Fit I implied $\Gamma^{\rm FIT\ I}_{K^\star\to K\pi} = 32.8$ MeV. Note that the PDG mass and decay width of the non-strange vector state $\rho(770)$ are implemented exactly in our model.
  - We obtain $\Gamma_{\varphi(1020)\to K^+K^-} = 2.33$ MeV whereas the PDG suggests $\Gamma^{\rm exp}_{\varphi(1020)\to K^+K^-} = (2.08 \pm 0.04)$ MeV [10]. Our result is slightly larger because $m_{\varphi(1020)}$ from our model is $\sim 20$ MeV heavier than the experimental value inducing an increase in phase space. It was not possible to calculate this decay width from Fit I because $\varphi(1020)$ was well below the $KK$ threshold.
  - The decay width $\Gamma_{a_1(1260)\to\rho\pi}$ is improved by two orders of magnitude and now has the value 861 MeV whereas Fit I yielded $\simeq 13$ GeV. The decay width is decreased once the $\rho$ meson is considered an off-shell state: $\Gamma_{a_1\to\rho\pi\to3\pi} = 706$ MeV. Nonetheless, it is still somewhat above the PDG interval $\Gamma_{a_1(1260)\to\rho\pi} = (250 - 600)$ MeV [10]. This may imply $(i)$ that one needs to consider the finiteness of the strong interaction using a suitable form factor or $(ii)$ that $a_1(1260)$ is not predominantly a quarkonium (although the overlap with the $\bar{q}q$ wave function is large, as suggested by our results). Alternatively, decreasing $\Gamma_{\rho\to\pi\pi}$ (the decay width determining the parameter $g_2$ that in turn decisively influences $\Gamma_{a_1(1260)\to\rho\pi}$) by $\sim 20$ MeV yields $\Gamma_{a_1(1260)\to\rho\pi} < 600$ MeV. Note that Fit I required decreasing $\Gamma_{\rho\to\pi\pi}$ by $\sim 100$ MeV for $\Gamma_{a_1(1260)\to\rho\pi} < 600$

MeV to be obtained. We also obtain $\Gamma_{a_1(1260)\to\bar{K}^\star K\to\bar{K}K\pi} = 0.55$ MeV and find $\Gamma_{a_1(1260)\to f_0(1370)\pi} \simeq 0$. Fit I implied $\Gamma^{\text{FIT I}}_{a_1(1260)\to\bar{K}^\star K\to\bar{K}K\pi} = 1.97$ GeV.

- Only one partial decay width of the $f_1(1285)$ resonance can be calculated within our model: $f_1(1285) \to \bar{K}^\star K \to \bar{K}K\pi$. The PDG does not cite a value for the decay width of the sequential decay but rather $\Gamma_{f_1(1285)\to\bar{K}K\pi} = (2.2 \pm 0.1)$ MeV, stating that no there is no contribution to this decay width from the stated sequential decay. Contrarily, we find $\Gamma_{f_1(1285)\to\bar{K}^\star K\to\bar{K}K\pi} = 0.9$ MeV, implying a 40% contribution to $\Gamma_{f_1(1285)\to\bar{K}K\pi}$. The result is obtained for $m_{f_1(1285)\equiv f_{1N}} = m_{a_1} = 1219$ MeV; increasing $m_{f_1(1285)\equiv f_{1N}}$ to the PDG value of 1281.8 MeV yields $\Gamma_{f_1(1285)\to\bar{K}^\star K\to\bar{K}K\pi} = \Gamma_{f_1(1285)\to\bar{K}K\pi}$. Note that Fit I yielded $\Gamma^{\text{FIT I}}_{f_1(1285)\to\bar{K}^\star K} \simeq 2.15$ GeV and thus Fit II represents a strong improvement of the results from Fit I.
- We also obtain $\Gamma_{f_1(1420)\to\bar{K}^\star K} = 274$ MeV. This result is two orders of magnitude smaller than the (unphysically large) value $\Gamma^{\text{FIT I}}_{f_{1S}\to\bar{K}^\star K} = 17.6$ GeV. Nonetheless, it is larger than the one reported by the PDG: $\Gamma^{\text{exp}}_{f_1(1420)} = (54.9 \pm 2.6)$ MeV. The reason is assumed to be the absence of the $1^{+-}$ nonet from our model expected to mix with the $1^{++}$ nonet already present in the model [and containing $f_1(1420)$].
- The full $K_1$ decay width is still larger than those of the two physical states: we obtain $\Gamma_{K_1} \sim 480$ MeV whereas the data suggest $\Gamma_{K_1(1400)} = (174 \pm 13)$ MeV and $\Gamma_{K_1(1270)} = (90 \pm 20)$ MeV. The reason has already been discussed: mixing of our $1^{++}$ nonet with the partner $1^{+-}$ nonet has to be implemented in the model. Nonetheless, Fit II improves not only the full decay widths but also the partial ones: we obtain $\Gamma_{K_1\to K^\star\pi} = 307$ MeV, $\Gamma_{K_1\to\rho K} = 128$ MeV, $\Gamma_{K_1\to\omega_N K} = 41$ MeV whereas Fit I yielded $\Gamma^{\text{FIT I}}_{K_1\to K^\star\pi} = 6.73$ GeV, $\Gamma^{\text{FIT I}}_{K_1\to\rho K} = 4.77$ GeV, $\Gamma^{\text{FIT I}}_{K_1\to\omega_N K} = 1.59$ GeV. Thus the full and partial $K_1$ decay widths, although still too large, have strongly improved in Fit II.

Thus Fit II accommodates the correct (axial-)vector phenomenology into the model [$\rho$, $K^\star$, $\varphi(1020)$, $f_1(1285)$], yields qualitative consistence [$a_1(1260)$] or suggests the necessity to include further states into the model [$f_1(1420)$, $K_1$].

Fit II yields a decisively better description of the overall phenomenology: meson masses and decay widths are either described correctly or stand closer to the data than in Fit I. For these reasons, the assumption of scalar $\bar{q}q$ states above 1 GeV is strongly preferred over the assumption that the same states are present below 1 GeV.

A comparison of results from the two fits is presented in Table 11.1; experimental uncertainties are omitted. Table 11.1 contains all the masses except $m_{\sigma_{1,2}}$ because of the experimental uncertainties (the $\sigma_{1,2}$ results are discussed above in this section).

| Observable | Fit I [MeV] | Fit II [MeV] | Experiment [MeV] |
|---|---|---|---|
| $m_\pi$ | 138.04 | 138.65 | 139.57 |
| $m_K$ | 490.84 | 497.96 | 493.68 |
| $m_\eta$ | 517.13 | 523.20 | 547.85 |
| $m_{K_S}$ | 1128.7 | 1550 | 676 (FitI)/1425 (FitII) |
| $m_{\eta'}$ | 957.78 | 957.78 | 957.78 |
| $m_\rho$ | 775.49 | 775.49 | 775.49 |
| $m_{K^\star}$ | 832.53 | 916.52 | 891.66 |
| $m_{a_0}$ | 978 | 1452 | 980 (Fit I)/1474 (FitII) |
| $m_{\varphi(1020)}$ | 870.35 | 1036.90 | 1019.46 |
| $m_{a_1(1260)}$ | 1396 | 1219 | 1230 |
| $m_{K_1}$ | 1520 | 1343 | 1272 or 1403 |
| $m_{f_1(1420)}$ | 1643.4 | 1457.0 | 1426.4 |
| $\Gamma_{a_1(1260)\to\pi\gamma}$ | 0.369 | 0.622 | 0.640 |
| $\Gamma_{\rho\to\pi\pi}$ | 149.1 | 149.1 | 149.1 |
| $\Gamma_{K^\star\to K\pi}$ | 32.8 | 44.2 | 46.2 |
| $\Gamma_{\varphi(1020)\to K^+K^-}$ | 0 | 2.33 | 2.08 |
| $\Gamma_{a_1(1260)\to\rho\pi}$ | $\sim 13000$ | 861 | $< 600$ |
| $\Gamma_{a_1(1260)\to\rho\pi\to 3\pi}$ | $\sim 11000$ | 706 | $< 600$ |
| $\Gamma_{a_1(1260)\to\bar{K}^\star K\to\bar{K}K\pi}$ | 1970 | 0.55 | small |
| $\Gamma_{f_1(1285)\to\bar{K}^\star K\to\bar{K}K\pi}$ | 1980 | 0.9 | $< 2.2$ |
| $\Gamma_{f_1(1420)\to\bar{K}^\star K\to\bar{K}K\pi}$ | 17600 | 274 | $\sim 54.9$ |
| $\Gamma_{K_1}$ | $\sim 13000$ | $\sim 480$ | $\lesssim 170$ |
| $a_0^0$ | 0.165 MeV$^{-1}$ | 0.158 MeV$^{-1}$ | 0.218 MeV$^{-1}$ |
| $a_0^2$ | $-0.0442$ MeV$^{-1}$ | $-0.0448$ MeV$^{-1}$ | $-0.0457$ MeV$^{-1}$ |

**Table 11.1:** Results from Fit I and Fit II compared with experiment.

# 12. Incorporating the Glueball into the Model

In the previous chapters we have discussed the phenomenology of states containing an antiquark and a quark. However, gluons – the gauge bosons of QCD – can also build composite states of their own: the so-called *glueballs*. Thus we expect in particular a scalar glueball to exist; if it does, then it could mix with the scalar $\bar{q}q$ states already presented in this work. The mixing is discussed in this chapter.

## 12.1 Introduction

Glueballs, bound states of gluons, are naturally expected in QCD due to the non-Abelian nature of the theory: gluons interact strongly with themselves and thus they can bind and form colorless states, analogously to what occurs in the quark sector. The existence of glueballs has been studied in the framework of the effective bag model for QCD already four decades ago [269] and it has been further investigated in a variety of approaches [142, 160, 270]. Numerical calculations of the Yang-Mills sector of QCD also find a full glueball spectrum in which the scalar glueball is the lightest state [271].

Glueballs can mix with quarkonium ($\bar{q}q$) states with the same quantum numbers. This makes the experimental search for glueballs more complicated, because physical resonances emerge as mixed states. The scalar sector $J^{PC} = 0^{++}$ has been investigated in many works in the past. The resonance $f_0(1500)$ is relatively narrow when compared to other scalar-isoscalar states: for this reason it has been considered as a convincing candidate for a glueball state. Mixing scenarios in which two quark-antiquark isoscalar states $\bar{n}n$ and $\bar{s}s$ and one scalar glueball $gg$ mix and generate the physical resonances $f_0(1370)$, $f_0(1500)$, and $f_0(1710)$ have been discussed in Refs. [206, 207].

In this chapter we discuss how to extend the calculations presented in this work to include a glueball field. The discussion will regard the $U(2) \times U(2)$ version of the model from Chapter 5 only; a corresponding extension of the $U(3) \times U(3)$ model is a very interesting project in itself that will be treated in a separate work [193].

The first attempt to incorporate a glueball into a linear sigma model was performed long ago in Ref. [272]. The novel features of the study in this chapter are the following: (*i*) The glueball is introduced as a dilaton field within a theoretical framework where not only scalar and pseudoscalar mesons, but also vector and axial-vector mesons are present from the very beginning. This fact allows also for a calculation of decays into vector mesons. As already indicated, the model is explicitly evaluated for the case of $N_f = 2$, for which only one scalar-isoscalar quarkonium state exists: $\sigma_N \equiv \bar{n}n$ which mixes with the glueball. The two emerging mixed states are assigned to the resonances $f_0(1370)$ which is, in accordance with Sec. 11.1.5, predominantly a $\bar{n}n$ state, and with $f_0(1500)$ which is predominantly a glueball state. (*ii*) We consequently test – to our knowledge for the first time – this mixing scenario above 1 GeV in the framework of a chiral model.

Let us emphasise again that our model is built in accordance with the symmetries of the QCD Lagrangian. It possesses the known degrees of freedom of low-energy QCD [(pseudo)scalar and (axial-)vector mesons] as well as the same global chiral invariance. In this chapter, we model

another feature of the QCD Lagrangian: the scale (or dilatation) invariance $x^\mu \to \lambda^{-1} x^\mu$ (where $x^\mu$ is a Minkowski-space coordinate and $\lambda$ the scale parameter of the conformal group), see Eq. (2.74) and the discussion thereafter. The scale invariance is realised at the classical level but broken at the quantum level due to the loop corrections in the Yang-Mills sector (scale anomaly). In this chapter the breaking of scale invariance is implemented at tree-level by means of a dilaton field (representing a glueball) with the usual logarithmic dilaton potential [272]. However, all the other interaction terms (with the exception of the chiral anomaly) are dilatation-invariant in the chiral limit.

Having constructed the Lagrangian of the effective model, we calculate the masses of the pure $\bar{n}n$ and glueball states in the $J^{PC} = 0^{++}$ channel, study their mixing and calculate the decay widths of the mixed states. Although we work with $N_f = 2$ in this chapter, the use of flavour symmetry enables us to calculate the decay widths of the scalar resonances into kaons and into both the $\eta$ and $\eta'$ mesons which contain the $s$-quark in their flavour wave functions. After the study of the already mentioned scenario where $f_0(1370)$ and $f_0(1500)$ are predominantly quarkonium and glueball, respectively, we also test the alternative scenario in which the resonance $f_0(1710)$ is predominantly glueball and scenarios in which $f_0(600)$ is predominantly quarkonium. They, however, lead to inconsistencies when compared to the present data and are therefore regarded as less favourable. Additionally, our results discussed in Sec. 11.4 also favour $f_0(1710)$ to be a predominantly $\bar{s}s$ state rather than a glueball.

## 12.2 The Model

The Yang-Mills (YM) sector of QCD (QCD without quarks) is classically invariant under dilatations [see Eqs. (2.74) – (2.80)]. This symmetry is, however, broken at the quantum level. The divergence of the corresponding current is the trace of the energy-momentum tensor $T^{\mu\nu}_{\rm YM}$ of the YM Lagrangian

$$(T_{\rm YM})^\mu_\mu = \frac{\beta(g)}{4g} G^a_{\mu\nu} G^{a,\mu\nu} \neq 0, \tag{12.1}$$

where $G^a_{\mu\nu}$ is the field-strength tensor of the gluon fields, $g = g(\mu)$ is the renormalised coupling constant at the scale $\mu$, and the $\beta$-function is given by $\beta(g) = \partial g / \partial \ln \mu$. At the one-loop level $\beta(g) = -bg^3$ with $b = 11N_c/(48\pi^2)$. This implies $g^2(\mu) = [2b \ln(\mu/\Lambda_{\rm YM})]^{-1}$, where $\Lambda_{\rm YM} \simeq 200$ MeV is the Yang-Mills scale. A finite energy scale thus emerges in a theory which is classically invariant under dilatation (dimensional transmutation). The expectation value of the trace anomaly does not vanish and represents the so-called gluon condensate:

$$\left\langle T^\mu_{{\rm YM},\mu} \right\rangle = -\frac{11N_c}{48} \left\langle \frac{\alpha_s}{\pi} G^a_{\mu\nu} G^{a,\mu\nu} \right\rangle = -\frac{11N_c}{48} C^4, \tag{12.2}$$

where [31, 32]

$$C^4 \simeq (300 - 600 \text{ MeV})^4. \tag{12.3}$$

At the composite level one can build an effective theory of the YM sector of QCD by introducing a scalar dilaton field $G$ which describes the trace anomaly. The dilaton Lagrangian reads [272]

$$\mathcal{L}_{dil} = \frac{1}{2}(\partial_\mu G)^2 - \frac{1}{4}\frac{m_G^2}{\Lambda^2}\left( G^4 \ln\left|\frac{G}{\Lambda}\right| - \frac{G^4}{4} \right). \tag{12.4}$$

The minimum $G_0$ of the dilaton potential is realised for $G_0 = \Lambda$. Upon shifting $G \to G_0 + G$, a particle with mass $m_G$ emerges, which is interpreted as the scalar glueball. The numerical value

has been evaluated in Lattice QCD and reads $m_G \sim 1.5$ GeV [271]. The logarithmic term of the potential explicitly breaks the invariance under a dilatation transformation. The divergence of the corresponding current reads $\partial_\mu J^\mu_{dil} = T^{\ \mu}_{dil,\,\mu} = -\frac{1}{4} m_G^2 \Lambda^2$. This can be compared with the analogous quantity in Eq. (12.2) which implies $\Lambda = \sqrt{11}\, C^2/(2m_G)$.

As demonstrated in Sec. 2.4, QCD with quarks is also classically invariant under dilatation transformations in the limit of zero quark masses (chiral limit). The scale of all hadronic phenomena is given by the previously introduced energy scale $\Lambda_{\rm YM}$. This fact holds true also when the small but nonzero values of the quark masses are considered. In order to describe these properties in a hadronic model we now extend the linear sigma model of the previous chapters by including the dilaton. To this end, the following criteria are applied [202]: $(i)$ With the exception of the chiral anomaly, the parameter $\Lambda$ from Eq. (12.4), which comes from the Yang-Mills sector of the theory in accordance with QCD, is the only dimensionful parameter of the Lagrangian in the chiral limit. $(ii)$ The Lagrangian is required to be finite for every finite value of the gluon condensate $G_0$. This, in turn, also assures that no singular terms arise in the limit $G_0 \to 0$. In accordance with the requirements $(i)$ and $(ii)$ only terms with dimension exactly equal to 4 are allowed in the chiral limit.

The hadronic Lagrangian obeying these requirements reads

$$
\begin{aligned}
\mathcal{L} = \mathcal{L}_{dil} &+ \mathrm{Tr}\left[(D^\mu\Phi)^\dagger(D_\mu\Phi) - m_0^2\left(\frac{G}{G_0}\right)^2\Phi^\dagger\Phi - \lambda_2(\Phi^\dagger\Phi)^2\right] - \lambda_1(\mathrm{Tr}\left[\Phi^\dagger\Phi\right])^2 \\
&+ c[\det(\Phi^\dagger) + \det(\Phi)] + \mathrm{Tr}\left[H\left(\Phi^\dagger + \Phi\right)\right] - \frac{1}{4}\mathrm{Tr}\left[(L^{\mu\nu})^2 + (R^{\mu\nu})^2\right] \\
&+ \mathrm{Tr}\left\{\left[\frac{m_1^2}{2}\left(\frac{G}{G_0}\right)^2 + \Delta\right](L_\mu^2 + R_\mu^2)\right\} + \frac{h_1}{2}\mathrm{Tr}[\Phi^\dagger\Phi]\mathrm{Tr}[L_\mu L^\mu + R_\mu R^\mu] \\
&+ h_2\mathrm{Tr}[\Phi^\dagger L_\mu L^\mu\Phi + \Phi R_\mu R^\mu\Phi^\dagger] + 2h_3\mathrm{Tr}[\Phi R_\mu\Phi^\dagger L^\mu] + \dots\ ,
\end{aligned}
\tag{12.5}
$$

where $\Phi$ denotes the $N_f \times N_f$ (pseudo)scalar multiplet and $L^\mu$ and $R^\mu$ the left- and right-handed vector multiplets, respectively. The dots represent further terms which do not affect the processes studied in this work.

The Lagrangian presented in Eq. (12.5) possesses the generic form for any number of flavours $N_f$. It is a generalisation of the Lagrangian (4.42) constructed in Chapter 4. In this chapter, the Lagrangian is evaluated for two flavours only. Consequently, as in Chapter 5, we define $\Phi = (\sigma_N + i\eta_N)\, t^0 + (\boldsymbol{a}_0 + i\boldsymbol{\pi}) \cdot \boldsymbol{t}$ ($\eta_N$ contains only non-strange degrees of freedom), $L^\mu = (\omega^\mu + f_1^\mu)\, t^0 + (\boldsymbol{\rho}^\mu + \boldsymbol{a}_1^\mu) \cdot \boldsymbol{t}$ and $R^\mu = (\omega_N^\mu - f_{1N}^\mu)\, t^0 + (\boldsymbol{\rho}^\mu - \boldsymbol{a}_1^\mu) \cdot \boldsymbol{t}$ ; $t^0$, $\boldsymbol{t}$ are the generators of $U(2)$. Moreover, $D^\mu\Phi = \partial^\mu\Phi - ig_1(L^\mu\Phi - \Phi R^\mu)$, $L^{\mu\nu} = \partial^\mu L^\nu - \partial^\nu L^\mu$, $R^{\mu\nu} = \partial^\mu R^\nu - \partial^\nu R^\mu$.

The explicit breaking of the global chiral symmetry is described by the term $\mathrm{Tr}[H(\Phi + \Phi^\dagger)] \equiv h\sigma$ ($h = const. \sim m_{u,d}^2$), which allows us to take into account the non-vanishing value $m_{u.d}$ of the non-strange quark mass. This term contains the dimensionful parameter $h$ with $[h] = [\text{energy}^3]$ and also explicitly breaks the dilatation invariance, just as the quark masses do in the underlying QCD Lagrangian. Finally, the chiral anomaly is described by the term $c\,(\det\Phi + \det\Phi^\dagger)$. This term corresponds to the one utilised in the model containing quarkonia only, see Chapter 5 (and also Sec. 6.4). For $N_f = 2$ the parameter $c$ carries the dimension $[\text{energy}^2]$ and represents a further breaking of dilatation invariance. This term arises from instantons which are also a property of the Yang-Mills sector of QCD.

The identification of the fields of the model with the resonances listed by the PDG [10] is the

same as in Chapter 5. We assign the fields $\boldsymbol{\pi}$ and $\eta_N$ to the pion and the $SU(2)$ counterpart of the $\eta$ meson, respectively, $\eta_N \equiv (\overline{u}u + \overline{d}d)/\sqrt{2}$, with a mass of about 700 MeV. This value can be obtained by 'unmixing' the physical $\eta$ and $\eta'$ mesons which also contain $\overline{s}s$ contributions. The fields $\omega_N^\mu$ and $\boldsymbol{\rho}^\mu$ represent the $\omega(782)$ and $\rho(770)$ vector mesons, respectively, while the fields $f_{1N}^\mu$ and $\boldsymbol{a}_1^\mu$ represent the $f_1(1285)$ and $a_1(1260)$ axial-vector mesons, respectively. [In principle, the physical $\omega(782)$ and $f_1(1285)$ states also contain $\overline{s}s$ contributions but their admixture is small.] As shown in Sec. 5.2.3, the $\sigma_N$ field should be interpreted as a $\bar{n}n$ state because its decay width decreases as $1/N_c$ in the limit of a large number of colors. The $\sigma_N$ and $G$ fields mix: the physical fields $\sigma'$ and $G'$ are obtained through an $SO(2)$ rotation, as we shall show in the following. Then the first and most natural assignment is $\{\sigma', G'\} = \{f_0(1370), f_0(1500)\}$, see Sec. 6.7. Note that the $\boldsymbol{a}_0$ state is assigned to the physical $a_0(1450)$ resonance in accordance with results of Sec. 5.4.1, confirmed by results from the $U(3) \times U(3)$ version of our model in Chapter 10. Other assignments for $\{\sigma', G'\}$ will be also tested in Sections 12.3.2 and 12.3.3 and turn out to be less favourable.

In order to study the non-vanishing vacuum expectation values (vev's) of the two $J^{PC} = 0^{++}$ scalar-isoscalar fields of the model $\sigma_N$ and $G$, we set all the other fields in Eq. (12.5) to zero and obtain:

$$\mathcal{L}_{\sigma G} = \mathcal{L}_{dil} + \frac{1}{2}(\partial^\mu \sigma_N)^2 - \frac{1}{2}\left[m_0^2 \left(\frac{G}{G_0}\right)^2 - c\right]\sigma_N^2 - \frac{1}{4}\left(\lambda_1 + \frac{\lambda_2}{2}\right)\sigma_N^4 + h\sigma_N. \tag{12.6}$$

Upon shifting the fields by their vacuum expectation values, $\sigma_N \to \sigma_N + \phi_N$ and $G \to G + G_0$, we obtain the masses of the states $\sigma_N = (\bar{u}u + \bar{d}d)/\sqrt{2}$ and $G = gg$,

$$M_{\sigma_N}^2 = m_0^2 - c + 3\left(\lambda_1 + \frac{\lambda_2}{2}\right)\phi_N^2\,, \qquad M_G^2 = m_0^2\,\frac{\phi_N^2}{G_0^2} + m_G^2\,\frac{G_0^2}{\Lambda^2}\left(1 + 3\ln\left|\frac{G_0}{\Lambda}\right|\right). \tag{12.7}$$

Note that the pure glueball mass $M_G$ depends also on the quark condensate $\phi_N$, but correctly reduces to $m_G$ in the limit $m_0^2 = 0$ (decoupling of quarkonia and glueball). In the presence of quarkonia, $m_0^2 \neq 0$, the vev $G_0$ is given by the equation

$$-\frac{m_0^2 \phi_N^2 \Lambda^2}{m_G^2} = G_0^4 \ln\left|\frac{G_0}{\Lambda}\right|. \tag{12.8}$$

The shift of the fields by their vev's introduces a bilinear mixing term $\sim \sigma_N G$ in the Lagrangian (12.6). The physical fields $\sigma'$ and $G'$ can be obtained through an $SO(2)$ rotation,

$$\begin{pmatrix} \sigma' \\ G' \end{pmatrix} = \begin{pmatrix} \cos\varphi_G & \sin\varphi_G \\ -\sin\varphi_G & \cos\varphi_G \end{pmatrix} \begin{pmatrix} \sigma_N \\ G \end{pmatrix}, \tag{12.9}$$

with

$$M_{\sigma'}^2 = M_{\sigma_N}^2 \cos^2\varphi_G + M_G^2 \sin^2\varphi_G + 2\,m_0^2\,\frac{\phi_N}{G_0}\sin(2\varphi_G), \tag{12.10}$$

$$M_{G'}^2 = M_G^2 \cos^2\varphi_G + M_{\sigma_N}^2 \sin^2\varphi_G - 2\,m_0^2\,\frac{\phi_N}{G_0}\sin(2\varphi_G), \tag{12.11}$$

where the mixing angle $\theta_G$ reads

$$\varphi_G = \frac{1}{2}\arctan\left[-4\,\frac{\phi_N}{G_0}\,\frac{m_0^2}{M_G^2 - M_{\sigma_N}^2}\right]. \tag{12.12}$$

The quantity $m_0^2$ can be calculated from the masses of the pion, $\eta_N$, and the bare $\sigma_N$ mass [Eqs. (5.14), (5.15) and (5.17)]:

$$m_0^2 = \left(\frac{m_\pi}{Z_\pi}\right)^2 + \frac{1}{2}\left[\left(\frac{m_{\eta_N}}{Z_\pi}\right)^2 - M_{\sigma_N}^2\right]. \tag{12.13}$$

If $m_0^2 - c < 0$, spontaneous breaking of chiral symmetry is realised.

## 12.3 Results and Discussion

The Lagrangian (12.5) contains the following twelve free parameters: $m_0$, $\lambda_1$, $\lambda_2$, $m_1$, $g_1$, $c$, $h$, $h_1$, $h_2$, $h_3$, $m_G$, $\Lambda = \sqrt{11}\,C^2/(2m_G)$. The processes that we shall consider depend only on the combination $h_1 + h_2 + h_3$, thus reducing the number of parameters to ten. We replace the set of ten parameters by the following equivalent set: $m_\pi$, $m_{\eta_N}$, $m_\rho$, $m_{a_1}$, $\phi_N$, $Z_\pi$, $M_{\sigma_N}$, $m_G$, $m_1$, $C$. The masses $m_\pi$ (= 139.57 MeV) and $m_\rho$ (= 775.49 MeV) are fixed to their PDG values [10].
As outlined in Sec. 7.1, the mass of the $\eta_N$ meson can be calculated using the mixing of strange and non-strange contributions in the physical fields $\eta$ and $\eta'$:

$$\begin{aligned} \eta &= \eta_N \cos\varphi_\eta + \eta_S \sin\varphi_\eta, \\ \eta' &= -\eta_N \sin\varphi_\eta + \eta_S \cos\varphi_\eta, \end{aligned} \tag{12.14}$$

where $\eta_S$ denotes a pure $\bar{s}s$ state and $\varphi_\eta \simeq -36°$ [227]. In this way, we obtain the value $m_{\eta_N} = 716$ MeV. [Given the well-known uncertainty of the value of the angle $\varphi_\eta$, one could also consider other values, e.g., our result $\varphi_\eta = -43.9°$ from Chapter 10 (see discussion of Table 10.3), which corresponds to $m_{\eta_N} = 764$ MeV, or the value $\varphi_\eta = -41.4°$ from the KLOE Collaboration [228], which corresponds to $m_{\eta_N} = 755$ MeV. Variations of the pseudoscalar mixing angle affect the results presented in this chapter only slightly.]
The value of $m_{a_1}$ is fixed to 1050 MeV according to the study of Ref. [47]. (We note that taking the value 1219 MeV from Sec. 10 or the present PDG estimate of 1230 MeV does not change the conclusions of this chapter.) The chiral condensate is fixed as $\phi_N = Z_\pi f_\pi$ and the renormalization constant $Z_\pi$ is determined by the study of the process $a_1 \to \pi\gamma$: $Z_\pi = 1.67 \pm 0.2$ in Sec. 5.2.5.

### 12.3.1 Assigning $\sigma'$ and $G'$ to $f_0(1370)$ and $f_0(1500)$

The $\sigma'$ field denotes an isoscalar $J^{PC} = 0^{++}$ state and its assignment to a physical state is a long-debated problem of low-energy QCD [58, 84, 142, 160, 206, 208, 210, 211, 270, 271]. The two major candidates are the $f_0(600)$ and $f_0(1370)$ resonances, see Sections 9.6 and 11.4. We have concluded in Sec. 11.4 that $f_0(1370)$ is favoured to be predominantly a $\bar{n}n$ state. As already stated, the resonance $f_0(1500)$ is a convincing glueball candidate. For these reasons we first test the scenario in which $\{\sigma', G'\} = \{f_0(1370), f_0(1500)\}$, which turns out to be phenomenologically successful, see below.
We are left with the following four free parameters: $C$, $M_{\sigma_N}$, $m_G$, $m_1$. They can be obtained by a fit to the five experimental quantities of Table 12.1: the masses of the resonances $f_0(1500)$ [$M_{G'} \equiv M_{f_0(1500)} = 1505$ MeV [10]] and $f_0(1370)$, for which we use the mean value $M_{\sigma'_N}^{\rm exp} = (1350 \pm 150)$ MeV taking into account the PDG mass range between 1200 MeV and 1500 MeV [10]), and

| Quantity | Our Value [MeV] | Experiment [MeV] |
|---|---|---|
| $M_{\sigma'}$ | $1191 \pm 26$ | 1200-1500 |
| $M_{G'}$ | $1505 \pm 6$ | $1505 \pm 6$ |
| $G' \to \pi\pi$ | $38 \pm 5$ | $38.04 \pm 4.95$ |
| $G' \to \eta\eta$ | $5.3 \pm 1.3$ | $5.56 \pm 1.34$ |
| $G' \to K\bar{K}$ | $9.3 \pm 1.7$ | $9.37 \pm 1.69$ |

**Table 12.1:** Fit in the scenario $\{\ \sigma', G'\} = \{\ f_0(1370), f_0(1500)\}$. Note that the $f_0(1370)$ mass ranges between 1200 MeV and 1500 MeV [10] and therefore, as an estimate, we are using the value $m_{\sigma'} = (1350 \pm 150)$ MeV in the fit.

the three well-known decay widths of the well-measured resonance $f_0(1500)$: $f_0(1500) \to \pi\pi$, $f_0(1500) \to \eta\eta$, and $f_0(1500) \to K\bar{K}$.

Using the Lagrangian (12.5), these observables can be expressed as functions of the parameters listed above. Note that, although our framework is based on $N_f = 2$, we can calculate the amplitudes for the decays into mesons containing strange quarks by making use of the flavour symmetry $SU(N_f = 3)$ [207]. It is then possible to calculate the following $f_0(1500)$ decay widths into pseudoscalar mesons containing $s$ quarks: $f_0(1500) \to K\bar{K}$, $f_0(1500) \to \eta\eta$, and $f_0(1500) \to \eta\eta'$.

The $\chi^2$ method yields $\chi^2/\text{d.o.f.} = 0.29$ (thus very small), $C = (699 \pm 40)$ MeV, $M_{\sigma_N} = (1275 \pm 30)$ MeV, $m_G = (1369 \pm 26)$ MeV and $m_1 = (809 \pm 18)$ MeV. We have also examined the uniqueness of our fit. To this end, we have considered $\chi^2$ fixing three of four parameters entering the fit at their best values and varying the remaining fourth parameter. In each of the four cases we observe only one minimum of the $\chi^2$ function; each minimum leads exactly to the parameter values stated in Table 12.1. We also observe no changes of the results for the errors of the parameters. These findings give us confidence that the obtained minimum corresponds to the absolute minimum of the $\chi^2$ function.

The consequences of this fit are the following:

(i) The quarkonium-glueball mixing angle reads $\theta_G = (29.7 \pm 3.6)^\circ$. This, in turn, implies that the resonance $f_0(1500)$ consists to 76% of a glueball and to the remaining 24% of a quark-antiquark state. An inverted situation holds for $f_0(1370)$. Given our results discussed in Sec. 11.4, we conclude that $f_0(1370)$ possesses admixtures from both $\bar{n}n$ and glueball; a detailed discussion will be presented in Ref. [193].

(ii) Our fit allows us to determine the gluon condensate: $C = (699 \pm 40)$ MeV. This result implies that the upper value in Eq. (12.2) is favoured by our analysis. It is remarkable that insights into this basic quantity of QCD can be obtained from the PDG data on mesons.

(iii) Further results for the $f_0(1500)$ meson are reported in the first two entries of Table 12.2. The decay into $4\pi$ is calculated as a product of an intermediate $\rho\rho$ decay. To this end the usual integration over the $\rho$ spectral function is performed. Our result yields 30 MeV in the $4\pi$ decay channel and is about half of the experimental value $\Gamma_{f_0(1500)\to 4\pi} = (54.0 \pm 7.1)$ MeV. However, it should be noted that an intermediate state consisting of two $f_0(600)$ mesons (which is also expected to contribute in this decay channel) is not included in the present model. The decay into the $\eta\eta'$ channel is also evaluated; this channel is subtle because it is exactly on the threshold of the $f_0(1500)$ mass. Therefore, an integration over the spectral function of the decaying meson $f_0(1500)$ is necessary. The result is in a qualitative agreement with the experiment. Note also

that the enhanced value of the $4\pi$ decay width is a consequence of the inclusion of the glueball field into the model [identified predominantly with $f_0(1500)$] as otherwise the $4\pi$ decay channel is known to be suppressed [see the note on $\sigma_{1,2} \to 4\pi$ decays in Sec. 11.1.2 for the case of our non-strange and strange quarkonia].

(iv) The results for the $f_0(1370)$ meson are reported in the last four rows of Table 12.2. They are in agreement with the experimental data regarding the full width: $\Gamma_{f_0(1370)} = (200 - 500)$ MeV [10]. Unfortunately, the experimental results in the different channels are not yet conclusive. Our theoretical results point towards a dominant direct $\pi\pi$ and a non-negligible $\eta\eta$ contribution; these results correspond well to the experimental analysis of Ref. [40] where $\Gamma_{f_0(1370)\to\pi\pi} = 325$ MeV and $\Gamma_{f_0(1370)\to\eta\eta}/\Gamma_{f_0(1370)\to\pi\pi} = 0.19 \pm 0.07$ are obtained. [Note that Ref. [40] also cites the Breit-Wigner mass of 1309 MeV whereas our result $M_{\sigma'\equiv f_0(1370)} = (1191 \pm 26)$ MeV is $\sim 100$ MeV smaller.] We find that the four-pion decay of $f_0(1370) \to \rho\rho \to 4\pi$ is strongly suppressed (as was also determined in Sec. 11.1.2). As stated in Sec. 3.3, the values of the $f_0(1370)$ decay widths are strongly mass-dependent with Ref. [40] citing the value of $\Gamma_{f_0(1370)\to\pi\pi} \sim 50$ MeV for $m_{f_0(1370)} \sim 1309$ MeV. The $4\pi$ phase space decreases rapidly with a decreasing resonance mass and is virtually negligible for our result $M_{\sigma'\equiv f_0(1370)} = (1191 \pm 26)$ MeV. For this reason, our results are qualitatively consistent with statements in Ref. [40]. Additionally, it should be noted that due to interference effects our result for this decay channel varies strongly when the parameters are even slightly modified.

(v) The mass of the $\rho$ meson can be expressed as $m_\rho^2 = m_1^2 + \phi^2 (h_1 + h_2 + h_3)/2$, see Eq. (6.40). In order that the contribution of the chiral condensate is not negative, the condition $m_1 \leq m_\rho$ should hold. In the framework of our fit this condition is fulfilled at the two-sigma level. This result points towards a dominant $m_1$ contribution to the $\rho$ mass. This property, in turn, means that the $\rho$ mass is predominantly generated from the gluon condensate and not from the chiral condensate, as confirmed by our result $m_1 = 762$ MeV in the $U(3)\times U(3)$ version of the model, see Table 10.3. It is therefore expected that the $\rho$ mass in the medium scales as the gluon condensate rather than as the chiral condensate. In view of the fact that $m_1$ is slightly larger than $m_\rho$ we have also repeated the fit by fixing $m_1 = m_\rho$: the minimum has a $\chi^2$/d.o.f. $\simeq 1$ and the results are very similar to the previous case. The corresponding discussion about the phenomenology is unchanged.

(vi) As already stressed in Refs. [52, 55], the inclusion of (axial-)vector mesons plays a central role to obtain the present results. The artificial decoupling of (axial-)vector states would generate a by far too wide $f_0(1370)$ state. For this reason the glueball-quarkonium mixing scenario above 1 GeV has been previously studied only in phenomenological models with flavour symmetry [142, 160, 207, 270] but not in the context of chirally invariant models.

| Quantity | Our Value [MeV] | Experiment [MeV] |
|---|---|---|
| $G' \to \rho\rho \to 4\pi$ | 30 | $54.0 \pm 7.1$ |
| $G' \to \eta\eta'$ | 0.6 | $2.1 \pm 1.0$ |
| $\sigma_N' \to \pi\pi$ | $284 \pm 43$ | - |
| $\sigma_N' \to \eta\eta$ | $72 \pm 6$ | - |
| $\sigma_N' \to K\bar{K}$ | $4.6 \pm 2.1$ | - |
| $\sigma_N' \to \rho\rho \to 4\pi$ | 0.09 | - |

**Table 12.2:** Further results regarding the $\sigma' \equiv f_0(1370)$ and $G' \equiv f_0(1500)$ decays.

Given that the resonance $f_0(1370)$ has a large mass uncertainty, we have also examined the behaviour of the fit at different points of the PDG mass interval. Considering the minimal value $m^{\rm min}_{f_0(1370)} = (1220 \pm 20)$ MeV we obtain $\chi^2 = 0.2$/d.o.f. The resulting value of the mixing angle $\theta_G = (30.3 \pm 3.4)^\circ$ is practically the same as the value $\theta_G = (29.7 \pm 3.6)^\circ$ obtained in the case where $m_{f_0(1370)} = (1350 \pm 150)$ MeV was considered. Other results are also qualitatively similar to the case of $m_{f_0(1370)} = (1350 \pm 150)$ MeV.

For the upper boundary of the $f_0(1370)$ mass, the error interval of $\pm 20$ MeV turns out to be too restrictive as it leads to unacceptably large $\chi^2$ values. Consequently, increasing the error interval decreases the $\chi^2$ values – we observe that $m^{\rm max}_{f_0(1370)} = (1480 \pm 120)$ MeV leads to an acceptable $\chi^2$ value of 1.14/d.o.f. Then we obtain $\theta_G = (30.0 \pm 3.5)^\circ$, practically unchanged in comparison with the value $\theta_G = (29.7 \pm 3.6)^\circ$ in the case where $m_{f_0(1370)} = (1350 \pm 150)$ MeV. Also other quantities remain basically the same as in the case of $m_{f_0(1370)} = (1350 \pm 150)$ MeV.

We have also considered the fit at several points between the lower and upper boundaries of the $m_{f_0(1370)}$ mass range. We have chosen points of 50 MeV difference starting at $m_{f_0(1370)} = 1250$ MeV (i.e., we have considered $m_{f_0(1370)} \in \{1250, 1300, 1350, 1400, 1450\}$ MeV) with errors chosen such that the $\chi^2$/d.o.f. becomes minimal (error values are between $\pm 30$ MeV for $m_{f_0(1370)} = 1250$ MeV and $\pm 100$ MeV for $m_{f_0(1370)} = 1450$ MeV). We observe that the previous results presented in this section do not change significantly; most notably, the mixing angle $\theta_G$ attains values between $30.2^\circ$ and $30.7^\circ$, with an average error value of $\pm 3.4^\circ$.

We therefore conclude that considering different values of $m_{f_0(1370)}$ within the $(1200-1500)$ MeV interval does not change the results significantly. In particular, the quarkonium-glueball mixing angle $\theta_G$ changes only slightly (by approximately $1^\circ$) and thus we confirm our conclusion that $f_0(1370)$ is predominantly a quarkonium and $f_0(1500)$ is predominantly a glueball.

### 12.3.2 Assigning $\sigma'_N$ and $G'$ to $f_0(1370)$ and $f_0(1710)$

Although the resonance $f_0(1710)$ has also been regarded as a glueball candidate in a variety of works [205], its enhanced decay into kaons and its rather small decay width make it compatible with a dominant $\bar{s}s$ contribution in its wave function. This was also confirmed by our results from the $U(3) \times U(3)$ version of the model, see Sec. 11.4. Nonetheless, we have also tested the assumption that the pure quarkonium and glueball states mix to produce the resonances $f_0(1370)$ and $f_0(1710)$.

Some experimental results regarding the resonance $f_0(1710)$ suffer from uncertainties stemming from the overlap with the nearby state $f_0(1790)$, see Sections 3.6 and 3.7. Decays of $f_0(1710)$ into $\pi\pi$, $\bar{K}K$, and $\eta\eta$ have been seen while no decays into $\eta\eta'$ and into $4\pi$ have been detected; partial decay widths of this resonance based on PDG-preferred results as well as those of the WA102 Collaboration have already been presented in Sections 3.7.1 and 3.7.3. The values of decay widths into $\pi\pi$, $\bar{K}K$, and $\eta\eta$ obtained in Sec. 3.7.3 are stated in Table 12.3.

A fit analogous to the one in Table 12.1 yields too large errors for the decay width $\sigma'_N \equiv f_0(1370) \to \pi\pi$. For this reason we repeat our fit by adding the following constraint: $\Gamma_{\sigma'_N \to \pi\pi} = (250 \pm 150)$ MeV. The large error assures that this value is in agreement with experimental data on this decay width. The results of the fit are reported in Table 12.3.

We obtain $C = (1070 \pm 65)$ MeV, $M_{\sigma_N} = (1483 \pm 47)$ MeV, $m_G = (1670 \pm 20)$ MeV and $m_1 = (817 \pm 16)$ MeV; Eq. (12.12) yields the mixing angle between the pure quarkonium and the pure glueball $\theta_G = (19.6 \pm 5.8)^\circ$. Note that the gluon condensate is in this case much larger

| Quantity | Our Value [MeV] | Experiment ($G'$ Decays from WA102 data, Sec. 3.7.3) [MeV] |
|---|---|---|
| $M_{\sigma'_N}$ | $1450 \pm 34$ | $1350 \pm 150$ |
| $M_{G'}$ | $1720 \pm 6$ | $1720 \pm 6$ |
| $G' \to \pi\pi$ | $16.0 \pm 3.6$ | $16.1 \pm 3.6$ |
| $G' \to \eta\eta$ | $4.1 \pm 1.0$ | $38.6 \pm 18.8$ |
| $G' \to K\bar{K}$ | $5.1 \pm 2.7$ | $80.5 \pm 30.1$ |
| $\sigma'_N \to \pi\pi$ | $313 \pm 49$ | $250 \pm 150$ |

**Table 12.3:** Fit in the scenario $\{\sigma', G'\} = \{f_0(1370), f_0(1710)\}$. Experimental data for $G'$ decays are from Sec. 3.7.3, other data from the PDG [10].

than what would be expected from the QCD sum rules or the lattice, see Eq. (12.3). The $\chi^2$ is worse than in the previous case: $\chi^2/\text{d.o.f.} = 2.5$. Additionally, $\Gamma_{\sigma'_N \to \pi\pi}$ is too large for the mass value $M_{\sigma'_N} \simeq 1450$ MeV, see Sec. 3.3 – the data suggest that the decay into $4\pi$ (and not into $2\pi$) is dominant at such large values of the $f_0(1370)$ mass. We also observe that both $\Gamma_{G' \to \eta\eta}$ and $\Gamma_{G' \to K\bar{K}}$ are by an order of magnitude smaller than their respective experimental values. Thus the WA102 data do not seem to favour a fit where $f_0(1370)$ and $f_0(1710)$ are, respectively, predominantly quarkonium and glueball. This statement is confirmed if further decays are considered: as evident from Table 12.4, $G' \equiv f_0(1710) \to 4\pi$ should be the largest contribution to the full $f_0(1710)$ decay width (branching ratio $\sim 2/3$) while experimentally it has not been seen.

| Decay Width | Our Value [MeV] | Experimental value [MeV] |
|---|---|---|
| $G' \to 4\pi$ | 41 | - |
| $G' \to \eta\eta'$ | 4.3 | - |
| $\sigma' \to \eta\eta$ | $100 \pm 8$ | - |
| $\sigma' \to K\bar{K}$ | $18.7 \pm 5.3$ | - |

**Table 12.4:** Further results from the fit with $\{\sigma', G'\} = \{f_0(1370), f_0(1710)\}$.

Note that a virtually unchanged picture emerges if the fit utilises the PDG-preferred data for the decays of $G' = f_0(1710)$, see Sec. 3.7.1. We then obtain $\chi^2/\text{d.o.f.} = 1.7$, $C = (764 \pm 256)$ MeV (now within expectations), $M_{\sigma_N} = (1516 \pm 80)$ MeV, $m_G = (1531 \pm 233)$ MeV and $m_1 = (827 \pm 36)$ MeV [203]. The mixing angle calculated from Eq. (12.12) is $\theta_G = (37.2 \pm 21.4)^\circ$. The mixing angle is large and could also overshoot the value of 45°, which would imply a somewhat unexpected and unnatural reversed ordering, in which $f_0(1370)$ is predominantly glueball and $f_0(1710)$ predominantly quarkonium. Additionally, we still obtain $\Gamma_{G' \to \eta\eta} = (6.9 \pm 5.8)$ MeV, five times smaller than $\Gamma^{\text{PDG}}_{f_0(1710) \to \eta\eta} = 34.26^{+15.4}_{-20.0}$ MeV in Eq. (3.20), and also $\Gamma_{G' \to K\bar{K}} = (16 \pm 14)$ MeV, again strongly suppressed in comparison with $\Gamma^{\text{PDG}}_{f_0(1710) \to KK} = 71.44^{+23.18}_{-35.02}$ MeV, Eq. (3.15). Finally, the $4\pi$ decay of $f_0(1710)$ should again be dominant ($\sim 115$ MeV), clearly at odds with the data.

Therefore, we conclude that this scenario is not favoured. Moreover, in this scenario the remaining resonance $f_0(1500)$ should then be interpreted as a predominantly $\bar{s}s$ state, contrary to what its experimentally dominant $\pi\pi$ decay pattern suggests. Consequently, $f_0(1710)$ is unlikely to be predominantly a glueball state; this is also in accordance with the results from the ZEUS Collaboration [182].

### 12.3.3 Scenarios with $\sigma' \equiv f_0(600)$

The scenarios $\{\sigma', G'\} = \{f_0(600),\ f_0(1500)\}$ and $\{\sigma', G'\} = \{f_0(600),\ f_0(1710)\}$ have also been tested. In both cases the mixing angle turns out to be small ($\lesssim 15^\circ$), thus the state $f_0(600)$ is predominantly quarkonium. Then, in these cases the analysis of Chapter 5 applies: a simultaneous description of the $\pi\pi$ scattering lengths and the $\sigma' \to \pi\pi$ decay width cannot be achieved. For these reasons the mixing scenarios with the resonance $f_0(600)$ as a quarkonium state are not favoured.

## 12.4 Summary of the Results with the Dilaton Field

Once a dilaton field is included into the chirally invariant linear sigma model with (axial-)vectors, a favoured scenario emerges: the resonance $f_0(1500)$ is predominantly a glueball with a subdominant $\bar{n}n$ component and, conversely, $f_0(1370)$ is predominantly a quark-antiquark $(\bar{u}u + \bar{d}d)/\sqrt{2}$ state with a subdominant glueball contribution. It is interesting to observe that the success of the phenomenological description of these scalar resonances is due to the inclusion of the (axial-)vector mesons in the model. The gluon condensate is also an outcome of our study and turns out to be in agreement with lattice QCD results. Different scenarios in which $f_0(1710)$ is predominantly glueball and/or $f_0(600)$ is predominantly quarkonium do not seem to be in agreement with the present experimental data.

# 13. Conclusions

In this thesis we have presented an effective model of Quantum Chromodynamics (QCD), the theory of strong interactions. The model was utilised to study all experimentally observed two-body decays of mesons for which there exist vertices in the model under the assumption that the said experimental states are of $\bar{q}q$ nature. In addition, three-body and four-body decay widths have also been calculated utilising sequential decays; $\pi\pi$ scattering lengths have been calculated as well. Particular attention was devoted to the question whether scalar $\bar{q}q$ states are located below or above 1 GeV in the physical spectrum. Our results clearly favour the scalar $\bar{q}q$ states to be above 1 GeV.

A realistic model of QCD with $N_f$ quark flavours should possess at least two features. Firstly, the model has to implement the symmetries present in QCD and described in Chapter 2, most notably the local $SU(3)_c$ colour symmetry, the discrete $CPT$ symmetry, the global $U(N_f)_L \times U(N_f)_R$ chiral symmetry and the breaking mechanisms of the latter symmetry: spontaneous (due to the chiral condensate), explicit (due to non-vanishing quark masses) as well as at the quantum level [the $U(1)_A$ anomaly]. Secondly, the model has to incorporate as many degrees of freedom as possible, within the energy interval of interest (typically determined by the mass of the highest resonance in the model, in our case $\sim 1.8$ GeV).
This also implies that the resonances should not be considered independently of each other – they may mix (if they possess the same quantum numbers) or stand connected via decay modes. For this reason, in the concrete case of our meson model, we have considered not only scalar and pseudoscalar but also vector and axial-vector mesons as well.

The model has implemented the linear realisation of the chiral symmetry of QCD [48] with two ($u$, $d$) and three flavours ($u$, $d$, $s$) – linear sigma model. The symmetry-breaking mechanisms have also been considered: the explicit symmetry breaking was modelled with terms proportional to (non-degenerate) quark masses, the chiral anomaly by a determinant term and the spontaneous symmetry breaking by means of condensation of the scalar isosinglet states: $\sigma_N \equiv (\bar{u}u + \bar{d}d)/\sqrt{2}$ in the $N_f = 2$ case and $\sigma_N$ as well as $\sigma_S \equiv \bar{s}s$ in the $N_f = 3$ case. Thus combining our meson states from constituent quarks and antiquarks we are able to construct two scalar isosinglet states $\sigma_{N,S}$. (Note that all the states present in our model are of $\bar{q}q$ structure, as we demonstrate in Sec. 4.3.)
However, as we have discussed in Chapter 3, current experimental data suggest that there are actually six non-strange scalar isosinglets: $f_0(600)$ or $\sigma$, $f_0(980)$, $f_0(1370)$, $f_0(1500)$, $f_0(1710)$ and $f_0(1790)$. At most two of them can be $\bar{q}q$ states – and the thesis has addressed the question *which two*. To this end, we have constructed three versions of the sigma model: in two flavours (Chapter 5), three flavours (Chapters 6 – 11) and two flavours + a scalar glueball state in Chapter 12.

In Chapter 5, the two-flavour version of the linear sigma model with vector and axial-vector mesons was discussed in two scenarios. In Scenario I, Sec. 5.3, we assigned our $\sigma_N$ state to the $f_0(600)$ resonance [or, in other words, $f_0(600)$ was assumed to be a $\bar{q}q$ state]. However, the

ensuing $f_0(600)$ decay width was several times smaller than the result suggested by the data [10, 41, 42]. For this reason we have considered an alternative scenario where $f_0(1370)$ was assumed to be of $\bar{q}q$ structure obtaining $\Gamma_{f_0(1370)\to\pi\pi} \simeq$ (300-500) MeV for $m_{f_0(1370)} =$ (1200-1400) MeV. Thus, already in the two-flavour model, the scenario in which the scalar states above 1 GeV, $f_0(1370)$ and $a_0(1450)$, are considered to be (predominantly) $\bar{q}q$ states appears to be favoured over the assignment in which $f_0(600)$ and $a_0(980)$ are considered (predominantly) $\bar{q}q$ states. It is important to stress that the role of the (axial-)vector states was crucial in obtaining these results because, in the (unrealistic) limit where the (axial-)vectors are removed from the model, we observed that the $f_0(600)$ decay width was within the data. Note also that we have calculated a range of other decay widths, in particular $\Gamma_{a_1(1260)\to\rho\pi}$, found to be consistent with experiment if $m_{a_1(1260)} \simeq 1130$ MeV.

In Chapters 6 – 11 we have addressed the question whether the conclusions from the two-flavour model remain the same once the model is generalised by inclusion of strange mesons (kaons). Thus, upon inclusion of the strange degrees of freedom we have again considered two possibilities: (*i*) that the scalar $\bar{q}q$ states are below 1 GeV and (*ii*) that the scalar $\bar{q}q$ states are above 1 GeV. We refer to these two possibilities as Fits I and II, respectively.

Although the phenomenology of scalar states is found to be acceptable, Fit I is nonetheless found to be strongly disfavoured for two reasons (see Sec. 9.6). Firstly, the obtained mass values deviate by up to $\sim 200$ MeV (for the $\kappa$ meson: $\sim 600$ MeV) from the experimental results (see Table 8.5). This is in particular problematic for the very narrow resonances $\varphi(1020)$ and $f_1(1420)$. Secondly, the axial-vector states are found to be extremely broad: $a_1(1260)$, $f_1(1285)$, $f_1(1420)$ and $K_1(1400)$ possess decay widths $\sim (1-10)$ GeV. These values are unphysically large. The only possibility to remedy these large decay widths would be to work with the $\rho$ meson that has a decay width $\lesssim 40$ MeV. However, then the $\rho$ meson would be too narrow.

We thus consider possibility (*ii*): scalar $\bar{q}q$ states above 1 GeV. All masses obtained from Fit II are within 3% of their respective experimental values with the exception of $m_\eta$ ($\simeq 4.5\%$ too small) and $m_{K_0^\star(1430)}$, found to be $\simeq 8.8\%$ too large because the pattern of explicit symmetry breaking in our model sets masses of strange states approximately 100 MeV ($\simeq$ strange-quark mass) heavier than their corresponding non-strange counterparts. Nonetheless, the phenomenology is massively improved in comparison with Fit I (see Sec. 11.4 and in particular Table 11.1). For example, our results for the (axial-)vector states are either within the data [$\rho$, $K^\star$, $\varphi(1020)$, $f_1(1285)$] or qualitatively consistent with the data [$a_1(1260)$]. The mixing of the pure-nonstrange and the pure-strange scalar isosinglet states allows us to determine $f_0(1370)$ as $91.2^{-1.7}_{+2.0}\%$ a $\bar{n}n$ state and $f_0(1710)$ as $91.2^{-1.7}_{+2.0}\%$ a $\bar{s}s$ state. Utilising only the ratio $\Gamma_{f_0(1710)\to\pi\pi}/\Gamma_{f_0(1710)\to KK} = 0.2 \pm 0.06$ [99] enables us to determine a large range of other observables with *no free parameters*. We calculate $\Gamma_{f_0(1370)\to\pi\pi}$, $\Gamma_{f_0(1370)\to KK}$, $\Gamma_{f_0(1710)\to\eta\eta}$, $\Gamma_{f_0(1370)\to\pi\pi}/\Gamma_{f_0(1370)\to KK}$, $\Gamma_{f_0(1370)\to\eta\eta}/\Gamma_{f_0(1370)\to\pi\pi}$, $\Gamma_{f_0(1710)\to\eta\eta}/\Gamma_{f_0(1710)\to\pi\pi}$, $\Gamma_{f_0(1710)\to\eta\eta}/\Gamma_{f_0(1710)\to KK}$ and $\Gamma_{K_0^\star(1430)\to K\pi}$ and their values are all within the data. We can even predict $\Gamma_{f_0(1370)\to\eta\eta}/\Gamma_{f_0(1370)\to KK} = 0.22 \pm 0.01$, $\Gamma_{f_0(1710)\to\eta\eta'}/\Gamma_{f_0(1710)\to KK} = 0.17^{+0.04}_{-0.03}$, $\Gamma_{f_0(1710)\to\eta\eta'}/\Gamma_{f_0(1710)\to\pi\pi} = 0.86^{-0.06}_{+0.11}$, $\Gamma_{f_0(1710)\to\eta\eta'}/\Gamma_{f_0(1710)\to\eta\eta} = 0.68 \pm 0.13$, $\Gamma_{f_0(1710)\to\eta\eta'} = 41^{+4}_{-5}$ MeV, $\Gamma_{f_0(1370)\to a_1(1260)\pi\to\rho\pi\pi} = 12.7^{+5.8}_{-4.2}$ MeV, $\Gamma_{f_0(1710)\to a_1(1260)\pi\to\rho\pi\pi} = 15.2^{+2.6}_{-3.1}$ MeV, $\Gamma_{f_0(1710)\to\omega\omega} \simeq 0.02$ MeV and also $\Gamma_{f_0(1710)\to\omega\omega\to 6\pi} \simeq 0.02$ MeV (the latter four strongly suppressed). Note, however, that the model also obtains too large absolute values of the $f_0(1710)$ decay widths (although, as already

mentioned, the ratios of the decay widths are correct).
A reason for this may be the missing glueball field as all the calculations described so far have only been performed with $\bar{q}q$ states. There are three nearby isoscalar singlet states above 1 GeV: $f_0(1370)$, $f_0(1500)$ and $f_0(1710)$. The $f_0(1500)$ state has long been discussed as a possible glueball candidate. In Chapter 12 we discuss the sigma model in two flavours + glueball to test this hypothesis. Indeed we find $f_0(1500)$ to be predominantly a glueball and $f_0(1370)$ to be predominantly a non-strange $\bar{q}q$ state. The study in Chapter 12 has been performed in the light-quark sector only and thus an extension of the study to $N_f = 3$ + glueball would represent a valuable continuation of the work presented in this thesis. Nonetheless, the scenario where $f_0(1710)$ is predominantly a glueball was also tested by a corresponding redefinition of our scalar states; the scenario was found to be not favoured.

Therefore, the main conclusion of this thesis is that the scalar $\bar{q}q$ states are strongly favoured to be above 1 GeV because then the description of the scalar but also of the vector and axial-vector phenomenology is decisively better than under the assumption that the scalar quarkonia are below 1 GeV.

We note that the work can be extended in many directions.

- An obvious point is to extend the $U(3) \times U(3)$ model of Chapter 10 to include the pure glueball field and implement the mixing of this field with the pure $\bar{n}n$ and $\bar{s}s$ to study the quarkonium/glueball content of $f_0(1370)$, $f_0(1500)$ and $f_0(1710)$.

- This work finds the scalars above 1 GeV to be predominantly quarkonia. This implies that the model can make no statement regarding the nature of the scalar states below 1 GeV [$f_0(600)$, $a_0(980)$, $\kappa$]. They may be interpreted as tetraquark states [58, 194]. Thus a further extension of the model would entail scalar $\bar{n}n$, $\bar{s}s$, glueball and tetraquark states (the latter with and without the $s$ quark) – six scalar states the mixing of which would be extremely interesting to study within a chiral model that contains vectors and axial-vectors as well.

- We have seen in Sec. 10.3 that the mass of the $K_1$ state obtained from our model corresponds neither to the mass of $K_1(1270)$ nor to that of $K_1(1400)$. The $K_1$ phenomenology is also not well described (see Sec. 11.4). The reason is that our model currently contains only an axial-vector nonet of states that is, however, expected to mix with a pseudovector nonet yielding the physical $K_1(1270)$ and $K_1(1400)$ states [247]. Building on this point, one can study the mixing of the pseudovector and axial-vector nonets within an extended version of the model in this thesis to determine the features of the $K_1(1270)$ and $K_1(1400)$ resonances.

- The model can be extended to the charm mesons [191].

- The hadronic decays of the $\tau$ lepton can also be studied within a version of the model incorporating the weak interaction (building on work in Ref. [245]).

- Further studies of the nucleon and its chiral partner (as well as, e.g., hyperons) can be performed on the line of Ref. [59].
  An important remark is in order about nucleon-nucleon scattering in the context of results

presented in this work. Baryon-baryon interaction is usually mediated by the exchange of scalar [$f_0(600)$] and vector [$\omega(782)$, $\rho(770)$] mesons [273]. Usually the $f_0(600)$ state is considered to be of $\bar{q}q$ structure. However, our results suggest the opposite: that the scalar $\bar{q}q$ state is actually in the region above 1 GeV. For this reason, nucleon-nucleon scattering does not appear to be performed by exchange of a quark and an antiquark; indeed if the states below 1 GeV are interpreted as tetraquarks then, consequently, exchange of a tetraquark state would occur [197].

- Finally, the issue of restoration of chiral symmetry at nonzero temperature and density is one of the fundamental questions of modern hadron and nuclear physics. Linear sigma models constitute an effective approach to study chiral symmetry restoration because they contain from the onset not only pseudoscalar and vector mesons, but also their chiral partners with which they become degenerate once the chiral symmetry has been restored. Given that the vacuum phenomenology is reasonably well reproduced within our model, then the model can also be applied to studies of chiral symmetry restoration at nonzero temperatures (similarly to Refs. [37, 194]) and densities (similarly to Ref. [274]).

And let us end this thesis along the line of Ref. [275]: "It took mankind only about one century to resolve the mystery of the spectral lines in visible light reported by Joseph Fraunhofer in 1814 [276]. The collection of sufficient data lasted several decades, during which some progress was made by the discovery of striking patterns in the spectra. An important step that provided the key to the analysis of spectra was the classification of hydrogen lines made by Johann Balmer in 1885 [277]. This allowed Niels Bohr [278] later on to account for those lines, resulting in a spectacular advance in our understanding of Nature." Nowadays the mysteries are related to far more miniature objects but they are nonetheless a large inspiration for anyone interested in understanding the way how nature functions.

# 14. Zusammenfassung

Die vorliegende Dissertation behandelt eine der grundlegenden Fragen der menschlichen Existenz: den Zustand der Materie im Universum kurz nach dem Urknall. Damals (vor ungefähr 13 Milliarden Jahren) war die Materie in ihre mikroskopischen Bauteile zerlegt: beispielsweise waren die Elektronen nicht an Atomkerne gebunden – es existierten keine Atome, sondern die Elektronenn stellten freie Teilchen dar. Die Elektronen waren indes nicht die einzigen freien Teilchen – auch andere so genannte *Leptonen* (mit den Elektronen verwandte Teilchen) bildeten keinerlei gebundene Zustände.

Der Materieaufbau im Universum in der jetzigen Zeit ist anders: beispielsweise sind Elektronen in einem Atom an den Atomkern gebunden (die entprechende elektrische Wechselwirkung wird als Coulomb-Kraft bezeichnet, nach dem französischen Physiker Charles Coulomb, der im 18. Jahrhundert lebte). Der Atomkern ist aber keine kompakte Einheit - er besitzt selbst eine innere Struktur, da er aus Protonen (positive eletrische Ladung) und Neutronen (keine elektrische Ladung) aufgebaut ist. Die Anzahl der Protonen im Atomkern ist für die Klassifikation der Atome von grundlegender Bedeutung: jedes Atom eines Naturelements besitzt eine genau festgelegte Anzahl von Protonen in seinem Kern (Wasserstoff: 1, Helium: 2, Lithium: 3, ..., Ununoctium: 118). Da die Protonen, wie erwähnt, elektrisch positiv geladen sind, müssen sie sich auch im Atomkern abstoßen; der Atomkern müsste folglich instabil sein, wodurch Atome (und Moleküle) ebenfalls instabil sein müssten. *Dies ist natürlich nicht der Fall* – stabile Materie ist auf der Erde (und, nach unserem Verständnis, auch im Universum) in der Tat vorhanden. Folglich ist also zu diskutieren, warum sich die Protonen in der Summe aller Kräfte doch anziehen (und stabile Atomkerne bilden können), obwohl sie sich elektrisch abstoßen.

Die Antwort liegt in der Betrachtung einer neuen Wechselwirkung: der so genannten *starken* Kraft. Diese ist nur auf den Atomkern beschränkt (also extrem kurzreichweitig), aber innerhalb des Kerns ist sie dominanter als die elektrische Abstoßung der Protonen. In der Summe ziehen sich also die Protonen in Atomkernen an und Atomkerne und Atome sind folglich stabil.

Die Protonen sind aber nicht die einzigen Teilchen, die der starken Wechselwirkung unterliegen. Schon die Neutronen, die anderen in Atomkernen präsenten Teilchen, sind ebenfalls stark wechselwirkend; dies ist auch der Fall für Hyperonen, Pionen, Kaonen und mehrere Hundert anderer Teilchen. Daher stellt es einen natürlichen Schritt dar, nach einem Klassifikationsschema für all diese Teilchen zu suchen. Dieses Klassifikationsschema erfordert die Annahme, dass die Protonen, Neutronen, Pionen, Kaonen, ..., eine innere Struktur besitzen - und aus noch elementareren Teilchen, den so genannteb Quarks, aufgebaut sind. Unterschiedliche Quark-Kombinationen ergeben dann unterschiedliche Teilchen, so wie unterschiedliche Quantitäten von Protonen unterschiedliche Atomkerne (und Atome) ergeben.

Die aus Quarks aufgebauten Teilchen werden als *Hadronen* bezeichnet. Die Hadronen unterteilen sich in zwei große Gruppen in Abhängigkeit von ihrem Spin: jene mitganzzahligem Spin (0, 1, 2, ...) werden als Mesonen bezeichnet (Pionen, Kaonen, ...), während die Hadronen mit halbzahligem Spin (1/2, 3/2, ...) als Baryonen bezeichnet werden (Protonen, Neutronen, ...). Die

Quarks kommen in der Natur nicht als freie Teilchen vor – sie sind immer in den Hadronen eigenschlossen. Diese experimentelle Beobachtung wird als Quark-Confinement bezeichnet; die Quarks können nur in hochenergetischen Protonen- oder Schwerionen-Stößen (wie gegenwärtig bei dem Large Hadron Collider am CERN in Genf oder bald bei der Facility for Antiproton and Ion Research bei der Gesellschaft für Schwerionenforschung in Darmstadt) erforscht werden.

Die Quarks waren nicht immer in den komplexeren Teilchen eingeschlossen: kurz nach dem Urknall waren die Quarks freie Teilchen, genau wie die Leptonen (wie schon erwähnt). Die Expansion des frühen Universums führte zu seiner Abkühlung; so konnte die gegenwärtig bekannte Materie nach ungefähr $10^{-10}$ Sekunden anfangen zu kondensieren. Mit anderen Worten: es entstanden Teilchen, die aus Quarks aufgebaut sind. Es ist klar, dass das einfachste aus Quarks aufgebaute Teilchen zwei Quarks besitzen musste - dies ist nach der obigen Definition ein Meson, und daher ist die Erforschung der Mesonen für die Erforschung des frühen Universums von außerordentlicher Bedeutung: sie ermöglicht uns, Kenntnisse über das Universum kurz nach dem Urknall zu erlangen.

Lassen Sie uns eine kurze Anmerkung einfügen. Mesonische Teilchen bestehen eigentlich nicht aus zwei Quarks, sondern aus einem Quark und einem Antiquark. Der Grund hierfür besteht in der Tatsache, dass die Quarks neben der elektrischen auch eine zusätzliche Ladungsform tragen: die Farbladung. (Dies ist nicht die Farbe im herkömmlichen Sinne, sondern eine Quanteneigenschaft der Quarks; die Farben werden trotzdem als rot, grün und blau bezeichnet und die Experimentaldaten deuten darauf hin, dass genau drei Quarkfarben existieren.) Die Quarks sind die einzigen bekannten Teilchen in der Natur, welche diese Farbladung besitzen; alle anderen Teilchen sind farbneutral und folglich ordnen sich die Quarks so an, dass das entstehende komposite Teilchen farbneutral ist. Konkret impliziert dies, dass ein Meson (wie zum Beispiel das Pion) aus einem Quark (mit Farbe) und einem Antiquark (mit Antifarbe) bestehen muss, damit sich die Farbe und die Antifarbe aufheben und das Meson, wie vom Experiment verlangt, keine Farbladung trägt. (Es kann im Rahmen der Gruppentheorie gezeigt werden, dass beispielsweise Protonen und Neutronen drei Quarks besitzen müssen, um farbneutral zu sein.)

Die Spins des Quarks und des Antiquarks in einem Meson können auf unterschiedliche Arten kombiniert werden. Die Quarks selbst sind Spin-1/2-Teilchen. Im Prinzip können sie also zu einem Spin-1-Teilchen (ein so genanntes Vektor-Meson) und zu einem Spin-0-Teilchen (skalares Meson) kombiniert werden. Die genaue Anzahl von so entstehenden Teilchen hängt von der Anzahl der Quarks ab, die in Betracht gezogen wurden. Gegenwärtige Experimentaldaten deuten darauf hin, dass es sechs Quarks in der Natur gibt: Up ($u$), Down ($d$), Strange ($s$), Charm ($c$), Bottom ($b$) und Top ($t$). Das u-Quark besitzt die kleinste Masse, während die Masse des schwersten Top-Quarks etwa 57000 Mal größer ist. Die Massen der Up- und Down-Quarks sind fast gleich (diese Quarks entarten also) und daher kann man sie als gleiche Teilchen betrachten. Das Strange-Quark unterscheidet sich in der Masse vom Up-Down-Paar um etwa Faktor 30. Die Up- und Down-Quarks werden oftmals als *nichtseltsame* Quarks bezeichnet (und die Mesonen, welche die Up- und Down-Quarks enthalten, als nichtseltsame Mesonen). Da die $c$-, $b$- und $t$-Quarks um eine bis drei Größenordnungen schwerer als das $s$-Quark sind, kann man diese als praktisch entkoppelt von den $u$-, $d$- und $s$-Quarks betrachten. Betrachten wir also die nichtseltsamen $u$- und $d$-Quarks sowie das seltsame $s$-Quark.

Wegen der erwähnten Massenentartung bei den nichtseltsamen Quarks werden nichtseltsame Mesonen immer sowohl aus $u$- als auch aus $d$-Quars gebildet. Für den konkreten Fall der skalaren Mesonen wird die Wellenfunktion wie folgt konstruiert:

$$\sigma_N \equiv (\bar{u}u + \bar{d}d)/\sqrt{2},$$

wo $\sigma_N$ das nichtseltsame skalare Meson und $\bar{u}$ und $\bar{d}$ respektive das Anti-Up- und das Anti-Down-Quarks kennzeichnen, und für ein seltsames
skalares Meson $\sigma_S$:

$$\sigma_S \equiv \bar{s}s,$$

wo $\bar{s}$ das seltsame Antiquark kennzeichnet.
Also würden wir nach einem Vergleich der oben genannten beiden Wellenfunktionen mit dem Experiment erwarten, dass die Experimentaldaten genau zwei nichtseltsame skalare Mesonen aufweisen. *Tatsächlich sind es sechs.* – **Und die Suche nach den Antiquark-Quark-Teilchen unter diesen sechs ist einer der Hauptarbeitspunkte der vorliegenden Dissertation.**

Die allgemein anerkannte physikalische Theorie, welche die Quarks und die aus den Quarks gebildeten Teilchen beschreibt, heißt

**Quantenchromodynamik (QCD).**

Die Quantenchromodynamik legt eine grundlegende Gleichung fest, den so genannten QCD-Lagrangian [siehe Gl. (2.18)]. Der QCD-Lagrangian zeigt gewisse Eigenschaften auf, die nicht nur eine elegante mathematische Konstruktion darstellen, sondern auch die tatsächlichen EIgenschaften physikalischer (aus Quarks gebildeter) Zustände widerspiegeln. Dies wurde durch viele Experimente bestätigt [10].

Falls man aber beabsichtigt, diese Zustände der Natur theoretisch näher zu behandeln, so bedient man sich der so genannten durch die QCD erlaubten Modelle. Diese Modelle müssen die erwähnten Eigenschaften (die *Symmetrien der QCD*, siehe Kapitel 2) erfüllen; alle Modelle der QCD erfüllen die QCD-Symmetrien, aber auf unterschiedliche Arten – dies stellt den Hauptunterschied zwischen ihnen dar.
Das in dieser Doktorarbeit vorgestellte Modell wird als das Lineare Sigma-Modell bezeichnet und es beinhaltet die in der Natur beobachteten mesonischen Teilchen. Wir beschreiben in Kapitel 4 die Konstruktion eines solchen Sigma-Modells. Die Implikationen des Modells werden in den Kapiteln 5 – 11 diskutiert. Insbesondere wird die Frage erforscht, wo sich die skalaren Antiquark-Quark-Teilchen $\sigma_N$ und $\sigma_S$ sich im physikalischen Spektrum befinden. Diese Frage ist aus mindestens zwei Gründen interessant:

- Da die experimentellen Messungen (wie erwähnt) mehr skalare Teilchen nachgewiesen haben als von der theoretischen Seite erwartet, stellt sich die Frage der Klassifikation solcher Teilchen, oder in anderen Worten derer Struktur: da höchstens zwei von diesen Teilchen von Antiquark-Quark-Struktur ($\bar{q}q$) sein können, stellt sich die Frage, welche von den gemessenen Teilchen tatsächlich die $\bar{q}q$-Teilchen sind und welche Struktur die übrig gebliebenen Teilchen besitzen.

- Das Pion ist ein wohlbekanntes $\bar{q}q$-Teilchen (dies ist seit langer Zeit sowohl theoretisch als auch experimentell bestätigt); die QCD sagt vorher, dass das Pion unter gewissen Bedingungen (sehr hohe Temperaturen von ungefähr einer Billion Grad Celsius) dieselbe Masse wie $\sigma_N$ besitzen muss – wir können aber zwischen *sechs* skalaren Teilchen wählen, die allesamt unserem $\sigma_N$-Teilchen entsprechen können. Die Frage ist also: *Welches von den skalaren Teilchen ist es?*

Allerdings wäre eine theoretische Betrachtung von nur Pionen und skalaren Teilchen nicht gerechtfertigt, da die experimentellen Daten eindeutig die Existenz anderer Teilchen nachweisen. Zum Beispiel ist experimentell wohlbekannt, dass auch Teilchen mit Spin 1 existieren (die so genannten *Vektoren*), welche mit den Pionen und den skalaren Teilchen wechselwirken. Aus diesem Grunde beinhaltet das in dieser Dissertation disktierte Modell sowohl die Skalaren als auch die Vektoren; ein Modell mit all diesen Teilchen muss mathematisch konsistent konstruiert werden, was im Kapitel 4 beschrieben wird.

Die skalaren Mesonen werden in zwei Gruppen geteilt: auf jene mit Ruheenergie unterhalb 1 GeV und auf jene mit Ruheenergie oberhalb 1 GeV (die Bezeichnung *GeV* bedeutet *Gigaelektronvolt*, also eine Milliarde Elektronvolt, wobei ein Elektronvolt der Energie eines Elektrons im elektrischen Feld von einem Volt Stärke entspricht). Im Kapitel 5 wird mittels Vergleich der theoretischen Ergebnissen mit Experimentaldaten diskutiert, ob sich unser skalares $\bar{q}q$-Teilchen unterhalb oder oberhalb 1 GeV befindet – und es scheint die Ruheenergie mehr als 1 GeV zu besitzen.
Dies ist eigentlich etwas überraschend. Üblich ist die Erwartung, dass ein Teilchen mit bloß einem Quark und einem Antiquark eher eine relativ kleine Ruheenergie besitzt (in unserem Fall also weniger als 1 GeV). Der Grund hierfür ist, dass alle anderen skalaren Teilchen, die *keine* Antiquark-Quark-Struktur besitzen, aus mehr als zwei Quarks bestehen und deren Ruheenergie folglich relativ größer ist. Die Ergebnisse des Kapitels 5 (und letztendlich dieser Dissertation) deuten auf ein umgekehrtes Bild hin.

Die Ergebnisse im Kapitel 5 sind aber nur unter Betrachtung der Mesonen zustande gekommen, die nur das Up- und das Down-Quark besitzen. Es ist folglich eine wohldefinierte Frage, ob sich die Ergebnisse womöglich ändern, wenn auch Teilchen mit seltsamen Quarks (die so genannten *Kaonen*) in das Modell hunzugefügt werden.
Aus diesem Grunde wird in den Kapiteln 6 – 11 eine ausführliche Diskussion des Linearen Sigma-Modells mit skalaren und vektoriellen Mesonen sowohl im nichtseltsamen als auch im seltsamen Sektor durchgeführt. Die Erörterungen über die skalaren Mesonen sind hierbei nicht die einzigen, welche behandelt werden – in den genannten Kapiteln werde *alle* hadronischen Zerfälle der Mesonen betrachtet, die aus dem Modell ausgerechnet werden können. Auf diese Weise entsteht eine breite phänomenologische Abhandlung der experimentell bekannten mesonischen Teilchen, die uns eine Klassifikation der Teilchen nach ihrer Quark-Struktur (ob $\bar{q}q$ oder nicht) durchzuführen, aber auch Einblicke in das Verhalten der Teilchen bei sehr hohen Temperaturen ermöglicht.

Die in den Kapiteln 6 – 11 durchgeführten Berechnungen bestätigen das (wie erwähnt) überraschende Ergebnis aus Kapitel 5: dass die skalaren $\bar{q}q$-Teilchen $\sigma_N$ und $\sigma_S$ eine Ruheenergie von mehr als 1 GeV besitzen. Diese Aussage hat mindestens zwei Implikationen:

- Das skalare Teilchen, welches bei sehr hohen Temperaturen ($\sim 10^{12}$ Grad Kelvin) die gleiche Masse wie das Pion besitzt, hat eine viel größere Ruheenergie als das Pion. Dies hat Konsequenzen für andere Signaturen des so genannten *Quark-Gluon-Plasmas*, eine Materieform, deren Entstehung bei den erwähnten sehr hohen Tenperaturen erwartet wird und die aus Quarks, aber auch Gluonen besteht – dabei sind die Gluonen Teilchen, welche die Wechselwirkung zwischen den Quarks übertragen (die *Botenteilchen*).

- Falls (nur) die skalaren Teilchen über 1 GeV die $\bar{q}q$-Struktur besitzen, dann bleibt die Frage offen, welche Struktur die (ebenfalls bekannten) Teilchen unter 1 GeV haben könnten. Dazu ist immer noch keine definitive Antwort vorhanden (auch nicht im Rahmen anderer Studien), es wird aber schon seit Langem darüber diskutiert, ob die Teilchen unterhalb 1 GeV aus zwei Quarks und zwei Antiquarks (statt wie bisher diskutiert aus einem Quark und einem Antiquark) bestehen könnten.

In der vorliegenden Dissertation wird aber noch eine zusätzliche Mesonenart diskutiert: die Gluebälle. Diese Mesonen bestehen nicht aus Quarks, sondern ausschließlich aus Gluonen, den (schon erwähnten) *Botenteilchen*, über welche die Quarks ihre Wechselwirkungen ausführen. In Kapitel 12 wird das skalare (also spinlose) Glueball-Teilchen in das Modell eingeführt und dessen Wechselwirkungen mit dem Antiquark-Quark-Teilchen $\sigma_N$ diskutiert. Es wird wiederum die Aussage bestätigt, das die Ruheenergie von $\sigma_N$ über 1 GeV liegt und zusätzlich die Folgerung diskutiert, dass die Ruheenergie des Glueball-Teilchens ebenfalls über 1 GeV ist.

Die Hauptaussage dieser Dissertation ist aber, dass die Spin-0-Teilchen aus einem Antiquark und einem Quark (die skalaren Mesonen) eine höhere Ruheenergie besitzen als gewöhnlich angenommen. Dies hat viele Implikationen für die weitere Mesonen- und, allgemeiner, Hadronenerforschung: die Frage nach der Struktur der skalaren Mesonen im Energiebereich unter 1 GeV bleibt offen genau so wie die Frage nach dem Materiezustand und -verhalten bei sehr hohen Temperaturen (also jenen wie kurz nach dem Urknall). Die Erforschung der Materie bei sehr hohen Temperaturen ist seit langer Zeit das hauptsächliche Thema vieler Projekte sowohl in der theoretischen als auch in der experimentellen Hadronenphysik, aber eine definitive Aussage über das Materieverhalten unter den extremen Bedingungen und bei einer großen Anzahl der mikroskopischen Teilchen (und folglich einer fast unendlichen Anzahl möglicher Wechselwirkungswege der betreffenden Teilchen und der Zerfallswege der instabilen Teilchen) kann noch nicht erfolgen. Aus diesem Grunde ist die theoretische und die experimentelle Erforschung der Elementarteilchenphysik bei sehr hohen Energien ein sehr spannendes Feld der Physik – mit vielfältigen Anwendungsmöglichkeiten der hier prsentierten Dissertation. Die vorliegende Dissertation bildet daher durch ihre Untersuchungen der Antiquark-Quark-Zustände genau die notwendige Basis für weitere Projekte bezüglich des Materiezustands bei sehr hohen Temperaturen und folglich für die Erforschung der Materie kurz nach dem Urknall und dem Anfang der noch unvollständig erforschten Phänomene der modernen Wissenschaft.

# Bibliography


[1] J. W. von Goethe, *Faust. – Ein Fragment von Goethe. – Aechte Ausgabe* (G. J. Göschen, Leipzig, 1790).

[2] V. I. Zakharov, JETP Lett. **12**, 312 (1970) [Pisma Zh. Eksp. Teor. Fiz. **12**, 447 (1970)]; V. A. Rubakov, M. V. Sazhin and A. V. Veryaskin, Phys. Lett. B **115**, 189 (1982); J. McGreevy, L. Susskind and N. Toumbas, JHEP **0006**, 008 (2000) [hep-th/0003075]; N. Arkani-Hamed, H. Georgi and M. D. Schwartz, Annals Phys. **305**, 96 (2003) [hep-th/0210184].

[3] P. T. Matthews and A. Salam, Phys. Lett. **8**, 357 (1964); A. Salam and J. C. Ward, Phys. Lett. **13**, 168 (1964); S. Weinberg, Phys. Rev. D **5**, 1962 (1972); S. Weinberg, Phys. Rev. D **7**, 1068 (1973).

[4] A. Pich, hep-ph/0502010.

[5] H. Miyazawa, Phys. Rev. **170**, 1586 (1968); G. Jungman, M. Kamionkowski and K. Griest, Phys. Rept. **267**, 195 (1996) [arXiv:hep-ph/9506380]; L. Randall and R. Sundrum, Nucl. Phys. B **557**, 79 (1999) [arXiv:hep-th/9810155].

[6] E. Farhi and L. Susskind, Phys. Rept. **74**, 277 (1981); M. Dine, W. Fischler and M. Srednicki, Nucl. Phys. B **189**, 575 (1981); D. D. Dietrich and C. Kouvaris, Phys. Rev. D **78**, 055005 (2008) [arXiv:0805.1503 [hep-ph]]; J. R. Andersen, O. Antipin, G. Azuelos, L. Del Debbio, E. Del Nobile, S. Di Chiara, T. Hapola and M. Jarvinen *et al.*, Eur. Phys. J. Plus **126**, 81 (2011) [arXiv:1104.1255 [hep-ph]]; A. Belyaev, M. T. Frandsen, S. Sarkar and F. Sannino, Phys. Rev. D **83**, 015007 (2011) [arXiv:1007.4839 [hep-ph]].

[7] T. A. Ryttov and F. Sannino, Phys. Rev. D **78**, 115010 (2008) [arXiv:0809.0713 [hep-ph]].

[8] M. Gell-Mann, Phys. Lett. **8**, 214 (1964).

[9] G. Zweig, In *Lichtenberg, D. B. ( Ed.), Rosen, S. P. ( Ed.): Developments In The Quark Theory Of Hadrons, Vol. 1*, 22-101 and CERN Geneva - TH. 401 (REC.JAN. 64) 24p

[10] K. Nakamura *et al.* (Particle Data Group), J. Phys. G **37**, 075021 (2010) and 2011 partial update for the 2012 edition.

[11] C. M. G. Lattes, H. Muirhead, G. P. S. Occhialini and C. F. Powell, Nature **159**, 694 (1947); C. M. G. Lattes, G. P. S. Occhialini and C. F. Powell, Nature **160**, 453 (1947); C. M. G. Lattes, G. P. S. Occhialini and C. F. Powell, Nature **160**, 486 (1947).

[12] M. Gockeler *et al.* [QCDSF and UKQCD Collaborations], Phys. Lett. B **639**, 307 (2006) [hep-ph/0409312]; M. Gockeler, R. Horsley, A. C. Irving, D. Pleiter, P. E. L. Rakow, G. Schierholz, H. Stuben and J. M. Zanotti, Phys. Rev. D **73**, 054508 (2006) [hep-lat/0601004]; Q. Mason *et al.* [HPQCD Collaboration], Phys. Rev. D **73**, 114501 (2006) [hep-ph/0511160]; Y. Nakamura *et al.* [CP-PACS Collaboration], Phys. Rev. D **78**, 034502 (2008) [arXiv:0803.2569

[hep-lat]]; C. Allton *et al.* [RBC-UKQCD Collaboration], Phys. Rev. D **78**, 114509 (2008) [arXiv:0804.0473 [hep-lat]]; C. T. H. Davies, C. McNeile, K. Y. Wong, E. Follana, R. Horgan, K. Hornbostel, G. P. Lepage and J. Shigemitsu *et al.*, Phys. Rev. Lett. **104**, 132003 (2010) [arXiv:0910.3102 [hep-ph]]; T. Blum, R. Zhou, T. Doi, M. Hayakawa, T. Izubuchi, S. Uno and N. Yamada, Phys. Rev. D **82**, 094508 (2010) [arXiv:1006.1311 [hep-lat]]; B. Blossier *et al.* [ETM Collaboration], Phys. Rev. D **82**, 114513 (2010) [arXiv:1010.3659 [hep-lat]].

[13] S. Narison, Phys. Lett. B **626**, 101 (2005) [hep-ph/0501208]; D. S. Gorbunov and A. A. Pivovarov, Phys. Rev. D **71**, 013002 (2005) [hep-ph/0410196]; E. Gamiz, M. Jamin, A. Pich, J. Prades and F. Schwab, Phys. Rev. Lett. **94**, 011803 (2005) [hep-ph/0408044]; P. A. Baikov, K. G. Chetyrkin and J. H. Kuhn, Phys. Rev. Lett. **95**, 012003 (2005) [hep-ph/0412350]; K. G. Chetyrkin and A. Khodjamirian, Eur. Phys. J. C **46**, 721 (2006) [hep-ph/0512295]; S. Narison, Phys. Rev. D **74**, 034013 (2006) [hep-ph/0510108]; M. Jamin, J. A. Oller and A. Pich, Phys. Rev. D **74**, 074009 (2006) [hep-ph/0605095]; A. Deandrea, A. Nehme and P. Talavera, Phys. Rev. D **78**, 034032 (2008) [arXiv:0803.2956 [hep-ph]]; C. A. Dominguez, N. F. Nasrallah, R. Rontsch and K. Schilcher, JHEP **0805**, 020 (2008) [arXiv:0712.0768 [hep-ph]]; C. A. Dominguez, N. F. Nasrallah, R. H. Rontsch and K. Schilcher, Phys. Rev. D **79**, 014009 (2009) [arXiv:0806.0467 [hep-ph]];

[14] R. Barate *et al.* [ALEPH Collaboration], Eur. Phys. J. C **11**, 599 (1999) [hep-ex/9903015].

[15] A. H. Hoang and M. Jamin, Phys. Lett. B **594**, 127 (2004) [hep-ph/0403083]; A. H. Hoang and A. V. Manohar, Phys. Lett. B **633**, 526 (2006) [hep-ph/0509195]; O. Buchmuller and H. Flacher, Phys. Rev. D **73**, 073008 (2006) [hep-ph/0507253]; R. Boughezal, M. Czakon and T. Schutzmeier, Phys. Rev. D **74**, 074006 (2006) [hep-ph/0605023]; J. H. Kuhn, M. Steinhauser and C. Sturm, Nucl. Phys. B **778**, 192 (2007) [hep-ph/0702103 [HEP-PH]]; A. Signer, Phys. Lett. B **672**, 333 (2009) [arXiv:0810.1152 [hep-ph]]; K. G. Chetyrkin, J. H. Kuhn, A. Maier, P. Maierhofer, P. Marquard, M. Steinhauser and C. Sturm, Phys. Rev. D **80**, 074010 (2009) [arXiv:0907.2110 [hep-ph]]; S. Narison, Phys. Lett. B **693**, 559 (2010) [Erratum-ibid. **705**, 544 (2011)] [arXiv:1004.5333 [hep-ph]]; C. McNeile, C. T. H. Davies, E. Follana, K. Hornbostel and G. P. Lepage, Phys. Rev. D **82**, 034512 (2010) [arXiv:1004.4285 [hep-lat]]; S. Bodenstein, J. Bordes, C. A. Dominguez, J. Penarrocha and K. Schilcher, Phys. Rev. D **82**, 114013 (2010) [arXiv:1009.4325 [hep-ph]];

[16] B. Aubert *et al.* [BABAR Collaboration], Phys. Rev. Lett. **93**, 011803 (2004) [hep-ex/0404017]; B. Aubert *et al.* [BABAR Collaboration], Phys. Rev. D **81**, 032003 (2010) [arXiv:0908.0415 [hep-ex]].

[17] T. Aaltonen *et al.* [CDF Collaboration], Phys. Rev. Lett. **105**, 252001 (2010) [arXiv:1010.4582 [hep-ex]].

[18] W. Pauli, Phys. Rev. **58**, 716 (1940).

[19] L. D. Roper, Phys. Rev. Lett. **12**, 340 (1964); M. G. Olsson and G. B. Yodh, Phys. Rev. **145**, 1309 (1966).

[20] S. Hands, S. Kim and J. I. Skullerud, Eur. Phys. J. C **48**, 193 (2006) [arXiv:hep-lat/0604004]; S. Hands, S. Kim and J. I. Skullerud, Eur. Phys. J. A **31**, 787 (2007) [arXiv:nucl-th/0609012];

S. Hands, P. Sitch and J. I. Skullerud, Phys. Lett. B **662**, 405 (2008) [arXiv:0710.1966 [hep-lat]]; S. Hands, T. J. Hollowood and J. C. Myers, JHEP **1012**, 057 (2010) [arXiv:1010.0790 [hep-lat]].

[21] G. 't Hooft, Nucl. Phys. B **72**, 461 (1974); E. Witten, Nucl. Phys. B **160**, 57 (1979); S. R. Coleman, "1/N," Published in Erice Subnuclear 1979:0011; R. F. Lebed, Czech. J. Phys. **49**, 1273 (1999) [arXiv:nucl-th/9810080].

[22] T. D. Cohen, Rev. Mod. Phys. **68**, 599 (1996); B. A. Gelman, UMI-30-78256; J. R. Pelaez, Mod. Phys. Lett. A **19**, 2879 (2004) [hep-ph/0411107]; F. Sannino and J. Schechter, Phys. Rev. D **76**, 014014 (2007) [arXiv:0704.0602 [hep-ph]]; O. Cata and V. Mateu, Phys. Rev. D **77**, 116009 (2008) [arXiv:0801.4374 [hep-ph]]; G. S. Bali and F. Bursa, JHEP **0809**, 110 (2008) [arXiv:0806.2278 [hep-lat]]; J. Nieves and E. Ruiz Arriola, Phys. Lett. B **679**, 449 (2009) [arXiv:0904.4590 [hep-ph]]; E. Ruiz Arriola and W. Broniowski, Phys. Rev. D **81**, 054009 (2010) [arXiv:1001.1636 [hep-ph]]; L. Bonanno and F. Giacosa, Nucl. Phys. A **859**, 49 (2011) [arXiv:1102.3367 [hep-ph]]; F. Giacosa, arXiv:1106.0523 [hep-ph]; J. Nieves, A. Pich and E. Ruiz Arriola, Phys. Rev. D **84**, 096002 (2011) [arXiv:1107.3247 [hep-ph]]; A. Heinz, F. Giacosa and D. H. Rischke, arXiv:1110.1528 [hep-ph]; E. R. Arriola and W. Broniowski, arXiv:1110.2863 [hep-ph].

[23] M. Y. Han and Y. Nambu, Phys. Rev. **139**, B1006 (1965).

[24] C. -N. Yang and R. L. Mills, Phys. Rev. **96**, 191 (1954).

[25] E. Noether, Gott. Nachr. **1918**, 235 (1918) [Transp. Theory Statist. Phys. **1**, 186 (1971)] [physics/0503066].

[26] J. S. Bell and R. Jackiw, Nuovo Cim. A **60**, 47 (1969); K. Fujikawa, Phys. Rev. Lett. **42**, 1195 (1979).

[27] R. D. Peccei, Lect. Notes Phys. **741**, 3 (2008) [arXiv:hep-ph/0607268].

[28] Y. Nambu and G. Jona-Lasinio, Phys. Rev. **122**, 345 (1961).

[29] C. Ratti, M. A. Thaler and W. Weise, Phys. Rev. D **73**, 014019 (2006) [hep-ph/0506234]; S. K. Ghosh, T. K. Mukherjee, M. G. Mustafa and R. Ray, Phys. Rev. D **73**, 114007 (2006) [hep-ph/0603050].

[30] D. J. Gross and F. Wilczek, Phys. Rev. Lett. **30**, 1343 (1973); D. J. Gross and F. Wilczek, Phys. Rev. D **8**, 3633 (1973); H. D. Politzer, Phys. Rev. D **9**, 2174 (1974); H. D. Politzer, Phys. Rept. **14**, 129 (1974).

[31] M. A. Shifman, A. I. Vainshtein and V. I. Zakharov, Nucl. Phys. B **147**, 385 (1979); L. J. Reinders, H. R. Rubinstein and S. Yazaki, Nucl. Phys. B **186**, 109 (1981); J. Marrow, J. Parker and G. Shaw, Z. Phys. C **37**, 103 (1987); B. V. Geshkenbein, Sov. J. Nucl. Phys. **51**, 719 (1990) [Yad. Fiz. **51**, 1121 (1990)]; D. J. Broadhurst, P. A. Baikov, V. A. Ilyin, J. Fleischer, O. V. Tarasov and V. A. Smirnov, Phys. Lett. B **329**, 103 (1994) [arXiv:hep-ph/9403274]; F. J. Yndurain, Phys. Rept. **320**, 287 (1999) [arXiv:hep-ph/9903457]; B. L. Ioffe and K. N. Zyablyuk, Eur. Phys. J. C **27**, 229 (2003) [arXiv:hep-ph/0207183]; K. Zyablyuk, JHEP **0301**, 081 (2003) [arXiv:hep-ph/0210103]; A. Samsonov, arXiv:hep-ph/0407199.

[32] J. Kripfganz, Phys. Lett. B **101**, 169 (1981); A. Di Giacomo and G. C. Rossi, Phys. Lett. B **100**, 481 (1981); A. Di Giacomo and G. Paffuti, Phys. Lett. B **108**, 327 (1982); E. M. Ilgenfritz and M. Muller-Preussker, Phys. Lett. B **119**, 395 (1982); S. s. Xue, Phys. Lett. B **191**, 147 (1987); M. Campostrini, A. Di Giacomo and Y. Gunduc, Phys. Lett. B **225**, 393 (1989); A. Di Giacomo, H. Panagopoulos and E. Vicari, Nucl. Phys. B **338**, 294 (1990); X. D. Ji, arXiv:hep-ph/9506413; G. Boyd and D. E. Miller, arXiv:hep-ph/9608482.

[33] V. Koch, Int. J. Mod. Phys. E **6**, 203 (1997) [nucl-th/9706075].

[34] F. Giacosa, *Glueball phenomenology within a nonlocal approach* (PhD Thesis), Faculty for Mathematics and Physics of Tübingen University (2005).

[35] J. Goldstone, Nuovo Cim. **19**, 154 (1961).

[36] Y. Nambu, Phys. Rev. Lett. **4**, 380 (1960); M. Kobayashi and T. Maskawa, Prog. Theor. Phys. **49**, 652 (1973); C. Vafa and E. Witten, Nucl. Phys. B **234**, 173 (1984); L. Giusti and S. Necco, JHEP **0704**, 090 (2007) [arXiv:hep-lat/0702013]; Y. Nambu, Int. J. Mod. Phys. A **24**, 2371 (2009) [Rev. Mod. Phys. **81**, 1015 (2009)].

[37] S. Strüber and D. H. Rischke, Phys. Rev. D **77**, 085004 (2008) [arXiv:0708.2389 [hep-th]].

[38] F. Giacosa and G. Pagliara, Mod. Phys. Lett. A **26**, 2247 (2011) [arXiv:1005.4817 [hep-ph]].

[39] W. R. Frazer and A. W. Hendry, Phys. Rev. **134**, B1307 (1964).

[40] D. V. Bugg, Eur. Phys. J. C **52**, 55 (2007) [arXiv:0706.1341 [hep-ex]].

[41] I. Caprini, G. Colangelo and H. Leutwyler, Phys. Rev. Lett. **96**, 132001 (2006) [hep-ph/0512364]; H. Leutwyler, AIP Conf. Proc. **1030**, 46 (2008) [arXiv:0804.3182 [hep-ph]].

[42] F. J. Yndurain, R. Garcia-Martin and J. R. Pelaez, Phys. Rev. D **76**, 074034 (2007) [hep-ph/0701025]; R. Kaminski, R. Garcia-Martin, P. Grynkiewicz and J. R. Pelaez, Nucl. Phys. Proc. Suppl. **186**, 318 (2009) [arXiv:0811.4510 [hep-ph]].

[43] B. Peyaud [NA48 Collaboration], Nucl. Phys. Proc. Suppl. **187**, 29 (2009).

[44] F. Giacosa, arXiv:1110.5923 [nucl-th].

[45] G. Pagliara and F. Giacosa, Acta Phys. Polon. Supp. **4**, 753 (2011) [arXiv:1108.2782 [hep-ph]].

[46] F. Giacosa, G. Pagliara, Phys. Rev. C **76**, 065204 (2007) [arXiv:0707.3594 [hep-ph]].

[47] M. Urban, M. Buballa and J. Wambach, Nucl. Phys. A **697**, 338 (2002) [arXiv:hep-ph/0102260].

[48] J. S. Schwinger, Annals Phys. **2**, 407 (1957); M. Gell-Mann and M. Levy, Nuovo Cim. **16**, 705 (1960); S. Weinberg, Phys. Rev. Lett. **18**, 188 (1967).

[49] S. Gasiorowicz and D. A. Geffen, Rev. Mod. Phys. **41**, 531 (1969).

[50] P. Gavillet *et al.* [Amsterdam-CERN-Nijmegen-Oxford Collaboration], Phys. Lett. B **69**, 119 (1977).

[51] D. Parganlija, F. Giacosa and D. H. Rischke, Acta Phys. Polon. Supp. **3**, 963 (2010) [arXiv:1004.4817 [hep-ph]]; P. Kovacs, G. Wolf, F. Giacosa and D. Parganlija, arXiv:1102.4732 [hep-ph]; D. Parganlija, Acta Phys. Polon. Supp. **4**, 727 (2011) [arXiv:1105.3647 [hep-ph]]; D. Parganlija, arXiv:1109.4331 [hep-ph].

[52] D. Parganlija, F. Giacosa, D. H. Rischke, Phys. Rev. D **82**, 054024 (2010) [arXiv:1003.4934 [hep-ph]].

[53] P. Ko and S. Rudaz, Phys. Rev. D **50**, 6877 (1994).

[54] D. Parganlija, F. Giacosa and D. H. Rischke, AIP Conf. Proc. **1030**, 160 (2008) [arXiv:0804.3949 [hep-ph]].

[55] D. Parganlija, F. Giacosa and D. H. Rischke, arXiv:0911.3996 [nucl-th].

[56] D. Parganlija, F. Giacosa, D. H. Rischke, P. Kovacs and G. Wolf, Int. J. Mod. Phys. A **26**, 607 (2011) [arXiv:1009.2250 [hep-ph]]; D. Parganlija, F. Giacosa, P. Kovacs and G. Wolf, AIP Conf. Proc. **1343**, 328 (2011) [arXiv:1011.6104 [hep-ph]].

[57] D. Parganlija, F. Giacosa and D. H. Rischke, PoS C**ONFINEMENT8**, 070 (2008) [arXiv:0812.2183 [hep-ph]].

[58] R. L. Jaffe, Phys. Rev. D **15**, 267 (1977).

[59] S. Gallas, F. Giacosa and D. H. Rischke, Phys. Rev. D **82**, 014004 (2010) [arXiv:0907.5084 [hep-ph]].

[60] G. Grayer *et al.*, Nucl. Phys. B **75**, 189 (1974).

[61] H. Becker *et al.* [CERN-Cracow-Munich Collaboration], Nucl. Phys. B **151**, 46 (1979).

[62] T. Akesson *et al.* [Axial Field Spectrometer Collaboration], Nucl. Phys. B **264**, 154 (1986); A. Breakstone *et al.* [Ames-Bologna-CERN-Dortmund-Heidelberg-Warsaw Collaboration], Z. Phys. C **31**, 185 (1986); A. Breakstone *et al.* [Ames-Bologna-CERN-Dortmund-Heidelberg-Warsaw Collaboration], Z. Phys. C **48**, 569-576 (1990).

[63] R. Kaminski, L. Lesniak, J. P. Maillet, Phys. Rev. D **50**, 3145 (1994) [hep-ph/9403264].

[64] M. Harada, F. Sannino and J. Schechter, Phys. Rev. D **54**, 1991 (1996) [hep-ph/9511335].

[65] S. Ishida, M. Ishida, H. Takahashi, T. Ishida, K. Takamatsu, T. Tsuru, Prog. Theor. Phys. **95**, 745 (1996) [arXiv:hep-ph/9610325].

[66] N. A. Tornqvist, M. Roos, Phys. Rev. Lett. **76**, 1575 (1996) [arXiv:hep-ph/9511210].

[67] C. Amsler *et al.* [Crystal Barrel Collaboration], Phys. Lett. B **355**, 425 (1995).

[68] A. Abele *et al.* [Crystal Barrel Collaboration], Phys. Lett. B **380**, 453 (1996).

[69] D. Alde *et al.* [GAMS Collaboration], Phys. Lett. B **397**, 350 (1997).

[70] E. M. Aitala *et al.* [E791 Collaboration], Phys. Rev. Lett. **86**, 770 (2001) [hep-ex/0007028].

[71] G. Bonvicini *et al.* [CLEO Collaboration], Phys. Rev. D **76**, 012001 (2007) [arXiv:0704.3954 [hep-ex]].

[72] M. Ablikim *et al.* [BES Collaboration], Phys. Lett. B **598**, 149 (2004) [hep-ex/0406038].

[73] Y. S. Jin and A. Martin, Phys. Rev. **135**, B1369 (1964); Y. S. Jin and A. Martin, Phys. Rev. **135**, B1375 (1964); S. M. Roy, Phys. Lett. B **36**, 353 (1971).

[74] L. Rosselet, P. Extermann, J. Fischer, O. Guisan, R. Mermod, R. Sachot, A. M. Diamant-Berger and P. Bloch *et al.*, Phys. Rev. D **15**, 574 (1977).

[75] A. V. Anisovich and A. V. Sarantsev, Phys. Lett. B **413**, 137 (1997) [hep-ph/9705401]; R. Delbourgo and M. D. Scadron, Int. J. Mod. Phys. A **13**, 657 (1998) [hep-ph/9807504]; D. Black, A. H. Fariborz, S. Moussa, S. Nasri and J. Schechter, Phys. Rev. D **64**, 014031 (2001) [hep-ph/0012278]; M. D. Scadron, F. Kleefeld, G. Rupp and E. van Beveren, Nucl. Phys. A **724**, 391 (2003) [hep-ph/0211275]; D. V. Bugg, Phys. Lett. B **572**, 1 (2003) [Erratum-ibid. B **595**, 556 (2004)].

[76] S. N. Cherry and M. R. Pennington, Nucl. Phys. A **688**, 823 (2001) [hep-ph/0005208]; J. M. Link *et al.* [FOCUS Collaboration], Phys. Lett. B **621**, 72 (2005) [hep-ex/0503043].

[77] C. R. Munz, Nucl. Phys. A **609**, 364 (1996) [arXiv:hep-ph/9601206].

[78] R. Delbourgo, D. s. Liu and M. D. Scadron, Phys. Lett. B **446**, 332 (1999) [arXiv:hep-ph/9811474];

[79] D. Morgan, Phys. Lett. B **51**, 71 (1974); A. Bramon and E. Masso, Phys. Lett. B **93**, 65 (1980) [Erratum-ibid. B **107**, 455 (1981)]; M. D. Scadron, Phys. Rev. D **26**, 239 (1982); E. van Beveren, T. A. Rijken, K. Metzger, C. Dullemond, G. Rupp and J. E. Ribeiro, Z. Phys. C **30**, 615 (1986) [arXiv:0710.4067 [hep-ph]]; D. Morgan and M. R. Pennington, Z. Phys. C **48**, 623 (1990); D. Morgan and M. R. Pennington, Nucl. Phys. Proc. Suppl. **21**, 37 (1991); D. Morgan and M. R. Pennington, Phys. Rev. D **48**, 1185 (1993); D. Morgan and M. R. Pennington, Phys. Rev. D **48**, 5422 (1993); N. A. Tornqvist and M. Roos, Phys. Rev. Lett. **76**, 1575 (1996) [arXiv:hep-ph/9511210]; V. Elias, A. H. Fariborz, F. Shi and T. G. Steele, Nucl. Phys. A **633**, 279 (1998) [arXiv:hep-ph/9801415]; M. Ishida, Prog. Theor. Phys. **101**, 661 (1999) [arXiv:hep-ph/9902260]; P. Minkowski and W. Ochs, Eur. Phys. J. C **9**, 283 (1999) [arXiv:hep-ph/9811518]; J. L. Lucio Martinez and M. Napsuciale, Phys. Lett. B **454**, 365 (1999) [arXiv:hep-ph/9903234]; A. V. Anisovich, V. V. Anisovich, D. V. Bugg and V. A. Nikonov, Phys. Lett. B **456**, 80 (1999) [arXiv:hep-ph/9903396]; E. van Beveren, G. Rupp and M. D. Scadron, Phys. Lett. B **495**, 300 (2000) [Erratum-ibid. B **509**, 365 (2001)] [arXiv:hep-ph/0009265]; A. Deandrea, R. Gatto, G. Nardulli, A. D. Polosa and N. A. Tornqvist, Phys. Lett. B **502**, 79 (2001) [arXiv:hep-ph/0012120]; F. De Fazio and M. R. Pennington, Phys. Lett. B **521**, 15 (2001) [arXiv:hep-ph/0104289]; A. M. Badalian and B. L. G. Bakker, Phys. Rev. D **66**, 034025 (2002) [arXiv:hep-ph/0202246]; M. D. Scadron, G. Rupp, F. Kleefeld and E. van Beveren, Phys. Rev. D **69**, 014010 (2004) [Erratum-ibid. D **69**, 059901 (2004)] [arXiv:hep-ph/0309109]; M. Koll, R. Ricken, D. Merten, B. C. Metsch and H. R. Petry, Eur. Phys. J. A **9**, 73 (2000) [arXiv:hep-ph/0008220].

[80] N. N. Achasov, S. A. Devyanin and G. N. Shestakov, Phys. Lett. B **96**, 168 (1980); D. Black, A. H. Fariborz, F. Sannino and J. Schechter, Phys. Rev. D **59**, 074026 (1999) [arXiv:hep-ph/9808415]; J. R. Pelaez, Mod. Phys. Lett. A **19**, 2879 (2004) [arXiv:hep-ph/0411107]; A. H. Fariborz, R. Jora and J. Schechter, Phys. Rev. D **77**, 034006 (2008) [arXiv:0707.0843 [hep-ph]]; A. H. Fariborz, R. Jora and J. Schechter, Phys. Rev. D **79**, 074014 (2009) [arXiv:0902.2825 [hep-ph]]; A. H. Fariborz, arXiv:1109.2630 [hep-ph].

[81] F. E. Close and N. A. Tornqvist, J. Phys. G **28**, R249 (2002) [arXiv:hep-ph/0204205].

[82] T. Teshima, I. Kitamura and N. Morisita, J. Phys. G **28**, 1391 (2002) [arXiv:hep-ph/0105107].

[83] J. R. Pelaez, Phys. Rev. Lett. **92**, 102001 (2004) [arXiv:hep-ph/0309292]; J. R. Pelaez, AIP Conf. Proc. **814**, 670 (2006) [arXiv:hep-ph/0510118]; J. R. Pelaez and G. Rios, Phys. Rev. Lett. **97**, 242002 (2006) [arXiv:hep-ph/0610397].

[84] M. Napsuciale and S. Rodriguez, Phys. Rev. D **70**, 094043 (2004) [arXiv:hep-ph/0407037].

[85] T. Barnes, Phys. Lett. B **165**, 434 (1985); T. Branz, T. Gutsche and V. E. Lyubovitskij, Phys. Rev. D **82**, 054010 (2010) [arXiv:1007.4311 [hep-ph]].

[86] J. D. Weinstein and N. Isgur, Phys. Rev. D **41**, 2236 (1990).

[87] M. P. Locher, V. E. Markushin and H. Q. Zheng, Eur. Phys. J. C **4**, 317 (1998) [arXiv:hep-ph/9705230]; V. Baru, J. Haidenbauer, C. Hanhart, Yu. Kalashnikova and A. E. Kudryavtsev, Phys. Lett. B **586**, 53 (2004) [arXiv:hep-ph/0308129]; D. V. Bugg, Eur. Phys. J. C **47**, 57 (2006) [arXiv:hep-ph/0603089].

[88] V. E. Markushin and M. P. Locher, Frascati Phys. Ser. **15**, 229 (1999) [arXiv:hep-ph/9906249].

[89] R. L. Jaffe, K. Johnson, Phys. Lett. **B60**, 201 (1976); D. Robson, Nucl. Phys. B **130**, 328 (1977).

[90] Yu. S. Surovtsev, P. Bydzovsky, R. Kaminski and M. Nagy, Phys. Rev. D **81**, 016001 (2010) [arXiv:0811.0906 [nucl-th]].

[91] M. Alston-Garnjost, A. Barbaro-Galtieri, S. M. Flatte, J. H. Friedman, G. R. Lynch, S. D. Protopopescu, M. S. Rabin, F. T. Solmitz, Phys. Lett. B **36**, 152 (1971); S. M. Flatte, M. Alston-Garnjost, A. Barbaro-Galtieri, J. H. Friedman, G. R. Lynch, S. D. Protopopescu, M. S. Rabin, F. T. Solmitz, Phys. Lett. **B38**, 232 (1972); S. D. Protopopescu, M. Alston-Garnjost, A. Barbaro-Galtieri, S. M. Flatte, J. H. Friedman, T. A. Lasinski, G. R. Lynch, M. S. Rabin *et al.*, Phys. Rev. D **7**, 1279 (1973).

[92] R. Bizzarri, M. Foster, P. Gavillet, G. Labrosse, L. Montanet, R. Salmeron, P. Villemoes, C. Ghesquiere *et al.*, Nucl. Phys. B **14**, 169 (1969).

[93] B. Hyams, C. Jones, P. Weilhammer, W. Blum, H. Dietl, G. Grayer, W. Koch, E. Lorenz *et al.*, Nucl. Phys. B **64**, 134 (1973).

[94] D. M. Binnie, J. Carr, N. C. Debenham, A. Duane, D. A. Garbutt, W. G. Jones, J. Keyne, I. Siotis *et al.*, Phys. Rev. Lett. **31**, 1534 (1973).

[95] G. Grayer, B. Hyams, C. Jones, P. Schlein, P. Weilhammer, W. Blum, H. Dietl, W. Koch *et al.*, AIP Conf. Proc. **13**, 117 (1973); R. J. Leeper, M. Buttram, H. B. Crawley, D. W. Duke, R. C. Lamb, F. C. Peterson, Phys. Rev. D **16**, 2054 (1977); M. Aguilar-Benitez, M. Cerrada, A. Gonzalez-Arroyo, J. A. Rubio, F. J. Yndurain, A. M. Cooper-Sarkar, A. Gurtu, P. K. Malhotra *et al.*, Nucl. Phys. B **140**, 73 (1978); N. N. Achasov, S. A. Devyanin, G. N. Shestakov, Sov. J. Nucl. Phys. **32**, 566 (1980); G. Gidal, G. Goldhaber, J. G. Guy, R. E. Millikan, G. S. Abrams, M. S. Alam, C. A. Blocker, A. Blondel *et al.*, Phys. Lett. B **107**, 153 (1981); S. Abachi, P. S. Baringer, B. G. Bylsma, R. DeBonte, D. S. Koltick, F. J. Loeffler, E. H. Low, R. L. McIlwain *et al.*, Phys. Rev. Lett. **57**, 1990 (1986); M. Aguilar-Benitez, W. W. W. Allison, A. A. Batalov, E. Castelli, P. Cecchia, N. Colino, R. Contri, A. De Angelis *et al.*, Z. Phys. C **50**, 405 (1991); D. Morgan, M. R. Pennington, Phys. Rev. D **48**, 1185 (1993); B. S. Zou, D. V. Bugg, Phys. Rev. D **50**, 591 (1994); V. V. Anisovich, A. V. Sarantsev, A. A. Kondashov, Y. .D. Prokoshkin, S. A. Sadovsky, Phys. Lett. B **355**, 363 (1995); M. P. Locher, V. E. Markushin, H. Q. Zheng, Eur. Phys. J. C **4**, 317 (1998) [arXiv:hep-ph/9705230]; J. A. Oller, E. Oset, J. R. Pelaez, Phys. Rev. D **59**, 074001 (1999) [arXiv:hep-ph/9804209]; R. Kaminski, L. Lesniak, B. Loiseau, Eur. Phys. J. C **9**, 141 (1999) [arXiv:hep-ph/9810386]; D. Barberis *et al.* [WA102 Collaboration], Phys. Lett. B **453**, 325 (1999) [arXiv:hep-ex/9903044]; E. M. Aitala *et al.* [E791 Collaboration], Phys. Rev. Lett. **86**, 765 (2001) [arXiv:hep-ex/0007027]; A. Bramon, R. Escribano, J. L. Lucio M, M. Napsuciale, G. Pancheri, Eur. Phys. J. C **26**, 253-260 (2002) [arXiv:hep-ph/0204339]; A. Garmash *et al.* [BELLE Collaboration], Phys. Rev. D **71**, 092003 (2005) [arXiv:hep-ex/0412066]; K. M. Ecklund *et al.* [CLEO Collaboration], Phys. Rev. D **80**, 052009 (2009) [arXiv:0907.3201 [hep-ex]]; G. Mennessier, S. Narison, X. G. Wang, Phys. Lett. B **688**, 59 (2010) [arXiv:1002.1402 [hep-ph]].

[96] T. A. Armstrong *et al.* [WA76 Collaboration], Z. Phys. C **51**, 351 (1991).

[97] D. Barberis *et al.* [WA102 Collaboration], Phys. Lett. B **453**, 305 (1999).

[98] D. Barberis *et al.* [WA102 Collaboration], Phys. Lett. B **453**, 316 (1999) [arXiv:hep-ex/9903043].

[99] D. Barberis *et al.* [WA102 Collaboration], Phys. Lett. B **462**, 462 (1999) [arXiv:hep-ex/9907055].

[100] B. S. Zou and D. V. Bugg, Phys. Rev. D **48**, 3948 (1993).

[101] V. V. Anisovich and A. V. Sarantsev, Eur. Phys. J. A **16**, 229 (2003) [arXiv:hep-ph/0204328].

[102] C. Amsler, D. S. Armstrong, I. Augustin, C. A. Baker, B. M. Barnett, C. J. Batty, K. Beuchert, P. Birien *et al.*, Phys. Lett. B **342**, 433 (1995).

[103] D. Alde *et al.* [GAMS Collaboration], Z. Phys. C **66**, 375 (1995).

[104] D. Alde *et al.* [GAMS Collaboration], Eur. Phys. J. A **3**, 361 (1998).

[105] R. Bellazzini *et al.* [GAMS Collaboration], Phys. Lett. B **467**, 296 (1999).

[106] N. N. Achasov, G. N. Shestakov, Phys. Rev. D **58**, 054011 (1998) [hep-ph/9802286].

[107] R. R. Akhmetshin *et al.* [CMD-2 Collaboration], Phys. Lett. **B462**, 371 (1999) [hep-ex/9907005].

[108] R. R. Akhmetshin *et al.* [CMD-2 Collaboration], Phys. Lett. B **462**, 380 (1999) [arXiv:hep-ex/9907006].

[109] F. Ambrosino *et al.* [KLOE Collaboration], Eur. Phys. J. C **49**, 473 (2007) [hep-ex/0609009].

[110] T. Mori *et al.* [Belle Collaboration], Phys. Rev. D **75**, 051101 (2007) [arXiv:hep-ex/0610038].

[111] S. Uehara *et al.* [Belle Collaboration], Phys. Rev. D **78**, 052004 (2008) [arXiv:0805.3387 [hep-ex]].

[112] K. L. Au, D. Morgan, M. R. Pennington, Phys. Rev. D **35**, 1633 (1987).

[113] G. Janssen, B. C. Pearce, K. Holinde, J. Speth, Phys. Rev. D **52**, 2690 (1995) [nucl-th/9411021].

[114] D. V. Bugg, V. V. Anisovich, A. Sarantsev and B. S. Zou, Phys. Rev. D **50**, 4412 (1994).

[115] N. A. Tornqvist, Z. Phys. C **68**, 647 (1995) [hep-ph/9504372]; R. Kaminski, L. Lesniak, B. Loiseau, Eur. Phys. J. C **9**, 141 (1999) [hep-ph/9810386].

[116] D. V. Bugg, B. S. Zou, A. V. Sarantsev, Nucl. Phys. B **471**, 59 (1996).

[117] V. V. Anisovich and A. V. Sarantsev, Phys. Lett. B **382**, 429 (1996) [arXiv:hep-ph/9603276]; V. V. Anisovich, Yu. D. Prokoshkin and A. V. Sarantsev, Phys. Lett. B **389**, 388 (1996) [arXiv:hep-ph/9610414].

[118] V. V. Anisovich, Phys. Usp. **41**, 419 (1998) [Usp. Fiz. Nauk **168**, 481 (1998)] [arXiv:hep-ph/9712504].

[119] V. V. Anisovich, A. V. Sarantsev, Int. J. Mod. Phys. A **24**, 2481 (2009).

[120] R. A. Donald *et al.*, Nucl. Phys. B **11**, 551 (1969).

[121] N. M. Cason, V. A. Polychronakos, J. M. Bishop, N. N. Biswas, V. P. Kenney, D. S. Rhines, W. D. Shephard, J. M. Watson, Phys. Rev. Lett. **36**, 1485 (1976).

[122] A. J. Pawlicki, D. S. Ayres, D. H. Cohen, R. Diebold, S. L. Kramer and A. B. Wicklund, Phys. Rev. Lett. **37**, 1666 (1976); A. J. Pawlicki, D. S. Ayres, D. H. Cohen, R. Diebold, S. L. Kramer and A. B. Wicklund, Phys. Rev. D **15**, 3196 (1977).

[123] D. H. Cohen, D. S. Ayres, R. Diebold, S. L. Kramer, A. J. Pawlicki and A. B. Wicklund, Phys. Rev. D **22**, 2595 (1980).

[124] A. Etkin *et al.*, Phys. Rev. D **25**, 1786 (1982).

[125] C. Amsler *et al.* [Crystal Barrel Collaboration], Phys. Lett. B **291**, 347 (1992).

[126] C. Amsler *et al.* [Crystal Barrel. Collaboration], Phys. Lett. B **322**, 431 (1994).

[127] V. V. Anisovich *et al.* [Crystal Barrel Collaboration], Phys. Lett. B **323**, 233 (1994).

[128] V. V. Anisovich, D. V. Bugg, A. V. Sarantsev, B. S. Zou, Phys. Rev. D **50**, 1972 (1994).

[129] A. Abele, J. Adomeit, D. S. Armstrong, C. A. Baker, C. J. Batty, M. Benayoun, A. Berdoz, K. Beuchert *et al.*, Nucl. Phys. A **609**, 562 (1996).

[130] C. Amsler *et al.* [Crystal Barrel. Collaboration], Phys. Lett. B **333**, 277 (1994).

[131] S. J. Lindenbaum, R. S. Longacre, Phys. Lett. B **274**, 492 (1992).

[132] A. D. Martin, E. N. Ozmutlu, Nucl. Phys. B **158**, 520 (1979).

[133] M. Gaspero, Nucl. Phys. A **562**, 407 (1993).

[134] A. Lanaro, A. Adamo, M. Agnello, F. Balestra, G. Bendiscioli, A. Bertin, P. Boccaccio, G. C. Bonazzola *et al.*, Nucl. Phys. A **558**, 13C (1993).

[135] J. Li *et al.* [Belle Collaboration], Phys. Rev. Lett. **106**, 121802 (2011) [arXiv:1102.2759 [hep-ex]].

[136] W. Ochs, AIP Conf. Proc. **619**, 167 (2002) [hep-ph/0111309]; W. Ochs, Nucl. Phys. Proc. Suppl. **174**, 146 (2007) [hep-ph/0609207].

[137] P. Minkowski, W. Ochs, Eur. Phys. J. C **9**, 283 (1999) [hep-ph/9811518].

[138] W. Ochs, AIP Conf. Proc. **1257**, 252 (2010) [arXiv:1001.4486 [hep-ph]].

[139] C. Amsler *et al.* [Crystal Barrel Collaboration], Phys. Lett. B **353**, 571 (1995).

[140] M. Ablikim *et al.* [BES Collaboration], Phys. Lett. B **607**, 243 (2005) [arXiv:hep-ex/0411001].

[141] C. A. Baker *et al.*, Phys. Lett. B **467**, 147 (1999) [arXiv:1109.2287 [hep-ex]].

[142] F. E. Close, Rept. Prog. Phys. **51**, 833 (1988).

[143] L. Gray, T. Kalogeropoulos, A. Nandy, J. Roy, S. Zenone, Phys. Rev. D **27**, 307 (1983).

[144] F. G. Binon *et al.* [Serpukhov-Brussels-Annecy(LAPP) Collaboration], Nuovo Cim. A **78**, 313 (1983); F. G. Binon *et al.* [Serpukhov-Brussels-Annecy(LAPP) Collaboration], Nuovo Cim. A **80**, 363 (1984); D. Alde *et al.* [Serpukhov-Brussels-Los Alamos-Annecy(LAPP) Collaboration], Phys. Lett. B **198**, 286 (1987); D. Alde *et al.* [Serpukhov-Brussels-Los Alamos-Annecy(LAPP)-Pisa Collaboration], Phys. Lett. B **201**, 160 (1988).

[145] D. Alde *et al.* [Serpukhov-Brussels-Los Alamos-Annecy(LAPP) Collaboration], Nucl. Phys. B **269**, 485 (1986).

[146] S. I. Bityukov, G. V. Borisov, N. K. Vishnevsky, E. V. Vlasov, Y. .P. Gouz, R. I. Dzhelyadin, A. M. Zaitsev, Y. .M. Ivanyushenkov *et al.*, Sov. J. Nucl. Phys. **55**, 1535 (1992).

[147] D. V. Amelin, E. B. Berdnikov, S. I. Bityukov, G. V. Borisov, Y. .P. Gouz, V. A. Dorofeev, R. I. Dzhelyadin, A. V. Ekimov *et al.*, Phys. Atom. Nucl. **59**, 976 (1996).

[148] F. G. Binon, A. M. Blik, S. V. Donskov, S. Inaba, V. N. Kolosov, A. A. Lednev, V. A. Lishin, Y. .V. Mikhailov *et al.*, Phys. Atom. Nucl. **68**, 960 (2005).

[149] T. A. Armstrong *et al.* [WA76 Collaboration], Phys. Lett. B **228**, 536 (1989).

[150] S. Abatzis *et al.* [WA91 Collaboration], Phys. Lett. B **324**, 509 (1994); F. Antinori *et al.* [WA91 Collaboration], Phys. Lett. B **353**, 589 (1995).

[151] D. Barberis *et al.* [ WA102 Collaboration ], Phys. Lett. B **413**, 217 (1997) [hep-ex/9707021].

[152] D. Barberis *et al.* [WA102 Collaboration], Phys. Lett. B **471**, 440 (2000) [hep-ex/9912005].

[153] D. Barberis *et al.* [WA102 Collaboration], Phys. Lett. B **479**, 59 (2000) [arXiv:hep-ex/0003033].

[154] C. Amsler *et al.* [Crystal Barrel Collaboration], Phys. Lett. B **340**, 259 (1994).

[155] A. Abele *et al.* [Crystal Barrel Collaboration], Eur. Phys. J. C **19**, 667 (2001).

[156] A. Abele *et al.* [Crystal Barrel Collaboration], Phys. Lett. B **385**, 425 (1996).

[157] C. Amsler *et al.* [ Crystal Barrel Collaboration ], Phys. Lett. B **639**, 165 (2006).

[158] A. Bertin *et al.* [OBELIX Collaboration], Phys. Lett. B **408**, 476 (1997).

[159] A. Bertin *et al.* [OBELIX Collaboration], Phys. Rev. D **57**, 55 (1998).

[160] E. Klempt and A. Zaitsev, Phys. Rept. **454**, 1 (2007) [arXiv:0708.4016 [hep-ph]]; M. Albaladejo and J. A. Oller, Phys. Rev. Lett. **101**, 252002 (2008) [arXiv:0801.4929 [hep-ph]].

[161] C. Edwards, R. Partridge, C. Peck, F. Porter, D. Antreasyan, Y. F. Gu, W. S. Kollmann, M. Richardson *et al.*, Phys. Rev. Lett. **48**, 458 (1982).

[162] A. Etkin, K. J. Foley, R. S. Longacre, W. A. Love, T. W. Morris, S. Ozaki, E. D. Platner, V. A. Polychronakos *et al.*, Phys. Rev. D **25**, 2446 (1982).

[163] D. L. Burke, G. Trilling, G. S. Abrams, M. S. Alam, C. A. Blocker, A. Boyarski, M. Breidenbach, W. C. Carithers *et al.*, Phys. Rev. Lett. **49**, 632 (1982).

[164] E. D. Bloom and C. Peck, Ann. Rev. Nucl. Part. Sci. **33**, 143 (1983).

[165] E. G. H. Williams, J. M. Marraffino, C. E. Roos, J. W. Waters, M. S. Webster, R. N. Diamond, C. C. Chang, T. C. Davis *et al.*, Phys. Rev. D **30**, 877 (1984).

[166] J. E. Augustin *et al.* [DM2 Collaboration], Z. Phys. C **36**, 369 (1987).

[167] J. E. Augustin *et al.* [DM2 Collaboration], Phys. Rev. Lett. **60**, 2238 (1988).

[168] A. Falvard *et al.* [DM2 Collaboration], Phys. Rev. D **38**, 2706 (1988).

[169] R. S. Longacre, A. Etkin, K. J. Foley, W. A. Love, T. W. Morris, A. C. Saulys, E. D. Platner, S. J. Lindenbaum *et al.*, Phys. Lett. **B177**, 223 (1986); J. Becker *et al.* [Mark-III Collaboration], Phys. Rev. D **35**, 2077 (1987); T. A. Armstrong *et al.* [ WA76 Collaboration ], Phys. Lett. B **227**, 186 (1989).

[170] B. V. Bolonkin *et al.*, Yad. Fiz. **46**, 799 (1987) [Nucl. Phys. B **309**, 426 (1988)].

[171] D. Alde *et al.* [Serpukhov-Brussels-Los Alamos-Annecy(LAPP) Collaboration], Phys. Lett. B **182**, 105 (1986).

[172] D. Alde *et al.* [ IFVE-Brussels-Annecy-Los Alamos Collaboration ], Phys. Lett. **B284**, 457 (1992).

[173] R. M. Baltrusaitis *et al.* [MARK-III Collaboration], Phys. Rev. D **33**, 1222 (1986); T. Bolton *et al.*, Phys. Lett. B **278**, 495 (1992).

[174] D. Bisello *et al.* [DM2 Collaboration], Phys. Rev. D **39**, 701 (1989).

[175] T. A. Armstrong *et al.* [E760 Collaboration], Phys. Lett. B **307**, 394 (1993).

[176] D. V. Bugg, I. Scott, B. S. Zou, V. V. Anisovich, A. V. Sarantsev, T. H. Burnett and S. Sutlief, Phys. Lett. B **353**, 378 (1995).

[177] J. Z. Bai *et al.* [BES Collaboration], Phys. Lett. B **472**, 207 (2000) [arXiv:hep-ex/9909040].

[178] B. S. Zou, Nucl. Phys. A **692**, 362 (2001) [arXiv:hep-ph/0011174].

[179] J. Z. Bai *et al.* [BES Collaboration], Phys. Rev. D **68**, 052003 (2003) [hep-ex/0307058].

[180] M. Ablikim *et al.* [BES Collaboration], Phys. Lett. B **603**, 138 (2004) [arXiv:hep-ex/0409007].

[181] M. Ablikim *et al.* [BES Collaboration], Phys. Rev. D **72**, 092002 (2005) [arXiv:hep-ex/0508050].

[182] S. Chekanov *et al.* [ZEUS Collaboration], Phys. Rev. Lett. **101**, 112003 (2008) [arXiv:0806.0807 [hep-ex]].

[183] A. V. Anisovich *et al.*, Phys. Lett. B **449**, 154 (1999).

[184] J. Z. Bai *et al.* [BES Collaboration], Phys. Rev. Lett. **77**, 3959 (1996).

[185] D. V. Bugg, arXiv:hep-ph/0603018.

[186] M. Ablikim *et al.* [Bes Collaboration], Phys. Rev. D **73**, 112007 (2006) [arXiv:hep-ex/0604045].

[187] M. Ablikim *et al.*, Phys. Lett. B **642**, 441 (2006) [arXiv:hep-ex/0603048].

[188] V. V. Anisovich, V. A. Nikonov and A. V. Sarantsev, Phys. Atom. Nucl. **65**, 1545 (2002) [Yad. Fiz. **65**, 1583 (2002)] [arXiv:hep-ph/0102338].

[189] J. S. Schwinger, Phys. Lett. B **24**, 473 (1967); S. Weinberg, Phys. Rev. **166**, 1568 (1968).

[190] F. Halzen and A. D. Martin, *Quarks And Leptons: An Introductory Course In Modern Particle Physics*, John Wiley & Sons (1984).

[191] W. Eshraim, PhD Thesis (in preparation).

[192] F. Giacosa, T. .Gutsche, V. E. Lyubovitskij and A. Faessler, Phys. Rev. D **72**, 114021 (2005) [hep-ph/0511171].

[193] S. Janowski, PhD Thesis (in preparation).

[194] A. Heinz, S. Struber, F. Giacosa and D. H. Rischke, Phys. Rev. D **79**, 037502 (2009) [arXiv:0805.1134 [hep-ph]]; A. Heinz, S. Struber, F. Giacosa and D. H. Rischke, Acta Phys. Polon. Supp. **3**, 925 (2010) [arXiv:1006.5393 [hep-ph]].

[195] S. Gallas, F. Giacosa and D. H. Rischke, PoS **CONFINEMENT8**, 089 (2008) [arXiv:0901.4043 [hep-ph]].

[196] L. R. Ram Mohan, Phys. Rev. D **14**, 2670 (1976); G. Baym and G. Grinstein, Phys. Rev. D **15**, 2897 (1977); H. Goldberg, Phys. Lett. B **131**, 133 (1983); P. K. Sahu, R. Basu and B. Datta, Astrophys. J. **416**, 267 (1993); D. Metzger, H. Meyer-Ortmanns and H. J. Pirner, Phys. Lett. B **321**, 66 (1994) [Erratum-ibid. B **328**, 547 (1994)] [hep-ph/9312252]; A. Bhattacharyya and S. Raha, J. Phys. GG **21**, 741 (1995); A. Bochkarev and J. I. Kapusta, Phys. Rev. D **54**, 4066 (1996) [hep-ph/9602405]; H. -S. Roh and T. Matsui, Eur. Phys. J. A **1**, 205 (1998) [nucl-th/9611050]; N. Petropoulos, J. Phys. GG **25**, 2225 (1999) [hep-ph/9807331]; J. Baacke and S. Michalski, Phys. Rev. D **67**, 085006 (2003) [hep-ph/0210060]; J. D. Shafer and J. R. Shepard, Phys. Rev. D **67**, 085025 (2003); J. Baacke and S. Michalski, Phys. Rev. D **70**, 085002 (2004) [hep-ph/0407152]; T. Herpay, A. Patkos, Z. .Szep and P. Szepfalusy, Phys. Rev. D **71**, 125017 (2005) [hep-ph/0504167]; J. Yasuda, arXiv:0801.0902 [hep-ph]; J. O. Andersen and T. Brauner, Phys. Rev. D **78**, 014030 (2008) [arXiv:0804.4604 [hep-ph]]; H. P. Tran, V. L. Nguyen, T. A. Nguyen and V. H. Le, Phys. Rev. D **78**, 105016 (2008); E. S. Bowman and J. I. Kapusta, Phys. Rev. C **79**, 015202 (2009) [arXiv:0810.0042 [nucl-th]]; F. Karsch, B. -J. Schaefer, M. Wagner and J. Wambach, Phys. Lett. B **698**, 256 (2011) [arXiv:1009.5211 [hep-ph]]; B. -J. Schaefer and M. Wagner, arXiv:1111.6871 [hep-ph].

[197] S. Gallas, F. Giacosa and G. Pagliara, Nucl. Phys. A **872**, 13 (2011) [arXiv:1105.5003 [hep-ph]].

[198] J. T. Lenaghan, D. H. Rischke and J. Schaffner-Bielich, Phys. Rev. D **62**, 085008 (2000) [nucl-th/0004006].

[199] O. W. Greenberg, Phys. Rev. Lett. **89**, 231602 (2002) [arXiv:hep-ph/0201258].

[200] U. G. Meissner, Phys. Rept. **161**, 213 (1988).

[201] J. Boguta, Phys. Lett. B **120**, 34 (1983); O. Kaymakcalan and J. Schechter, Phys. Rev. D **31**, 1109 (1985); R. D. Pisarski, arXiv:hep-ph/9503330.

[202] F. Giacosa, Phys. Rev. D **80**, 074028 (2009) [arXiv:0903.4481 [hep-ph]].

[203] S. Janowski, D. Parganlija, F. Giacosa and D. H. Rischke, Phys. Rev. D **84**, 054007 (2011) [arXiv:1103.3238 [hep-ph]].

[204] C. Amsler and F. E. Close, Phys. Lett. B **353**, 385 (1995) [arXiv:hep-ph/9505219].

[205] W. J. Lee and D. Weingarten, Phys. Rev. D **61**, 014015 (2000) [arXiv:hep-lat/9910008]; H. Y. Cheng, C. K. Chua and K. F. Liu, Phys. Rev. D **74**, 094005 (2006) [arXiv:hep-ph/0607206].

[206] C. Amsler and F. E. Close, Phys. Rev. D **53**, 295 (1996) [arXiv:hep-ph/9507326]; F. E. Close and A. Kirk, Eur. Phys. J. C **21**, 531 (2001) [arXiv:hep-ph/0103173]; F. Giacosa, T. Gutsche and A. Faessler, Phys. Rev. C **71**, 025202 (2005) [arXiv:hep-ph/0408085]; T. Teshima, I. Kitamura and N. Morisita, J. Phys. G **30**, 663 (2004) [arXiv:hep-ph/0305296].

[207] F. Giacosa, T. Gutsche, V. E. Lyubovitskij and A. Faessler, Phys. Rev. D **72**, 094006 (2005) [arXiv:hep-ph/0509247]; F. Giacosa, T. Gutsche, V. E. Lyubovitskij and A. Faessler, Phys. Lett. B **622**, 277 (2005) [arXiv:hep-ph/0504033]; A. H. Fariborz, Phys. Rev. **D74**, 054030 (2006) [hep-ph/0607105].

[208] R. L. Jaffe, Phys. Rev. D **15**, 281 (1977); A. H. Fariborz, Int. J. Mod. Phys. A **19**, 2095 (2004).

[209] L. Maiani, F. Piccinini, A. D. Polosa and V. Riquer, Phys. Rev. Lett. **93**, 212002 (2004) [arXiv:hep-ph/0407017]; F. Giacosa, Phys. Rev. D **74**, 014028 (2006) [arXiv:hep-ph/0605191]; A. H. Fariborz, R. Jora and J. Schechter, Phys. Rev. D **76**, 114001 (2007) [arXiv:0708.3402 [hep-ph]]; G. 't Hooft, G. Isidori, L. Maiani, A. D. Polosa and V. Riquer, Phys. Lett. B **662**, 424 (2008) [arXiv:0801.2288 [hep-ph]]; T. Kojo and D. Jido, Phys. Rev. D **78**, 114005 (2008) [arXiv:0802.2372 [hep-ph]]; T. Kojo and D. Jido, arXiv:0807.2364 [hep-ph].

[210] A. H. Fariborz, R. Jora and J. Schechter, Phys. Rev. D **72**, 034001 (2005) [arXiv:hep-ph/0506170].

[211] F. Giacosa, Phys. Rev. D **75**, 054007 (2007) [hep-ph/0611388].

[212] F. Giacosa, *Ein effektives chirales Modell der QCD mit Vektormesonen, Dilaton und Tetraquarks: Physik im Vakuum und bei nichtverschwindender Dichte und Temperatur* (Habilitation Thesis), Institute for Theoretical Physics of Frankfurt University (2011).

[213] G. 't Hooft, Phys. Rev. D **14**, 3432 (1976) [Erratum-ibid. D **18**, 2199 (1978)]; G. 't Hooft, Phys. Rept. **142**, 357 (1986).

[214] G. Ecker, J. Gasser, A. Pich and E. de Rafael, Nucl. Phys. B **321**, 311 (1989); G. Ecker, J. Gasser, H. Leutwyler, A. Pich and E. de Rafael, Phys. Lett. B **223**, 425 (1989).

[215] M. Bando, T. Kugo and K. Yamawaki, Phys. Rept. **164**, 217 (1988).

[216] M. C. Birse, Z. Phys. A **355**, 231 (1996) [arXiv:hep-ph/9603251].

[217] H. B. O'Connell, B. C. Pearce, A. W. Thomas and A. G. Williams, Prog. Part. Nucl. Phys. **39**, 201 (1997) [arXiv:hep-ph/9501251].

[218] J. J. Sakurai, Annals Phys. **11**, 1 (1960).

[219] D. Lurie, *Particles and Fields*, John Wiley & Sons (1968).

[220] D. Parganlija, *Pion-Pion-Streuung in einem geeichten linearen Sigma-Modell mit chiraler $U(2)_R \times U(2)_L$-Symmetrie* (Diploma Thesis), Institute for Theoretical Physics of Frankfurt University (2007).

[221] L. Roca, E. Oset and J. Singh, Phys. Rev. D **72**, 014002 (2005) [arXiv:hep-ph/0503273].

[222] L. S. Geng, E. Oset, J. R. Pelaez and L. Roca, Eur. Phys. J. A **39**, 81 (2009) [arXiv:0811.1941 [hep-ph]].

[223] M. Wagner and S. Leupold, Phys. Lett. B **670**, 22 (2008) [arXiv:0708.2223 [hep-ph]].

[224] S. Schael *et al.* [ALEPH Collaboration], Phys. Rept. **421**, 191 (2005) [arXiv:hep-ex/0506072].

[225] M. Harada and K. Yamawaki, Phys. Rept. **381**, 1 (2003) [arXiv:hep-ph/0302103].

[226] K. Kawarabayashi and M. Suzuki, Phys. Rev. Lett. **16**, 255 (1966); Riazuddin and Fayyazuddin, Phys. Rev. **147**, 1071 (1966).

[227] F. Giacosa, arXiv:0712.0186 [hep-ph].

[228] F. Ambrosino *et al.*, JHEP **0907**, 105 (2009) [arXiv:0906.3819 [hep-ph]].

[229] B. Ananthanarayan, G. Colangelo, J. Gasser and H. Leutwyler, Phys. Rept. **353**, 207 (2001) [arXiv:hep-ph/0005297].

[230] A. H. Fariborz, N. W. Park, J. Schechter and M. Naeem Shahid, Phys. Rev. D **80**, 113001 (2009) [arXiv:0907.0482 [hep-ph]].

[231] M. S. Bhagwat, L. Chang, Y. X. Liu, C. D. Roberts and P. C. Tandy, Phys. Rev. C **76**, 045203 (2007) [arXiv:0708.1118 [nucl-th]].

[232] M. Harada, F. Sannino and J. Schechter, Phys. Rev. D **69**, 034005 (2004) [arXiv:hep-ph/0309206].

[233] N. Mathur *et al.*, Phys. Rev. D **76**, 114505 (2007) [arXiv:hep-ph/0607110]; T. Draper, T. Doi, K. F. Liu, D. Mankame, N. Mathur and X. f. Meng, PoS **LATTICE2008**, 108 (2008) [arXiv:0810.5512 [hep-lat]].

[234] C. S. Fischer and R. Williams, Phys. Rev. Lett. **103**, 122001 (2009) [arXiv:0905.2291 [hep-ph]].

[235] B. Bloch-Devaux [NA48 Collaboration], Nucl. Phys. A **827**, 234C (2009).

[236] S. Weinberg, Phys. Rev. Lett. **17**, 616 (1966).

[237] E. Santini, M. D. Cozma, A. Faessler, C. Fuchs, M. I. Krivoruchenko and B. Martemyanov, Phys. Rev. C **78** (2008) 034910 [arXiv:0804.3702 [nucl-th]]; W. Peters, M. Post, H. Lenske, S. Leupold and U. Mosel, Nucl. Phys. A **632** (1998) 109 [arXiv:nucl-th/9708004]; M. Post, S. Leupold and U. Mosel, Nucl. Phys. A **689**, 753 (2001) [arXiv:nucl-th/0008027].

[238] C. A. Baker *et al.*, Phys. Lett. B **563**, 140 (2003).

[239] A. Abele *et al.* [CRYSTAL BARREL Collaboration], Eur. Phys. J. C **21**, 261 (2001).

[240] G. Veneziano, Nucl. Phys. B **159**, 213 (1979); E. Witten, Nucl. Phys. B **156**, 269 (1979);

[241] C. Rosenzweig, J. Schechter and C. G. Trahern, Phys. Rev. D **21**, 3388 (1980); J. Schechter, Phys. Rev. D **21**, 3393 (1980); P. Di Vecchia and G. Veneziano, Nucl. Phys. B **171**, 253 (1980); E. Witten, Annals Phys. **128**, 363 (1980); A. Aurilia, Y. Takahashi and P. K. Townsend, Phys. Lett. B **95**, 265 (1980); K. Kawarabayashi and N. Ohta, Nucl. Phys. B **175**, 477 (1980); R. Alkofer, M. A. Nowak, J. J. M. Verbaarschot and I. Zahed, Phys. Lett. B **233**, 205 (1989); R. Alkofer and I. Zahed, Phys. Lett. B **238**, 149 (1990); S. D. H. Hsu, F. Sannino and J. Schechter, Phys. Lett. B **427**, 300 (1998) [arXiv:hep-th/9801097]; A. H. Fariborz, R. Jora and J. Schechter, Phys. Rev. D **77**, 094004 (2008) [arXiv:0801.2552 [hep-ph]].

[242] M. Kobayashi, H. Kondo and T. Maskawa, Prog. Theor. Phys. **45**, 1955 (1971).

[243] J. Schaffner-Bielich, Phys. Rev. Lett. **84**, 3261 (2000) [hep-ph/9906361].

[244] E. Klempt, B. C. Metsch, C. R. Munz and H. R. Petry, Phys. Lett. B **361**, 160 (1995) [arXiv:hep-ph/9507449]; V. Dmitrasinovic, Phys. Rev. C **53**, 1383 (1996); C. Ritter, B. C. Metsch, C. R. Munz and H. R. Petry, Phys. Lett. B **380**, 431 (1996) [arXiv:hep-ph/9601246]; V. Dmitrasinovic, Phys. Rev. D **56**, 247 (1997).

[245] A. Habersetzer, *Spectral Densities of the $\tau$ Lepton in a Global $U(2)_L \times U(2)_R$ Linear Sigma Model with Electroweak Interaction* (Diploma Thesis), Institute for Theoretical Physics of Frankfurt University (2011).

[246] G. Wolf, private communication.

[247] L. Burakovsky and J. T. Goldman, Phys. Rev. D **57**, 2879 (1998) [arXiv:hep-ph/9703271].

[248] S. Godfrey and N. Isgur, Phys. Rev. D **32**, 189 (1985); M. Suzuki, Phys. Rev. D **47**, 1252 (1993); M. Suzuki, Phys. Rev. D **50**, 4708 (1994) [Erratum-ibid. D **51**, 1428 (1995 PHRVA,D51,1428.1995)]; L. Burakovsky and J. T. Goldman, Phys. Rev. D **56**, 1368 (1997) [arXiv:hep-ph/9703274].

[249] H. J. Lipkin, Phys. Lett. B **72**, 249 (1977); H. J. Lipkin, Phys. Lett. B **303**, 119 (1993) [arXiv:hep-ph/9301206].

[250] H. Y. Cheng, arXiv:1110.2249 [hep-ph].

[251] R. K. Carnegie, R. J. Cashmore, W. M. Dunwoodie, T. A. Lasinski and D. W. G. Leith, Phys. Lett. B **68**, 287 (1977); J. L. Rosner, Comments Nucl. Part. Phys. **16**, 109 (1986); N. Isgur and M. B. Wise, Phys. Lett. B **232**, 113 (1989); H. G. Blundell, S. Godfrey and B. Phelps, Phys. Rev. D **53**, 3712 (1996) [arXiv:hep-ph/9510245]; D. M. Asner *et al.* [CLEO Collaboration], Phys. Rev. D **62**, 072006 (2000) [arXiv:hep-ex/0004002]; H. Y. Cheng, Phys. Rev. D **67**, 094007 (2003) [arXiv:hep-ph/0301198]; T. Barnes, N. Black and P. R. Page, Phys. Rev. D **68**, 054014 (2003) [arXiv:nucl-th/0208072]; J. Vijande, F. Fernandez and

A. Valcarce, J. Phys. G **31**, 481 (2005) [arXiv:hep-ph/0411299]. D. M. Li, B. Ma and H. Yu, Eur. Phys. J. A **26**, 141 (2005) [arXiv:hep-ph/0509215]; D. M. Li and Z. Li, Eur. Phys. J. A **28**, 369 (2006) [arXiv:hep-ph/0606297]; H. Hatanaka and K. C. Yang, Phys. Rev. D **77**, 094023 (2008) [Erratum-ibid. D **78**, 059902 (2008)] [arXiv:0804.3198 [hep-ph]]; H. Y. Cheng and C. K. Chua, Phys. Rev. D **81**, 114006 (2010) [Erratum-ibid. D **82**, 059904 (2010)] [arXiv:0909.4627 [hep-ph]].

[252] F. E. Close and A. Kirk, Z. Phys. C **76**, 469 (1997) [arXiv:hep-ph/9706543]; D. M. Li, H. Yu and Q. X. Shen, Chin. Phys. Lett. **17**, 558 (2000) [arXiv:hep-ph/0001011]; W. S. Carvalho, A. S. de Castro and A. C. B. Antunes, J. Phys. A **35**, 7585 (2002) [arXiv:hep-ph/0207372]; D. M. B. Li, B. Ma, Y. X. Li, Q. K. Yao and H. Yu, Eur. Phys. J. C **37**, 323 (2004) [arXiv:hep-ph/0408214]. K. -C. Yang, Phys. Rev. D **84**, 034035 (2011) [arXiv:1011.6113 [hep-ph]].

[253] G. D. Tikhomirov, I. A. Erofeev, O. N. Erofeeva and V. N. Luzin, Phys. Atom. Nucl. **66**, 828 (2003) [Yad. Fiz. **66**, 860 (2003)];

[254] J. A. Oller, E. Oset, Phys. Rev. D **60**, 074023 (1999) [arXiv:hep-ph/9809337].

[255] M. N. Achasov, S. E. Baru, K. I. Beloborodov, A. V. Berdyugin, A. V. Bozhenok, A. D. Bukin, D. A. Bukin, S. V. Burdin *et al.*, Phys. Lett. B **485**, 349 (2000) [arXiv:hep-ex/0005017].

[256] B. Aubert *et al.* [BABAR Collaboration], Phys. Rev. D **74**, 032003 (2006) [arXiv:hep-ex/0605003].

[257] B. Aubert *et al.* [BABAR Collaboration], Phys. Rev. D **76**, 012008 (2007) [arXiv:0704.0630 [hep-ex]].

[258] J. A. Oller, E. Oset, Nucl. Phys. A **620**, 438 (1997) [arXiv:hep-ph/9702314].

[259] V. A. Polychronakos *et al.*, Phys. Rev. D **19**, 1317 (1979).

[260] A. B. Wicklund, D. S. Ayres, D. H. Cohen, R. Diebold and A. J. Pawlicki, Phys. Rev. Lett. **45**, 1469 (1980).

[261] V. V. Vladimirsky *et al.*, Phys. Atom. Nucl. **69**, 493 (2006) [Yad. Fiz. **69**, 515 (2006)];

[262] M. Bargiotti *et al.* [OBELIX Collaboration], Eur. Phys. J. C **26**, 371 (2003).

[263] D. Aston, N. Awaji, T. Bienz, F. Bird, J. D'Amore, W. M. Dunwoodie, R. Endorf, K. Fujii *et al.*, Nucl. Phys. B **296**, 493 (1988).

[264] D. M. Asner *et al.* [CLEO Collaboration], Phys. Rev. D **61**, 012002 (2000) [hep-ex/9902022].

[265] T. E. Coan *et al.* [CLEO Collaboration], Phys. Rev. Lett. **92**, 232001 (2004) [hep-ex/0401005].

[266] A. Drutskoy *et al.* [Belle Collaboration], Phys. Lett. B **542**, 171 (2002) [hep-ex/0207041].

[267] R. Nacasch *et al.*, Nucl. Phys. B **135**, 203 (1978).

[268] P. Achard *et al.*[L3 Collaboration], JHEP **0703**, 018 (2007).

[269] R. L. Jaffe and K. Johnson, Phys. Lett. B **60**, 201 (1976); R. Konoplich and M. Shchepkin, Nuovo Cim. A **67**, 211 (1982); M. Jezabek and J. Szwed, Acta Phys. Polon. B **14**, 599 (1983); R. L. Jaffe, K. Johnson and Z. Ryzak, Annals Phys. **168**, 344 (1986); M. Strohmeier-Presicek, T. Gutsche, R. Vinh Mau and A. Faessler, Phys. Rev. D **60**, 054010 (1999) [arXiv:hep-ph/9904461].

[270] S. Godfrey and J. Napolitano, Rev. Mod. Phys. **71**, 1411 (1999) [arXiv:hep-ph/9811410]; C. Amsler and N. A. Tornqvist, Phys. Rept. **389**, 61 (2004).

[271] C. Morningstar and M. J. Peardon, AIP Conf. Proc. **688**, 220 (2004) [arXiv:nucl-th/0309068]; M. Loan, X. Q. Luo and Z. H. Luo, Int. J. Mod. Phys. A **21**, 2905 (2006) [arXiv:hep-lat/0503038]; E. B. Gregory, A. C. Irving, C. C. McNeile, S. Miller and Z. Sroczynski, PoS **LAT2005**, 027 (2006) [arXiv:hep-lat/0510066]; Y. Chen *et al.*, Phys. Rev. D **73**, 014516 (2006) [arXiv:hep-lat/0510074].

[272] C. Rosenzweig, A. Salomone and J. Schechter, Phys. Rev. D **24**, 2545 (1981); A. Salomone, J. Schechter and T. Tudron, Phys. Rev. D **23**, 1143 (1981); C. Rosenzweig, A. Salomone and J. Schechter, Nucl. Phys. B **206**, 12 (1982) [Erratum-ibid. B **207**, 546 (1982)]; A. A. Migdal and M. A. Shifman, Phys. Lett. B **114**, 445 (1982); H. Gomm and J. Schechter, Phys. Lett. B **158**, 449 (1985); R. Gomm, P. Jain, R. Johnson and J. Schechter, Phys. Rev. D **33**, 801 (1986).

[273] J. Schaffner and I. N. Mishustin, Phys. Rev. C **53**, 1416 (1996) [nucl-th/9506011]; S. Weissenborn, D. Chatterjee and J. Schaffner-Bielich, arXiv:1112.0234 [astro-ph.HE].

[274] P. Papazoglou, D. Zschiesche, S. Schramm, J. Schaffner-Bielich, H. Stoecker and W. Greiner, Phys. Rev. C **59**, 411 (1999) [nucl-th/9806087]; N. K. Glendenning and J. Schaffner-Bielich, Phys. Rev. C **60**, 025803 (1999) [astro-ph/9810290]; D. Zschiesche, P. Papazoglou, S. Schramm, J. Schaffner-Bielich, H. Stoecker and W. Greiner, Phys. Rev. C **63**, 025211 (2001) [nucl-th/0001055]; D. Zschiesche, L. Tolos, J. Schaffner-Bielich and R. D. Pisarski, Phys. Rev. C **75**, 055202 (2007) [nucl-th/0608044]; V. Dexheimer, G. Pagliara, L. Tolos, J. Schaffner-Bielich and S. Schramm, Eur. Phys. J. A **38**, 105 (2008) [arXiv:0805.3301 [nucl-th]].

[275] E. van Beveren and G. Rupp, Mod. Phys. Lett. A **19**, 1949 (2004) [hep-ph/0406242].

[276] J. von Fraunhofer, Denkschriften der Königlichen Akademie der Wissenschaften zu München, **V**, 193-226 (1814-15).

[277] J. Balmer, Annalen der Physik und Chemie **25**, 80 (1885).

[278] N. Bohr, Philosophical Magazine **26**, 1 (1913).